

AGARD CP No. 37

AD 68 56665

AGARD CONFERENCE PROCEEDINGS No. 37

AGARD

ADVISORY GROUP FOR AEROSPACE RESEARCH & DEVELOPMENT

7 RUE ANCELLE 92 NEUILLY SUR SEINE FRANCE

## Scatter Propagation of Radio Waves

PART 1



AUGUST 1968

NORTH ATLANTIC TREATY ORGANIZATION



AGARD Conference Proceedings No. 37

NORTH ATLANTIC TREATY ORGANIZATION  
ADVISORY GROUP FOR AEROSPACE RESEARCH AND DEVELOPMENT  
(ORGANISATION DU TRAITE DE L' ATLANTIQUE NORD)

SCATTER PROPAGATION OF RADIO WAVES

Published in Two Parts

P A R T   1

Papers presented at the XIVth Symposium of the Electromagnetic Wave Propagation Committee  
of the Avionics Panel of AGARD, held at Sandefjord, Norway, 19th - 23rd August 1968.

## SUMMARY

The volume contains 50 authoritative papers on various aspects of scatter propagation of radio waves. The importance of scatter propagation for communication purposes, as well as the use of scattered radio waves as diagnostic tools for studying the scattering media, are discussed.

The book deals with scatter from the ionospheric D-, E- and F-regions, with scatter from the troposphere, and with scatter from the earth's surface. A record of the discussions on the various topics is included in the book.

## RESUME

Le présent volume contient 50 exposés autoritaires sur divers aspects de la propagation par diffusion des ondes radioélectriques. L'importance de la propagation par diffusion pour les besoins de la communication et l'utilisation des ondes radioélectriques diffusées, comme outils diagnostiques pour étudier les moyens de diffusion, sont examinées.

L'ouvrage traite de la diffusion provenant des zones D, E et F ionosphériques, de la diffusion provenant de la troposphère et de celle provenant de la surface de la Terre. Il comporte également le texte des discussions sur les divers sujets présentés.

## **FOREWORD**

This volume contains the proceedings of the 14th annual technical meeting of the Electromagnetic Wave Propagation Committee of the Avionics Panel of AGARD. It has been the policy of the EPC to choose for its technical meetings rather specialised topics of current interest, to bring together competent workers in those areas to present and discuss the latest developments, and to make the information gathered in this way available through publication of a series of conference proceedings. This policy is clearly reflected in the titles of the books now printed, the latest of which are: "Spread-F and its Effects on Radio Communications", "Propagation Factors in Space Communications", and "Propagation Near the Lowest Usable High Frequency", from the EPC Symposia in 1964, 1965 and 1966 respectively.

The present book deals with "Scatter Propagation of Radio Waves", a topic of interest for the geophysicist as well as the communication engineer. Some fifty papers, including eight invited review papers, were presented at the meeting, treating various theoretical and experimental aspects of scattering from the ground, the sea, and from irregularities in the troposphere and ionosphere. The plan of the book closely follows the conference programme, including records of the discussion periods which were held at the end of each session, or after a group of papers dealing with a specific topic. A summing-up and evaluation of the scientific programme by four of the participants will be found as the last item in the book.

A committee with the following members was responsible for the scientific programme of the symposium:

E.S. Warren, Defence Research Telecommunication Establishment,  
Ottawa, Canada (Programme Chairman)

P.J. Bartholomé, SHAPE Technical Centre, The Hague, Netherlands

R. Cohen, Aeronomy Laboratory, ERL/ESSA, Boulder, Colorado, USA

H. Jeske, Meteorologisches Institut, Universität Hamburg, Germany

G. Lange-Hesse, Max Planck Institut für Aeronomie, Lindau/Harz,  
Germany

E.V. Thrane, Institute for Telecommunication Sciences, ERL/ESSA,  
Boulder, Colorado, USA.

The editor feels strongly that, if proceedings of this type are to be useful, they must appear in print very soon after the conference. An effort has therefore been made by all parties concerned to speed up the publication procedure. To obtain speed, however, certain sacrifices are necessary. For example, it has not been possible to send the papers out to independent referees, nor has it been considered practical to send galley proofs to individual authors. But then the purpose of this book is not to compete with standard scientific journals, but to supplement these by providing the participants, as well as other workers, with a useful reference record of the meeting and an up-to-date survey of work in the field. As such, it is the editor's hope that the book will be a success.

Eivind Thrane.

## CONTENTS

	Page
SUMMARY	11
RESUME	11
FOREWORD	111

## PART 1

### SESSION 1 - GROUND SCATTER

Paper

GROUND SCATTER IN REVIEW by Edgar C. Hayden	1
SURFACE SCATTERING IN OCEAN ROUGHNESS AND SEA ICE STUDIES by Albert W. Biggs	2
ANALYSE DES PHENOMENES DE DIFFUSION LATERALE DANS UNE EXPERIENCE BISTATIQUE A L'AIDE DE DEUX RADARS MONOSTATIQUES DECAMETRIQUES par M. Crochet	3
SOME FEATURES OF HF BACKSCATTER IONOGRAMS by L. W. Barclay	4
DISCUSSION	5

### SESSION 2 - GROUND SCATTER AND SCATTER BY PARTICULATE SUSPENSIONS

LA REFLEXION EN ONDES DECAMETRIQUES PAR LA SURFACE TERRESTRE EN EMISSION IMPULSIONNELLE ET SON ROLE DANS L'INTERPRETATION DES SPECTRES DE FREQUENCE DES ECHOS OBTENUS DANS LES SONDAGES PAR RETRODIFFUSION par Claude Goutelard	6
HF GROUND BACKSCATTER ANALYSIS WITH THE AID OF COMPUTER RAY TRACING by R. G. Maliphant	7
INTERFERENCE PATTERNS IN HF SIGNALS BACKSCATTERED FROM OCEAN WAVES by D. B. Muldrew	8
SOME CHARACTERISTICS OF GROUND SIDE-SCATTER AT 20 MHZ by D. W. Rice	9
FADING AMPLITUDE DUE TO INTERFERENCE FROM FORWARD SEA SCATTER by G. C. Rider	10

Paper

APERTURE SYNTHESIS IN IONOSPHERIC GROUND BACKSCATTER RADAR by E. D. R. Shearman and J. Clarke	11
COURTE NOTE SUR LES ECHOS 2 × F DIFFUS OBSERVES A DJIBOUTI par A. M. Bourdila et J. Odoux	12
SCATTERING OF ELECTROMAGNETIC RADIATION BY PARTICULATE SUSPENSIONS IN THE ATMOSPHERE by Kurt Bullrich	13
DISCUSSION	14

SESSION 3 - TROPOSPHERIC SCATTER

SCATTERING OF RADIO WAVES FROM REGULAR AND IRREGULAR TIME VARYING REFRACTIVE INDEX STRUCTURES IN THE TROPOSPHERE by Dag T Gjessing	15
THEORETICAL ANALYSIS MEDIUM-DEPENDENT FLUCTUATIONS WITH TROPOSPHERIC SCATTER LINKS, AND COMPARISON WITH NEW EXPERIMENTAL DATA, INCLUDING SIDE-SCATTER CHARACTERISTICS by H. J. Albrecht	16
PHASE QUADRATURE COMPONENTS OF THE MICROWAVE SCATTERED FIELD IN A SHORT TROPOSPHERIC PATH AS RELATED TO THE METEOROLOGICAL PARAMETERS by C. I. Beard, W. T. Kreiss, and W. G. Tank	17
PHASE AND AMPLITUDE MEASUREMENTS OF TRANSHORIZON MICROWAVES WITH A MULTI-DATA-GATHERING ANTENNA ARRAY by Donald C. Cox and Alan T. Waterman, Jr	18
THE WAVELENGTH DEPENDENCE OF TROPOSPHERIC BEYOND-THE-HORIZON PROPAGATION by Folke Eklund	19
THE THEORY OF TROPOSPHERIC SCATTERING IN THE LIGHT OF NEW PROPAGATION MEASUREMENTS by L. Fehlhaber	20
MICROWAVE PROPAGATION INFLUENCED BY INTERNAL GRAVITY WAVES by Gerda Fengler and Gerd Stilke	21
INVESTIGATION OF THE RECEIVING FIELD FOR SCATTER PROPAGATION by J. Grosskopf	22
ELECTROMAGNETIC SCATTERING FROM AIR CURRENTS by H. N. Kritikos	23
TROPOSPHERIC SCATTER PROPAGATION AT 16 GHZ OVER A 500 KM PATH by Uwe H. W. Lammers, Edward E. Altshuler and John W. B. Day	24
USING THE TROPOSPHERIC VOLUME OF A QUASI-BACKSCATTER LINK TO INVESTIGATE THE SCATTER MECHANISM by R. Menzel and Kh. Rosenbach	25

**Paper**

**NOTES ON THE THEORY OF TROPOSCATTER MODULATION DISTORTION**  
by A. Wasiljeff

**26**

**DISCUSSION**

**27**

**SESSION 4 - D-REGION PARTIAL REFLECTIONS AND THOMSON SCATTER**

**RADIO WAVE SCATTERING FROM THE IONOSPHERIC D-REGION**  
by J. B. Gregory

**28**

**DRIFT MEASUREMENTS BY USE OF D-REGION PARTIAL REFLECTIONS**  
by Arne Haug and Olav Holt

**29**

**DISCUSSION**

**30**

**THOMSON SCATTER AS A COMMUNICATION MODE**  
by Allen M. Peterson

**31**

**INCOHERENT SCATTER OBSERVATIONS OF THE E-REGION**  
by G. N. Taylor

**32**

**DISCUSSION**

**33**

**PART 2**

**SESSION 5 - AURORAL SCATTER AND VHF FORWARD SCATTER**

**AURORAL SCATTER**  
by P. A. Forsyth

**34**

**A NOTE ON A PARTICULAR TYPE OF SCATTERING ECHOES OBSERVED  
AT HIGH LATITUDES**  
by Kristen Folkestad

**35**

**FIELD-ALIGNED IONIZATION SCATTER GEOMETRY**  
by George H. Millman

**36**

**DISCUSSION**

**37**

**REVIEW OF VHF FORWARD SCATTER**  
by Richard C. Kirby

**38**

**ELECTROMAGNETIC SCATTERING FROM A PLASMA SLAB HAVING LARGE SCALE,  
RANDOM ELECTRON DENSITY FLUCTUATIONS**  
by Adolf R. Hochstim and Charles P. Martens

**39**

**CONTROLLABILITY ASPECTS OF SCATTER PROPAGATION OF RADIO WAVES**  
by M. Z. von Krzywoblocki

**40**

**VHF IONOSPHERIC SCATTER PROPAGATION VIA THE EQUATORIAL ELECTROJET**  
by Carlos A. Romero, Alberto A. Giesecke, Jr and  
Oscar Pérez

**41**

**Paper**

<b>MICROWAVE SCATTERING FROM SPHERICAL ELECTRON CLOUDS</b>	
by N. W. Rosenberg, M. M. Klein and G. Anderson	<b>42</b>
<b>STOCHASTIC THEORY OF THE SCATTERING OF ELECTROMAGNETIC WAVES FROM A RANDOM MEDIUM</b>	
by C. M. Tchen	<b>43</b>
<b>DISCUSSION</b>	<b>44</b>

**SESSION 6 - TRANSEQUATORIAL PROPAGATION AND F-REGION SCATTER**

<b>A REVIEW OF VHF TRANSEQUATORIAL PROPAGATION</b>	
by D. L. Nielson	<b>45</b>
<b>THE IMPORTANCE OF HORIZONTAL F-REGION DRIFTS TO TRANSEQUATORIAL VHF PROPAGATION</b>	
by D. L. Nielson	<b>46</b>
<b>ETUDE D'UNE PROPAGATION TRANSEQUATORIALE EN DEHORS DU GRAND CERCLE EN PERIODE D'OCCURRENCE DE F DIFFUS</b>	
par M. Crochet et P. Broche	<b>47</b>
<b>RAY TRACING OVER A TRANSEQUATORIAL PATH</b>	
by N. C. Gerson	<b>48</b>
<b>TRANSEQUATORIAL PROPAGATION IMPLICATIONS OF EQUATORIAL VERTICAL DRIFT MEASUREMENTS</b>	
by Robert Cohen and J. P. McClure	<b>49</b>
<b>DISCUSSION</b>	<b>50</b>
<b>F-REGION SCATTER</b>	
by Robert Cohen	<b>51</b>
<b>RADIO-DOPPLER OBSERVATIONS OF THE IONOSPHERE NEAR THE MAGNETIC EQUATOR</b>	
by Kenneth Davies and Norman J. F. Chang	<b>52</b>
<b>JOINT PROBABILITY DENSITY OF SIGNAL FADING AT SPACED RECEIVERS</b>	
by T. J. Elkins	<b>53</b>
<b>SATELLITE SCINTILLATION AT HIGH LATITUDES</b>	
by Jon Frihagen	<b>54</b>
<b>HF RADAR SIGNATURES OF TRAVELING IONOSPHERIC IRREGULARITIES</b>	
<b>3D RAY-TRACING SIMULATION</b>	
by T. M. Georges and Judith J. Stephenson	<b>55</b>
<b>NATURE OF F-REGION IRREGULARITIES INFERRED FROM OBLIQUE REFLECTION MEASUREMENTS</b>	
by L. C. Humphrey, C. R. Roberts and R. Mather	<b>56</b>
<b>DISCUSSION</b>	<b>57</b>

SESSION 7 - F-REGION SCATTER

Paper

**BACKSCATTER OBSERVATIONS FROM DISTANT FIELD-ALIGNED  
IRREGULARITIES**

by H. Kopka and H.G. Möller

58

**RESEARCH ON FIELD-ALIGNED PROPAGATION OF HF RADIOWAVES  
USING ALOUETTE 2 TOPSIDE SOUNDER DATA AND DIGITAL  
RAY-TRACING TECHNIQUES**

by Jayaram Ramasastri, Edward J. Walsh and John R. Herman

59

**DISCUSSION**

60

**GROUND SCATTER IN REVIEW**

by

**Edgar C. Hayden**

**Institute for Telecommunication Sciences  
Environmental Science Services Administration  
Boulder, Colorado 80302, USA**

## SUMMARY

The possibility of HF radio wave transmission by scatter processes apparently was suspected as early as 1926. In the late 1920s and the 1930s the scattering of signals into the skip zone, in fact directly back to the point of emission, was noted frequently. During the 1940s and the first half of the 1950s, the surface of the earth was convincingly identified as the scattering agent responsible for one major form of scatter transmission, that now called "ground backscatter." Concurrently the role of ground scatter in certain off-great-circle transmissions - "ground side-scatter" was demonstrated.

Several applications which exploit ground scatter have been at least partially developed, e.g., current estimation of the primary coverage of an HF broadcast transmitter, methods for real-time choice of operating frequency in the HF band, studies of the structure of the ionosphere-- especially its irregularities and motions, and communication at frequencies above those normally usable.

A number of problems remain unsolved, or incompletely solved. Perhaps the most notable is the relationship of the backscatter coefficient to physical terrain features, including ocean surface features. A second is the interpretation of amplitude and frequency spectrum information in the backscattered signal as functions of arrival angle, time of flight, and time of observation. Interpretation is especially difficult in the presence of irregular structure (e.g., travelling disturbances) in the ionosphere. Digital ray-tracing techniques promise to be of great utility in helping to visualize and understand the relationship between ionosphere structure and observed ground scatter phenomena. The application of some of the more sophisticated radar techniques to the study of ground scatter - especially ground backscatter - is clearly indicated. Needed are improvements in angular resolution and range resolution, and better exploitation of the frequency-spectrum information in the backscattered signal.

## GROUND SCATTER IN REVIEW

Edgar C. Hayden

### 1. INTRODUCTION

It is inevitable that each person who attempts to prepare a review paper on a given subject will color it a different hue. What one sees in a subject, and his manner of viewing it, will be influenced by his particular interests, knowledge, and experience, and by the resource material available to him. Each of us would bring to the task a different combination of these factors, this author being no exception. "Ground scatter" is here interpreted to mean the nonspecular propagation of radio energy incident on the ground - "ground" meaning "surface of the earth", both land and sea. The emphasis will be primarily on energy propagated in directions other than the forward, or specular, direction though the latter will receive some mention. More emphasis will probably fall on propagation of energy back along or near the direction of incidence - backscatter - than on propagation in other directions - side-scatter. Attention will be focused almost exclusively on the HF portion of the spectrum.

Looking through the old papers has produced for me an impression akin to that of a time-lapse motion picture by which, for example, one can show the blossoming of a flower condensed into a period of a minute or less. The visibility of trends and actions, not easily discerned at the slower real-time pace, is thus enhanced. It is a temptation to dwell for a time on this aspect of the subject. However the present and future must also be given their due, so we shall have to be content with setting out a few of the landmarks along the way.

### 2. FROM THE PAST

The study of ground scatter has a fascinating history. It has roots reaching back into the mid-1920s when the exploitation of the HF band for commercial radio telegraphy was expanding rapidly. Magneto-ionic theory had developed to a surprising state. Theory predicted, and experiment, primarily by amateur operators, demonstrated the HF skip phenomenon. High power transmitters and improved receivers were coming into use. One of the consequences was that a number of phenomena not previously observable were discovered.

One of the first of the newly observed phenomena was simultaneous two-way transmission, by both the long and short great-circle paths, between the new Rocky Point transmitters in the United States and receivers in Geltow, Germany, as well as complete round-the-world transmissions from German transmitters to German receivers. In 1926 Quäck<sup>1</sup> reported such observations, and gave the figure 0.138 s for the round-the-world propagation time. At about the same time, Taylor<sup>2</sup> in the United States reported observations of signals received within the skip zone, but without offering any explanation. Apparently Mögel and others in Germany<sup>9, 23</sup> made similar observations in the same period. These observations represent the beginnings of the study of scatter transmission in the HF band.

It was Eckersley<sup>3</sup>, in 1927, who gave convincing evidence that signals such as those observed by Taylor and Mögel were propagated by scatter processes. Other observations and observers added detail to the developing picture<sup>4-8</sup>. At this point most of the explanations for the anomalous transmissions involved scattering from the upper atmosphere

"as from a light beam passing through a turgid medium", or scattering from auroral structures.

Taylor and Young<sup>8</sup>, in 1928, did suggest as a plausible explanation for some of their observations of reception in the skip zone that "The nearby set of echoes might be thought of as being due to reflections of the wave from rough portions of the earth's surface directly back on itself, so to speak, and coming from the first zone of reception; namely from just above the edge of the first skipped distance."

It becomes obvious at this point that a number of different scatter phenomena were being observed, a certain amount of confusion being the consequence (Refs. 10-30, 32). In retrospect, many of the observations seem from their descriptions almost certainly to have involved ground scatter. However, little attention was given this possibility, the preponderance of weight being given to scatter from the upper atmosphere. The new theories of propagation in the ionized upper atmosphere, and Eckersley's convincing identification of "short scatter" with ionic structures (meteors?) seemed predominant in the minds of most workers. Taylor and Young<sup>14</sup> did, in 1929, reiterate their suggestion, and added the observation that energy seemed also to be scattered back from the sea surface, perhaps better than from land. Mögel<sup>20, 21</sup> scored a close miss, getting the timing of certain scattered signals properly related to the skip distance, but attributing the scattering to a "turn-around zone" (or scatter zone) in the ionosphere, lying on rays from the transmitter between the tangential and critical rays, near the top of the ray trajectories.

The ground scatter tide began to turn in 1941 with the observations by Edwards and Jansky<sup>31</sup> of off-great-circle trans-Atlantic transmission, and their analysis of the observations in terms of side-scatter from the various skip zones. In 1945 Smith<sup>33</sup> proposed a backscatter technique for determining MUF and skip distance. However, it is revealing to note that in one of the diagrams in his report the backscattered energy is depicted as coming from the distant E-region just before the skip boundary, rather than from the ground. Benner<sup>35</sup> made a similar proposal in 1949 on a similar, but more nearly correct, basis.

It was primarily in the years between 1945 and 1955 that convincing evidence of the reality and prevalence of ground backscatter was given. It came through the efforts of a number of workers (Refs. 34, 36-41, 45, 47, 49, 51, 60, 68, 92, 93, 114-117, 127, 128). During the same period additional evidence for the existence of ground side-scatter was presented (Refs. 42, 43, 48, 71, 72), as was evidence for significant scattering at the ground reflection point of normal two-hop transmissions<sup>46, 66</sup>. With the reality and nature of ground scatter firmly established, numerous applications for the phenomenon blossomed. Techniques were developed and hardware constructed to exploit its potential in many ways, both for the study of the ionosphere itself and for demonstrating and studying propagation phenomena. Beyond this point developments became too numerous and varied to be discussed individually, at least within the scope of this paper.

For the most part, transmission situations involving ground scatter fall easily into one of two major classes. The first of these (I) is a communication-type situation in which the transmitter and receiver are generally not co-located, and the purpose for transmission between them is (Ia) point-to-point communication or broadcasting or (Ib) examination of the character of the signal propagated between them. The second (II) is a radar-type situation in which the transmitter and receiver are frequently, but not necessarily, co-located, are under common control, and the purpose of transmission between them is (IIa) to examine the structure of the intervening propagation medium, or (IIb) to detect or examine objects - in our case the surface of the earth - from which energy is scattered back. It is of the essence of IIa that the ground is acting as a nondistorting, matte (nonspecular) reflector, or at least that it introduces only known distortions (e.g., a smooth variation with incidence angle), thus permitting observation of irregular propagation phenomena. It is of the essence of IIb, in contrast to IIa, that propagation be sufficiently regular to allow detection and evaluation of the scatter.

Class Ia includes two-hop (or more) off-great-circle transmission at frequencies above

the maximum transmittable on the direct great-circle path. The existence of such a transmission mechanism has been clearly demonstrated and proposals made for its practical application (Refs. 71, 72, 79, 81, 94, 118, 119, 129, 132, 138, 139, 170, 176). In class Ib are a number of one-way schemes for determining the current status of a transmission path or the optimum frequency for use on such a path (Refs. 125, 131, 144, 178). Into class IIa fall ground backscatter techniques for estimating or monitoring the current coverage of broadcast transmissions (Refs. 44, 50, 54, 59, 64, 65, 73, 82, 92, 93, 102, 103, 105, 105, 114 - 117, 122, 125 - 128, 144, 156, 164, 165, 181, 202, 203, 223, 224, 233, 236, 239, 240). Also in this class are many instances of the use of techniques involving ground backscatter for study of the structure and motions of the ionosphere (Refs. 53, 55 - 58, 61 - 63, 78, 82 - 84, 95 - 99, 104, 105, 107, 108, 111 - 113, 123, 134 - 137, 140 - 142, 144 - 146, 148, 150, 151, 154, 155, 157, 159, 162, 163, 167, 175, 177, 178, 180, 186). This, perhaps, has been the most widely exploited application for ground backscatter. In class IIb, the principal unclassified application has been to attempt remote determination of sea state (Refs. 67, 69, 88 - 91, 109, 120, 149, 152, 158, 160, 161, 199, 210, 218, 232, 235). Detection of objects beyond the horizon has also been investigated<sup>77, 100</sup>.

### 3. AT THE PRESENT

Ground scatter has, so far, found use primarily in research applications. Commercial or operational usage has been developed little, if at all, with some minor exceptions noted below.

Though ground side-scatter transmission (class Ia of Section 2) has been suggested as a means to extend the capacity of the HF part of the spectrum, it has not found appreciable acceptance or usage on a regular, planned, basis. Its use has been mostly accidental or fortuitous, except for intercept of signals at locations other than those at which they were intended to be received.

The potential for such use seems to exist rather regularly, but procedures for predicting path characteristics have not yet been reduced to practice, making transmission circuit planning and frequency management difficult. Since a scatter mechanism is involved, channel character may be such as to limit signaling rates or information handling capacity. In some situations, for example when the skip distance is considerably greater than the transmitter-to-receiver distance, the active side-scatter area may be quite large (but dependent on antenna characteristics). Time dispersion of the signal can then be considerable. As the skip distances about the transmitter and receiver vary, the optimum location for side-scatter will move. The transmission channel will thus have not only a time-varying transfer characteristic but also a time-varying location! Antennas with steerable beams will undoubtedly be required. The degree of steerability (maximum angle of slew) necessary would be rather large, especially if the same antenna were also to be used for normal on-path operation. Slewing of the transmitting and receiving antenna beams will have to be coordinated to ensure that both are always "looking" at the same area. If the antenna slewing is not controlled by some real-time channel sampling process, it must be pre-programmed, which again requires path prediction. Additionally, it might well be advantageous to use antennas having small beamwidths to restrict the size of the relevant side-scatter area in order to minimize time dispersion of the signal (but at the cost of raising the required steering accuracy).

None of these factors seem to be insuperable problems; they could be solved by proper application of engineering principles. However, they (especially the antenna requirements) do tend to restrict the range of suitable applications on either engineering or economic grounds.

Side-scatter is anathema to those doing HF radiolocation (D/F). After cases of operator error and signal misidentification have been deleted, it seems probable that the majority of the remaining "wild" bearings are examples of side-scatter transmission. It

is important in this application to be able to predict or identify such situations. The author, while at the University of Illinois, has observed on the Wullenweber receiving antenna there a number of cases of side-scatter transmission from stations of known location. Often the signal would have been difficult to distinguish from a more normal multi-hop signal.

Ground backscatter transmission (class IIa of Section 2) is, in at least two cases known to the author, in limited operational use for determining or monitoring the coverage of HF broadcasts (Refs. 164, 165, 181, 223, 224, 236, 240). Reduction of this technique to practice has been facilitated by development of circuitry for using the broadcast transmitter itself to do the sounding without appreciable or obnoxious interruption of the program material<sup>164, 165</sup>. Two advantages thereby accrue, a substantial saving of equipment cost, and use of the same antenna for the sounding as for the broadcasting. The technique promises to be quite successful and useful. It should provide a coverage monitoring service for areas from which it is difficult to get signal reports. After initial test and validation it should eliminate the necessity for maintaining a dispersed coverage monitoring network. If interpretation does not prove too difficult, the system may be able to provide warning of transmission failure due to causes such as change in transmission mode or severe sporadic-E. An alternate choice of antenna beam configuration, especially elevation angle, may thereby be signaled.

It does not appear that the system will be of great use in real-time frequency selection. Changes in frequency are inhibited by the necessity for adhering to a predetermined schedule in order that listeners know on what frequency to expect the program. A cause for some concern on the part of one user<sup>240</sup> is that, while the system can define the near border of the coverage zone, it gives little information about the depth of coverage beyond this border.

Research on the ionosphere (class IIa) continues to be a major use of ground backscatter. Attempts are being made or proposed for remote determination of certain parameters of the regular ionosphere, notably height, maximum ion density, and perhaps ion density profile. The technique is also being applied to observation of disturbances of the F-region, both those of atmospheric origin and those of solar origin. A tremendous amount of information on sporadic-E has been obtained by this means. The method seems especially attractive for detection and observation of the irregular ionosphere features and their motions. Most of this work is based on the assumption that the ground acts as a smooth (without outstanding glints or highlights), but matte (nonspecular) scattering surface. Its effect is merely to redirect energy back along the direction of incidence without impressing a pattern of its own.

To a surprising extent (at least to this author) this effect seems to be so. On displays of backscatter amplitude versus range and frequency, or versus range and azimuth, it is quite difficult to identify reliably and positively any sort of terrain feature. This covers such things as mountain ranges or coast lines, or the difference between land and sea, to say nothing of more subtle features. This result is perhaps a bit less surprising when one considers that, at a range of 2500 km, an antenna beamwidth of 2.3° used with a pulse duration of 667 μs produces a resolution cell 100 km square. To reduce this cell size to 10 km square would require a beamwidth of 0.23° and a pulse duration of 67 μs. Within a resolution cell, with radar operating parameters in common use, the scattered signal is averaged over an area large compared to individual terrain features, though not large compared to the extent of relatively homogeneous terrain types. The amplitude effects produced by focusing in the ionosphere seem on the average greatly to overshadow those produced by terrain type. This is, of course, a fortunate circumstance for ionosphere studies.

Except for the simplest regular features, the interpretation of backscatter data in terms of ionosphere structure has proved to be extraordinarily complex. The development of accurate and versatile ray-tracing procedures has provided a tool of tremendous power (Refs. 173, 179, 190, 211, 222, 234). With such procedures comes the ability to produce

synthetic backscatter records of a variety of types from known ionosphere models. These synthetic records may be compared with actual records to aid in interpretation of the latter. The problem has now come to be to define an ionosphere model, based on physically reasonable principles or observations, which will reproduce the observed backscatter record. As a specific example, it has been shown by this method that certain physically reasonable ionosphere models produce returns of nearly constant range, independent of frequency<sup>175, 234</sup>. The temptation has been strong in the past to ascribe such returns to terrain features<sup>47, 60</sup>.

The question of backscatter coefficient cannot be completely dismissed (bibliography references in category [3]). Because of the effects produced by the ionosphere, it has so far seemed impractical to determine it, except roughly, through use of an ionospherically propagated signal (class IIb). Fortunately, an increasing amount of data measured by other methods has recently been appearing in the literature (Refs. 116, 187, 188, 200, 216, 217, 221, 225, 231). The observed variation with terrain type is not negligible. The variation with incidence angle is for some cases quite large. For some terrain types and polarization conditions a critical angle exists, on the grazing side of which the coefficient drops very rapidly. Many articles have been published treating the subject at microwave frequencies. However, the direct application of these methods to the HF range has so far shown less than satisfactory agreement with experiment.

Some progress has been reported recently in the use of backscatter for remote estimation of the state of the sea (class IIb). Crombie<sup>235</sup> has produced diffraction patterns related to sea wave structure. Frequencies used were in the 2 - 5 MHz range, and propagation was by groundwave. Thus the range is rather limited but is of the order of 200 km, depending on frequency. Tveten<sup>232</sup> shows some evidence for Doppler shift, perhaps due to sea wave structure, in ionospherically propagated ground backscatter (note that the two figures in this reference are interchanged with respect to the captions).

#### 4. FOR THE FUTURE

Many avenues are open to future development of the technology involving ground scatter. The author would like to single out just four which seem of particular importance, or perhaps seem especially troublesome. They are matters of technique rather than of application.

In the pursuit of better resolution in studies of the ionosphere which make use of backscatter, antenna systems are becoming quite large and expensive or, alternatively, needed performance is being sacrificed. Additional resolution is desirable and useful. For example, in a number of applications it would be desirable to have high resolution in two dimensions, a "pencil beam" analogous to a bundle of rays in a ray-tracing procedure. To attempt this by brute force with normal linear arrays (linear in the sense of linear phasor addition of signal components) might well be to price oneself out of the game. In another application it would be desirable to have a beam very narrow, say 1° - 2° in azimuthal width and scanable through 360° for use with PPI-type systems, in contrast to the 30° - 60° Yagi arrays commonly used.

A first possible route to cost reduction is to take advantage of recent advances in "thinned" or nonuniform arrays. The price of the simplification for a given resolution would be some loss of sensitivity. The development of such antennas would be a fairly straightforward problem in array design. It might be possible to use the array for transmitting as well as receiving - a definite advantage. A second route would be to employ either linear aperture synthesis techniques, or nonlinear multiplicative (data-processing) array techniques<sup>237</sup>. Proper application of these last two techniques requires adequate knowledge of the degree of correlation of the backscatter field over the spatial angular spectrum. Thus more exact knowledge of the general character of the backscattered field (Refs. 159, 169, 204) would be of considerable value.

The second item is in some respects related to the first. It seems evident that something is being missed by generating backscatter displays or records using either amplitude or frequency spectrum information alone. These two parameters of the backscatter signal both need to be used, and in suitable juxtaposition, perhaps in the manner of a multi-parameter terrain-differentiation radar. Employment of such measures seems crucial to development of any terrain differentiation or target detection capability.

The third item is the ground scatter coefficient. It is possible to fit a multi-parameter theoretical model to empirical data, thereby providing a formula for calculation but no satisfactory physical explanation. Backscatter models which have been based on essentially topographical descriptions of terrain surface have fallen short of explaining the experimental observations, usually underestimating the signal returned from smoother terrain types. Attempts to extrapolate theories developed for microwave frequencies down to HF have run into difficulty. The author would like to suggest further investigation of the possibility that at HF the inhomogeneity of surface and subsurface electrical parameters<sup>200</sup>, rather than surface contour, is the important factor.

The fourth item is to develop further the versatility and capability of ray-tracing procedures in producing synthetic backscatter records. As an aid to visualization and interpretation, they should be almost indispensable.

To this short list the reader will undoubtedly be able to add many items, some of which may well seem more urgent to him than these.

### 5. BIBLIOGRAPHY ON HF GROUND SCATTER

The compilation of a bibliography involves a selection of material from all that is available and relevant. The content is circumscribed by the interests of its author and the resources available to him. The chief criterion for inclusion of each of the references below is its relationship to the scattering of radio energy from the ground (the term "ground" is interpreted to mean "the surface of the earth", including both land and sea). Articles dealing exclusively with scattering from upper-atmosphere ionic structures have not been included, except in one or two cases needed to complete the historical sequence. Chief emphasis has been on ground scatter in the HF range. However, in the case of category [3], references to some work at higher frequencies have been given because of the dearth of material treating the HF case. The bibliography, though extensive, is not exhaustive. Suggestions of additional significant and relevant references would be welcomed by the author.

Articles will fall into one of the following five categories: [1] those of historical interest, giving background to the discovery and study of ground scatter, [2] those dealing with the theory and observation of radio transmission involving ground scatter, [3] those treating the ground scatter coefficient explicitly, [4] those discussing engineering or scientific applications of ground scatter phenomena or equipment development, and [5] references to other related bibliographies.

The references are grouped by year of publication to highlight the historical development of the subject, especially that during the early years. Full titles of papers are given to assist the reader in utilizing the bibliography. In a number of cases it has been possible to give two or more sources for essentially the same material. Where this occurs, a single author entry will be followed by two or more references, listed under the year in which the material first appeared. In a very few cases this procedure leads to the anomaly of a reference apparently listed in the wrong year. The numbers in square brackets, e.g., [3, 4], which precede the author's name, indicate this author's classification of the reference according to the five categories above. An author index to the references follows the chronological list.

## CHRONOLOGICAL LIST

## 1926

1. [1] Quäck, E. *Neues über die Ausbreitung von kurzen Wellen, mit Kurzwellen rund um die Erde.* Jahrbuch der Drahtlosen Telegraphie und Telephonie.: Zeits. Hochfrequenztechnik, Vol. 28 (6), Dec. 1926, pp. 177-178.

2. [1] Taylor, A.H. *Relation Between the Height of the Kennelly-Heaviside Layer and High Frequency Radio.* Proceedings, Institute of Radio Engineers, Vol. 14 (4), Aug. 1926, pp. 521-540.

## 1927

3. [1] Eckersley, T.L. *Short Wave Wireless Telegraphy.* Journal, Institution of Electrical Engineers, Vol. 65 (366), June 1927, pp. 600-638. (Discussion on pp. 638-644.)

4. [1] Quäck, E. *Die Ausbreitung kurzer Wellen rund um die Erde.* Elekt. Nachrtech., Vol. 4 (1), Jan. 1927, pp. 74-76.

5. [1] Quäck, E. *Weitere Mitteilungen über die Ausbreitung der Kurzwellen.* Elekt. Nachrtech., Vol. 4 (7), July 1927, pp. 308-312.

6. *Weitere Mitteilungen über die Ausbreitung der Kurzwellen.* Jahrbuch der Drahtlosen Telegraphie und Telephonie.: Zeits. Hochfrequenztechnik, Vol. 30 (2), Aug. 1927, pp. 41-42.

## 1928

7. [1] Hoag, J.B. *A Study of Short-Time Multiple Signals.* Proceedings, Institute of Radio Engineers, Vol. 16 (10), Oct. 1928, pp. 1368-1374.

8. [1] Taylor, A. Hoyt  
Young, L.C. *Studies of High-Frequency Radio Wave Propagation.* Proceedings, Institute of Radio Engineers, Vol. 16 (5), May 1928, pp. 561-578.

## 1929

9. [1] Böhm, O. *Mehrfachwege und Dopplereffekt bei der Ausbreitung der Kurzen Wellen".* Telefunken Zeitung, Vol. 10 (53), Dec. 1929, pp. 9-22.

10. [1] Eckersley, T.L. *An Investigation of Short Waves.* Journal, Institute of Electrical Engineers, Vol. 67 (392), Aug. 1929, pp. 992-1032.

11. [1] Quäck, E.  
Mögel, H. *Doppel - und Mehrfachzeichen bei Kurzwellen.* Elekt. Nachr. Tek. Vol. 6 (2), Feb. 1929, pp. 45-79.

12. *Double and Multiple Signals with Short Waves.* Proceedings, Institute of Radio Engineers, Vol. 17 (5), May 1929, pp. 791-823.

13. [1] Quäck, E.  
Mögel, H. *Short Range Echoes with Short Waves.* Proceedings, Institute of Radio Engineers, Vol. 17 (5), May 1929, pp. 824-829.

1-8

14. [1] Taylor, A. Hoyt  
Young, L.C. *Studies of Echo Signals.* Proceedings, Institute of Radio Engineers, Vol. 17 (9), Sept. 1929, pp. 1491-1507.

1930

15. [1] Mögel, H. *Betriebskontrolle von Kurzwellensendern.* Telefunken Zeitung, Vol. 11 (55), Oct. 1930, pp. 8-21.

16. *Betriebskontrolle von Kurzwellensendern.* Elektr. Nachr. Tek., Vol. 7 (9), Sept. 1930, pp. 333-348.

17. *Monitoring the Operation of Short Wave Transmitters.* Proceedings, Institute of Radio Engineers, Vol. 19 (2), Feb. 1931, pp. 214-232.

1931

18. [1] Editor *Scattered Radiation from Short-Wave Beams.* Wireless Engineer and Experimental Wireless, Vol. 8 (98), Nov. 1931, pp. 579-580.

19. [1] Kenrick, G.W.  
et. al. *Notes on High-Frequency Transmission During the Summer of 1930.* Proceedings, Institute of Radio Engineers, Vol. 19 (2), Feb. 1931, pp. 252-255.

20. [1] Mögel, H. *Feldstärkemessungen deutscher Kurzwellensender in England; Vergleich von Fernfrequenzmessungen zwischen New York, London and Berlin.* Elekt. Nachr. Tek., Vol. 8 (8), Aug. 1931, pp. 321-330.

21. *Field Strength Measurements in England of German Short-Wave Stations: Comparison of Distant Frequency Measurements Made in New York, London and Berlin.* Wireless Engineer, Vol. 8 (98), Nov. 1931, p. 604. (Abstract).

1932

22. [1] Eckersley, T.L. *Studies in Radio Transmission.* Journal, Institution of Electrical Engineers, Vol. 71 (429), Sept. 1932, pp. 405-459.

23. [1] Mögel, H. *Weitere Mitteilungen über Nahechos.* Telefunken Zeitung, Vol. 13 (60), Mar. 1932, pp. 29-32.

1934

24. [1] Kirby, S.S.  
et. al. *Studies of the Ionosphere and their Application to Radio Transmission.* Proceedings, Institute of Electrical Engineers, Vol. 22 (4), Apr. 1934, pp. 481-521.

25. [1] Mimno, H.R. *Wireless Echoes from Regions above the F Layers.* Nature (London), Vol. 134 (3376), 14 July, 1934, pp. 63-64.

1937

26. [1] Eckersley, T.L. *Ultra-Short-Wave Refraction and Diffraction.* Journal, Institution of Electrical Engineers, Vol. 80 (483), Mar. 1937, pp. 286-304.

27. [1] Eckersley, T.L. *Irregular Ionic Clouds in the E Layer of the Ionosphere.* Nature (London), Vol. 140 (3550), 13 Nov. 1937, pp. 846-847. (Letter).

## 1939

28. [1] Eckersley, T.L. *Scattering of Wireless Waves in the Ionosphere.* Nature (London), Vol. 143 (3610), 7 Jan. 1939, pp. 33-34.

29. [1] Feldman, C.B. *Deviations of Short Waves from the London-New York Great-Circle Path.* Proceedings, Institute of Radio Engineers, Vol. 27 (10), Oct. 1939, pp. 635-645.

## 1940

30. [1] Eckersley, T.L. *Analysis of the Effect of Scattering in Radio Transmission.* Journal, Institution of Electrical Engineers, Vol. 86 (522), June, 1940, pp. 548-567.

## 1941

31. [1] Edwards, C.F. Jansky, K.G. *Measurements of the Delay and Direction of Arrival of Echoes from Near-By Short-Wave Transmitters.* Proceedings, Institute of Radio Engineers, Vol. 29 (6), June, 1941, pp. 322-329.

## 1944

32. [1] Eckersley, T.L. et al. *Ground and Cloud Scatter of Electromagnetic Radiation.* Nature (London), Vol. 153 (3881), 18 Mar. 1944, pp. 341. (Letter).

## 1945

33. [1, 4] Smith, Newbern *An Automatic Instantaneous Indicator of Skip Distance and MUF.* US National Bureau of Standards, Report, IRPL-R9, 5 Feb. 1945.

## 1948

34. [1, 2] Hartsfield, W.L. et al. *Back-Scatter Observations by the Central Radio Propagation Laboratory: August 1947-March 1948.* Central Radio Propagation Laboratory, US National Bureau of Standards, Report, CRPL-5-5, 7 Oct. 1948.

## 1949

35. [1, 2] Benner, A.H. *Predicting Maximum Usable Frequency from Long-Distance Scatter.* Proceedings, Institute of Radio Engineers, Vol. 37 (1), Jan. 1949, pp. 44-47.

36. [1, 2] Peterson, A.M. *The Interpretation of Long Scatter Echo Patterns.* Technical Report on Proceedings of the Conference on Ionospheric Research, edited by B.B. Underhill, Pennsylvania State College, 27-29 June, 1949, Basic Ionospheric Research Technical Report No. 5, July, 1949, Contract AF 19 (122)-44, Radio Propagation Laboratory, Pennsylvania State College. Section F.

37. *The Interpretation of Long Scatter Echo Patterns.* Journal of Geophysical Research, Vol. 54 (3), Sept. 1949, p. 284. (Abstract).

38. [1, 2] Silberstein, R. *Oblique-Incidence Propagation Work at the Central Radio Propagation Laboratory.* In "Technical Report on Proceedings of the Conference on Ionospheric Research", edited by B.B. Underhill, Pennsylvania State College, 27-29 June, 1949, Basic Ionospheric Research Technical Report No. 5, Contract AF 19(122)-44, Radio Propagation Laboratory, Pennsylvania State College. Section N.

39. *Oblique Incidence Propagation Work of the Central Radio Propagation Laboratory.* Journal of Geophysical Research, Vol. 54 (3), Sept. 1949, p. 288. (Abstract).

**1950**

40. [1, 2] de Bettencourt, J.T. *The Beacon Technique as Applied to Oblique Incidence Ionosphere Propagation.* Proceedings, Institute of Radio Engineers, Vol. 38 (7), July 1950, pp. 791-792.

41. [1, 2] Hartsfield, W.L. et al. *Back-Scatter-Observations by the Central Radio Propagation Laboratory — August 1947 to March 1948.* Journal of Research, National Bureau of Standards, Vol. 44 (2), Feb. 1950, pp. 199-214.

42. [1, 2] Kōno, Tetsuo *Experimental Study on Scattered Echoes (No. 1).* Report of Ionosphere Research in Japan, Vol. 4 (3), 1950, pp. 127-135.

43. [1, 2] Kōno, Tetsuo *Experimental Study on Scattered Echoes (No. 2).* Report of Ionosphere Research in Japan, Vol. 4 (4), 1950, pp. 189-199.

**1951**

44. [1, 4] Abel, W.G. *Use of Long-Distance Back-Scatter to Determine Skip Distance and Maximum Usable Frequency.* URSI Spring Meeting, 16-18 April, 1951.

45. [1, 2] Abel, W.G. Edwards, L.C. *The Source of Long Distance Backscatter.* Proceedings, Institute of Radio Engineers, Vol. 39 (12), Dec. 1951, pp. 1538-1541.

46. [2, 3] Bramley, E.N. Ross, W. *Measurements of the Direction of Arrival of Short Radio Waves Reflected at the Ionosphere.* Proc. Roy. Soc., London, Series A, Vol. 207, 22 June 1951, pp. 251-267.

47. [2] Dieminger, W. *The Scattering of Radio Waves.* Proceedings of the Physical Society, Vol. 64B (2), Feb. 1951, pp. 142-158.

48. [2, 3] Miya, K. et al. *The Field Intensity of Scattered Wave in Radio Wave Propagation.* Report of Ionosphere Research in Japan, Vol. 5 (2), June 1951, pp. 55-73.

49. [2] Peterson, A.M. *The Mechanism of F-layer Propagated Back-scatter Echoes.* Journal of Geophysical Research, Vol. 56 (2), June 1951, pp. 221-237.

**1952**

50. [4] de Bettencourt, J.T. *Instantaneous Prediction of Ionospheric Transmission Circuits by the Communication Zone Indicator.* Institute of Radio Engineers, Transactions, Antennas and Propagation, PGAP-3, Aug. 1952, pp. 202-209.

51. [2] Hartsfield, W.L. Silberstein, R. *A Comparison of CW Field Intensity and Backscatter Delay.* Proceedings, Institute of Radio Engineers, Vol. 40 (12), Dec. 1952, pp. 1700-1706.

52. [3] Lysanov, V.P. *On The Scattering of Electromagnetic Waves from a Rough Surface.* Doklady Akademii Nauk SSSR, Vol. 87, 1952, pp. 719-722.

53. [2] Peterson, A.M. *Scatter-Sounding Ionosphere Investigations by Back-Scatter Techniques.* PhD Dissertation, Stanford University, California. May 1952.

54. [4] Villard, O.G. Jr. Peterson, A.M. *Instantaneous Prediction of Radio Transmission Paths.* QST, Vol. 36 (3), Mar. 1952, pp. 11-20.

55. [2,4] Villard, O.G. Jr. Peterson, A.M. *Scattersounding: A Technique for Study of the Ionosphere at a Distance.* Technical Report 54, Contract N6onr-251, Electronics Research Laboratory, Stanford University, California, Aug. 1952.

56. *Scatter-sounding: A Technique for Study of the Ionosphere at a Distance.* Institute of Radio Engineers, Transactions, Antennas and Propagation, PGAP-3, Aug. 1952, pp. 186-201.

57. [2,4] Villard, O.G. Jr. Peterson, A.M. *Scatter Sounding: A New Technique in Ionospheric Research.* Science, Vol. 116 (3009), 29 Aug. 1952, pp. 221-224.

58. [2,4] Villard, O.G. Jr. et al. *A Method for Studying Sporadic-E Clouds at a Distance.* Proceedings, Institute of Radio Engineers, Vol. 40 (8), Aug. 1952, pp. 992-994. (Correspondence).

**1953**

59. [4] Edwards, L.C. *COZI -Communications Zone Indicator.* Electronics, Vol. 26 (8), Aug. 1953, pp. 152-155.

60. [2] Silberstein, R. *High-Frequency Scatter Sounding Experiments at the National Bureau of Standards.* Science, Vol. 118 (3078), 25 Dec. 1953, pp. 759-763.

**1954**

61. [2,4] Dieminger, W. *New Knowledge of the Scattering of Short Waves and Its Practical Importance.* Umschau, Vol. 54 (10), 15 May, 1954, pp. 300-303.

62. [2] Silberstein, R. *A Note on Sweep-Frequency Backscatter Observations.* Journal of Geophysical Research, Vol. 59 (1), Mar. 1954, pp. 138-139.

63. [2] Silberstein, R. *Sweep-Frequency Back-Scatter - Some Observations and Deductions.* Institute of Radio Engineers, Transactions, Antennas and Propagation, AP-2 (2), Apr. 1954, pp. 56-63.

**1955**

64. [2,4] Beckman, B. Vogt, K. *Über Beobachtungen der Rückstreuung (Backscatter) im Kurzwellengebiet an kommerziellen Telegraphiesignalen.* Fernmeldetechnische Zeitschrift. Vol. 8 (9), Sept. 1955, pp. 473-481.

65. *Observations on Back-scattering with Commercial Telegraph Signals in the HF Band.* Proceedings, Institute of Radio Engineers, Vol. 44 (4), Apr. 1956, p. 593. (Abstract).

66. [2,3] Bramley, E.N. *Some Comparative Directional Measurements on Short Radio Waves over Different Transmission Paths.* Proceedings, Institution of Electrical Engineers, Vol. 102B (4), July 1955, pp. 544-549.

67. [3] Crombie, D.D. *Doppler Spectrum of Sea Echo at 13.56 Mc/s.* Nature, (London), Vol.175 (4459), 16 Apr. 1955, pp.681-682.

68. [2] Hartsfield, W.L. *Observations of Distant Meteor-Trail Echoes Followed by Ground Scatter.* Journal of Geophysical Research, Vol.60 (1), Mar. 1955, pp.53-56.

69. [3] Hoffman, W.C. *A Theoretical Model for High-Frequency Backscatter from the Sea Surface via the Ionosphere.* Journal of Atmospheric and Terrestrial Physics, Vol.7 (415), Nov. 1955, pp.278-284.

70. [3] Hoffman, W.C. *Back-Scatter from Perfectly-Conducting Doubly-Trochoidal and Doubly-Sinusoidal Surfaces.* Institute of Radio Engineers, Transactions, Antennas and Propagation, AP-3 (3), July 1955, pp.96-100.

71. [2,4] Mitchell, J.D. Jr. *Radio Communication and Scatter Propagation.* Technical Report 87, Contract N6onr-25107, Stanford University, California, 15 Aug. 1955, AD-68060.

72. [2,4] Miya, K. Kanaya, S. *Radio Propagation Prediction Considering Scattering Wave on the Earth's Surface.* Report of Ionosphere Research in Japan, Vol.9 (1), 1955, pp.1-15.

**1956**

73. [2,4] Allock, G. McK. *The Prediction of Maximum Usable Frequencies for Radio Communication over a Transequatorial Path.* Proceedings, Institution of Electrical Engineers, Vol.103B (10), July 1956, pp.544-552.

74. [3] Ament, W.S. *Forward-and Back-Scattering from Certain Rough Surfaces.* Institute of Radio Engineers, Transactions, Antennas and Propagation, AP-4 (3), July 1956, pp.369-373.

75. [3] Beckman, B. Vogt, K. *Über die Messung des Streukoeffizienten bei der Rückstreuung von Kurzwellen-Telegraphiesignalen.* Nachrichtentechnische Zeitschrift. Vol.9 (10), Oct. 1956, pp.441-448

76. *Measurement of the Scattering Coefficient in the Back-Scattering of Short-Wave Telegraphy.* Proceedings, Institute of Radio Engineers, Vol.45 (7), July, 1957, 1050. (Abstract).

77. [2,4] de Bettencourt, J.T. Whitcraft, W.A. Jr. *Long Range Meteoric Echoes via F-Layer Reflections.* Institute of Radio Engineers, Transactions, Antennas and Propagation, AP-4 (1), Jan. 1956, pp.72-76.

78. [4] Clark, C. Peterson, A.M. *Motion of Sporadic-E Patches Determined from High-Frequency Backscatter Records.* Nature (London), Vol.178 (4531), 1 Sept. 1956, pp.486-487.

79. [4] Hedlund, D.A. et al. *Some Ionosphere Scatter Techniques.* Institute of Radio Engineers, Transactions, Communication Systems, CS-4 (1), Mar. 1956, pp.112-117.

80. [3] McCue, C.G. *High-Frequency Back-Scatter Observations at Salisbury, South Australia.* Australian Journal of Physics, Vol.9 (4), Dec. 1956, pp.454-470.

81. [2] Miya, K.  
Kanaya, S. *On the Lateral Deviation of Radio Waves Coming from Europe.* Report of Radio Research in Japan, Vol.10 (1), 1956, pp. 1-8.

82. [2] Shearman, E.D.R. *A Study of Ionospheric Propagation by Means of Ground Back-Scatter.* Proceedings, Institution of Electrical Engineers, Vol.103B (8), Mar. 1956, pp.203-209.

83. [2] Shearman, E.D.R. *The Technique of Ionospheric Investigation Using Ground Back-Scatter.* Proceedings, Institution of Electrical Engineers, Vol.103B (8), Mar. 1956, pp.210-221.

84. [4] Shearman, E.D.R.  
Martin, L.T.J. *Back-Scatter Ionosphere Sounder.* Wireless Engineer, Vol.33 (8), Aug. 1956, pp.190-201.

**1957**

85. [2,3] Beckman, B.  
Vogt, K. *Über den Gewinn einer Empfangsrichtantenne bei Rückstreuung im Kurzwellengebiet.* Nachrichtentechnische Zeitschrift. Vol.10 (2), Feb. 1957, pp.90-91.

86. *The Gain of a Directive Receiving Aerial for Short-Wave Back-Scatter.* Proceedings, Institute of Radio Engineers, Vol.45 (11), Nov. 1957, pp.1578. (Abstract).

87. [3] Beckman, P. *A New Approach to the Problem of Reflection from a Rough Surface.* Acta Technica (Praha), Vol.4, 1957, pp.311-355.

88. [2,3] Dowden, R.L. *Short-Range Echoes Observed on Ionospheric Recorders.* Journal of Atmospheric and Terrestrial Physics, Vol.11 (2), 1957, pp.111-117.

89. [3] Ingalls, R.P.  
Stone, M.L. *Characteristics of Sea Clutter at HF.* URSI/Institute of Radio Engineers Symposium, Berkeley, California, 11-12 Oct. 1956.

90. *Characteristics of Sea Clutter at HF.* Institute of Radio Engineers, Transactions, Antennas and Propagation, AP-5 (1), Jan. 1957, pp.164-165. (Abstract).

91. [3] Katzin, M. *On the Mechanism of Sea Clutter.* Proceedings, Institute of Radio Engineers, Vol.45 (1), Jan. 1957, pp.44-54.

92. [1,2] Kazantsev, A.N. *USSR Research Into Radio Wave Propagation in the Ionosphere.* Radiotekhnika i Elektronika, Vol.2 (11), 1957, pp.1360-1374.

93. *USSR Research Into Radio Wave Propagation in the Ionosphere.* Radio Engineering and Electronics, Vol.2 (11), 1957, pp.62-83.

94. [2,3] Miya, K.  
et al. *On the Bearing of Ionospheric Radio Waves.* Report of Ionosphere Research in Japan, Vol.11 (3), Sept. 1957, pp.130-144.

95. [2] Peterson, A.M. *Ionospheric Back-scatter.* In "Annals of IGY, III (IV)." Pergamon Press, 1957, pp.361-381.

96. [2,4] Silberstein, R. *Comments on Studies of Transequatorial Ionospheric Propagation by the Scatter-Sounding Method.* Journal of

Geophysical Research, Vol. 64 (4), Dec. 1957, pp. 645-646.  
(See Reference 97).

97. [2,4] Villard, O.G. Jr.  
et al. *Studies of Transequatorial Ionospheric Propagation by the Scatter-Sounding Method.* Journal of Geophysical Research, Vol. 62 (3), Sept. 1957, pp. 399-412. (See Reference 96).

98. [2,4] Wilkins, A.F.  
Shearman, E.D.R. *Back-Scatter Sounding: An Aid to Radio Propagation Studies.* Journal of the British Institution of Radio Engineers, Vol. 17 (11), Nov. 1957, pp. 601-616.

99. [2,4] Widdel, H.U. *Beobachtungen an rückgestreuten Echos bei Kurzwellen-Fernübertragung.* Archiv der Elektrischen Übertragung, Vol. 11 (11), Nov. 1957, pp. 429-439.

**1958**

100. [2,4] Dieminger, W. *Ground Scatter by Ionospheric Radar.* In "Satellites and Problems of Long Range Detection and Tracking". AGARDograph 40, AGARD Avionics Panel Meeting, Copenhagen, 20-25 Oct. 1958, Pergamon, 1960, pp. 29-43.

101. [3] Katz, I.  
Spetner, L.M. *A Functional Relationship Between Radar Cross-Section of Terrain and Depression Angle.* Institute of Radio Engineers, Transactions, Antennas and Propagation, AP-6 (3), July, 1958, p. 310. (Abstract).

102. [4] Osetrov, B.I. *Some Problems Relating to the Return-Inclined Sounding of the Ionosphere.* Radiotekhnika i Elektronika (Moscow), Vol. 13 (12), Dec. 1958, pp. 3-10.

103. *Some Problems Relating to the Return-Inclined Sounding of the Ionosphere.* Radio Engineering, Vol. 13 (12), 1958, pp. 1-13.

104. [4] Shearman, E.D.R.  
Harwood, J. *Sporadic E as Observed by Back-Scatter Techniques in the United Kingdom.* In "Sporadic E Ionization," edited by B. Landmark, AGARDograph 34, Ionospheric Research Meeting, AGARD Avionics Panel, Cambridge, England, Sept. 1958, NATO, Paris, 1958, pp. 111-128. (See also Reference 137).

105. [4] Silberstein, R. *The Use of Sweep-Frequency Backscatter Data for Determining Oblique-Incidence Ionospheric Characteristics.* Journal of Geophysical Research, Vol. 63 (2), June 1958, pp. 335-351.

106. [3] Spetner, L.M. *A Statistical Model for Forward Scattering of Waves off a Rough Surface.* Institute of Radio Engineers, Transactions, Antennas and Propagation, AP-6 (1), Jan. 1958, pp. 88-94.

107. [2,4] Stein, S. *The Role of Ionospheric Layer Tilts in Long-Range High-Frequency Radio Propagation.* Journal of Geophysical Research, Vol. 63 (1), Mar. 1958, pp. 217-241.

108. [4] Valverde, J.F. *Motions of Large-Scale Travelling Disturbances Determined from High-Frequency Backscatter and Vertical Incidence Records.* Scientific Report No. 1, May, 1958. Contract AF19(604)-1830, Electronics Research Laboratories, Stanford University, California.

## 1959

109. [3,4] Barber, N.F. *A Proposed Method of Surveying the Wave State of the Open Ocean.* New Zealand Journal of Science, Vol.2 (1), Mar. 1959, pp.99-108.

110. [5] Brown, A.K. *Abstracts of Articles on Ground Backscatter Propagated by the Ionosphere.* Technical Report No.4, July 1959. Contract Nonr 225 (33), NR 087 090, Radio Propagation Laboratory, Stanford University, California.

111. [2] Dominici, P. *Comparison Between Ionospheric Sounding by Backscatter and Sounding Vertically.* Proceedings, 8th Annual Convention, Italian Geophysical Association, 12-14 Feb. 1959, Rome, Italy, pp.159-164.

112. [4] Egan, R.D. *N(h) Profiles Deduced from Oblique Incidence Backscatter.* In "Some Ionospheric Results Obtained During the IGY", edited by W.J.G. Beynon, URSI/AGI Committee Symposium, Brussels, Belgium, Sept. 1959, Elsevier, Amsterdam, 1960, pp.231-238.

113. [4] Harwood, J. *A Preliminary Report on Observations of Sporadic-E by the Backscatter Technique.* In "Some Ionospheric Results Obtained During the IGY", edited by W.J.G. Beynon, URSI/AGI Committee Symposium, Brussels, Belgium, Sept. 1959, Elsevier, Amsterdam, 1960, pp.231-238.

114. [1,2] Kabanov, N.I. *Long-Distance Shortwave Scattering from the Earth, 1946-1958.* Report at the IXth Plenary Assembly of CCIR, Los Angeles, Apr. 1959.

115. [2,4] Kosikov, K.M. *Ground Backscatter and the Problems of Radio Communications and Broadcasting over Great Distances.* Elektrosvyaz, Vol.7, July 1959, pp.10-16.

116. *Oblique-Return Sounding and Problems of Radio Communication and Broadcasting over Long Distances.* Telecommunications, Vol.7, 1959, pp.699-708.

117. *Ground Backscatter and the Problems of Radio Communications and Broadcasting over Great Distances.* Electrical Communication, Vol.7, July 1959, (Abstract).

118. [2,3] Miya, K. *Propagation of Long-Distance H.F. Signals.* Electronics and Radio Engineer, Vol.36 (7), July 1959, pp.263-271.

119. [4] Peterson, A.M. et al. *The IGY Three-Frequency Back-Scatter Sounder.* Proceedings, Institute of Radio Engineers, Vol.47 (2), Feb. 1959, pp.300-314.

120. [2,3] Ranzi, I. *HF Backscatter from Land and Sea.* Scientific Note 1, 30 May, 1959. Contract AF61(052)-139. Centro Radio-elettrico Sperimentale "G. Marconi", Rome, Italy.

1960

121. [3] Ament, W.S. *Reciprocity and Scattering by Certain Rough Surfaces.* Institute of Radio Engineers, Transactions, Antennas and Propagation, AP-8 (2), Mar. 1960, pp.167-174.

122. [2,4] Beckman, B.  
Vogt, K.  
*Observations of Back-Scattering on Telegraph Signals.* In "Electromagnetic Wave Propagation", edited by M. Desirant and J.L. Michiels, Academic Press, London, 1960, pp.157-166.

123. [2] Bibl, K.  
*Experimental Proof of Focusing at the Skip Distance by Backscatter Records.* Proceedings, Institute of Radio Engineers, Vol.48 (5), May 1960, pp.956-957. (See Reference 141).

124. [3] Cosgriff, R.L.  
et al.  
*Terrain Scattering Properties for Sensor System Design (Terrain Handbook II).* Engineering Experimental Station Bulletin, May 1960, Ohio State University, Columbus, Ohio. Vol.XXIX (3).

125. [2,4] Dieminger, W.  
et al.  
*Results from Combined Backscatter and Impulse Long Range Transmission Experiments.* In "Electromagnetic Wave Propagation", edited by M. Desirant and J.L. Michiels, Academic Press, London, 1960, pp.699-718.

126. [4] Edwards, L.C.  
Hedlund, D.A.  
*COZI Oblique Incidence Ionospheric Soundings Using Normal Communications Transmissions.* Institute of Radio Engineers, Transactions, Communication Systems, CS-8 (3), Sept. 1960, pp.160-164.

127. [1,2] Kabanov, N.I.  
*Long-Distance Shortwave Scattered Ground Reflection.* Radiotekhnika i Elektronika, Vol.5 (10), Oct. 1960, pp.1576-1592.

128.  
*Long-Distance Shortwave Scattered Ground Reflection.* Radio Engineering and Electronics, Vol.5 (10), Oct. 1960, pp.29-53.

129. [2] Kanaya, S.  
Yakoi, H.  
*The Lateral Deviation of Radio Waves Propagated Along the Great-Circle Path from Europe.* Report of Ionosphere Research in Japan, Vol.14 (2), 1960, pp.192-195.

130. [3] Katz, I.  
Spetner, L.M.  
*Polarization and Depression-Angle Dependence of Radar Terrain Return.* Journal of Research, National Bureau of Standards, Vol.64D (5), Sept.-Oct. 1960, pp.483-486.

131. [2] Kift, F.  
*Propagation of High-Frequency Radio Waves to Long Distances.* Proceedings, Institution of Electrical Engineers, Vol.107B, Mar. 1960, pp.127-140.

132. [2] Miya, K.  
Ueno, K.  
*Influence of Directivity of Transmitting Antenna on the Bearing of HF Signals.* Report of Ionosphere Space Research in Japan, Vol.14 (2), 1960, pp.187-191.

133. [3] Nielson, D.  
et al.  
*An Investigation of the Backscatter of High-Frequency Radio Waves from Land, Sea-Water, and Ice.* Final Report, May 1960. Contract Nonr 2917 (00), Stanford Research Institute, Menlo Park, California. AD-238 811.

134. [2] Phillips, M.L.  
*Theoretical Evaluation of HF-Backscatter Observations.* Technical Memorandum E-13, 1 Dec. 1960, Electro-Physics Laboratories, ACF Industries, Hyattsville, Maryland, AD 403 501. (See Reference 176).

135. [2] Ranzi, I. *Tropospheric Influence on H.F. Backscatter Near the Sea.* Scientific Note No.2, 30 Mar. 1960, Contract AF61 (052)-139, Centro Radioelettrico Sperimentale "G. Marconi", Rome, Italy.

136. [2] Ranzi, I. *Researches on Backscattering of Radiowaves.* In "Electromagnetic Wave Propagation", edited by M. Desirant and J.L. Michiels. Academic Press, London, 1960, pp.29-35.

137. [4] Sherman, E.D.R. Harwood, J. *Sporadic-E as Observed by Backscatter Techniques in the United Kingdom.* Journal of Atmospheric and Terrestrial Physics, Vol.18 (1), 1960, pp.29-42. (See also Reference 104).

138. [2] Wolfram, Russell T. *An Examination of Backscatter Propagation Between Bozeman, Montana, and Palo Alto, California.* Scientific Report No.1, Jan. 1960, Contract AF 19-(604)-5571, Stanford Research Institute, Menlo Park, California.

139. [4] Wolfram, R.T. *Improved Communications Using Groundscatter Propagation.* Electronics, Vol.33 (44), 28 Oct. 1960, pp.74-78.

**1961**

140. [2,3] Barry, G.H. Widess, P.R. *Use of a Phase-Sensitive Backscatter Sounder to Deduce Ionospheric Changes Associated with a Solar Flare.* Technical Report 37, 12 Dec. 1961, Contract Nonr 225(33), ARPA Order 196-61, Radioscience Laboratory, Stanford Electronics Laboratories, Stanford University, California.

141. [2] Bates, H.F. et al. *Comments on Experimental Proof of Focusing at the Skip Distance by Backscatter Records.* Proceedings, Institute of Radio Engineers, Vol.49 (1), Jan. 1961, p.369. (See Reference 123).

142. [4] Bibl, K. *Neuartige Backscatter-Registrierungen und - Ergebnisse.* Vortrage und Berichte der gemeinsamen Tagung der Arbeitsgemeinschaft Ionosphäre, des Deutschen URSI - Landesausschusses und der Fachgruppe Wellenausbreitung der NTG, Kleinheubach, 1961, Fernmeldetechnisches Zentralamt, Darmstadt, pp.111-114.

143. [3] Daniels, F.B. *A Theory of Radar Reflection from the Moon and Planets.* Journal of Geophysical Research, Vol.66 (6), June 1961, pp. 1781-1788.

144. [2,4] Dieminger, W. et al. *On the Influence of Disturbances of Solar Origin on Oblique Incidence Pulse Transmission.* In "The Effect of Disturbances of Solar Origin on Communications", edited by G.J. Gassmann, AGARDograph 59, Symposium of the Ionospheric Research Committee, AGARD Avionics Panel, Naples, Italy, May 1961, Macmillan, 1963, pp.193-206.

145. [2,4] Egan, R.D. Peterson, A.M. *The Influence of Sudden Ionospheric Disturbances on Backscatter Sounding.* In "The Effect of Disturbances of Solar Origin on Communications", edited by G.J. Gassmann, AGARDograph 59, Symposium of the Ionospheric Research Committee, AGARD Avionics Panel, Naples, Italy, May 1961, Macmillan, 1963, pp.155-165.

146. [4] Egan, R.D.  
Peterson, A.M. *Backscatter Observations of Sporadic-E.* Technical Report No.2, 30 May, 1961, NSF Grant Y 22-10/309, Radioscience Laboratories, Stanford University, California.

147. [5] Hagn, G.H.  
et al. *Backscatter Literature Survey.* June 1961, Contract SD66, Stanford Research Institute, California. AD 264 460.

148. [4] Harwood, J. *Some Observations of the Occurrence and Movement of Sporadic-E Ionization.* Journal of Atmospheric and Terrestrial Physics, Vol.20 (4), Apr. 1961, pp.243-262.

149. [3] Ranzi, I. *Doppler Frequency Shift of HF to SHF Radio Waves Returned from the Sea.* Technical Note No.6, 15 Sept. 1961, Contract AF61 (052)-139, Centro Radioelettrico Sperimentale "G. Marconi", Rome, Italy.

150. [2] Ranzi, I. *An Error Cause in Ionospheric Sounding Near the Sea.* Technical Note No.7, 15 Sept. 1961, Contract AF61 (052)-139, Centro Radioelettrico Sperimentale "G. Marconi", Rome, Italy.

151. [2,4]Ranzi, I. *Backscatter Echo Pattern and Vertical Radiation Diagram.* Technical Note No.8, 1 Oct. 1961, Centro Radioelettrico Sperimentale "G. Marconi", Rome, Italy. AD-277 983. (See also Reference 167).

152. [2,3]Ranzi, I. *Experiments on Backscatter of HF Radiowaves from Open and Coastal Sea.* Scientific Note No.3, 1 Mar. 1961, Contract AF 61(052)-139, Centro Radioelettrico Sperimentale "G. Marconi", Rome, Italy.

153. [2,3]Ranzi, I. *Backscatter of HF Radio Waves from Coastal and Continental Ground Reliefs.* Scientific Note No.4, 15 Apr. 1961, Contract AF 61(052)-139, Centro Radioelettrico Sperimentale "G. Marconi", Rome, Italy. AD-268-075.

154. [2,4]Ranzi, I. *Radiocommunication by Backscatter, 1 Dec. 1959-31 May 1961.* Annual Summary Report No.2, 30 June, 1961, Contract AF 61(052)-139, Centro Radioelettrico Sperimentale "G. Marconi", Rome, Italy. Ad-268 010.

155. [2,4]Ranzi, I.  
Dominici, P. *Backscatter Sounding During Ionospheric Storms,* In "The Effect of Disturbances of Solar Origin on Communications", edited by G.J. Gassmann, Symposium of the Ionospheric Research Committee, AGARD Avionics Panel, Naples, Italy, May 1961, Macmillan. 1963, pp.143-154.

156. [4] Shearman, E.D.R. *An Investigation of the Usefulness of Backscatter Sounding in the Operation of High-frequency Broadcast Services.* Proceedings, Institution of Electrical Engineers, Vol.108B (40), July 1961, pp.361-374.

157. [4] Tveten, L.H. *Ionospheric Motions Observed with High-frequency Backscatter Sounders.* Journal of Research, National Bureau of Standards, Vol.65D (2), Mar.-Apr. 1961, pp.115-127.

1962

158. [3,4]Barber, N.F. *Detecting Sea Waves by Their Diffraction of a Radio Wave.* Technical Report, Reference No.62-39, Sept. 1962, Contract Nonr-3351(00), NR 083-501, Woods Hole Oceanographic Institution, Woods Hole, Massachusetts.

159. [2,4] Barry, G.H.  
Widess, P.R. *The Effect of a Solar Flare on the Frequency of HF Ground Backscatter.* Journal of Geophysical Research, Vol. 67 (7), July, 1962, pp. 2707-2714.

160. [3,4] Braude, S.Ya. *The Radio Oceanographic Investigation of Sea Swells.* Akademiya Nauk Ukrains. SSR, Kiev, Institut Radiofiz. Electron. 1962, 116 pp.

161. *The Radio Oceanographic Investigation of Sea Swells.* US Office of Naval Intelligence, Translation No. 2067, 1962, 158 pp.

162. [4] Dueno, B. *Sporadic E as Observed from Mayaguez, Puerto Rico, by Backscatter Sounders.* In "Ionospheric Sporadic E", edited by E.K. Smith, Jr. and S. Matsushita, Pergamon Press, 1962, pp. 110-122.

163. [3,4] Egan, R.D.  
Peterson, A.M. *Backscatter Observations of Sporadic-E.* In "Ionospheric Sporadic E", edited by E.K. Smith, Jr. and S. Matsushita, Pergamon Press, 1962, pp. 89-109.

164. [4] Fenwick, R.B. *A Test of the Frequency-Shift-Pulse Backscatter Sounding Technique in Short Wave Broadcasting.* Report SU-SEL-62-130, Final Report, Oct. 1962, Contract IA-8513, Stanford Electronics Laboratories, Stanford University, California.

165. [4] Fenwick, R.B.  
Villard, O.G. Jr. *FM Backscatter Sounding as a Means for Monitoring Propagation Conditions during Short-Wave Broadcasts.* Institute of Radio Engineers, International Convention Record, Pt. 1, Vol. 10, 1962, pp. 136-144.

166. [3] Hagn, G.H. *An Investigation of the Direct Backscatter of High-Frequency Radio Waves from Land, Sea Water, and Ice Surfaces.* Final Report II, May 1962, Contract Nonr 2917(00), Stanford Research Institute, Menlo Park, California.

167. [4] Ranzi, I. *Backscatter Study of Ionospheric Irregularities by Using a Vertically Split Beam.* Proceedings, International Conference on the Ionosphere, edited by A.C. Stickland, Imperial College, London, July, 1962, Institute of Physics and the Physical Society, London, 1963, pp. 285-287. (See also Reference 151).

168. [2,4] Ranzi, I. *Radio Communication by Backscatter.* Final Technical Report, 31 Dec. 1962, Contract AF 61(052)-139, Centro Radioelettrico Sperimentale "G. Marconi", Rome, Italy. AD 404 270.

169. [2] Shearman, E.D.R. *The Amplitude and Spectrum of Ground Backscatter Echoes.* Proceedings, International Conference on the Ionosphere, edited by A.C. Stickland, Imperial College, London, July, 1962, The Institute of Physics and the Physical Society, 1963, pp. 293-300.

170. [2] Triskova, L. *Reception of Signals at the Frequency of 21 Mc/s in the Skip Region.* Slaboproudny Obzor. (Czechoslovakia), Vol. 23, 1962, pp. 558-561.

**1963**

171. [3] Beckman, P.  
Spizzichino, A. *The Scattering of Electromagnetic Waves from Rough Surfaces.* International Series of Monographs on Electromagnetic Waves, Vol. 4, Pergamon Press, 1963.

172. [3] Clarke, R.H. *Theoretical Characteristics of Radiation Reflected Obliquely from a Rough Conducting Surface.* Proceedings, Institution of Electrical Engineers, Vol. 110 (1), Jan. 1963, pp. 91-100.

173. [2] Croft, T.A. Gregory, L. *A Fast, Versatile Ray-Tracing Program for IBM 7090 Digital Computers.* Report SU-SEL-63-108, Technical Report 82, Oct. 1963, Electronics Laboratories, Stanford University, California.

174. [3] Daniels, F.B. *Radar Reflections from a Rough Moon Described by a Composite Correlation Function.* Journal of Geophysical Research, Vol. 68 (23), 1 Dec. 1963, pp. 6251-6254.

175. [2] Dueno, B. *Interpretation of Some Sweep-frequency Backscatter Echoes.* Journal of Geophysical Research, Vol. 68 (12), 15 June, 1963, pp. 3603-3610.

176. [2] Hagg, E.L. Rolfe, W. *A Study of Transatlantic Radio Propagation Modes at 41.5 Mc/s.* Canadian Journal of Physics, Vol. 41 (2), Feb. 1963, pp. 220-233.

177. [2] Phillips, M.L. *Auxiliary Procedures Used in Theoretical Evaluation of HF Backscatter Observations and Other Communications Problems.* Electro Physics Laboratory, ACF Electronics, Inc., Bladensburg, Md., 22 Apr. 1963, AD 407 187. (See Reference 134).

178. [2,4] Werle, H. *Backscatter and Long-Distance Pulse Propagation Investigations Between Lindau (Hartz) and Tsumeb (Southwest Africa).* Archiv der Elektrischen Übertragung, Vol. 17 (3), Mar. 1963, pp. 121-130.

**1964**

179. [2] Croft, T.A. *The Synthesis of Oblique Ionograms by Digital Computer.* Report SU-SEL-64-106, Electronics Laboratories, Stanford University, California, Sept. 1964.

180. [4] Davis, J.R. et al. *A HF Backscatter Study of Solar Eclipse Effects upon the Ionosphere.* Journal of Geophysical Research, Vol. 69 (1), 1 Jan. 1964, pp. 190-193.

181. [4] Fenwick, R.B. *Operational Use of Backscatter-Sounding in Broadcasting.* Report SU-SEL-64-100, Contract IA-9039, Electronics Laboratories, Stanford University, California, Sept. 1964.

182. [3] Fung, A.K. *Theory of Radar Scatter from Rough Surfaces, Bistatic and Monostatic, with Application to Lunar Radar Return.* Journal of Geophysical Research, Vol. 69 (6), 13 Mar. 1964, pp. 1063-1073.

183. [3] Hagfors, T. *Backscattering from an Undulating Surface with Applications to Radar Returns from the Moon.* Journal of Geophysical Research, Vol. 69 (18), 15 Sept. 1964, pp. 3779-3784.

184. [5] Hagn, G.H. McAfee, L.R. *Backscatter Literature Survey.* Contract SD66 Stanford Research Institute, Oct. 1964, AD 474 163.

185. [4] Heisler, I.H. Whitehead, J.D. *The Correlation Between the Occurrence of Sporadic-E and the Horizontal Component of the Earth's Magnetic Field.* Journal of Atmospheric and Terrestrial Physics, Vol. 26, Apr. 1964, pp. 437-444.

186. [3,4] Steele, J.G. *The Effect of the Ground Backscatter Coefficient on Observations of Sporadic-E over Sea, Land and Mountains.* Journal of Atmospheric and Terrestrial Physics, Vol.26 (2), 1964, pp.322-324.

187. [3] Steele, J.G. *Backscatter of Radio Waves from the Ground.* PhD Thesis, 1964, University of Queensland, Brisbane, Australia.

188. *Backscatter of Radio Waves from the Ground.* Technical Report 109, Contracts Nonr-225(64), NR 088 019, Stanford University, California, June 1965, AD 464699. (Reprint of Reference 187).

189. [4] Wickersham, A.F. Jr. *Identification of Ionospheric Motions Detected by the High-Frequency Backscattering Technique.* Journal of Geophysical Research, Vol.69 (3), 1 Feb. 1964, pp.457-463.

**1965**

190. [2] Croft, T.A. *The Synthesis of Sweep-Frequency Ground Backscatter by Digital Computer.* Report SU-SEL-65-002, Technical Report 84, Contract Nonr 225(64), NR 088 019 and ARPA Order 196-65, Radioscience Laboratory, Electronics Laboratories, Stanford University, California, Jan. 1965, AD-46593.

191. [3] Beckman, Petr *Radar Backscatter from the Surface of the Moon.* Journal of Geophysical Research, Vol. 70 (10), 15 May, 1965, pp.2345-2350.

192. [3] Beckman, Petr *Scattering by Composite Rough Surfaces.* Proceedings, Institute of Electrical and Electronic Engineers, Vol.53 (8), Aug. 1965, pp.1012-1015.

193. [3] Chaevskii, E.V. *Energy Characteristics of the Field Scattered by a Rough Surface.* Izvestiya VUZ Radiofizicheskaya, Vol.8 (6), Nov.-Dec. 1965, pp.1128-1133.

194. *Energy Characteristics of the Field Scattered by a Rough Surface.* Soviet Radiophysics, Vol.8 (6), Nov. - Dec. 1965, pp.811-815.

195. [2,3] Chia, R.C. et al. *High Frequency Backscatter from the Earth Measured at 1000 km. Altitude* Radio Science, 69D (4), Apr. 1965, pp. 641-649.

196. [5] Corriher H.A. Jr. Pyron, B.O. *A Bibliography of Articles on Radar Reflectivity and Related Subjects 1957-1964.* Proceedings, Institute of Electrical and Electronic Engineers, Vol.53 (8), Aug. 1965, pp.1025-1064.

197. [4] Gilliland, C.R. *Sweep-Frequency Backscatter with Calibrated Amplitude.* Report SU-SEL-65-095, Technical Report 111, Electronics Laboratories, Stanford University, California, 1965.

198. [3] Kaufman, D.E. Hayre, H.S. *Electromagnetic Wave Scattering from Very Rough Surfaces Composed of Correlated Large and Small Scale Roughness.* Proceedings, Institute of Electrical and Electronic Engineers, Vol.53 (8), Aug. 1965, pp.1157-1158.

199. [3] Steele, J.G. *Backscatter of 16 Mc/s Radio Waves from Land and Sea.* Australian Journal of Physics, Vol. 18 (4), Aug. 1965, pp. 317-327.

200. [3] Steele, J.G. *Influence of Electrical Properties of the Ground on the Backscatter Coefficient at High Frequencies.* Technical Report 121, Contracts Nonr-225(64), NR 088 019, ARPA Order 196-65, Stanford University, California, Dec. 1965.

**1966**

201. [3] Brockelman, R.A. Hagfors, T. *Note on the Effect of Shadowing on the Backscattering of Waves from a Random Rough Surface.* Proceedings, Institute of Electrical and Electronic Engineers, Transactions, Antennas and Propagation, AP-14 (5), Sept. 1966, pp. 621-626. (Discussion on pp. 626-629).

202. [2,4] CCIR *Backscattering (Report 261-1).* Documents of the XIth Plenary Assembly, II, Oslo, 1966. International Telecommunication Union, 1967, pp. 283-288.

203. [2,4] Delloue, J. Goutelard, C. *Sur l'Interprétation des Échos de Rétrodiffusion par la Méthode des Courbes de Transmission.* Comptes Rendus, Académie des Sciences, Paris, Series B, Vol. 263 (3), 18 July, 1966, pp. 256-259.

204. [2] Dueno, B. *Phase Fluctuations of Ground Backscattered Signals.* Journal of Geophysical Research, Vol. 71 (13), 1 July, 1966, pp. 3281-3283.

205. [3] Floyd, W.L. Lund, T.J. *Scatterometer Program.* Proceedings, Institute of Electrical and Electronic Engineers, Transactions, Aerospace Electronics Systems, AES-2 (6) (Supplement) Nov. 1966, pp. 323-328.

206. [3] Fung, A.K. *On Depolarization of Electromagnetic Waves Backscattered from a Rough Surface.* Planetary and Space Science, Vol. 14, July 1966, pp. 563-568.

207. [3] Katz, I. *Wavelength Dependence of the Radar Reflectivity of the Earth and the Moon.* Journal of Geophysical Research, Vol. 71 (2), 15 Jan. 1966, pp. 361-366.

208. [3] Kumar, V.R. et al. *Backscatter of Electromagnetic Waves from a Rough Layer.* Proceedings, Institute of Electrical and Electronic Engineers, Vol. 54 (9), Sept. 1966, pp. 1191-1193.

209. [3] DeLorenzo, J.D. Cassedy, E.S. *A Study of the Mechanism of Sea Surface Scattering.* Proceedings, Institute of Electrical and Electronic Engineers, Transactions, Antennas and Propagation, AP-14 (5), Sept. 1966, pp. 611-620.

210. [3,4] McKee, R. et al. *Ionospheric Sporadic-E Backscatter Return from Land Versus Sea.* Journal of Atmospheric and Terrestrial Physics, Vol. 28, June/July, 1966, pp. 661-662.

211. [2] Martin, J.J. *Structure of an Ionospherically Reflected Backscattered Radar Pulse.* Journal of Geophysical Research, Vol. 71 (2), 15 Jan. 1966, pp. 357-360.

212. [3] Rosenberg, A.D.  
et al. *Frequency Shift of Radiation Scattered from a Rough Sea Surface.* Izvestiya VUZ Radiofizicheskaya, Vol. 9 (2), Mar./Apr. 1966, pp. 334-340.

213. *Frequency Shift of Radiation Scattered from a Rough Sea Surface.* Soviet Radiophysics, Vol. 9 (2), Mar./Apr. 1966, pp. 161-164.

214. [3] Semenov, B.I. *Approximate Calculation of E.M. Wave Scattering at the Surface of a Rough Terrain.* Radiotekhnika i Elektronika, Vol. 11 (8), Aug. 1966, pp. 1351-1361.

215. *Approximate Computation of Scattering of Electromagnetic Waves by Rough Surface Contours.* Radio Engineering and Electronic Physics, Vol. 11 (8), Aug. 1966, pp. 1306-1308.

216. [3] Steele, J.G. *High-Frequency Backscatter from Terrain with Trees.* Technical Note 128, Contracts Nonr-225(64), NR 088 019, ARPA Order 196-65, Electronics Laboratories, Stanford University, California, Apr. 1966. (See also Reference 231).

217. [3] Steele, J.G.  
Barnum, J.B. *High-Frequency Measurement of Radar Cross Section Using the Standing-Wave Method.* Report SU-SEL-66-021, Technical Report 127, Contract Nonr-225(64), ARPA Order 196-65, Electronics Laboratories, Stanford University, California, Mar. 1966, AD-481 748.

218. [3] Wait, J.R. *Theory of HF Ground Wave Backscatter from Sea Waves.* Journal of Geophysical Research, Vol. 71 (20), 15 Oct. 1966, pp. 4839-4842.

219. [3] Walker, B. *An Analogue Method of Studying the Angular Spectrum of Radiation Reflected from Rough Surfaces.* Radio and Electronic Engineer, Vol. 32 (6), Dec. 1966, pp. 363-370.

220. [3] Wright, J.W. *Backscattering from Capillary Waves with Application to Sea Clutter.* Institute of Electrical and Electronic Engineers, Transactions, Antennas and Propagation, AP-14 (6), Nov. 1966, pp. 749-754.

**1967**

221. [3] Barnum, J.R. *High-Frequency Backscatter from Terrain with Buildings.* Technical Report 130, Contracts Nonr-225(64), NR 088019, ARPA Order 196-67, Stanford University, California, Jan. 1967.

222. [2] Croft, T.A. *Computation of HF Ground Backscatter Amplitude.* Radio Science (New Series), Vol. 2 (7), July 1967, pp. 739-746.

223. [4] Fenwick, R.B. *Backscatter-Sounding Tests in Southeast Asia Using VOA Broadcasts.* Report SU-SEL-67-012, Technical Report IA-2, Contract IA-10180, Electronics Laboratories, Stanford University, California, Jan. 1967.

224. [4] Fenwick, R.B. *Backscatter-Sounding Study of Coverage of VOA Broadcasts to Brazil.* Report SU-SEL-67-016, Technical Report IA-4, Contract IA-10180, Electronics Laboratories, Stanford University, California, Nov. 1967.

225. [3] Hagn, G.H. *The Direct Backscatter of High-Frequency Radio Waves from Land, Sea-Water and Ice Surfaces.* Institute of Electrical and Electronic Engineers, International Convention Record, Part 2, Vol. 15, 1967, pp. 150-159.

226. [4] Hunsucker, R.D. Tveten, L.H. *Large Traveling Ionospheric Disturbances Observed at Midlatitudes Utilizing the High Resolution HF Backscatter Technique.* Journal of Atmospheric and Terrestrial Physics, Vol. 29, Aug. 1967, pp. 909-916.

227. [3] Ott, R.H. Schlak, G.A. *Backscattering from Rough Terrain.* Technical Report RL60-ITS 57, ESSA Research Laboratory, US, Department of Commerce, Sept. 1967.

228. [3,4] Schindler, J.K. *Electromagnetic Scattering Phenomena Associated with Extended Surfaces.* Institute of Electrical and Electronic Engineers, International Convention Record Part 2, Vol. 15, 1967, pp. 136-149.

229. [2,4] Shepherd, E.G. *HF Ground Backscatter.* Technical Note CDD(T) 139, Weapons Research Establishment, Australian Defence Scientific Establishment, Salisbury, South Australia, Aug. 1967.

230. [3] Smith, B.G. *Geometrical Shadowing of a Random Rough Surface.* Institute of Electrical and Electronic Engineers, Transactions, Antennas and Propagation AP-15 (5), Sept. 1967, pp. 668-671.

231. [3] Steele, J.G. *High Frequency Backscatter from Terrain with Trees.* Proceedings, Institute of Electrical and Electronic Engineers, Vol. 55 (9), Sept. 1967, pp. 1583-1590. (See also Reference 216).

232. [2,4] Tveten, L.H. *Ionospherically Propagated Sea Scatter.* Science, Vol. 157 (3794), 15 Sept. 1967, pp. 1302-1304.

**1968.**

233. [2,4] Barclay, L.W. *Field Strength Predictions for Backscatter Ionospheric Sounding.* Marconi Review, Vol. 31 (168) (First Quarter 1968), pp. 32-42.

234. [2,4] Croft, T.A. *The Influence of Ionospheric Irregularities on Sweep-Frequency Backscatter.* Journal of Atmospheric and Terrestrial Physics, Vol. 30 (5), May 1968, pp. 1051-1063.

235. [3,4] Crombie, D.D. Watts, J.M. *Observations of Coherent Backscatter of 2-10 MHz Radio Surface Waves from the Sea.* Deep-Sea Research, Vol. 15, 1968, pp. 81-87.

236. [4] Lomasney, J.M. Fenwick, R.B. *Elevation Steering of HF Broadcasting Antennas Using Backscatter Sounding.* Report SU-SEL-68-031, Technical Report IA-5, Contract IA-10180, Electronics Laboratories, Stanford University, California, June 1968.

237. [2,4] Shearman, E.D.R. Clarke, J. *Aperture Synthesis in Ionospheric Radar.* Nature (London), Vol. 219 (5150), 13 July, 1968, pp. 143-144.

238. [2,4] Surtees, W.J. *An Approximate Synthesis of HF Backscatter Considering Ionospheric Motions.* Radio Science (New Series), Vol. 3 (1), Jan. 1968, pp. 57-67.

239. [2,4] Treharne, R.F. *Triangulation of High Frequency Backscatter Returns.* Proceedings, Institution of Radio and Electronic Engineers of Australia, Vol.29 (4), Apr. 1968, pp.109-114.

240. [4] Wright, C.S. Moffatt, H. Private Communication, 16 Apr. 1968, Trial Use of Backscatter Sounding by Radio Free Europe.

241. [3] Wright, W.J. *A New Model for Sea Clutter.* Institute of Electrical and Electronic Engineers, Transactions, Antennas and Propagation, AP-16 (2), Mar. 1968, pp.217-223.

#### Author Index

Abel, W.G. 44,45  
 Ahearn, J.L. 180  
 Allock, G. McK. 73  
 Ament, W.S. 74,121  
 Andrew, V.J. 7  
 Barber, N.F. 109,158  
 Barclay, L.W. 233  
 Barnum, J.R. 217,221  
 Barry, G.H. 140,159  
 Bates, H.F. 141  
 Beckman, B. 64,65,75,76,85,86,122  
 Beckman, P. 87,171,191,192  
 Benner, A.H. 35  
 Berkner, L.V. 24  
 deBettencourt, J.T. 40,50,77  
 Bibl, K. 123,142  
 Böhm, O. 9  
 Bramley, E.N. 46,66  
 Braude, S. Ya. 160,161  
 Brockelman, R.A. 201  
 Brown, A.K. 110  
 Cassedy, E.S. 209  
 CCIR 202  
 Chaevskii, E.V. 193,194  
 Chia, R.C. 195  
 Clark, C. 78,210  
 Clark, N. 133  
 Clarke, J. 237  
 Clarke, R.H. 172  
 Corriher, H.A., Jr. 196  
 Cosgriff, R.L. 124  
 Cox, J.W. 32  
 Croft, T.A. 173,179,190,222,234  
 Crombie, D.D. 67,235  
 Daniels, F.B. 143,174  
 Davis, J.R. 180  
 Delloue, J. 203  
 Dieminger, W. 47,61,100,125,144  
 Dominici, P. 111,120,155  
 Dowden, R.L. 88  
 Duino, B. 162,175,204  
 Durrani, S. 208  
 Eckersley, T.L. 3,10,22,26,27,28,30,32  
 Editor 18  
 Edwards, C.F. 31  
 Edwards, L.C. 45,59,79,126  
 Egan, R.D. 112,119,145,146,163  
 Feldman, C.B. 29  
 Fenwick, R.B. 164,165,181,223,224,236  
 Floyd, W.L. 205  
 Fung, A.K. 182,195,206  
 Gilliland, C.R. 197  
 Goutelard, C. 203  
 Gregory, L. 173  
 Hagg, E.L. 176  
 Hagfors, T. 183,201  
 Hagn, G.H. 133,147,166,184,225  
 Harris, R.D. 210  
 Hartsfield, W.L. 34,41,51,68  
 Harwood, J. 104,113,137,148  
 Hayre, H.S. 198  
 Headrick, W.C. 180  
 Hedlund, D.A. 79,126  
 Heisler, L.H. 185  
 Hoag, J.B. 7  
 Hoffman, W.C. 69,70  
 Hunsucker, R.D. 141,226  
 Ingalls, R.P. 89,90  
 Ishikawa, M. 94  
 Jansky, K.G. 31  
 Kabanov, N.I. 114,127,128  
 Kalmykov, A.I. 212,213  
 Kanaya, S. 72,81,94,129  
 Katz, I. 101,130,207

Katzin, M. 91  
 Kaufman, D.E. 198  
 Kawai, M. 118  
 Kazantsev, A.N. 92, 93  
 Kenrick, G.W. 19  
 Kift, F. 131  
 Kirby, S.S. 24  
 Klemperer, H. 40  
 Kobayashi, T. 48  
 Koepsel, W.W. 208  
 Kōno, T. 42, 43  
 Kosikov, K.M. 115, 116, 117  
 Kumar, V.R. 208  
 Lomasney, J.M. 236  
 deLorenzo, J.D. 209  
 Lund, T.J. 205  
 Lysanov, Y.P. 52  
 McAfee, L.R. 184  
 McCue, C.G. 80  
 McKee, R. 210  
 Manning, L.A. 58  
 Martin, J.J. 211  
 Martin, L.T.J. 84  
 Millington, G. 32  
 Mimno, H.R. 25  
 Mitchell, J.D., Jr. 71  
 Miya, K. 48, 72, 81, 94, 118, 132  
 Moffatt, H. 240  
 Mögel, H. 11, 12, 13, 15, 16, 17, 20, 21, 23  
 Möller, H.G. 125, 144  
 Moore, R.K. 195  
 Nielson, D.L. 133, 147  
 Osetrov, B.I. 102, 103  
 Ostrovskii, I.E. 212, 213  
 Ostrow, S.M. 34, 41  
 Ott, R.H. 227  
 Owren, L. 141  
 Peake, W.H. 124  
 Peterson, A.M. 36, 37, 49, 53, 54, 55, 56, 57, 58,  
     78, 95, 119, 145, 146, 163  
 Phillips, M.L. 134, 177  
 Pratt, D.S. 119  
 Pyron, B.O. 196  
 Quäck, E. 1, 4, 5, 6, 11, 12, 13  
 Ranzi, I. 120, 135, 136, 149, 150, 151, 152, 153,  
     154, 155, 167, 168  
 Rolfe, W. 176  
 Rorden, L. 133  
 Rose, G. 125, 144  
 Rosenberg, A.D. 212, 213  
 Ross, W. 46  
 Schindler, J.K. 228  
 Schlak, G.A. 227  
 Semenov, B.I. 214, 215  
 Shearman, E.D.R. 82, 83, 84, 98, 104, 137, 156,  
     169, 237  
 Shepherd, E.G. 229  
 Silberstein, R. 34, 38, 39, 41, 51, 60, 62, 63,  
     96, 105  
 Smith, B.G. 230  
 Smith, F.H. 147  
 Smith, N. 33  
 Spetner, L.M. 101, 106, 130  
 Spizzichino, A. 171  
 Steele, J.G. 186, 187, 188, 199, 200, 216, 217, 231  
 Stein, S. 97, 107  
 Stone, M.L. 89, 90  
 Stuart, D.M. 24  
 Surtees, W.J. 238  
 Taylor, A.H. 2, 8, 14, 19  
 Taylor, R.C. 124  
 Treharne, R.F. 239  
 Triskova, L. 170  
 Tveten, L.H. 157, 226, 232  
 Ueno, K. 132  
 Valverde, J.F. 108  
 Villard, O.G., Jr. 54, 55, 56, 57, 58, 97, 165  
 Vogt, K. 64, 65, 75, 76, 85, 86, 122  
 Wait, J.R. 218  
 Wakai, N. 48  
 Walker, B. 219  
 Watts, J.M. 235  
 Werle, H. 178  
 Whitcraft, W.A., Jr. 77, 79  
 Whitehead, J.D. 185  
 Wickersham, A.F., Jr. 189  
 Widdel, H.U. 99  
 Widdess, P.R. 140, 159  
 Wilkins, A.F. 98  
 Wolfram, R.T. 138, 139  
 Wright, C.S. 240  
 Wright, J.W. 220, 241  
 Yakoi, H. 129  
 Yeh, K.C. 97  
 Young, L.C. 8, 14, 19

**SURFACE SCATTERING IN OCEAN ROUGHNESS  
AND SEA ICE STUDIES**

by

**Albert W. Biggs**

**Center for Research in Engineering Science  
The University of Kansas  
Lawrence, Kansas 66044, USA**

## SUMMARY

Scattering from rough surfaces is reviewed in terms of analytical and experimental results. The angle of incidence and wavelength of the incident electromagnetic wave, polarization of the wave with respect to the surface, effective dielectric constant and conductivity at the surface, and the surface roughness spectrum relative to wavelength are parameters introduced in descriptions of backscatter variations. The rough surfaces include ocean roughness in the form of sea states generated by different wind speeds and sea ice in the Arctic regions. The sea states were observed with radar scatter techniques over ocean sectors offshore from Bermuda, Newfoundland, and Iceland. Sea ice, separated into polar (several years old) and winter (less than one season old) ice, was observed in the Beaufort Sea near Point Barrow, Alaska.

Measurements of the variations of the radar scattering coefficient with the above parameters are made with the radar scatterometer. Correlations of the scattered signal with the terrain are achieved with ground truth observations of terrain characteristics.

## SURFACE SCATTERING IN OCEAN ROUGHNESS AND SEA ICE STUDIES

Albert W. Biggs

### 1. INTRODUCTION

A broad discussion of all aspects of radar scattering research - theory, computation, and experiment - is presented in the August 1965 issue of the IEEE Proceedings. Analytical discussions by Beckmann<sup>1</sup> and Kodis<sup>2</sup> cover scattering from rough surfaces in contrast with scattering from discrete objects such as spheres, finite cones, and similar symmetrical ground-plane shapes. Beckmann derives an expression for mean backscattered power per unit power as a function of the angle of incidence. His results compare favorably with experimental measurements by Evans and Pettergill<sup>3</sup>. Although the other papers in this issue are concerned with discrete object backscatter, a bibliography by Corriher and Pyron<sup>4</sup> of approximately 1500 papers is useful for additional radar scatter papers. A more current bibliography on rough surface scatter has been prepared by Walters<sup>5</sup> for backscatter from the earth's surface.

Scattering from a surface with a roughness small in comparison with the incident wavelength<sup>6</sup> represents a low frequency spectral response, while that from a surface with a roughness large in comparison with the incident wavelength<sup>7</sup> represents high frequency spectral response. The theories covering the frequency spectrum from smooth to rough surfaces are described in detail by Fung<sup>8</sup>.

Backscatter measurements of rough surfaces have been made with radar imagery and scatterometry<sup>9</sup>. An imaging radar measures the same backscatter as that seen by a scatterometer, but only at one angle. The scatterometer is more versatile in examining the scattering properties of the earth's surface because they can be measured at angles ranging from 60° forward to 60° aft. Since more information is obtained on roughness with scatterometers, the measurements described subsequently will be limited to scatterometry.

The terrain investigated by scatterometry can include oceans, sea ice, coastal regions, forests, agricultural regions, and geological areas. The results from scatterometer measurements over the ocean can be used to provide information on sea states and winds<sup>10</sup>. Flights over sea ice with scatterometers will indicate ice thickness and surface features. Agricultural scatter can differentiate various stages of growth of grain crops (wheat or barley) and types of crops (grain, corn, and beans). Timber cruising on foot can be replaced by flights over inaccessible growth. Identification of geological characteristics is achieved in Pisgah Crater in Reference 11.

### 2. SCATTEROMETERS

A scatterometer is a radar developed to obtain backscatter characteristics, the scattering coefficients, of a sector of the earth's surface for a wide range of incidence angles. The variation is achieved with a fan beam antenna pattern, wide along the direction of the flight path and very narrow across the flight path. The nature of the return signal produces a Doppler frequency dependent upon the angle of incidence. The resolution cell sampled has a width established by the antenna pattern and a length (along the flight path) fixed by the bandwidths of the filters for each increment of incidence angle.

Parameters influencing the backscatter in a particular resolution cell include

wavelength  
polarization  
incidence angle.

In addition to the surface roughness variations with frequency, the dielectric properties (including losses) of different materials change with frequency. The combination of these effects creates variations in scattering coefficient with frequency. The influence of both specular and non-specular reflection is also found in polarization variations. The specular effect creates different reflection coefficients for horizontal and vertical polarization, and the non-specular effect creates de-polarization. Coupled with these is the influence of incidence angle. Return drops with larger angles, but the rate is frequency-dependent.

The above parameters are dependent on the terrain characteristics,

surface roughness  
dielectric constant  
conductivity or loss factor  
stratification  
inhomogeneities or mixed paths.

The surface roughness will predominate over any subsurface properties at the high frequency end of radar scatterometry operation. As the frequency decreases, the dielectric constant and loss factor (or conductivity) of the region near the surface have an effect which eventually dominates the backscatter. Since no terrain is homogeneous over practical depths, the stratification must be considered. This factor increases in importance with decreasing frequency because the skin depth senses more layers with diverging properties. Inhomogeneities or changes in dielectric properties along the flight path also influence the return when the mixed path occurs in a given resolution cell.

These parameters and characteristics are indicated as aids in interpreting anomalous results and in developing analytical models. They introduce methods for evaluating and interpreting scatterometry results.

### 3. SEA STATES

The surface of the sea over a prescribed resolution cell can be described with a spectrum depending upon the winds and their past histories. The scattering coefficient curve, as a function of incidence angle, also depends upon the surface of the sea. Since the scatterometer measures only ocean roughness, and this is a sea state, the winds can be inferred. The dielectric properties of the sea are homogeneous and do not influence the scattering coefficient.

Representative sea state measurements are shown in Figure 1. The scattering coefficient is plotted in decibels versus the incidence angles. The dynamic range required for a scatterometer is determined by the lowest sea state desired. An extremely rough sea would have a constant scattering coefficient from  $0^\circ$  to  $70^\circ$  (or  $90^\circ$ ). A smooth sea will have almost all specular reflection and negligible scatter. Three sea states have been identified in flights offshore from Bermuda, Newfoundland, and Iceland.

### 4. SEA ICE

The only scatterometry data taken over sea ice are shown in Figures 2 and 3. The sea ice consists of winter ice and polar ice. Winter ice is relatively smooth and thin

because it is less than a year in age. Polar ice is rougher, thicker, and more than a year in age. The ground truth along the flight path is presented with the scatter return for two typical angles of incidence. The scattering coefficient is plotted as a function of distance to illustrate the variation in roughness along the path.

## 5. CONCLUSIONS

Some of the aspects of radar scatterometry have been described. Although parameters and characteristics have been discussed, additional data are needed at lower frequencies with multi-polarization capabilities. Analytical studies of the influence of dielectric properties will avoid anomalous results when the data is interpreted.

## ACKNOWLEDGMENTS

R.L.Walters provided necessary and valuable coordination in the planning phases of the scatterometer flights and flew on the Newfoundland flight, and W.P.Waite aided in data collection and flew on the Iceland flight for sea state data. J.W.Rouse flew on the Point Barrow flight and also directed the excellent effort on data presentation.

This research was supported by the Naval Oceanographic Office, Washington, DC, and the Naval Ordnance Laboratory, White Oak, Maryland, under Contract N 62306-67-C-0044.

## REFERENCES

1. Beckmann, P. *Scattering by Composite Rough Surfaces.* Proceedings, Institute of Electrical and Electronic Engineers, Vol.53, August 1965, pp. 1012-1015.
2. Kodis, R.D. *Propagation and Scattering Plasmas.* Proceedings, Institute of Electrical and Electronic Engineers, Vol.53, August 1965, pp. 1016-1024.
3. Evans, J.V.  
Pettengill, G.H. *The Scattering Behavior of the Moon at Wavelengths of 3.6, 68 and 784 Centimeters.* Journal of Geophysical Research, Vol.68, January 1963, pp. 423-447.
4. Corriher, H.A., Jr  
Pyron, B.O. *A Bibliography of Articles on Radar Reflectivity and Related Subjects: 1957-1964.* Proceedings, Institute of Electrical and Electronic Engineers, Vol.53, August 1965, pp.1025-1064.
5. Walters, R.L. *Radar Bibliography for Geoscientists.* CRES Report 61-30, Center for Research in Engineering Science, University of Kansas, Lawrence, Kansas, March 1968.
6. Rice, S.O. *Reflection of Electromagnetic Waves from Slightly Rough Surfaces.* Communications in Pure and Applied Mathematics, Vol.4, 1951, pp.351-378.
7. Beckmann, P.  
Spizzichino, A. *The Scattering of Electromagnetic Waves from Rough Surfaces.* Pergamon Press, London; Macmillan, New York, 1963.
8. Fung, A. *Scattering Theories and Radar Return.* CRES Report 48-3, Center for Research in Engineering Science, University of Kansas, Lawrence, Kansas, May 1965.
9. Moore, R.K. *Radar Scatterometry - an Active Remote Sensing Tool.* Proceedings, Fourth Symposium on Remote Sensing of Environment, University of Michigan, Ann Arbor, Michigan, April 1966.
10. Moore, R.K.  
Pierson, W.J. *Measuring Sea State and Estimating Winds from a Polar Orbiting Satellite.* International Symposium on Electromagnetic Sensing of the Earth from Satellites, Miami Beach, Florida, November 1965.
11. Dalke, G.W. *Identification of Remote Objects by Means of Scatterometry Data and Application to Pisgah Crater.* CRES Report 61-17, Center for Research in Engineering Science, University of Kansas, Lawrence, Kansas, 1967.

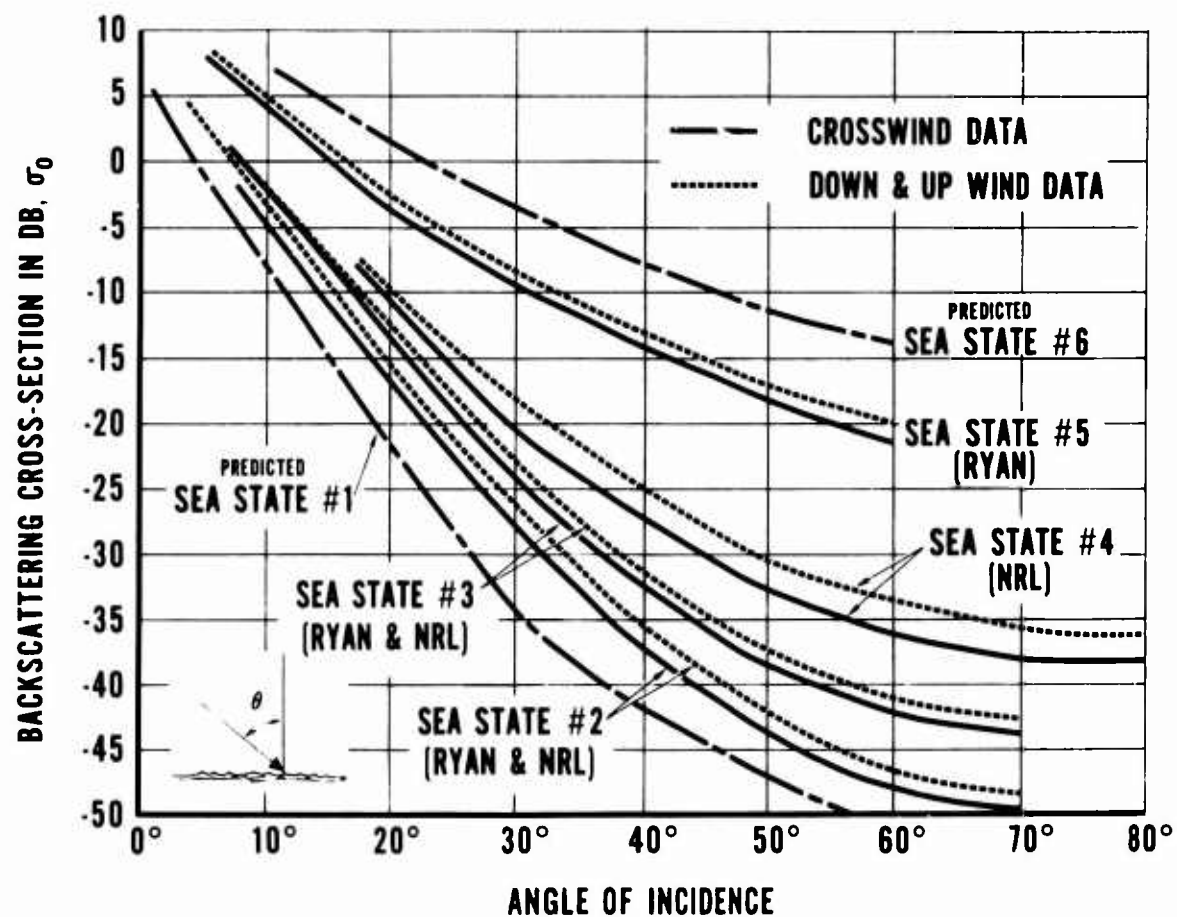
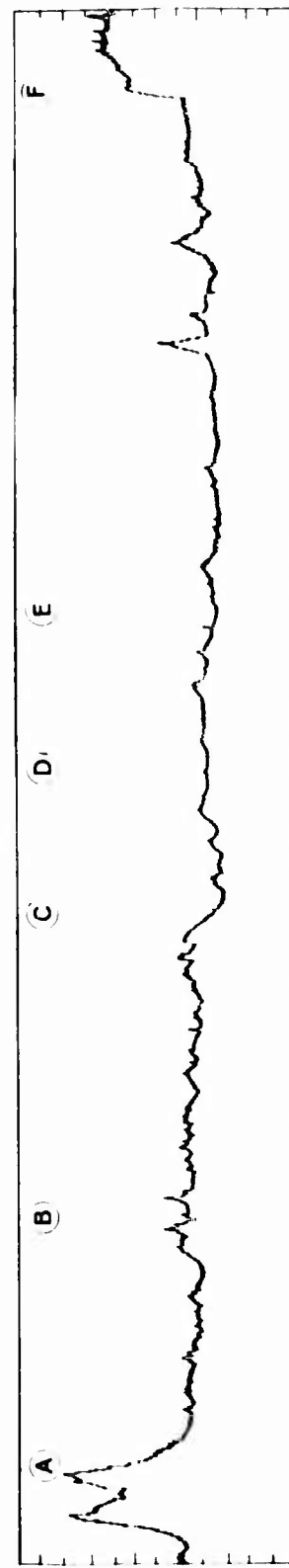
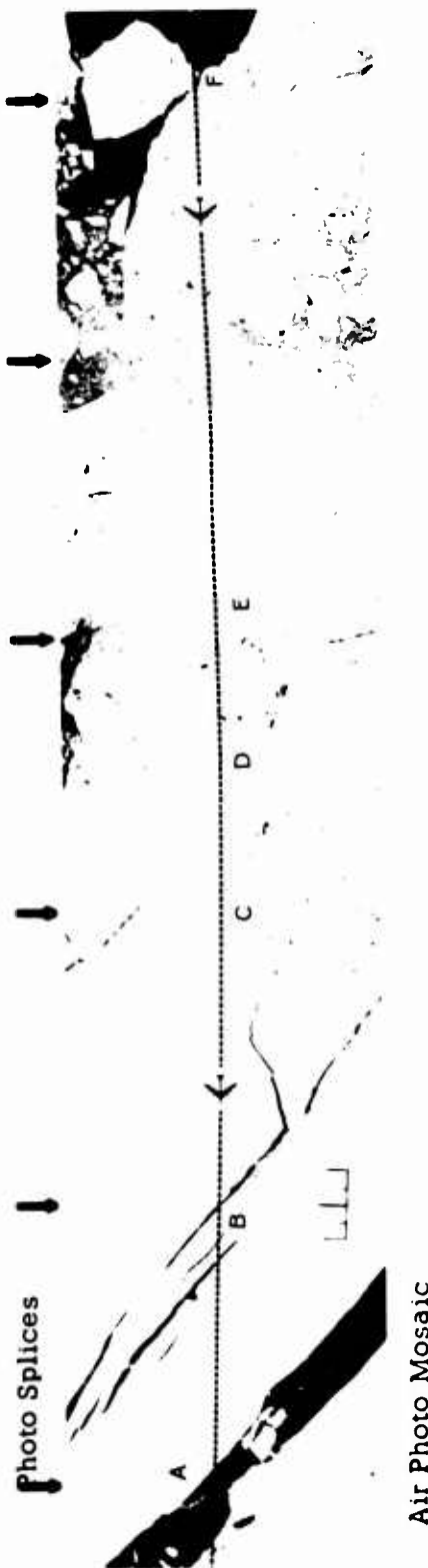


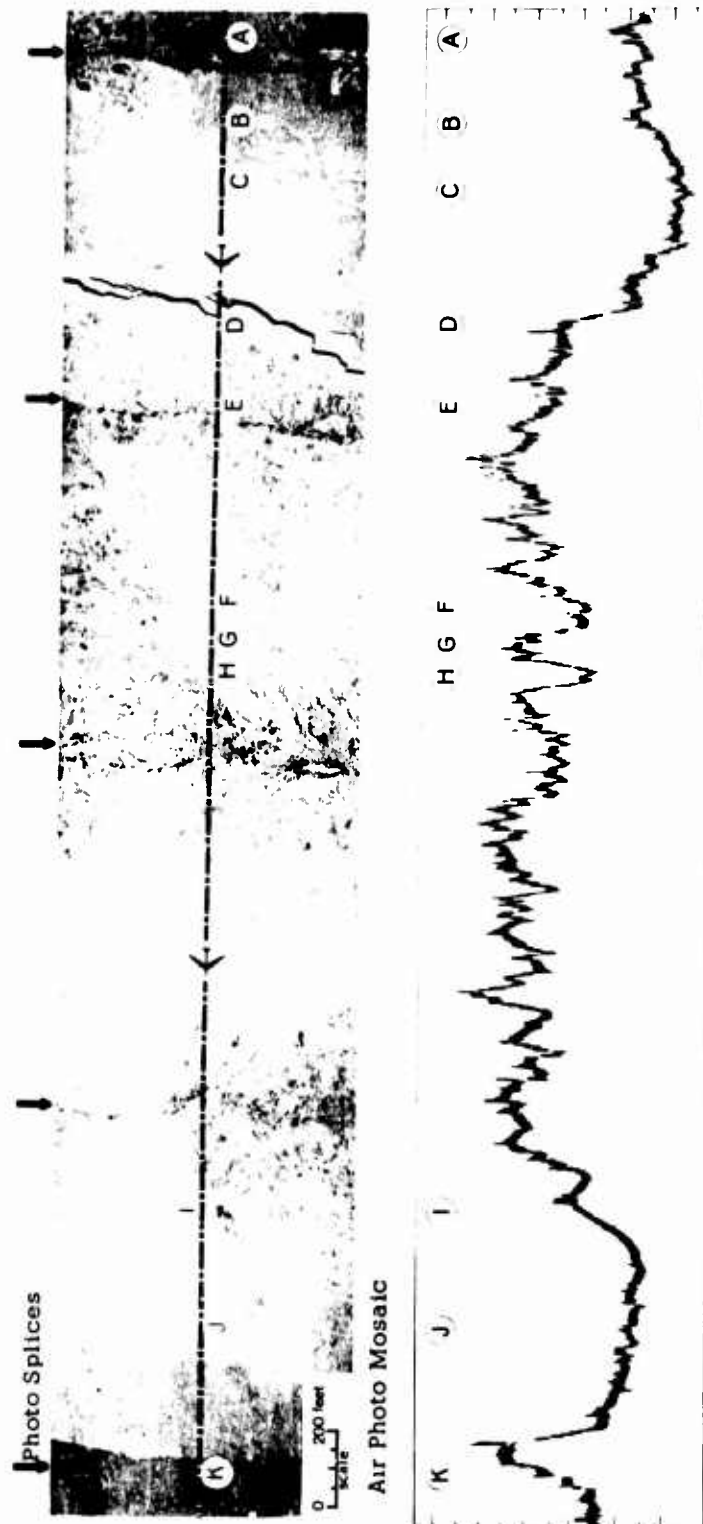
Fig. 1 Representative sea state measurements



Radar Return at  $6.7^{\circ}$  Incidence Angle

- A- Open lead.
- B- Crack in smooth winter ice.
- C- Heavy pressure ridging at boundary of smooth winter ice.
- D- Smooth winter ice in field of dense pressure ridging.
- E- Field of ridged ice.
- F- Boundary ridged ice and open water.

Fig. 2 Ice-type identification by radar. Arctic Ice. Off shore of Barrow, Alaska. 12 May 1967. NASA/MSC Mission 47, Site 93, Line 91, Run 1, 1500 ft altitude



- A - Polar ice fragments imbedded in field of rough winter ice.
- B - Boundary between winter ice with polar ice fragments and winter ice.
- C - Smooth winter ice.
- D - Crack at boundary of winter ice and polar ice.
- E - Polar ice.
- F-G-H - Example of texture changes on surface of polar ice. Transition is from smooth-to-rough-to-smooth.
- I - Boundary between polar ice and winter ice. A polar ice fragment is imbedded in the winter ice near the boundary.
- J - Winter ice.
- K - Area of extensive pressure ridging on winter ice.

Fig. 3 Ice-type identification by radar. Arctic polar ice pack. Beaufort Sea. 15 May 1967. NASA/MSC Mission 47, Site 93, Line 94, Run 1, 1000 ft altitude

ANALYSE DES PHENOMENES DE DIFFUSION LATERALE  
DANS UNE EXPERIENCE BISTATIQUE A L'AIDE DE DEUX  
RADARS MONOSTATIQUES DECAMETRIQUES

par

M. Crochet

Laboratoire de Physique de l'Exosphère.  
Faculté des Sciences de Paris, France

## RESUME

Une expérimentation bistatique Valensole (France) - Guadeloupe (Antilles) a permis d'analyser des propagations par diffusion latérale à l'aide de sondages par rétrodiffusion. Les zones de diffusion sont déterminées à l'aide du retard des signaux et différents types de propagation (régulière ou par supermodes) sont analysés. Le coefficient de diffusion latérale sur mer, pour des élévations d'une dizaine de degrés, est trouvé de l'ordre de - 22 dB et sensiblement indépendant de l'azimut.

**ANALYSE DES PHENOMENES DE DIFFUSION LATÉRALE  
DANS UNE EXPÉRIENCE BISTATIQUE A L'AIDE DE DEUX  
RADARS MONOSTATIQUES DECAMÉTRIQUES**

M. Crochet

**1. INTRODUCTION**

De nombreuses recherches ont été poursuivies sur la nature des propagations hors du grand cercle 1-4 en ondes décimétriques. L'importance des phénomènes de diffusion au sol a été mise en évidence par la détermination des directions d'arrivée et des études de "fréquence maximum utilisable" sur les différentes trajectoires<sup>1, 2</sup>.

Les zones de diffusion latérale pour une trajectoire particulière ont été localisées par Wolfram par une détermination originale des azimuts à l'émission et à la réception. Dans la technique des émissions pulsées, l'étude des retards relatifs des différentes parties du signal permet de définir les accroissements de trajets dus aux diffusions latérales, alors que des informations obtenues par rétrodiffusion aux deux extrémités de la liaison conduisent à la localisation des zones de silence<sup>3</sup>. C'est cette dernière méthode qui a été utilisée et dont les résultats vont être présentés.

**2. DESCRIPTION DE L'EXPÉRIENCE**

L'existence de deux stations équipées pour les sondages par rétrodiffusion à Valensole ( $6^{\circ}$ E,  $45^{\circ}$ N) et à la Guadeloupe ( $67^{\circ}$ W,  $16^{\circ}$ N) a permis des expériences en bistatique (où l'on utilise à l'une des stations les impulsions émises par l'autre) complétée par des informations obtenues en monostatique (où chaque station fonctionne en radar à rétrodiffusion) aux deux extrémités de la liaison.

A la Guadeloupe, station du Centre National d'Etudes et Télécommunications, un aérien log-périodique, utilisé en émission-réception, est pointé dans le N - NW, présentant une largeur de lobe d'environ  $120^{\circ}$  à 12 dB pour une fréquence de 10 Mhz. A cet aérien est couplé un émetteur AME de puissance de crête 150 kW.

A la station de Valensole, un réseau de radiateurs biconiques présentant un maximum de rayonnement pour un azimut de  $285^{\circ}$  et une largeur de lobe de  $15^{\circ}$  à 12 dB à une fréquence de 10 Mhz, est associé à un amplificateur HF Granger de puissance de crête 100 kW.

Les émissions des deux stations sont pulsées à une cadence de 5 Hz avec une durée d'impulsion  $\tau$  de 1 milliseconde. Les cadences de pulsage présentant un écart de l'ordre de  $10^{-4}$ , une dérive relative des signaux reçus en fonctionnement bistatique par rapport aux signaux rétrodiffusés permet de les distinguer (Fig.5b).

On remarque (Fig.1) que pour chaque station la direction de l'autre station est située en dehors des maxima de rayonnement. Les puissances reçues par le trajet direct seront donc faibles (-38 dB par rapport à l'optimum). Cette orientation relative des aériens est donc particulièrement propice à l'étude des propagations hors du grand cercle.

### 3. METHODE D' INTERPRETATION DES RESULTATS

#### 3.1 Localisation de Zones de Diffusion Latérale

A une heure donnée et pour une fréquence de fonctionnement fixée les régions du globe qui vont contribuer à la formation des échos par diffusion latérale sont celles qui peuvent recevoir de l'énergie des deux stations du fait des diagrammes de rayonnement des deux aériens et des conditions de propagation.

Ces zones pourront être définies à partir des enregistrements par rétrodiffusion pour une fréquence donnée en corrigeant les trajet de groupe observés pour obtenir les distances au sol.

Les situations géographiques différentes des deux stations conduisent à des aspects différents de la propagation. La Guadeloupe, station tropicale, est dans une zone où les fréquences critiques sont nettement plus élevées que pour Valensole (zone tempérée). La fréquence de fonctionnement commune ayant été en général déterminée par les conditions de propagation à partir de Valensole, la première zone de silence est plus étroite autour de la Guadeloupe qu'autour de Valensole. D'autre part, les zones de silence d'ordre supérieur n'existent pas autour de la Guadeloupe car les distances de premier bond pour les angles bas sont supérieures au double du rayon de la zone de silence.

L'aérien de la Guadeloupe étant, de plus, nettement moins directif que celui de Valensole, on considérera que les zones possibles de diffusion latérale sont pratiquement définies par le seul diagramme de l'aérien de Valensole. Les enregistrements de rétrodiffusion obtenus à Valensole à une heure donnée (Fig.1) permettent ainsi de placer ces zones en distance par rapport à cette station.

Par superposition d'une famille de courbes "isodistance" (courbes lieux des points dont la somme des distances aux deux stations est constante), on déterminera les retards des différents modes que l'on doit observer par diffusion latérale en fonctionnement bistatique. On a représenté sur la Figure 3 les retards et les angles de diffusion latérale en fonction de la distance de la zone de diffusion à Valensole.

#### 3.2 Effect de la Durée Finie de l'Impulsion

A un instant  $t$ , défini par un retard  $\Delta t$ , donné par rapport au front avant de l'onde directe, le niveau instantané d'énergie dans l'écho reçu par diffusion est la résultante de tous les rayons diffusés latéralement au sol à l'intérieur d'un anneau limité par les courbes isodistance de paramètre  $\Delta T$  et  $\Delta T - \tau$ ,  $\tau$  étant la durée de l'impulsion émise. Les zones communes à ces anneaux et au diagramme de rayonnement de l'aérien de Valensole conduisent à des configurations nettement différentes selon la position géographique des zones considérées, et en particulier, selon la distance à la station de Valensole: pour de faibles retards, par exemple  $\Delta T = 2$  ms, et une durée d'impulsion de 1 ms la zone possible de diffusion (Fig.2, zone B) s'étend entre 2000 et 6000 km le long de la trajectoire, alors que pour des retards importants de l'ordre de 30 ms (Fig.2, zone A) la zone de diffusion n'a qu'une profondeur de 300 km le long de la trajectoire et une largeur égale à celle du diagramme de rayonnement. Pratiquement on déterminera aisément la zone de diffusion pour des retards importants, alors qu'une superposition de signaux provenant de zones situées à des distances notablement différentes pourra exister pour les faibles retards.

#### 3.3 Détermination du Coefficient de Diffusion Latérale

Le coefficient de diffusion latérale  $\sigma(\Delta, \phi)$  sera déterminé en comparant à Valensole les niveaux relatifs de l'onde directe et de l'onde diffusée.

Les conditions de propagation et de rayonnement des aériens imposent des angles d'élévation  $\Delta$  compris entre  $5^\circ$  et  $15^\circ$ , à une fréquence de 10 Mhz pour les heures d'observation. On pourra donc considérer que les valeurs obtenues pour  $\sigma$  seront valables pour des élévations de l'ordre de  $10^\circ$ .

La puissance directe reçue en V peut s'écrire

$$P_{r_1} = \frac{P_e G_{T_1}}{4\pi r_1^2} A_{r_1}. \quad (1)$$

La puissance diffusée en un point défini par les distances  $r_2, r_3$  (Fig.4) s'écrit

$$P_{r_{23}} = \frac{P_e G_{T_2}}{4\pi r_2^2} \frac{S_{\text{diff}} \sin \Delta \sigma(\Delta, \phi)}{2\pi r_3^2} A_{r_3}. \quad (2)$$

Notations:  $P_e$  puissance émise en G

$G_{T_1}$  gain en G selon  $r_1$

$G_{T_2}$  gain en G selon  $r_2$

$A_{r_1}$  surface de captation en V selon  $r_1$

$A_{r_3}$  surface de captation en V selon  $r_3$

$S_{\text{diff}}$  surface efficace de diffusion au sol.

On en déduit

$$\sigma(\Delta, \phi) = \frac{G_{T_1} A_{r_1} \left( \frac{r_2}{r_1} \right)^2}{G_{T_2} A_{r_3}} \frac{2\pi r_3^2}{S_{\text{diff}} \sin \Delta} \frac{P_{r_{23}}}{P_{r_1}}, \quad (3)$$

avec

$$\frac{A_{r_1}}{A_{r_3}} = -20 \text{ dB}.$$

Cette expression est valable de nuit lorsque l'absorption est négligeable. De jour, il est nécessaire d'introduire un facteur correctif égal au rapport des atténuations sur les deux trajectoires.

#### 4 RESULTATS EXPERIMENTAUX

Au cours de deux périodes d'expérimentation, en mars 1966 et en juin 1967, un certain nombre d'enregistrements ont été obtenus. Pour un jour et une heure donnés, les principales caractéristiques de la propagation sont classées dans un tableau. Pour une zone de diffusion repérée par le type d'écho auquel elle correspond en rétrodiffusion et par les paramètres  $r_2, r_3$  (Fig.4) le retard  $\Delta T_c$  est déterminé à l'aide des courbes "isodistance" et comparé au retard observé  $\Delta T_o$ . Le paramètre  $\rho$ , rapport entre l'énergie d'un signal propagé par diffusion et l'énergie du signal direct est exprimé en décibels, ainsi que le paramètre  $\eta$ , rapport des absorptions non déviatives sur les deux trajectoires. Pour de faibles retards le coefficient de diffusion  $\sigma$  n'a pas été déterminé car des modes d'ordre supérieur de l'onde directe peuvent se superposer aux signaux diffusés.

Le 16/3/1966 entre 21 h et 22 h TU, pour une propagation de type normal, l'écho observé en liaison point à point a une structure très flouante (Figs.5a et 5b), dans laquelle deux maxima,  $m_1$  et  $m_2$ , persistent pour des retards de 4 et 7,5 ms. La méthode d'analyse décrite précédemment permet d'associer au premier maximum  $m_1$  (Tableau I) la zone correspondant à l'écho localisé à 6000 km en  $M_1$  sur l'enregistrement par rétrodiffusion obtenu à Valensole (Fig.5c).

Dans ce cas particulier, les coefficients de diffusion calculés pour les différentes zones présentent une certaine dispersion. L'existence d'absorption sur une partie de la trajectoire

et les phénomènes de focalisation, difficiles à évaluer, ne permettent pas une grande précision dans le calcul.

Le 23/3/1966 entre 06 h et 07 h 15 TU, la propagation vers l'ouest au lever du soleil est caractérisée par l'existence de "supermodes"<sup>5</sup>. Un écho produit par un tel mode est visible à une distance de 11.500 à 13.500 km sur la Figure 6b où il se différencie des échos normaux par le fait que sa distance ne change pas quand la fréquence varie. La zone de diffusion correspondante produit, en fonctionnement bistatique, un signal S retardé de 40 ms (Fig. 6a).

Le Tableau II résume les résultats relatifs à l'ensemble des modes normaux et anormaux observés: la dispersion dans les coefficients est beaucoup plus faible et montre en particulier que ce paramètre est peu sensible à l'azimut.

Le 30/7/67 des situations analogues à la précédente ont été observées avec présence de modes anormaux. Les résultats correspondants sont rassemblés dans le Tableau III et font apparaître un coefficient de diffusion latérale du même ordre.

Les résultats du calcul du coefficient de diffusion latérale conduisent à une même valeur moyenne  $\sigma = -22\text{dB}$ , pour une surface diffusante qui, d'après la configuration de la trajectoire (Fig.1), est généralement la mer.

Il est possible que les valeurs plus fortes ( $\sigma = -16\text{ dB}$ ) du Tableau I proviennent d'une diffusion sur la côte Est de l'Amérique du Nord qui, par son orientation favorable en bordure de trajectoire, entre 6000 et 8000 km, introduirait une modification importante des coefficients de diffusion.

### 5. CONCLUSION

L'étude d'une liaison bistatique pulsée s'appuyant sur des sondages par rétrodiffusion permet de définir les zones diffusantes au sol qui contribuent à la formation du signal complexe reçu.

Les phénomènes de focalisation par les couches et d'absorption non déviative peuvent rendre difficiles l'évaluation du coefficient de diffusion. Cependant les résultats moyens, voisins de  $-22\text{ dB}$ , pour des élévations d'une dizaine de degrés, quelque soit l'azimut de déviation, semblent indiquer une certaine isotropie dans le diagramme de diffusion de la surface de la mer.

### REMERCIEMENTS

Ce travail a été accompli dans le Cadre des Conventions 67-232 et 68-217 du Centre National d'Etudes Spatiales et des Conventions 66-342 et 174-68 de la Direction des Recherches et Moyens d'Essais.

Nous remercions le Centre National d'Etudes et Télécommunications (Département TDA) et en particulier Monsieur Viossat dont la coopération a permis l'exécution d'un programme d'observations simultanées à la Guadeloupe.

## REFERENCES

1. Miya, K.  
Kanaya, S.  
*Radio Propagation Considering Scattering Waves on the Earth's Surface.* Report of Ionosphere (and Space) Research in Japan, Vol.9, 1955, p.1.
2. Miya, K.  
et al.  
*On the Bearing of Ionospheric Radio Waves.* Report of Ionosphere (and Space) Research in Japan. Vol.11, 1957, p.130.
3. Hedlung, D.A.  
et al.  
*Some Ionosphere Scatter Techniques.* Institute of Radio Engineers, Transactions. PGCS-4, Vol.1, March 1956, p.112.
4. Wolfram, R.T.  
*Improved Communications Using Groundscatter Propagation*  
*Electronics,* Vol.28, October 1960, p.74.
5. Crochet, M.  
Delloue, J.  
*Sur la Variabilité des Propagations Anormales Longue Distance Observées par Rétrodiffusion.* Comptes Rendus de l'Académie des Sciences, Vol.263, 1966, pp.517-520.

mode	1F		2F		3F+echos E			
$r_3$ (km)	2500	-3700	4000	-4800	5000	6150	7000	8000
$r_2$ (km)	5000	-3900	3700	-3100	3100	2200	2200	2500
$\Delta T_c$ (ms)	1,6	2	2,3	-3	3	4,1	8	12
$\Delta T_o$ (ms)			2,5		4	7,5	9,5	-13
$\rho$ (dB)			-12		-7,2	-10	-18	
$\eta$ (dB)			+4		+6	+6	+7	
$\phi$ (deg)			40		55	65	85	
$\sigma$ (dB)			-26		-15	-16	-26	

Tableau I 16.03.1966 soir  $f = 10 \text{ MHz}$ 

mode	1F		2F		$^3F$		$^4F$				
$r_3$ (km)	2400	-3300	4800	-7000	7800	-10.000	11.500	-13.000			
$r_2$ (km)	5000	-4200	3000	-2200	2500	-3700	4800	-6000			
$\Delta T_c$ (ms)	1,3	-1,8	2,8	-7,1	11	-22	31	-40			
$\Delta T_o$ (ms)	1,86		5	-6	16	-18,5	-20,5	32,6	-34	-38	-40
$\rho$ (dB)	-6		-5		-9		-18	-20			
$\eta$ (dB)	0		0		0		0	0			
$\phi$ (deg)			60°		100°		150°				
$\sigma$ (dB)			-22		-25		-21				

Tableau II 23.03.1966 matin  $f = 10 \text{ MHz}$ 

mode	1F		2F		$^3F$	
$r_3$ (km)	2000	-3200	4500	-7000	9000	-10.800
$r_2$ (km)	5300	-4200	3300	-2200	3000	-4300
$\Delta T_c$ (ms)	1	-1,8	2,8	-7,1	16	-27
$\Delta T_o$ (ms)	0	-5			17	
$\rho$ (dB)			-6		-12	
$\eta$ (dB)	0		0		0	
$\phi$ (deg)			60		135	
$\sigma$ (dB)			-21		-22	

Tableau III 30.06.1967 matin  $f = 10 \text{ MHz}$

## LEGENDE DES FIGURES

**Figure 1** Diagrammes de rayonnement (projection Mercator)

- - - - - limites de la zone éclairée (à 12 dB) par l'aérien de Valensole.

- . - . - - limites de la zone éclairée (à 12 dB) par l'aérien de la Guadeloupe.

6..... distance depuis Valensole (en milliers de kilomètres)



Zone recevant de l'énergie à 10 Mhz le 23/3/1966 à 00400 TU.



Zone donnant des échos de sol à Valensole.

**Figure 2** Courbes isodistances Valensole-Guadeloupe (projection Mercator)

- - - - - courbes isodistances (retard en millisecondes)



zones éclairées par des impulsions de 1 milliseconde A : 11,500 km,  
B : 2000 à 5500 km

**Figure 3** Retard et angle de diffusion latérale en fonction de la distance de la zone de diffusion à Valensole

Résultats expérimentaux

**Figure 4** Géométrie de la diffusion**Figure 5** (pas de légende)**Figure 6** (pas de légende)

3-8

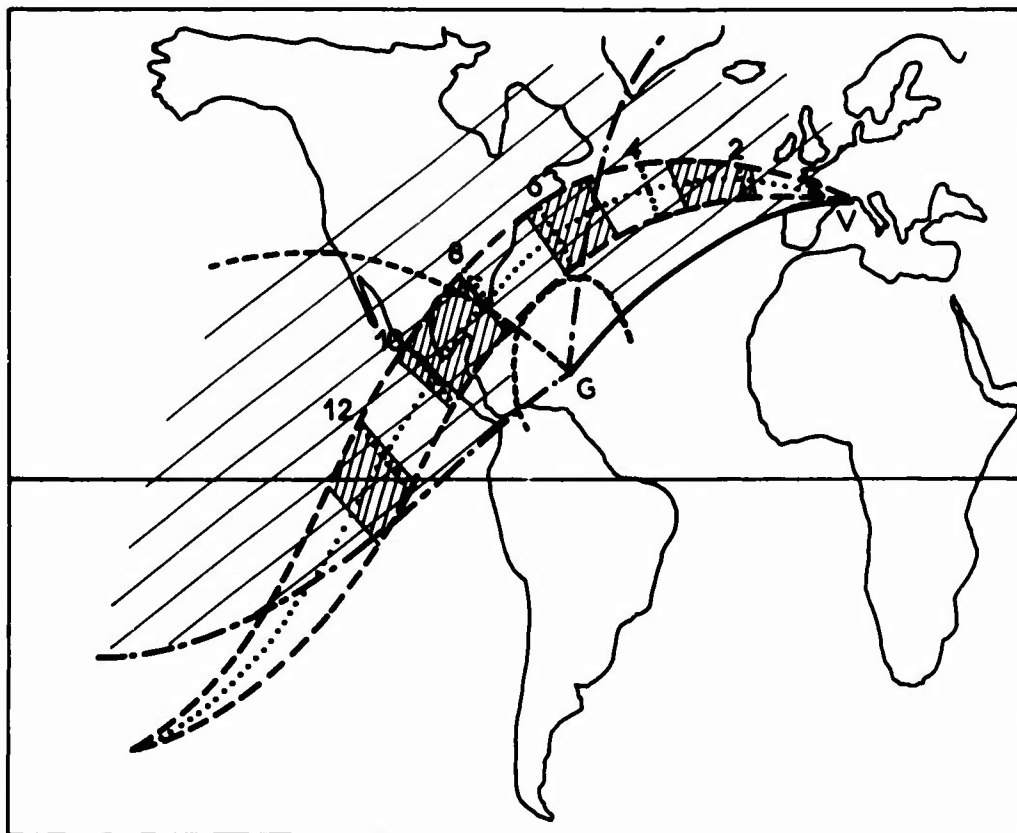


Figure 1

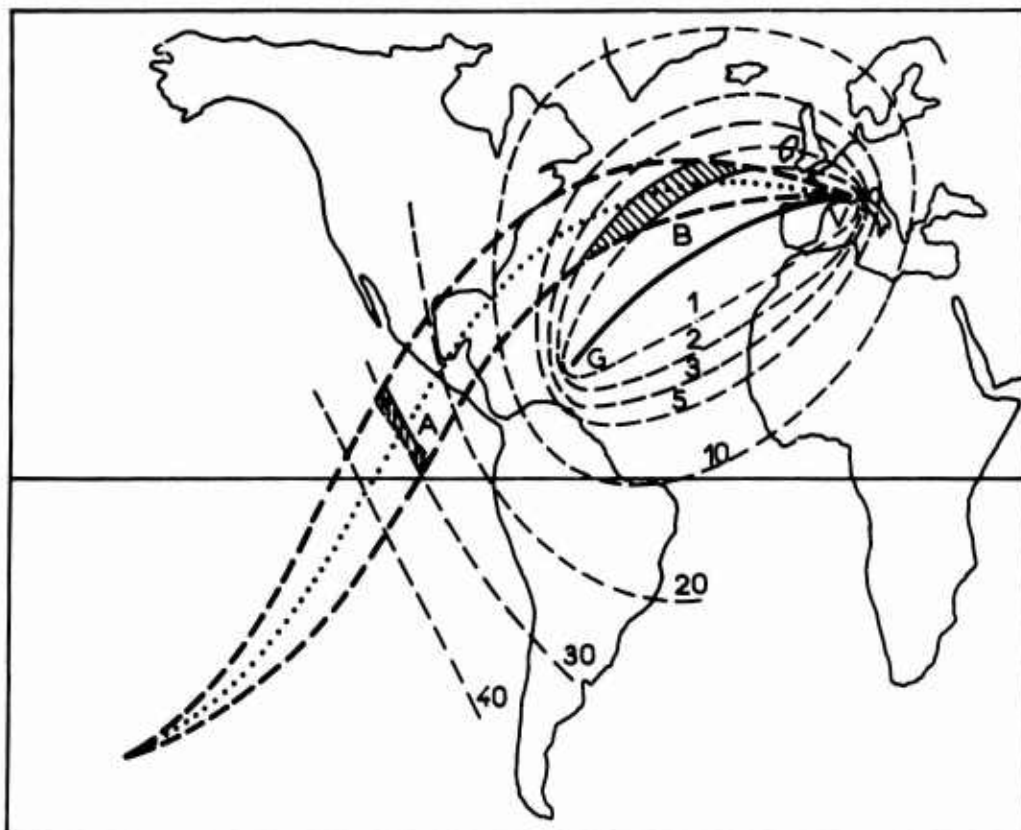


Figure 2

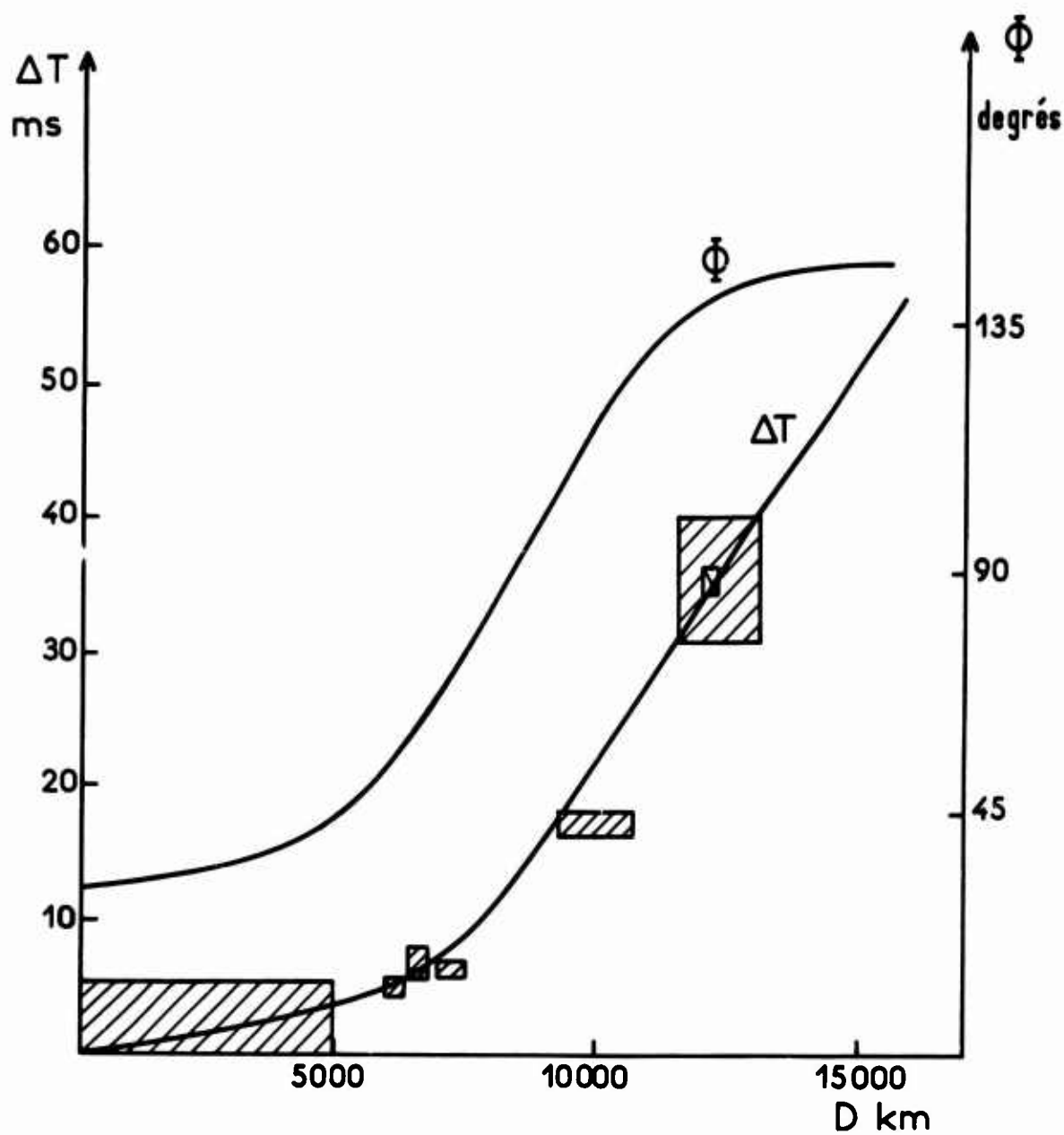


Figure 3

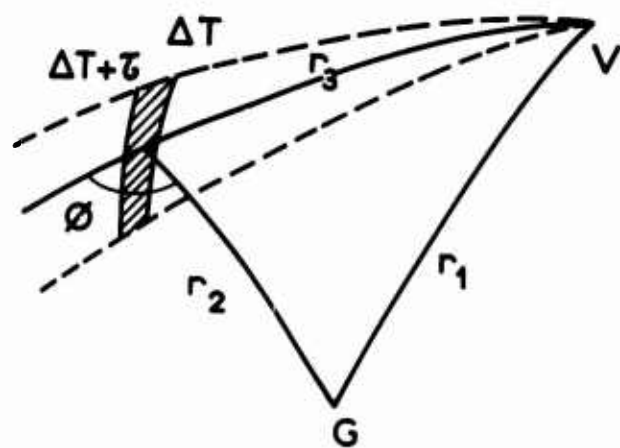


Figure 4

3-10

16.03.1966  
21:06 à 22:06 TU

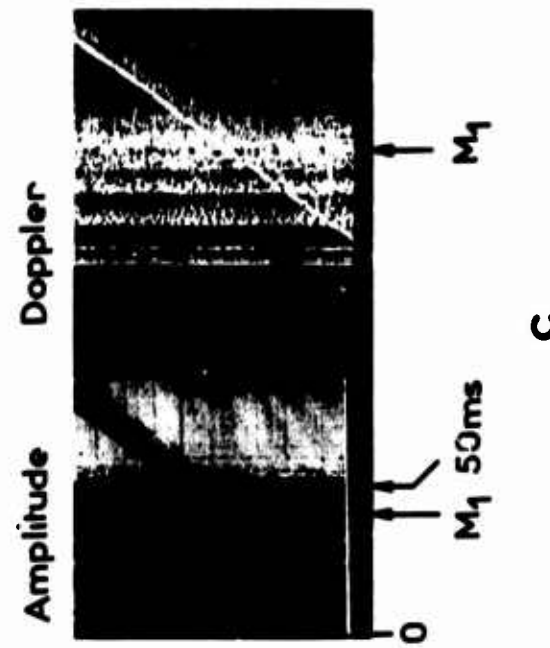
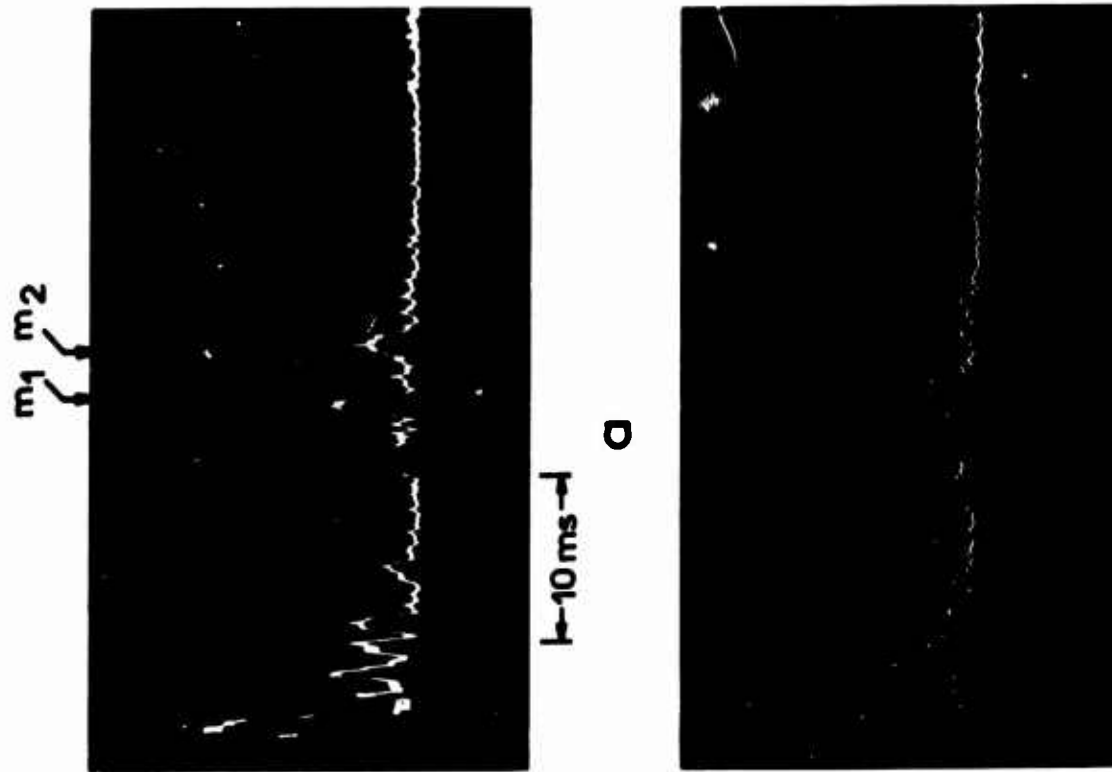
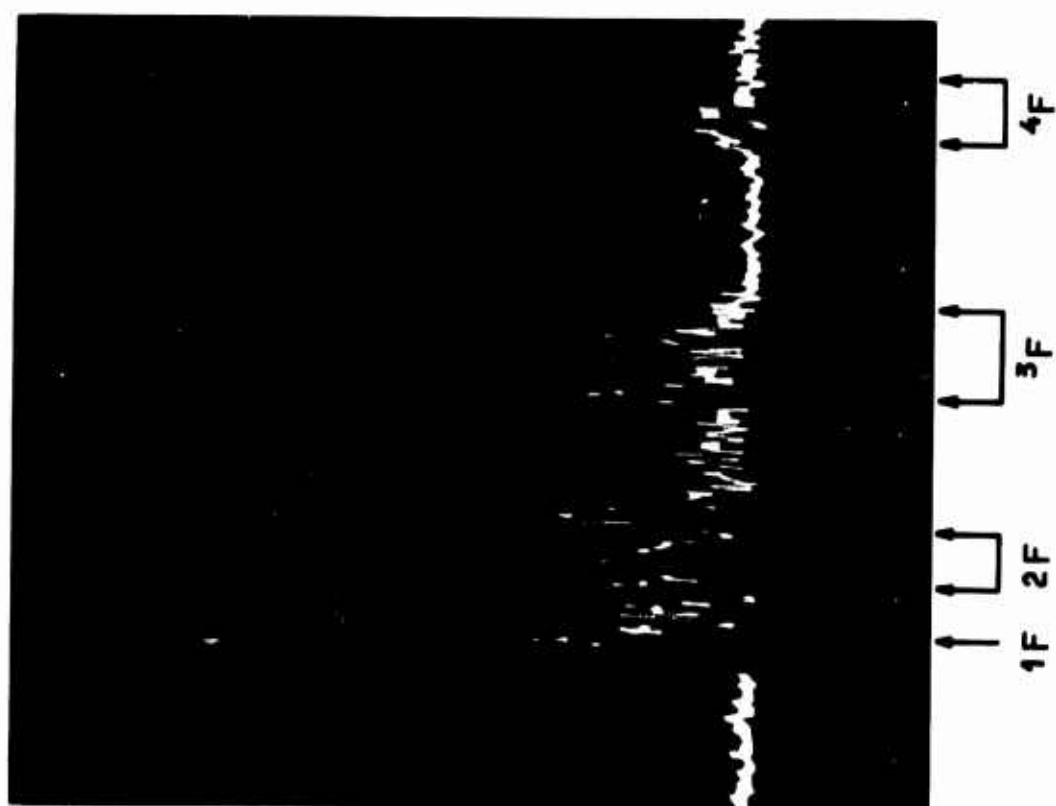


Figure 5

23.03.1966  
06:00 à 07:15 TU



b



d

Figure 6

## SOME FEATURES OF HF BACKSCATTER IONOGRAMS

by

L. W. Barclay

The Marconi Company Limited  
Baddow Research Laboratories,  
Great Baddow, Essex,  
England.

## SUMMARY

On several days the backscattered returns from swept-frequency fixed-azimuth HF pulse transmissions have been recorded on P'f ionograms at one-minute intervals. The rapid sequence allows an examination of changes of detail in the backscatter signals. Usually the returns indicated have a range spread of little more than a pulse width. The predominant feature is a return with a range which increases with increasing frequency; this is ascribed to focusing of the minimum time paths via the F-region. Other returns are observed at greater ranges and these often have a range which is approximately independent of frequency. It is suggested that these are due to travelling disturbances in the ionosphere.

Detailed examination has not indicated any preferred ranges for backscatter returns and it is concluded that, for a path which traverses land without outstanding profile features, the ionospheric variations are more important than ground scatter variations in determining the ranges at which returns are observed.

## SOME FEATURES OF HF BACKSCATTER IONOGRAMS

L. W. Barclay

### 1. INTRODUCTION

A Granger 100 kW peak power backscatter sounder has been operated at a site in Essex, England, for several years. The sounder feeds an antenna array comprising 18 vertically-polarised log-periodic aerials arranged broadside, so that the main radiation is at an azimuth of  $88^{\circ}$ . This array has a nominal azimuthal beamwidth of  $5^{\circ}$  at 10 MHz. The transmission path is almost entirely overland and avoids any large-scale ground features, such as mountain ranges or coast lines, apart from the nearby North Sea coasts. Recently an interference suppression unit has been constructed and this has allowed the photographic recording of P'f ionograms. Recordings have been made at one-minute intervals for several 24-hour periods and also at other times. These rapid ionograms show features which have not been apparent in the longer duration ionograms published by other workers. This contribution is intended only to provide a qualitative description of some of the ionogram features observed.

The ionograms extend from 4 to 32 MHz in three linear octave bands and allowance must be made for the 2 to 1 changes in frequency scale at one-third and two-thirds along the ionogram; a frequency scale is included in Figure 1. Range marks are included at the interval noted in the caption to each figure. The standard pulse width has been  $500 \mu\text{s}$ . Up to five sweeps on each channel, depending on the operation of the interference suppressor, are recorded in ionograms taken in one minute. Longer duration ionograms have been made by recording several frequency sweeps on one exposure.

### 2. IONOGRAM FEATURES

Most backscatter ionograms featured in the literature have a minimum slant range which increases with frequency and also have returns extending beyond this minimum range. Figure 1 is an example of such an ionogram which was recorded in ten minutes. Even this ionogram shows a more limited range spread than might have been expected and this may be due in part to the narrow azimuthal beam and to poor low angle radiation from the antenna. However, ionograms taken in one or two minutes invariably show returns which are even more restricted. An extreme example is shown in Figure 2 where, at a time shortly after sunrise, the returns are confined to a single pulse width. Such a limited response may be ascribed to minimum-time (loosely, "skip-distance") focusing in conjunction with a very poor ground scattering coefficient. Previous work<sup>1</sup> attempted to explain the limited nature of the returns by conventional HF prediction technique, without reference to focusing effects, but such methods cannot explain the rapid decrease in signal beyond the first return.

Usually ionograms are more complex than that shown in Figure 2, and show some structure beyond the minimum-time returns. An example is given in Figure 3, where the changes in successive two-minute intervals may also be seen. The sum of these intermittent and variable returns may also account for part of the range extension seen on long duration ionograms. The minimum-time returns in Figure 3 do not show the smooth increase with frequency expected from a simple consideration of a smooth ionosphere. This is a common occurrence which is also illustrated in Figure 4.

Examination of a long sequence of one-minute ionograms shows the presence of "flat" returns, which have a range which is constant or which decreases slightly with increasing frequency. Usually these traces decrease in range in successive ionograms. An example which shows two such features, one of which extends through the minimum time return at high frequency, is shown in Figure 5. Figure 6 shows a sequence of ionograms through which the progression of one of these features may be followed.

Such moving features have been examined in detail in the recordings made on the 17/18 November 1966. They occurred most frequently in the afternoons and the ranges at which they were observed are shown in Figure 7. Although it was difficult at times to positively relate the traces seen in successive ionograms, the tendency shown in Figure 7 is for several groups of points to decrease in range with time. The range-change is 800-1200 km per hour. These features are probably due to focusing caused by travelling ionospheric disturbances, which would have speeds from east to west of about half the rate of range-change observed.

A few particular features could be followed with reasonable certainty for 10 to 15 minutes and the rate of range-change of one of these is approximately 960 km per hour (Fig. 8).

Some moving features were also observed in the morning period, but these were less distinct and had a range which increased with frequency. One of these was followed for 12 minutes (Fig. 9) and showed a range increase at a rate of 1140 km per hour.

The records have been examined for any indications of preferred ranges of the returns, but none were found. As stated earlier, the path observed has no large-scale topographical variations and the smaller features are apparently masked, either by ionospheric variability or by the 500  $\mu$ s pulse length. The predominant cause of the observed backscatter returns is focusing due to ionospheric variations. This conclusion is contrary to that of some other workers and it may be a fruitful subject for discussion.

#### ACKNOWLEDGMENTS

The interference suppression unit was designed by Mr. A.B.E. Ellis and most of the observations were made by Mr. B.J. Peters and Mr. I.M. Kibble. The work was undertaken on a Ministry of Technology contract and the installation was made available under this contract. This contribution is presented by permission of the Director of Research of the Marconi Company Limited.

#### REFERENCE

1. Barclay, L.W.

*Field Strength Predictions for Backscatter Ionospheric Sounding.*  
Proceedings of the 11th AGARD/EPC Meeting, Leicester, 1966,  
in course of publication.

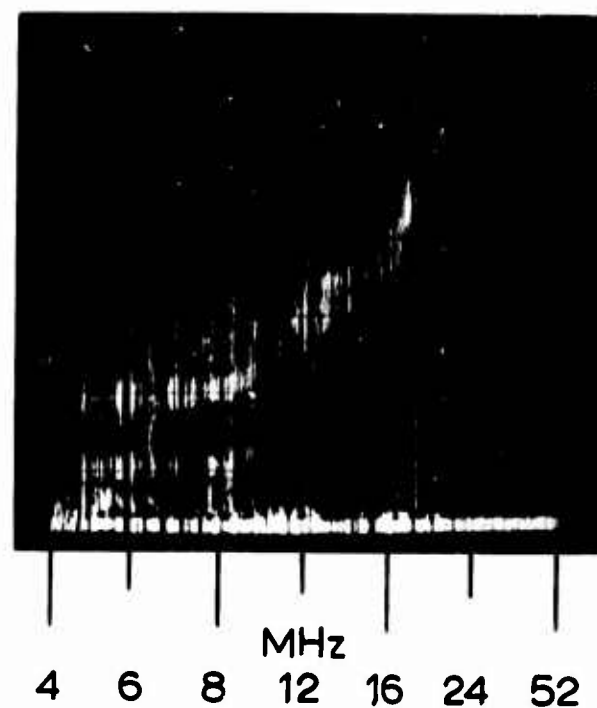


Fig. 1. A 10-minute backscatter ionogram, 14.15-25 h GMT, 21/3/68.  
(Range mark interval 300 km)

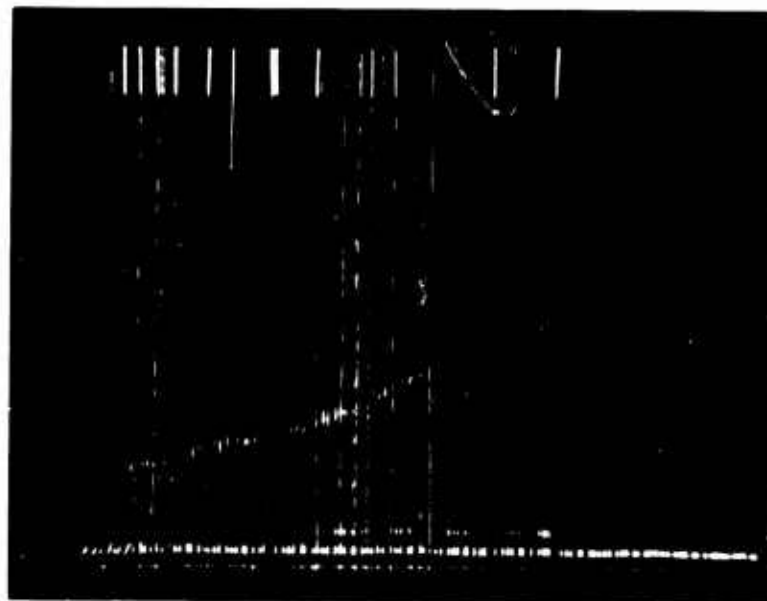
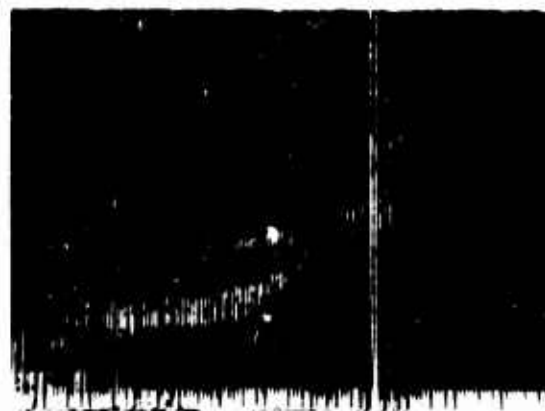
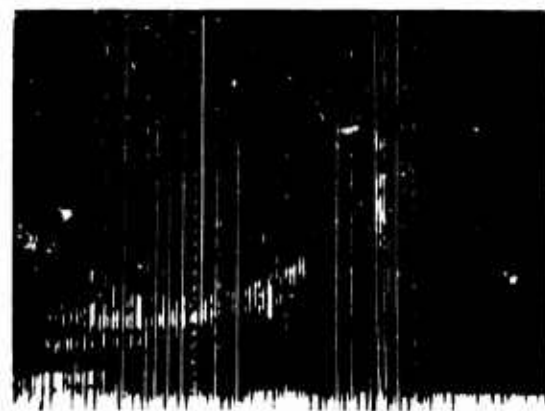


Fig. 2. 07.33 h GMT, 18/11/66. (Range mark interval 1500 km)

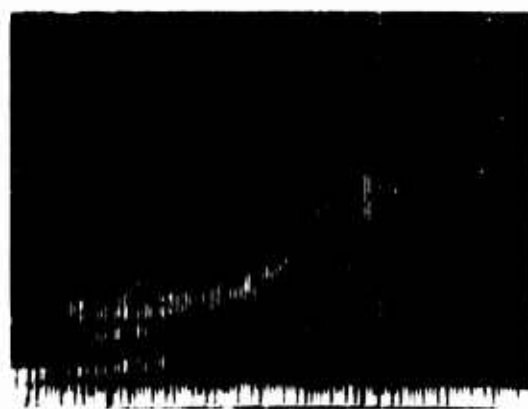
4-4



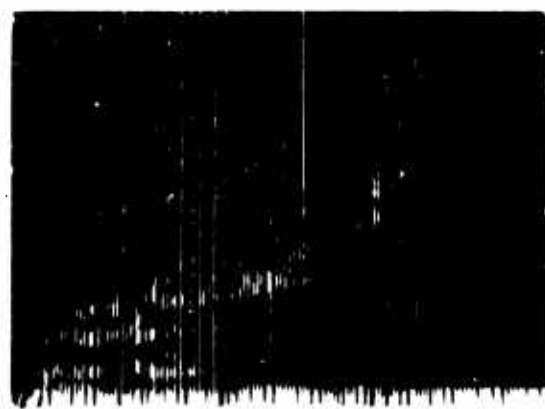
10.13 h GMT



10.15 h GMT



10.17 h GMT



10.19 h GMT

Fig. 3. Change in ionograms during 7 minutes, 1/12/66. (Range mark interval 300 km)



Fig. 4. 11.57 h GMT, 1/12/66. (Range mark interval 300 km)



Fig. 5. "Flat" features in ionogram, 11.11 h GMT, 1/12/66.  
(Range mark interval 300 km)

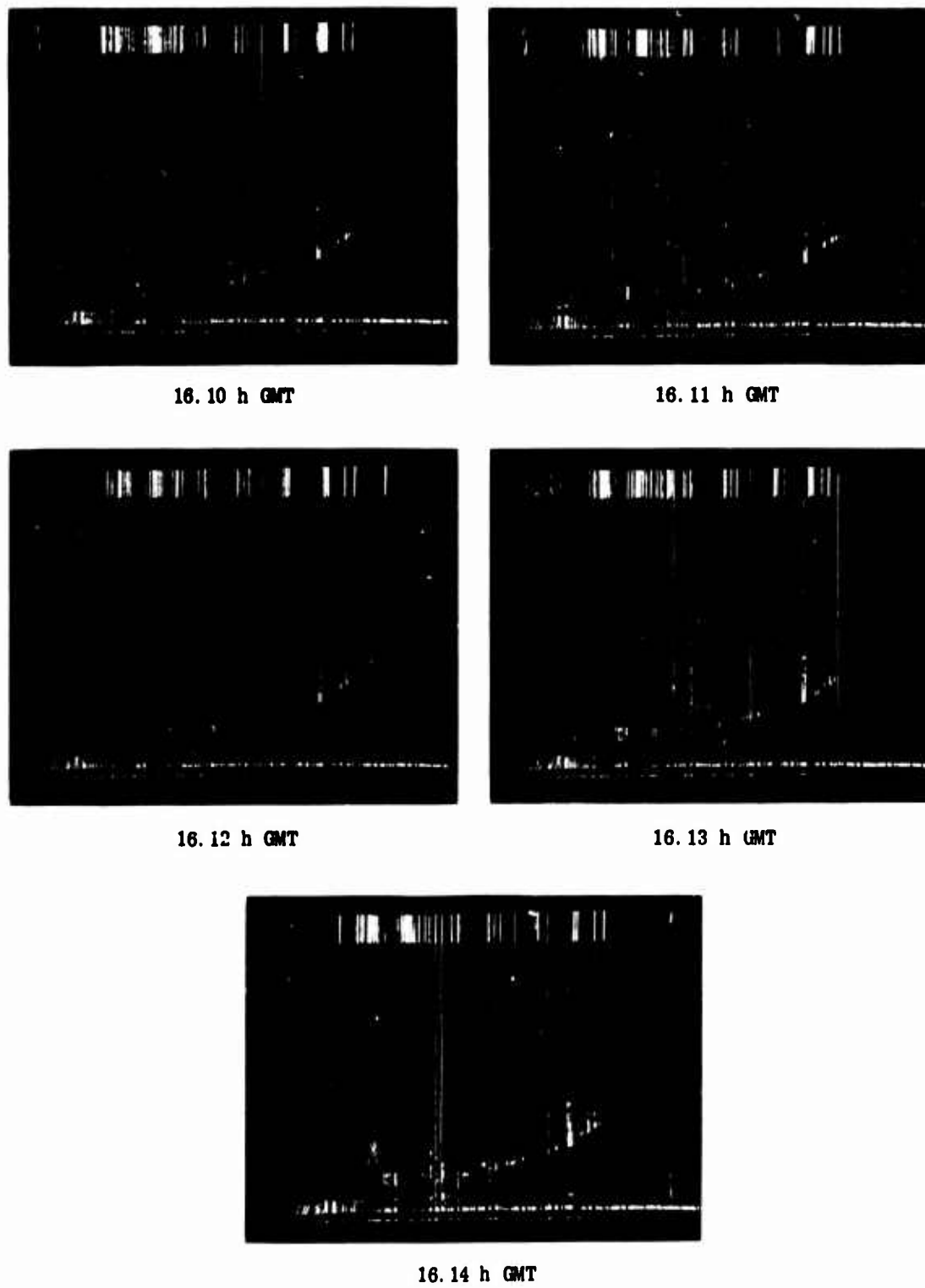
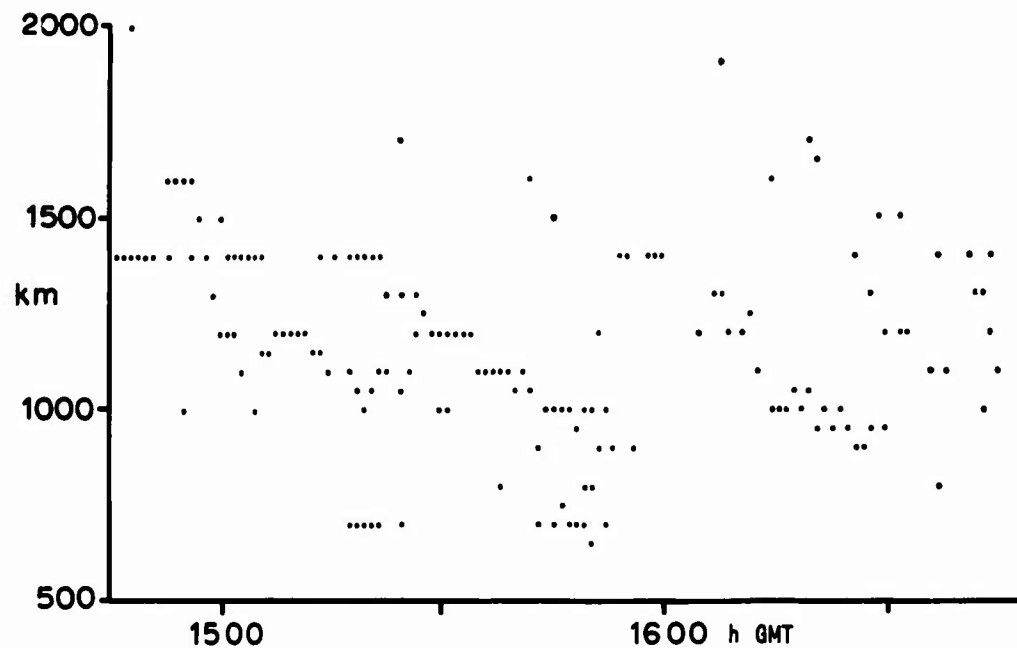


Fig. 6. The movement of an ionospheric feature. 16. 10-14 h GMT, 17/11/66.  
(Range mark interval 1500 km)

NOVEMBER 17th 1966  
1445-1645 h GMT



NOVEMBER 18th 1966  
1310-1510 h GMT

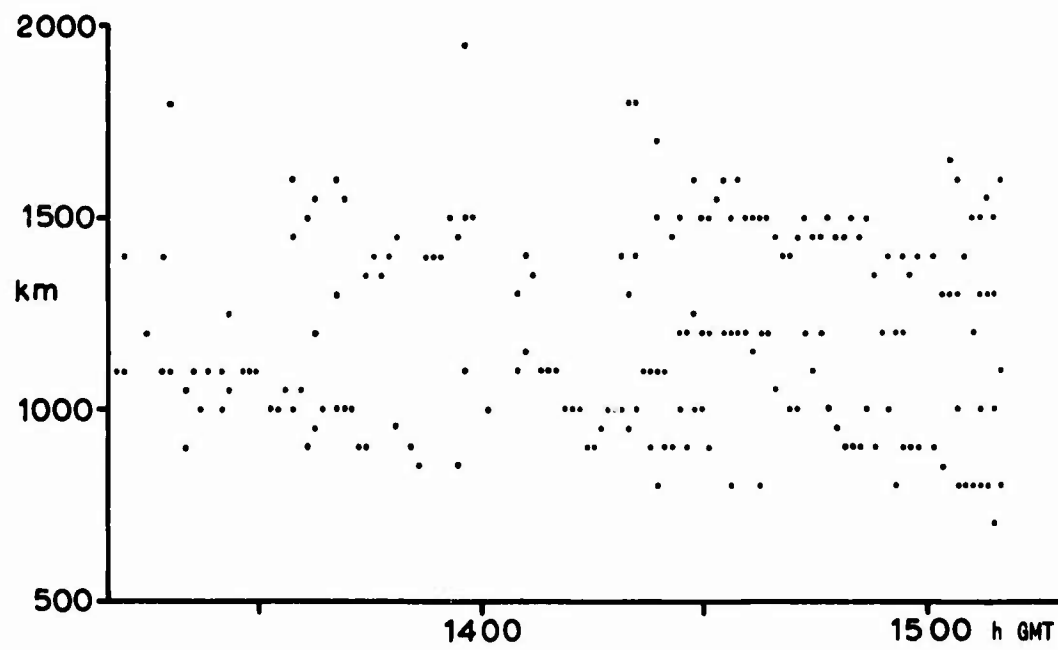


Fig. 7. The observed ranges of "flat" ionospheric features

4-8

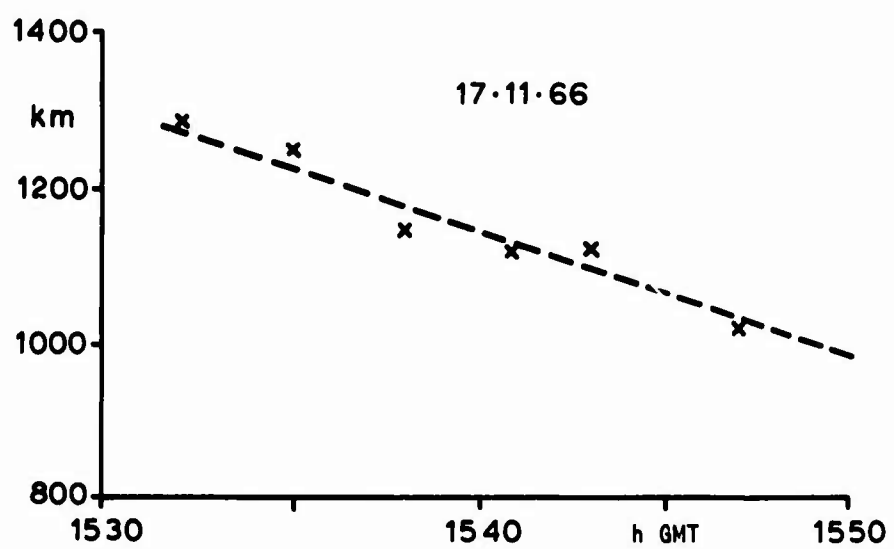


Fig. 8. Change of the observed range of a moving ionospheric feature

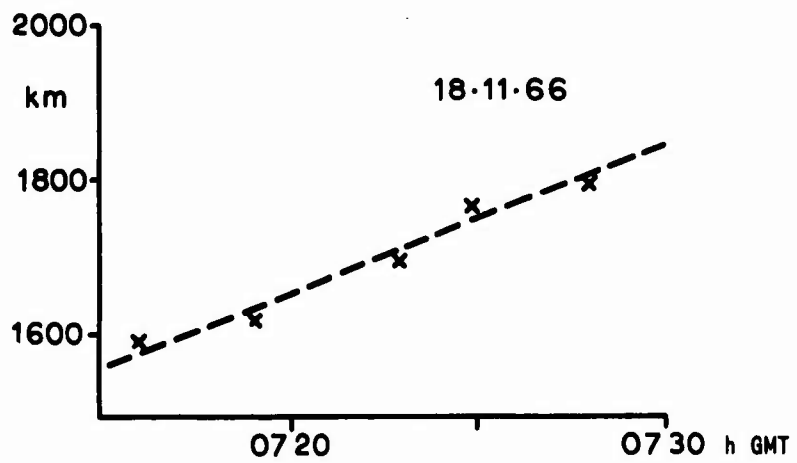


Fig. 9. Change of the observed range of a moving ionospheric feature

**DISCUSSION ON THE PAPERS PRESENTED IN SESSION I (GROUND SCATTER)**

*Discussion on Paper 1, "Ground Scatter in Review" by E.C.Hayden.*

**Dr Phillip Newman:** Dr Hayden has managed to speak at length about the subject of ground scatter without using the word "clutter", which would detract perhaps from the "respectability" of the subject. Another term one misses is "Rayleigh's criterion" for smoothness of an area.

**Dr E.C.Hayden:** Perhaps this is because ground scatter primarily has been used as a tool for the study of other phenomena, and hence has been considered a desirable phenomenon, rather than something which obscures. One exception is the study of remote meteor incidence, i.e. meteor incidence above the scattering region, or detection of other remote targets above the surface of the earth. With respect to Rayleigh's criterion for roughness, I pointed out that backscattering models based just on surface contour, or descriptions of surface roughness, do not appear to suffice in explaining the observed behavior.

**Question to Dr Hayden:** Regarding your comment on the role of subsurface features, is there any research relating ground backscatter to ground surface conductivity maps, seasonal rainfall, ground-water table features, etc?

**Dr E.C.Hayden:** See the second paper in this session for microwave data. I know of only one source that seems to treat the subject at HF directly, Reference 200 in the bibliography in my paper (*J.G.Steele, Influence of Electrical Properties of the Ground on the Backscatter Coefficient at High Frequencies*, Technical Report 121, Stanford University, Calif, Dec. 1965). Related material is given in Reference 225 in the bibliography (*G.H.Hagn, The Direct Backscatter of High-Frequency Radio Waves from Land, Sea-Water, and Ice Surfaces*. Institute of Electrical and Electronic Engineers, Int. Convention Records, Vol. 15, 1967, pp.150-159). My purpose was to point out the dearth of such data, and the desirability that some be obtained.

**Dr K.Davies:** Can ionospherically propagated backscattered echoes be used to study the ground characteristics?

**Dr E.C.Hayden:** Results to this date have been generally negative. In fact, one of the points of my presentation is that, so far, the greatest application of ground scatter has been to the study of the ionosphere, rather than conversely, e.g. to the study of Sporadic-E or F-regions traveling irregularities rather than the scattering target itself. In examining the ITS (Boulder, Colo.) range/azimuth backscatter recordings, I have yet to see any certainly identifiable evidence of terrain features. Certainly the opportunity to do so exists, because within view are such divergent terrain types as the central Plain, the Ozark Hills, the Appalachian Mountains, the Atlantic Ocean, the Florida peninsula, and the Gulf of Mexico. At best, it seems to me that discrimination of terrain types, let alone individual features, is likely to require exploitation of some of the techniques mentioned in the last part of the paper, namely reduction in resolution cell size, and use of multi-parameter recordings or displays, perhaps, for example, utilizing spectral as well as amplitude information. Specifically, it was my intention to convey the impression that attempts at measuring backscatter coefficient using ionospherically propagated signals have not had marked success, and that a need exists for other methods to be developed and used. One must realize that if one did succeed in rendering distinct some terrain feature, say a coastline, that it would be distorted by the ionospheric focusing - just that same mechanism that produces the uneven distribution of amplitude - and that the nature and degree of distortion would vary with time. It would be a bit like putting a map at the bottom of a pan of water, then viewing it through the water as the surface is disturbed. Nonetheless, the capability to recognize terrain features would be useful for purposes of calibration, as well as other obvious applications.

**Professor E.D.R. Shearman:** Although I agree that little success has rewarded attempts to recognize terrain features, it should surely be possible to see, with sufficient resolution, a rocky island in a calm sea. Another possibility is to distinguish sea from land by the characteristic fading of sea echo. Unfortunately, F-layer propagated echoes fade at a similar rate and make identification difficult, but I have observed very slow-fading,  $E_s$ -propagated, echoes in a landward direction and, on rotating the aerial to look at sea echoes propagated by the same  $E_s$  cloud, I have seen fast-fading echoes.

**Professor I. Ranzi:** I would like to stress the importance of the presence of metallic objects (power lines, rails, etc.) on the direct HF backscatter. Using some experimental results obtained in Italy in 1960-1964, we calculated that a highly industrialized area may present an average HF backscatter coefficient much higher than the one presented by a similar area, not covered by metallic structures. We also observed that the coastal sea is a stronger backscatterer than the open sea (with the same roughness); this is due to the system of stationary sea waves, which appears near the coast.

**Professor E.D.R. Shearman:** Further valuable results on backscattering cross-sections have been given recently by Steele (Proceedings, Institute of Electrical and Electronic Engineers, Vol. 55, 1967, p. 1583). He has described the measurement of the backscattering cross-section of a single tree for downcoming waves by a most ingenious and simple technique.

**Dr D.Nielson:** From experience obtained in a direct groundscatter measurement at 30 MHz from an aircraft, there is much difficulty in drawing significant conclusions regarding the detailed characteristics of land or sea. At the longer wavelengths that must be used in ionospherically propagated backscatter, both the dielectric properties and the land or sea contours become important. This fact plus the large land areas involved for obtainable beamwidths, and the time variation of the ionosphere, argue against the use of ionospherically propagated backscatter for detailed terrain return analysis.

**Dr A.W. Biggs:** The use of microwave radar imagery and scatterometry for making observations of forested areas is already underway at the University of Kansas. Multifrequency measurements are also planned to yield information on the subsurface dielectric properties of the earth and their associated backscatter cross-section.

**Dr E.C. Hayden:** It is my suggestion that persons interested in backscatter coefficients at HF should take note of the microwave techniques Dr. Biggs mentioned to see whether or how some of them might be "borrowed" or adapted. I doubt that the microwave results are themselves applicable at HF. At HF the depth of penetration is significant, and inhomogeneities of conductivity and dielectric constant could well cause non-specular transmission of energy incident on even a flat ground surface. It is for the smoother terrain types that the microwave models seem least successful in predicting HF behavior. Perhaps also, as Dr. Ranzi suggested, the effect of man-made structures such as powerlines is important.

**Dr H. Kopka:** Groundscatter observation also gives information about the state of the ionosphere. For instance: we often see on  $p'$ - $f$  diagrams the splitting of the backscatter traces into magnetoionic components. Since the pattern width of the aerial is about  $36^\circ$ , the ionosphere must be very uniform in azimuthal variation to produce distinct magnetoionic traces on the record.

*Discussion on Paper 2: "Surface Scattering in Ocean Roughness and Sea Ice Studies," by A.W. Biggs.*

**Dr J. Ramasastry:** Dr Biggs, when you mentioned "lower frequencies", how much lower is the frequency? Have you made any calculations for the optimum minimum frequency that could be used which will still give accurate information about the scattering surface?

**Dr Albert W. Biggs:** Lower frequencies extend from 13.3 GHz to 400 MHz, about two orders of magnitude. With regard to your second question, these calculations will be made in the form of empirical analyses based on experimental measurements.

**Mr S. B. Levin:** At what frequencies are you observing the sea ice? At considerably lower frequencies (e.g. <0.5 GHz) you will penetrate the ice and observe primarily the sea water surface.

**Dr A. W. Biggs:** Sea ice is presently being observed at 13.3 GHz. At lower frequencies, we hope to examine the dielectric properties of the ice and the ice-sea interfaces. This permits a qualitative indication of ice thickness as well as roughness.

**Dr N. C. Gerson:** Sea ice over the Arctic Ocean has a general average thickness of about 3-5 m. Employing the proper frequency is it possible to obtain reflections from both the top and bottom surfaces of the sea ice, and thus "map" the sea ice over extended areas of the ocean?

**Dr A. W. Biggs:** HF techniques don't work because of the large wavelengths; the other problems are tied in with high absorption in the ice-sea water transition region. The lower structure of polar ice is stalagmite in nature, and very lossy due to brine deposits. When ice thickness exceeds 5 m, it is too thick for current interest.

*Discussion on Paper 4: "Some Features of HF Backscatter Ionograms" by L. W. Barclay (presented by A. N. Peters).*

**Dr E. C. Hayden:** In connection with Mr Barclay's paper I should like you to note the paper by T. A. Croft, *The Influence of Ionospheric Irregularities on Sweep-Frequency Backscatter*, Journal of Atmospheric and Terrestrial Physics, Vol. 30(5), May 1968, pp. 1051-1063. He has shown synthesized range-frequency ionograms, done by digital ray-tracing techniques which exhibit the constant-range feature. The ionosphere model involved a perturbation of the gravity-wave type. He did not treat, however, the question of motion.

**Professor I. Ranzi:** I was surprised to hear that the prevailing direction of the movement of the large-scale traveling disturbances observed by Mr Barclay was along West-to-East or reverse. We, in Italy, always observe a well-defined movement from the North magnetic pole towards the equator.

**Dr E. N. Bramley:** The observations of Mr Barclay on traveling disturbances are consistent with those made in the UK by direction-finding techniques, some fifteen years ago. These also showed a tendency for movements from West to East in the morning and from East to West in the afternoon. There was no limitation on the directions which could be observed by this technique.

**LA REFLEXION EN ONDES DECAMETRIQUES PAR  
LA SURFACE TERRESTRE EN EMISSION IMPULSIONNELLE ET  
SON ROLE DANS L'INTERPRETATION DES SPECTRES DE FREQUENCE  
DES ECHOS OBTENUS DANS LES SONDAGES PAR RETRODIFFUSION**

**par**

**Claude Goutelard**

**Laboratoire de Physique de l'Exosphère  
Faculté des Sciences de Paris, France**

## RESUME

La réflexion des ondes décamétriques sur la surface terrestre est marquée par le relief dont les dimensions sont souvent de l'ordre de grandeur de la longueur d'onde.

Les sols et la mer peuvent être représentés par des modèles théoriques, aléatoires dans les premiers cas, avec une composante périodique représentant la houle, dans le second.

En émission impulsionnelle, trois phénomènes peuvent apparaître simultanément: diffusion, diffraction et interférence. L'énergie n'est pas transmise uniquement dans la direction de réflexion spéculaire. Dans le cas d'une réflexion sur la mer, une grande partie de l'énergie est transmise dans des directions particulières dont certaines peuvent donner lieu à des propagations hors du grand cercle. Dans le cas d'une réflexion sur le sol, un phénomène de diffusion entraîne, en général, un affaiblissement important de la transmission de l'énergie dans la direction de réflexion spéculaire. Ces résultats théoriques peuvent expliquer les différences systématiques observées dans les propagations ionosphériques multibonds où les réflexions successives s'effectuent toutes sur le sol ou la mer.

Dans tous les cas, une petite partie de l'énergie est diffusée dans les autres directions. En particulier, au voisinage de la direction d'incidence, la quasi-isotropie du rayonnement diffusé permet d'interpréter la formation des échos obtenus dans les sondages par rétrodiffusion par l'interférence de plusieurs trajectoires différentes de l'énergie.

Une méthode graphique permet d'en déduire les composantes spectrales des informations doppler et fading à partir des profils réels et de lier simplement leurs variations à celles des paramètres ionosphériques. L'analyse de cas concrets montre le bon accord obtenu entre les déterminations théoriques des spectres et les relevés expérimentaux.

**LA REFLEXION EN ONDES DECAMETRIQUES PAR  
LA SURFACE TERRESTRE EN EMISSION IMPULSIONNELLE ET  
SON ROLE DANS L'INTERPRETATION DES SPECTRES DE FREQUENCE  
DES ECHOS OBTENUS DANS LES SONDAGES PAR RETRODIFFUSION**

Claude Goutelard

**1. ASPECT PARTICULIER DU PROBLEME**

Une onde plane est réfléchie dans la direction de réflexion spéculaire par une surface plane infinie. Dans les sondages impulsionsnels par rétrodiffusion cette loi est modifiée à cause des deux points suivants:

- la surface terrestre instantanément illuminée  $S$  est limitée, en particulier par la durée de l'impulsion. Il existe donc un phénomène de pupille donnant un champ de diffraction.
- la surface illuminée peut présenter des aspérités périodiques, telle la houle, qui produisent des phénomènes d'interférence, ou réparties au hasard et qui produisent une diffusion.

Les réflexions pouvant se produire sur la mer ou sur la terre, on a été conduit à rechercher deux types de modèles théoriques pour les représenter.

**2. CHOIX DES MODELES**

Si on définit le plan horizontal par les axes de coordonnée  $Ox, Oy$ , il est possible de représenter localement le sol ou la mer par la superposition de deux surfaces,

$$\tau(xy) = \tau_1(xy) + \tau_2(xy),$$

où  $\tau_1(xy)$  représente les ondulations lentes auxquelles se superposent des ondulations plus rapides  $\tau_2(xy)$ .

**2.1 Cas des Sols**

Dans le cas des sols,  $\tau_1(xy)$  représente les accidents à grande échelle constitués par le relief et  $\tau_2(xy)$  les aspérités telles que la végétation ou les constructions. Ces surfaces peuvent être représentées par des modèles aléatoires définis:

- soit par des aspérités, de forme particulière, réparties au hasard<sup>1,2</sup>
- soit, d'une manière plus générale, par des aspérités de forme indéterminée mais pour lesquelles on admet une distribution normale définie par l'écart type  $\sigma$  et une distance de corrélation  $T$  (Réf. 3).

Cette dernière définition a été adoptée pour cette étude. Ainsi, pour représenter le relief on est conduit à choisir  $T$  et  $\sigma$  grands, tandis que pour représenter la végétation  $T$  et  $\sigma$  sont plus petits:

Des études de coupe de terrains ont permis de déterminer:

- pour la région parisienne (plaine)  $\sigma = 30 \text{ m}$   $T = 6 \text{ km}$
- pour la région de Valensole (plateaux montagneux)  $\sigma = 50 \text{ m}$   $T = 1500 \text{ m}$

D'autre part, on a pu estimer:

- pour une végétation pauvre:  $\sigma = 1,5 \text{ m}$   $T = 7,5 \text{ m}$
- pour une forêt dense ou une agglomération  $\sigma = 5 \text{ m}$   $T = 30 \text{ m}$ .

## 2.2 Cas de la Mer

Dans le cas de la mer, si on accepte de représenter la houle par une sinusoïde,

$$\tau_1(xy) = h \cos 2\pi \left( \frac{x}{\Lambda_x} + \frac{y}{\Lambda_y} \right), \quad (1)$$

$\Lambda_x$  et  $\Lambda_y$  étant liés à la longueur d'onde de la houle  $\Lambda$  par la relation

$$\frac{1}{\Lambda^2} = \frac{1}{\Lambda_x^2} + \frac{1}{\Lambda_y^2}. \quad (2)$$

Son inclinaison peut être repérée par l'angle  $\psi$  formé par la normale à la crête des vagues et l'axe  $Ox$ , tel que

$$\operatorname{tg} \psi = \Lambda_x / \Lambda_y. \quad (3)$$

La longueur d'onde  $\Lambda$  est comprise entre 75 et 150 m (Réf. 4) et  $2h$ , qui représente le creux de la houle, n'excède pas 10 m.

$\tau_2(xy)$  représente l'agitation qui s'y superpose et que l'on peut définir par une surface aléatoire pour laquelle

$T = 7,5 \text{ m}$  et  $\sigma = 0,07 \text{ m}$  pour une faible agitation

$T = 7,5 \text{ m}$  et  $\sigma = 0,5 \text{ m}$  pour une forte agitation.

## 3. DIAGRAMMES DE RAYONNEMENT

Les modèles choisis sont définis par la superposition de deux surfaces dont les distances de corrélation des aspérités sont très différentes.

Il peut être montré alors que celle dont la distance de corrélation est la plus grande est responsable du rayonnement au voisinage de la direction de réflexion spéculaire tandis que celle dont la distance de corrélation est la plus faible a une action prédominante dans les autres directions<sup>5</sup>.

Cette propriété a été appliquée aux modèles représentant la mer et la terre.

### 3.1 Méthode de Calcul (Fig. 1)

Soit une onde plane définie par le vecteur d'onde  $k_1$  contenue dans le plan  $xOz$  et diffractée par une aire  $S$  du sol dans une direction définie par le vecteur d'onde  $k_2$ . Le champ  $E_2$  reçu en un point  $P$  situé en dehors des zones de Fraunhofer est<sup>3</sup>

$$E_2 = j \frac{E_1 \exp(jkr_0)}{4\pi r_0} \iint_S (Rv - p)n \exp(v \cdot r) ds, \quad (4)$$

avec  $E_1$  = amplitude du champ incident  
 $r$  = rayon vecteur joignant l'origine à un point de la surface  $z = \tau(xy)$   
 $R$  = coefficient qui dépend de la nature du sol et de sa forme, de la polarisation de l'onde et de son angle d'incidence.  
et  $r_0 = OP$ ,  $v = k_1 - k_2$ ,  $p = k_1 + k_2$ ,  $k = |k_1| = |k_2| = 2\pi/\lambda$   
 $\lambda$  = longueur d'onde de l'onde électromagnétique.

$v$  ayant pour composantes

$$\left. \begin{aligned} v_x &= k(\sin \theta_1 - \sin \theta_2 \cos \theta_3) \\ v_y &= -k \sin \theta_2 \sin \theta_3 \\ v_z &= -k(\cos \theta_1 + \cos \theta_2) \end{aligned} \right\} \quad (5)$$

La surface illuminée  $S$  a été supposée limitée à  $-X < x < X$  et  $-Y < y < Y$ .

### 3.2 Cas de la Mer

En ondes décamétriques, la mer peut être assimilée à un conducteur parfait puisqu'à 20 MHz  $|R| = 0,98$  en incidence verticale et l'angle pseudo-Brewster est  $50'$  (Réf. 1). Dans une direction donnée, le rayonnement est produit par la réflexion du champ incident sur des surfaces élémentaires parallèles. La direction du plan de polarisation de l'onde varie mais l'amplitude du champ n'est pas altérée. On peut donc, si l'on ne s'intéresse qu'à la valeur scalaire du champ, poser dans (4),  $R = 1$ .

#### 3.2.1 Action de la Houle

Si on pose  $X = M\Lambda_x$ ,  $Y = N\Lambda_y$ ,  $M$  et  $N$  entiers, l'expression (4) se simplifie et le rapport

$$\rho = \frac{E_2}{E_{20}} \quad (6)$$

dans lequel  $E_{20}$  est le champ rayonné dans la direction de réflexion spéculaire par la surface  $S$  supposée plane et infiniment conductrice, s'exprime par

$$\rho = \frac{K}{S} \int_{-X}^X \int_{-Y}^Y \exp(jv \cdot r) dx dy \quad (7)$$

avec

$$K = \frac{1 + \cos \theta_1 \cos \theta_2 - \sin \theta_1 \sin \theta_2 \cos \theta_3}{\cos \theta_1 (\cos \theta_1 + \cos \theta_2)} \quad (8)$$

$$S = 4XY.$$

Compte tenu de la double périodicité, par rapport à  $\Lambda_x$  et  $\Lambda_y$  il vient, après un arrangement,

$$\rho = \frac{K}{S} \sum_{\mu=-M}^{M-1} \sum_{\nu=-N}^{N-1} \exp(j2\pi p\mu) \exp(j2\pi q\nu) \int_0^{\Lambda_x} \int_0^{\Lambda_y} \exp(jv \cdot r) dx dy \quad (9)$$

avec

$$2\pi p = v_x \Lambda_x = k \Lambda_x (\sin \theta_1 - \sin \theta_2 \cos \theta_3) \quad (10a)$$

$$2\pi q = v_y \Lambda_y = -k \Lambda_y \sin \theta_2 \sin \theta_3. \quad (10b)$$

Enfin, en effectuant les sommes,

$$\rho = j^{p+1} K \frac{\sin 2Nq\pi}{2N \sin q\pi} \frac{\sin 2Mp\pi}{2M \sin p\pi} \frac{\sin(p-q)\pi}{\pi(p-q)} \left[ J_{-p}(-hv_z) + \frac{\sin p\pi}{\pi} \int_0^\infty \exp(pt + hv_z \sin t) dt \right] \quad (11)$$

$J_{(-p)}(-hv_z)$  est une fonction de Bessel de première espèce d'ordre  $-p$ .

Cette relation met en évidence l'existence de trois phénomènes différents: interférence, diffraction et diffusion.

#### Phénomène d'interférence constructive

Il apparaît que  $\rho$  est inversement proportionnel à  $S$ , donc très petit, sauf lorsque  $p = q = m$  ( $m$  entier), cas pour lesquels se produit un phénomène d'interférences constructives dans les directions particulières  $\theta_{2m}$  et  $\theta_{3m}$  définies par l'égalité des relations (10a) et (10b) et où le module du coefficient  $\rho$  s'exprime simplement

$$|\rho| = K |J_{-m}(-hv_z)| . \quad (12)$$

#### Position des lobes (Fig.2)

Les directions de rayonnement sont des arêtes d'un cône de sommet  $O$ . Elles peuvent être représentées commodément au moyen de vecteurs unités issus de  $O$  dont les projections des extrémités sont sur une droite  $\Delta$  d'équation

$$x \sin \psi - y \cos \psi = \sin \theta_1 \sin \psi \quad (13)$$

et séparées par des longueurs égales à  $\lambda/\Lambda$  à partir du point  $A$  correspondant à la réflexion spéculaire. Lorsque les crêtes de la houle sont normales au plan d'incidence ( $\psi = 0$ ), tous les lobes sont contenus dans ce plan. On retrouve alors les résultats donnés par Brekhovskikh<sup>7</sup>. Pour les autres directions de la houle, seul le lobe correspondant au mode  $m = 0$  dont la direction est celle de la réflexion spéculaire, demeure dans le plan d'incidence.

#### Application aux cas usuels en rétrodiffusion

Pour un angle  $\psi$  défini:  $|\rho|$ , donné par (12), ne dépend que des trois paramètres:

$$m; \quad H = kh; \quad L = \lambda/\Lambda.$$

En rétrodiffusion,  $\lambda$  est compris entre 10 et 30 m.

La Figure 3 montre l'influence de  $\psi$  pour  $\theta_1 = 45^\circ$ .

Figure 4 montre l'influence du creux de la houle pour  $\theta_1 = 60^\circ$  et  $\psi = 60^\circ$ . Pour les commodités de la représentation on a porté les enveloppes des amplitudes des lobes et tracé la droite  $\Delta$ , le cercle extérieur figurant le cercle de rayon 1. Par exemple, à 20 MHz, les valeurs  $H = 0,1; 0,2; 0,5; 1; 2$ , correspondent à des creux de la houle égaux respectivement à  $2h = 0,5$  m, 1 m, 2,4 m, 4,8 m, 9,6 m.

#### Interprétation

La structure périodique de la houle introduit une compression spatiale dans la transmission de l'énergie et son orientation introduit les propagations en dehors du plan d'incidence.

Pour des mers agitées, les lobes latéraux contigus à la direction de réflexion spéculaire peuvent devenir prédominants.

Engin, les lobes pour lesquels  $\theta_2 < \theta_1$ , correspondent, en général, à une perte d'énergie puisqu'ils sont susceptibles de traverser les couches.

### 3.2.2 Diffraction dans le Plan d'Incidence

Il est important pour les études de rétrodiffusion de connaître le rayonnement dans le plan d'incidence. L'expression de  $\rho$  est obtenue dans ce cas en portant, dans (11),

$$\theta_3 = 0 \quad \text{ou} \quad \pi.$$

On obtient la figure de diffraction d'une pupille marquée par la structure périodique de la houle. Il est significatif de déterminer la valeur moyenne de  $|\rho|^2$  qui est proportionnelle à la puissance:

$$\overline{|\rho|^2} = \frac{K^2}{8\pi^2 M^2 p^2} \left| J_{-p}(-hv_z) + \frac{\sin \rho\pi}{\pi} \int_0^\infty \exp(pt + hv_z \operatorname{sh} t) dt \right|^2 \quad (14)$$

La Figure 5 représente les résultats obtenus pour un angle d'incidence  $\theta_1 = 60^\circ$  et  $\psi = 60^\circ$ , dans le cas d'une durée d'impulsion  $T = 700\mu s$  et pour une largeur azimutale du lobe d'antenne  $\omega_A = 8^\circ$ . Cet exemple correspond à une propagation ionosphérique typique caractérisée par la portée  $D = 1200$  km et une hauteur virtuelle de réflexion de 300 km. On remarque dans ces conditions  $|\rho|^2$  dans la direction d'incidence est de l'ordre de -120 dB.

### 3.2.3 Influence de l'Agitation

Le problème de la diffusion des ondes électromagnétiques par une surface aléatoire définie par  $\sigma$  et  $T$  a été traitée par P. Beckmann<sup>3</sup>.

Pour une surface parfaitement conductrice, la valeur moyenne de  $|\rho|^2$  est

$$\overline{|\rho|^2} = \exp(-g) \left[ \rho_0^2 + \frac{\pi T^2 K^2}{S} \sum_{m=1}^{\infty} \frac{g^m}{m! m} \exp\left(\frac{-v_{xy}^2 T^2}{4m}\right) \right] \quad (15)$$

avec

$$g = (\sigma v_z)^2 = \frac{2\pi\sigma}{\lambda} (\cos \theta_1 + \cos \theta_2)^2 \quad (16)$$

$$\rho_0 = \frac{\sin Xv_x}{Xv_x} \frac{\sin Yv_y}{Yv_y} \quad (17)$$

$$v_{xy}^2 = (v_x^2 + v_y^2). \quad (18)$$

Sur la Figure 5, on a porté les valeurs de  $10 \log \overline{|\rho|^2}$  données pour les deux cas suivants:  $\sigma/\lambda = 0,333$  et  $\sigma/\lambda = 0,010$  avec  $T/\lambda = 0,5$ , ce qui correspond à 20 MHz à  $\sigma = 0,5$  m et 0,07 m avec  $T = 7,5$  m.

Dans les directions voisines de l'incidence la diffusion donne un coefficient  $\overline{|\rho|^2}$  voisin de -100 dB dans les deux cas, alors que le phénomène de diffraction n'est que -120 dB.

L'agitation superposée paraît donc être à l'origine du phénomène de formation des échos observés par rétrodiffusion. Il est intéressant de remarquer qu'en voisinage de la direction d'incidence, la diagramme de rayonnement est quasi isotrope.

### 3.3 Cas des Sols

Les surfaces  $\tau_1(xy)$  et  $\tau_2(xy)$  sont représentées par des modèles aléatoires dont les valeurs types de  $\sigma$  et  $T$  ont pu être définies.

La valeur de  $\overline{|\rho|^2}$  est donnée par (15) et la Figure 6 montre les diagrammes de diffusion obtenus à partir des modèles donnés en exemple, les conditions de propagation étant celles définies pour la Figure 5.

Il apparaît que l'énergie transmise dans la direction d'incidence est comparable à celle obtenue dans le cas de la mer. Par contre, l'énergie transmise dans la direction de réflexion spéculaire est plus faible et la perte d'énergie due à la traversée des couches après réflexion est d'autant plus grande que le sol est plus rugueux. Ces résultats établis pour un sol parfaitement conducteur doivent être corrigés pour tenir compte de la conductivité réelle. Cette correction se traduit par un affaiblissement supplémentaire qui peut être accru par une inclinaison moyenne du sol pouvant également donner des propagations hors du grand cercle.

La Figure 7 représente deux exemples de propagations typiques obtenus de nuit dans des conditions ionosphériques similaires à la station de Valensole (France). Dans la direction Ouest, les réflexions successives se font sur la mer et dans la direction Est sur la terre.

Dans le premier cas les échos observés, nombreux et réguliers, montrent une faible perte de transmission. Dans le second cas, où les réflexions se font sur un sol montagneux, la décroissance des échos successifs est très rapide.

## 4. CALCUL DU CHAMP REÇU

La puissance reçue par rétrodiffusion peut être évaluée à partir de l'équation du radar.

On appellera

$P$ : la puissance crête de l'émetteur

$G_e$ : le gain d'antenne dans la direction d'émission

$G_r$ : le gain d'antenne dans la direction de réception

$S'_r$ : la surface équivalente de l'antenne de réception,  $G_r = 4\pi S'_r / \lambda^2$

$\omega_A$ : la largeur azimutale du lobe d'antenne d'émission

$\tau$ : la durée de l'impulsion d'émission.

En rétrodiffusion, les rayons qui contribuent au champ reçu  $E_r$  sont ceux dont la différence de temps de propagation n'excède pas  $\tau$ . Le rayon correspondant au temps de propagation le plus court a une portée  $D_1$  et celui dont le temps de propagation est le plus grand a une portée  $D_2$ . L'aire  $S$  a donc pour dimensions

$$X = \frac{D_2 - D_1}{2} = \frac{\Delta D}{2} \quad (19)$$

$$Y = \frac{\omega_A R}{2} \sin\left(\frac{D_{moy}}{R}\right) \quad (20)$$

avec

$$D_{moy} = \frac{D_1 + D_2}{2}$$

Cette surface est vue de l'émetteur sous un angle solide  $d\Omega_1$  délimité par les rayons extrêmes et dans lequel la puissance émise  $dP_1$  est

$$dP_1 = \frac{PG_e}{4\pi} d\Omega_1 . \quad (21)$$

A partir de la relation (6) en remplaçant  $E_{20}$  par sa valeur, il vient

$$|E_2|^2 = |\rho|^2(\theta_1, \theta_2) \frac{s^2 \cos^2 \theta_2}{\lambda^2 r^2} E_1^2 . \quad (22)$$

La puissance  $dP_2$  transmise dans un angle solide  $d\Omega_2$  est liée à la puissance incidente  $dP_1$  par la relation

$$dP_2 = |\rho|^2(\theta_1, \theta_2) \frac{s \cos^2 \theta_2}{\lambda^2} \frac{dP_1}{\cos \theta_1} d\Omega_2 . \quad (23)$$

On peut définir une surface radar équivalente

$$\sigma(\theta_1, \theta_2) = 4\pi |\rho|^2(\theta_1, \theta_2) \frac{s \cos^2 \theta_2}{\lambda^2 \cos \theta_1} . \quad (24)$$

La puissance  $dP_2$  est répartie, après réfraction ionosphérique, sur une surface  $S_2$  du sol, que les rayons atteignent avec un angle d'incidence  $\theta_4$ .

La puissance  $dP_r$  interceptée par les antennes de réception vaut alors

$$dP_r = dP_2 \frac{S'_r}{S_2 \cos \theta_4} = dP_2 \frac{G_r \lambda^2}{4\pi S_2 \cos \theta_4} . \quad (25)$$

En groupant (21) à (25), et en exprimant les angles solides  $d\Omega_1$  et  $d\Omega_2$ , il vient

$$dP_r = \frac{P}{(4\pi)^2 R \sin\left(\frac{D_{moy}}{R}\right)} \frac{G_e \omega_A \sin \theta_1 \Delta D}{dD/d\theta_1} \frac{|\rho|^2 \cos^2 \theta_2}{\cos \theta_1} \frac{G_r \sin \theta_2}{\cos \theta_4 (dD/d\theta_2)} . \quad (26)$$

Cette relation qui a été établie en négligeant les absorptions et pertes dues aux réflexions sur le sol dans le cas de propagations multibonds, peut être corrigée par l'utilisation de relations classiques<sup>9,10</sup>. Le calcul du champ reçu s'effectue simplement à partir des courbes  $D_{(t)}$  et  $D_{(1)}$  ( $i = \pi/2 - \theta_1$ ).

Pour un temps de propagation  $t$ , et une durée d'impulsion  $\tau$  donnés on peut trouver par une construction évidente,  $D_{moy}$ ,  $\Delta D$ ,  $\theta_1$ ,  $\theta_2$ ,  $\theta_4$ ,  $dD/d\theta_1$  et  $dD/d\theta_2$ . La surface  $S$ , le coefficient  $|\rho|^2$  et enfin  $dP_r$  s'en déduisent.

La Figure 8 montre un exemple traité à partir d'un sondage par rétrodiffusion à plusieurs fréquences. Une méthode graphique<sup>6,9</sup> a permis d'en déduire les courbes  $D_{(t)}$  et  $D_{(1)}$ . Le calcul a été appliqué au rayon bas en supposant l'ionosphère horizontalement stratifiée ( $\theta_1 = \theta_2 = \theta_4$ ) et en prenant pour  $|\rho|^2$  la valeur standard -100 dB. Cette détermination graphique donne un champ maximum de  $70 \mu V$  très voisin de celui relevé expérimentalement. Le bon accord entre les valeurs paraît justifier les hypothèses de départ. En fait, le calcul complet du champ est compliqué comme nous allons le voir, par le mécanisme de formation des échos dû à la quasi isotropie du diagramme de rayonnement au voisinage de la direction d'incidence.

## 5. FREQUENCE DOPPLER ET FADING

### 5.1 Rôle du Sol

Pour la clarté de l'exposé, on négligera tout d'abord l'influence du champ magnétique.

Si l'ensemble émetteur-récepteur de la station de sondage par rétrodiffusion est situé en A, un point B au sol peut être atteint, dans le cas général, par un rayon bas et par un rayon haut, pour lesquels les temps de parcours sont respectivement  $t_B$  et  $t_H$ . La trajectoire de retour B-A peut se faire également par ces deux chemins. La quasi-isotropie du diagramme de diffusion au voisinage de la direction d'incidence permet donc d'imaginer les quatre trajectoires possibles pour les rayons issus de A et y revenant après avoir atteint B:

Trajet A-B	Trajet B-A	Temps Propagation
1 Rayon bas	Rayon bas	$2t_B$
2 Rayon bas	Rayon haut	$t_B + t_H$
3 Rayon haut	Rayon bas	$t_H + t_B$
4 Rayon haut	Rayon haut	$2t_H$

On appellera

- Type bas      Trajet 1
- Type haut      Trajet 4
- Type mixte      Trajet 2 et 3.

Le type mixte (2+3) correspond à deux modes de transfert de l'énergie. En fait, les échos de rétrodiffusion sont formés par l'ensemble des rayons ayant le même temps de transit. Dans le cas général, les trois types interviennent, les rayons correspondants atteignent des distances différentes (Fig. 9).

Le champ magnétique et la dépolarisation introduite par le sol compliquent encore le phénomène d'interférence et l'on peut dénombrer 16 types de trajectoires possibles (Fig. 10), dont les contributions dans la formation de l'écho sont heureusement très différentes. Tout d'abord, si le sol est assez conducteur on peut admettre que l'effet de dépolarisation est faible, ce qui supprime les croisements de modes et une étude des amplitudes relatives permet, comme il va être vu, de ne retenir finalement que deux modes principaux.

### 5.2 Importance Relative des Rayons Interférents

La puissance interceptée par les antennes de réception dans le cas général est donnée par (26). Si on s'intéresse au cas d'une ionosphère stratifiée horizontalement,  $\theta_2 = \theta_4$  et, en admettant pour simplifier que  $G_e = G_r = G$ ,

$$dP_r = \frac{PG^2\omega_A}{2\pi^2R} \frac{S|\rho|^2 \operatorname{tg}\theta_1 \sin 2\theta_2}{\sin(D_{moy}/R)} \frac{d\theta_1 d\theta_2}{dD}. \quad (27)$$

La puissance transportée par chaque type de propagation peut être déterminée par la méthode exposée au paragraphe précédent. La Figure 11 schématisse la construction opérée pour chacun des trois et l'application à un cas classique. En prenant pour  $|\rho|^2$  la valeur standard -100 dB, on obtient, pour un temps de propagation de 15 ms,

- pour le type bas       $P_{r1} = 313 \times 10^{-12} W$
- pour le type mixte       $P_{r2} = 124 \times 10^{-12} W$
- pour le type haut       $P_{r3} = 12 \times 10^{-12} W$ .

Le type haut peut, comme il l'est souvent admis, être négligé, mais il apparaît clairement sur cet exemple qu'il convient de retenir les types bas et mixte.

### 5.3 Détermination des Fréquences Doppler et Fading

Le "chemin de phase"  $P$  et le "chemin de groupe"  $P'$  sont liés par la relation classique

$$P' = \frac{d}{d\omega} (\omega P) \quad (28)$$

dans le cas où les chocs sont négligés et en l'absence de champ magnétique.

On peut montrer que cette relation est utilisable avec une très bonne approximation<sup>9</sup>, dans les cas usuels de propagation en rétrodiffusion, en l'appliquant le long des trajectoires  $\Gamma_0$  et  $\Gamma_x$  des modes ordinaires et extraordinaires.

En posant  $t_p = P/c$  et  $t = P'/c$ , que nous appellerons respectivement temps de phase et temps de groupe, la relation (28) devient

$$d(ft_p) = t df. \quad (29)$$

Enfin, l'angle  $V$  entre le rayon et la normale au plan d'égale phase étant toujours très petit, on peut écrire au second ordre près<sup>9</sup>, en appelant  $\mu$  l'incidice de phase:

Pour le mode ordinaire:

$$P_0 = \int_{\Gamma_0} \mu_0 ds. \quad (30)$$

Pour le mode extraordinaire:

$$P_x = \int_{\Gamma_x} \mu_x ds. \quad (31)$$

Pour un type de propagation donné, le champ reçu par des aériens à polarisation rectiligne vaut

$$E_r = e_0 \exp(j\psi_0) + e_x \exp(j\psi_x) \quad (32)$$

avec

$$\psi_0 = \omega \left( t - \frac{P_0}{c} \right) \text{ se rapportant au mode ordinaire}$$

$$\psi_x = \omega \left( t - \frac{P_x}{c} \right) \text{ se rapportant au mode extraordinaire.}$$

La relation (32), qui peut aussi s'écrire

$$E_r = E_0 \exp(j\psi_0) \quad (33)$$

avec

$$E_0 = e_0 + e_x \exp(j\Omega) \quad (34)$$

et

$$\Omega = \frac{\omega}{c} (P_0 - P_x), \quad (35)$$

montre qu'il existe deux composantes spectrales

$$\omega_0 = \frac{d\psi_0}{dt} = \omega - \frac{\omega}{c} \frac{dP_0}{dt} \quad (36)$$

$$\omega_x = \frac{d\psi_x}{dt} = \omega - \frac{\omega}{c} \frac{dP_x}{dt}; \quad (37)$$

l'écart

$$\Delta\omega = \omega_0 - \omega_x = \frac{d\Omega}{dt} \quad (38)$$

traduisant l'effet Faraday demeure dans la gamme des fréquences utilisées inférieur à 0,06 ( $\omega_0 - \omega$ ) .

Si on considère les deux types principaux de propagation, auxquels on affectera les indices 1 et 2, le champ total est

$$E_r = e_{01} \exp(j\psi_{01}) + e_{x1} \exp(j\psi_{x1}) + e_{02} \exp(j\psi_{02}) + e_{x2} \exp(j\psi_{x2}) . \quad (39)$$

Le spectre du signal reçu est donc constitué par quatre raies spectrales formant deux doublets (Fig. 12) qui permettent d'interpréter simplement les spectres Doppler et fading.

### 5.3.1 Spectre Doppler

L'effet Doppler fait apparaître quatre raies spectrales principales

$$\omega_{d1} = \omega_{01} - \omega; \quad \omega'_{d1} = \omega_{x1} - \omega; \quad \omega_{d2} = \omega_{02} - \omega; \quad \omega'_{d2} = \omega_{x2} - \omega,$$

formant deux doublets. Il est commode de les définir par les deux pulsations  $\omega_{d1}$  et  $\omega_{d2}$  (Fig. 12), qui s'expriment facilement, à partir de (36),

$$\omega_{d1} = \frac{\omega}{c} \left| \frac{dP_{01}}{dt} \right| \quad (40)$$

$$\omega_{d2} = \frac{\omega}{c} \left| \frac{dP_{02}}{dt} \right| \quad (41)$$

et auxquelles, compte tenu de (29) à (31), on peut faire correspondre les fréquences  $f_{d1}$  et  $f_{d2}$ .

$$f_{d1} = \frac{d}{dt} \left( \int_0^t t df \right) \quad \text{à } D_1 \text{ constant} \quad (42)$$

$$f_{d2} = \frac{d}{dt} \left( \int_0^t t df \right) \quad \text{à } D_2 \text{ constant}, \quad (43)$$

$D_1$  et  $D_2$  étant respectivement les portées des trajets bas et mixtes correspondant au même temps de propagation  $t$ .

$f_{d1}$  et  $f_{d2}$  peuvent être calculées graphiquement à partir des courbes  $t(f)$  à  $D_1$  et  $D_2 = \text{constante}$  (Fig. 15), puisqu'on verra sans peine que

$$f_{d1} = 2 \frac{d}{dt} (S_1) \quad (44)$$

$$f_{d2} = \frac{d}{dt} (2S_2 - S'_2) . \quad (45)$$

### 5.3.2 Spectre Fading

Le champ  $E_r$  peut, compte tenu de (33) à (35), s'écrire

$$E_r = \Sigma_1 \exp \left( j \frac{P_{01}}{c} \right) + \Sigma_2 \exp \left( j \frac{P_{02}}{c} \right) \quad (46)$$

et la tension détectée est

$$E_d = \left| E_1 + E_2 \exp \left[ j \frac{\omega}{c} (P_{01} - P_{02}) \right] \right|. \quad (47)$$

Si l'effet Faraday n'était pas sensible, la pulsation fading serait

$$\omega_f = \frac{\omega}{c} \frac{d}{dt} (P_{01} - P_{02}), \quad (48)$$

à laquelle, par un raisonnement identique à celui du paragraphe précédent, on peut faire correspondre la fréquence de fading

$$f_f = \frac{d}{dt} [2(S_1 - S_2) + S'_2]. \quad (49)$$

L'effet Faraday se traduit en fait par une pluralité des raies spectrales due à la présence des doublets.

### 5.3.3 Conclusion

L'effet Faraday qui est à l'origine du dédoublement des raies spectrales, est difficile à mettre en évidence expérimentalement à cause de la trop faible résolution des analyseurs de spectres usuels et de l'élargissement des raies causé par la durée de l'impulsion d'émission.

Un exemple particulièrement caractéristique est représenté sur la Figure 13. Sur la piste "Doppler" on observe les fréquences doppler qui sont de l'ordre de 0,3 Hz et un battement - qu'on peut attribuer à l'effet Faraday - dont la fréquence est de l'ordre de 0,008 Hz. Sur la "piste amplitude" la fréquence de fading, de l'ordre de grandeur de la fréquence Doppler, est décelable.

Un second exemple a été reproduit sur les figures suivantes à partir d'un enregistrement effectué le 8.11.1966 entre 20 h 11 et 21 h 00 TU à la station de Valensole. Durant cette période, le coucher du soleil entraîne une variation rapide des paramètres des couches, qui apparaissent sur la Figure 14 où les résultats donnent les fréquences Doppler et fading (ordonnée) en fonction du temps de propagation (abscisse).

La Figure 16, où l'on a reporté les résultats expérimentaux pour les confronter avec les résultats théoriques, montre un bon accord entre eux.

## REFERENCES

1. Twersky, V.

*Multiple Scattering of Radiation by an Arbitrary Plane Configuration of Parallel Cylinder and by Two Parallel Cylinders.* Journal of Atmospheric and Terrestrial Physics, Vol. 23, 1952, pp. 407-414.

2. Twersky, V.

*On Scattering of Waves by the Infinite Grazing of Circular Cylinders.* Institute of Radio Engineers, Transactions, Antennas and Propagation, Vol. 10, November 1962, pp. 737-765.

3. Beckmann, P.,  
Spizzichino, A.

*The Scattering of Electromagnetic Waves from Rough Surfaces.* Pergamon Press, Oxford, New York, 1963.

4. Bruhat, G.

*Cours de Physique Générale - Optique.* Masson.

5. Voge, J.

*Réflexion Partielle et Réflexion Diffuse sur des Feuilles Atmosphériques.* Annales de Télécommunication, Vol. 15, 1968, pp. 38-47.

6. Al'pert, Ya. L.

*Radio Wave Propagation and the Ionosphere.* Plenum Press, New York, 1968.

7. Brekhovskikh, L.M.

*Waves in Layered Media.* Academic Press, New York, 1960.

8. Delloue, J.,  
Goutelard, C.

*Sur l'Interprétation des Echos de Rétrodiffusion par la Méthode des Courbes de Transmission.* Compte Rendu, Académie des Sciences, Paris, Vol. 263, No. 3, Juillet 1966, p. 256.

9. Goutelard, C.

*Thèse d'Etat.* Faculté des Sciences de Paris, Mars 1968.

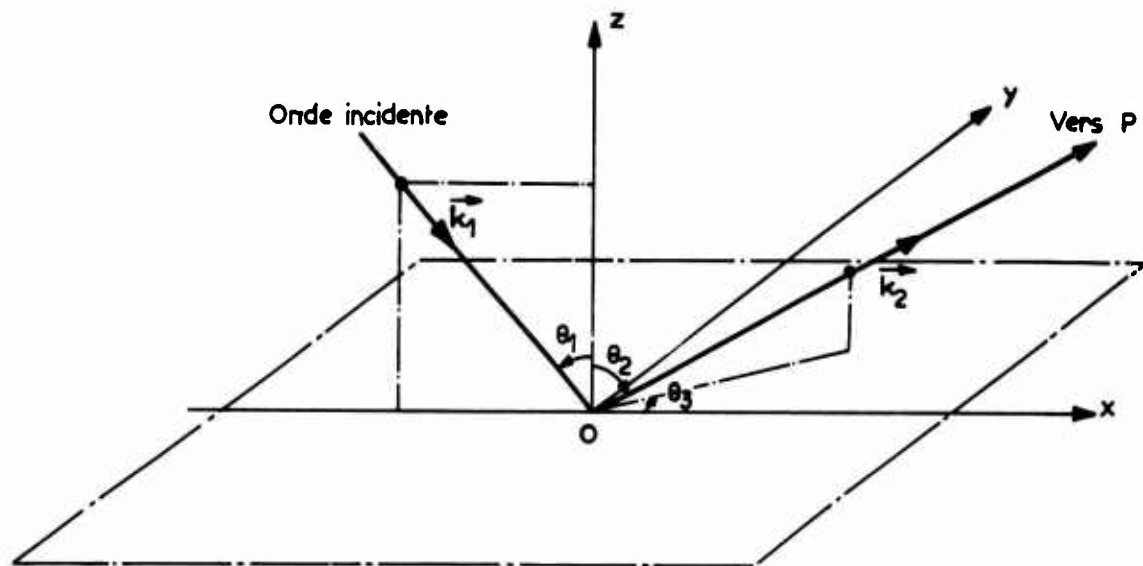


Figure 1

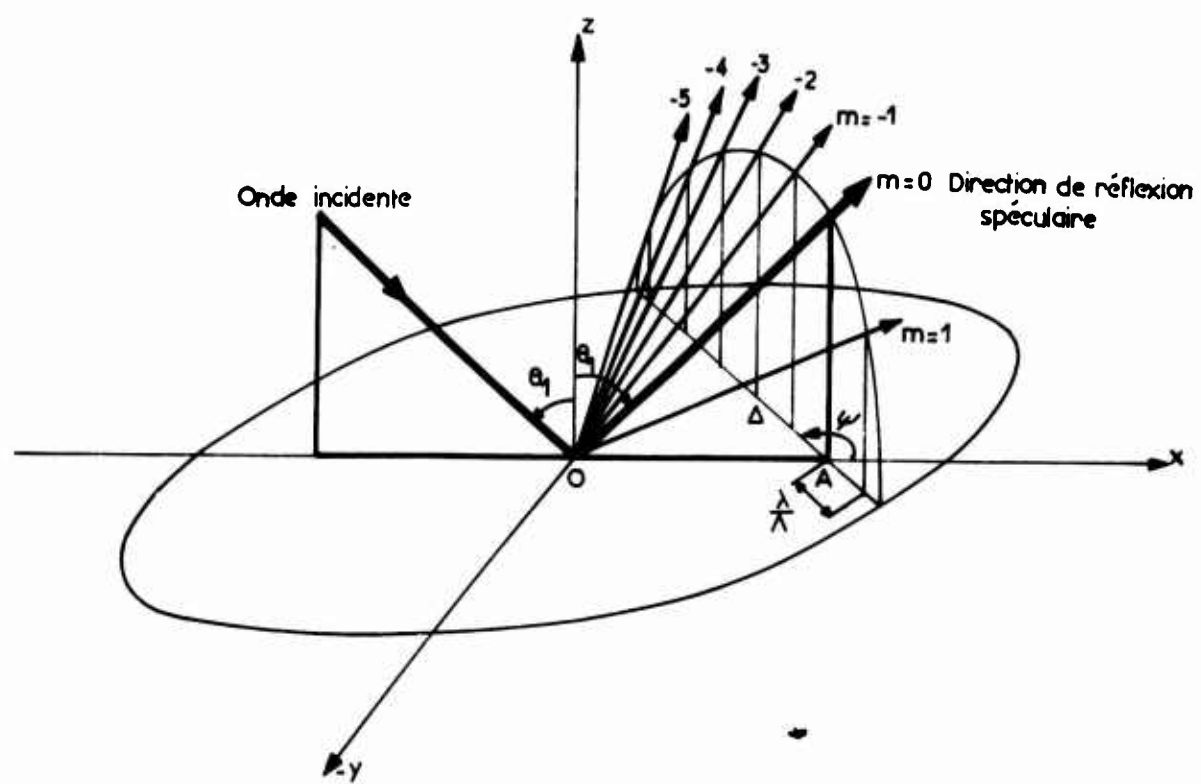


Figure 2

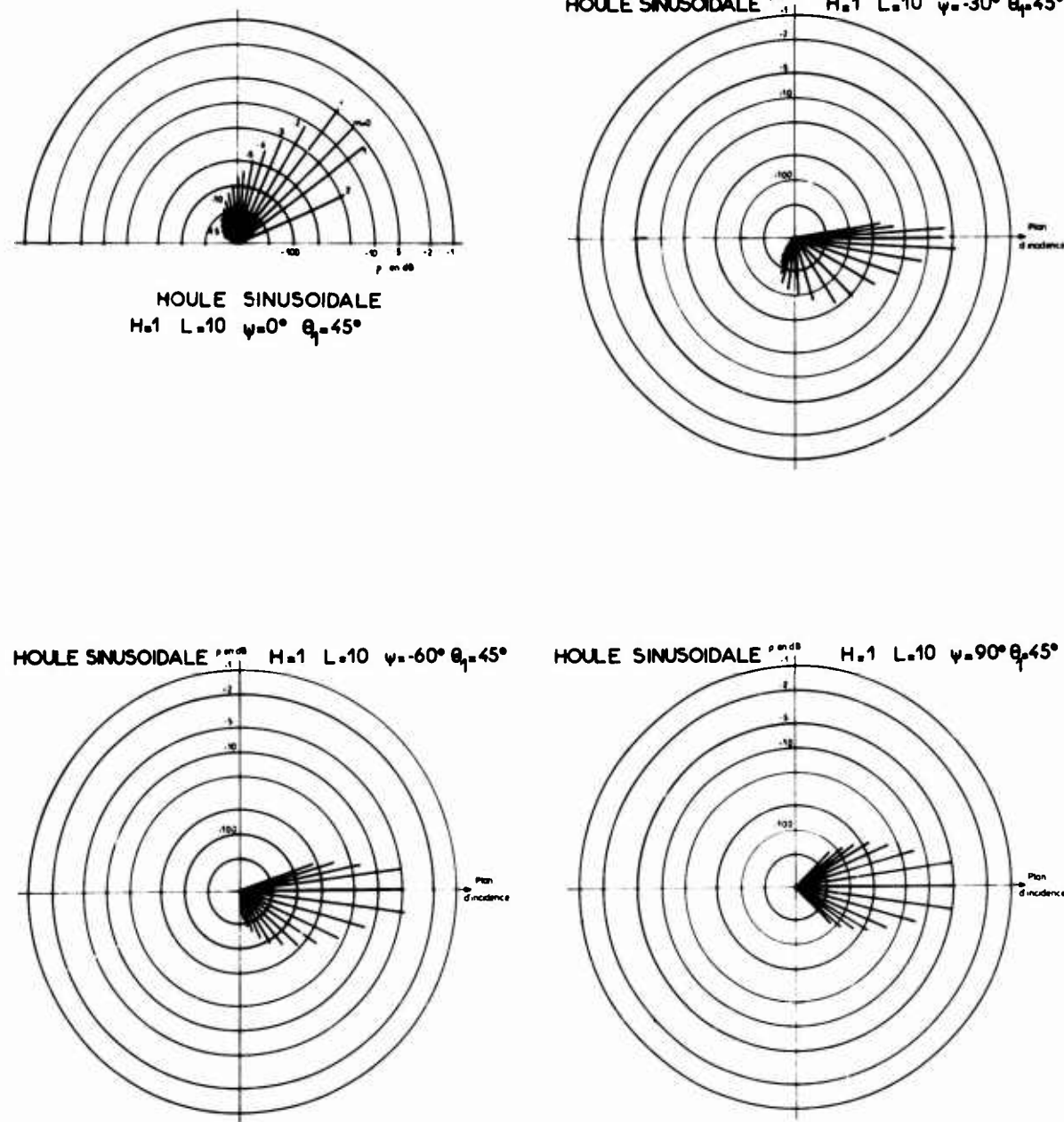


Figure 3

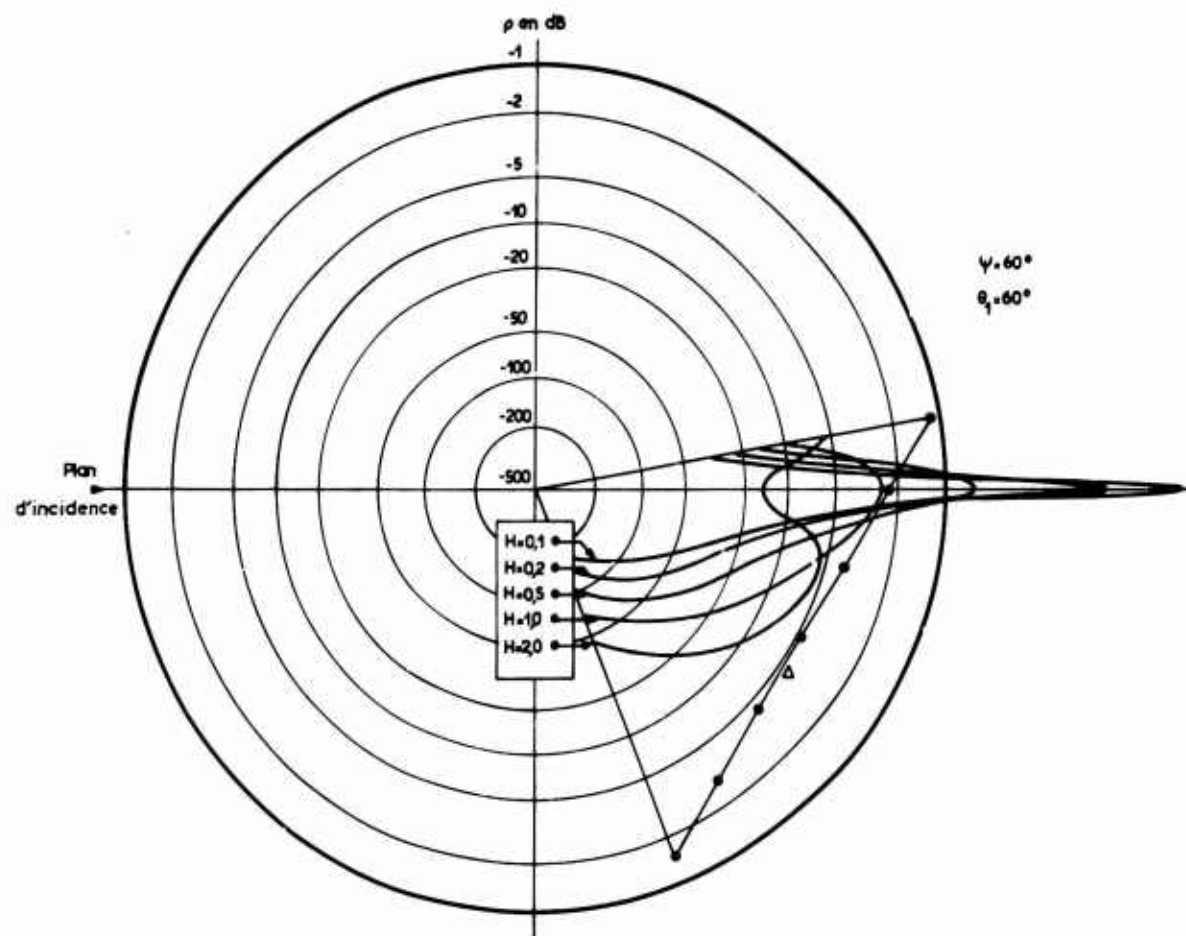


Figure 4

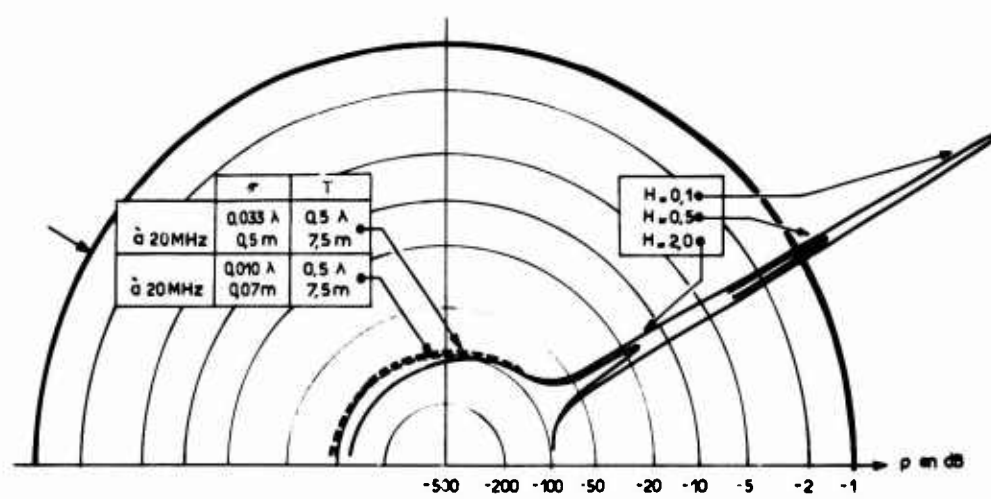


Figure 5

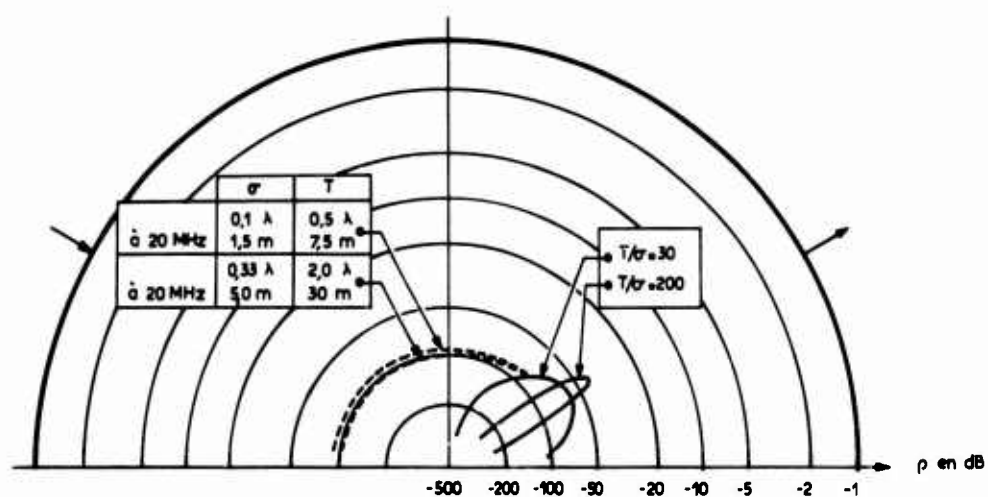


Figure 6

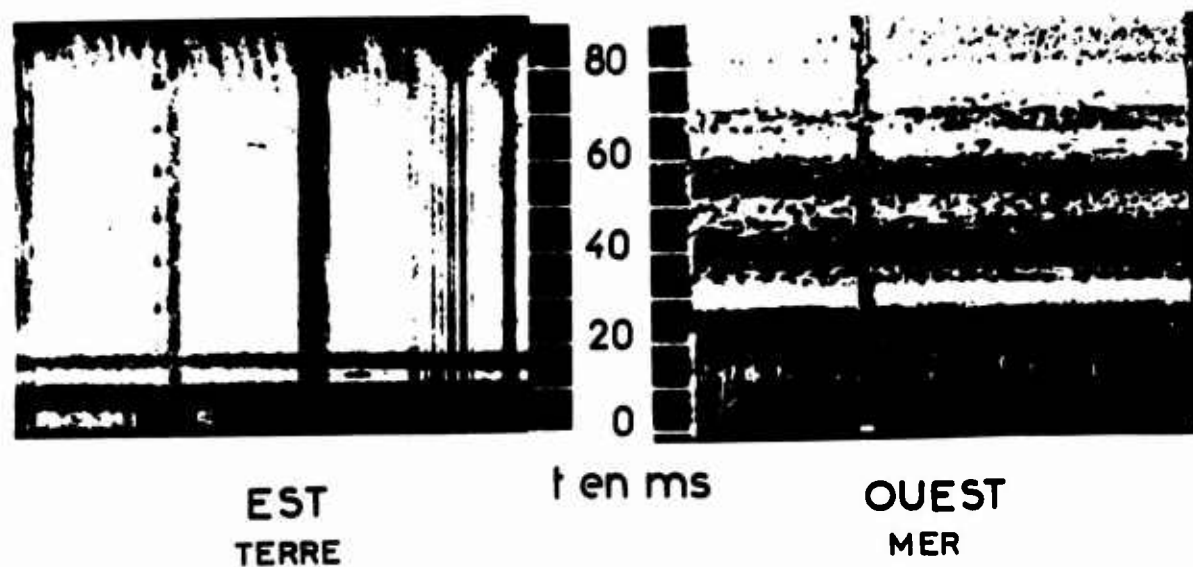


Figure 7

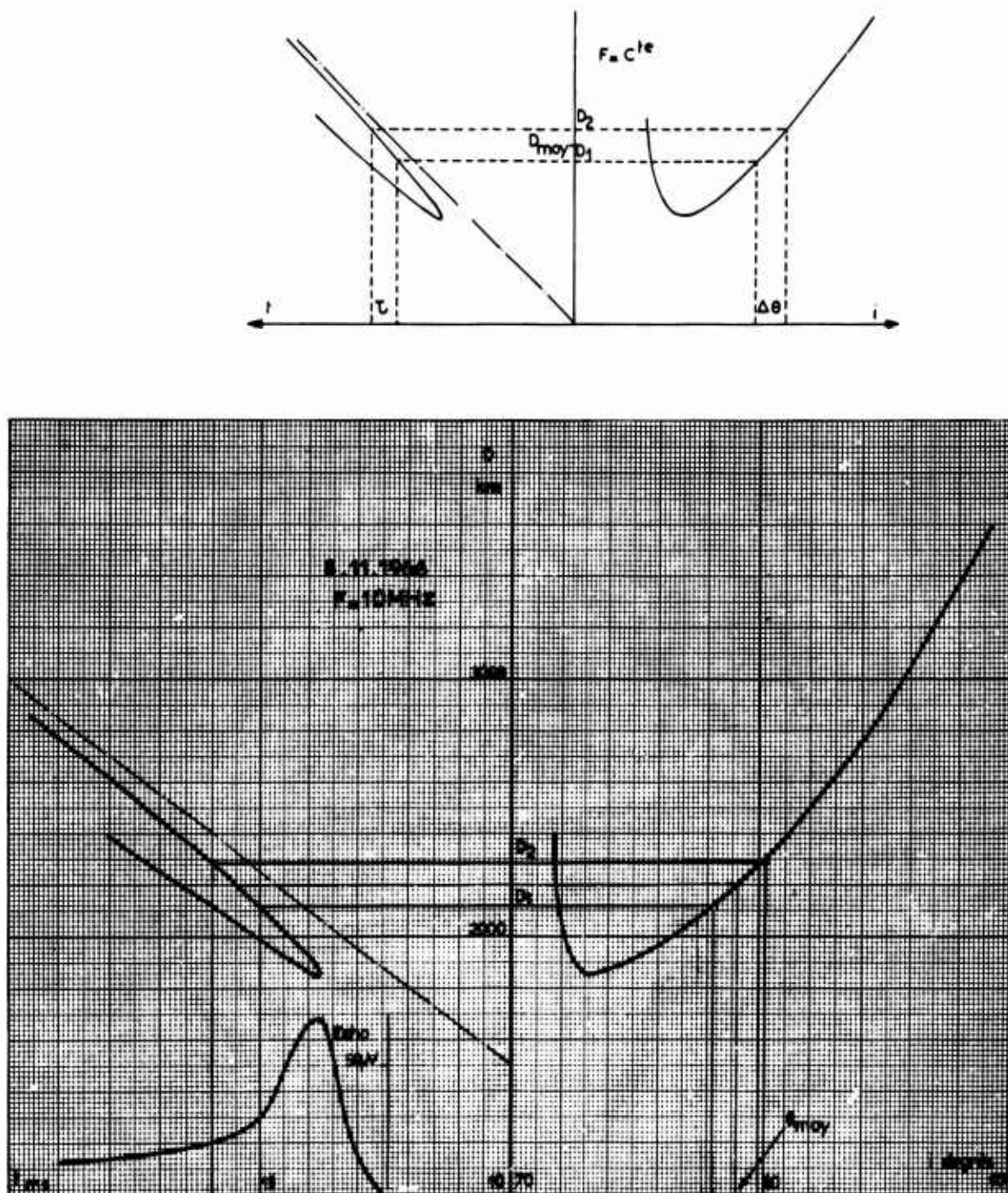


Figure 8

6-18

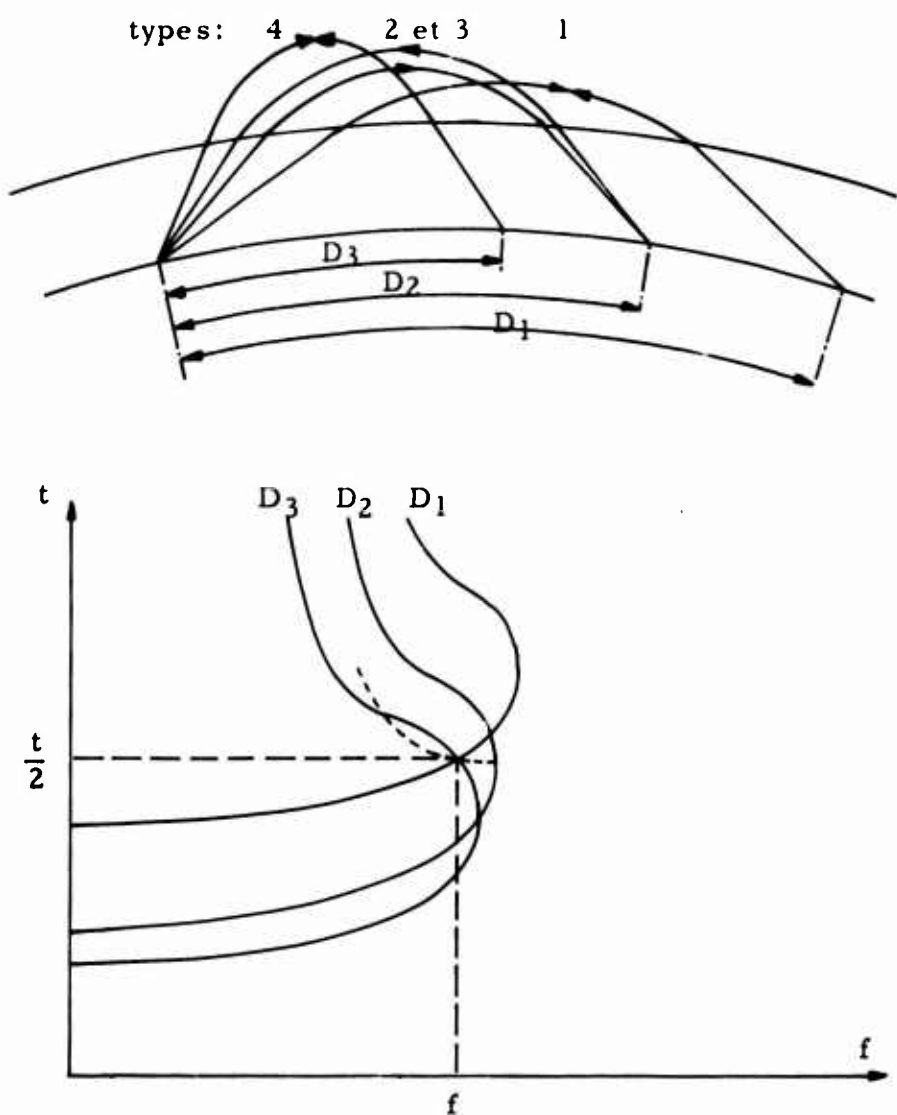


Figure 9

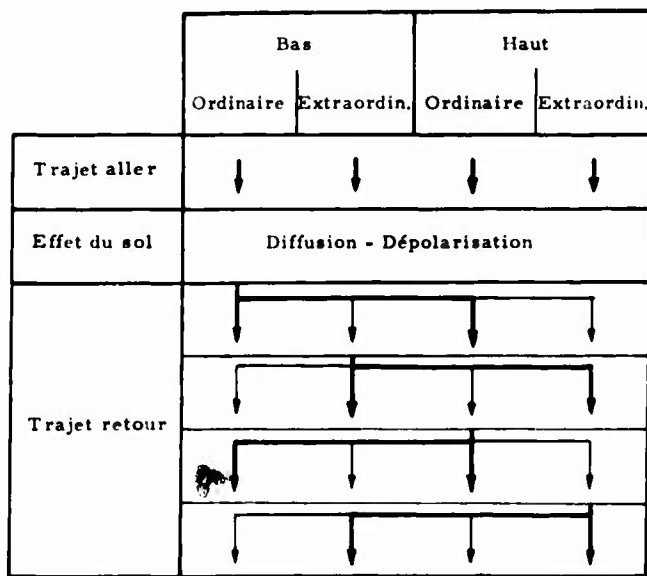


Figure 10

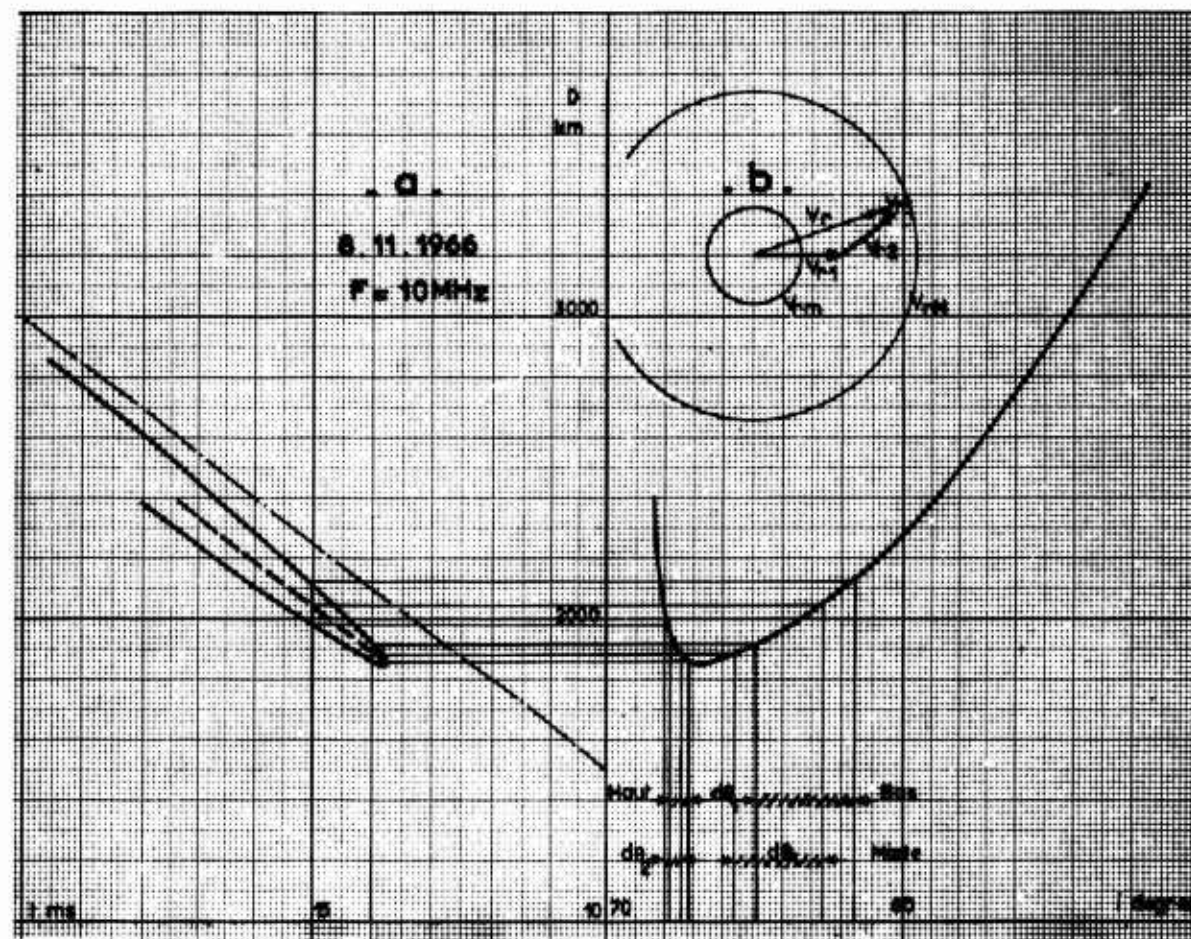
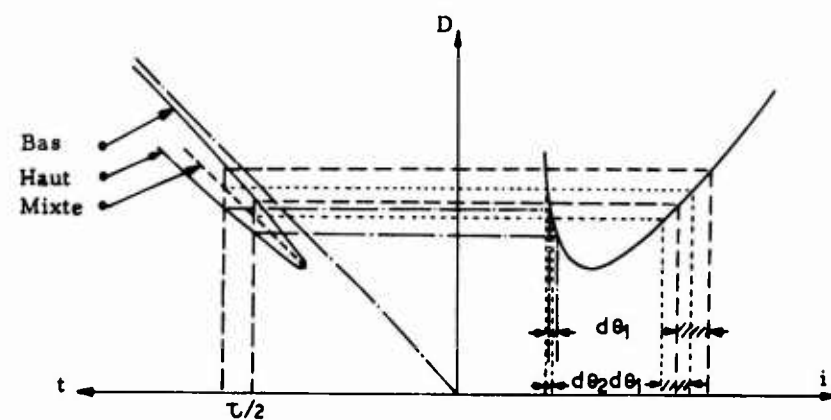


Figure 11

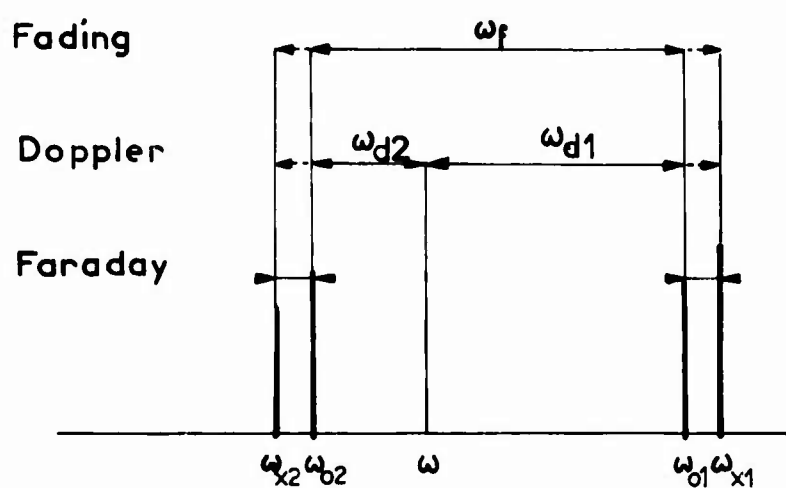


Figure 12

NOT REPRODUCIBLE

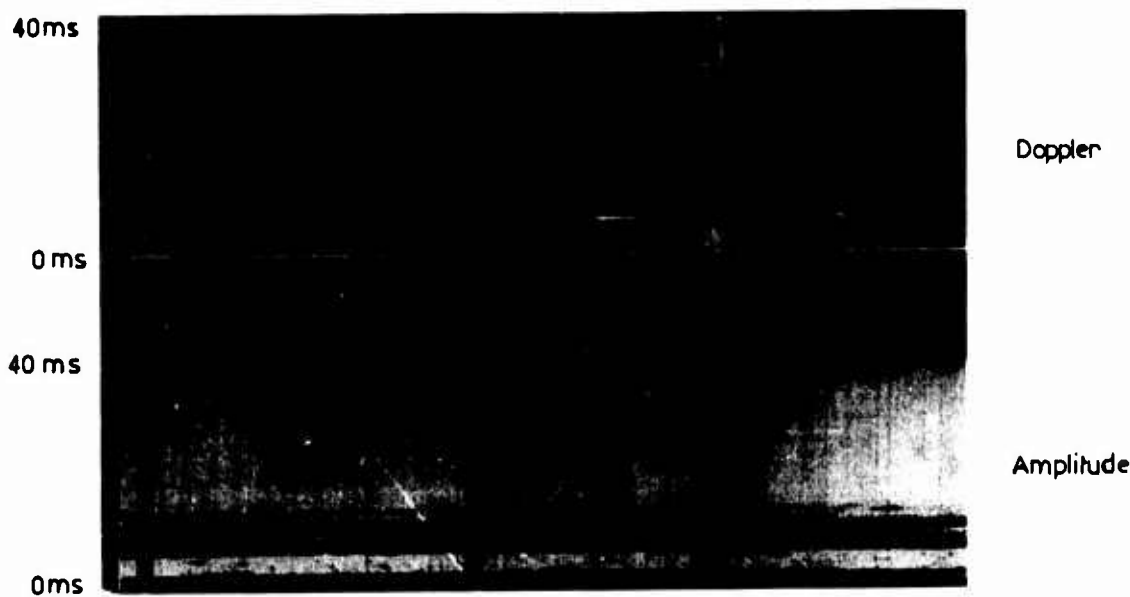
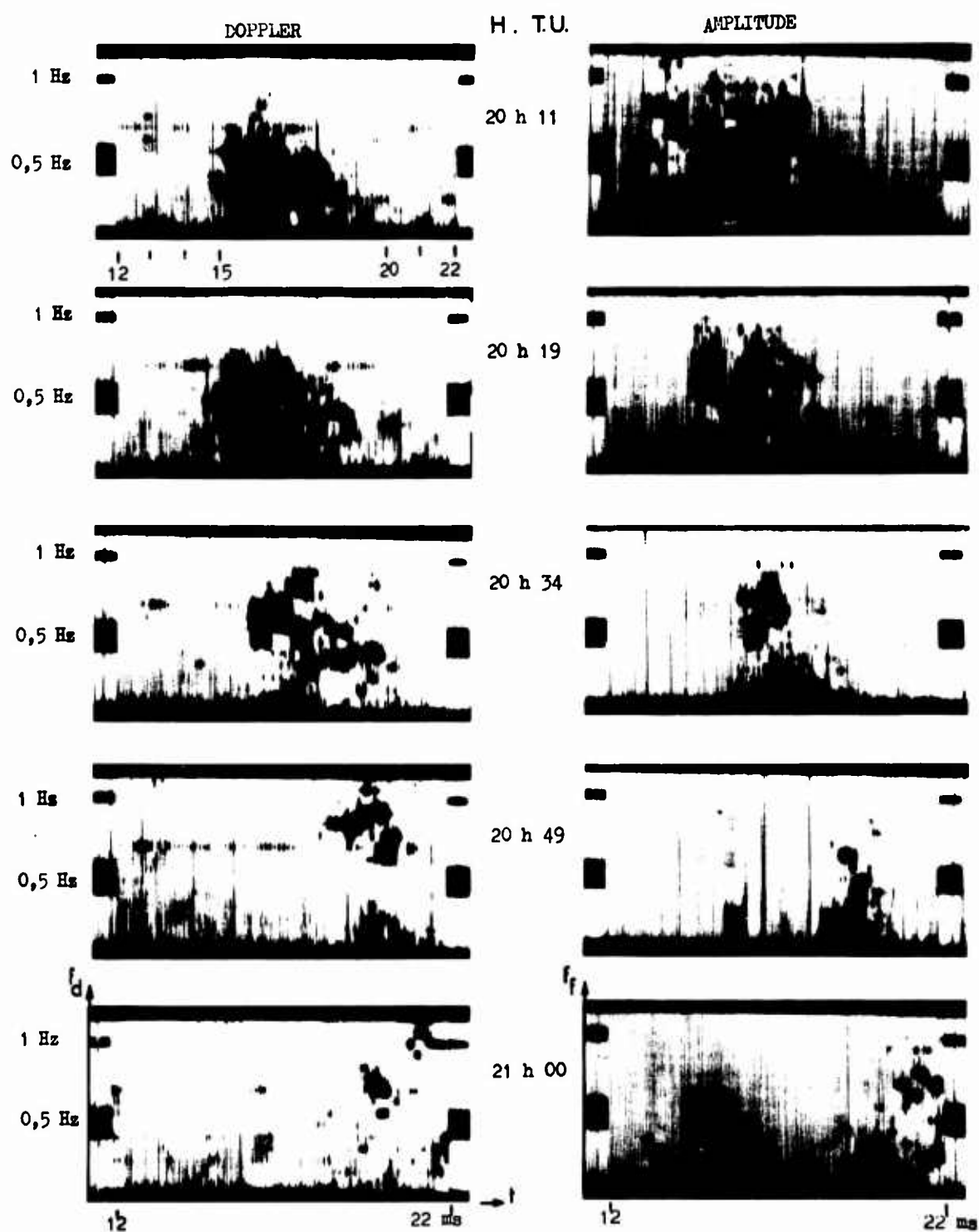
14. 3. 1966,  $f = 9 \text{ MHz}$ 

Figure 13



8. 11. 1966, f = 10 MHz

Figure 14

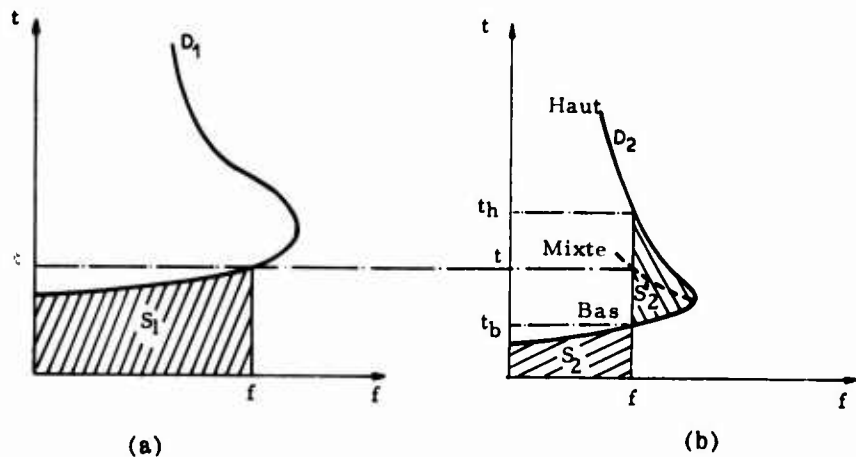
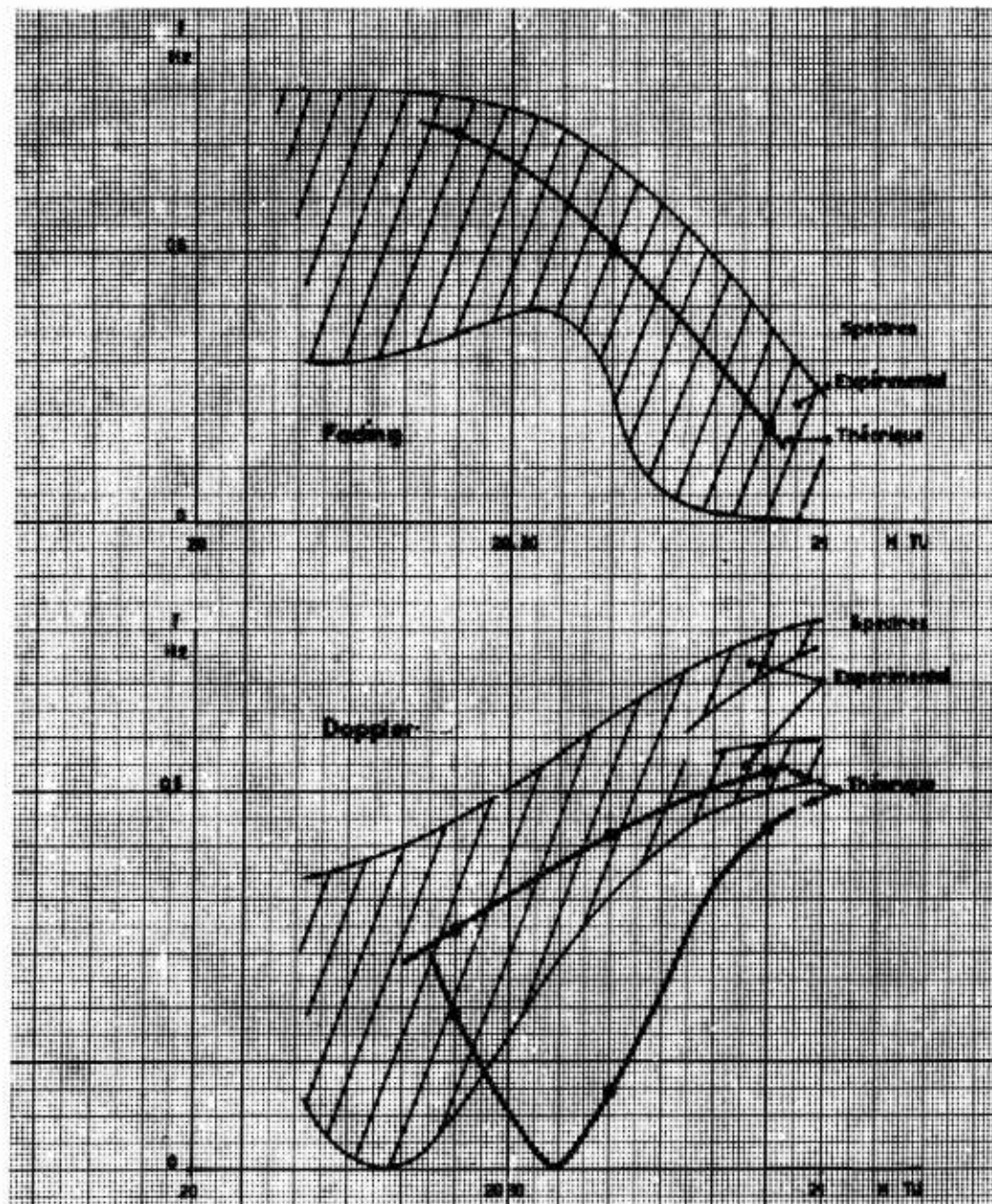


Figure 15



**HF GROUND BACKSCATTER ANALYSIS WITH THE  
AID OF COMPUTER RAY TRACING**

by

**R. G. Maliphant**

**Government Communications Headquarters  
Cheltenham, England**

#### SUMMARY

A computer program is described which fits any electron density distribution with the minimum number of line segments required to meet a specified tolerance while preserving continuity of slope throughout the height range of the profile. The equation for the line segments is such that analytic expressions may be obtained for the various propagation parameters required in a ray-tracing program. The high speed with which ray paths may be calculated by the use of this technique permits stepped-frequency backscatter records to be synthesised and plotted directly on the computer output form. A description is given of some of these plots and the general features are discussed. The possibility of reversing the process is then considered and the final section is devoted to a discussion of the problems involved in translating experimental backscatter records into synthetic oblique incidence ionograms for particular paths.

**HF GROUND BACKSCATTER ANALYSIS WITH THE  
AID OF COMPUTER RAY TRACING**

R. G. Maliphant

**1. INTRODUCTION**

In principle, backscatter sounding provides a convenient method of calibrating the ionosphere over regions where vertical incidence measurements are impracticable. However, the technique has been difficult to implement satisfactorily for a number of reasons. With the transmitter and receiver co-located, backscattered echoes may be received from many different areas of the earth's surface. The strength of these signals varies considerably, according to the degree of focusing or defocusing by the ionosphere, radio wave absorption, and the topography of the ground in the scattering region. The polar diagrams of the transmitting and receiving aerials largely determine the azimuthal coverage of the backscatter and also modify the variation of field intensity with angle of elevation. Traditionally, backscatter records have taken the same form as vertical and oblique incidence ionograms, that is a plot of propagation time versus frequency. However, whereas ionograms for fixed ground ranges display clearly delineated traces, the variable ranges from which backscatter echoes are received result in a continuum of energy with a much larger spread of propagation times recorded for any given frequency. The information taken from such recordings has usually been limited to the minimum propagation times, and these measurements have been used to estimate skip distance as a function of transmitted frequency. Thus a large part of the total information content of backscatter records remains unused.

By employing computer ray tracing, it is possible to simulate the backscatter process and produce synthetic backscatter records directly on the computer output form. Thus, the effects produced by different ionospheric distributions may readily be observed in the resultant backscatter plots. In the formats to be described, either angle of elevation or mode of propagation is printed at each backscatter data point. If required, the data may be limited to field intensities above some specified threshold. Study of these records suggests ways in which backscatter data may be used to measure the properties of the ionosphere along a particular bearing from the sounding station. This requirement is discussed in a later section, together with a brief description of an associated routine for simulating oblique incidence ionograms for particular paths from the results obtained by ray tracing through the derived model of the ionospheric distribution.

**2. THE RAY TRACING PROGRAM**

The path of a ray through the ionosphere is represented schematically in Figure 1. From this diagram, it may be seen that

$$d\theta = \frac{\tan i}{r} dr, \quad (1)$$

where  $i$  is the angle of incidence of the ray at the height  $r$  measured from the centre of the earth, and  $d\theta$  is the angle subtended at the centre of the earth by the limits of the ray path over the height increment  $dr$ .

By applying Snell's law and neglecting the effect of the earth's magnetic field (see Reference 1 for further details), one may derive from Equation (1) an expression for the distance ( $D = R\theta$ ) propagated over the curved earth's surface (where  $R$  is the radius of the earth).

Thus,

$$D = \frac{R}{2} \cos \Delta \int_{\text{Path}} \frac{d(\rho^2)}{\rho^2 \sqrt{(\rho^2 - \rho^2 f_N^2/f^2 - \cos^2 \Delta)}} \quad (2)$$

where  $\rho$  is the normalised radius  $r/R$ ,  $f_N$  is the plasma frequency (proportional to the square root of the electron density),  $f$  is the wave frequency and  $\Delta$  is the angle of elevation at the earth's surface.

The value of the integral in Equation (2) is normally calculated numerically by approximating the ionosphere with a large number of thin laminations within which the plasma frequency  $f_N$  is considered to be constant. However, in 1953, de Voogt<sup>2</sup> published a paper in which the ionospheric layers were each represented by two segments, within which the plasma frequency distribution was of a form yielding an analytic solution of the distance integral. Muldrew<sup>3</sup> later adopted a similar approach, using a simplified form for the segments (electron density practically a linear function of height) which enabled real ionospheric distributions to be synthesised. In the work described here, the advantages of both methods have been retained through the use of segments of the form

$$f_N^2 = a/\rho^2 + b + g\rho^2, \quad (3)$$

where  $a$ ,  $b$  and  $g$  are constants calculated to fit the segment to part of the required distribution while retaining continuity of both value and slope at the junctions with adjacent segments. The differential  $(df_N^2/d\rho)$  is assumed to be zero at the highest point on the profile ( $\rho_m$ ) so that, for the top ( $n^{th}$ ) segment,

$$g_n = a_n/\rho_m^4$$

and

$$b_n = f_c^2 - 2a_n/\rho_m^2,$$

where  $f_c$  is the plasma frequency at  $\rho_m$ .

The value of  $a_n$  is then calculated to minimise the quantity

$$S_i = \sum_j [f_{Nj}^2 - (a_i/\rho_j^2 + b_i + g_i\rho_j^2)]^2.$$

Thus

$$a_n = \left[ \sum_j f_{Nj}^2 \gamma_j - \sum_j f_c^2 \gamma_j \right] / \sum_j \gamma_j^2.$$

where

$$\gamma_j = 1/\rho_j^2 - 2/\rho_m^2 + \rho_j^2/\rho_m^4.$$

The summations are carried out with progressively larger numbers of input data points,  $f_{Nj}(\rho_j)$ , until the lowest point is reached for which the segment fits all the data points in its height range within some specified tolerance level.

The requirements of continuity set the constants for the lower segments as

$$g_i = g_{i+1} + (a_i - a_{i+1})/\rho_k^4$$

and

$$b_i = b_{i+1} - 2(a_i - a_{i+1})/\rho_k^2.$$

where  $\rho_k$  is the upper limit of the  $i^{th}$  segment.

The value of  $a_i$  is then calculated as before, by minimising  $S_i$ .

Thus

$$a_i = a_{i+1} + \left[ \sum_j f_{Nj}^2 \beta_j - \sum_j (a_{i+1}/\rho_j^2 + b_{i+1} + g_{i+1}\rho_j^2) \beta_j \right] / \sum_j \beta_j^2.$$

where

$$\beta_j = 1/\rho_j^2 - 2/\rho_k^2 + \rho_j^2/\rho_k^4.$$

The number of segments required to fit real-height profiles derived from actual vertical incidence ionograms varies typically between five and fifteen. The complete curve-fitting process is required only once for each profile; in all subsequent ray tracing, on any frequency, the profile is referred to in terms of the segment constants. In practice, it was found that certain precautions were required in order to guarantee a sensible fit to the original profile. Tests had to be included in the computer program to check whether the differential  $(df_N/d\rho)$  inappropriately passed through zero within the effective height range of the segment. If this occurred, intermediate points were interpolated and the segment constants re-calculated. The degree of smoothing achieved by the segmented curve was set at a reasonable level by extending the fitting process to include one or, where possible, two data points just below the height range of each segment.

Analytic solutions of the distance integral (Equation (2)) for segments of the form described by Equation (3) are given in the Appendix.

### 3. BACKSCATTER SIMULATION

Since only a small number of segments is required in order to fit the ionospheric distribution up to the height of maximum electron density, relatively few calculations are needed to evaluate the distance a ray is propagated. The consequent high speed of the computer ray-tracing program makes it very suitable for simulating backscatter sounding records, for which a large number of ray paths need to be traced.

In order to synthesise a backscatter record, it is necessary to calculate the time of propagation ( $t$ ) or the virtual path length ( $P' = ct/2$ , where  $c$  is the velocity of electromagnetic waves in free space). These quantities may be obtained by solving expressions similar to the distance equations. However, the similarity of the integrals suggests a simpler approach. Thus, Equation (2), re-written as

$$D = \frac{R}{2} \cos \Delta \int_{\text{Path}} I d(\rho^2).$$

may be compared with the virtual path length equation

$$P' = \frac{R}{2} \int_{\text{Path}} \rho^2 I d(\rho^2).$$

where

$$I = \rho^{-2} (\rho^2 - \rho^2 f_N^2/f^2 - \cos^2 \Delta)^{-1/2}.$$

Application of the second law of the mean for integrals then yields

$$P' = \xi D / \cos \Delta,$$

where  $\xi$  is some value between the limits of  $\rho^2$  over the integration range.

The lower limit of  $\rho^2$  is unity (value at the earth's surface) and the upper limit of  $\rho^2$  is  $(1 + h_r/R)^2$ , where  $h_r$  is the height of reflection measured from the earth's surface. Since  $h_r$  is small relative to  $R$ , the upper limit may be approximated by  $(1 + 2h_r/R)$ , which yields

$$1 \leq \xi \leq 1 + 2h_r/R.$$

From ray-tracing results,  $\xi$  was invariably found to be within 1% of the mean value of this range.

Hence

$$\xi \approx 1 + h_r/R = \rho_r$$

and

$$P' \approx \rho_r D / \cos \Delta. \quad (4)$$

This equation is used in the computer program to calculate virtual path length at a number of frequencies from the results of ray tracing with a variety of initial elevation angles. The results are printed in the form of a synthetic backscatter record, as represented by Figure 2. The angle of elevation is indicated by a letter, the key for which is given at the side of the graph. In this example, rays were traced at  $2\frac{1}{2}^{\circ}$  intervals of elevation angle. The effect of ionospheric focusing is apparent from the separation of the letters: as the minimum virtual path length is approached, differences between the path lengths for adjacent ray paths become so small that several angles of elevation need to be indicated at the same position on the graph. In such cases, only the highest angle of elevation in the group is printed; the included angles can be determined from the continuity of traces for constant angles of elevation. Figure 3 shows a plot of virtual path lengths for four selected angles. The original vertical incidence ionogram would be obtained by halving the path lengths given by ray tracing at  $90^{\circ}$  angle of elevation (although Equation (4) breaks down at this limit). The graphs obtained for other angles of elevation clearly display the same features as the original ionogram.

The original ray-tracing program (see Maliphant<sup>1</sup>) included a routine for calculating the effect of focusing and defocusing on a forward path. For this calculation, it was necessary to evaluate the differential  $(dD/d\Delta)$ . The analytic expression for  $D$  in the type of ray-tracing program described makes it possible to evaluate this differential directly. Earlier methods required additional ray tracing to calculate this quantity. The field strengths thus calculated have been used to approximate the effect of ionospheric focusing on the backscatter data: Figure 4 shows the same output as Figure 2, except that printing was suppressed whenever the calculated field intensity fell below a prescribed threshold. Thus, the diagram more closely represents the type of backscatter record obtained experimentally, although the results may be modified significantly by the effects of absorption, the nature of the ground in the scattering region, and the polar diagrams of the transmitting and receiving aerials. Figure 5 repeats the data given in Figure 4 but, instead of elevation angle, each letter represents the layer in which the ray was reflected. The leading edge of the separate returns from the E- and F-layers are clearly distinguishable.

#### 4. IONOSPHERIC CALIBRATION

Many methods are available for deriving the real-height electron density distribution from information given by a vertical incidence ionogram (see, for example, Wright and Smith<sup>4</sup>). It has been shown here that ray tracing at any fixed angle of elevation produces a  $P'(f)$  trace displaying similar features to those observed on a vertical incidence ionogram. In fact, any perturbation of the ionospheric distribution is more apparent on the  $P'(f)$  traces obtained at lower angles of elevation. It follows therefore that, in the case of a concentric ionosphere the real-height electron density distribution should be derivable from  $P'(f)$  data obtained at any fixed angle of elevation. A method of performing this reduction for the simplified case of a plane-stratified ionosphere with no magnetic field has been described by Unz<sup>5</sup> and in a later paper by Gething and Maliphant<sup>6</sup>. However, experimental backscatter data, by its nature, is incomplete and it is unlikely that adequate information could be obtained at a fixed angle of elevation. Most of the measurements will be restricted to backscatter near the leading edge of returns from the various ionospheric layers. These ray paths are found to have a rather constant height of reflection at a level defined by the condition  $f_N \approx 0.85 f_c$ , which is generally fairly near the height

of maximum electron density of the layer concerned. Since the minimum virtual path length for a given frequency is a function of the electron density distribution up to the height of reflection of the ray, measurements of the minimum virtual path lengths at a number of frequencies should be adequate to define the electron density distribution in the absence of any horizontal gradients. In the practical use of backscatter sounding, however, it can not be assumed that the ionosphere is concentric with the earth. In this case it may be acceptable to assume a constant gradient near the mid-point of the ray paths, but a more general solution is possible by describing the ionosphere in terms of an "equivalent concentric distribution". This term will be explained by reference to Figure 6, which shows the locus of apparent heights of reflection, described as a reflectrix by Lejay and Lepechinsky<sup>7</sup>, constructed for ray paths in a non-concentric ionosphere. The apparent height of reflection is defined as the height at which the straight line portion of the ray path, when extended from the origin, intersects the perpendicular erected from the surface of the earth at the centre of the ground range. A reflectrix refers to propagation at a fixed frequency. The equivalent concentric distribution is the distribution which, in the absence of horizontal gradients, yields an identical reflectrix for the same frequency. The effect of the non-concentric ionosphere on propagation ranges may thus be completely described by the equivalent concentric distribution. The extent of any horizontal gradients may be judged by comparing the equivalent concentric distributions determined for different frequencies. If there are no horizontal gradients, these distributions will be identical and will then represent the actual ionospheric distribution.

The type of ray-tracing program described in this paper is well suited to the requirements of ionospheric calibration, since it is necessary only to adjust the segment constants until the results of ray tracing are the same as the measurements taken from an experimental backscatter record. Use of the method of steepest descents to determine the segment constants is under study and the results will be described in a future paper. Before using this technique as a refinement process, it is necessary to obtain a reasonable approximation of the required distribution. When angle of elevation measurements are available, an approximate vertical incidence ionogram [ $h'(f_v)$ ] may be obtained by using plane-ionosphere theory, which yields

$$h' = R\{\sqrt{1 + \frac{1}{4}(P'/R)^2 + (P'/R) \sin \Delta} - 1\} \quad (5)$$

$$\text{and } f_v = f/\sqrt{[1 - \cos^2 \Delta/(1+h'/R)^2]} . \quad (6)$$

This ionogram may then be reduced by one of the simpler methods to obtain a first approximation of the real-height profile.

To illustrate the use of this technique, data from five points on the backscatter plot shown in Figure 4 have been used to calculate points on an approximate vertical incidence ionogram and the real-height equivalents plotted on Figure 7 for comparison with the original profile. The virtual path length obtained by using the approximate profile in the ray-tracing program are compared with the required values in Table I. The refinement process involves adjusting the constants for each of the profile segments in turn to determine the effect on the resultant path lengths and then using this information to modify the profile to obtain a closer fit to the experimental data.

A similar procedure may be used when measurements have been obtained at different frequencies; however, in this case the validity of the equivalent concentric distribution is lost and the accuracy of the resultant profile depends on the magnitude of any horizontal gradients of electron density. When horizontal gradients are fairly small, the minimum virtual path lengths recorded over a small frequency range may be used to derive an average profile applicable to locations near the region from which these signals have been returned.

### 5. OBLIQUE INCIDENCE IONOGRAMS FOR FIXED GROUND RANGES

Backscatter data may be used most efficiently when a number of communication circuits terminate near the sounding station. In such cases, the information contained in fixed-frequency reflectrices calculated by ray-tracing through profiles which yield the observed backscatter data may be stored in three-dimensional arrays ( $f, \Delta, h'$ ) applicable to particular bearings at the time of measurement. The required information on frequency, angle of elevation and path length for a fixed ground range may then be obtained by interpolation. If desired, synthetic oblique incidence ionograms may be produced to provide information which could otherwise only be obtained by oblique incidence sounding between the two terminals. (It is relevant here to note that, for a concentric ionosphere, the apparent path length for F-layer returns appears generally to be larger than the virtual path length but remains within about 1% of that value.)

On occasions when backscatter data are to be applied to a single communication circuit, one profile may often be sufficient to describe the effect of the ionosphere between the two terminals. It is then convenient to use a homing technique in the ray-tracing program to synthesise an oblique incidence ionogram for the required ground range.

An efficient interpolation process has been developed in which the height of reflection is held constant by varying frequency as the angle of elevation is adjusted to yield the required ground range. The required relation between angle and frequency is given by the equation

$$f = f_v \left( 1 - \frac{\cos^2 \Delta}{\rho_r^2} \right)^{-1/2} \quad (7)$$

(see Reference 8 for derivation).

The relationship between angle of elevation and distance propagated, for a constant height of reflection, is then represented empirically by the equation

$$D = u \tan^v \left( \frac{\Delta - 90}{w - 1} \right) \quad (8)$$

where  $\Delta$  is measured in degrees and the constants  $u$ ,  $v$  and  $w$  are calculated to fit the ray-tracing results. It may be seen that in this equation  $D$  is a monotonic function of  $\Delta$ , which is zero when  $\Delta = 90^\circ$  and infinity when  $(\Delta/90) = w$ . The constant  $w$  is positive only when the height of reflection is near the height of maximum electron density; in this height range, the value may be obtained directly from the equation

$$w = \frac{1}{90} \text{arc cos} \sqrt{\left( \frac{g_1 \rho_r^u - a_1}{2g_1 \rho_r^2 + b_1} \right)} . \quad (9)$$

In order to synthesise an oblique incidence ionogram, ray-tracing results are required for a number of reflection heights. The first estimate of  $\Delta$  is derived from values previously calculated for the lower heights of reflection, the distance resulting from the subsequent ray tracing being used together with any results closer to the required value to modify the constants  $u$ ,  $v$  and  $w$ . The interpolated value of  $\Delta$  is then given by the equation

$$\Delta = 90 - (1-w) \text{arc tan} (D_0/u)^{1/v} , \quad (10)$$

where  $D_0$  is the required value of  $D$ .

Using the method described, homing within 0.5 km of the required range is usually accomplished with only one to three range calculations. Typical results for the profile shown in Figure 7 are given in Table II.

**ACKNOWLEDGEMENT**

This paper is published by permission of the Director, Government Communications Headquarters, Cheltenham.

**REFERENCES**

1. Maliphant, R.G. *The Control of F-Layer LUFs by the Defocusing Effect of the Lower Layer.* Proceedings of the XIth Symposium of the AGARD Electromagnetic Wave Propagation Committee, Leicester, England, 25th-29th July, 1966.
2. de Voogt, A.H. *The Calculation of the Path of a Radio-Ray in a Given Ionosphere.* Proceedings, Institute of Radio Engineers, Vol. 41, September 1953, pp. 1183-1186.
3. Muldrew, D.B. *An Ionospheric Ray-Tracing Technique and its Application to a Problem in Long-Distance Radio Propagation.* Institute of Radio Engineers, Transactions on Antennas and Propagation, Vol. AP-7, October 1959, pp. 393-396.
4. Wright, J.W., Smith, G.H. *Review of Current Methods of Obtaining Electron Density Profiles from Ionograms.* Radio Science, Vol. 2, October 1967, pp. 1119-1282.
5. Unz, H. *Schlomilch's Integral Equation for Oblique Incidence.* Journal of Atmospheric and Terrestrial Physics, Vol. 28, 1966, pp. 315-316.
6. Gething, P.J.D., Maliphant, R.G. *Unz's Application of Schlomilch's Integral Equation to Oblique Incidence Observations.* Journal of Atmospheric and Terrestrial Physics, Vol. 29, 1967, pp. 599-600.
7. Lejay, P., Lepechinsky, D. *Field Intensity at the Receiver as a Function of Distance.* Nature, Vol. 165, February 1950, pp. 306-307.
8. Maliphant, R.G. *The Refractive Deviation of Radio Waves that Penetrate the Earth's Ionosphere.* Defence Research Telecommunications Establishment, Ottawa, Canada, DRTE Report 1090, Appendix A, September 1962.

## APPENDIX

The total range propagated along the curved earth's surface is given by

$$D = D_0 + \sum_{i=1}^n D_i ,$$

where  $D_i$  is the contribution due to the ray travelling through the  $i^{th}$  segment, and  $D_0$  is the distance along the ground covered by the ray in traversing the un-ionised regions below the ionosphere, given by

$$D_0 = 2R \left\{ \arccos \left( \frac{\cos \Delta}{\rho_0} \right) - \Delta \right\} ,$$

where  $\rho_0$  is the value of  $\rho$  at the lower limit of the ionosphere.

The ground range covered by the ray travelling through the  $i^{th}$  segment is given by

$$D_i = A \int_{z_j}^{z_k} \frac{dz}{\sqrt{(Uz^2 + Vz + W)}} ,$$

where  $z_j$  and  $z_k$  represent the height limits of the  $i^{th}$  segment,

$$x = \rho^2$$

$$A = (R/2)f \cos \Delta$$

$$U = -g_i$$

$$V = f^2 - b_i$$

$$\text{and } W = -(a_i + f^2 \cos^2 \Delta) .$$

Solution of the integral yields

$$D_i = \frac{A}{\sqrt{W}} \log \left\{ \frac{\rho_k}{\rho_j} \frac{\frac{1}{\rho_j} + \sqrt{X_j} + (V/2W)\rho_j}{\frac{1}{\rho_k} + \sqrt{X_k} + (V/2W)\rho_k} \right\} , \quad \text{when } W > 0$$

where

$$X_j = 1/\rho_j^2 + (U/W)\rho_j^2 + V/W ,$$

or

$$D_i = \frac{A}{\sqrt{(-W)}} \left[ \arcsin \sqrt{\left\{ 1 + \left( \frac{2W}{V\rho_k} \right)^2 \frac{X_k}{1 - 4UW/V^2} \right\}} - \arcsin \sqrt{\left\{ 1 + \left( \frac{2W}{V\rho_j} \right)^2 \frac{X_j}{1 - 4UW/V^2} \right\}} \right] ,$$

when  $W < 0$

or

$$D_i = \frac{2A}{\sqrt{|V|}} \{ \sqrt{[1/\rho_k^2 + U/V]} - \sqrt{[1/\rho_j^2 + U/V]} \} , \quad \text{when } W = 0 .$$

The value of  $x$  at the height of reflection is used as the upper limit for the  $n^{th}$  segment, given by

$$x_r = -(V/2U) \{ 1 \pm \sqrt{1 - 4UW/V^2} \} .$$

In practice, this expression is evaluated for each segment in turn until the value of  $x_r$  thus obtained falls within the effective height range of the segment. This value is then used as the upper limit for the ray path. If two such values are found for the same segment, the lower of these represents the correct solution.

Since the ray path is symmetrical in a concentric ionosphere with no magnetic field, the distance calculated by summing  $D_i$  up to the height of reflection is doubled to obtain the total ground range covered by the ray while travelling through the ionosphere.

**TABLE I**

**Virtual Path Lengths Obtained by Ray-Tracing Through an Approximate Profile  
Compared with the Values Used to Derive the Distribution.**

Frequency (MHz)	Elevation Angle (degrees)	Reflection Height (km)	Virtual Path Length (km)	
			Required Value	Approximate Value
10	6	88	1358	1394
10	30	160	927	811
10	42	184	747	720
10	50	198	709	688
10	60	216	706	714

**TABLE II**

**Ray-Tracing Results for a Ground Range of 1500 km.**

Frequency (MHz)	Elevation Angle (degrees)	Reflection Height (km)	Virtual Path Length (km)	Number of Range Calculations Required
9.46	4.25	90	1525	2
10.68	7.16	100	1536	3
7.50	16.15	130	1594	4
8.72	14.18	140	1581	3
9.61	13.92	150	1582	2
10.46	14.17	160	1586	2
11.57	14.32	170	1590	2
12.94	14.53	180	1593	2
14.65	14.78	190	1598	2
17.07	14.93	200	1601	3

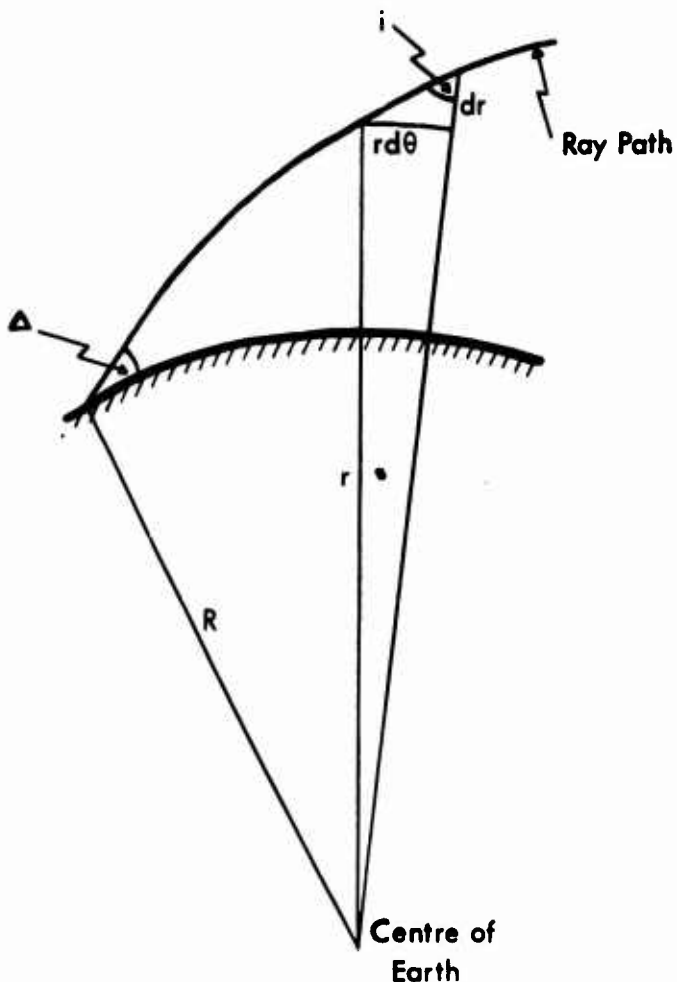


Fig. 1 Schematic representation of ray path through the ionosphere

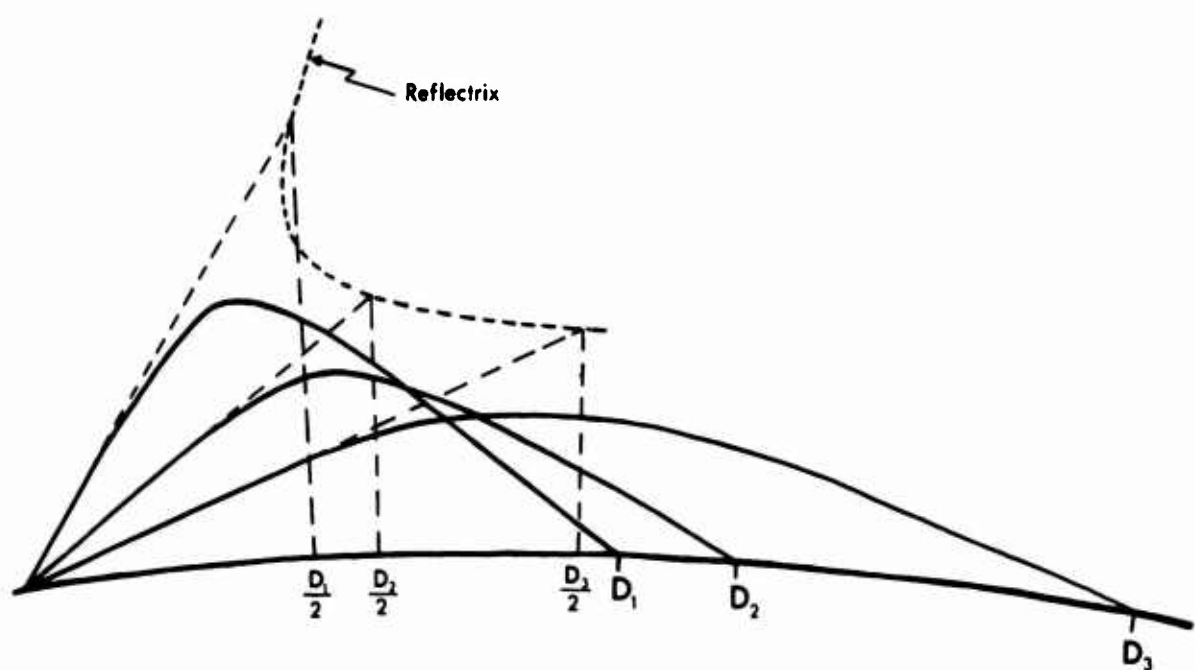


Fig. 6 The locus of apparent heights of reflection for ray paths in a non-concentric ionosphere

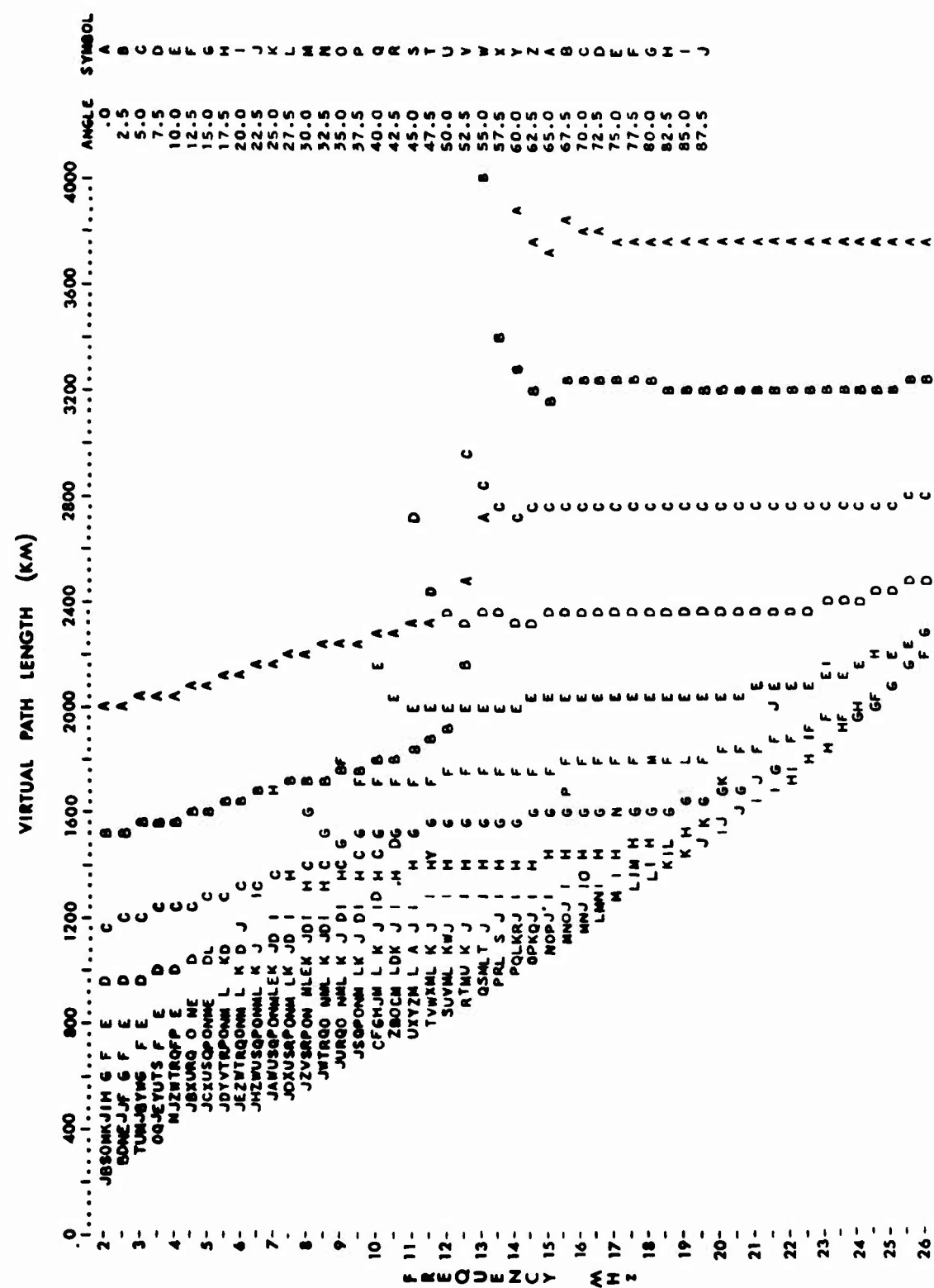


Fig. 2 Synthetic backscatter record. The angle of elevation is indicated by a letter, the key for which is given to the right of the graph

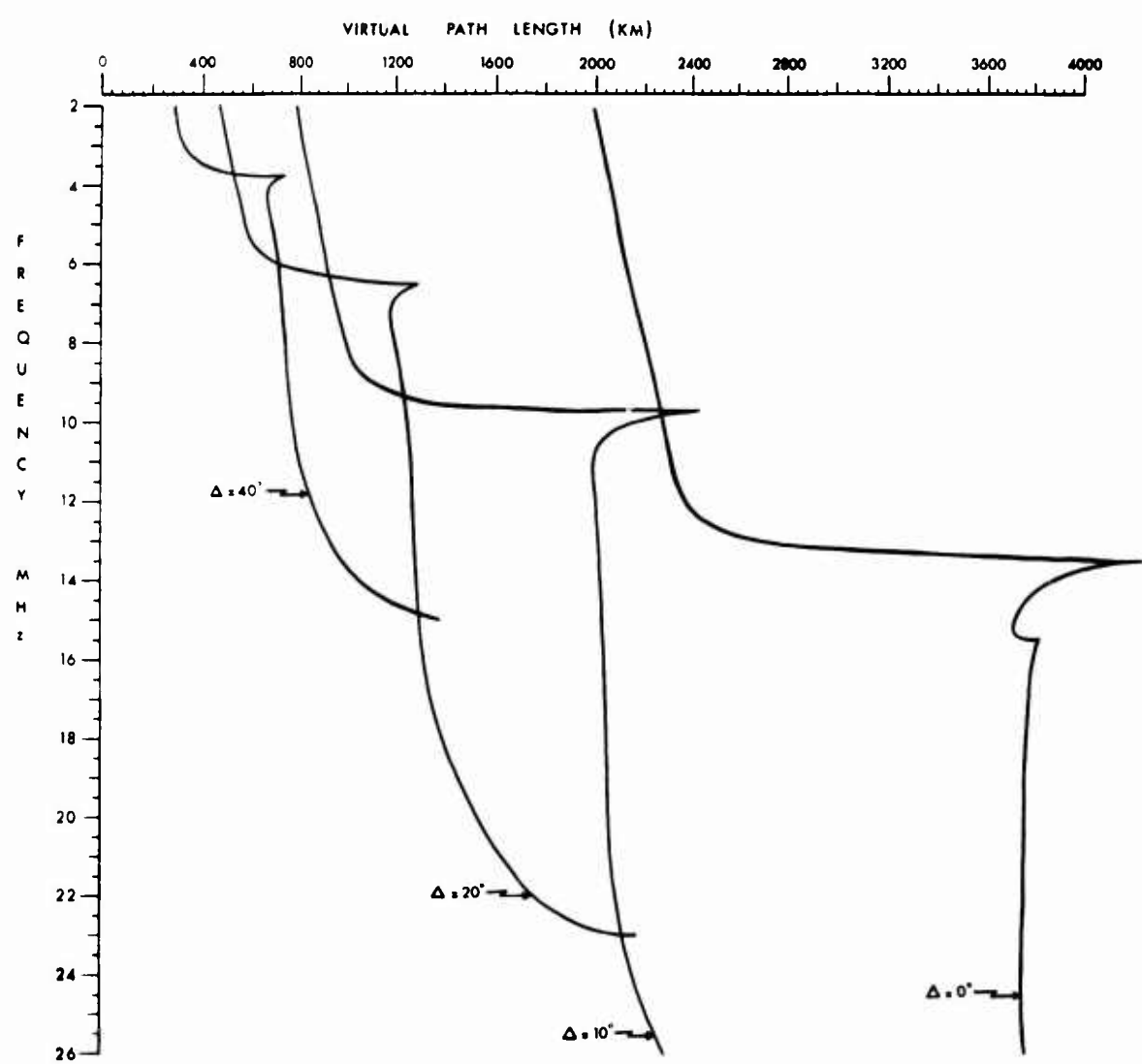


Fig. 3 Virtual path lengths for four selected angles

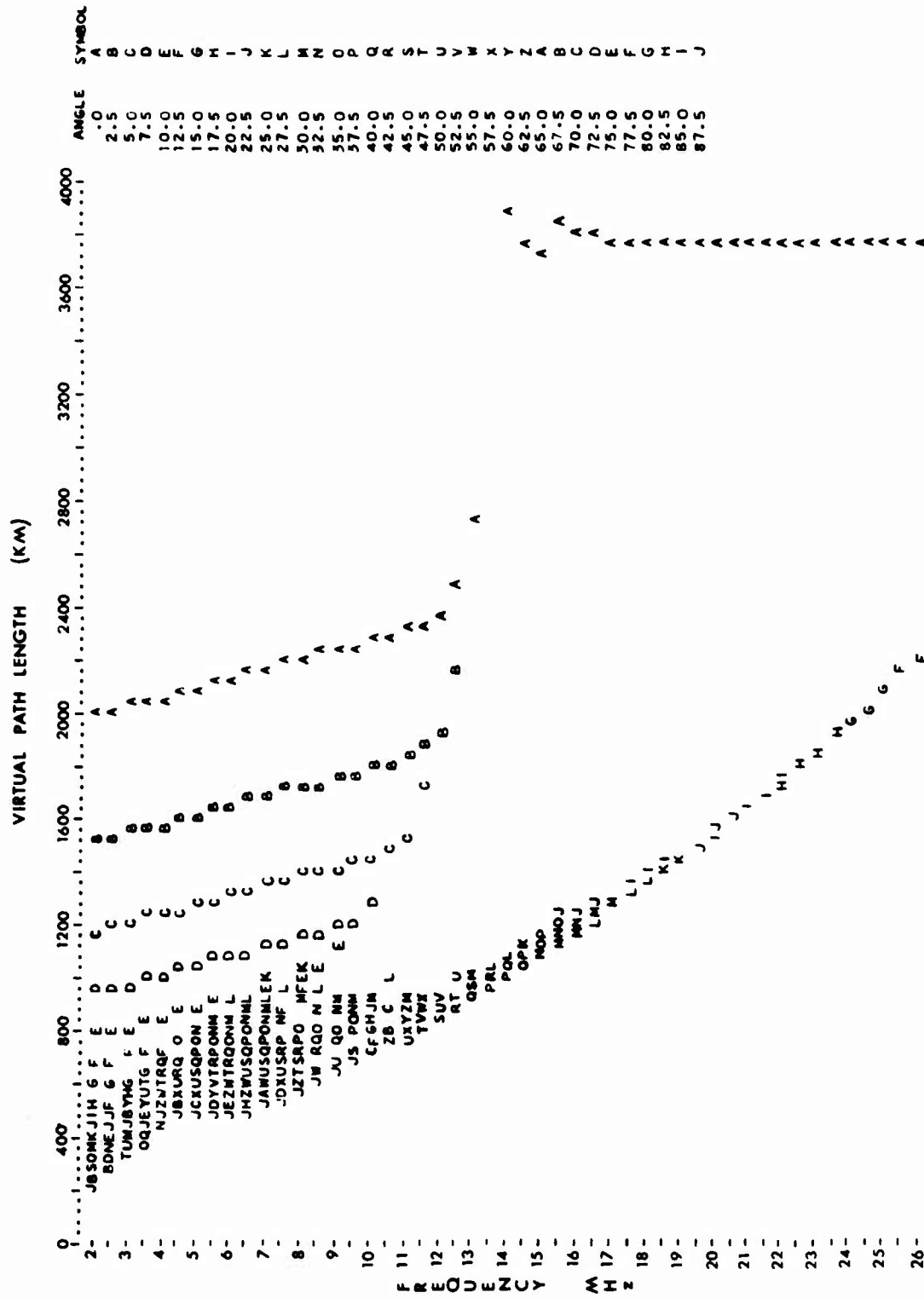


Fig. 4 Synthetic backscatter record. Printing was suppressed whenever calculated field intensity fell below a prescribed threshold

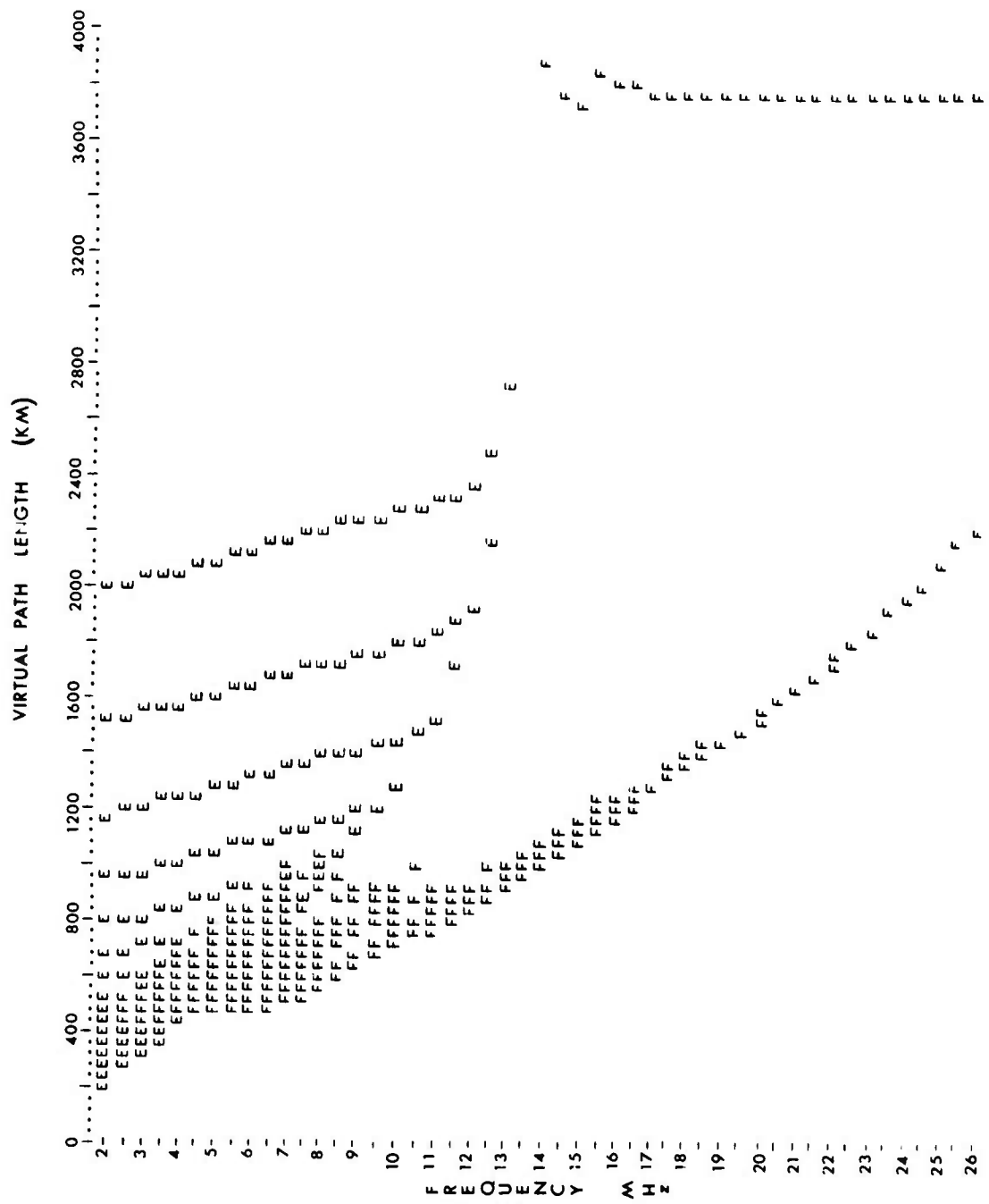


Fig. 5 Synthetic backscatter record. Each letter represents the layer from which the ray was reflected

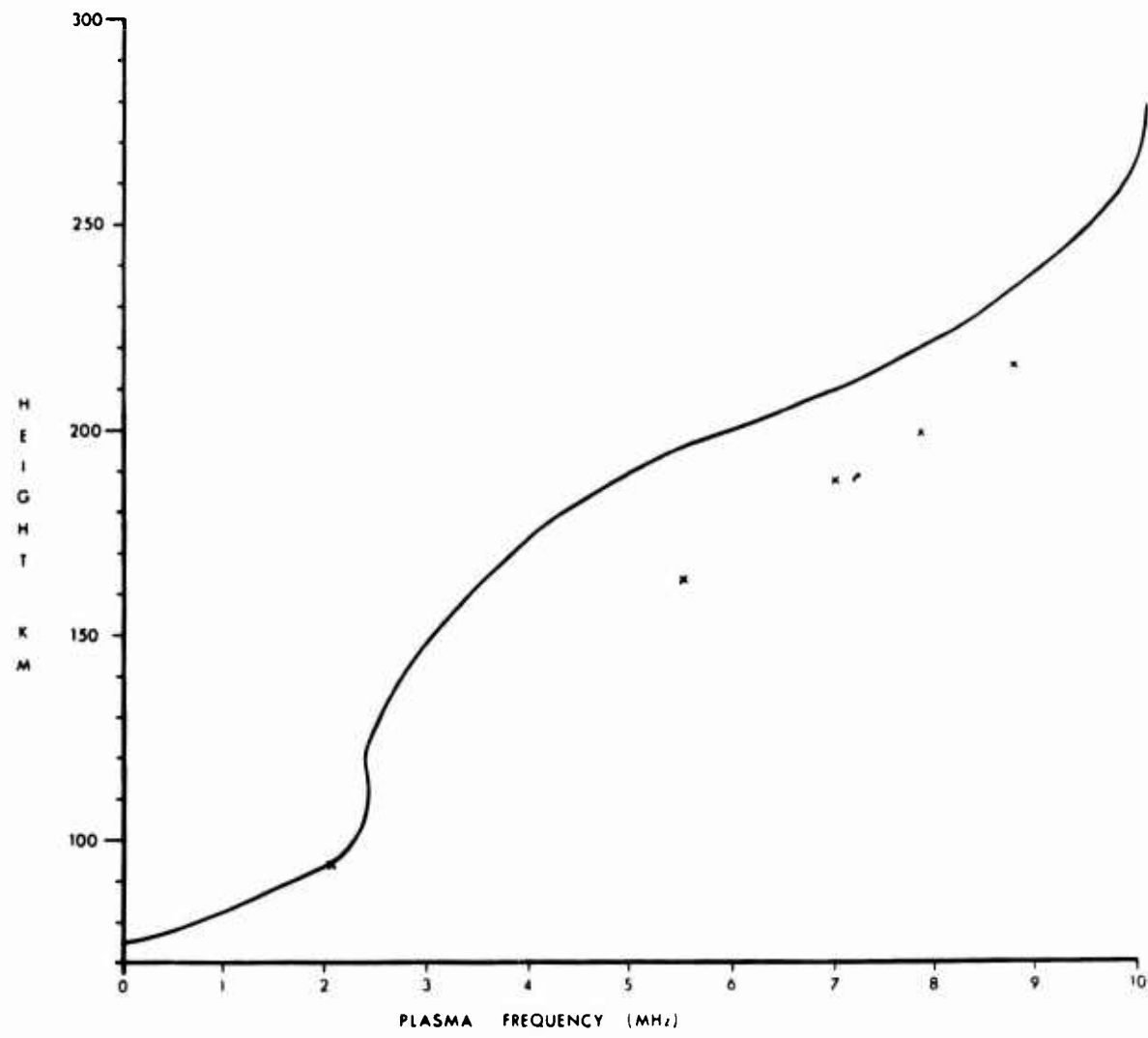


Fig. 7 Comparison of real height profile computed from the backscatter plot in Figure 4 (crosses) with original profile (solid line)

**INTERFERENCE PATTERNS IN HF SIGNALS  
BACKSCATTERED FROM OCEAN WAVES**

by

**D. B. Muldrew**

**Radio Physics Laboratory  
Defence Research Telecommunications Establishment,  
Ottawa, Canada**

## SUMMARY

Signals backscattered from the North Atlantic Ocean were occasionally observed at Ottawa from 1957 to 1964 at frequencies in the range from 25 to 40 MHz using an oblique-incidence ionospheric sounder. Enhancement of the backscatter signal by skip-distance or time-delay focusing is evident on most of the ionogram records containing backscatter signals. In addition patterns consisting of up to six parallel ridges appear. It is thought that these patterns are caused by interference of radio waves backscattered from spatially coherent waves on the ocean surface at distances of a few thousand kilometers from the transmitter. The frequency separation of the interference ridges indicates that the ocean-wave components which are responsible for the ridges have a wavelength of about 50 to 200 m; such waves can occur in ocean swell generated by gales on the ocean. From the orientation of the ridges on the ionogram, the change in wavelength, with distance from the transmitter, of the ocean swell responsible for the ridges can be deduced.

## INTERFERENCE PATTERNS IN HF SIGNALS BACKSCATTERED FROM OCEAN WAVES

D.B. Muldrew

## 1. INTRODUCTION

The backscatter of radio waves from the sea surface may be studied by direct illumination of the sea, or by using an ionospheric mode of propagation. On occasion, strong coherent components appear in the backscatter signals. When the sea is illuminated directly, coherent backscatter provides information on the state of the sea surface. If, however, an ionospheric mode of propagation is used, the interpretation of coherent backscatter observations is more difficult since, in principle, ionospheric structures could also cause coherent scatter signals.

Using a vertical-incidence HF sounder, Ellyett<sup>1</sup> recorded radio-wave echoes which he thought were reflected from an apparent height of about 50 km. These echoes occurred 65% of the time during daytime and had a strength of approximately one-third of the E-layer echo. Major<sup>2</sup> pointed out that all the ionospheric stations which recorded echoes similar to those reported by Ellyett were on islands or near the sea.

Crombie<sup>3</sup> recorded the Doppler shift of CW radio waves backscattered from the sea surface at 13.56 MHz. The received signal had been scattered mainly by those ocean waves that travelled directly away from or toward the receiver and transmitter (see Figure 1). In one case Crombie showed that his data were consistent with a theoretical model based upon coherent reflection from about six consecutive ocean waves of length  $\lambda/2$  where  $\lambda$  is the radio wavelength.

Dowden<sup>4</sup>, using a vertical-incidence ionospheric sounder at Macquarie Island, received strong vertically polarized echoes at very low elevation angles, with apparent ranges from 20 to 100 km. He concluded that these echoes (and similar echoes recorded by Ellyett and others) were caused by coherent backscatter from the sea of the type described by Crombie. Dowden, and later Haubert<sup>5</sup>, obtained a beat frequency on the records of twice the Doppler frequency. They concluded that this beat was caused by interference between the radio waves backscattered from the ocean waves travelling directly away from and those travelling directly toward the ionosonde (see Figure 1).

Coherent backscatter from ocean waves at about 50 MHz was reported by Sofaer<sup>6</sup>.

Ranzi<sup>7</sup> studied HF backscatter signals from sea waves and noted that the signals were especially strong when the backscatter occurred near the sea coast. He observed that when the sea was rough the 4 and 28 MHz signals were of similar strength; however, for a calm sea the voltage-reflection coefficient was about 10 times greater on 28 MHz than on 4 MHz. He also found that on 28 MHz horizontally polarized waves were about 26 dB weaker than vertically polarized waves.

Wait<sup>8</sup> derived an equation for the voltage-reflection coefficient relative to a mirror-type reflection for backscatter from coherent ocean waves. For 10 successive infinite ocean waves of 20 m wavelength having a height of 1 m and at a range of 20 km from the transmitter (the range determines the size of the Fresnel zone), he obtained a reflection coefficient for radiowaves of 40 m wavelength of 0.05 in agreement with Dowden's<sup>4</sup> measurements.

From Wait's equation it would be expected that a 28 MHz wave would have a voltage-reflection coefficient about 15 times greater than that for a 4 MHz wave. This is in good agreement with Ranzi's<sup>7</sup> experimental results for a calm sea. On calm seas backscatter likely occurs from low-amplitude swell waves.

Crombie and Watts<sup>9</sup> noted that HF sea-backscatter data obtained by direct illumination of the sea could be used to study the sea-wave spectrum and its variation with direction and distance up to about 200 km from the transmitter. The present paper indicates that oblique-incidence HF sounders could be used to study the sea surface at distances up to a few thousand kilometers.

## 2. OBLIQUE SOUNDER CIRCUIT

Between September 1957 and March 1964 an oblique-incidence sounder was operated between Ottawa, Canada and two sites in Europe. The transmitters and receivers at both ends of the path stepped nearly simultaneously in frequency from 3 to 49 MHz at a rate of 100 kHz sec<sup>-1</sup>. The European site was changed from Slough, England (5300 km path) to The Hague, Netherlands (5600 km path) in March 1959 (see Figure 2). The beamwidth of the rhombic antenna used in the circuit varies with frequency; a horizontal beam width of 60° is probably a reasonable central value and is used in the figure. Between 2000 and 4000 km the elevation angle of one-hop ionospherically reflected radio waves incident on the sea surface is less than 20°.

## 3. OBSERVATIONS

Figure 3 is part of an oblique-incidence ionogram recorded at Ottawa on January 25, 1958 at about 1700 GMT. The apparent range ( $ct/2$ , where  $c$  is the free-space velocity of light and  $t$  is the time interval measured from transmission of a pulse from the Ottawa terminal) is given on the vertical scale and frequency on the horizontal scale. The vertical scale is correct for signals backscattered to Ottawa but, because the transmitter pulses at the two terminals do not occur at precisely the same time, this apparent range scale should not be applied to the signals received from Slough. Traces resulting from propagation which required two and three hops to travel between Slough and Ottawa are labelled. Both the high-angle and low-angle branches of these traces can be seen. It is well known that focusing of radio waves occurs at the skip distance (LeJay and Lepechinsky<sup>10</sup>; Warren and Muldrew<sup>11</sup>); the signal backscattered from this distance and which arrives at the transmitter-receiver terminal will have been focused twice. Time-delay focusing can also occur (Peterson<sup>12</sup>). The 'skip-distance' and/or 'time-delay' focus ridge can be clearly seen in Figure 3. For a given frequency no backscatter signal is observed at ranges less than the range of the skip distance. In the backscatter region (above and to the left of the focus ridge) of the ionogram of Figure 3, three ridges can be seen. Other examples of such ridges appear in Figure 4, recorded on January 11, near 2000 GMT, 1958. Two sets of ridges can be seen at frequencies between 25 and 28 MHz and another set at frequencies between 29 and 32 MHz. The focus ridge is clearly visible.

In this paper a probable explanation of the sets of ridges will be presented.

## 4. INTERPRETATION OF THE INTERFERENCE RIDGES

In this section it is assumed that radio waves are scattered by a periodic ocean surface with waves of length  $L$  oriented orthogonally to the plane of incidence of the radio waves. Reinforcement of the radio wave scattered from the ocean surface can then occur in the plane of incidence. If the elevation angle of the radio waves to the mean ocean surface is  $\kappa$ , then reinforcement of the backscattered radio waves will occur at a radio wave length  $\lambda_n$  such that

$$n\lambda_n/2 = L \cos \kappa, \quad (1)$$

where  $n$  is an integer (see Figure 1). The frequencies at which reinforcement can occur for a given ocean wave length are

$$f_n = \frac{nc}{2L \cos \kappa}, \quad n = 1, 2, 3, \dots, \quad (2)$$

where  $c$  is the free-space velocity of light. At a given range on the ionogram the frequency difference  $\Delta f$  between two consecutive ridges is given by

$$\Delta f = f_{n+1} - f_n = \frac{c}{2L \cos \kappa}. \quad (3)$$

From (2) and (3),

$$n = \frac{f_n}{\Delta f}. \quad (4)$$

Using (4) it is possible to determine  $n$  with an accuracy of only about 10%, due to the uncertainty in measuring  $\Delta f$ . The probable values of  $n$  for the three ridges in the ionogram of Figure 3 are thought to be 10, 11 and 12 although 9, 10, 11 or 11, 12, 13 are also possible.

It is desirable to know the ocean wavelength in the backscatter region and also the rate of change of this wavelength with distance on the ocean surface. The approximate rate of change can be found by differentiating (2) with respect to the apparent range  $r'$ . This yields

$$\frac{df_n}{dr'} = - \frac{nc}{2(L \cos \kappa)^2} \frac{d(L \cos \kappa)}{dr'}. \quad (5)$$

Using (2),  $L \cos \kappa$  can be determined at any apparent range  $r'$  on one of the ridges of the interference patterns; for example for the  $n = 11$  ridge at 2800 km apparent range,  $f_{11} = 35.0$  MHz and, from (2),  $L \cos \kappa = 47$  m. The slope of the ridges obtained from the ionogram  $df_n/dr'$  is about 2.1 MHz per 100 km apparent range at 35 MHz. Thus for  $n = 11$ , substitution into (5) gives  $d(L \cos \kappa)/dr' \approx -2.8$  m/100 km. The values for  $L \cos \kappa$  and its slope  $d(L \cos \kappa)/dr'$  have about the same error as  $n$ , i.e. about 10%. Because  $\kappa$  is small and the real range  $D$  is nearly equal to  $r'$ , the change of ocean wavelength with real range from the transmitter,  $dL/dD$ , can be approximated by  $d(L \cos \kappa)/dr'$  with an error which is much smaller than the error of about 10% in  $d(L \cos \kappa)/dr'$ .

Using sliders (Smith<sup>13</sup>) or ray tracing (Muldrew<sup>14</sup>) and the appropriate vertical-incidence ionogram from Ottawa, Ontario or St. John's, Newfoundland, it is possible to estimate the elevation angle  $\kappa$  and the apparent height of reflection  $h'$  of the radio waves in the ionosphere for any frequency on a given interference ridge. The values obtained for  $f = 35.0$  MHz at an apparent range of 2800 km on the ionogram of Figure 3 are  $h' \approx 320$  km and  $\kappa \approx 7^\circ$ . Hence it can be shown that, at an apparent range of 2800 km,  $L \cos \kappa$ , equal to 47 m, corresponds to an ocean wave length  $L$  of about 47.5 m at a real range  $D$  of about 2670 km from the sounder.

There appear to be three independent interference patterns labelled A, B and C in the ionogram of Figure 4. These ridges are sketched at the bottom of the figure. Similar analyses to that given above for the set of ridges in the ionogram of Figure 3 are summarized in Table T.

### 5. SIGNAL STRENGTH

From Equation (17) of Wait<sup>8</sup> (1966) an estimation of the backscatter voltage-reflection coefficient  $|R|$  relative to a mirrortype reflection can be made from a series of ocean waves aligned orthogonally to the plane of radio-wave propagation. Wait's Equation (17) may be written

$$|R| \simeq \left( \frac{2}{\lambda d} \right)^{\frac{1}{2}} \frac{2\pi d_0 h}{\lambda} . \quad (6)$$

where  $\lambda$  is the radio wavelength,  $d$  is the distance from the sounder to the scatter area and can be approximated by  $r'$ ,  $d_0$  is the extent of the coherent ocean waves in the direction of radio-wave propagation and  $h$  is the height amplitude (one half the height from trough to crest) of the ocean waves. Equation (6) is only valid if  $|R| \ll 1$ . The corresponding values of  $\lambda$  and  $d$  for the ridges in the ionogram of Figure 3 are 9 m and 2800 km respectively. If the number of coherent ocean waves  $p$  is taken to be 10 then, since  $L = 47$  m,  $d_0 \simeq pL \simeq 470$  m. The height amplitude of swell waves can have a wide range of values for a given wavelength; however, some observations reported by Neumann<sup>15</sup> give  $h \simeq 0.006L$  and this value will be used here. Using these values for  $\lambda$ ,  $d$ ,  $d_0$  and  $h$ , Equation (6) yields  $|R| \simeq 0.03$ . This simple calculation gives a signal strength which is about 30 dB below a specular reflection. The sounder system could detect signals down to about 2  $\mu$ V (E.L. Hagg, private communication) and backscatter signals 30 dB below a specular reflection give signals of about 10  $\mu$ V from a range of 2500 km. The value of  $|R|$  calculated here is by no means a maximum since  $h$  might reasonably be increased by a factor of about three (Bigelow and Edmondson, p.71, of Reference 16),  $p$  could be larger, and there could exist several independent coherent scattering areas that contribute to the backscattered signal.

### 6. DISCUSSION

#### 6.1 Ocean Waves and Season

In Table I the ocean wavelengths obtained vary from about 50 to 200 m. Waves of this length can be obtained from winds of 18 to 40 knots blowing for about 25 to 30 hours over a fetch of 170 to 500 miles (Vine and Volkman<sup>17</sup>). In January in the North Atlantic, gales with winds greater than 34 knots blow 20 to 30% of the time; about 50% of these gales last 12 hours or more and about 10% last 24 hours or more (US Navy Hydrographic Office<sup>18</sup>). Thus, in January, it appears that there are regions of the North Atlantic suitable for producing backscatter ridges of the type observed. In the summer backscatter is not usually observed on the oblique ionograms; this is probably because the sea surface is considerably less active (US Navy Hydrographic Office<sup>18</sup>).

#### 6.2 Swell

The radio-wave energy responsible for the interference ridges on the ionograms is not necessarily backscattered directly from the area of a gale on the ocean, but may be backscattered from the swell which is generated by the gale. This is illustrated in Figure 1. A gale on the ocean, near the region marked 'X' in the figure, may generate swell which travels circularly outward from the gale area. The swell can extend continuously for many hundreds or thousands of kilometers and may propagate away from its source and still be observable for several days. Longer ocean waves travel faster than shorter waves and, consequently, at a given point on the ocean the frequency of the swell increases gradually with time (Dinger<sup>19</sup>). In one particular set of Dinger's data (see Neumann and Pierson, p.359, of Reference 20) the peak in the frequency spectrum of swell increases linearly over a three-day period from about 0.070 Hz to about 0.110 Hz. From the equation for group velocity of ocean waves and the relation between ocean wavelength and frequency (Neumann and Pierson, p.280, of Reference 20), the change in frequency with

time at a given point can be related to the change in wavelength with distance on the ocean surface at a given time. The frequency of 0.110 Hz corresponds to an ocean wavelength  $L = 150 \text{ m}$  and at this frequency the change in frequency of 0.040 Hz ( $0.110 \text{ Hz} - 0.070 \text{ Hz}$ ) in three days found by Dinger corresponds to a change in  $L$  of about 5.7 m in a 100 km range (see the Appendix) on the ocean surface. In Table I, the values of  $|dL/dD|$  obtained for patterns B ( $L = 115 \text{ m}$ ) and C ( $L = 204 \text{ m}$ ) of Figure 4 are both 6.6 m/100 km. The good agreement here is likely fortuitous; nevertheless, it indicates that the swell explanation for the backscatter ridges is not unreasonable.

Since the swell spreads out circularly from the source there will be two zones in the swell for which the radio waves from the sounder will be orthogonal to the ocean waves. In one zone the ocean waves will be travelling toward the sounder and in the other case they will be travelling away from the sounder. In the former case the corresponding ridges on the ionogram will have a positive slope (i.e.  $df_n/dr' > 0$ ) and in the latter case they will have a negative slope. Figure 4 illustrates that both positive and negative sloped interference ridges are observed. Positive sloped interference ridges occur more often than negatively sloped ridges. This is consistent with the idea that the backscatter responsible for the ridges occurs from swell since, in the 2000 to 4000 km zone (Fig. 2) from which backscatter occurs, swell travelling toward the sounder can be generated almost anywhere in the North Atlantic whereas swell in this zone, travelling away from the sounder, must originate near the North American coast.

### 6.3 Ocean-wave Spectrum

Oceanographers generally consider ocean waves to have a continuous spectrum of wavelengths (Neumann and Pierson, p.334 of Reference 20). An analysis of western North Atlantic wave records by Seiwell and Wadsworth<sup>21</sup>), however, indicates that ocean wave spectra frequently consist of one dominant frequency on which random components of lesser amplitude are superimposed. The dominant frequency appears to be that generated under the influence of a controlling meteorological situation and the random components by local winds. The work of Seiwell<sup>22</sup> is disregarded by Neumann and Pierson<sup>20</sup>. Neumann and Pierson may be right in general but there may also be isolated patches of ocean in which coherence is approximated. It would be difficult to explain the interference ridges of the ionogram of Figures 3 and 4 if Neumann and Pierson were right, since the occurrence of ridges implies that in at least some cases there is a dominant sinusoidal component in the ocean wave spectrum. As mentioned above, Crombie<sup>3</sup> could explain his data in some detail from the assumption that backscatter was occurring from six coherent waves.

## 7. CONCLUSIONS

This paper has indicated that interference patterns resulting from coherent backscatter from ocean waves are occasionally observed on oblique-incidence ionograms. The possibility that these interference patterns are due to ionospheric structure rather than to sea scatter cannot be ruled out by the present observations, but the probability of this is considered to be small. The earlier work of Ellyett', Crombie<sup>3</sup> and others demonstrated that backscatter of this type is to be expected. It has also been shown that ocean conditions required to produce the observed patterns occur frequently in January, when most of the ionograms containing backscatter are recorded, and that the backscatter signals should be of sufficient strength to be detected.

A narrow-beam backscatter radar would be a much better instrument than the oblique-incidence sounder described here for detecting interference patterns resulting from backscatter of radio waves from coherent ocean waves, and hence for studying the wave structure of the sea surface.

Assuming that the present explanation of the interference ridges observed on oblique HF ionograms is essentially correct, then in at least some small areas of the ocean there appears to be a single dominant component in the ocean wave spectrum. As mentioned

above, Crombie<sup>3</sup> and Seiwell and Wadsworth<sup>21</sup> also indicate this, although this view is not commonly accepted. The wavelength of this dominant component would change gradually with distance on the ocean surface.

## REFERENCES

1. Ellyett, C.D., *Echoes at D-Heights with Special Reference to the Pacific Islands. Terrestrial Magnetism and Atmospheric Electricity*, Vol. 52, 1947, pp. 1-13.
2. Major, G. *D-Layer Ionospheric Echoes at Macquarie Island*. Nature, Vol. 175, 1955, pp. 862-863.
3. Crombie, D.D., *Doppler Spectrum of Sea Echo at 13.56 Mc/s.* Nature, Vol. 175, 1955, pp. 681-682.
4. Dowden, R.L., *Short-Range Echoes Observed on Ionospheric Recorders*. Journal of Atmospheric and Terrestrial Physics, Vol. 11, 1957, pp. 111-117.
5. Haubert, A., *Échoes Radioélectriques Observés sur la Houle à la Station de Sondages Ionosphériques de Casablanca*. Annales de Géophysique, Vol. 14, 1958, pp. 368-372.
6. Sofaer, E., *Phase-Coherent Backscatter of Radio Waves at the Surface of the Sea*. Proceedings, Institution of Electrical Engineers, Vol. 105B, 1958, pp. 383-394.
7. Ranzi, I., *Experiments on Backscatter of HF Radiowaves from Open and Coastal Sea*. Scientific Note No. 3, Centro Radioelettrico Sperimentale, G. Marconi, Rome, Italy, March 1, 1961.
8. Wait, J.R., *Theory of HF Ground Wave Backscatter from Sea Waves*. Journal of Geophysical Research, Vol. 71, 1966, pp. 4839-4842.
9. Crombie, D.D., Watts, J.W., *Observations of Coherent Backscatter of 2-10 MHz Radio Surface Waves from the Sea*. Deep-Sea Research, Vol. 15, 1968, pp. 81-87.
10. Lejay, P., Lepechinsky, D., *Field Intensity at the Receiver as a Function of Distance*. Nature, Vol. 165, February 1950, pp. 306-307.
11. Warren, E., Muldrew, D., *A method for Computing Ionospheric Focusing of Radio Waves, Using Vertical Incidence Ionograms*. Institute of Radio Engineers, Transactions on Antennas and Propagation, Vol. AP-9, 1961, pp. 403-409.
12. Peterson, A.M., *The Mechanism of F-Layer Propagated Backscatter Echoes*. Journal of Geophysical Research, Vol. 56, 1951, pp. 221-237.
13. Smith, N., *The Relation of Radio Sky-Wave Transmission to Ionospheric Measurements*. Proceedings, Institute of Radio Engineers, Vol. 27, 1939, pp. 332-347.

14. Muldrew, D.B.,  
*An Ionospheric Ray-Tracing Technique and its Application to a Problem in Long Distance Radio Propagation.* Institute of Radio Engineers, Transactions on Antennas and Propagation, Vol. AP-7, 1959, pp. 393-396.

15. Neumann, G.,  
*On Ocean Wave Spectra and a New Method of Forecasting Wind-Generated Sea.* New York University Report, 1953.

16. Bigelow, H.B.,  
Edmondson, W.T.,  
*Wind Waves at Sea, Breakers and Surf.* Hydrographic Office, US Navy, Washington, DC. 1947.

17. Vine and Volkmann.  
*Woods Hole Oceanographic Institution.* 1950.

18. Weather Bureau,  
US Navy Hydrographic Office.  
*Climatological and Oceanographic Atlas for Mariners.* Vol. 1, North Atlantic Ocean, US Government Printing Office, Washington, 1959.

19. Dinger, J.E.,  
*Spectra of Ocean Waves and Microseisms as Related to Storm at Sea.* NRL Report 5804, US Navy Research Laboratory, Washington, DC., 1962.

20. Neumann, G.,  
Pierson, W.J., Jr  
*Principles of Oceanography.* Prentice-Hall, Englewood Cliffs, NJ., 1966.

21. Seiwell, H.R.,  
Wadsworth G.P.,  
*A New Development in Ocean Wave Research.* Science, Vol. 109, 1949, pp. 271-274.

22. Seiwell, H.R.  
*The Principles of Time Series Analysis Applied to Ocean Wave Data.* Proceedings, National Academy of Sciences (USA), Vol. 35, 1949, p. 518.

## APPENDIX

## Distance Rate of Change of Ocean Wavelength in Swell

From Neumann and Pierson (p. 280 of Reference 20), the relationship between wavelength  $L$  and wave frequency  $f$  is given by

$$L = \frac{g}{2\pi f^2} . \quad (A1)$$

where  $g$  is the acceleration of gravity. The group velocity  $v_g$  of deep water waves is given by

$$v_g = \frac{1}{2} Lf . \quad (A2)$$

The distance  $D$  travelled by a group of waves is

$$D = v_g t . \quad (A3)$$

where  $t$  is the time. Substituting (A1) and (A2) into (A3), to eliminate  $f$  and  $v_g$ , and differentiating, holding  $t$  constant, gives

$$\left( \frac{\partial L}{\partial D} \right)_t = \frac{2L}{D} . \quad (A4)$$

Substituting (A1) and (A2) into (A3), to eliminate  $L$  and  $v_g$ , and differentiating, holding  $D$  constant, gives

$$\left( \frac{\partial f}{\partial t} \right)_D = \frac{g}{4\pi D} . \quad (A5)$$

Thus, from (A4) and (A5),

$$\left( \frac{\partial L}{\partial D} \right)_t = \frac{8\pi L}{g} \left( \frac{\partial f}{\partial t} \right)_D . \quad (A6)$$

For  $L = 150 \text{ m}$ ,  $g = 9.8 \text{ m sec}^{-2}$  and  $(\partial f / \partial t)_D = 0.040 \text{ Hz per 3 days} = 1.5 \times 10^{-7} \text{ Hz sec}^{-1}$ ,  $(\partial L / \partial D)_t = 5.7 \times 10^{-5} = 5.7 \text{ m}/100 \text{ km}$ .

TABLE I

Results for a given frequency on a ridge of the interference patterns shown in Figures 3 and 4.

	Fig. 3	Fig. 4, A	Fig. 4, B	Fig. 4, C
$f$ (MHz)	35.0	28.0	27.7	30.5
Apparent range, $r'$ (km)	2800	2375	2550	2650
$n = f/\Delta_f$ , 10% error	11	12	21	41
$L \cos \kappa$ (m), 10% error	47	64	114	202
$h'$ (km)	320	310	305	320
$\kappa$ (deg)	7	10	8	8
$D$ (km)	2670	2240	2420	2520
$L$ (m), 10% error	47	65	115	204
$\frac{dL}{dD} \approx \frac{d(L \cos \kappa)}{dr'}$ (m/100 km), 10% error	-2.8	2.2	-6.6	-6.6

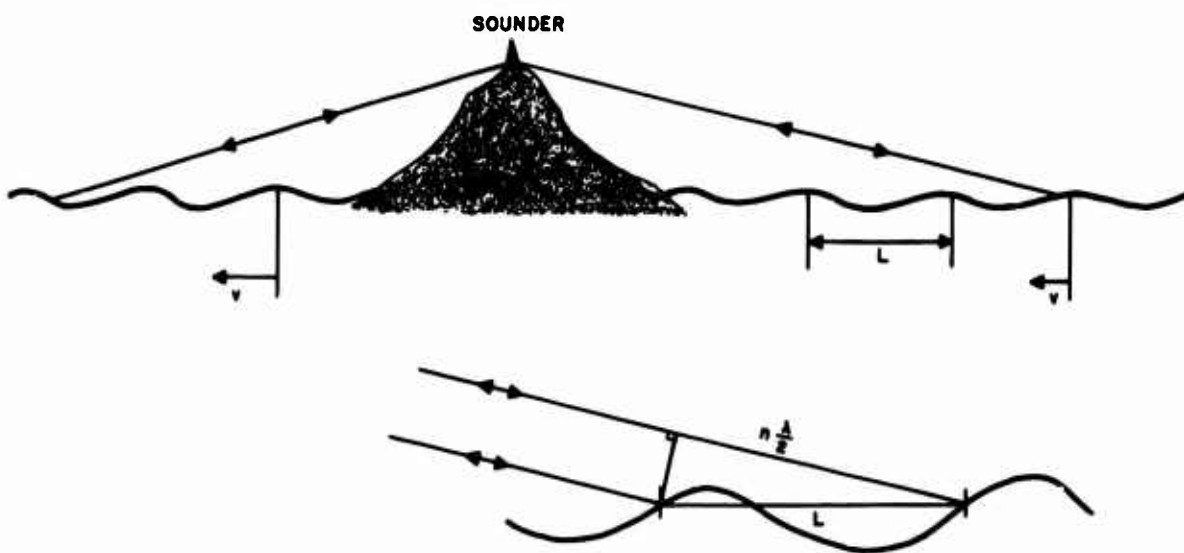


Fig. 1. Coherent backscatter of radio waves of wavelength  $\lambda$  from ocean waves of wavelength  $L$ . The transmitter and receiver are located on an island and the backscatter is occurring from waves moving with velocity  $v$  toward and away from the sounder

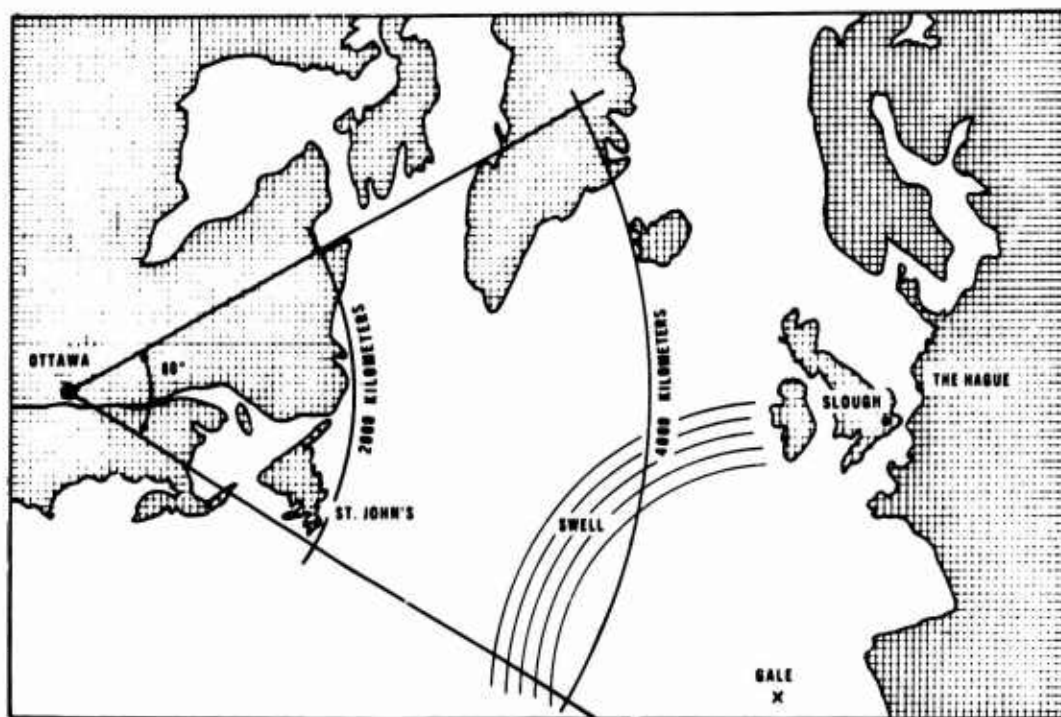


Fig. 2. Gnomonic-projection map, showing area of North Atlantic where most of the backscatter observed on the Ottawa oblique-incidence ionograms probably occurs

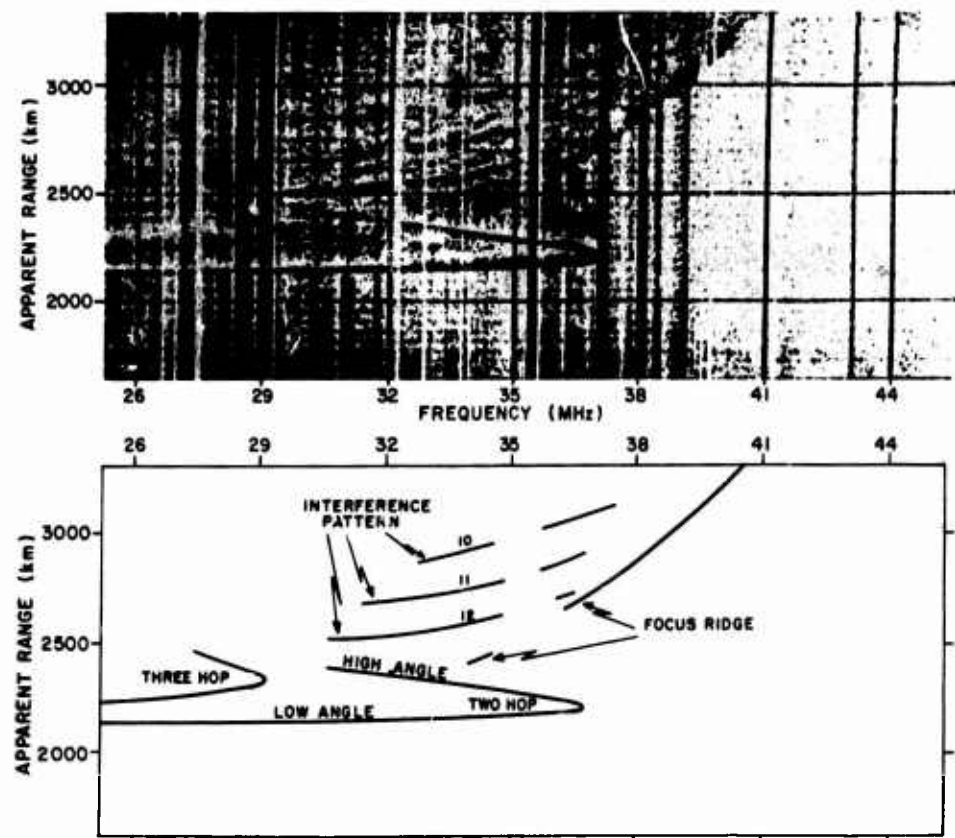


Fig. 3. Oblique-incidence ionogram, recorded at Ottawa on January 25, 1958, at about 1700 GMT, showing two-hop and three-hop traces, backscatter focus ridge, and interference ridges

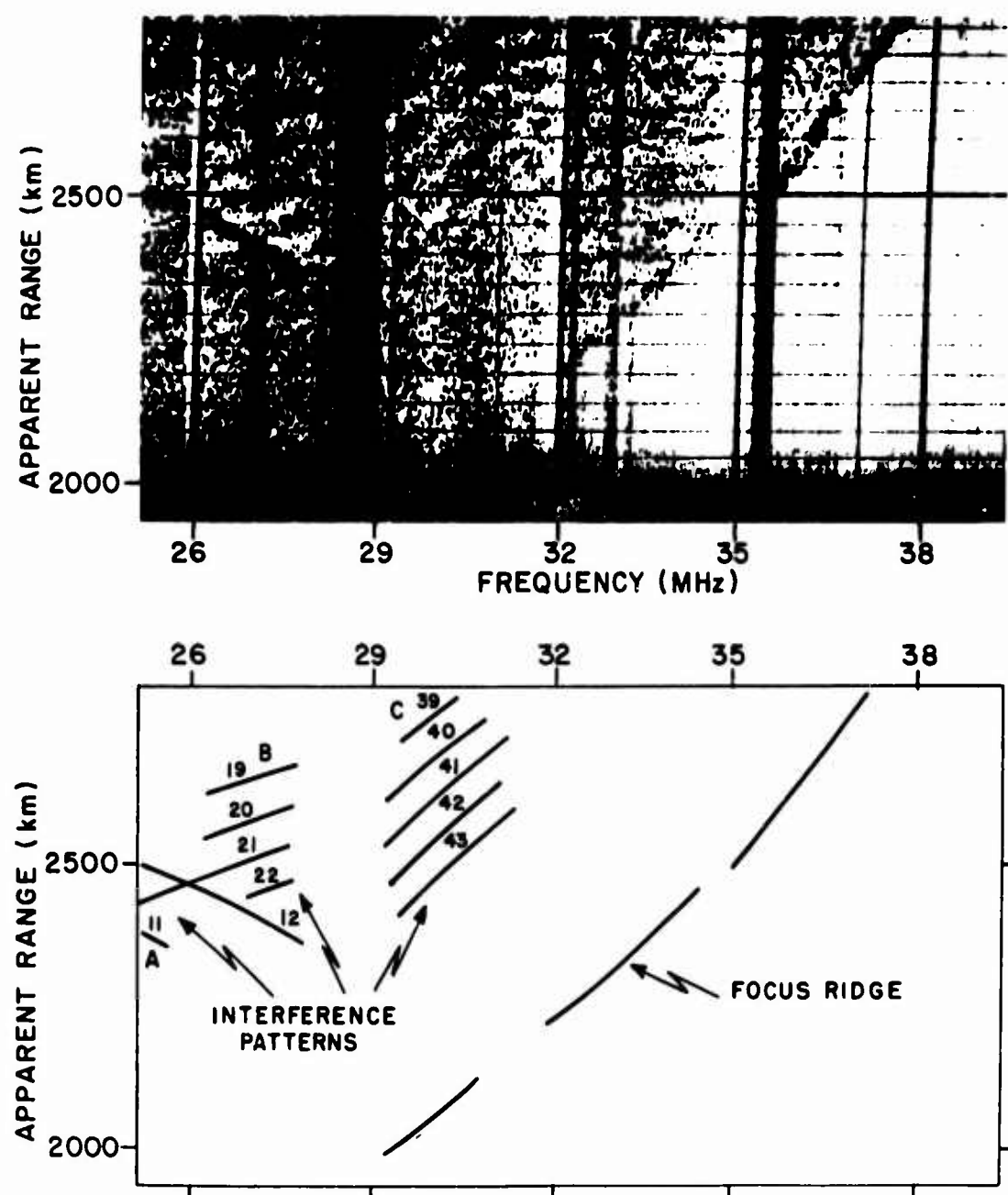


Fig. 4. Oblique-incidence ionogram recorded at Ottawa on January 11, 1958, at about 2000 GMT, showing focus ridge and three sets of interference ridges

**SOME CHARACTERISTICS OF GROUND  
SIDE-SCATTER AT 20 MHz**

by

**D. W. Rice**

Radio Physics Laboratory  
Defence Research Telecommunications Establishment  
Ottawa, Canada

## SUMMARY

Observations were made at Ottawa of the time delay, horizontal angle of arrival, and amplitude of 20 MHz WWV time standard transmissions from Washington. These observations are interpreted in terms of two-hop propagation over a non-great-circle path, with scatter occurring from the ground beyond the transmitter and receiver one-hop skip distances. Due to the relatively small transmitter-receiver separation (710 km), these skip focusing regions nearly coincide. The observed signals arrive over an azimuthal range of  $270^{\circ}$  or more, with transit times 10 to 20 milliseconds in excess of that expected for great-circle propagation (3 milliseconds). It is often observed that time delay dispersion adds additional cycles to the transmitted one second "ticks", which are 5 cycles of 1 kHz tone. It is shown that this extension in time of the modulation is due to scattering from two or more areas simultaneously, rather than from one extended area.

## SOME CHARACTERISTICS OF GROUND SIDE-SCATTER AT 20 MHz

D. W. Rice

### 1. INTRODUCTION

It has long been recognized that radio waves propagated via one or more ionospheric reflections do not always travel from transmitter to receiver along the great-circle path. These non-great-circle modes of propagation may manifest themselves in various ways; for example, signals may be received from a transmitter located within the receiver skip zone<sup>1</sup>, with time delays in excess of that expected<sup>2</sup>, and from directions other than the great circle direction to the transmitter<sup>3</sup>.

While early workers agreed that these anomalous signals were due to propagation over unusually long paths, the nature of these paths and the reasons for them remained in dispute for some time. Explanations usually involved one or more ionospheric reflections, combined with scattering either at the ground or in the ionosphere<sup>2,4,5</sup>. Our present understanding is that either of these may occur, depending upon path geometry and the current ionospheric conditions<sup>6,7</sup>.

Figure 1 illustrates the situation of interest here, in which signals are received by way of scattering from an area on the ground. This ground side-scatter mode, as it is called, results from propagation to, and scatter from, a region at or beyond the skip distances from both the transmitter and the receiver<sup>7,8</sup>. Because of skip distance focusing, the strongest signals are scattered from regions where the skip distances intersect.

### 2. EXPERIMENTAL EQUIPMENT AND PROCEDURE

Ground side-scatter signals at 20 MHz originating from WWV at Washington, DC, were recorded at Ottawa, Canada, a great-circle distance of 710 km. The transmitting antenna was omni-directional. The receiving antenna was a three-element Yagi rotated in a horizontal plane at one revolution per minute, thus providing an indication of the azimuthal direction of signal arrival.

Due to severe fading of the 20 MHz signal, the amplitude versus azimuth data was averaged over 15-minute intervals in order to obtain representative results. The analysis procedure was to scale the original strip-chart records and then enter these data into a computer along with receiver calibration data. The subsequent computer processing included conversion of the experimental data to decibels relative to 1  $\mu$ V at the receiver input, averaging of the corrected data, computation of the root-mean-square deviations of the averages, and output of the data in graphical and tabulated form.

The 5 MHz WWV signal was also recorded, so that the time delay between the arrival of the 5 and 20 MHz signals could be determined. A local frequency standard was used to trigger an oscilloscope display of the 1-second "ticks" (which are 5 cycles of 1 kHz tone) that modulate the 5 and 20 MHz transmissions. The oscilloscope display was then photographed.

### 3. TIME DELAY AND SIGNAL AMPLITUDE RESULTS

Figure 2(a) shows the results of a series of measurements made on March 8, 1966. These results are typical of those obtained on 14 magnetically quiet (planetary magnetic index  $K_p < 4$ ) days during February, March and November, 1966. Shown is a series of graphs of signal strength versus azimuth, the signal strength being indicated in decibels relative to a reference level of  $1 \mu\text{V}$  across 50 ohms at the receiver input. The signal strength in the direction of signal maximum is in the range 5 to 20 dB above the reference level. This is 45 to 60 dB below the free-space propagation value for the great-circle propagation-path distance, or 30 to 45 dB below the free-space value for a distance equal to the side-scatter path length.

The graphs of Figure 2(a) may be compared with Figure 2(b), which shows the measured receiving antenna pattern. It is evident that, during most of the day, the signals arrive from a range of azimuths much greater than the  $60^\circ$  beamwidth of the antenna. Signal amplitude is a minimum to the north, where the skip zones retreat to great distances because of the lower ionization density normally found in this direction. In contrast, near sunrise (1200 - 15 GMT) scattering tends to be more concentrated towards the south-east where ionization is highest and at sunset (2330 - 45 GMT) the last signals received are scattered from the south-west. During the night, the ionization density remained too low to support a detectable side-scatter signal.

Each polar diagram in Figure 2(a) is an average of 15 azimuth scans of the antenna; the r.m.s. deviations of the measurements from their averages is noted on each diagram. These r.m.s. deviations are in the range 3 to 4 dB. Also noted on each of the diagrams (except for two in which relative time delay was not measured) are the observed average time delays between the initial arrivals of the 5 and 20 MHz signals. These time delays are in the range 14 to 16.5 milliseconds. As the one-hop great-circle propagation time from Washington to Ottawa is 3 milliseconds (assuming that the 5 MHz signal propagates along the great circle), the 20 MHz signal has a total transit time of 17 to 19.5 milliseconds.

If the side-scatter mode depicted in Figure 1 is assumed, then the measured propagation time may be used to locate a scattering point on an ellipse about the transmitter-receiver axis. (This ellipse is nearly circular in the present case.) If it is further assumed that all signals are received via the antenna main lobe, then the azimuth of the antenna at the instant of reception may be taken as a rough indication of the direction to the scattering point. Figure 3 shows individual scattering points located in this manner, for a 12-minute period near local noon. While the location in azimuth of an individual point has considerable uncertainty, the distribution of the points is a good indicator of the location of the scattering areas. This is because points could be located only when the signal was sufficiently above the noise level, so that there are more points in the directions of the stronger signals.

Figure 3 also indicates the transmitter and receiver skip zones computed on the basis of ionospheric predictions. Such predictions are based on average conditions for a given month, time of day, and sunspot number; ionosonde data taken at seven North American stations showed that the actual F-layer critical frequencies were on the average 10% lower than the predicted values. If this were uniformly true over the entire relevant area, the skip zones would be increased in distance by about 600 km. This would improve the agreement with the locations of the scattering points, particularly to the south-west. Taking this into account, the agreement between the computed skip zones and the measured scattering areas is quite good for the latitudes south of Ottawa. Those points appearing to the north and north-west are believed to be due to reception of signals by the back lobe of the antenna; the relatively small amplitudes of these signals correspond to those expected from the back lobe.

Since the skip zone computations are based on average conditions, the zones at a given time are likely to depart in detail from that shown. In particular, they may intersect

at points other than the two indicated. The areas of such crossings would be preferred for scattering because the signal is doubly focused there.

#### 4. TIME DELAY DISPERSION

Important information regarding the number and extent of ground scattering areas can be obtained from the observed time delay dispersion of the signals. The 1-second "ticks" of the 20 MHz signal often appear to have more than 5 cycles. Some examples of this phenomenon are shown in Figure 4, which shows successive 1-second ticks for both 5 and 20 MHz signals. It will be shown that this extra modulation is likely due to scattering from two or more well separated areas providing different path lengths, and not due to a single extended scattering region, as might at first be thought.

Consider the geometry shown in Figure 5. For simplicity, the transmitter and receiver are both considered to be located at the origin. As with a conventional backscatter radar, power is returned to the receiver after scattering from the distant ground area, with the greatest signal power being received from just beyond the skip distance because of skip-distance focusing<sup>9</sup>. Assuming plane earth geometry, the power incident on ground area  $dA$  is

$$dP_1 = \frac{P_T G_T dA \sin \delta}{4\pi r^2} \quad (1)$$

and, assuming that the incident power is scattered into a hemisphere, the portion of the scattered power received back at the receiver is

$$dP_{rec} = \frac{\rho dP_1}{2\pi r^2} \frac{G_R \lambda^2}{4\pi} \quad (2)$$

where, in Equations (1) and (2),

$P_T$  = transmitted power

$G_T$  = transmitting antenna gain

$\delta$  = elevation angle of the radiation incident on the ground

$r$  = effective path length from the transmitter-receiver combination to the scattering area

$\rho$  = apparent ground reflection coefficient, which includes the effects of ionospheric focusing

$G_R$  = receiving antenna gain

$G_R \lambda^2 / 4\pi$  = effective area of the receiving antenna.

Substituting Equation (1) and the equations

$$\sin \delta = \frac{2h}{r}$$

$$dA = x dx d\phi$$

$$x dx = r dr$$

into Equation (2) and integrating with respect to  $\phi$ , one obtains

$$dP_{rec} = \frac{\rho K P_T dr}{r^4} \quad (3)$$

where  $\int d\phi = \pi/3$  for the antenna used, and

$$K = \frac{G_T G_R \lambda^2 h}{48\pi^2}.$$

The apparent ground reflection coefficient  $\rho$  is a complicated function of the nature of the ground, the angle of incidence, the polarization, and ionospheric focusing. As a first approximation, assume that skip-distance focusing is the only significant source of variation, and that the variable  $\rho$  has the form

$$\rho = \begin{cases} 0, & \text{for } r < r_0 \\ \rho_0 \exp - \left[ \frac{r - r_0}{L} \right] & \text{for } r > r_0. \end{cases} \quad (4)$$

where  $r_0$  is the effective path length to the skip distance, and  $\rho_0$  is the reflection coefficient at the skip distance.  $L$  is the "scattering length", the distance in which the scattered power decreases by the factor  $e$ . It is also necessary to specify the transmitted power  $P_T$  as a function of time and space. The modulation waveform of WWV in the vicinity of the 1-second "ticks" may be described as

$$P_T = \begin{cases} P_0 & \text{for } t - \frac{2r}{c} \leq 0 \\ P_0 \left[ 1 + \sin w_m \left( t - \frac{2r}{c} \right) \right]^2 & \text{for } 0 < t - \frac{2r}{c} < 0.005 \\ P_0 & \text{for } t - \frac{2r}{c} \geq 0.005, \end{cases} \quad (5)$$

where  $w_m$  is the modulation angular frequency, i.e.  $w_m/2 = 1$  kHz, and  $P_0$  is a constant.

Assuming incoherent scatter, the total power received is the integral of Equation (3) over all ranges from the skip distance to infinity, with  $\rho$  and  $P_T$  as given by Equations (4) and (5) respectively,

$$P_{rec} = K \rho_0 \int_{r_0}^{\infty} P_T \frac{1}{r^4} \exp - \left[ \frac{r - r_0}{L} \right] dr. \quad (6)$$

The integral in Equation (6) was evaluated directly on a digital computer; Figure 6 shows some of the results. The computed modulation envelopes are for various values of the ratio  $L/\lambda_m$ , that is, the ratio of scattering length to modulation wavelength. The result for  $L/\lambda_m = 0.01$  corresponds very nearly to the result for a point scatterer (the 100% modulation of the transmitted signal is reproduced) whereas, for increasing scattering length, the modulation smears and the depth of modulation of the received signal decreases. A comparison of these results with the observed signals indicates a scattering length  $L$  of the order of one-tenth of the modulation wavelength ( $L \approx 30$  km). This is in reasonable agreement with detailed focusing calculations<sup>9</sup>.

A further computational result is shown in Figure 7, which shows the signal amplitude received from two scattering regions such that the two returns overlap. The different cases show the signal for different phases between the two signals in the region of overlap. The similarity between the calculations and the signals shown in Figure 4 is obvious. Due to the low signal-to-noise ratio of the recorded signals, it does not seem worthwhile to attempt a more detailed comparison.

These computational results indicate that returns from two or more scattering areas, at different ranges, are required in order to explain the observed time-delay dispersion. Although it is possible that two scattering areas could exist at nearly the same azimuth, it seems more likely that the scattering areas are well separated in azimuth, with large scale ionization gradients causing a variation of skip distance with azimuth. Thus some of the returns at a given instant are likely to be received well off the axis of the main lobe or by the back lobe of the antenna. The observational effect could be quite different if an antenna with more azimuthal discrimination were used.

### 5. CONCLUDING REMARKS

Differences in the propagation delays of 5 and 20 MHz transmissions over a 710 km path, together with direction-of-arrival measurements of the higher-frequency signal, are found to be consistent with a model of ground side-scatter of the 20 MHz signal from just beyond the one-hop skip distance. The observed time-delay dispersion indicates that scattering often occurs from two or more areas simultaneously. This is a consequence of the near coincidence of the transmitter and receiver skip zones because of the relatively small transmitter-receiver separation.

While the relatively low signal levels and the time-delay dispersion are limitations insofar as communications use of side-scatter is concerned, side-scatter may provide an attractive alternative in some instances. It could be used to extend the period of time each day when a given frequency may be utilized, providing the necessary adjustments in antenna orientations are made. It could also be used to provide HF communications around areas of ionospheric disturbance, such as the auroral zones, or areas of nuclear detonation. The exploitation of side-scatter in situations such as these could lead to an increase in the overall reliability of HF communications.

## REFERENCES

1. Taylor, A.H. *Relation Between the Height of the Kennelly-Heaviside Layer and High Frequency Radio Transmission Phenomena.* Proceedings, Institute of Radio Engineers (USA), Vol. 14, 1926, p. 521.
2. Taylor A.H. Young, L.C. *Studies of High Frequency Radio Wave Propagation.* Proceedings, Institute of Radio Engineers (USA), Vol. 16, 1928, p. 561.
3. Friis, H.T. *Oscillographic Observations on the Direction of Propagation and Fading of Short Waves.* Proceedings, Institute of Radio Engineers (USA), Vol. 16, 1928, p. 658..
4. Hoag, J.B. Andrew, V.J. *A Study of Short-Time Multiple Signals.* Proceedings, Institute Radio Engineers (USA), Vol. 16, 1928, p. 1368.
5. Eckersley, T.L. *Studies in Radio Transmission.* Journal of Institution of Electrical Engineers (GB), Vol. 71, 1932, p. 405.
6. Feldman, C.B. *Deviations of Short Radio Waves from the London - New York Great Circle Path.* Proceedings, Institute of Radio Engineers (USA), Vol. 27, 1939, p. 635.
7. Hagg, E.L. Rolfe, W. *A Study of Transatlantic Radio Propagation Modes at 41.5 Mc/s.* Canadian Journal of Physics, Vol. 41, 1963, p. 220.
8. Silberstein R. Dickson, F.H. *Great-Circle and Deviated-Path Observations on CW Signals Using a Simple Technique.* Institute of Electrical and Electronic Engineers, Transactions, Antennas and Propagation (USA), Vol. AP-13, 1965, p. 52.
9. Warren, E. Muldrew, D. *A Method for Computing Ionospheric Focusing of Radio Waves, Using Vertical Incidence Ionograms.* Institute of Radio Engineers, Transactions, Antennas and Propagation, Vol. AP-9, 1961, p. 403.

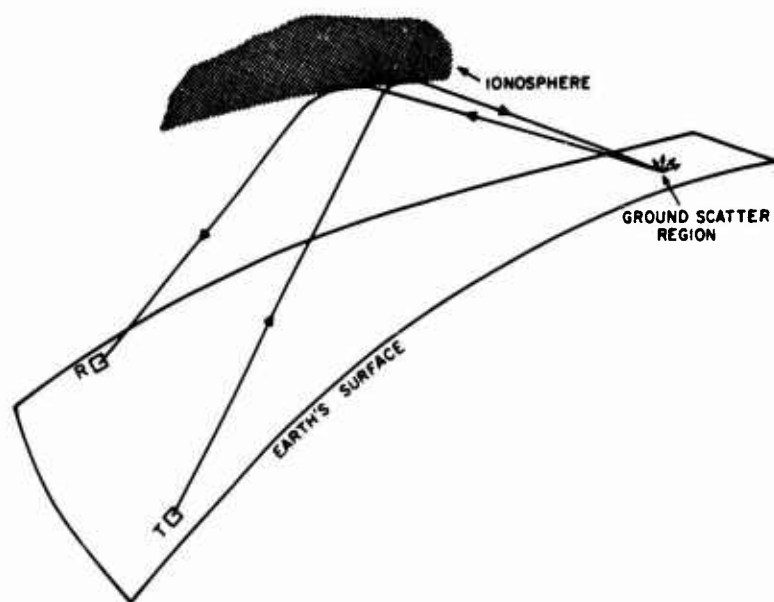
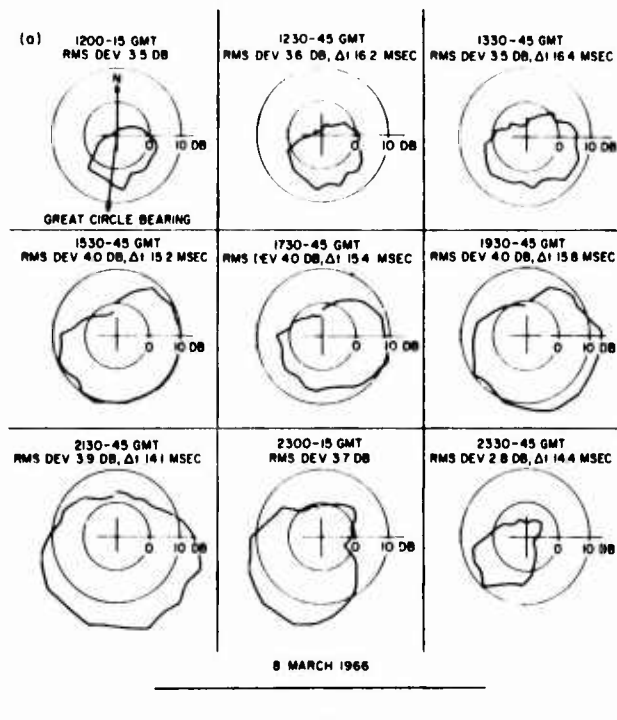


Fig.1 Pictorial representation of propagation from T to R via ground side-scatter



(b)

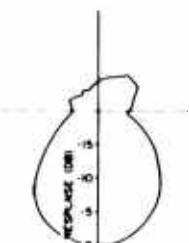


Fig.2(a) Polar plots of averaged signal strength versus azimuth. The root-mean-square deviation of the experimental points from the average is indicated.  $\Delta t$  is the average time delay between the reception of the 5 and 20 MHz signals  
 (b) 20 MHz horizontal antenna pattern, as measured at  $10^{\circ}$  elevation angle. This antenna was rotated at 1 revolution per minute

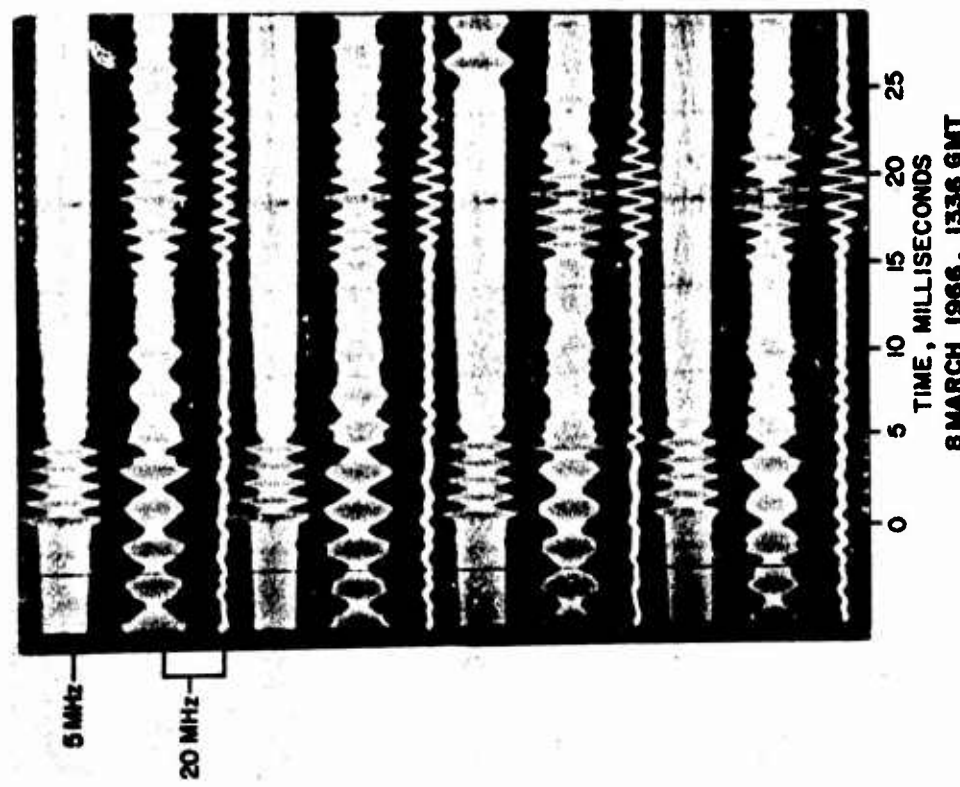


Fig. 4 Photograph of an oscilloscope display of the receiver IF output for the 5 and 20 MHz signals, and the detected 20 MHz signal. The time scale origin is arbitrary. The 5 MHz "ticks" appear between 0 and 5 milliseconds; the 20 MHz ticks begin at 15 milliseconds. Note the extra cycles on the 2C MHz signal

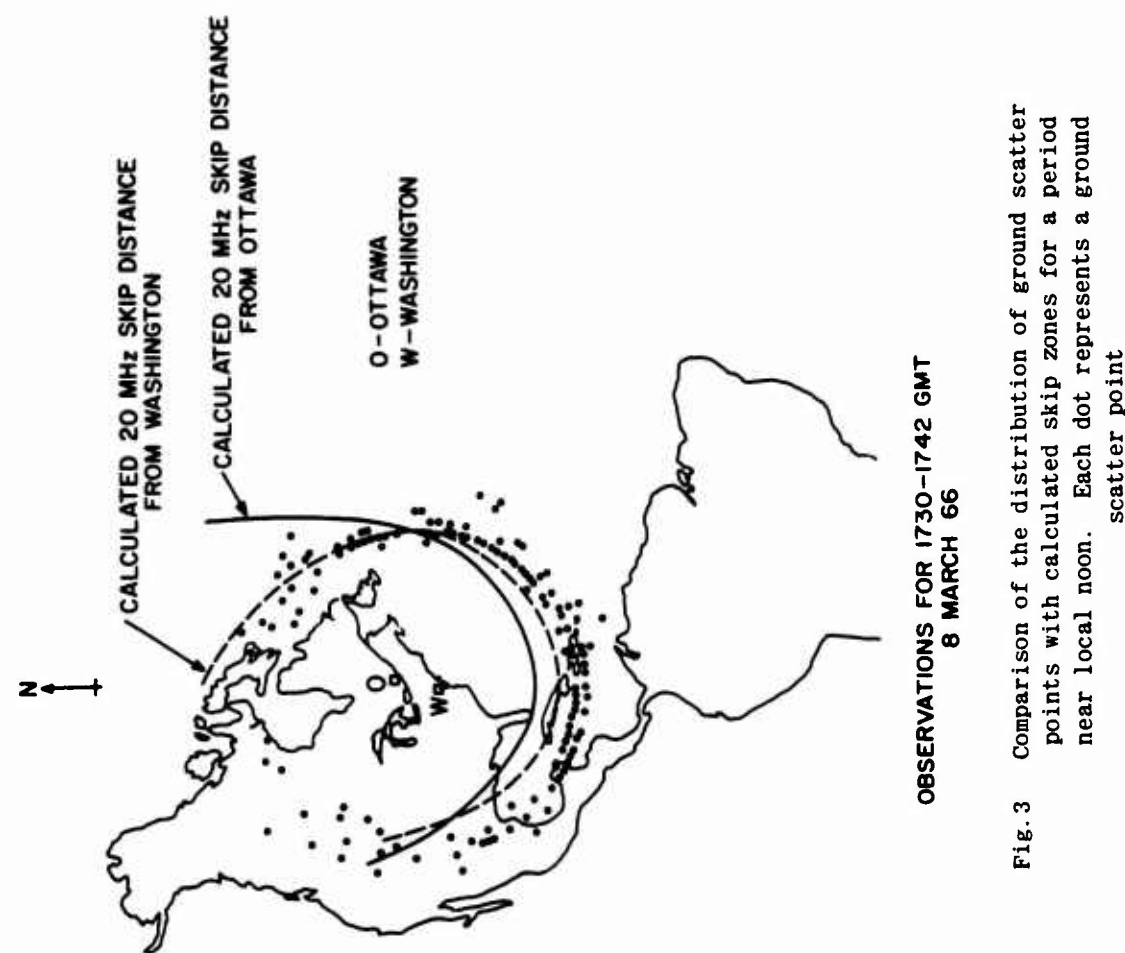


Fig. 3 Comparison of the distribution of ground scatter points with calculated skip zones for a period near local noon. Each dot represents a ground scatter point

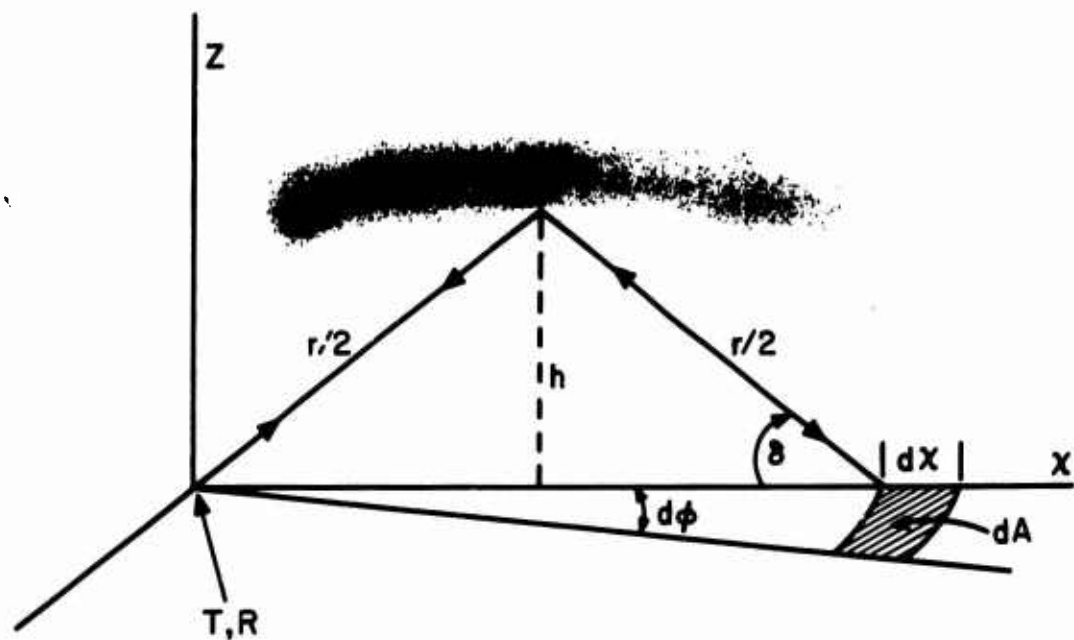


Fig. 5 Geometry assumed for calculation of side-scattered signal modulation envelope

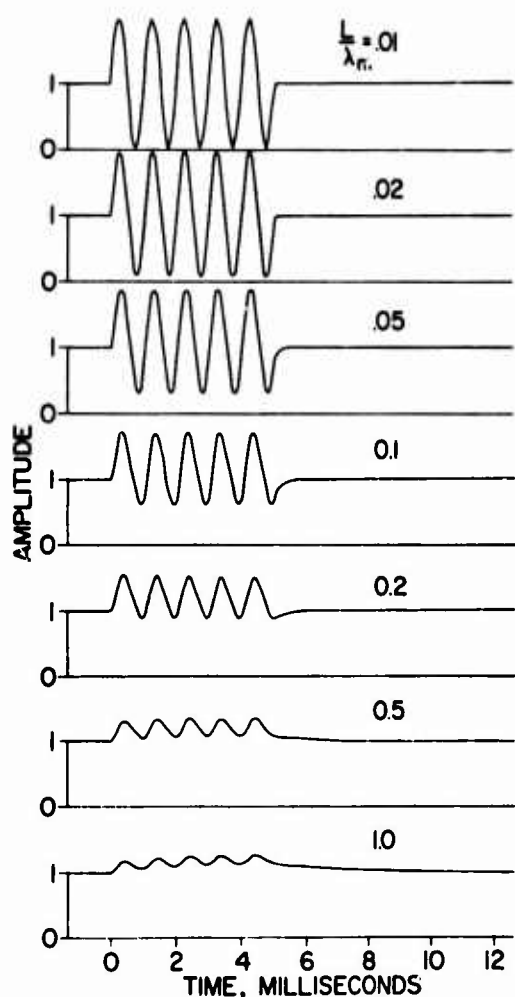


Fig. 6 Computed modulation envelopes for various ratios of scattering length to modulation wavelength  $L/\lambda$ . (Only one-half of the modulation envelope is shown)

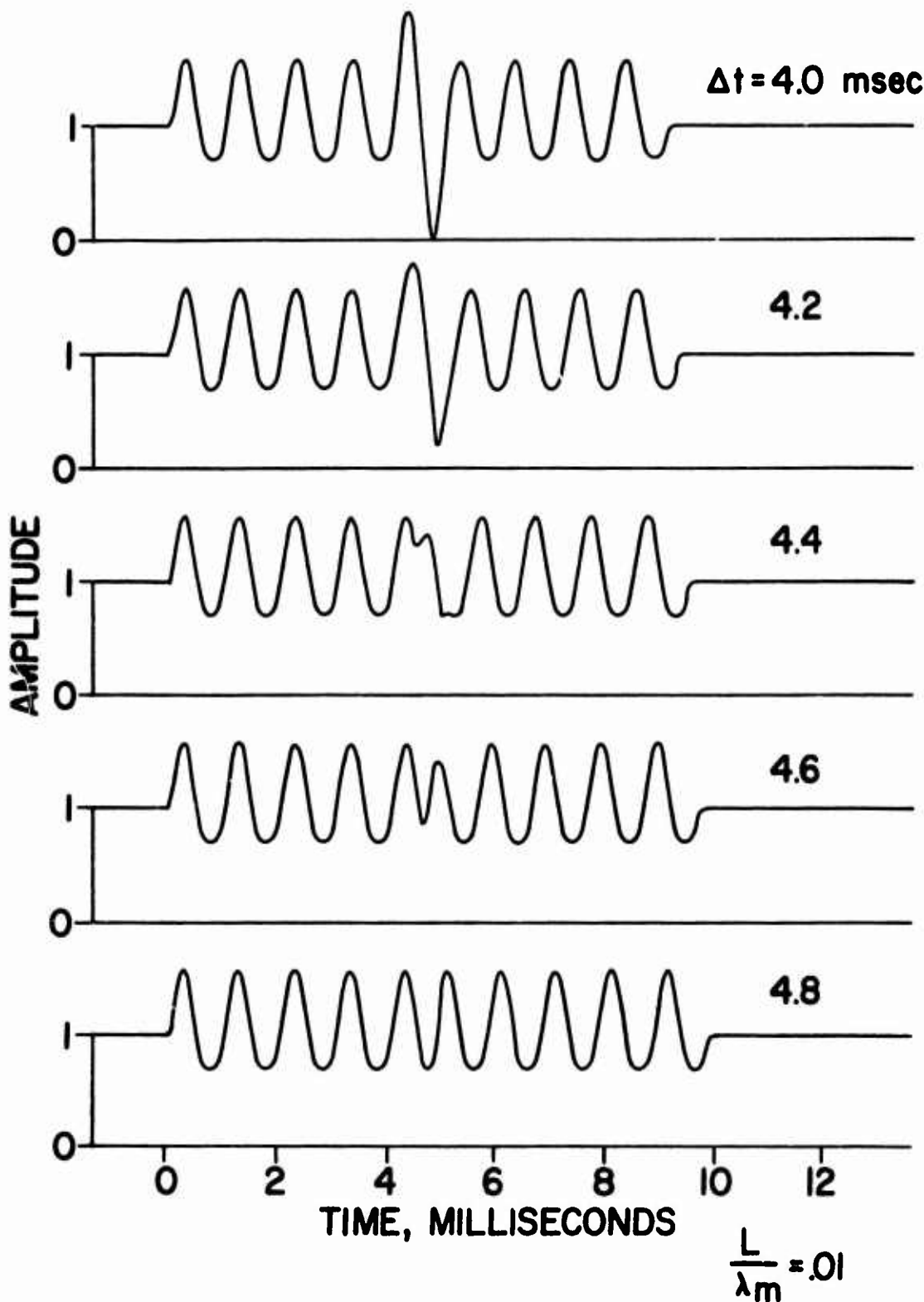


Fig. 7 Computed modulation envelopes for the resultant of two scattered returns which overlap.  $\Delta t$  is the difference between the arrival times of the two signals

FADING AMPLITUDE DUE TO INTERFERENCE FROM  
FORWARD SEA SCATTER

by

G. C. Rider, B.Sc.

The Marconi Company Limited,  
Research Laboratories,  
Great Baddow, Essex,  
England.

## SUMMARY

In most cases of oversea propagation in the visual range the interfering effect of energy reflected and scattered from the sea surface has to be taken into account. The effect is of most importance when the sea is fully illuminated by the transmitting beam, either because the aerial beamwidth is wide, or because small grazing angles make discrimination against reflected energy impossible for even a high gain aerial.

In this paper the energy from the sea surface is assumed to be composed of a coherent reflected ray and incoherent scattered energy having a Rayleigh amplitude distribution. This model of the propagation is discussed in terms of the experimental and theoretical work of Beard and others, and curves are presented displaying simply the calculation of probability of fade depth.

Low level ground-to-air propagation tests are described on three frequencies, bracketing the UHF and SHF bands, and the fading amplitudes which were measured are shown to be in acceptable agreement with the model.

## FADING AMPLITUDE DUE TO INTERFERENCE FROM FORWARD SEA SCATTER

G.C. Rider

### 1. INTRODUCTION

A specification of the energy arriving at the receiver from the sea surface is required in most cases of oversea propagation in the visual range, and is of most importance when the sea surface is fully illuminated by the aerial beams, either because the beamwidths are wide or because small grazing angles make discrimination against reflected energy impossible even for high gain aerials.

This paper is concerned with the prediction or statistics of fade depth for a ground-to-air propagation path, the end product being a plot of signal strength probability versus range or time, of the form illustrated in Figure 1. A model of the propagation mechanism is first described and the fade depth calculations which arise from it are set out for straightforward calculation. Finally the results of some flight tests are presented and shown to be in accord with the theory.

### 2. THE MODEL

The scatter model is presented in the terminology of C.I. Beard<sup>1</sup>, since the experiments which he describes provide its most extensive validation, and his graphs are reproduced for use in computation. Other presentations, for example by Clarke<sup>2</sup>, lead to analogous conclusions.

It is usual to consider the fading within the visual range to be due to the interference between a direct ray and a sea-reflected ray, and the present model extends this treatment by introducing an additional vector. Thus the reflected ray is represented by two vectors, one with phase as for reflection in a smooth sea and amplitude dependent upon roughness and the other an incoherent or "noise" vector with random phase and with amplitude also dependent upon the roughness of the surface.

Referring to Figure 2,  $D$  is the direct or free space vector, used as unit reference for the fading calculation. The coherent reflected vector  $C$  is shown both theoretically and experimentally to be a function of the Rayleigh roughness parameter,  $h\psi/\lambda$ , where  $h$  is the r.m.s. deviation of the sea surface from its mean level and  $\psi$  is the grazing angle of reflection (in milliradians). Figure 3, due to Beard, shows this dependence. The ordinate is the coherent ray normalised with respect to its smooth sea value, that is, incident vector times smooth earth reflection coefficient  $D\rho$ .

The incoherent component is the vector sum of reflections from numerous small facets of the sea surface in the vicinity of the geometrical reflection point. The height relative to mean sea level, and also the inclination of these facets, is taken to vary in a random manner, giving numerous vectors in random phase and amplitude, and a Rayleigh amplitude distribution is assumed for the incoherent component, with random phase.

A Rayleigh amplitude distribution may be resolved into two orthogonal Gaussian distributions ( $I_x$ ,  $I_y$  in Figure 2) having equal standard deviations,  $\sigma = \sigma_x = \sigma_y$ , and zero mean. Beard<sup>3</sup> and Clarke<sup>2</sup> discuss this assumed equality,  $\sigma_x = \sigma_y$ , which is not

physically realised under all conditions, but the errors involved in making this assumption are small in practice compared with uncertainty with respect to  $h$ , and a Rayleigh amplitude distribution is assumed here for the vector  $I$ . The mean incoherent power is  $2\sigma^2$  and Figure 4 (also due to Beard) shows the dependence of  $\sigma$  upon the Raleigh roughness parameter  $h\psi/\lambda$ . As in Figure 3, the ordinate is normalised in terms of  $D\rho$ .

The points plotted in Figures 3 and 4 are from the experiments which Beard describes, which were made across the Golden Gate in California and between two drilling rigs in the Gulf of Mexico. The roughness parameter was varied by the use of two frequencies, in X and Q band, by variation in aerial height, and by natural variations in the sea state.

### 3. CALCULATION OF FADE STATISTICS

Figure 5 is a flow diagram for the calculation, with inputs  $h$ ,  $\psi$  and  $\lambda$ .  $h$  is obtained from sea measurement in an experiment, or from known sea state statistics in the prediction case; for example, Hogben and Lumb<sup>4</sup> have published extensive data for all the oceans.

The grazing angle  $\psi$  is obtained from the path geometry as a function of range or time as desired, taking into account the effect of earth curvature.

The roughness parameter  $h\psi/\lambda$  and the smooth sea reflection coefficient  $\rho$  are next found.  $\rho$  is the Fresnel reflection coefficient dependent upon  $\psi$ ,  $\lambda$ , polarisation, and the electrical constants of the sea. Graphs of values are available, for example Reference 5.  $D'$ , the divergence factor, and the correction to the flat-earth value of  $\psi$  to allow for earth curvature may be obtained from Millington<sup>6</sup>.

The quantities  $r_h$  and  $s_h$  may be termed "coherent" and "effective incoherent" ray amplitude. They are derived from Figures 3 and 4, being defined as

$$r_h = \frac{C}{D} \quad (1)$$

$$s_h = \frac{(\sqrt{2})\sigma}{D} \quad (2)$$

The total coherent amplitude has maximum values  $D + C$  and  $D - C$  ( $1 + r_h$  and  $1 - r_h$ , since  $D$  is considered as a unit reference vector).

Having determined the effect of the surface reflection on the vectors  $C$  and  $I$ , any effect of aerial misalignment may be included; it is shown as  $f(\theta)$  in Figure 5. It is convenient to retain  $D$  as a unit reference vector and multiply  $s_h$  and  $r_h$  by the appropriate factor to give  $s'_h$  and  $r'_h$ .

The coherent and incoherent components are next summed. Norton<sup>7</sup> has fully tabulated the summation of a constant vector with a vector of Rayleigh amplitude distribution, and the required level is immediately obtained from his curves in terms of the chosen probability and the parameter  $K$ , the ratio of incoherent to coherent power. For the peak to trough fading range calculation outlined in Figure 5, values of  $K$  are required at the maximum and minimum of the coherent fading pattern.

$$\text{Thus } K_{\max} = 20 \log_{10} \frac{s'_h}{1 + r'_h} \quad (3)$$

$$\text{and } K_{\min} = 20 \log_{10} \frac{s'_h}{1 - r'_h} \quad (4)$$

" $T_{\max}$ " and " $T_{\min}$ " on Figure 5 are thus the levels, relative to free space, exceeded at the peak of the coherent fading pattern with a probability of 5% and at the trough of the coherent pattern with a probability of 95%, and these values enable the fading envelope to be sketched adequately through the flight. These percentage values have been arbitrarily selected; it was thought that they would be appropriate for the method of record analysis described below. The final block in Figure 5, "peak to trough" fading, is included since this is the fading parameter obtained in the experiments to be described.

#### 4. PRACTICAL CALCULATION METHOD

$\psi$  is first determined in terms of range or time, using Reference 6 to correct the flat-earth value of  $\psi$  for earth curvature and to determine the divergence factor. Tables have been prepared by computer to give  $r_h$  and  $s_h$  from  $h$ ,  $\psi$  and  $\lambda$ . Nominal wavebands and coarse intervals of  $h$  are used in the tables, with  $\psi$  tabulated in  $0.1^\circ$  intervals. The effect of aerial polar diagrams, misalignments and divergence factor upon the relative strength of direct and reflected rays, is next introduced ( $f(\theta)$  in Figure 5) to modify  $r_h$  and  $s_h$ . Finally Figure 6 summarises the remainder of the calculation, giving a direct reading of peak-to-trough fading (95% to 5% levels).

#### 5. EXPERIMENTAL CONFIRMATION

##### 5.1 Test Configuration

Flying tests have been carried out using similar flight profiles on several frequencies at a coastal site. In each case the receiver and recording equipment was on a cliff-top site at a height of 220 ft, overlooking the sea. The transmitting equipment was airborne, the aircraft flying at 2000 ft above sea level and flying directly out to sea away from the receiver to a range of 15 to 20 miles. Tests were made at 400 MHz, and at 3 and 10 GHz, and although moderately high gain receiving aerials were used at the receiver the beamwidth, about  $12^\circ$  at the higher frequencies, was such that the sea and the aircraft were both fully illuminated. Very wide beam transmitting aerials were used.

Paper chart recordings of signal strength were made for each frequency, and Figure 7 shows four samples of S band recordings arranged in order of increasing sea roughness. The "peak-to-trough" fading parameter was obtained by noting the highest and lowest signal levels within a period covering 0.5 miles of flight centered upon the range giving the nominal value of  $\psi$  required. Ideally the recordings should be analysed to give the probability of definite high and low signal levels being exceeded, but this was not feasible with the rapidly changing value of  $\psi$  found in these tests. The sea state was observed on each occasion but no instrumental indication of sea state was available and the quality of the sea state data is not good.

##### 5.2 Experimental Results

For each waveband the expected peak to trough fading has been plotted against sea state for three selected values of grazing angle, and the observed fading at these  $\psi$  values is plotted, on the curves where possible, in Figures 8, 9, 10. This presentation allows computed and observed values to be compared without giving much weight to the observed sea state. On each calculated curve the observed points have been placed where their ordinate value is correct, in order to show what sea state is called for, theoretically, to give this value. The points on each curve are numbered in order of reported roughness, beginning with the smoothest reported sea state.

In the UHF case the predicted dependence on sea state is so slight that it may merely be noted that the points for those single runs which were classified clearly by sea state are in reasonable agreement with theory, whilst the range of values obtained for a number of other runs which were not clearly classified for sea state brackets the expected value

(Boxed point in Figure 8). The general values at S band (Fig. 9) are also reasonably close to expectation except for the two runs at the smallest grazing angle. The X band points fit the calculated curves best. The boxed points are median values for a number of runs with different instrumentation but with the same path geometry. It is of interest to note the maxima in the predicted fade curves (Fig. 9 and 10) for the smaller grazing angles. These occur at higher sea states for longer wavelengths. The smoothest sea is thus not necessarily a "worst case" for fade depth. In general the calculated values are high in each waveband. This is possibly because the method of reading the charts corresponded to the 90% to 10% fading range rather than to the 95% to 5% range. With this adjustment the general range of sea states indicated by fitting the points to the lines is much more self-consistent and covers the range of sea states over which the flights were made. It is clearly unprofitable to pursue the sea state data further without good instrumental observations, since the reported sea states have not led to success even in arranging the runs in order of fade depth. The boxed points on the X band curves (Fig. 10), which are more consistent in this respect, are each the median values of about a dozen flights grouped, for sea state, into smooth and not-smooth sea.

#### 6. CONCLUSION

If a tolerance of even a decibel is allowed on the individual measurements the agreement between observation and theory is quite acceptable and is better in the case of the higher frequency where the expected effect of sea roughness is greatest. The calculation outlined may thus be usefully employed to predict fading probability envelopes for propagation over a non-smooth sea.

#### ACKNOWLEDGEMENTS

Acknowledgement is made to the Ministry of Technology who supported this work and to the Director of Research, Marconi Company, for permission to publish this paper. Thanks finally to the very many colleagues involved in making these measurements.

## REFERENCES

1. Beard, C.I. *Coherent and Incoherent Scattering of Microwaves from the Ocean.* Institute of Radio Engineers, Transactions, AP-9, September 1961, p. 470.
2. Clarke, R.H. *Theoretical Characteristics of Radiation Reflected Obliquely from a Rough Conducting Surface.* Proceedings, Institution of Electrical Engineers, Vol. 110, January 1963, p. 91.
3. Beard, C.I. *Behaviour of Non-Rayleigh Statistics of Microwave Forward Scatter from a Random Water Surface.* Institute of Electrical and Electronic Engineers, Transactions, AP-15, No. 5, September 1967, p. 649.
4. Hogben, N. Lumb, F.E. *Ocean Wave Statistics.* H.M. Stationery Office, 1967.
5. *Atlas of Radio Wave Propagation Curves for Frequencies between 30 and 10,000 Mc/s.* Radio Research Laboratory, Ministry of Postal Services, Tokyo, 1957.
6. Millington, G. *Curved Earth Geometrical Optics.* Marconi Review, No. 80 Jan/Mar. 1946, p. 1.
7. Norton, K.A. et al. *The Probability Distribution of the Amplitude of a Constant Vector plus a Rayleigh Distributed Vector.* Proceedings, Institute of Radio Engineers, Vol. 43, October 1955, p. 1354.

10-6

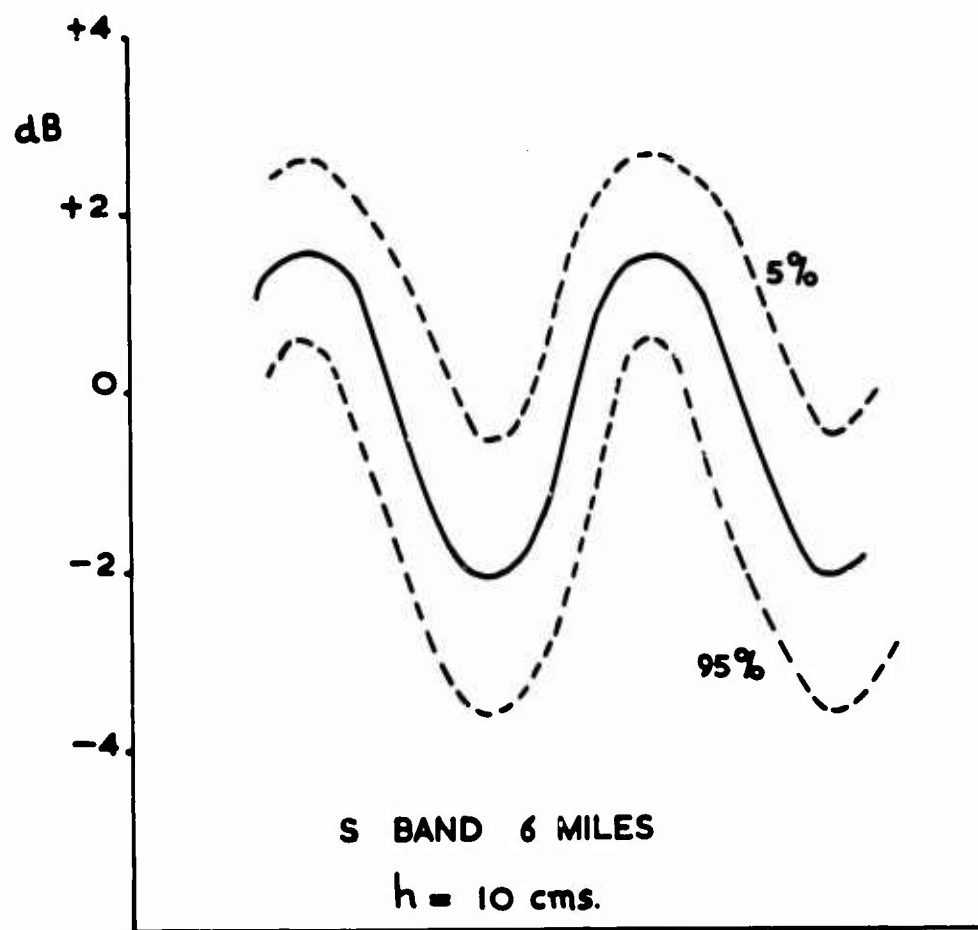


Fig. 1 Predicted fading structure

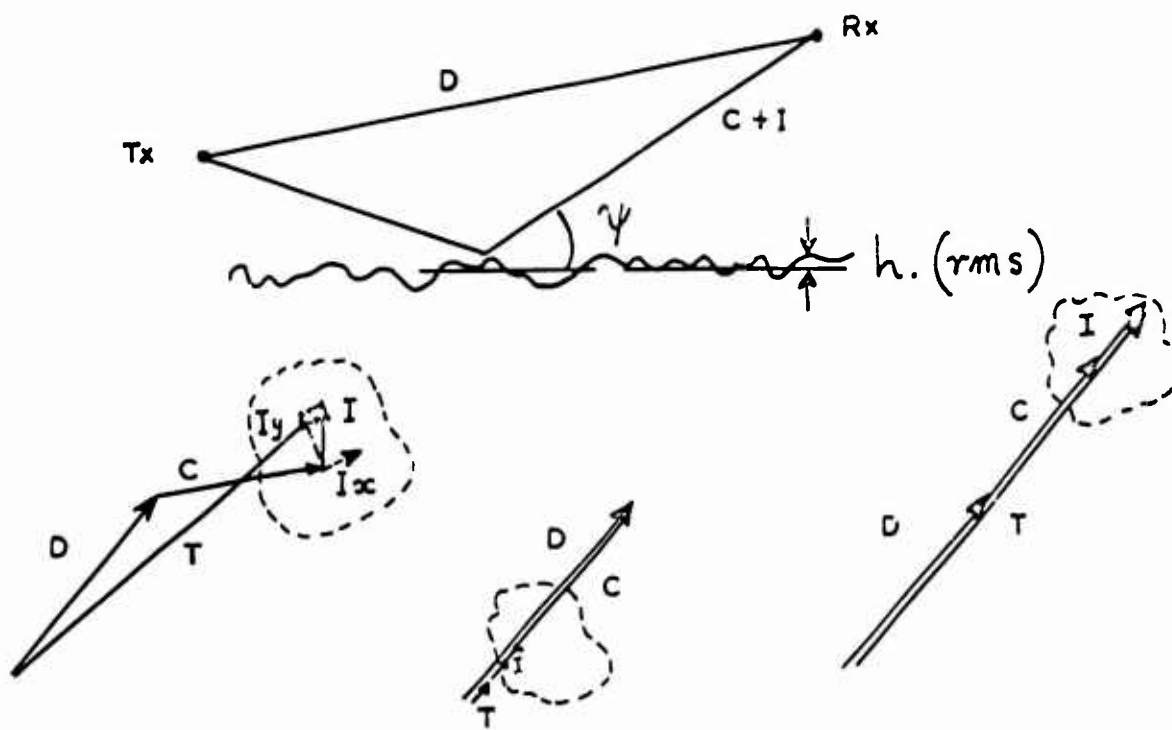


Fig. 2 Symbols used and vector diagrams

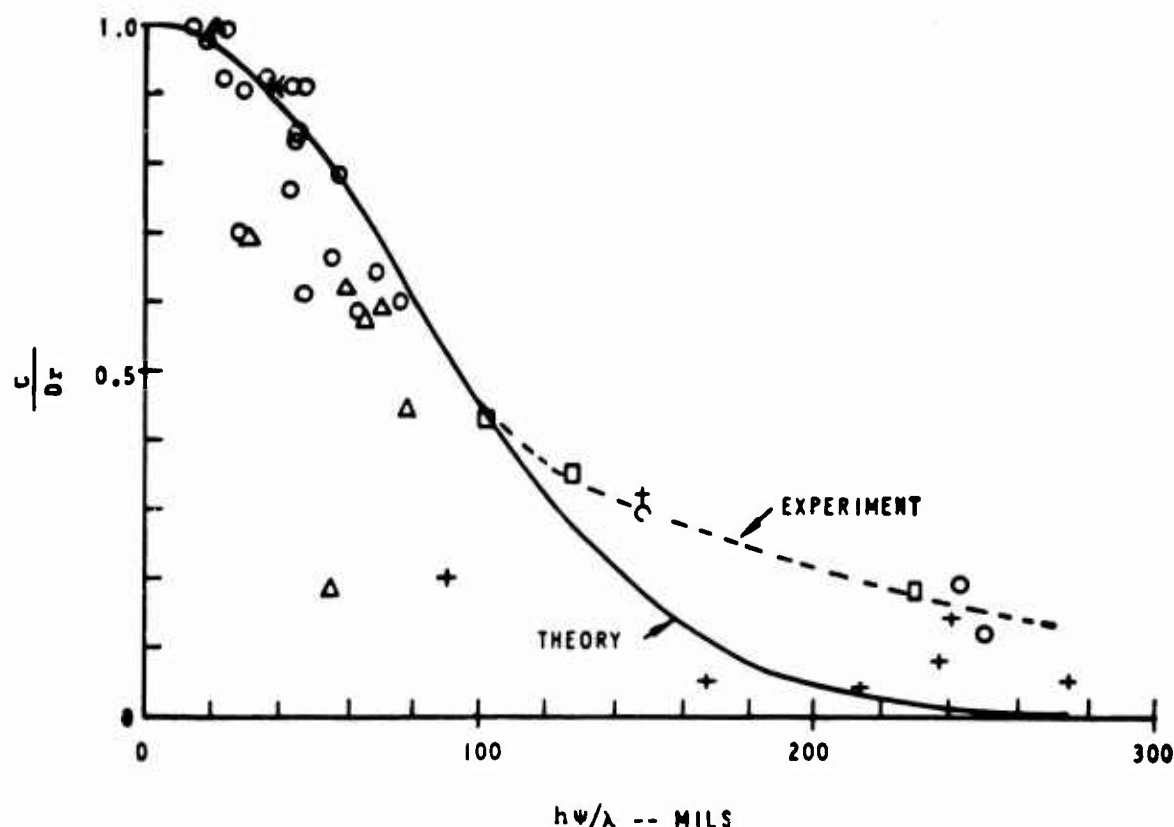
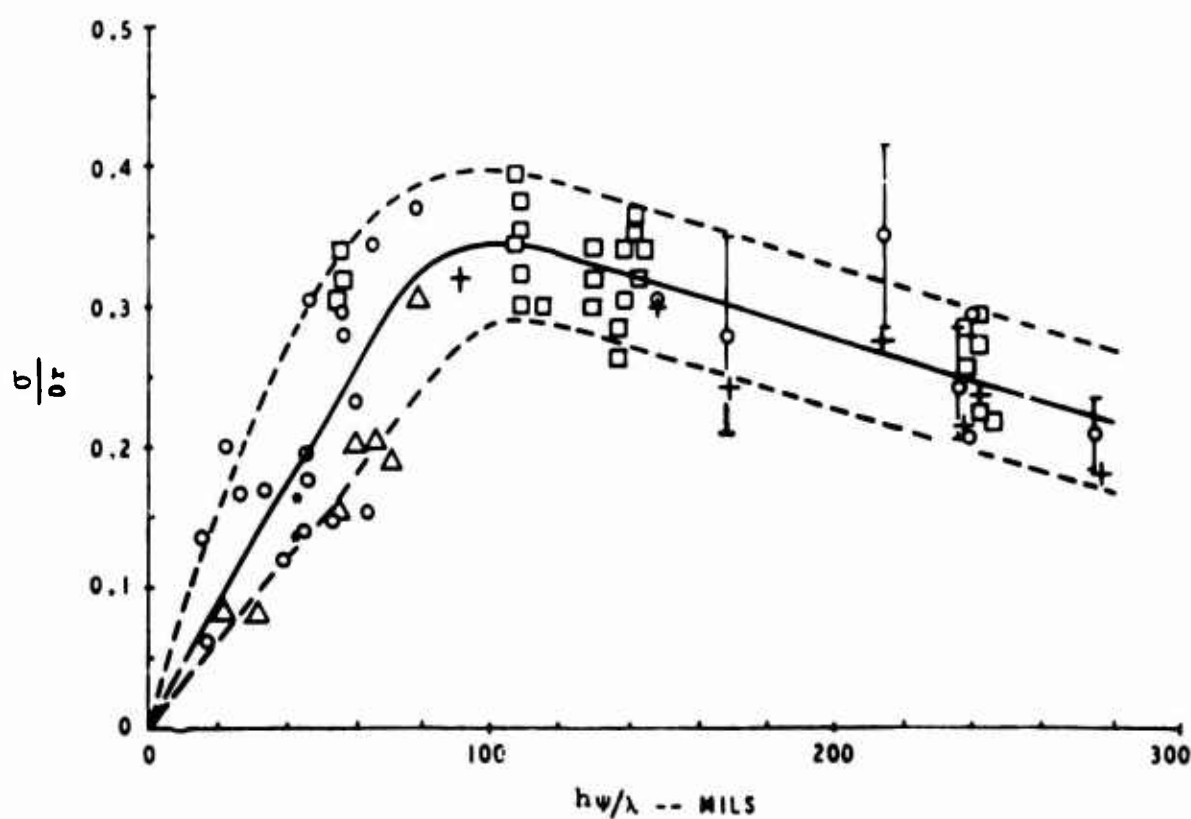


Fig. 3 Coherent field versus apparent ocean roughness

Fig. 4 Incoherent field versus apparent ocean roughness. Incoherent power =  $2\sigma^2$ .

10-8

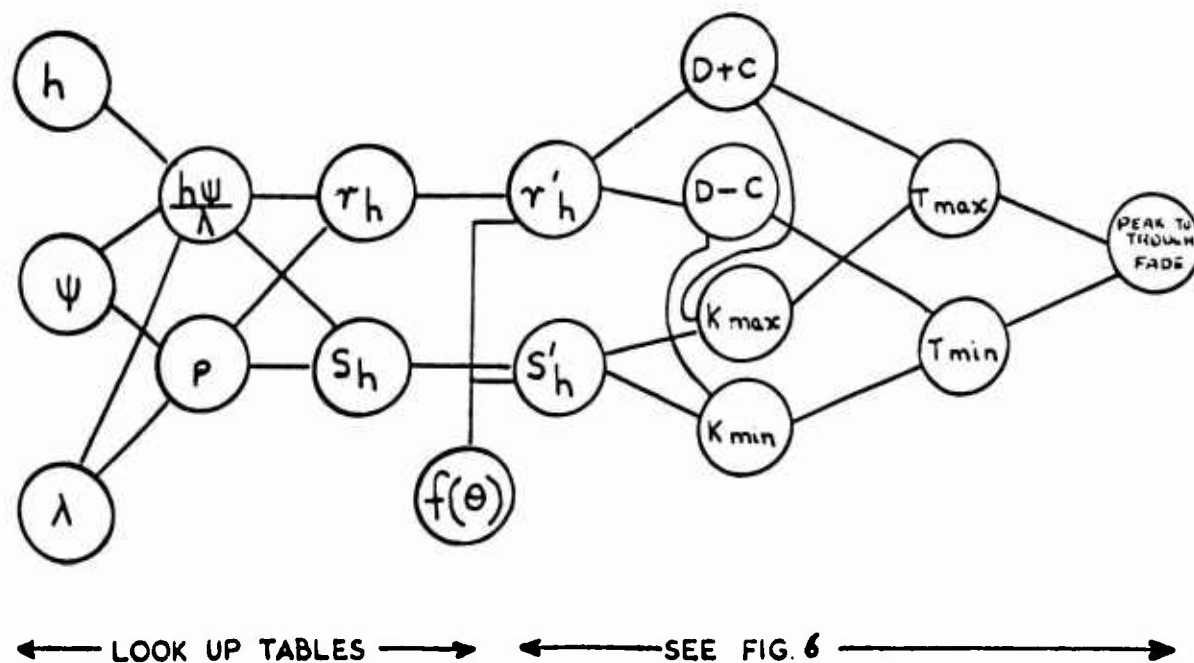


Fig. 5 Calculation flow diagram

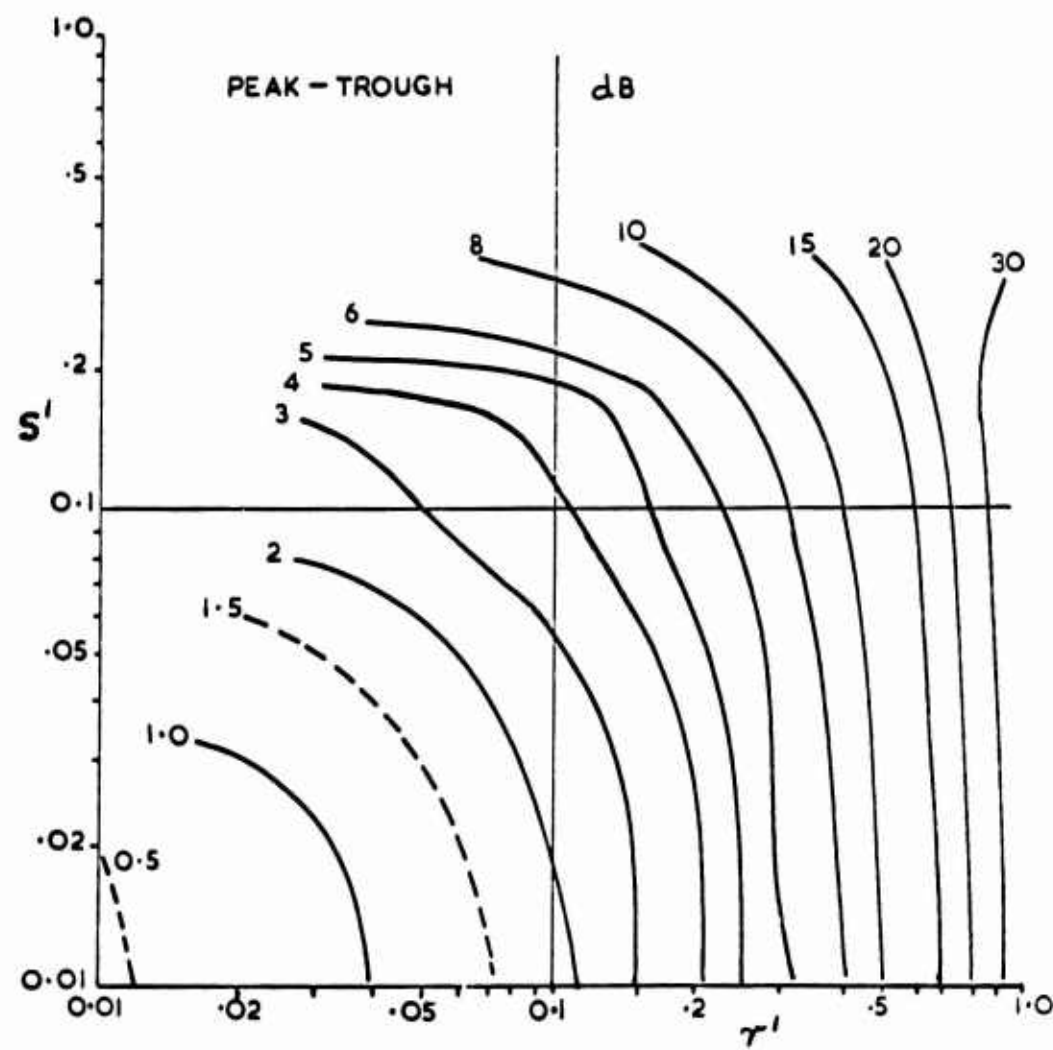


Fig. 6 Peak to trough fade versus ' $r'$  and ' $s'$

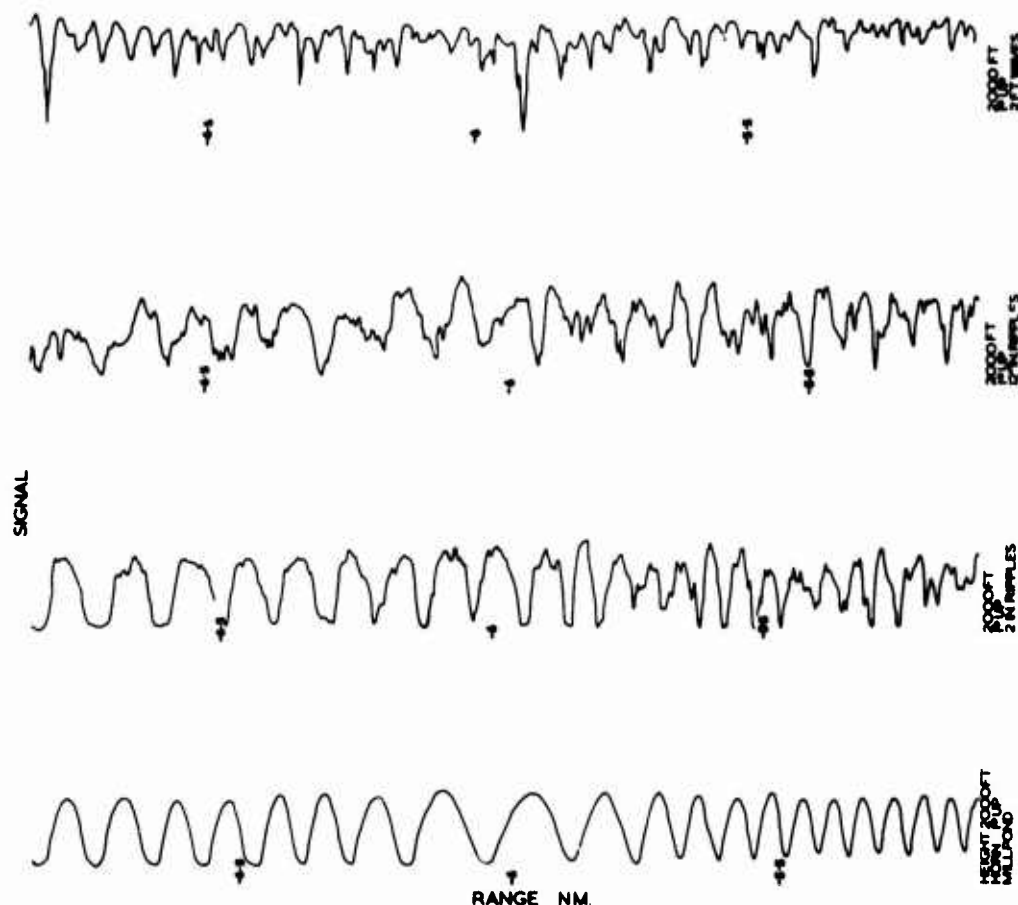


Fig. 7 Sample S band recordings, showing effect of increasing sea roughness

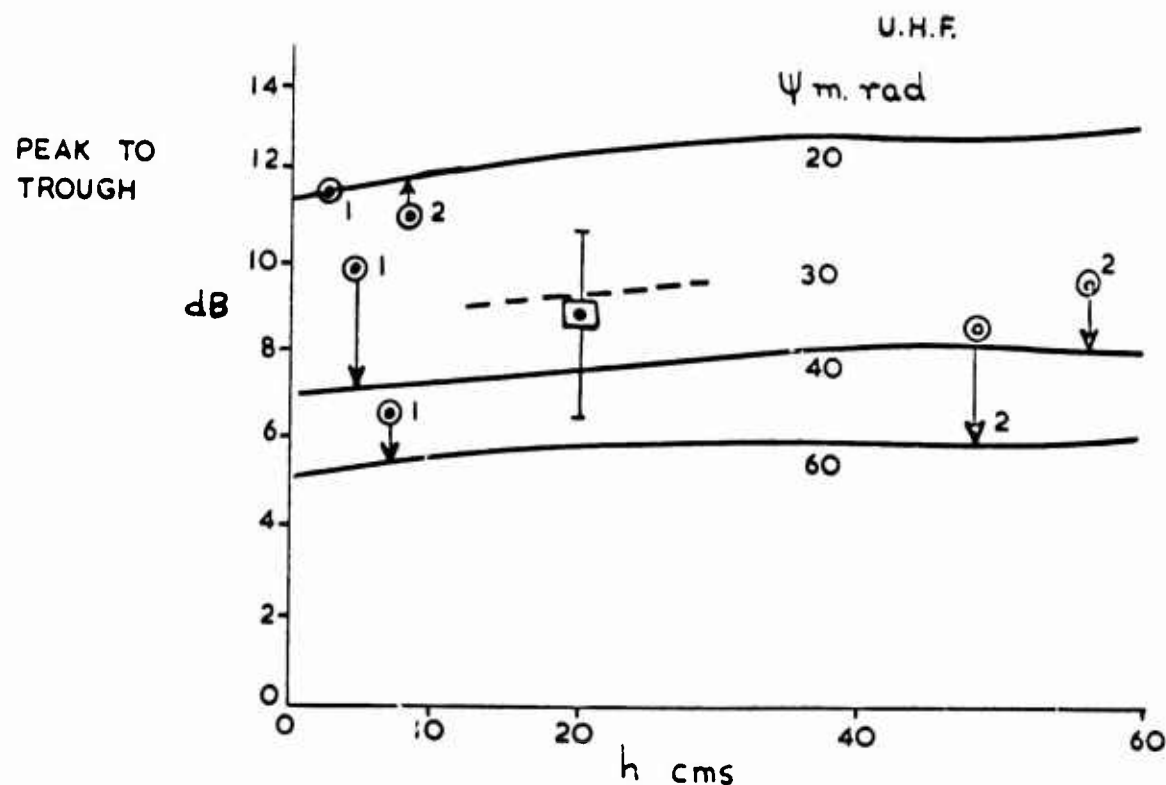


Fig. 8 Fading versus sea state. UHF band

10-10

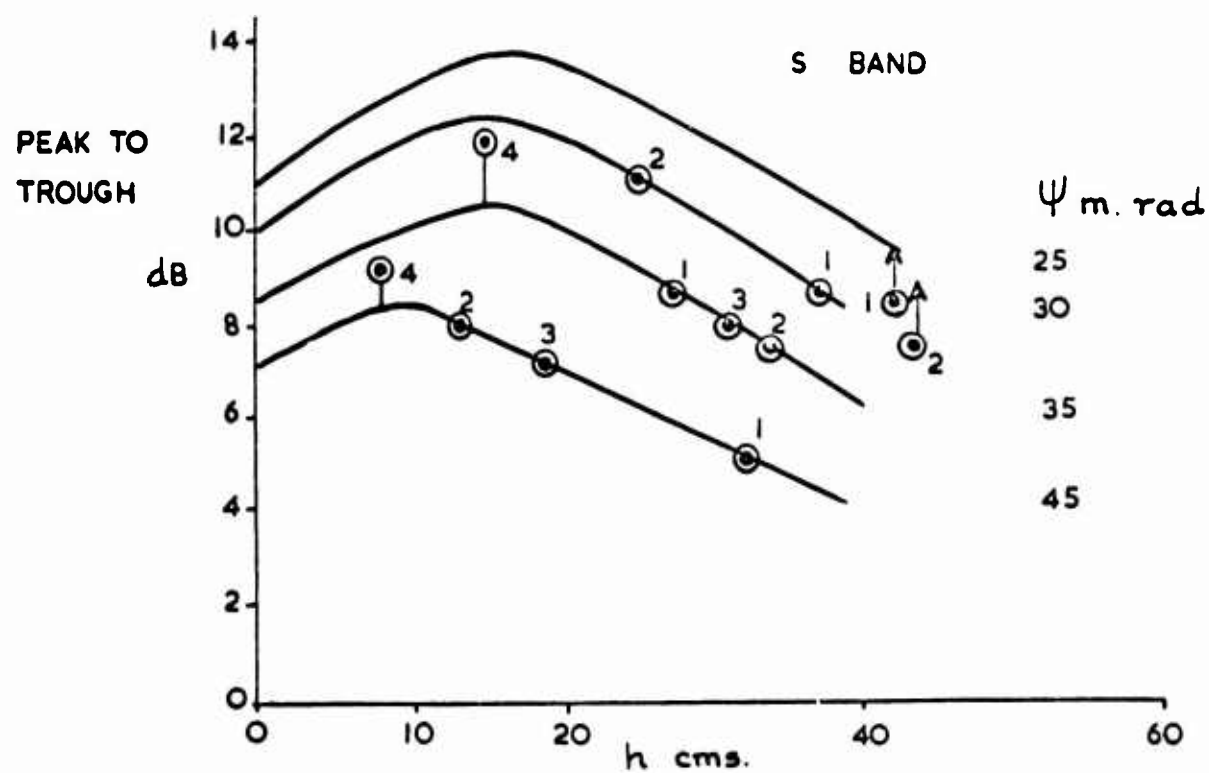


Fig. 9 Fading versus sea state. S band

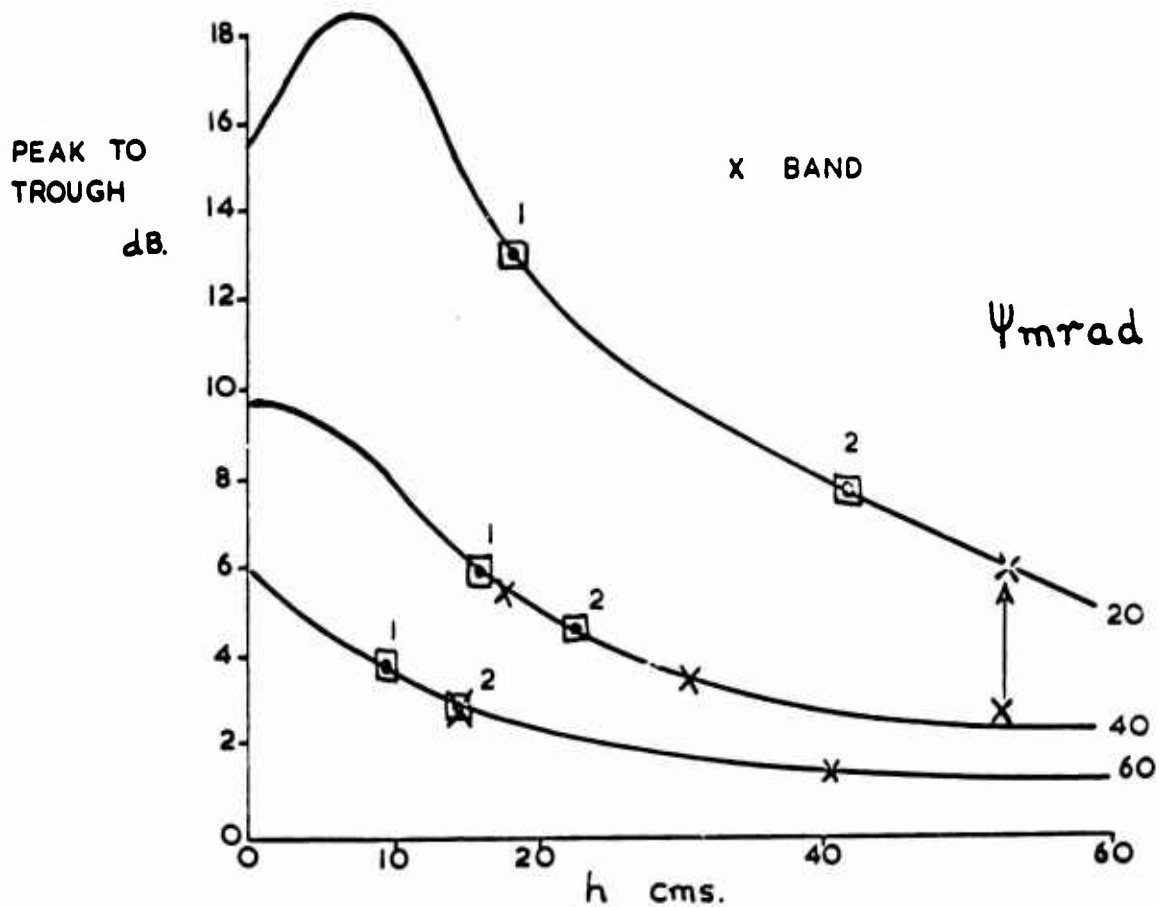


Fig. 10 Fading versus sea state. X band

**APERTURE SYNTHESIS IN IONOSPHERIC GROUND  
BACKSCATTER RADAR**

by

**Professor E.D.R. Shearman and J. Clarke**

**Department of Electronic and Electrical Engineering,  
University of Birmingham, UK**

## SUMMARY

The usefulness of backscatter radars for observing the properties of ionospheric layers over a large geographical area are at present limited by the great size needed for a directional array of narrow beamwidth. For a  $1^{\circ}$  beam at 15 MHz a 1 km aperture with some 100 elements in the array is needed. The present proposal is to use two aerials only, one fixed and one moving along a track, to record the time-averaged product of the two received backscattered signals and then to synthesise by computation the range/azimuth display which could have been obtained with a filled broadside array the length of the track.

The recording of time-averaged product as a function of range and aerial separation is made photographically in the form of density variation over a two-dimensional raster. After processing, the photographic transparency is put in a multi-channel one-dimensional optical Fourier transformer to yield the required range/azimuth map of ground targets.

Results are given which have been obtained with an ultrasonic model using two separable transducers under water to detect targets illuminated by way of reflection at the rippled surface of the water.

## NOTATION

$m, n$	element numbers in an array
$I_m, I_n$	current in $m^{\text{th}}$ and $n^{\text{th}}$ element
$\omega$	angular frequency of wave
$t$	time
$\phi_m, \phi_n$	phase of currents in $m^{\text{th}}$ and $n^{\text{th}}$ elements
$j$	$= \sqrt{(-1)}$
$P$	received power
$\lambda$	wavelength of radio wave
$\theta$	angle of incidence
$\Lambda$	coherence length
$s$	$= \sin \theta$
CRT	cathode ray tube
$X$	aerial spacing

## APERTURE SYNTHESIS IN IONOSPHERIC GROUND BACKSCATTER RADAR

Professor E. D. R. Shearman and J. Clarke

### 1. INTRODUCTION

Rotating-aerial backscatter radars with plan position displays have proved very useful tools for observing the regular and irregular variations of the ionospheric layers over an area a few thousand kilometres across<sup>1,2</sup>. The typical beamwidths of 40° or so obtainable with Yagi or log-periodic arrays give poor resolution, however, and narrower-beam rotating arrays become very unwieldy<sup>3</sup>. Sector-scanning with a stationary broadside array permits narrower beamwidths<sup>4</sup>, but the scale, complexity and cost of such an installation can be seen from an example; for a 1° beam at 15 MHz, a 1 km-long broadside array of some 100 elements is needed.

Radio astronomers presented with similar difficulties have made use of the technique of aperture synthesis<sup>5,6</sup>, in which high angular resolution is obtained with the use of two simple aerials, moving their locations so as to occupy different relative positions in a large area which it would otherwise be necessary to fill completely with physical elements. The unchanging angular distribution of the incoming radio wave flux is then computed from the measurements, the process being somewhat analogous to synthesising multiple beams in a beam-forming matrix attached to a real filled array.

The purpose of the present paper is to describe work on a synthetic aperture system for backscatter radar. The requirement here has the difference that the synthesis must be completed before the ionospheric features have drifted by a distance comparable with the beamwidth of the system, a time of the order of 5 or 10 minutes.

The work has reached the stage at which a sound-in-water analogue of an HF backscatter radar has been used to verify the theory evolved and to evaluate the performance of the electronic and optical signal processing system. Preliminary radio experiments in the field are now beginning.

An account of earlier experiments with the ultrasonic model has been published elsewhere<sup>7</sup>.

### 2. APERTURE SYNTHESIS: THE BASIC PRINCIPLE

We first consider a complex monochromatic wave field incident on a normal, filled, linear receiving array. Such a field might arise from a distribution of transmitters of common frequency around the sky, ("coherent radio stars"), or from backscattered echoes from complex spatially-distributed targets illuminated by a CW radar. The field will, in general, vary along the array in amplitude and phase as determined by the interference of the criss-crossing waves travelling inwards from the distant transmitters or targets.

Following Ryle<sup>5</sup> let the currents set up at typical elements  $m$ ,  $n$  be  $(\sqrt{2})I_m \cos(\omega t + \phi_m)$  and  $(\sqrt{2})I_n \cos(\omega t + \phi_n)$  when terminated in a matched load ( $I_m$ ,  $I_n$  being the root-mean-square values). We shall represent these currents by the phasor quantities  $(\sqrt{2})I_m e^{j\phi_m}$ ,  $(\sqrt{2})I_n e^{j\phi_n}$ , suppressing the common time factor  $e^{j\omega t}$  and the implied operator, "take the real part of".

If the outputs of all the elements in the array are taken by equal-length cables to a receiver matched to the array impedance, then the receiver current is given by the sum of the phasor element currents,

$$(\sqrt{2})I = \sum_{-r}^{+r} (\sqrt{2})I_n e^{j\phi_n}.$$

(The common phase retardation in the cables has been suppressed.)

The receiver power (assuming the receiver to be of unit resistance) is

$$P = |I|^2 = I \cdot I^* = \sum_{-r}^{+r} I_n e^{j\phi_n} \cdot \sum_{-r}^{+r} I_n e^{-j\phi_n}. \quad (1)$$

We now inspect Equation (1) to see whether we could have calculated the same power from individual measurements of the element currents. We note that Equation (1) may be rewritten as

$$P = \sum I_n^2 + \sum_{m \neq n} \sum I_m I_n e^{j(\phi_m - \phi_n)} \quad (2)$$

The first term in Equation (2) is merely the sum of the powers from individual elements. The second term appears at first sight to be a complex quantity and therefore not meaningful as power. However, we note that, for each term of the form  $I_m I_n e^{j(\phi_m - \phi_n)}$ , there is a paired term of the form  $I_n I_m e^{j(\phi_n - \phi_m)}$ , which may be written  $I_m I_n e^{-j(\phi_m - \phi_n)}$ . Equation (2) thus becomes

$$P = \sum I_n^2 + \frac{1}{2} \sum_{m \neq n} \sum I_m I_n [e^{j(\phi_m - \phi_n)} + e^{-j(\phi_m - \phi_n)}]$$

or

$$P = \sum I_n^2 + \sum_{m \neq n} \sum I_m I_n \cos(\phi_m - \phi_n). \quad (3)$$

Thus measurements which are sufficient to calculate the total power which would be received by the complete array can be made by moving a single pair of elements about, placing them successively in all possible relative positions (except coincident), and measuring the power received from one of the elements,  $I_n^2$ , and the "cross-power", or scalar product,  $I_m I_n \cos(\phi_m - \phi_n)$ , from the element-pair. The "cross-power" may be found by multiplying the two currents in an analogue multiplier, and filtering out the unwanted second harmonic term (as indicated in Figure 2).

We may now relax the condition that the sources are coherent since the phase measurement is of relative phase between elements in the array,  $(\phi_m - \phi_n)$ . Thus, provided the coherence length is greater than the array length and the signal is band-limited, measurements of the quantities in Equation (3) taken in time sequence will be satisfactory.

The computation process necessary to find the distribution of sources is a Fourier transformation process and can best be seen from Figure 1, which illustrates an incoherent plane wave of mean wavelength  $\lambda$  incident at an angle  $\theta$  on an aperture. The mean wavelength of the field distribution along the aperture is  $\lambda/\sin\theta$ , and for this single incident wave the cross-power of spaced elements as a function of spacing (autocorrelation function of the aperture field) is as shown in Figure 1. The periodicity of the sinusoidal function is  $\lambda/\sin\theta$  and the length of the wave packet is  $\Lambda/\sin\theta$ , where  $\Lambda$  is the coherence length, here assumed to be very large.

To find the direction of the source, therefore, we merely identify the spatial frequency  $\sin\theta/\lambda$  cycles/metre and thus obtain  $\sin\theta$  by multiplying by the known mean wavelength. For a complex incident wavefield we must first Fourier analyse the complicated autocorrelation function into its sinusoidal components and multiply the spatial frequencies by  $\lambda$  to obtain the incident angular power spectrum (or angular distribution of the sources  $F(s)$  as a function of  $s = \sin\theta$ ). This is the process of aperture synthesis.

A factor glossed over above is that the form of the real autocorrelation function depicted in Figure 1 is the same for waves incident from left and right of the normal. To resolve this ambiguity the imaginary part,  $\sum I_m I_n \sin(\phi_m - \phi_n)$ , of the complete complex autocorrelation function must also be measured and the Fourier transformation carried out on this complex function.

### 3. IONOSPHERIC RADAR SYSTEM

Vertical movements in the ionosphere cause the echoes of a ground backscatter radar to be partially coherent in nature and, because of this, the above two-transducer method of aperture synthesis is suggested rather than a single-transducer method possible with a coherent wavefield<sup>8</sup>. The proposal of the authors is as follows: A radar transmitter uses a wide beamwidth aerial which "floodlights" the surveyed area with HF pulses. Two aerials are used for reception, one fixed and one movable along a track hundreds of meters in length. The receiver beamwidths will also be large in order to "see" the whole of the illuminated area. Ideally, to form the spatial autocorrelation function of the aperture field, the signals received on the two receiving aerials should be multiplied together and the product averaged over all space for the particular aerial separation considered. Since the incident field is not coherent it is permissible to time-average the product instead, and this forms the spatial autocorrelation function. The averaging time necessary to produce a reasonably accurate approximation to the autocorrelation function sets a minimum time for the synthesis period.

The autocorrelation function is recorded on photographic film. This is accomplished by using the correlator output signal to intensity-modulate a cathode ray tube spot about some bias brightness, and photographing the face of the tube. The spot of the CRT is swept vertically in synchronism with the transmitted pulse to sort the information with respect to the range of the echo, and is swept slowly horizontally in exact synchronism with the separation of the aerials to record the correlation function against separation. The receiving system thus has the form indicated in Figure 2.

An analysis of the above system shows that the information on the film is the one-dimensional Fourier transform of the radar echo pattern (one-dimensional since no transformation has taken place in the range direction). Discrete targets ("lines" in the angular spectrum) give rise to fringes of a particular periodicity on the record. The inverse transformation can be performed fairly easily in an optical data processor and the radar map is produced. The film from the camera is developed to produce a transparency and this is then placed in the parallel, monochromatic, coherent beam of light of the data processor. The processor comprises little more than one spherical lens and one cylindrical lens and the output consists of a light distribution in the plane giving imaging in the range co-ordinate and Fourier transformation in the separation co-ordinate. This is the synthetic aperture radar map of range versus  $\sin\theta$ . (The optical method has similarities to that used by Cutrona et al<sup>8</sup>, in side-looking airborne radar, though avoiding the complications introduced by near-field operation.)

### 4. EXPERIMENTAL WORK

At the University of Birmingham an ultrasonic model of a synthetic aperture radar system has been built which employs a carrier frequency of 1 MHz in water. Figure 3 shows results obtained for the case of two point targets present. Figure 3(a) shows the

field of view and aerial configuration, and Figure 3(b) the corresponding film picture taken of the CRT face, where the correlation function for each target can be seen. To overcome the bearing ambiguity problem mentioned above the correlation function is translated in frequency before recording thus avoiding the necessity for recording real and imaginary functions. (This frequency translation is achieved by the continuously-rotating phase shifter shown in Figure 2). When the transparency is processed, the "map" shown in Figure 3(c) is obtained. The map is that distribution within the white rectangle, the other features of the display are a bright distribution of light (b) on the axis of the data processor and a mirror image (m) of the radar map to the left of this axis. The displacement of the map from the data processor axis is a direct result of frequency-translating the correlation function before recording. In the map the two targets can clearly be seen at the bearing and range appropriate to each.

An important factor in the application of this system to ionospheric backscatter sounding is clearly the nature of the partial coherence of the target returns and the effect of averaging. Ionospheric measurements have shown the oblique signals reflected at parts of the ionosphere separated by some kilometres (as are the returns from ground targets in neighbouring beamwidths of the above radar system) to be phase-incoherent over a time scale of a few seconds. This is sufficient to achieve the necessary phase averaging.

The ultrasonic analogue has been used to simulate this effect by reflecting the transmitted and received signals internally at the surface of the water in the tank. The sonar transducers are placed near the bottom of the tank pointing obliquely upwards and the rippled surface of the water simulates the wrinkled, drifting reflecting surface of the ionosphere, reflecting the signals to and from the targets, located near the floor at the other end of the tank.

Figure 4 shows two targets clearly resolved with this arrangement with no spurious target returns evident. Figure 5 shows a "distributed target", actually a row of five point targets which have in fact not been placed close enough and have been partially resolved.

##### 5. CONCLUSIONS

The ultrasonic analogue of the proposed synthetic aperture ionospheric radar has verified the predicted performance in resolving multiple targets reflected by way of a rippled surface. Preliminary radio experiments at 20 MHz are now in progress in preparation for the construction of a synthetic aperture array, of  $\frac{1}{2}$  to 1 km length, with a synthesis time of the order of 5 minutes.

## REFERENCES

1. Shearman, E. D. R.  
Martin, L. T. J.  
*Backscatter Ionospheric Sounder.* Wireless Engineer, Vol. 33, 1956, p. 190.
2. Peterson, A. M.  
et al.  
*The IGY Three-Frequency Backscatter Sounder.* Proceedings, Institute of Radio Engineers, Vol. 47, 1959, p. 300.
3. Thomas, J. A.  
McNicol, R. W. E.  
*Nature*, Vol. 187, 30 July, 1960, p. 398.
4. Cotton, H. V.  
*Current Development in an Electronically Scanned Antenna.* Symposium on Electromagnetic Theory and Antennas, Copenhagen 1962. Pergamon, 1963.
5. Ryle, M.  
Hewish, A.  
*The Synthesis of Large Radio Telescopes.* Monthly Notices, Royal Astronomical Society, Vol. 120, 1960, p. 220.
6. Hewish, A.  
*The Realization of Giant Radio Telescopes by Synthesis Techniques.* Proceedings, Institute of Radio Engineers of Australia, February 1963, p. 255.
7. Shearman, E. D. R.  
Clarke, J.  
*Aperture Synthesis in Ionospheric Radar.* Nature, Vol. 219, 13 July 1968, p. 143.
8. Cutrona, L. J.  
et al.  
*On the Application of Coherent Optical Processing Techniques to Synthetic Aperture Radar.* Proceedings, Institute of Electrical and Electronic Engineers, Vol. 54, 1966, p. 1026.

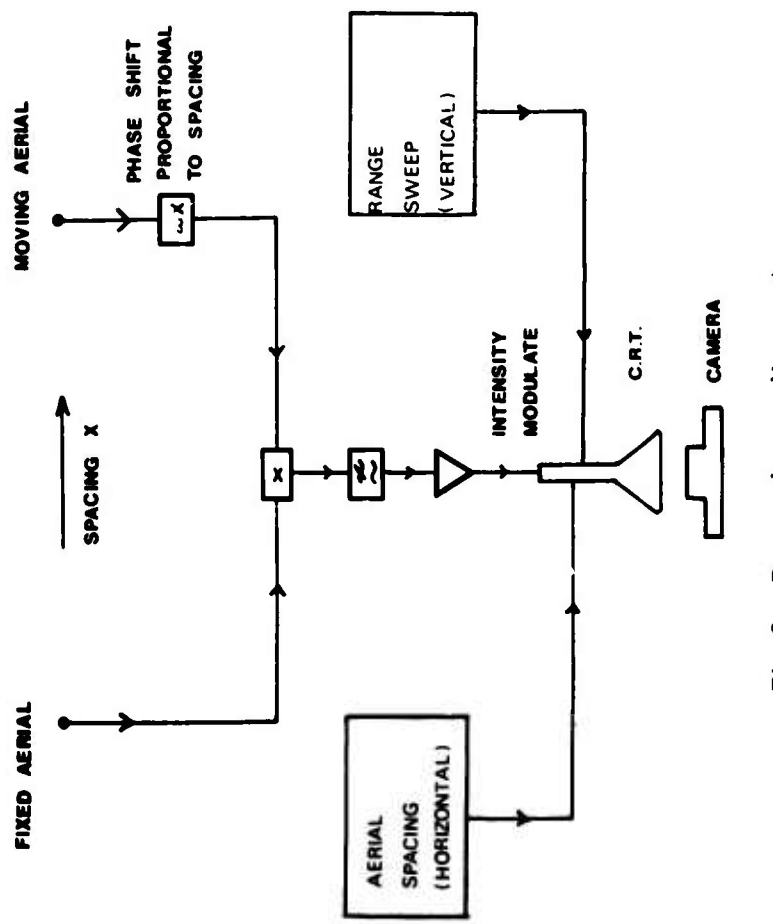
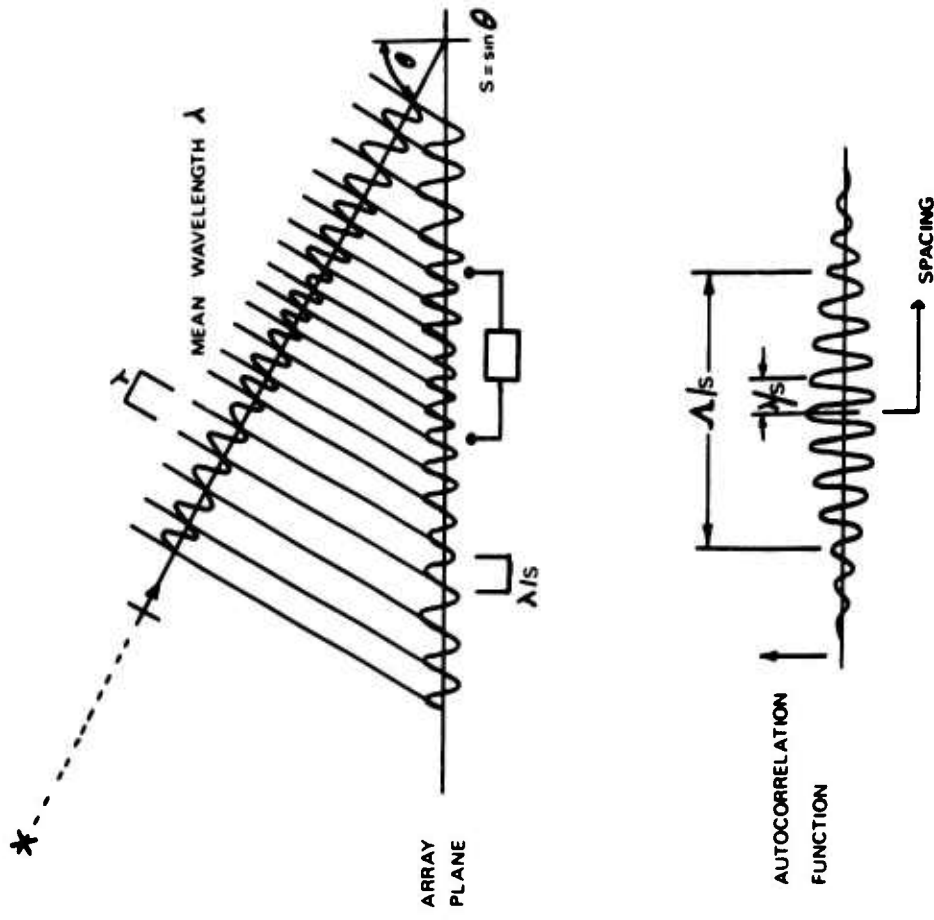


Fig. 1 Autocorrelation function for incoherent wave

Fig. 2 Proposed recording system

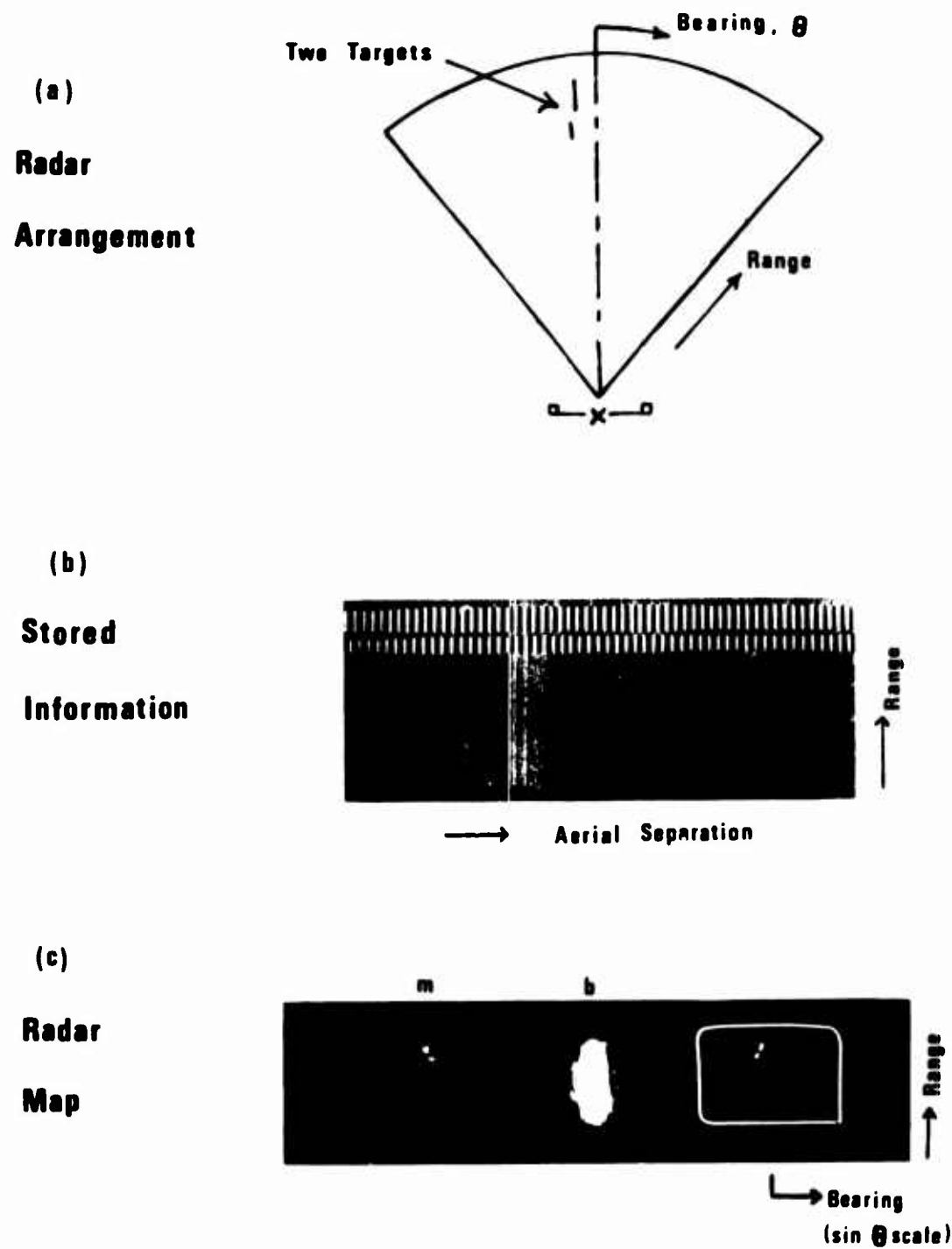


Fig. 3 Signal processing sequence



Fig. 4 Two targets in model



Fig. 5 Distributed target in model

COURTE NOTE SUR LES ECHOS 2 x F DIFFUS OBSERVES A DJIBOUTI

par

A.M. Bourdila et J. Odoux

Division des Prévisions Ionosphériques  
du  
Centre National d'Etudes des Télécommunications  
Saclay, 91, Orsay, France.

## COURTE NOTE SUR LES ECHOS $2 \times F$ DIFFUS OBSERVÉS À DJIBOUTI

A.M. Bourdila et J. Odoux

### 1.

Les ionogrammes zénithaux de la station française de Djibouti ( $11^{\circ}31' N$ ,  $42^{\circ}50' E$ ), présentent quotidiennement des traces diffuses correspondant aux échos réfléchis deux fois par la couche F ( $2 \times F$ ), sans que la trace  $1 \times F$  soit affectée (Fig.1). Afin de déterminer la nature du phénomène (cause technique, diffusion par le sol ou diffusion ionosphérique), la Division des Prévisions Ionosphériques du CNET a effectué une étude statistique de l'année 1964. ( $\overline{R}_5 = 6$  à 22).

### 2.

La Figure 2 présente les pourcentages d'apparition du phénomène décrit ci-dessus, en fonction de l'heure, et pour les 12 mois de l'année 1964. Sur ces graphiques, l'influence de l'heure et de la saison apparaît nettement. En été, deux maximums sont mis en évidence, l'un à 08 h.00 l'autre entre 16 et 22 h.00. Au mois d'octobre, l'aspect de la courbe change, et il apparaît un troisième maximum, vers 13 h.00, que l'on retrouve l'hiver, en novembre et décembre. Au solstice de printemps, du mois de mars au mois d'avril, la courbe reprend l'aspect qu'elle présente en été.

Il paraît donc certain que le phénomène ne peut être attribué, ni à une cause technique, ni à la diffusion par le sol seule, laquelle ne pourrait avoir qu'un effet permanent. L'influence de l'ionosphère est donc bien mise en évidence.

### 3.

La Figure 3 présente les coupes schématiques, dans les plans verticaux Nord-Sud et Est-Ouest d'une surface d'égal densité électronique dans la couche F, estimée d'après les cartes d'ionisation de W.B. Jones et R. Gallet pour un indice d'activité solaire  $\overline{R}_{12} = 0$  et pour 6 mois caractéristiques<sup>1</sup>. En juin (13 h.00) et janvier (23 h.00), le  $2 \times F$  diffus est peu fréquent, et l'on voit qu'au dessus de Djibouti, la pente de l'ionosphère est faible.

Au contraire, en mai (07 h.00 et 17 h.00) et décembre (07 h.00 et 13 h.00), le phénomène est très fréquent (Fig.2) et l'on voit que l'ionosphère, au dessus de Djibouti, présente une pente importante, soit Est-Ouest (à 07 h.00), soit Nord-Sud (en mai 17 h.00 et décembre 13 h.00).

Bien que quelques réserves doivent être faites, du fait du caractère sommaire du tracé de ces coupes ionosphériques, il semble cependant que l'on puisse lier l'apparition du  $2 \times F$  diffus à la présence d'une pente de l'ionosphère au dessus de la station de sondage.

### 4.

Pour les mois de mai (17 h.00) et décembre (13 h.00), on peut expliquer le phénomène sans faire intervenir la diffusion par le sol, ainsi qu'on peut le voir sur la Figure 4.

A 07 h.00, le schéma de la Figure 4 ne s'applique plus. La pente maximum de l'ionosphère étant alors Est-Ouest, le point de réflexion spéculaire au sol du bond  $2 \times F$  se trouve alors sur la mer, dans le golfe d'Aden. On peut alors penser que la rétrodiffusion sur la mer agitée (houle des vagues), puisse être en partie responsable du  $2 \times F$  diffus (Fig.5).

Cependant, nul n'ignore que la structure de l'ionosphère, du lever du soleil, n'est pas aussi simple que celle que l'on a représentée sur la Figure 5, et les mesures d'effets Doppler, en particulier, présentent des oscillations qui traduisent sans doute l'existence de 'vagues' d'ionisation en mouvement, lesquelles peuvent être, elles aussi, à l'origine du  $2 \times F$  diffus, suivant le processus décrit par la Figure 4. On notera enfin qu'aucune influence notable de l'activité magnétique n'a pu être mise en évidence.

## REFERENCES

# 1. CCIR Rapport 340, Oslo, 1966.

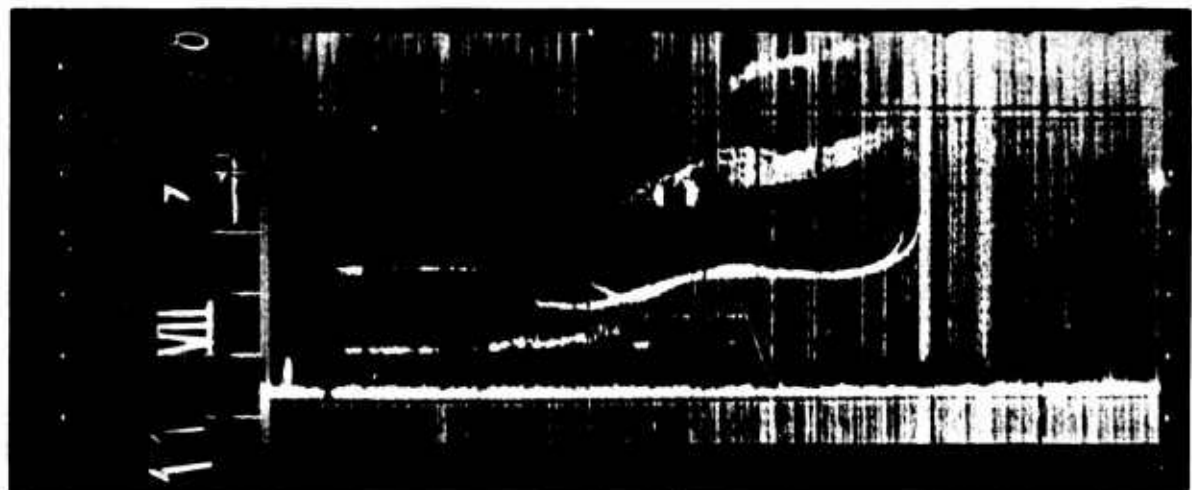


Fig. 1. Ionogramme zénithal enregistré à la station d'Arta (Djibouti), le 11 juillet 1964 à 07 h.58 (temps du fuseau)

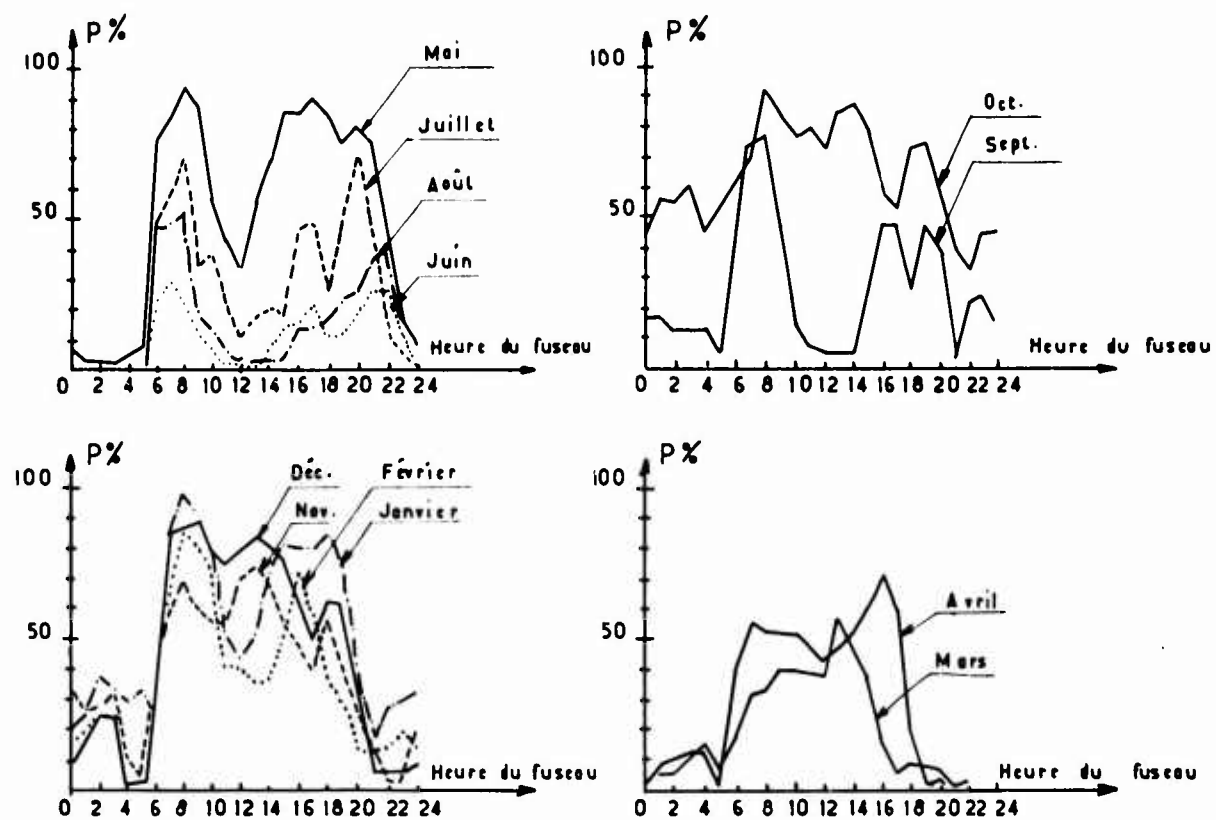


Fig. 2. Pourcentage P d'apparition, à Djibouti, d'une trace diffuse sur le deuxième écho seul, en fonction de l'heure locale, et pour les 12 mois de l'année 1964 (activité solaire:  $\overline{IR}_5 = 6 \text{ à } 22$ )

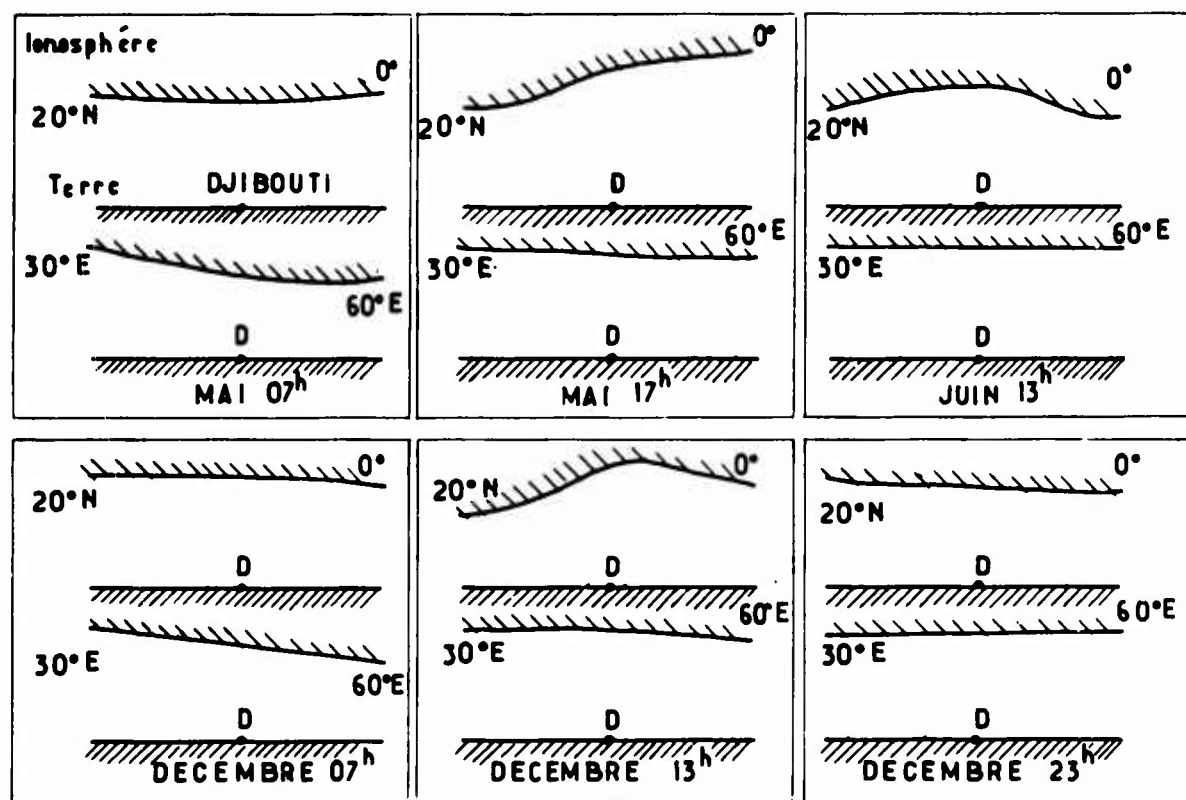


Fig. 3. Coupes schématique de la cavité terre-ionosphère, dans le plan vertical Nord-Sud ( $20^{\circ}$  N à  $0^{\circ}$  S) et dans le plan vertical Est-Ouest ( $30^{\circ}$  E à  $60^{\circ}$  E), montrant les pentes de l'ionosphère, pour 6 mois et heures de l'année. La station de Djibouti est indiquée par la lettre D

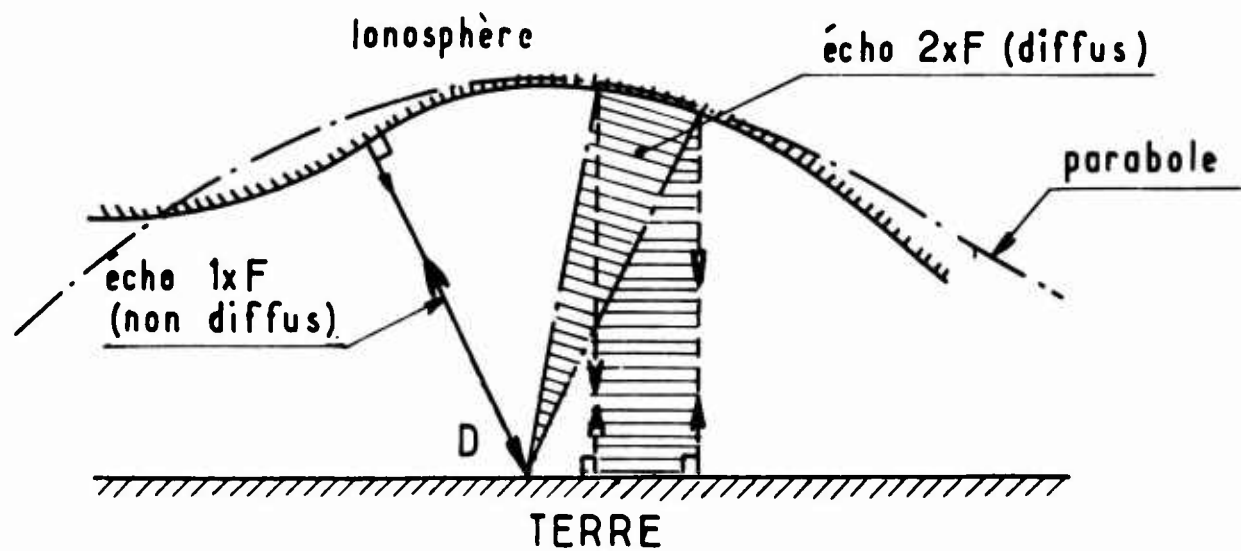


Fig.4. Schéma illustrant la production de l'écho  $2 \times F$  diffus, sans diffusion par le sol

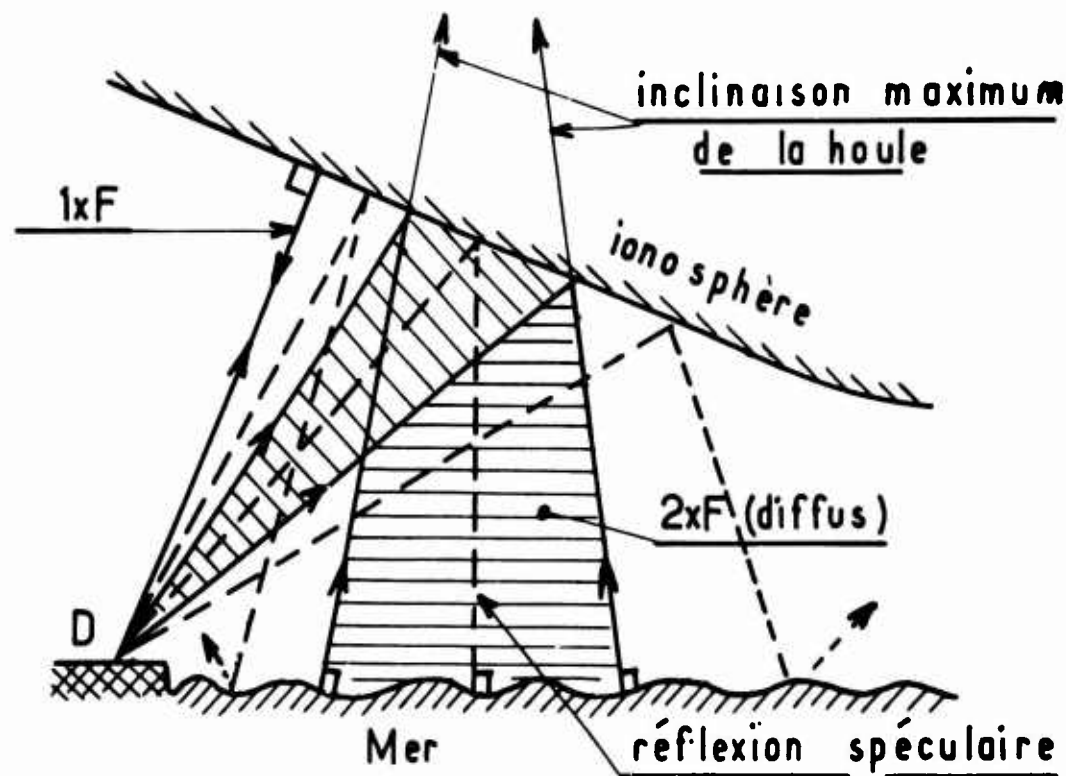


Fig.5. Schéma illustrant la production du  $2 \times F$  diffus, par les effets combinés du sol et de l'ionosphère

**SCATTERING OF ELECTROMAGNETIC RADIATION BY  
PARTICULATE SUSPENSIONS IN THE ATMOSPHERE**

by

**Kurt Bullrich**

Meteorologisches Institut der  
Johannes Gutenberg-Universität  
Mainz, Germany

#### **SUMMARY**

The paper gives a survey on the scattering parameters in the turbid atmosphere. In particular the role of the aerosol particles are described: size distribution, structure and refractive index. The behaviour of the atmospheric aerosol and the scattering of higher orders are problems which cannot be neglected in the consideration of scattering processes in the atmosphere. Some of them are not yet solved.

## SCATTERING OF ELECTROMAGNETIC RADIATION BY PARTICULATE SUSPENSIONS IN THE ATMOSPHERE

Kurt Bullrich

### 1. INTRODUCTION

The electromagnetic radiation which is emitted by the sun, the moon, the stars and artificial terrestrial light sources undergoes modification while passing through the atmosphere, owing to absorption and scattering processes. The effects of these processes are (i) the extinction, i.e. the attenuation, of this radiation and (ii) the deflection from the direction in which the incident radiation was advancing. In the case of absorption, absorbent gases in the atmosphere convert radiant energy into heat in specific wavelength ranges. This energy may appear again as infrared, i.e. longwave radiation. In the case of scattering, however, the light is only deflected from its original direction of propagation so that the amount of its total energy can be reproduced by measurements at various so-called scattering angles. A good example is the visible scattered radiation outside the water vapour absorption bands, which is propagated in all directions of the atmosphere almost without undergoing absorption. A portion of the incident radiation reaches the observer directly or is scattered towards him, another portion reappears as sky radiation or diffuse radiation scattered by the clouds, and the rest is scattered into space.

### 2. THE GASEOUS ATMOSPHERE

We now consider the scattering processes within the atmosphere. Of course, the question arises of the constituents of the scattering medium which is called the atmosphere, most of which are gases. This gaseous proportion is called the molecular atmosphere because in it the incident electromagnetic radiation is scattered exclusively by gas molecules. The mean state of the gaseous atmosphere is well known. However, the variations of its temperature, i.e. of its density, must be taken into account. This includes variations in time as well as in the vertical distribution. Many meteorological computations are based upon the hypothesis of the homogeneous atmosphere without biasing the results unduly. The vertical extent of the homogeneous atmosphere is approximately 8 km and the hypothesis is made that the density is constant with height. The molecular atmosphere may be assumed to be almost isotropic. Its molecules are nearly spherical and their spatial distribution is independent of direction. The individual molecules are so far from each other that no phase relationship of their scattered radiation exists.

### 3. THE AEROSOL

Solid and liquid or two-phase particles are suspended in the gaseous atmosphere. They also scatter the incident electromagnetic radiation. This suspension is called the atmospheric aerosol and the aerosol particles alone represent the haze. The precipitation elements are excluded. The aerosol particles play an important role in the scattering processes of the atmosphere, although their proportion of concentration is less than that of the gaseous phase by several powers of ten.

#### 4. AEROSOL PARTICLE SIZE DISTRIBUTION

If the molecular atmosphere alone is considered, it is sufficient to know the number of molecules per cubic centimetre for the turbid atmosphere; however, it is necessary to know not only the number of aerosol particles per cubic centimetre but also their radii, in order to assess their effects. During the last 15 years numerous investigations into the aerosol particle size distribution have been carried out. Figure 1 shows a size distribution which was first measured by Junge<sup>1</sup> in 1952 and which is typical for Central Europe. The abscissa shows the radius on a logarithmic scale, the ordinate shows the particle number per cubic centimetre referring to the radius range,  $d \log r$ . The particle numbers vary within a range covering 8 powers of ten, and the radii of the particles vary within a range covering 3 to 4 powers of ten. Jaenicke<sup>2</sup> has measured particles up to  $150 \mu$ . An upper limitation was not evident. The explanation of the existence of the coarse particles of mainly mineral origin is still pending.

There is a better insight into the nature of the lower limitation, which is due to the genesis of the particles. The fairly continuous decrease might be due to the statistical distribution of the variety of aerosol sources which contribute to the formation of the natural atmospheric aerosol.

This size distribution is expressed by the equation

$$\frac{dN(r)}{d \log r} \propto r^{-\nu^*}. \quad (1)$$

The exponent  $\nu^*$  varies within the range 2.5 to 4. If it is 2.5, the proportion of large aerosol particles is great; if it is 4, the proportion of small aerosol particles is great. Figure 2 shows also the volume distribution of the particles. It is identical with a mass distribution under the assumption that the exponent  $\nu^* = 3$  and the density is constant. However, direct and optical radiation measurements have revealed noticeable deviations from this relationship. Figure 1 shows that the size distribution over the oceans differs from that over the continents. The sea salt particles are characterised by smaller concentrations and smaller radii. But deviations have been also found over the continents. Figures 3 and 4 show some of these types of deviations in the measurements taken by Fenn<sup>3</sup> in the USA and Jaenicke<sup>4</sup> on Maui, Hawaii.

#### 5. REGIONAL AND VERTICAL DISTRIBUTION OF THE AEROSOL PARTICLES

Particle numbers of the order of magnitude of  $10^5$ /cubic centimetre are measured in densely populated areas. From these source regions the particles spread out over the entire globe so that, including the regions which are not influenced by human activity, the measurements yield particle numbers of the order of  $10^2$ .

The decrease in the particle number with height is not fully known yet. A rapid decrease with height up to about 5 km can be observed, then the number remains constant up to the stratosphere. There is evidence of the existence of an aerosol layer at a height of about 20 km ( $\pm 3$  km), which is subject to an annual variation and the height of which depends on the geographical latitude. It is worth mentioning that the variation with height does not refer only to the number, but also to the size distribution of the aerosol particles. Furthermore, the existence of an accumulation of particles at a height of 80 km is evident. The existence of a dust layer at a height of 40 km seems probable.

#### 6. STRUCTURE OF THE AEROSOL PARTICLES

The mixed structure is one of the most important features of the aerosol particles; this is also true of their chemical composition. As aerosol particle consists of various

constituents, which might be soluble or insoluble on the one hand and organic or inorganic on the other hand. This mixed structure is due to the formation of the particles. Small particles may result from the condensation and sublimation of various combustion products which are due either to natural events or human activity; these small particles coagulate and agglomerate. It also happens that the products of chemical reactions of trace gases come in contact with the aerosol particles, thus changing their composition and expediting their mixed structure. The aerosol particles can be roughly broken down into three groups;

Inorganic and insoluble in water, about 60%.

Organic and insoluble in water, about 15% .

Inorganic and water-soluble, about 25% .

$\text{SO}_4$  originates when  $\text{SO}_2$  is transformed into sulphuric acid by means of oxidation, either in a photochemical process or on cloud droplets, so that positive hydrogen ions are always present in the aerosol. The life-span of the aerosol particles is about 4 weeks. This time is sufficient for a worldwide spreading of the particles from out of the continents.

## 7. REFRACTIVE INDEX $m$ OF THE AEROSOL PARTICLES WITH REFERENCE TO AIR

The refractive index is a material property of the aerosol particles. Thus it must be known for interpreting the processes of radiation scattering in the atmosphere, but it is difficult to determine its amount. First, knowledge of the chemical composition of the aerosol particles is very inadequate so far; secondly, the mixed structure of the aerosol particles is a handicap in determining their refractive index; thirdly,  $m$  varies as a function of the relative humidity. In 1966, Hanel<sup>5</sup>.<sup>6</sup> found a method of measuring the refractive index at various relative humidities. These results are presented in Figure 5. It can be seen that the refractive index varies within the values 1.67 and 1.33 (water) according to the variation of the relative humidity.

## 8. SCATTERING OF RADIATION IN THE MOLECULAR ATMOSPHERE

As a physical explanation of blue sky, Lord Rayleigh put forward his theory of the primary scattering of radiation in the molecular atmosphere which is free of haze. Therefore, the latter is often called the Rayleigh atmosphere. Rayleigh has expressed the scattering coefficient under the condition that  $r$  is much smaller than  $\lambda$  as

$$\sigma_R(\lambda) = \frac{32\pi^3(m-1)^2}{2N\lambda^4} , \quad (2)$$

where  $m$  is the refractive index,  $N$  the number of molecules per cubic centimetre and  $\lambda$  is the wavelength. This is the well known Rayleigh's law, which says that the scattering coefficient varies inversely with the fourth power of the wavelength.

Furthermore, it must be remembered that the  $\text{O}_2$  and  $\text{N}_2$  molecules are not spherical. Therefore, the so-called anisotropic coefficient has to be applied. Kasten<sup>7</sup> recently gave new values. Under normal pressure at  $\lambda = 0.55 \mu$ ,  $\sigma_R$  results in a visual range of 390 km, using Koschmieder's formula. The angular dependence of the scattered radiation in a molecular atmosphere is expressed by a scattering function

$$f_R(\phi) = \frac{3}{16\pi} \frac{1}{\sigma_R(\lambda)} (1 + \cos^2\phi) , \quad (3)$$

where  $\phi$  is the scattering angle. This functional relationship implies that as much energy is scattered into the forward hemisphere of space as into the backward one.

It became apparent that Rayleigh's Law did not give the full explanation for the dis-

tribution of the radiance of the sky, for two reasons:

- (a) scattering by aerosol particles has been neglected,
- (b) scattering of higher orders has been neglected.

It is possible that a beam of light does not reach the observer until after it has undergone multiple scattering as well as reflection by the ground. In the early fifties, Chandrasekar forwarded a theory which enables one to compute the scattering of higher order. The results were published in tabular form by Coulson, Dave and Sekera<sup>8</sup> in 1960.

However, these values do not agree with the observations either. Even in areas which are far away from any aerosol particle source region, e.g. in Greenland, aerosol particles have been detected by means of optical radiation measurements. And in densely populated areas the scattering due to aerosol particles is predominant. Therefore, it was essential to look for physical and mathematical ways of finding an approximation for the various types of aerosol particles and their scattering coefficient  $\sigma_A$ . However, there are still many problems in this field.

#### 9. SCATTERING COEFFICIENT OF THE AEROSOL PARTICLES

In 1908 Mie derived integro-differential equations in order to compute the angular-dependent intensities of radiation scattered by spherical particles, the radii of which are assumed to be of a size comparable with the wavelength of the incident electromagnetic radiation. These equations include the Rayleigh scattering. They can be solved only if the quantitative values of both the size parameter,  $\alpha = 2\pi r/\lambda$ , and the refractive index  $m$  are known. For values of  $m$  ranging between 1.33 and 1.486, the so-called scattering cross-sections have been computed by several authors, Penndorf, Giese et al<sup>9</sup>. The scattering cross-section is expressed as

$$\kappa(\alpha) = \frac{\sigma_A(r, \lambda)}{\pi r^2} . \quad (4)$$

Some results are presented in Figure 6. It can be seen that small variations in  $m$  result in the shifting of the periodic oscillations of  $\kappa(\alpha)$ .

We have seen from the Figure 1 that the atmosphere contains aerosol particles of different sizes. The size interval ranges approximately from  $r = 0.04 \mu$  up to  $r = 150 \mu$ . This means that the numerical values of  $\kappa(\alpha)$  have to be computed by the Mie theory for this size range. This could not be done until electronic computers of great capacity were available. Figure 6 shows the values of  $\kappa(\alpha)$  from  $\alpha = 0$  up to  $\alpha = 159$ , for the case  $m = 1.5$ , corresponding to the particle size range of the radii from zero to  $10 \mu$ .

For a volume of 1 cubic centimetre of air, the scattering coefficient is modified to

$$\sigma'_A(r, \lambda) = \sigma_A(r, \lambda) dN(r) , \quad (5)$$

where  $dN(r) \propto cr^{-\nu^*} d \log r$  or  $dN(r) \propto 0.434 r^{-(\nu^*+1)} dr$ .

Integration taken over all the radii  $r$  leads to

$$\sigma'_A(\lambda) = 0.434 \int_{r_1}^{r_2} \frac{\sigma_A(r, \lambda)}{r^{(\nu^*+1)}} dr . \quad (6)$$

Substitution with

$$\alpha = \frac{2\pi r}{\lambda} \quad \text{and} \quad \kappa(\alpha) = \sigma_A(r, \lambda)/r^2\pi ,$$

gives Equation (6) which, in addition, gives the tabulated values of  $\kappa(g)$ .

For both the air molecules and the aerosol particles the scattering coefficient reads

$$\sigma_R + \sigma'_A = \sigma' \quad (7)$$

It can be seen that

$$\sigma'_A \propto \lambda^{2-\nu^*} \quad (8)$$

This implies that, for  $\nu^* = 3$ , the scattering coefficient of the aerosol particles is inversely proportional to the wavelength  $\lambda$ . Previously, we have seen that in the molecular atmosphere the scattering coefficient is inversely proportional to the fourth power of the wavelength  $\lambda$ .

If the scattering coefficient is to refer to the whole atmosphere, it is necessary to integrate over the vertical distribution.

#### 10. THE SCATTERING FUNCTION OF THE AEROSOL PARTICLES

The method of determining the scattering function is analogous to the method of determining the scattering coefficient. Figure 7 gives an example of the intensities of scattered radiation which have been computed by the Mie theory for the scattering angles from  $0^\circ$  up to  $180^\circ$  and for various values of  $a$ . The abscissa shows the values of  $a$ , and the ordinate represents one of the two components of the polarised scattered radiation on a logarithmic scale for  $\phi = 90^\circ$ . The large variations with  $a$  are smoothed away by the integration over  $a$ . This integration must be taken, as before, over all the values of  $a$  which correspond to the radii of all the aerosol particles occurring in the atmosphere. Then the scattering function is transformed into

$$b'_A(\lambda, \phi) \propto \left(\frac{2\pi}{\lambda}\right)^{\nu^*-2} \int_{a_1}^{a_2} \frac{i_1 + i_2}{a^{\nu^*-2}} da, \quad (9)$$

shown in Figure 8. Its form differs considerably from that of the air molecules. The limiting radii and the refractive index have to be taken into account. Figure 9 shows the strong influence of the real and imaginary part of the refractive index of the aerosol particles on the scattering function.

For both the air molecules and the aerosol particles the scattering function is

$$f_R(\phi) + f_A(\phi) = f(\phi). \quad (10)$$

If the investigation is restricted to an air volume, the theoretical values of the scattering coefficient and the scattering function agree fairly well with the measurements (Bullrich<sup>10</sup>).

#### 11. RATIO OF RAYLEIGH SCATTERING TO TOTAL SCATTERING

This ratio depends very much on the number of aerosol particles in the atmosphere and, of course, it also depends on the wavelength. Figure 10 gives an example for  $\nu^* = 2.5$  and various visibilities. The relationship between the scattering coefficient  $\sigma'$  and the visibility  $V$  is

$$\sigma' = 3.91: V; \quad (11)$$

thus, the scattering coefficient can be expressed in terms of the visibility. For large

visibilities molecular scattering predominates in the short-wave portion of the visible spectrum, in the scattering angle range from  $120^\circ$  to  $150^\circ$ , with 7% of the total energy, whereas forward scattering is the domain of the aerosol particles<sup>10</sup>.

## 12. SCATTERING OF HIGHER ORDER IN THE TURBID ATMOSPHERE

The scheme of the scattering of higher order has already been demonstrated for the molecular atmosphere. For the aerosol particles in the turbid atmosphere, the scheme is the same; however, no exact method of computation has been found so far. An approximation, which cannot be explained in full detail here, has been put forward by de Bary<sup>11</sup>; this procedure gives at least the order of magnitude of the influence of the scattering of higher order. Heger<sup>12, 13</sup> has provided values of the influence of secondary scattering. Figure 11 shows the ratio of the sky radiation due to primary scattering to the sky radiation due to secondary scattering for a specific turbidity, solar elevation and wavelength. Obviously, the secondary scattering has a great influence on the sky radiance. Thus, scattering of higher order must not be neglected in the consideration of scattering processes in the atmosphere.

## 13. POLARISATION PHENOMENA

All the considerations on the scattering of incident radiation in the atmosphere, given previously, apply separately for both the polarised components  $i_1$  and  $i_2$ , or  $i_r$  and  $i_t$ , respectively. It is known that the complete investigation into the scattering processes in the atmosphere requires the computation or the measurement of the four Stokes parameters. As mentioned previously<sup>8</sup>, the computation has been fully accomplished only for the molecular atmosphere. As for the primary scattering by aerosol particles, detailed tabulations are available for the radiance of the atmosphere and its degree of polarization (de Bary, Braun, Bullrich<sup>14</sup>). It is worth mentioning that the polarization phenomena show large variations which are caused by the different sizes of the aerosol particles. Thus, the polarization phenomena enable one to furnish proof of the existence of atmospheric particles of specific sizes. The polarization of the scattered radiation cannot be dealt with in detail here.

Finally, it should be mentioned that all these theoretical reflections are valid only for spherical particles. The spherical shape of the aerosol particles is also the prerequisite for any type of evaluation of direct measurements which are based upon the collection of aerosol particles in the atmosphere; the same is true with optical radiation measurements. There is no doubt about the fact that deviations from the spherical shape exist especially in dense aerosol which is due to human activity. Figure 12 shows as an example an electron micrograph of solid particles which were taken in Los Angeles in smog (Bowler<sup>15</sup>).

## 14. SCATTERING OF RADIATION BY PRECIPITATION ELEMENTS IN THE ATMOSPHERE

The scattering process of radiation in fog raises problems which are similar to those connected with the scattering by aerosol particles. If the sizes and the number of droplets are known, the Mie theory enables one to compute the scattered radiation of a volume element of foggy air according to the laws of geometric optics.

When haze in the atmosphere turns into fog, owing to the increase of the relative humidity, some aerosol particles of specific size do not undergo any change due to hygroscopic effects. These non-hygroscopic particles remain in the fog; those aerosol particles which have turned into droplets are characterised by a size distribution which approximates to a Gaussian distribution. The relevant scattering functions and polarization effects have been computed and measured for a small volume of air.

The penetration of a beam of light into fog or clouds very quickly results in the occurrence of scattering of higher order. The mechanism of propagation of collimated light differs from that of diffuse light. The collimated sun beams have a penetration of 5 km in normal clouds. The backward scattering of higher order plays an important role in clouds. It is usually called the reflectivity of the cloud and it depends on the thickness of the cloud and the size of the cloud droplets. Incidentally, diffraction and refraction phenomena are the almost whitish fogbow and the coloured rainbows. Diffraction and refraction on and in the crystals of ice clouds produce a variety of well-known coloured and uncoloured phenomena.

Research in the field of cloud and precipitation physics is often based on the investigation of radiation which is scattered on snow and ice particles as well as on water droplets. This means the use of the well-known radar technique, which is formed from "radio detection and ranging". Radar is based on a pulse timing method. A powerful radio transmitter of more than 100 kW emits short pulses between 0.25 and 1 microseconds in length. The time interval between the individual pulses is about 1000 microseconds. The echoes from cloud droplets or precipitation elements are recorded up to  $10^{-14}$  watt. The weather radar frequency band lies in between 1.5 and 30 GHz.

Since  $\lambda = c/\nu$ , the related wavelengths lie between 1 and 20 cm, that means the wavelength is of the order of magnitude of the droplet diameter. Thus, again, the Mie theory is valid.

### 15. TWILIGHT

Scattering by particles at a height of about 80 km results in the phenomena of the noctilucent clouds. The measurements of their scattering functions and polarisation imply that the scattering particles are covered by an ice film. Samples which have been collected with rockets and brought down to the ground have been analysed without clear-cut results so far. Radiation measurements during twilight provide at least a qualitative contribution to knowledge of the variations in space and time of the aerosol particles in the high atmosphere. The twilight phenomena are sensitive indicators of the composition of the atmospheric aerosol in the stratosphere, especially the purple light. It is due to the interaction of scattering on molecules and aerosol particles. Volz<sup>16</sup> and other authors have observed the spreading of volcanic dust in the stratosphere. For instance, after the eruption of the volcano Agung the particle number at a height of about 20 km increased from 1 to 10 per cubic centimetre.

### 16. LIDAR

As a final observation the measuring methods which have been developed for the detection of particles in the atmosphere by means of the effects of scattered radiation should be mentioned. By analogy with radar the abbreviation "Lidar" is formed from "light detection and ranging". It comprises coherent parallel and strongly monochromatic radiation which is emitted from a point source. Most popular is the abbreviation "laser" which means "light amplification by stimulated emission of radiation". The most powerful radiation is emitted by the ruby laser stick at the wavelength  $\lambda = 0.694 \mu$ , which, by a lucky chance, is free from absorption by atmospheric gases, as can be seen in Figure 13 (Long<sup>17</sup>). However, there are also gas lasers with weaker emission in other wavelength ranges.

In the case of a small particle concentration, for instance in the stratosphere, powerful lasers must be used. But their application covers also general and tropospheric problems. Thus it was possible to investigate the Cabannes anisotropic coefficient, that means the deviation of the molecules from the spherical shape which plays an important role in Rayleigh's theory. Moreover, Harris et al.<sup>18</sup> could prove that a mono-dispersive system has the same scattering properties in coherent as well as in noncoherent light.

Tropospheric backscatter signals give information on aerosol particles which are accumulated underneath inversions. Furthermore, this method enables one to detect cirrus veils (Masterson et al.<sup>19</sup>), which are invisible because of their small concentration, as can be seen in Figure 14. The same is true with the spreading of smoke plumes. Last but not least, laser is a very useful tool for detecting aerosol layers in the stratosphere as shown in Figure 15 (Kent et al.<sup>20</sup>) and Collins et al.<sup>21</sup>. It would be highly desirable to extend this method to those heights in which extraterrestrial material is encountered. Of course this would require tracking under specific angles; thus laser and receiver should be located at a great distance from each other.

## REFERENCES

1. Junge, C. *Air Chemistry and Radioactivity. International Geophysics Series, Vol.4.* Academic Press, 1963.
2. Jaenicke, R. Junge, C. *Studien zur oberen Grenzgrösse des natürlichen Aerosols. Beiträge zur Physik der Atmosphäre, Vol.40,* 1967, p.129.
3. Fenn, R. *Aerosolverteilungen und atmosphärisches Streulicht. Beiträge zur Physik der Atmosphäre, Vol.37,* 1964.
4. Bullrich, K. et al. *Solar Radiation Extinction, Sky Radiation, Sky Light Polarization and Aerosol Particle Total Number and Size Distribution on the Island Maui, Hawaii. PAGEOPH, Vol.69,* 1968, p.280.
5. Hänel, G. *Master Theses, University Mainz, 1966.*
6. Eiden, R. *The Elliptical Polarization of Light Scattered by a Volume of Atmospheric Air. Applied Optics, Vol.5,* 1966, p.569.
7. Kasten, F. *Rayleigh-Cabannes-Streuung in trockener Luft unter Berücksichtigung neuerer Depolarisierungs-Messungen. Optik, Vol.27,* 1968, p.155.
8. Coulson, K.L. et al. *Tables Related to Radiation Emerging from a Planetary Atmosphere with Rayleigh Scattering. University of California Press, 1960.*
- 9a. Penndorf, R. *New Tables of Mie Scattering Functions. Geophysical Research Papers, Vol.45,* 1956, Part 6.
- 9b. Giese, R.H. et al. *Tables of Mie Scattering Functions and of the Mie Cross-Section for Spherical Particles. Abhandlung der Deutschen Akademie der Wissenschaften zu Berlin. Klasse für Mathematik, Physik und Technik, No.6,* 1961.
10. Bullrich, K. *Scattered Radiation in the Atmosphere and the Natural Aerosol. Advances in Geophysics, Vol.X,* 1964, p.99.
11. de Bary, E. *Influence of Multiple Scattering of the Intensity and Polarization of Diffuse Sky Radiation. Applied Optics, Vol.3,* 1964, p.1293.
12. Heger, K. *Die von der trüben Atmosphäre nach aussen gestreute Strahlung, II. Beiträge zur Physik der Atmosphäre, Vol.39,* 1966, p.11.
13. Bullrich, K. et al. *Research on Atmospheric Radiation Transmission. Air Force Cambridge Research Laboratories, Scientific Report No.6, AFCRL, Bedford, F 61052 67 C 0046,* 1968.
14. de Bary, E. et al. *Tables Related to Light Scattering in a Turbid Atmosphere. Air Force Cambridge Research Laboratories, Vols.15. I - III, AFCRL-65-710, Special Reports, No.33,* 1965.
15. Bowler, E.C.S. *Electron Micrographs of Backyard Incinerators. Engineering Department, University of California at Los Angles,* 1958.

16. Volz, F. *Twilight Phenomena Caused by the Eruption of the Volcano Agung.* Science, Vol.144, 1964, p.1121.
17. Long, R.K. *Atmospheric Attenuation of Ruby Lasers.* Proceedings, Institute of Electrical and Electronic Engineers, Vol.51, 1963, p.859.
18. Harris, F.S. et al. *Experimental Comparison of Scattering of Coherent and Incoherent Light.* Institute of Electrical and Electronic Engineers, Transactions on Antennas and Propagation, AP-15 (1), 1967, p.141.
19. Masterson, J.E. et al. *The Laser as an Operational Meteorological Tool.* Bulletin of the American Meteorological Society, Vol.47, 1966, p.695.
20. Kent, G.S. et al. *High Altitude Atmospheric Scattering of Light from a Laser Beam.* Journal of Atmospheric and Terrestrial Physics, Vol.29, 1967, p.169.
21. Collins, R.T.H. Ligda, M.G.H. *Note on Lidar Observations of Particulate Matter in the Stratosphere.* Journal of Atmospheric Science, Vol.23, 1966, p.121.

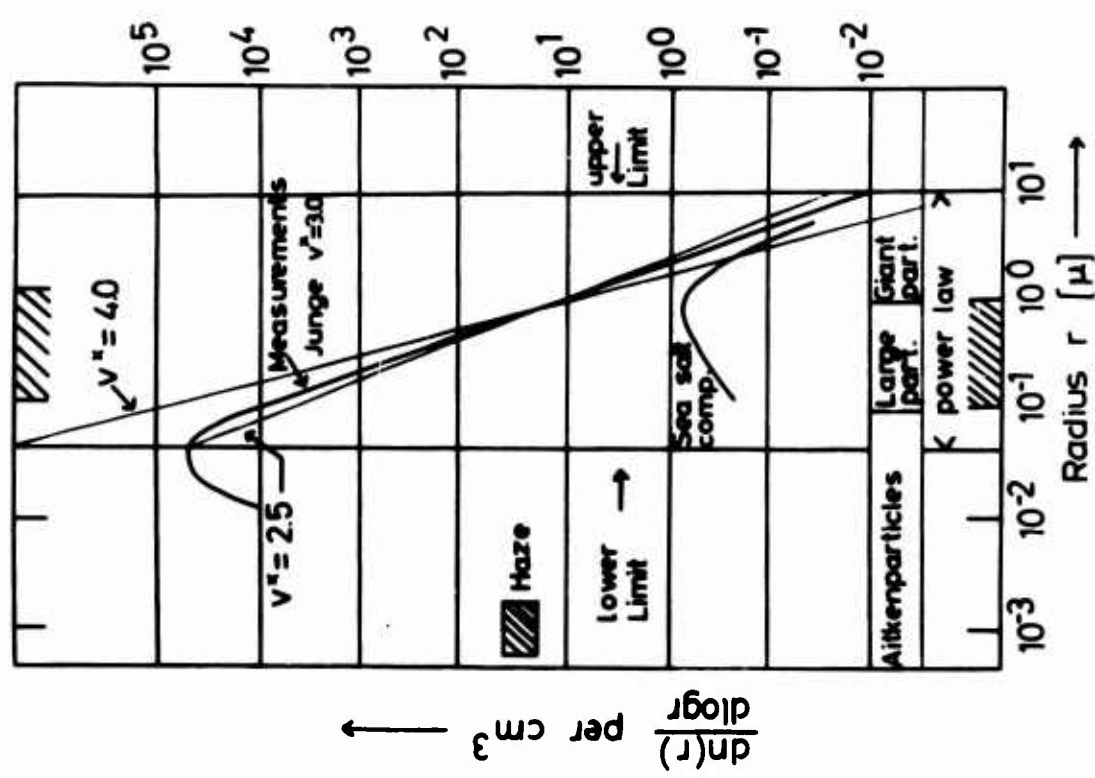


Fig. 1. Normal aerosol size distribution in the continental atmosphere (Junge) (Equation (1)).

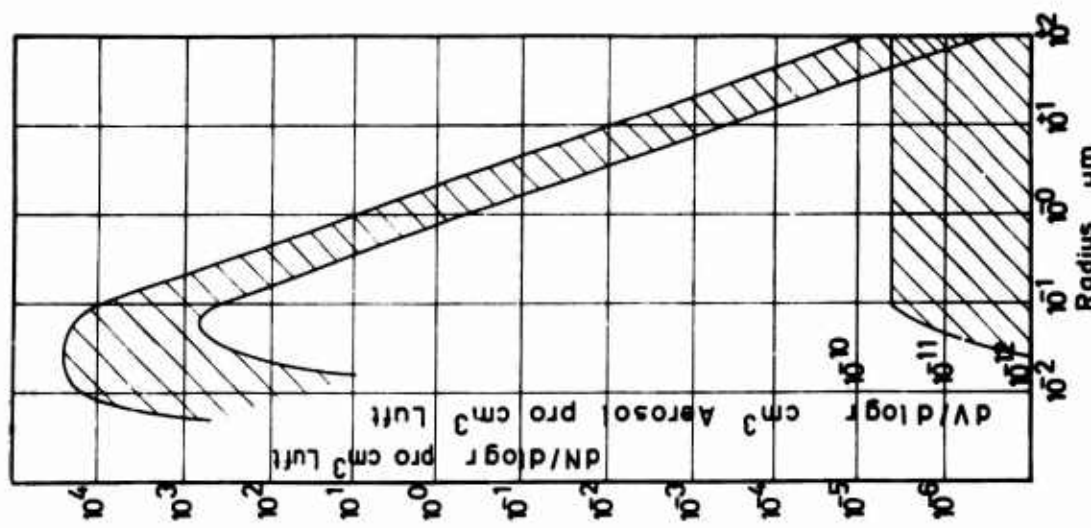


Fig. 2. Size distribution and volume distribution of the aerosol particles (Junge).

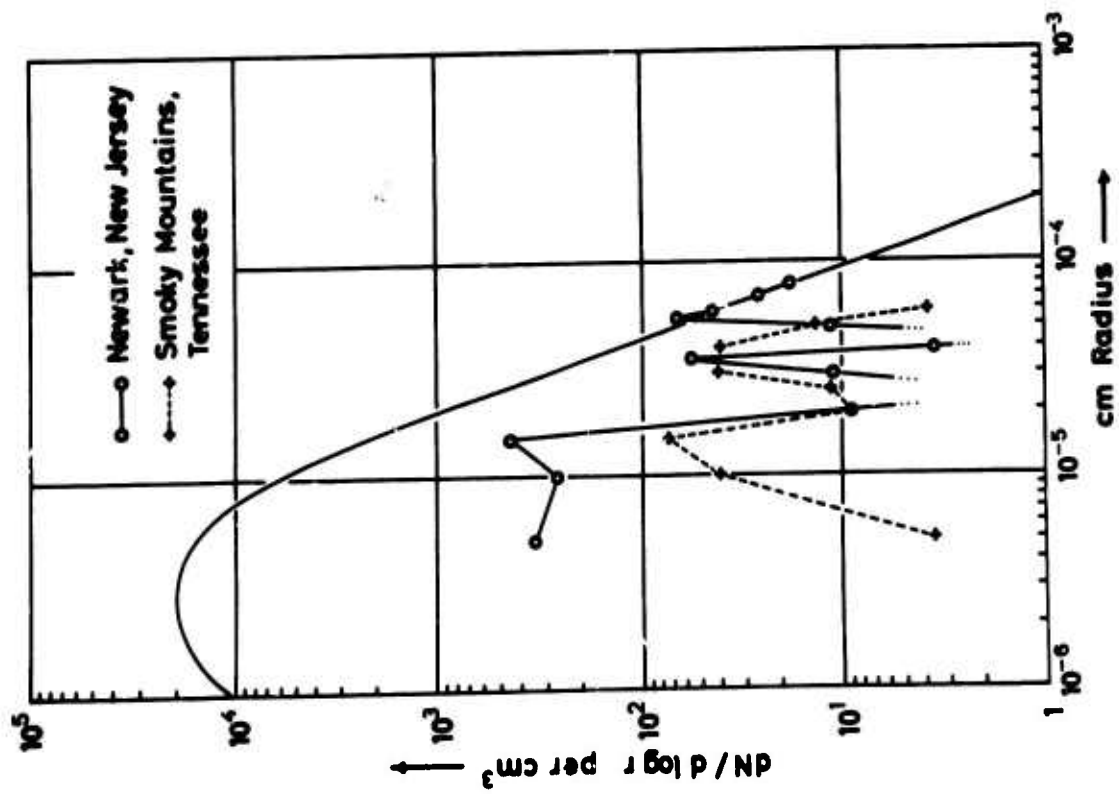


Fig. 3. Deviations of the normal aerosol size distribution (Penn<sup>3</sup>).

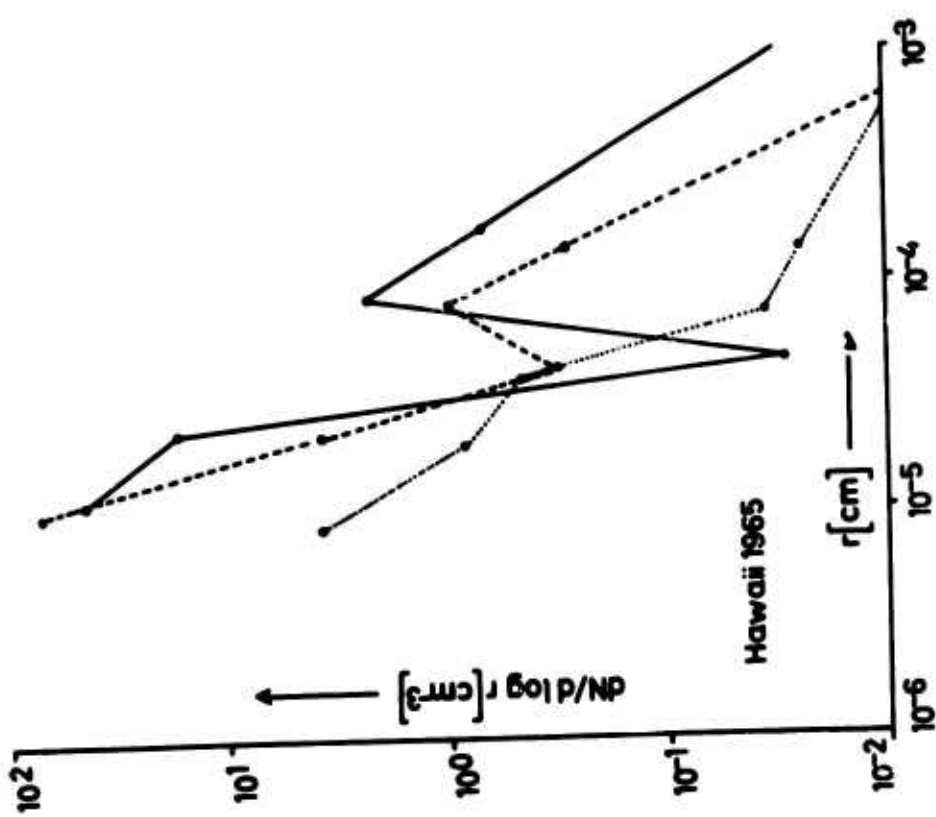
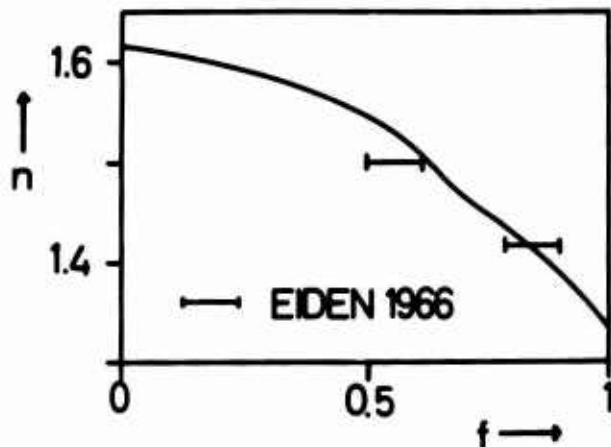


Fig. 4. Aerosol size distribution measured on Maui, Hawaii (Jaenicke<sup>4</sup>).



$$n = n_{12} + \frac{n_2 - n_1}{n_1 V_1} g$$

Empirical rule for the real part of the refractive index  
of mixtures by ARAGO and BIOT.

- $n$  real part of the mean refractive index of atmospheric aerosol particles
- $g$  mean density of atmospheric aerosol particles
- $n_{12}$  real part of the refractive index of the mixture
- $n_1$  real part of the refractive index of the liquid
- $m$  mass of atmospheric aerosol particles
- $V_1$  volume of the liquid

Fig. 5 Refractive index of atmospheric aerosol particles versus relative humidity (Hänel<sup>5</sup>). (Eiden's<sup>6</sup> results have been added. They are based on measurements of elliptical polarisation).

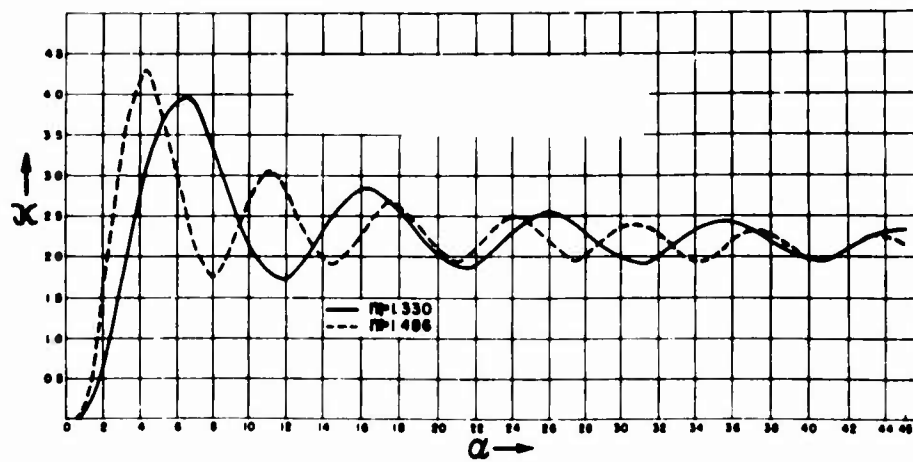
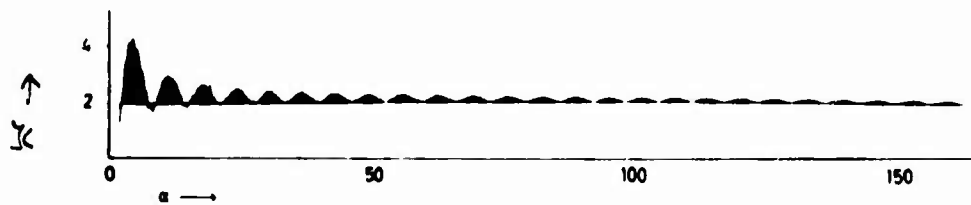


Fig. 6 Scattering cross-section versus  $\alpha = 2\pi r/\lambda$ . (Equation (4)).

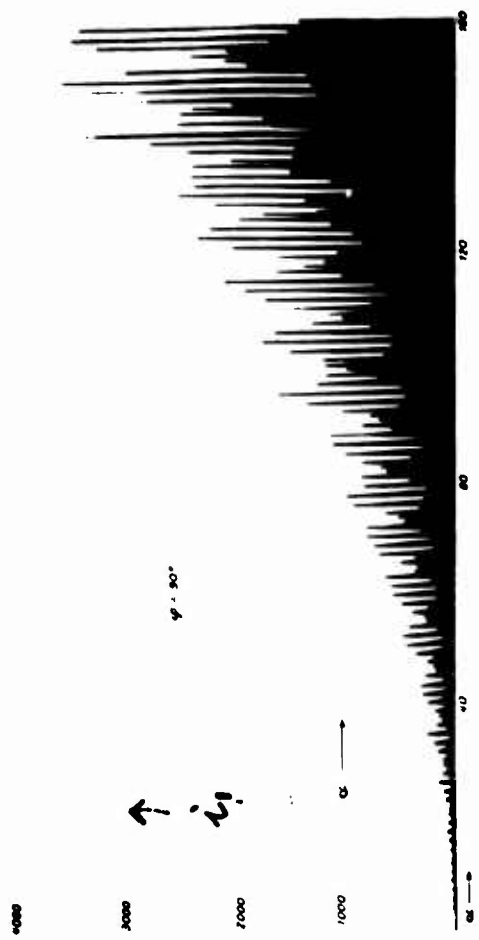


Fig. 7. Intensities of scattered radiation versus  
 $\alpha = 2\pi r/\lambda$ , according to the Mie theory.  
 $i_1$ -component (above),  
 $i_2$ -component (below).  
Scattering angle  $\varphi = 90^\circ$ .

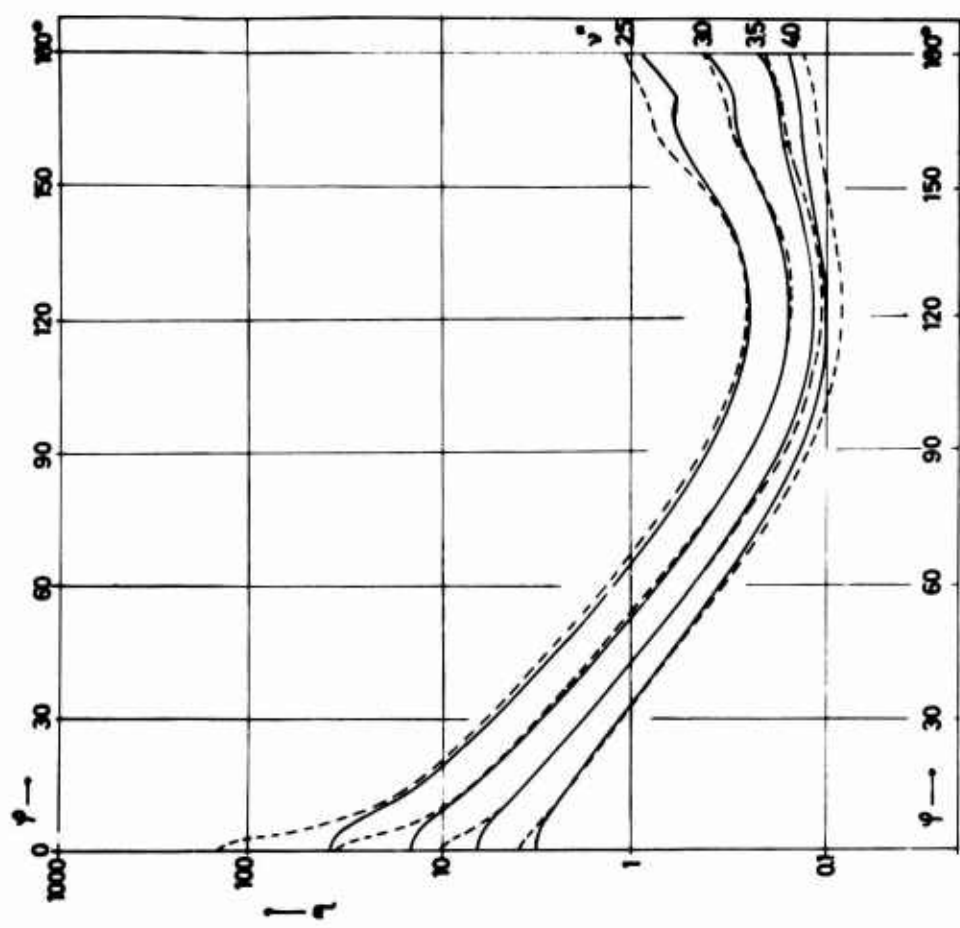


Fig. 8. Angular function of the scattering function of  
aerosol particles for different  $v_*$ ,  
with  $\lambda = 0.4\mu$ .  
(Equations (9) and (10)).

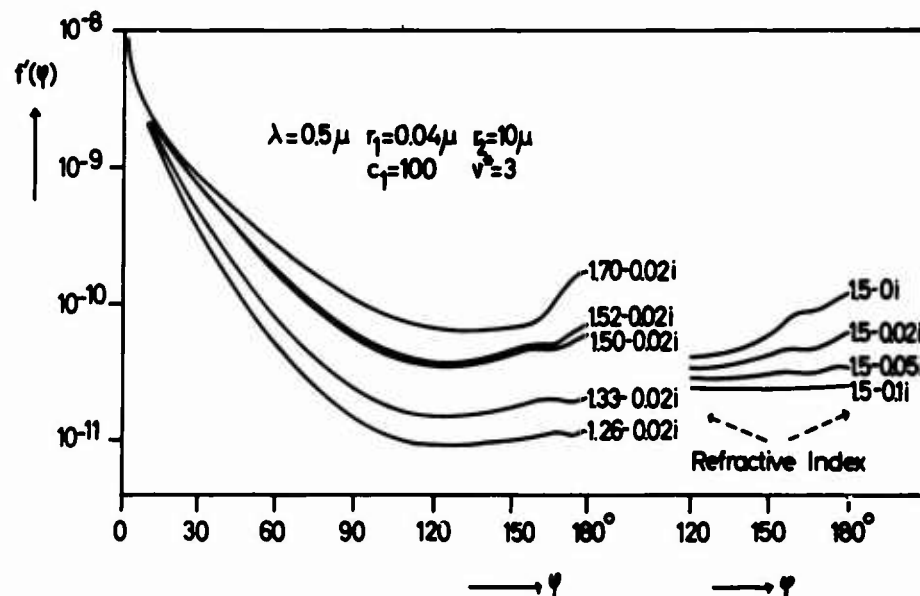


Fig. 9. Scattering function for various refractive indices (Hänel).

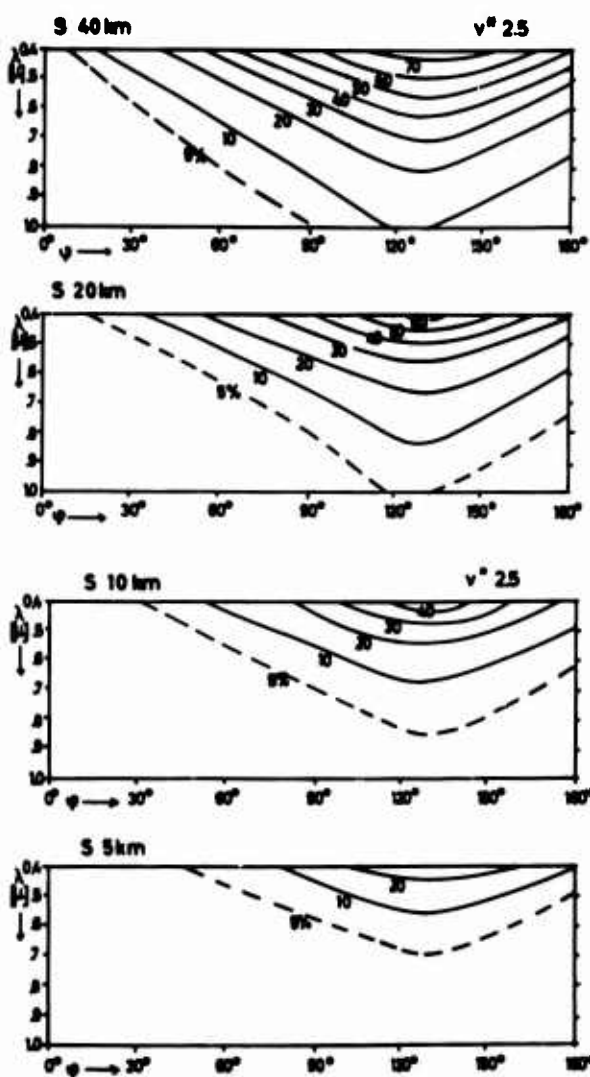


Fig. 10 Ratio of Rayleigh scattering to the total scattering for  $v^* = 2.5$  and various visual ranges.

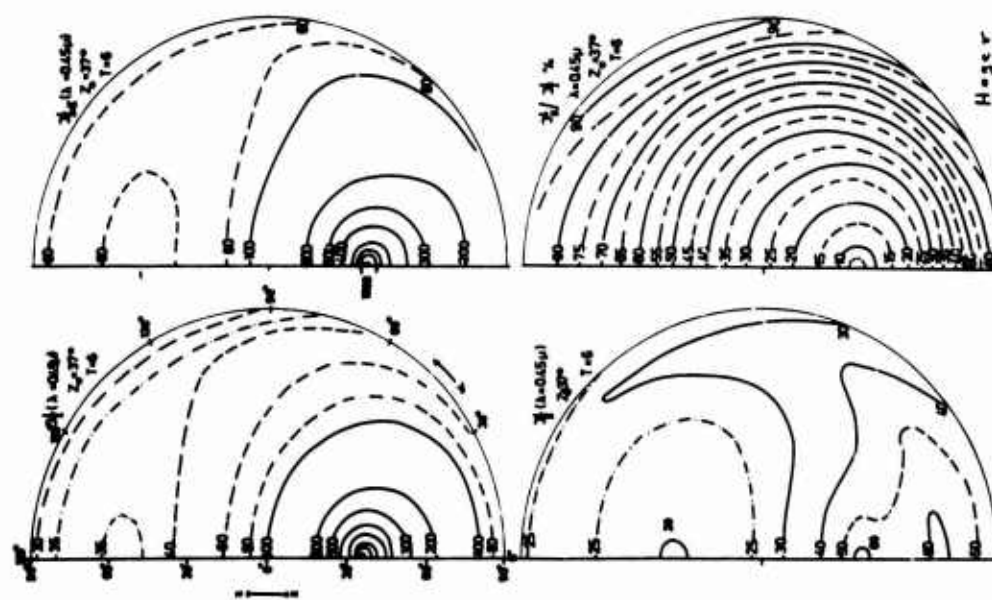


Fig. 11 Ratio of the sky radiation due to primary scattering to the sky radiation due to secondary scattering (Heger<sup>12, 13</sup>).  $Z_0$  = zenith distance of the sun.  $T$  = turbidity factor according to Linke.  $I_1$  = primary scattering,  $I_{II}$  = secondary scattering,  $I_1/I_{II}$  = ratio.



Fig. 12 Electron micrograph of solid particles taken at Los Angeles in smog (Bowler<sup>15</sup>).

### RELATIVE INTENSITY

Fig. 14 Detecting cirrus clouds by using laser  
(Masterson<sup>19</sup>).

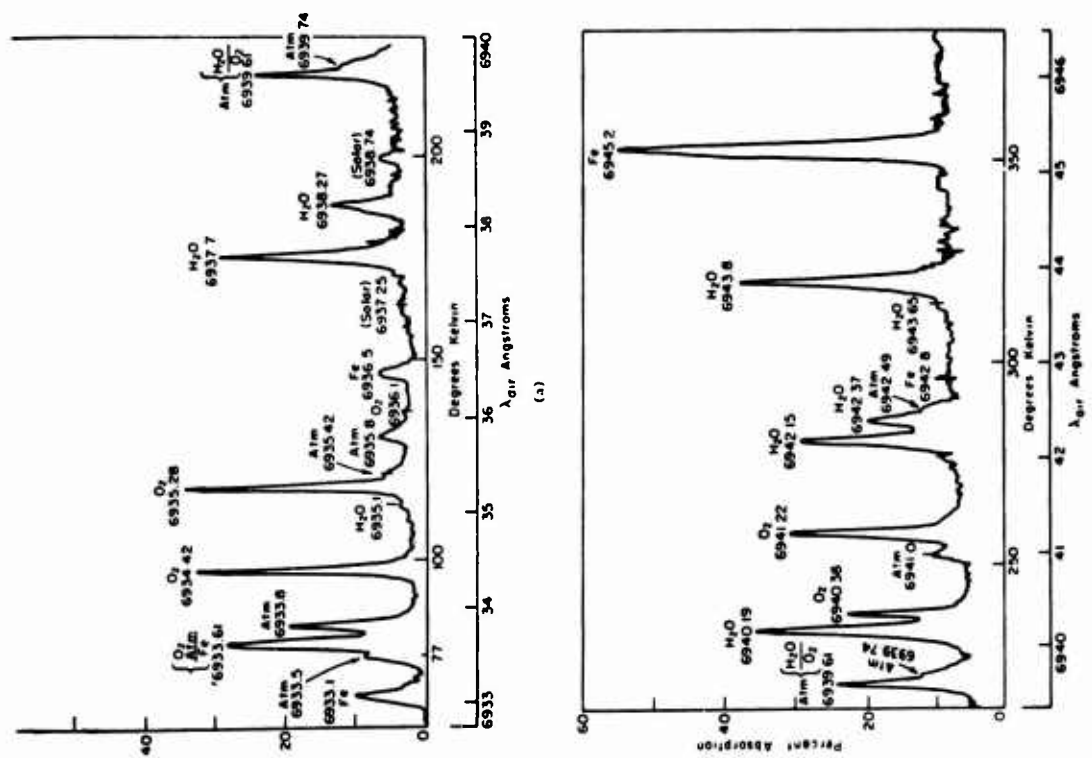
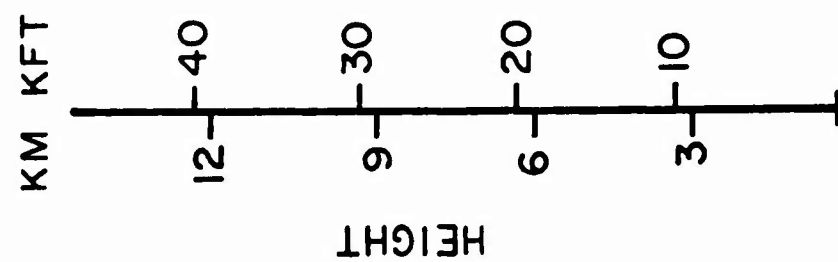
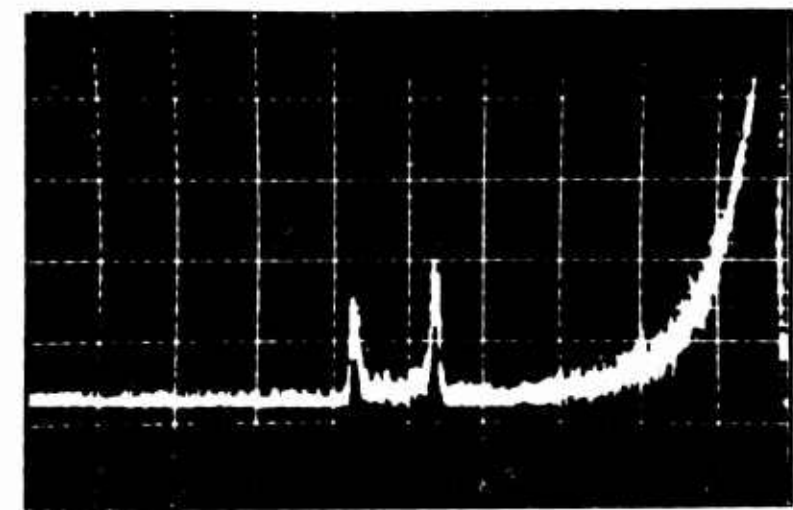


Fig. 13 Spectrum of absorption around the Ruby-laser emission (Long<sup>17</sup>).

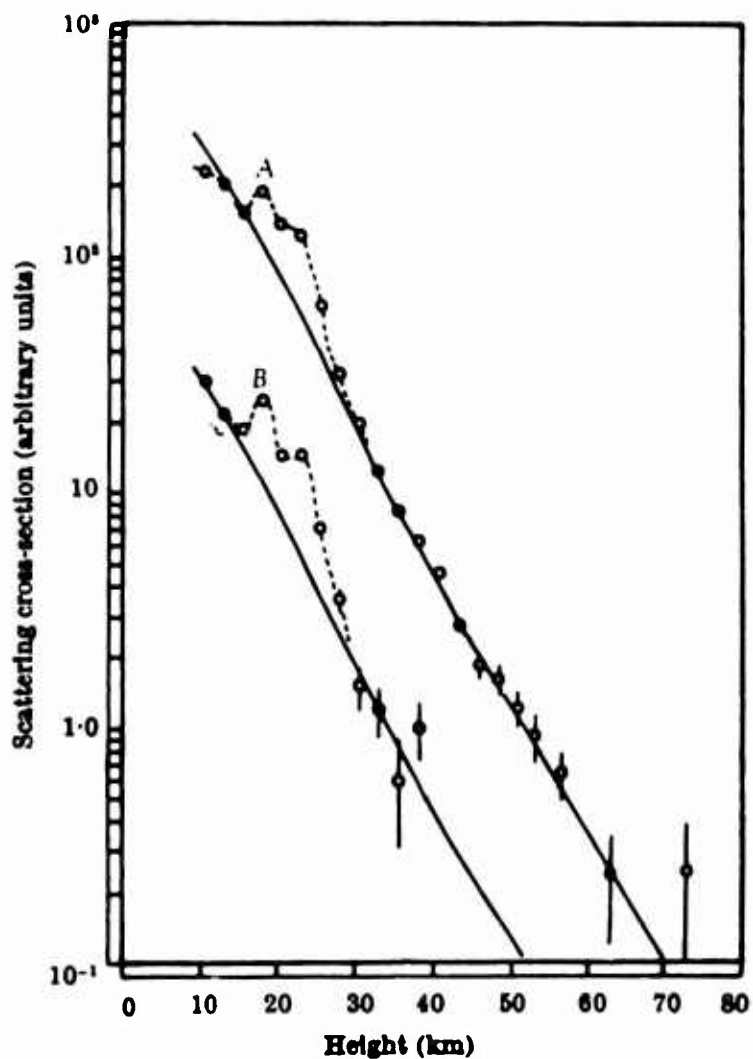


Fig. 15 Detecting aerosol layers in the stratosphere by using laser  
(Kent et al.<sup>20</sup>, Collins<sup>21</sup>)

— standard atmosphere  
---○--- experimental observations

**DISCUSSION ON THE PAPERS PRESENTED IN SESSION II (GROUND SCATTER)**

A considerable part of this discussion was concerned with the results given in *Paper 8 "Interference Patterns in HF Signals Backscattered from Ocean Waves"* by D.B. Muldrew (presented by D.W. Rice). In the general discussion after Session IV the question of scatter from ocean waves was raised again, and for completeness the relevant part of this discussion is also recorded here.

There were several questions concerning the uniqueness of the interpretation suggested by Mr Muldrew:

**Dr J. Ramasastry:** Unless it can be shown that the phenomenon described in Mr Muldrew's paper was either repetitive in time or extended over a period of time, his explanation can only be accepted as tentative. I also believe that the ionospheric effects due to irregularities cannot be excluded. Is it possible to obtain such wavelengths in the irregularities in the F-layer of the ionosphere?

**Dr H.G. Möller** also asked if ionospheric effects could be excluded.

**Dr D.W. Rice:** The explanation of Muldrew is offered as a tentative one which seems to fit the experimental data; however, it is not claimed to be a unique explanation.

**Dr E.N. Bramley:** If the observed effects were due to ionospheric phenomena, these would produce characteristic patterns on first-order ionospheric echoes where ground reflection is not involved.

**Dr C.R. Roberts:** In one of your oblique ionograms there was a trace whose slope was negative with respect to frequency. Would you repeat your explanation of this? Does the amplitude of the coherent returns compare with what would be expected from the suggested target?

**Dr D.W. Rice:** The negative slope would be a result of a positive ocean wavelength gradient with increasing range from the radar; either slope is possible. Your second question is dealt with in the written paper; the answer is yes.

**Dr J. Ramasastry:** Since it is a fixed transmitter-receiver experiment, what is the time dependence of such events that you discussed? How long did each event persist? How do your calculated results of ocean wavelengths and gradients compare with those generally accepted?

**Dr D.W. Rice:** Mr Muldrew will be asked to provide the answer to your first questions after the conference. The answer to your last question is that the agreement is excellent in the limited number of cases that have been analyzed in detail.

**Professor I. Ranzi:** I have the following question on the papers by D.W. Rice and D.B. Muldrew: Did you observe any effects due to large-scale traveling disturbances? As they have a wave-like structure, with wavelengths of the order of 200-400 km, their influence may be important. In other words, did you observe any seasonal variation that might be due to the seasonal variation of the ionospheric irregularities?

**Dr D.W. Rice:** We did not observe any seasonal effect.

*The following discussion on sea scatter took place during the general discussion after Session IV.*

**Professor I. Ranzi:** My main objection to Mr Muldrew's interpretation of his observed backscattered echo pattern is that the Doppler frequency shift of the radio waves back-

scattered from the sea waves is always a well defined one, and it corresponds to a coherent backscatter from sea waves having a length equal to  $\lambda/2$ , and never to  $n\lambda/2$  ( $n$  is an integer). Furthermore, we never observed any "aspect sensitivity" of the backscattered echoes (with respect to the direction of propagation of the sea waves). These facts may be explained by assuming that the backscatter occurs from the small sea surface ridges rather than from the sloping surfaces of regular sinusoidal sea waves.

**M. C. Goutelard:** Les calculs que nous avons faits à propos de la rétrodiffusion sur la mer montrent que l'énergie rétrodiffusée est causée par l'agitation de la mer superposée à la houle. Malgré la simplicité des modèles choisis, les résultats experimentaux paraissent confirmer cette interprétation. On constate, par exemple, que les amplitudes des échos reçus par rétrodiffusion sur la mer ne présentent pas des grandes variations auxquelles on aurait pu s'attendre si le creux de la mer intervenait directement dans ce phénomène. Je pense que la houle introduit un phénomène d'interférence dont l'influence est importante dans la transmission de l'énergie vers l'avant, tandis que dans la rétrodiffusion ce phénomène apparaît, selon nos calculs, de plusieurs dizaines de dB en dessous du phénomène de diffusion. Ces résultats sont en accord avec les idées exposées par le Professeur Ranzi, et je voulais le signaler.

**Dr E.S. Warren:** The question arises of whether the experiments made by Dr Muldrew and by Professor Ranzi are compatible and should be compared. I should like to ask Professor Ranzi what the elevation angle was for the measurements he has quoted.

**Professor Ranzi:** The measurements were also made from a mountain, and the elevation angle ranges should therefore presumably be adequate.

**Dr. E. S. Warren:** The areas of the ocean scanned by the two experiments are dramatically different, and therefore the probability of observing regular structure may be very different.

**Professor I. Ranzi:** I think we may conclude that further experimental and theoretical studies are needed to clarify this question.

*The author of Paper 8, Mr Muldrew, who was not present at the meeting, was later invited by the editor to give his comments on the discussion on sea scatter.*

**Mr Muldrew:** Most of Dr Ramasastry's comments have been answered either in the text or by those present at the meeting. With regard to his first comment the explanation in my paper is still considered tentative, although the phenomenon does extend over a period of time. Interference ridges can be frequently followed from ionogram to ionogram over a period of hours. The ionograms were recorded at a rate which changed from time to time but was either 1, 2, or 3 ionograms per hour. The location of the ridges is slightly different on consecutive ionograms; this is an area of study which has not yet been sufficiently investigated to discuss here.

In reply to Prof Ranzi's question on seasonal variations, no attempt has yet been made to correlate traveling disturbances with the occurrence of interference patterns on the ionograms. Since the meeting in Norway, a statistical study has been made on the occurrence of ordinary backscatter and on the occurrence of backscatter containing interference patterns. The results of this study are shown in Figure 1. The number associated with each month is the number of usable ionograms recorded during the month. In general backscatter occurs in the fall and winter months. During those months storms are generally prevalent in the North Atlantic. However, the ionosphere also has the highest critical frequencies during this period and the seasonal variation may be due to the seasonal variation in critical frequency. The figure shows that, where backscatter occurs, there is a fair chance that interference patterns will be observable in the backscatter. The percentages for the winter of 1957-58 are considerably higher than for the winter of 1959-60; this may not be a real effect but may be due to the ionogram recording technique. Because of this, it

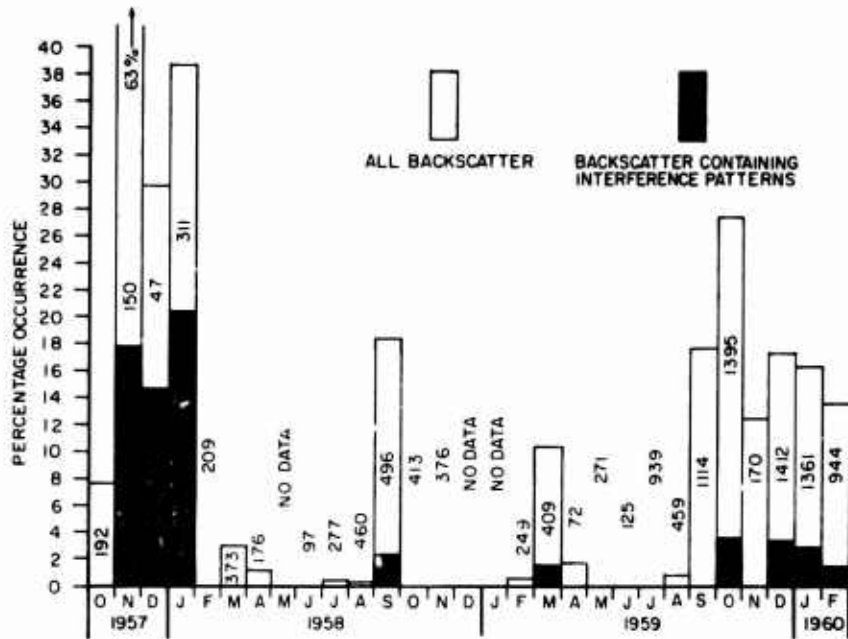


Fig. 1 Percentage occurrence of backscatter and percentage occurrence of backscatter interference patterns, observed on oblique-incidence ionograms recorded at Ottawa.

would be difficult to relate the seasonal variation of travelling disturbances to the statistical seasonal variation of the interference patterns.

With regard to Prof Ranzi's second comment, evidence for coherent backscatter from ocean waves of length  $\lambda$  ( $n = 2$ ) is given in an excellent paper by D.D.Crombie (Nature, Vol. 175, 1966, p. 681). In fact, the voltage-reflection coefficient  $|R|$  of Wait (see Equation (6) of text) is not even a function of  $n$ ;  $|R|$  is only a function of the radio wavelength, the size of the coherent region and the height of the ocean waves. Hence, it is not unlikely that coherent backscatter could occur from ocean waves of length  $n\lambda/2$ , when  $n$  is large.

*Discussion on Paper 11 "Aperture Synthesis in Ionospheric Ground Backscatter Radar," by E.D.R.Shearman.*

**Dr K. Davies:** Radio astronomers use techniques similar to those used by Professor Shearman. They record the data on magnetic tape and feed the tapes into digital computers. I should like to ask Professor Shearman if he has tried this technique?

**Professor E. D. R. Shearman:** The data rate in radio astronomy is considerably lower than for our experiment, low enough in the Cambridge and Jodrell Bank experiments to use punched paper tape. Because we have to process some tens of range resolution cells simultaneously with a fast data rate per cell, optical recording is a very convenient solution. It fits in ideally with optical processing in which parallel Fourier transformation in a number of channels is practicable.

**Dr I. Paghis:** You mentioned an integration time of 5 to 10 minutes. However, it was not clear to me whether this integration time was based on what you found practically feasible in instrumentation or whether the prime consideration was the behavior of a specific ionospheric model.

**Professor E. D. R. Shearman:** There is no inherent instrumentation limit, but there is a compromise between a synthesis time which is fast enough to be complete before the ionospheric pattern viewed has moved by one azimuth resolution cell and one which is slow enough to permit phase averaging for the incoherent signals from targets in adjacent cells. Study of this compromise indicates that 5 to 10 minutes is adequate.

*Discussion on Paper 12 "Courte Note sur les Echos 2XF Diffus Observés à Djibouti" by A.M.Bourdila and J.Odoux (presented by Commandant P.Halley).*

**M. C.Goutelard:** Vous dites que l'étalement de l'écho ne peut être expliqué totalement par les modèles que vous proposez. Pensez-vous que, dans le cas de la Figure 5, un second mode 2F situé de l'autre côté de celui indiqué et pour lequel existe un phénomène de divergence expliquerait, par combinaison avec le premier, l'étalement des échos observés?

**Commandant P.Halley:** Non, j'ai dit que la variabilité dans le temps de l'effet constaté, c'est à dire de l'étalement de l'écho en hauteur virtuelle ne peut être expliquée par les seules irrégularités du sol terrestre ou maritime. Il faut supposer une variabilité de l'ionosphère. Le miroir équivalent concave, plan, ou convexe présente une normale dont la direction varie, si bien que la surface du sol intéressée varie. Les irrégularités du sol, telles que de faibles changements, de pente, expliquent bien l'étalement de l'écho constaté.

*Discussion on Paper 13 "Scatter by Particulate Suspensions" by K.Bullrich.*

There was some discussion on the possibility of detecting the nature of the suspended particles (that is their composition, shapes and sizes) from scatter measurements.

**Dr K.Davies:** Do you imply, Professor Bullrich, that the scattering properties of aerosols depend only on their size and shape and not on their chemical composition? It is possible to determine the chemical composition from the shape of atmospheric (pollution) particles?

**Dr J.Ramasastri:** In connection with Dr Davies's question about the determination of the chemical composition by backscatter measurements, I am aware of results determined by aerosol particle analysers in balloons and rockets.

**Professor K.Bullrich:** The chemical analysis of atmospheric aerosol particles is difficult because of their mixed structure, that is, one particle may consist of several constituents. The analysis of rain water is not representative. In the particle analysis sulfur compounds like  $\text{SO}_2$  and  $\text{SO}_4$  have been found to be important, but  $\text{NH}_4$ , Ca, Si and others have also been detected.

**Dr H.J. Albrecht:** I should like to ask Professor Bullrich the following questions:

Regarding your statement that scattering of higher orders is more pronounced during certain types of meteorological conditions (clouds etc), have there been any supporting measurements?

What is the influence of particle shape on scattering of higher orders?

With reference to backscattered laser signals from clouds, is there any relationship between the scattered signal and other (meteorological) parameters, if measured at all, within the same cloud?

**Professor K.Bullrich:** Numerous measurements have been done which give indirect information about the multiple scattering in the atmosphere. The deviations from the measurements of theoretical values which do not include the higher order scattering were used to estimate the scattering of higher order.

The answer to your second question is not known for the atmosphere so far. Probably the influence of particle shape on multiple scattering is small if the air is not too turbid. The influence is great on the measured results for particles using impactor systems.

In the laser beam experiments, profiles of temperature were measured simultaneously. Very thin clouds and aerosol particle layers were found in inversions.

**SCATTERING OF RADIO WAVES FROM REGULAR  
AND IRREGULAR TIME VARYING REFRACTIVE  
INDEX STRUCTURES IN THE TROPOSPHERE**

by

**Dag T Gjessing**

Norwegian Defence Research Establishment,  
P O Box 25, Kjeller,  
Norway

## SUMMARY

The aim of this paper is to review the problems related to tropospheric radio scatter propagation. It is intended to give a unified treatment of the phenomena encountered, in the sense that scattering from turbulent irregularities and scattering (reflection) from layers are not treated as separate phenomena using the two "classical" sets of mathematical tools. Starting from first principles, we shall briefly show that any atmospheric structure, random (turbulent) or ordered (layered), can be expressed in general terms in the form of a three-dimensional refractive index spectrum and, when investigating the characteristic properties of the scattered radio wave (angular power spectrum, bandwidth, frequency and space diversity properties, antenna-to-medium coupling loss, etc), the calculations are based on this general three-dimensional refractive index spectrum. An attempt is made to treat the problems in such a way as to ensure a physical understanding of the phenomena encountered, giving first-order results rather than lengthy and very accurate expressions.

## NOTATION

$A$	antenna aperture
$a$	radius of earth
$\beta$	the radio beamwidth
$\gamma$	direction of $\mathbf{k} = \mathbf{k}_0 - \mathbf{k}_s$ relative to the vertical direction
$c$	a constant (usually velocity of light)
$C_n^2$	Tartarskis' scatter coefficient
$d$	distance between transmitter and receiver
$de$	complex e.m.f.
$E(S, t)$	complex field strength
$E_0$	incident field strength
$E_s$	scattered field strength
$\overline{\delta\epsilon^2}$	standard deviation of permittivity fluctuations
$\epsilon_0$	permittivity (average value)
$F$	Doppler shift
$\delta F$	width of the Doppler spectrum
$\Delta f$	bandwidth of scattering mechanism
$f_\epsilon(r, t)$	function describing the refractive index irregularities in time space
$G$	antenna gain
$\theta$	scattering angle
$k_0$	wavenumber of the incident field
$k_s$	wavenumber of the scattered field
$l$	diameter of the first Fresnel zone
$\Delta l$	width of the delay spectrum
$L$	correlation distance
$\lambda$	radio wavelength
$m$	coefficient of anisotropy
$P$	power transmitted or received
$dP$	dipole moment
$d\pi$	polarisation potential
$R(\xi)$	spatial autocorrelation function of the field strength
$\tau$	position vector of the scattering element
$\rho$	phase coherent distance

$\sigma$  scattering cross-section  
 $dv$  a volume element  
 $V$  scattering volume  
 $\phi(K)$  spatial power spectrum of the refractive index field

## SCATTERING OF RADIO WAVES FROM REGULAR AND IRREGULAR TIME VARYING REFRACTIVE INDEX STRUCTURES IN THE TROPOSPHERE

Dag T Gjessing

### 1. INTRODUCTION

During the past decade several theories ostensibly explaining the phenomena encountered in trans-horizon propagation have been advanced. Although there are certain similarities and intermingling of the theoretical foundations between all the theories, they can be roughly classified according to the type of model they employ. One may of course question this classification scheme or, in fact, the models themselves, for a model may be anything from a fictitious mathematical artifice to a plausible explanation of the actual mechanisms involved. Nonetheless, there appear to be three distinct groups of theoretical work.

- (i) Theories based on turbulence. Booker-Gordon<sup>1</sup>, Villars-Weisskopf<sup>2</sup>, Megaw<sup>3</sup>, Batchelor<sup>4</sup> and many others.
- (ii) 'Mode-theories'. Carroll-Ring<sup>5</sup>, Bullington<sup>6</sup>.
- (iii) Reflection theories. Friis-Crawford-Hogg<sup>7</sup>, Waterman<sup>8</sup> and others.

These different groupings automatically demand that any complete experimental verification of all the theories is quite extensive<sup>9</sup>. Surprisingly enough, each theory has, to a greater or lesser extent, been verified by experimental results. This apparent paradox of seemingly different theories all being experimentally confirmed can be simply explained by noting that in all cases only simple experiments could be explained. This then leads to the conclusion that the differences between the various theories is really only superficial, and that the sometimes "equal" experimental confirmation is in most cases simply a confirmation of the underlying similarities and not in any way a substantial proof of the validity of an individual theory.

With the knowledge that we possess today, it seems reasonable to conclude that whether we support theories based on scattering from turbulent irregularities or theories based on "reflections" from layered structures depends on the ambient atmospheric conditions and on the radio wavelength used.

In this paper we shall try to give a unified treatment of tropospheric scatter problems. We shall not treat scattering from turbulent irregularities and scattering (reflection) from layers separately, using the two "classical" sets of mathematical tools. Starting from first principles we shall briefly show that any atmospheric structure, random (turbulent) or ordered (layered) can be expressed in general terms in the form of a three-dimensional refractive index spectrum and, when investigating the characteristic properties of the scattered radio wave (angular power spectrum, bandwidth, frequency and space diversity properties, antenna to medium coupling loss), we shall base our calculations on this general three-dimensional refractive index spectrum. We shall attempt to treat the problem in such a way as to ensure a physical understanding of the phenomena encountered, giving first-order results rather than complicated expressions of optimum accuracy, knowing that such detailed treatments will be given in contributions following this introductory paper.

## 2. ANGULAR SCATTERED POWER SPECTRUM IN RELATION TO REFRACTIVE INDEX STRUCTURE

Consider a volume element  $dv = dx dy dz = d^3 r$ , within the scattering volume  $V$ , this scattering volume being confined to the spatial region in the troposphere illuminated by the transmitting antenna and "seen" by the receiving antenna. If the permittivity (refractive index) within the elementary volume differs by an amount  $\Delta\epsilon$  from the average value of the permittivity  $\epsilon_0$  the element of dielectric becomes polarised, giving rise to a dipole moment ( $dP = \Delta\epsilon dv \cdot E_0$ ) when under the influence of an electric field  $E_0$ . Distant  $R$  from the scattering element the dipole moment results in a polarisation potential  $d\psi$  and, provided  $k^2 \nabla \gg \nabla \nabla \cdot \nabla$  (which requires  $R \gg V^{1/3}$ ), the scattered field strength  $E_s = k^2 \nabla \psi$ , where  $k$  is the wavenumber of the electric field. The scattered field resulting from the integral of elementary scattering elements is then given by

$$E_s = \frac{k_s^2}{4\pi R} \int E_0 f(r, t) e^{-jk_r r} d^3 r, \quad (1)$$

omitting the time-factor  $e^{j\omega t}$ .

Here

$$k = k_0 - k_s$$

$k_0$  = wavenumber of incident field

$k_s$  = wavenumber of scattered field

$$|k_0| = |k_s| = 2\pi/\lambda$$

$\lambda$  = radio wavelength.

Thus

$$|k| = \frac{4\pi}{\lambda} \sin \theta/2,$$

where  $\theta$ , the scattering angle, is the angle between  $k_s$  and  $k_0$ . The vector  $r$  is the position vector of the scattering element and  $f_\epsilon(r, t)$  is the space-time function of the normalised permittivity  $\Delta\epsilon/\epsilon_0$ .

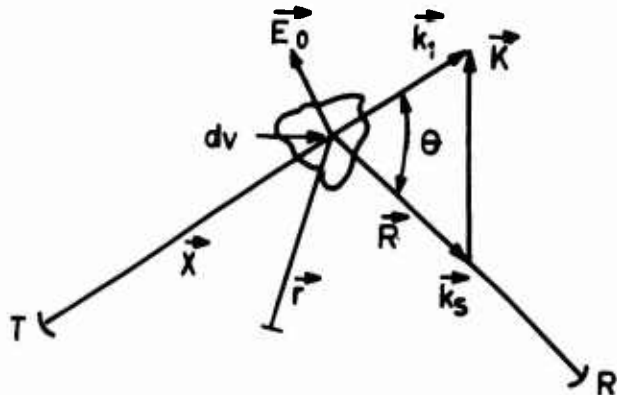


Fig.1 The fundamental geometry

Note that Equation (1), which is derived from Maxwell's equation, is perfectly general and does not consider the nature of the refractive index irregularities described by the function  $f_\epsilon(r, t)$ . This function may be a stochastic one, in which case the refractive

index field is conveniently described by the spatial autocorrelation function of refractive index, or we may be dealing with an ordered variation in  $\epsilon$ , say a horizontal layer through which the refractive index varies in a systematic fashion expressible as a well behaved function.

In order to ensure a thorough physical understanding of the problem, let us discuss Equation (1) in some detail.

(a) Let us first assume that the wave incident on the scattering volume is a plane one and that the linear extension of the scattering volume  $V^{1/3}$  is very small compared with the distance from the transmitter to the scattering volume (and similarly small compared with the distance  $R$  from the scattering volume to the receiving antenna). This means that we must assume that the curvature of the wave front is large, such that the first Fresnel zone in a vertical plane normal to the transmission path is large compared with the linear extension of the scattering volume as measured in this plane. Under such conditions we can exclude the  $E_0$  factor from the integrand of Equation (1), the result being that the scattered field is simply the Fourier transform with respect to space of the  $f_\epsilon(r)$  function. In order to obtain an expression for the angular power spectrum of the scattered wave, we shall have to multiply  $E_s$  by its complex conjugate, thus obtaining the scattering cross-section  $\sigma$  given by

$$\sigma(\theta) = \frac{\pi k^4}{2} \phi(K) , \quad (2)$$

where  $\phi(K)$  is the spatial "power spectrum" of the refractive index field such that  $\phi(K)$  is the Fourier transform of the spatial autocorrelation function of  $f_\epsilon(r)$ .

(b) Then let us consider the opposite case where the incident field  $E_0$  varies far more rapidly with  $r$  than does the refractive index. In the extreme case we assume that  $f_\epsilon(r)$  is a constant throughout the scattering volume. Equation (1) then takes the form

$$E_s = c \int_V E_0(r) e^{-jk\cdot r} d^3r , \quad (3)$$

stating that the diffraction field is the Fourier transform of the field strength distribution in the plane in which  $r$  is measured. For a symmetrical radio path this plane is the vertical cross-path plane illuminated by the transmitter and seen by the receiver.

In the general case, as already noted, Equation (1) applies, so that the angular spectrum of scattered field strength is the Fourier transform of the product  $E(r) \cdot f_\epsilon(r)$ . It should be quite clear then, from the foregoing arguments, that  $E(r)$  can only be excluded from the Fourier integral if the  $E(r)$  function is "wide" in comparison with the  $f_\epsilon(r)$  function.

Then let us consider these two functions in turn.

(i) The "width" of the  $f_\epsilon(r)$  function is easily defined if we are dealing with a non-stochastic function, say a layer through which the refractive index varies systematically. The width of the  $f_\epsilon(r)$  function is then simply the thickness of the layer. If we are dealing with a random function of  $f_\epsilon(r)$ , it seems clear that the width of the  $f_\epsilon(r)$  function is comparable with the correlation distance  $L$  of the refractive index field. This we define as the distance we shall have to move before the autocorrelation coefficient of refractive index drops to  $1/e$ .

Practical experiments (see, for example, Reference 10) shows that  $L$  varies with time and position in space. A correlation distance of some 10 m appears to be the right order of magnitude for  $L$ .

(ii) Then let us consider the "width" of the  $E(r)$  function. Here there are two factors which must be considered. If we are neglecting the influence of the irregular refractive index structure on the phase front of the radio beam as this propagates from the transmitter to the common volume, the  $E(r)$  function is determined entirely by the curvature of the phase front in the scattering volume, i.e., the "width" of the  $E(r)$  function is essentially the first Fresnel zone as measured in a vertical cross-path plane through the centre of the scattering volume.

If  $R_1$  is the distance from the transmitter to this plane, then the diameter of the first Fresnel zone is given by

$$l = \sqrt{(2R_1\lambda)} , \quad (4)$$

where  $\lambda$  is the radio wavelength.

A typical value of  $\lambda$  is 5 cm and  $R_1$  may typically be 100 km. Hence the diameter of the first Fresnel zone may typically be 100 m.

However, in order for the radio wave to reach the scattering volume, it will have to propagate through the refractive index irregularities. Hence the phase front in the scattering volume is a perturbed one. In other words, superimposed on the spherical phase front with radius of curvature equal to  $R_1$ , we have random phase fluctuations resulting from the fact that the phase at a point  $P$  in the scattering volume is given by the refractive index integral

$$\frac{\pi}{\lambda} \int_T^P n(x) dx ,$$

$T$  being the transmitter and  $dx$  a line element.

Introducing then the concept of "phase coherence distance", which is the distance measured in the vertical cross-path plane distant  $R$  from the transmitter at which the coherence is  $1/e$ , it can be shown<sup>11</sup> that the phase coherence distance is given by

$$\rho = \left( \frac{1.84}{k^2 R C_n^2} \right)^{3/5} , \quad (5)$$

where  $k = 2\pi/\lambda$  and  $C_n^2$  is Tatarski's scatter coefficient. Putting  $\lambda = 5$  cm,  $C_n^2 = 10^{-12}$  and  $R = 100$  km, we find that the coherence distance is 10 m.

Consequently, the Fresnel zone does not constitute a limiting factor and the  $E(r)$  function is limited by the antenna beams.

In conclusion, therefore, we note that in general it is permissible to exclude the  $E(r)$  term from the integrand. Consequently, if we write the refractive index spectrum (see Equation (2)) in the form

$$\phi(K) \sim K^{-n} ,$$

the angular power spectrum of the scattered wave is given by

$$P(\theta) \sim \theta^{-n}$$

when we assume an isotropic refractive index field.

Before we proceed to consider the characteristic properties of a radio wave scattered from a refractive index structure whose spectral distribution is characterised by the  $\phi(K)$  function, let us briefly consider the form of the  $\phi(K)$  function.

### 3. THE FORM OF THE REFRACTIVE INDEX STRUCTURE

During the last decade a whole spectrum of seemingly different models characterising the tropospheric refractive index field has been advanced. In this presentation we shall consider three such models (three different plausible atmospheric situations) and we shall discuss the form of the refractive index spectrum  $\phi(K)$  appropriate to each model, basing the mathematical treatment solely on the basic Equation (1).

#### 3.1 Scattering by Homogeneous Turbulence

The theory of small-scale turbulence developed by Kolmogorov, Oboukhov and others, based, on natural physical ideas, gives quite definite conclusions on spatial spectra of air velocity fluctuations. A very close relationship is also established between the spectrum of air velocity fluctuations and that of temperature and humidity. Since there is a simple relationship between refractive index  $N$  and temperature  $T$  and humidity  $e$ , the spatial refractive index spectrum can be represented as a linear combination of the  $T$  and  $e$  spectra.

When seeking an expression for the refractive index spectrum  $\phi(K)$ , our first problem is to find the air velocity spectrum appropriate to a specific location in the troposphere and to a specific atmospheric situation.

In the wavenumber range ( $K$ -range) corresponding to the inertial sub-range, this being a limited range between that at which energy is being fed into the turbulence field and that at which energy is being extracted in the form of energy dissipation, the refractive index spectrum  $E(K)$  can, according to turbulence theory (see, for example, Reference 4), be written in the form

$$E(K) \sim \overline{\delta\epsilon^2} l^{-2/3} K^{-5/3}, \quad (6)$$

where  $\overline{\delta\epsilon^2}$  = standard deviation of permittivity fluctuations

$l$  = input scale, i.e.,  $l = 2\pi/K_m$  where  $K_m$  is the wavenumber for maximum  $E(K)$ .

The spectrum  $E(K)$  is the one-dimensional "power" spectrum obtained from an integration of  $\phi(K)$  over all directions of  $K$ .

If the refractive index field is isotropic, then

$$E(K) = 4\pi K^2 \phi(K). \quad (7)$$

In the inertial sub-range we therefore have the following expression for the refractive index spectrum:

$$\overline{\delta\epsilon^2} \phi(K) = 0.033 C_n^2 K^{-11/3}, \quad (8)$$

where  $C_n^2 = 5.3 \overline{\delta\epsilon^2} l^{-2/3}$  as introduced by Tatarski on the basis of structure function considerations.

The expression for the scattering cross-section (see Equation (2)) then takes the form

$$\sigma = 0.03 C_n^2 \lambda^{-1/3} (\sin \theta/2)^{-11/3}. \quad (9)$$

Remembering that the scattering cross-section is defined as the power density of the scattered wave per unit solid angle in the direction of  $k_s$  per unit scattering volume per unit power density of incident wave at the position of the scattering volume, the angular power spectrum of the scattered wave is found directly from Equation (9).

Then let us consider the other extreme case where we are dealing with a layered atmospheric structure.

### 3.2 Scattering from a Layer through which the Refractive Index Varies Systematically

To illustrate the principles involved, let us consider one horizontal layer through which the refractive index varies according to the function  $f_\epsilon(z)$ ,  $z$  being the vertical coordinate. Writing Equation (1) as

$$E_s = \frac{k^2 E_0}{4\pi R} A(K), \quad (10)$$

we can express  $A(K)$  as

$$A_\epsilon(K) = \int_{-\infty}^{\infty} f_\epsilon(r) e^{-j(K_x x + K_y y + K_z z)} dx dy dz.$$

But with a horizontal layer,  $f_\epsilon(r)$  reduces to  $f_\epsilon(z)$ . the permittivity being constant in the  $x$  and  $y$  directions. Thus we have

$$A_\epsilon(K) = \int_{-\infty}^{\infty} f_\epsilon(z) e^{-jK_z z} dz \int_{-\infty}^{\infty} e^{-jK_y y} dy \int_{-\infty}^{\infty} e^{-jK_x x} dx.$$

The integrals having  $x$  and  $y$  arguments are immediately recognised as the Fourier integral representations of the Dirac delta function, so that this expression may be written

$$A_\epsilon(K) = \left\{ \int_{-\infty}^{\infty} f_\epsilon(z) e^{-jK_z z} dz \right\} \delta(K_y y) \delta(y). \quad (11)$$

The function  $A_\epsilon(K)$ , and thus  $E_s$ , then vanishes unless both  $K_x$  and  $K_y$  are zero. Hence  $A(K) = 0$  unless  $K$  is normal to the layer boundary.

In order to obtain an expression for the scattering cross-section, we shall have to form the product  $A_\epsilon(K) A_\epsilon^*(K)$ , obtaining

$$\sigma = \frac{\pi k^2}{2} \left| \int f_\epsilon(z) e^{-jK_z z} dz \right|^2, \quad (12)$$

since  $f_\epsilon(z)$  is a known real function. To obtain the transmission loss relative to the free-space loss, we shall have to perform an integration over the appropriate illuminated layer area, thus obtaining<sup>12</sup>

$$T \sim (\sin \theta/2)^{-2} \left| \int f_\epsilon(z) e^{-jK_z z} dz \right|^2. \quad (13)$$

The flat layer, however, constitutes the simplest, and most unrealistic, of the models involving systematic layers. In order to include the case of a rippled layer, we shall have to consider beam focusing effects, complicating the issue considerably<sup>12, 13</sup>.

In this survey, this case will be not be included.

Then let us replace the smooth layer by a turbulent one.

### 3.3 Scattering from a Turbulent Layer

With turbulent layer we here refer to the case where the intense turbulence affecting radio wave propagation is confined to one or more strata of extremely limited vertical extent as opposed to the case treated in Section 3.1, where it was assumed that the scattering occurred within a great vertical depth of the atmosphere.

A distinct difference between this type of layer and that just discussed is that when we are dealing with turbulent strata, the layer boundaries are not likely to be smooth (smooth in terms of the radio wavelength). This means that mirror reflection, as inferred in Section 3.1, will not take place.

Now, these atmospheric layers are generally associated with a large degree of local stability. Hence it is reasonable to expect the mean temperature and humidity, and hence also the mean refractive index, to vary in a systematic fashion through the layer. On this systematic refractive index profile the random fluctuations of refractive index caused by turbulence are superimposed. Thus there are two factors contributing to the scattered radio power. One is the scattering from the mean profile (partial reflection) as discussed in Section 3.1, the other is the scattering from the random refractivity fluctuations caused by turbulence. Since the two contributions to the scattered field bear random phase relationship, the total resulting scatter field is obtained by simple summation. If then the random refractivity fluctuations obey the inertial sub-range  $K^{-5/3}$  law, and if the mean refractive index profile can be expressed by the function  $f_\epsilon(z)$ ,  $z$  being the vertical coordinate, then the resultant scattering cross-section is given by the sum of Equations (9) and (12). Thus

$$\sigma_T = 0.03 C_n^2 \lambda^{-1/3} (\sin \theta/2)^{11/3} + \frac{\pi k^2}{2} \left| \int f_\epsilon(z) e^{-jkz} dz \right|^2. \quad (14)$$

The relative importance of the two terms of this equation depends on

- (a) the relative magnitude of the root-mean-square random refractivity fluctuations and the degree to which the mean refractive index varies through the layer,
- (b) the thickness of the layer in relation to the quantity  $\lambda/\sin(\theta/2)$ ,
- (c) the radio wavelength  $\lambda$  in relation to the input scale  $l$  of the turbulence field.

Having discussed various plausible atmospheric structures, various forms of the refractive index spectrum  $\phi(K)$ , we shall consider the relationship between this general refractive index spectrum and the characteristic properties of the scattered radio wave.

### 4. PROPERTIES OF A SCATTERED RADIO WAVE

It is the purpose of this section of the presentation to discuss the relationship between the refractive index structure and the characteristic properties of the scattered radio wave. Such an investigation may serve two different purposes. The radio engineer requires information about the transmission loss, the bandwidth limitation, the advantages of space and frequency diversity reception, etc., whereas the radiophysicist would like to know what conclusions can be drawn about the atmospheric structure on the basis of radio measurements.

We have seen that the scattering cross-section is proportional to the refractive index spectrum  $\phi(K)$  and we have shown that the  $\phi(K)$  spectrum takes very different forms, depending on the atmospheric conditions.

To simplifying the mathematics related to a discussion of the characteristic properties of the scattered radio wave, we shall express the spectrum function  $\phi(K)$  in the form

$$\phi(K) \sim \nu(x, y, z) [K]^{-[n-m\gamma/90]} . \quad (15)$$

Here the  $\nu(x, y, z)$  function describes the spatial homogeneity properties of the refractive index field<sup>14</sup>, whereas the coefficient  $m$  is a measure of the degree of anisotropy, the angle  $\gamma$  being the direction of the  $K$  vector relative to the vertical direction<sup>15, 16</sup>. Thus, if the refractive index field is homogeneous and isotropic and governed by the inertial sub-range turbulence law,

$$\phi(K) \sim K^{-11/3} .$$

If, however, we are dealing with a layered structure such that  $\phi(K) = 0$  unless  $K$  is normal to the layer boundary (see Equation (11)), then the coefficient  $m$  in Equation (15) approaches minus infinity and the coefficient  $n$  is determined by the layer thickness and by the profile of the refractive index through the layer.

Experiments<sup>17, 18</sup> shows that the exponent  $n$  is strongly dependent on the atmospheric stability. For low values of the stability,  $n$  may typically be  $6/3$ , whereas  $n$  may be as high as  $21/3$  under very stable conditions<sup>18</sup>.

#### 4.1 Distance Dependence of Scattered Radio Wave

The scattering cross-section is defined as the power density of the scattered wave per unit solid angle in the direction of  $k_s$  per unit scattering volume per unit power density of incident wave at the position of the scattering volume. The scattered power received over a receiving aperture  $A_R$  from an element of the scattering volume  $dV$ , distant  $R_T$  from the transmitter (having gain  $G_T$  and power output  $P_T$ ) and distant  $R_R$  from the receiving antenna, is thus given by

$$dP_R = \frac{P_T G_T}{4\pi R_T^2} \sigma dV \frac{A_R}{R_R^2} . \quad (16)$$

The total power received is thus the integral of Equation (16) over the scattering volume  $V$ .

Our next problem then is to determine the scattering volume, which depends on the atmospheric structure. We shall refrain from going into detail here and confine ourselves to the case of narrow antenna beams such that the factors  $\sigma$ ,  $G$  and  $R$  of Equation (16) can be taken as constant within the scattering volume.

Under these conditions the scattering volume can be written as<sup>14</sup>

$$V = \frac{2 D^2 \beta^2}{3 \sin \theta} , \quad (17)$$

where  $D = 2R$  (for  $R_S = R_T$ ) and  $\beta$  is the beamwidth of the transmitting and the receiving antennas.

Writing then  $\sigma = \pi/2 K^4 \phi(K)$  and  $\phi(K) \sim K^{-n}$ , our expression for the received power reduces to

$$\frac{P_R}{P_T} \sim \frac{(\sqrt{G}) \lambda^{n-2}}{R^{n+2}} , \quad (18)$$

where we have substituted for

$$K = \frac{4\pi}{\lambda} \sin \theta/2 \approx \frac{2\pi}{\lambda} \theta \text{ and } \theta = \frac{2R}{a}$$

where  $a$  is the radius of the earth.

If, however, we are dealing with wide beam antennas, the situation is somewhat different. Since, as we have seen (Equation (9)), the scattered angular power spectrum falls off rapidly with scattering angle, the effective scattering volume is limited to the lower part of the common volume. Accordingly, for wide beam antennas, the scattering volume is smaller than the common volume. An estimate of the scattering volume under such conditions can be obtained by using Equation (17) and substituting for the effective beamwidth  $\beta_{\text{eff}}$ . This is defined as half the difference between the minimum scattering angle ( $\theta_{\min} = 2R/a$ ) and the scattering angle corresponding to a position in space (height) of the scattering element where the contribution to the scattered power is negligible.

Writing then the angular power spectrum in the form  $P \sim \theta^{-n}$  and  $\theta = 2(\alpha_0 + \alpha)$ , where  $\alpha_0$  is half the angle between the earth's tangent planes at the receiver and transmitter respectively, we have

$$\frac{P_\alpha}{P_0} = \left( \frac{\alpha_0 + \alpha}{\alpha_0} \right)^{-n} . \quad (19)$$

Letting then the effective scattering volume be limited to the region within which the scattered power is larger than 1/10 of the maximum value obtained for a scattering angle  $\theta_0 = 2\alpha_0 = R/a$ , we have

$$\frac{P_\alpha}{P_0} = \frac{1}{10} = \left( \frac{\alpha_0 + \beta_{\text{eff}}}{\alpha_0} \right)^{-n}$$

and

$$\beta_{\text{eff}} = \frac{R}{a} (n/(10) - 1) . \quad (20)$$

#### 4.2 Wavelength Dependence of Scattered Radio Wave

Using narrow beam antennas, the wavelength dependence is given by Equation (18). Thus, for large scaled antennas, the scattered power is proportional to  $\lambda^{n-2}$ . This is also seen directly from the basic equation for the scattering cross-section (Equation (2)) putting  $\phi(K) \sim K^{-n}$ . For wide beam antennas, however, the situation is different unless the form of the  $\phi(K)$  spectrum is such that the effective scattering volume for scaled antennas is independant of wavelength.

#### 4.3 Bandwidth Limitations of a Scattered Radio Wave (Frequency Diversity Properties)

Our interest is now focused on the correlation function in the frequency domain. The wavelength dependence, in the way just discussed, has thus no bearing on our problem. To illustrate the issue, let us consider a practical experiment.

We have a scatter connection making use of antenna beams which have large vertical extension and which are narrow in the horizontal plane. Thus, for the vertical direction, it is the  $\phi(K)$  function that limits the upper boundary of the effective scattering volume. The lower boundary is determined by the earth's tangent planes through the transmitter and the receiver respectively.

The transmitter frequency is varied over a small frequency band (some 1% frequency deviation) at a rate which is large in comparison with the rate at which the atmospheric structure changes. At the receiver we measure the field strength as a function of frequency, sweep by sweep, and in general we then find that this is a strongly varying function.

Measuring then the difference in frequency  $\Delta f$  between successive amplitude minima, we obtain a measure of the maximum difference in path length  $\Delta l$  for the waves that reach the receiver via the scattering elements in the scattering volume. Using then, to simplify the discussion, beams which are narrow in the horizontal plane, the difference in path length is a result of scattering from irregularities (scattering element) which are located at different heights in the scattering volume. Note that scattering elements which lie on the same ellipsoidal surface, the foci being at the position of the transmitter and the receiver respectively, give rise to the same delay. Consequently, the width of the delay spectrum is essentially determined by the height distribution of the contributing scattering elements. The delay spectrum is thus determined by  $\phi(K)$  for  $K$  vertical.

In order to ensure a physical understanding of the problems involved, let us seek an approximate expression for the bandwidth capability of the scattering mechanism. In terms of the width of the delay spectrum  $\Delta l$ , the bandwidth  $\Delta f$  is given by

$$\Delta f = \frac{c}{\Delta l} . \quad (21)$$

where  $c$  is the velocity of light.

For a given geometry (i.e., given distance between transmitter and receiver) there is a direct relationship between the width of the delay spectrum  $\Delta l$  and the thickness of the effective scattering volume  $\Delta z$ . Here  $\Delta z$  is approximately equal to the product  $R\beta_{\text{eff}}$ , where  $R$  is half the path length and  $\beta_{\text{eff}}$  is the effective beamwidth as expressed in Equation (20). Measuring thus  $\Delta f$  we obtain a measure of the width of the  $\phi(K)$  function for  $K$  vertical.

Referring to Figure 2, we find that  $\Delta l$  is given by

$$\Delta l = R(\theta\beta + \beta^2) . \quad (22)$$

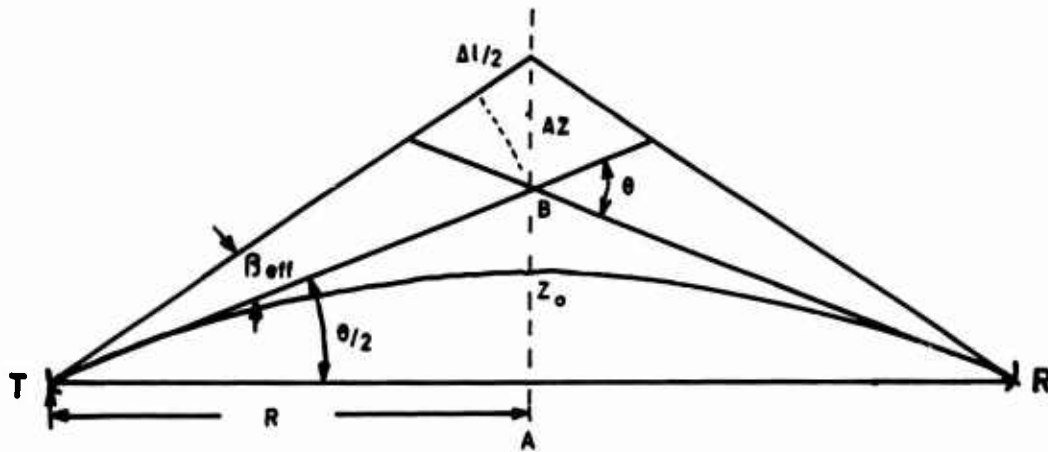


Fig. 2 Bandwidth limitations of the scattering mechanism

Substituting then for  $\theta = R/a$ , where  $a$  is the earth's radius, and for the effective beamwidth as given by Equation (20), our expression for bandwidth takes the form

$$\Delta f = \frac{c}{\Delta l} = \frac{a^2 c}{R^3 (10^{2/n} - 10^{1/n})} . \quad (23)$$

We see that, if the scattering mechanism is such that the  $\phi(K)$  function is narrow, in the limit a delta function, the exponent  $n$  approaches infinity and the bandwidth approaches infinity. If, however, the  $\phi(K)$  function is wide,  $n$  is small and the bandwidth is limited.

Experiments show (see, for example, Reference 10) that the median value of  $n$  is near 4 in accordance with the inertial sub-range  $K^{-5/3}$  law for the  $E(K)$  spectrum. For a 100 mile scatter circuit the bandwidth is then, as given by Equation (23), approximately 9 MHz.

The general expression for the autocorrelation function in the frequency domain is obtained from the fundamental expression for the scattered field (Equation (1)) by forming the product  $E(\omega) E^*(\omega + \Delta\omega)$  and normalising this by  $|E(\omega)|^2$ .

This derivation is analogous to that used in connection with field strength spatial correlation properties to be discussed shortly. It will be seen that the correlation of field strength with spaced antennas, as well as that of field strength with spaced frequency, is obtained by a simple Fourier transformation of the angular power spectrum, i.e., a Fourier transformation of the refractive index spectrum  $\phi(K)$ .

#### 4.4 Field Strength Spatial Correlation Properties of a Scattered Radio Wave

In this section attention is focused on the spatial field strength correlation properties of a scattered wave. We have a wide beam transmitter radiating its power essentially in a horizontal direction. The scattered wave resulting from this transmitter impinges on two nearly identical wide beam receiving antennas positioned beyond the horizon relative to the transmitter. The receiving antennas are placed a distance  $\xi$  wavelengths apart along a direction which may be horizontal or vertical but is always normal to the line joining the transmitter and the receivers. We want to calculate the complex e.m.f. (pre-detection) induced in these antennas.

At an instant  $t$  the complex field strength from the direction  $\alpha$  (where  $\alpha$  is measured in a plane containing the transmitter and the two receiving antennas) is taken to be  $E(S, t)$  at the mid-point of the receiving antenna baseline. Here  $S = \sin \alpha$ .

The complex e.m.f. induced in the two antennas from this direction is thus given by

$$\left. \begin{aligned} de_1 &\sim E(S, t) e^{-j\pi\xi S} dS \\ de_2 &\sim E(S, t) e^{+j\pi\xi S} dS \end{aligned} \right\} \quad (24)$$

Integrating over all values of  $S$  we obtain the total e.m.f. in the two antennas:

$$e_1 \sim \int E(S, t) e^{-j\pi\xi S} dS$$

$$e_2 \sim \int E(S, t) e^{+j\pi\xi S} dS.$$

The normalised complex correlation of these two voltages is thus

$$R(\xi) = \frac{\overline{e_1 e_2^*}}{\overline{|e_2|^2}} = \frac{\int |E(S)|^2 e^{-j2\pi\xi S} dS}{\int |E(S)|^2 dS}. \quad (25)$$

(Bars refer to time averaging.)

Equation (25) states that the spatial autocorrelation function  $R(\xi)$  of field strength is the Fourier transform of the angular power spectrum.

Note, again, that if  $\xi$  is measured along a horizontal direction, the angle of arrival spectrum is measured in a horizontal plane. If  $\xi$  is measured vertically, the angle of arrival spectrum is measured in the vertical plane.

Thus from horizontal and vertical correlation measurements (averaging in time) we obtain exactly the same information as that which would be obtained from an experiment using one directional antenna swinging the beam in azimuth and elevation respectively.

Having obtained the required relationship between the refractive index structure and the angular spectrum of the scattered wave, and also the relationship between angular power spectrum and spatial field strength correlation, we are in the position to present definite and practical results regarding the field strength correlation distance as measured by ground-based spaced receivers.

We shall first consider an isotropic refractive index structure. Specifying the angle of arrival of a particular scattered wave by an elevation angle  $\alpha$  (relative to the line joining the transmitter T and the receiver R) and an azimuth angle  $\beta$  relative to the great-circle plane through T and R, we can write the scattering angle  $\theta$  as<sup>15</sup>

$$\theta \sim (\beta^2 + \alpha^2)^{1/2}, \quad (26)$$

such that the angular power spectrum in accordance with Equation (2) becomes

$$P(\alpha, \beta) \sim (\beta^2 + \alpha^2)^{-n/2}. \quad (27)$$

Note, then, that in order to calculate the correlation properties of the field strength with horizontally spaced antennas, we shall have to take the Fourier transform of the  $P(\beta)$  angular spectrum, whereas vertically spaced antennas require a Fourier transformation of the  $P(\alpha)$  spectrum.

In order to be in closer contact with the physics of the problem throughout the mathematical manipulations, let us briefly consider a simple approximate method by the application of which the field strength correlation distance can be calculated. The correlation distance we define as the antenna spacing required for the correlation coefficient to drop to 1/e.

We have already noted the close relationship between angular power spectrum and field strength correlation.

Diverting for a moment to some fundamental relationships applicable to antenna problems, some striking similarities are readily seen.

We know that the angular power spectrum (antenna radiation pattern) of an antenna is the Fourier transform of the illuminating field strength distribution over the antenna aperture. For a rectangular illumination function, the 3 dB width of the resulting angular power spectrum is given by

$$\theta_{1/2} = \frac{0.88\lambda}{L}, \quad (28)$$

where L is the width of the illuminating field strength distribution<sup>19</sup>.

Applying these results to our problem, we have that the 3dB width of the scattered beam, as measured in the vertical plane, is given by

$$\frac{P_{1/2}}{P_0} = \frac{1}{2} = \left( \frac{\alpha_0 + \alpha_1}{\alpha_0} \right)^{-n}, \quad (29)$$

where  $\alpha_{1/2}$  is the 3dB beamwidth and  $\alpha_0 = d/2a$ , where  $d$  is distance between transmitter and receiver and  $a$  is the radius of the earth. Solving for  $\alpha_{1/2}$  and substituting this in Equation (28), we have

$$\frac{L_v}{\lambda} = \frac{0.44}{n\sqrt{2}} \frac{a}{d}. \quad (30)$$

In order to find an approximate expression for the horizontal correlation distance, we use the same approach as before, now in terms of the angular power spectrum as measured in the horizontal plane.

We then find that the correlation distance is given by

$$\frac{L_h}{\lambda} = \frac{0.44}{(n\sqrt{4}) - 1} \frac{a}{d}. \quad (31)$$

Note that the result of Equations (30) and (31) are in very good accord with the result based on rigorous Fourier transformations of the angular power spectra.

So far we have limited our attention to the isotropic case; let us finally include the more general situation of anisotropy.

Referring to Reference 15 for details, we write the refractive index spectrum in the form

$$\phi(|K|, \gamma) \sim |K|^{-n + (m\gamma/90)},$$

where  $\gamma$  is the direction of  $K$  relative to the vertical direction and  $m$  is a measure of the degree of anisotropy. We see that when  $K$  is vertical  $\phi(K) \sim K^{-n}$ , whereas when  $K$  is horizontal (i.e., scattering takes place in a horizontal plane)  $\phi(K) \sim K^{-n + m}$ .

It can be shown<sup>15</sup> that the angle  $\gamma$  is given approximately by  $\tan \gamma = \beta/(\alpha + \alpha_0)$ . We see that the vertical correlation distance is not affected by the anisotropy, whereas the horizontal correlation of field strength is given by

$$R(\xi_h) = \text{Fourier transform of } \left( \frac{\alpha_0^2 + \beta^2}{\alpha_0^2} \right)^{-\frac{1}{2}[n + (m\gamma/90)}.$$

This expression, however, does not readily lend itself to approximate solutions. A procedure involving direct numerical Fourier transformation is therefore necessary<sup>20</sup>.

#### 4.5 Antenna Gain Degradation in Scatter Propagation

When calculating the power received over a scatter path, knowledge about the antenna gain is a requirement (see, for example, Equation (16)). From basic antenna theory, we know that the antenna gain is proportional to the antenna aperture ( $G = 4\pi A/\lambda^2$ ). When dealing with large antennas in connection with scatter propagation, however, this linear relationship is not fulfilled. If the antenna aperture is increased by a factor  $k$ , the received power is in general increased by a factor which is less than  $k$ . This apparent gain degradation is commonly referred to as antenna-to-medium coupling loss<sup>21</sup>.

The phenomenon can be explained in several different ways (see, for example, References 22 and 23). One may base the discussion on the width of the angular power spectrum of the scattered wave relative to angular reception capability of the receiving antenna, or one may base the argument on the scattered field strength spatial correlation properties over the receiving aperture. In this review we shall discuss the latter method, briefly to illustrate the principles involved rather than to seek an expression of optimum accuracy.

Basing the discussion on the results of Section 4.4, we note that, at the receiving site, the area (normal to the direction of propagation) over which the field strength is correlated is given by  $L_V L_H$ . This area may then be considered as being the effective receiving antenna aperture, provided the actual aperture is larger than  $L_V L_H$ . If the actual aperture area  $D^2 < L_V L_H$ , we do not experience a gain degradation. The effective antenna gain is thus

$$G_{\text{eff}} = \frac{4\pi L_V L_H}{\lambda^2},$$

whereas the plane wave gain is

$$G = \frac{4\pi D^2}{\lambda^2}.$$

The gain loss is thus

$$G_L = \frac{D}{L_V L_H} = \frac{5 [n\sqrt{2} - 1] [n\sqrt{4} - 1]^{1/2} D^2}{(a/d)^2 \lambda^2}. \quad (32)$$

We see that, if  $n$  is large (narrow  $\phi(K)$  function), the correlation area is large and thus the real aperture is realised, giving no coupling loss. If we use a typical value for  $n$ , for example  $n = 4$ , the expression for the gain loss reduces to

$$G_L = 0.65 \frac{D^2}{(a/d)^2 \lambda^2} \quad (33)$$

This expression is in good agreement with experimental results (see, for example, Reference 24) provided the ratio between the scattering angle  $a/d$  and the beamwidth  $\lambda/D$  is larger than approximately 2.

#### 4.6 Time Dependence of a Scattered Radio Wave

Up to this point we have not concerned ourselves with time variations of the refractive index field. We shall now study the time fluctuations of the electromagnetic wave received via a scattering medium in the troposphere. We have previously shown that it is irregularities (scattering elements) in the troposphere of linear extension  $2\pi/K$  (where  $K = k_1 - k_s$ ) that contribute to the power density at the receiver. Consider, now, one such scattering element within the scattering volume. This element is generally in motion (velocity  $V$ ), giving rise to a Doppler shift of  $\Delta f$ , the radio wave scattered from the element.

If  $k_1$  be the wavenumber of the wave incident on the scattering element and  $k_s$  be the wavenumber of the scattered wave, the Doppler shift of this scattered wave is given by

$$\Delta f = \frac{1}{2\pi} (k_1 - k_s) \cdot V. \quad (34)$$

We see, then, that the scattering elements give rise to different Doppler shifts, depending on the position of the element in question (determined by  $k_1 - k_s$ ) within the scattering volume and depending on the velocity of this element. The power density at the receiver is thus a result of a number of electromagnetic waves having random mutual phase, different frequency and, in general, different amplitude. This situation leads to fading.

Obviously, then, it is the width of the Doppler spectrum that is of importance to the speed of fading. The position of the Doppler spectrum on the frequency axes relative to the transmitting frequency has no influence on the fading. It is the size of the effective scattering volume (variation in  $k_1 - k_s$ ) and the variation in the velocity of the various contributing scattering elements which has an influence on the Doppler spectrum width.

As regards the amplitude distribution of the received signal, it can readily be shown that this is independant of the shape of the Doppler spectrum and of the position of this on the frequency axes. Indeed, the amplitude distribution is affected only by the number of incoherent scattering elements present. If this number is larger than 5-6, the amplitude distribution is a Rayleigh distribution.

Returning then to the Doppler spectrum, it can be shown on the basis of Equation (34) (Reference 9) that the width of this is given by

$$\delta F = \frac{2}{\lambda} (V\beta + \delta V(\gamma)\theta) . \quad (35)$$

where  $\beta$  is the beamwidth (if this is large we shall have to use the effective beamwidth  $\beta_{eff}$ ) and  $\delta V$  is the deviation from the mean velocity  $V$  of the scattering elements. The angle  $\gamma$  specifies the direction of  $k_1 - k_s$  relative to the vertical direction and  $\theta$  is the scattering angle. If the scattering takes place in a great-circle plane, then  $\gamma = 0$  and it is the vertical component of the fluctuating air velocity that is influencing the fading speed. Note that the mean velocity  $V$  in Equation (35) is the cross-path velocity component.

#### 4.7 Backscatter in Relation to Forward Scatter

In the preceeding discussions we have not explicitly stressed the difference between forward scatter and pure backscatter. The expressions derived, however, are in most cases perfectly general and their application is not limited to small values of the scattering angle  $\theta$ . Thus the case of backscatter where the scattering angle  $\theta = \pi$  does not constitute a singularity. In order to illustrate the difference between forward scatter and backscatter from the point of view of the influence of a given atmospheric irregularity structure on the scattered radio power, the expression for the scattering cross-section, as presented in Equation (9), may conveniently form the basis.

Substituting for  $\theta = \pi$  in Equation (9) we find that the scattering cross-section for backscatter is given by

$$\sigma_{Back} = 0.03 C_n^2 \lambda^{-1/3} . \quad (37)$$

Thus the ratio of the forward scattering cross-section and that associated with backscatter is given by

$$\frac{\sigma_{Forw}}{\sigma_{Back}} = (\sin \theta/2)^{-11/3} . \quad (38)$$

This expression states that, for a given path length (range), the bistatic situation leads to a scattered power intensity which is several orders of magnitude larger than that corresponding to a situation where the transmitter and the receiver are located at the same point.

## REFERENCES

1. Booker, H.G.  
Gordon, W.E.  
*A Theory of Radio Scattering in the Troposphere.* Proceedings, Institute of Radio Engineers, Vol.38, April 1950, pp.401-412
2. Villars, F.  
Weisskopf, V.F.  
*The Scattering of Electromagnetic Waves by Turbulent Atmospheric Fluctuations.* Physical Review, Vol.94, April 1954, p. 232.
3. Megaw, E.C.S.  
*Fundamental Radio Scatter Propagation Theory.* Proceedings, Institution of Electrical Engineers, Vol.104C, September 1957, pp. 411-455.
4. Batchelor, G.K.  
*The Scattering of Radio Waves in the Atmosphere by Turbulent Fluctuations in Refractive Index.* School of Electrical Engineering, Cornell University, Ithaca, New York, Research Report EE 262, 1955.
5. Carroll, T.S.  
*Propagation of Short Waves in a Normally Stratified Troposphere.* Proceedings, Institute of Radio Engineers, Vol.43, October 1955, pp. 1384- 1390.
6. Bullington, K.  
*A Quantitative Explanation of Tropospheric and Atmospheric Scatter Transmission.* Paper presented at URSI-IRE meeting, Boulder, Colorado, December 1960.
7. Friis, H.T.  
et al.  
*A Reflection Theory for Propagation Beyond the Horizon.* Bell Systems Technical Journal, Vol.3C, May 1957, pp.627-644.
8. Waterman, A.T. Jr.  
*A Rapid Beamswinging Experiment in Transhorizon Propagation.* Institute of Radio Engineers, PGAP, Vol. AP-C, October 1958, pp. 338- 340.
9. Gjessing, Dag T.  
*Determination of Permittivity Variations in the Troposphere by Scatter-Propagation Methods.* Proceedings, Institution of Electrical Engineers, Part C, September 1962.
10. Gjessing, Dag T.  
J.Børresen.  
*Beamswinging and Supplementary Experiments.* Proceedings of NATO Advanced Study Institute, Wales, 1967.
11. Fried, D.L.  
*Limiting Resolution Through the Atmosphere.* Journal, Optical Society of America, Vol. 56, p. 1382.
12. Gjessing, Dag T.  
Irgens, F.  
*On the Scattering of Electromagnetic Waves by a Moving Tropospheric Layer having Sinusoidal Boundaries.* Institute of Electrical and Electronic Engineers, PTGAP, Vol. AP-13, January 1964.
13. Gjessing, Dag T.  
Irgens, F.  
*Scattering of Radio Waves by a Moving Tropospheric Layer: A Simple Model-experiment.* Institute of Electrical and Electronic Engineers, PTGAP, Vol. AP-12, Nov 1964.
14. Gjessing, Dag T.  
*An Experimental Study of the Variation of the Scattering Cross-section and Air Velocity with Position in Space.* Institute of Electrical and Electronic Engineers, PTGAP, Vol. AP-12, January 1964.

15. Gjessing, Dag T. *On the Scattering of Electromagnetic Waves by Nonisotropic Inhomogeneities in the Atmosphere.* Journal of Geophysical Research, Vol. 67, 1962, pp. 1017-1026.

16. Gjessing, Dag T. *Determination of Isotropy Properties of the Tropospheric Permittivity and Wind Velocity Fields by Radio-propagation Methods.* Journal of Geophysical Research, Vol. 69, 1964, pp. 569-581.

17. Bolgiano, Ralph Jr. *A Theory of Wavelength Dependence in Ultrahigh Frequency Trans-horizon Propagation based on meteorological Considerations.* Journal of Research, National Bureau of Standards, D, Radio Propagation, Vol. 64D, 1960, No. 3.

18. Gjessing, Dag T. et al. *Spectral Measurements and Atmospheric Stability.* Submitted for Publication.

19. Gordon, W.E. *Radio Scattering in the Troposphere.* Proceedings, Institute of Radio Engineers, Vol. 43, January 1955.

20. Gjessing, Dag T. Børresen, J. *The Influence of an Irregular Refractive Index Structure on the Spatial Field-strength Correlation of a Scattered Radio Wave.* Institution of Electrical Engineers, Proceedings of a Conference on "Tropospheric Wave Propagation", London, 30th September - 2nd October, 1968.

21. Booker, H.G. Bettencourt de J.T. *Theory of Radio Transmission by Tropospheric Scattering using Very Narrow Beams.* Proceedings, Institute of Radio Engineers, Vol. 43, March 1955, pp. 281-290.

22. Waterman, A.T. Jr. *Some Generalized Scattering Relationships in Transhorizon Propagation.* Proceedings, Institute of Radio Engineers, Vol. 46, November 1958.

23. Grosskopf, J. *Loss in Antenna Gain Due to Scattering.* National Bureau of Standards, Translation T4-60, Technical Report 5552, October 1959.

24. Yeh, L.P. *Experimental Aperture-to-Medium Coupling Loss.* Contribution to USA CCIR Study Group IX, October 1965.

THEORETICAL ANALYSIS MEDIUM-DEPENDENT FLUCTUATIONS  
WITH TROPOSPHERIC SCATTER LINKS, AND COMPARISON WITH  
NEW EXPERIMENTAL DATA, INCLUDING SIDE-SCATTER CHARACTERISTICS

by

H. J. Albrecht

Department of Telecommunications,  
Forschungsinstitut für Hochfrequenzphysik - FHP  
5321 Werthhoven, nr. Bonn, Germany

## SUMMARY

This contribution refers to a more detailed study of the effect of weather disturbances upon scatter links, including medium-dependent tropospheric side-scatter. Fundamental results may be found in the author's previous work on the subject.

New results to be presented in this contribution concern a thorough theoretical analysis of possible effects of frontal disturbances passing through a scatter volume as well as a general comparison of side-scatter data. Among them are those obtained by another experimental scatter link, employing quasi-backscatter signals of a tropospheric scatter volume. A detailed contribution on this subject by R. Menzel and Kh. Rosenbach appears elsewhere in this volume.

A theoretical analysis of parameters affecting the strengths of signal attenuation caused by certain weather situations yields values corresponding to the Kolmogorov-Obukhov "two-thirds-law", generally accepted for the interdependence of turbulence scale and the mean square of velocity differences. The resultant expression contains the general temperature structure and permits an explanation of seasonal effects found experimentally and reported upon by the author in the EPC/AGARD Symposium in 1967.

The good agreement between theoretical and experimental values is illustrated by new experimental data, including additional scatter links which also form part of the overall research programme.

In conclusion, the paper mentions new aspects of forecasting weather-dependent conditions interfering with a normal behaviour of tropospheric scatter links.

**THEORETICAL ANALYSIS OF MEDIUM-DEPENDENT FLUCTUATIONS  
WITH TROPOSPHERIC SCATTER LINKS, AND COMPARISON WITH  
NEW EXPERIMENTAL DATA, INCLUDING SIDE-SCATTER CHARACTERISTICS**

H.J. Albrecht

**1. INTRODUCTION**

The problem of scatter propagation by means of scatter volumes in the troposphere has been dealt with by a large number of authors in equally numerous papers during two decades. Only a few items seem to be unsolved at this juncture, and these aspects all appear to be connected with the meteorological structure of the troposphere, which represents an equally difficult subject.

One of the problems still existing is the predictability of the diurnal variation of field strength. This may vary by more than 20 dB. However, a reasonably reliable method of prediction requires adequate knowledge of physical processes causing changes in the propagation medium. Historically, the majority of the earlier research papers on tropospheric scatter propagation by Booker and Gordon, Villars and Weisskopf, Megaw<sup>1-3</sup> and others all mention certain assumptions with regard to the behaviour of the medium. In quite a few cases, experimental data on the meteorological parameters have been dealt with. They are useful as long as the methods of measurement permitted by the characteristics of the medium yield adequately representative information.

This paper aims at a further discussion of relevant parameters. It is based on the author's previous papers on the subject and presents some new results. A previous contribution dealt with the conditions to be fulfilled by a scatter link for a turbulent scatter mechanism to exist<sup>4</sup>. Thus the mechanism within an effective scatter volume located above hilly terrain and with its lower portion within the planetary boundary layer may be considered turbulent. Other papers presented statistical results on the effect of weather disturbances on a scatter volume<sup>5</sup>, on a phenomenological method of predicting such changes<sup>6</sup>, as well as on related subjects<sup>7</sup>.

The present contribution mentions some of the effort undertaken by the Department of Telecommunications at Werthhoven towards determining the effect of medium-dependent variations by using quasi-forward and side-scatter links on different frequencies.

**2. THEORETICAL ANALYSIS OF TROPOSPHERIC EFFECTS**

Based upon the concept of a well-defined region up to an altitude of 1 or 2 km above land surface, the so-called planetary boundary layer, the effective scatter volume may be considered to be limited by it. Depending upon the roughness of the earth's surface, this upper limit of the effective volume may reach 3 to 4 km if no abrupt discontinuity is assumed.

In an attempt to investigate medium effects upon scatter propagation, clearly defined changes of meteorological conditions were carefully monitored and interpreted in their effect upon scatter links<sup>5</sup>. In order to reduce the ambiguity in the analysis, particular attention has to be paid to the type of meteorological effect selected. If anticyclonic high pressure conditions are considered representative of an undisturbed behaviour, the passage of a cyclonic system through the effective scatter volume may be assumed to cause a disturbance which may also be recognised and interpreted in a definite way. Of the

frontal system accompanying a cyclone, the cold front is the more suitable part, due to its relatively definite behaviour. It should be emphasised generally that the selection of typical conditions, of text-book appearance, is important when using such medium changes caused by nature.

As has already been published, cold fronts were found to cause definite and unambiguous changes to an effective scatter volume if its altitude and the ground underneath fulfilled the conditions representative of a predominantly turbulent scatter mechanism<sup>4</sup>. The passage of fronts in general, and cold fronts in particular, is connected with a decrease in field strength. Correlation studies concerned with the amount of signal change and the relevant frontal parameters, yielded a particularly good result with frontal age, which may be expressed in terms of an appropriate scale<sup>6</sup>.

Side-scatter experiments have shown a general tendency of signal increase coincident with frontal passage at a location situated at a scatter angle towards the back of the scatter volume. Changes in field strength may be attributed to dimensional variations of turbulence blobs, i.e. an abrupt decrease in the scale of turbulence<sup>7</sup>.

In a recent contribution, the author presented a theoretical approach based on concepts of dynamic meteorology<sup>8</sup>. The front was assumed to be represented by an inclined discontinuity passing through the scatter volume, with conditions as indicated in Figure 1a.

If  $v_x$ ,  $v_y$ ,  $v_z$  represent the velocity of air in the three directions and if suffixes 1 and 2 indicate the warm air above and the cold air below this inclined boundary layer, respectively, an expression may be found for the angle of inclination  $\alpha$ , in terms of  $\tan \alpha$  (Ref. 9)

$$dp = \left( \frac{\partial p}{\partial x} \right) dx + \left( \frac{\partial p}{\partial y} \right) dy + \left( \frac{\partial p}{\partial z} \right) dz \quad (1)$$

$$\left[ \left( \frac{\partial p}{\partial x} \right)_1 - \left( \frac{\partial p}{\partial x} \right)_2 \right] dx + \left[ \left( \frac{\partial p}{\partial y} \right)_1 - \left( \frac{\partial p}{\partial y} \right)_2 \right] dy = - \left[ \left( \frac{\partial p}{\partial z} \right)_1 - \left( \frac{\partial p}{\partial z} \right)_2 \right] dz. \quad (2)$$

Considering the Coriolis force,

$$\tan \alpha \approx \frac{2\omega T \sin \varphi}{g} \frac{v_{y2} - v_{y1}}{T_1 - T_2}, \quad (3)$$

where  $\varphi$  = geographical latitude

$\omega$  = angular velocity of point on earth

$g$  = acceleration of gravity.

Equation (3) represents the conditions of a cold front which may be considered stationary; this well-known Margules Equation is valid if the difference in wind velocity along the  $y$ -axis is a decisive factor. Extending the theoretical approach used previously<sup>9</sup>, the following expression is obtained for a non-stationary front:

$$\tan \alpha_1 \approx \frac{2\omega \sin \varphi (v_{y2} - v_{y1}) - (\dot{v}_{x2} - \dot{v}_{x1})}{g(\Delta T/T) - v_{z1}}. \quad (4)$$

Provided that  $g \frac{\Delta T}{T} \gg \dot{v}_{x1} \tan \alpha$  (Ref. 10) and  $\dot{v}_{x2} = -\dot{v}_{x1}$  (Ref. 11),

$$\dot{v}_{x_1} = -g \frac{\Delta T}{2T} (\tan \alpha - \tan \alpha_1) \quad (5)$$

or

$$\dot{v}_{x_2} = g \frac{\Delta T}{2T} (\tan \alpha - \tan \alpha_1) \quad (6)$$

after G. Stuve<sup>12</sup>.

As far as general turbulence is concerned, the so-called "two-thirds-law" by Kolmogorov-Obukhov<sup>13,14</sup>,

$$\overline{(v_2 - v_1)^2} \propto l^{2/3}, \quad (7)$$

may be considered representative,

with  $l$  = scale of turbulence

$v_1, v_2$  = wind velocities at two points.

Turbulence blobs responsible for the scatter mechanism are found within a range of sizes which is limited, at its upper end, by eddies produced by external energy and, at its lower end, by the conversion to thermal energy with the smallest turbulence cells. This lower value is connected to the so-called micro-scale of turbulence  $l_0$ , defined by G. I. Taylor<sup>15</sup>. It is a function of the kinematic viscosity and heat conversion, which is proportional to the wind velocity  $V$ . R. J. Taylor computed this length dimension from the shearing effect of the wind<sup>16</sup> while the expression was completed by T. B. MacCready<sup>17</sup>:

$$l_0 = \frac{c_1}{V^{3/4}} \quad (8)$$

C. H. B. Priestley used a compilation of several data<sup>18</sup> to derive  $l_0$  as a function of altitude with a wind velocity assumed to be 5 m/sec. This yields  $c_1 = 0.184$  as a value of the constant in Equation (8) for an altitude of 1000 m.

With reference to the previous paper on the use of a cyclonic age scale<sup>6</sup>, the changes of the angle of inclination during the period of life of a weather front may be expressed in terms of age "A", shown in Figure 1(b). Following general assumptions in meteorological work, this angle may be assumed to increase from about  $0.5^\circ$  to  $1^\circ$  in the effective portion of the inclined boundary layer. If this variation is considered linear we obtain

$$\alpha = \alpha_0 - kt, \quad (9)$$

where  $\alpha_0 = 0.0175$  rad

$t = 5.0 - A$

$A$  = frontal age

$k = 1.85 \times 10^{-3}$ .

Combining Equations (3) and (7), the predominant scale of turbulence may be expressed as a function of the relative frontal age<sup>8</sup>:

$$l \approx \left[ \frac{\Delta T}{T} \frac{g[\alpha_0 - k(5.0 - A)]}{2\omega c \sin \varphi} \right]^{3/4}. \quad (10)$$

With the introduction of some constants, and assuming  $\Delta T$  to be constant ( $= 6^{\circ}\text{C}$ ) ,

$$l \approx 1.46 \times 10^4 \left[ \frac{4.46 - A}{T} \right]^3 \quad (11)$$

with  $c = 40$ ,  $\varphi = 50^{\circ}$ .

On the other hand, Equations (5) and (6) may be integrated to yield an expression for the difference of air velocity in the x direction:

$$(v_{x_1} - v_{x_2}) = g \frac{\Delta T}{2 T} k (5.0 - A)^2 . \quad (12)$$

Figure 2 illustrates the scattering of values of  $l$  derived from measured values about the theoretical curve given by the scatter coefficient due to Booker and Gordon. In addition, Equations (8) and (12) yield an increase of  $l_0$  for increasing  $A$ , which also corresponds to the behaviour shown by experimental data. Reasonable agreement is shown for the entire curve in Figure 2, although the theoretical method should yield somewhat unreliable data for smaller eddies.

### 3. ADDITIONAL EXPERIMENTAL DATA

More experimental data refer in particular to side-scatter measurements on a quasi-forward scatter-link on 900 MHz and to side-scatter data obtained by means of a vertical scatter system on 140 MHz, both operated by the Department of Telecommunications, Forschungsinstitut für Hochfrequenzphysik, Werthhoven. Figure 3 depicts the systems used to gain forward scatter and side-scatter data on different frequencies. Figure 3(a) shows the quasi-forward scatter link with a secondary receiving terminal almost underneath the scatter volume. In Figure 3(b) a vertical scatter sonde is depicted, with quasi-backscatter reception at locations particularly suitable for this type of research work. Figure 4 shows the geographical relationship.

As an evaluation aid, the nomogram shown in Figure 5 has been constructed for the scatter coefficient. The frequency on the left-hand side and the scale of turbulence indicated along diagonal lines permit the  $l/\lambda$  ratio to be found on the bottom scale. On the other hand, the vertical line from this value intersects with the scatter angle at which the scatter coefficient is required. This is further calculated by a horizontal line from the last-mentioned intersection to the outer right-hand scale and then with the nomogram built into the net: the connecting line between the appropriate point on the outer right-hand scale and the frequency on the left-hand scale cuts the inner vertical scale at the desired value of scatter coefficient (calculated for two different values of  $\Delta n$ ), which may also be determined relatively on its dB scale with an arbitrary zero. This chart was constructed to allow a quick estimate on average conditions; it has been used successfully. The scatter volume can be determined by the usual, approximate methods, limiting the effective scatter volume to a maximum altitude of 3 to 4 km.

With regard to the vertical scatter system on 140 MHz, in this paper use will be made of some data only, since a detailed description of the system, and first results obtained on diffraction and scatter paths, is the subject of a contribution by R. Menzel and Kh. Rosenbach in this volume<sup>19</sup>.

Particular attention has again been paid to the passage of cold fronts. A signal decrease by 2 dB in the quasi-forward direction coincided with a signal increase of 9 dB at a secondary receiving terminal on 900 MHz and with a signal increase of 2.5 dB at a side-scatter terminal of the 140 MHz system. Taking all factors into account, these changes would yield a change in the predominant scale of turbulence from 2 to 1 m. On the other hand, on another occasion a similarly small change in the forward direction was

accompanied by a 5 dB increase at its secondary terminal and by a 2 dB increase on the other frequency, thus yielding a change from perhaps 4 to 2 m. In contrast, another frontal passage yielded a signal decrease by 5 dB in the quasi-forward direction and an increase of 10 dB at the appropriate secondary receiving location, thus indicating a change from a normal scale of turbulence of 2 m down to about 30 cm or from 1 m down to about 10 cm.

#### 4. GENERAL INTERPRETATION OF RESULTS

Summarising the results described in this paper, and those mentioned in the author's previous contributions, the effect of cold front passages through a scatter link fulfilling the conditions of a turbulent scatter mechanism has been shown to coincide with changes in the predominant scale of turbulence. The theoretical analysis has yielded feasible results and reasonable agreement between measured and calculated data, if turbulence within the actual boundary layer between warm and cold air can be considered essential. On the other hand, there is the possible explanation of strong ascending and descending winds within thunder clouds\* accompanying cold fronts<sup>6</sup>.

There is reason to believe that changes in field strength effective upon a diurnal variation of this parameter generally coincide with changes in the scale of turbulence, again lower field strength correlating with the predominant existence of small turbulent blobs. However, smaller turbulent blobs are connected with an abrupt change in the polar diagram of the scatter mechanism, such that these blobs display a more omni-directional pattern. With regard to this condition having a somewhat stimulating effect upon the occurrence of multiple scattering, the amount of intermodulation on a scatter link would thus increase with lower field strength. On the other hand, such a negative correlation between field strength and intermodulation is mentioned in relevant literature<sup>20</sup> and was recently confirmed for the 900 MHz scatter link by F. Schmitt of the Department of Telecommunications at Werthhoven<sup>21</sup>.

It would be of interest to compare the results obtained here with those gained by several research workers in radar measurements of tropospheric backscatter<sup>22,23</sup>, provided that sufficient data material were available for the types of weather disturbances discussed in this paper. In this connection, the rather high frequency (usually around 3 GHz) may be considered a disadvantage on account of precipitation and not turbulence causing the backscatter. Also, attention should always be paid to meteorological measurements in the altitude range of the actual volume and not to those taken at standard altitude of 2 m above the ground.

#### 5. PREDICTION OF FIELD STRENGTH IN SCATTER LINKS

In a further extension of the prediction method already published<sup>6,8</sup>, more accurate forecasts may be obtained by determining the predominant value of turbulence scale by Equations (10) and (11), or (8) and (12), and substituting this value into appropriate approximate methods of calculating the scatter coefficient, from which the signal received may be determined.

Existing scatter theories differ only slightly in their power spectra if they are referred to the accuracy of measurement obtainable with modern methods. The frequent use of the approach by Booker and Gordon<sup>1</sup> thus appears to be justified for the purpose of this work.

---

\*Suggested by H J. aufm Kampe, see Reference 4.

## 6. CONCLUSIONS

The present paper contains several new results on medium effects upon tropospheric links. Among these, changes in the medium coincident with field-strength variations and the prediction of such conditions are of particular interest, while some other relevant parameters may also be explained by the results shown. Investigations are continuing and more data will be presented at some future date.

## ACKNOWLEDGEMENTS

The author wishes to acknowledge the assistance rendered by Messrs. Schneider and Stumm, of the Geophysical Measuring Unit at Idar-Oberstein, Federal Republic of Germany, in the operation of a secondary receiving terminal, as well as the conscientious work done by Mr. Niephaus and Miss Fassbender in preparing the paper for printing.

The work was sponsored by the Ministry of Defence, Federal Republic of Germany, under Research Contract T-831-1-203 and T 833-1-203/5.1, and the paper is published by permission of the Ministry.

## REFERENCES

1. Booker, H. G.  
Gordon, W. E.  
*A Theory of Radio Scattering in the Troposphere.* Proceedings, Institute of Radio Engineers, Vol. 38, 1950, pp. 401-412.
2. Villars, V.  
Weisskopf, V.F.  
*On the Scattering of Radio Waves by Turbulent Fluctuations of the Atmosphere.* Proceedings, Institute of Radio Engineers, Vol. 43, 1955, pp. 1232-1239.
3. Megaw, E.C.S.  
*Fundamental Radio Scatter Propagation Theory.* Proceedings, Institution of Electrical Engineers, Vol. 104C, 1957, p. 441.
4. Albrecht, H.J.  
*Feldstärkeinbrüche bei Streuausbreitung über hügeligem Gelände.* National URSI Convention, Germany, 1967.  
Kleinheubacher Berichte, Bd. 12, 1967, pp. 153-158.
5. Albrecht, H.J.  
*Correlating Tropospheric Scatter Data and Cyclonic Parameters.* Proceedings, Institute of Electrical and Electronic Engineers, Vol. 55, 1967, pp. 1768-1769.
6. Albrecht, H.J.  
*Variations of Tropospheric Scatter Propagation Caused by Changing Weather Situations and Problems of Relevant Predictions.* EPC/AGARD Symposium, Ankara, Turkey, October 1967.
7. Albrecht, H.J.  
*Coincidence Tests in Tropospheric Side-scatter Propagation.* Proceedings, Institute of Electrical and Electronic Engineers, Vol. 54, 1966, pp. 1982-1983.
8. Albrecht, H.J.  
*Theoretical Analysis of a Variable Scatter Mechanism in a Tropospheric Propagation Medium.* URS Symposium, Stresa, Italy, June 1968.

9. Margules, M. *Über Temperaturschichtung in Stationär Bewegter und in Ruhender Luft.* Met. Zs., 1906, pp. 243-254.

10. Bjerknes, J. *Diagnostic and Prognostic Application of Mountain Observations.* Geofysiske Publikasjoner, Vol. 111, 1924, No. 6.

11. Exner, E. M. *Über den Aufbau hoher Zyklonen und Antizyklonen in Europa.* Met. Zs., Vol. 38, 1921, pp. 296-299.

12. Stüve, G. *Gleitflächen und Pilotwindmessungen.* Met. Zs., Vol. 42, 1925, pp. 98-103.

13. Kolmogorov, A. N. *Doklady Akad. Nauk. SSSR.* Vol. 32, 1941, p. 16.

14. Oboukhov, A. M. *Izv. Akad. Nauk. SSSR. Ser. Geograf. Geofiz.*, Vol. 5, 1941, p. 453.

15. Taylor, G. I. *Diffusion by Continuous Movement.* Proceedings, London Mathematical Society, Vol. 20, 1922, pp. 196-212.

16. Taylor, R. J. *The Dissipation of Kinetic Energy in the Lowest Layers of the Atmosphere.* Quarterly Journal of the Royal Meteorological Society, Vol. 78, 1952, pp. 179-185.

17. MacCready, P. B. *Structure of Atmospheric Turbulence.* Journal of Meteorology, Vol. 10, 1953, pp. 434-449.

18. Priestley, C. H. B. *Turbulent Transfer in the Lower Atmosphere.* University of Chicago Press, 1959.

19. Menzel, R. Rosenbach, Kh. *Using the Tropospheric Volume of a Quasi-backscatter Link to Investigate the Scatter Mechanism.* EPC/AGARD Symposium, Oslo, Norway, in August 1968 (in this volume).

20. Clutts, C. E. et al. *Results of Bandwidth Tests on the 185 Mile Florida - Cuba Tropospheric Scatter System.* Transactions, Institute of Radio Engineers, CS-9, 1961, p. 434.

21. Schmitt, F. *Über Intermodulationsmessungen bei troposphärischer Streuausbreitung.* National URSI Convention, Germany, 1967. Kleinheubacher Berichte, Bd. 12, 1967, pp. 139-145.

22. Saxton, J. A. et al. *Layer Structure of the Troposphere.* Proceedings, Institution of Electrical Engineers, Vol. 111, 1964, pp. 275-283.

23. Stratmann, E. *Ergebnisse der Troposondenmessungen in Darmstadt.* National URSI Convention, Germany, 1967. Kleinheubacher Berichte, Bd. 12, 1967, pp. 131-138.

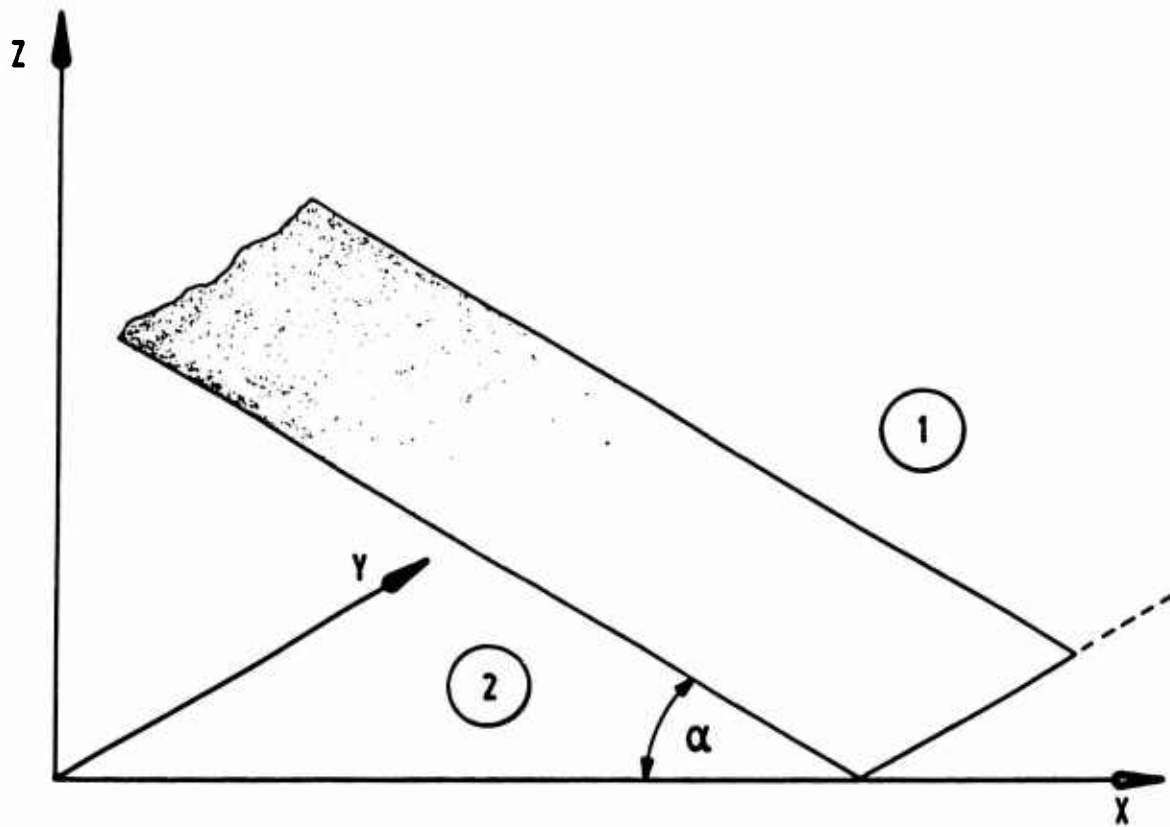


Fig. 1(a) A front represented by an inclined discontinuity through the scatter volume.

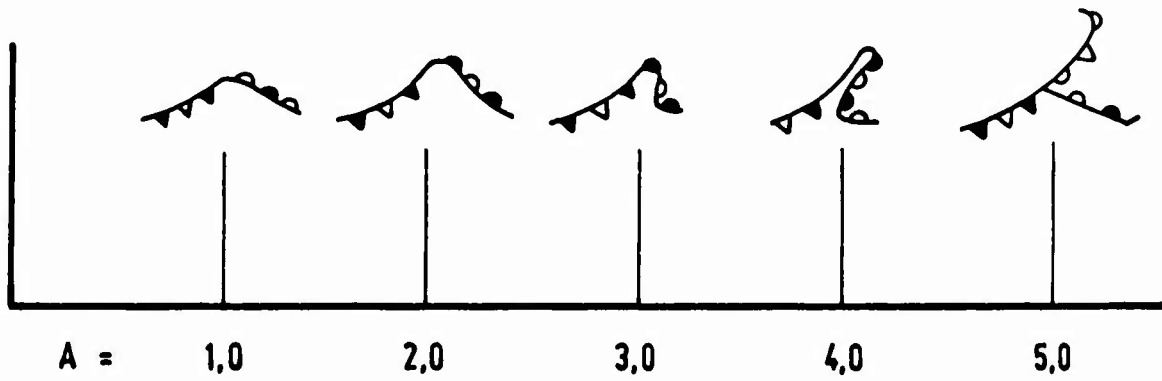


Fig. 1(b) The development of a front with cyclonic age  $A$ .

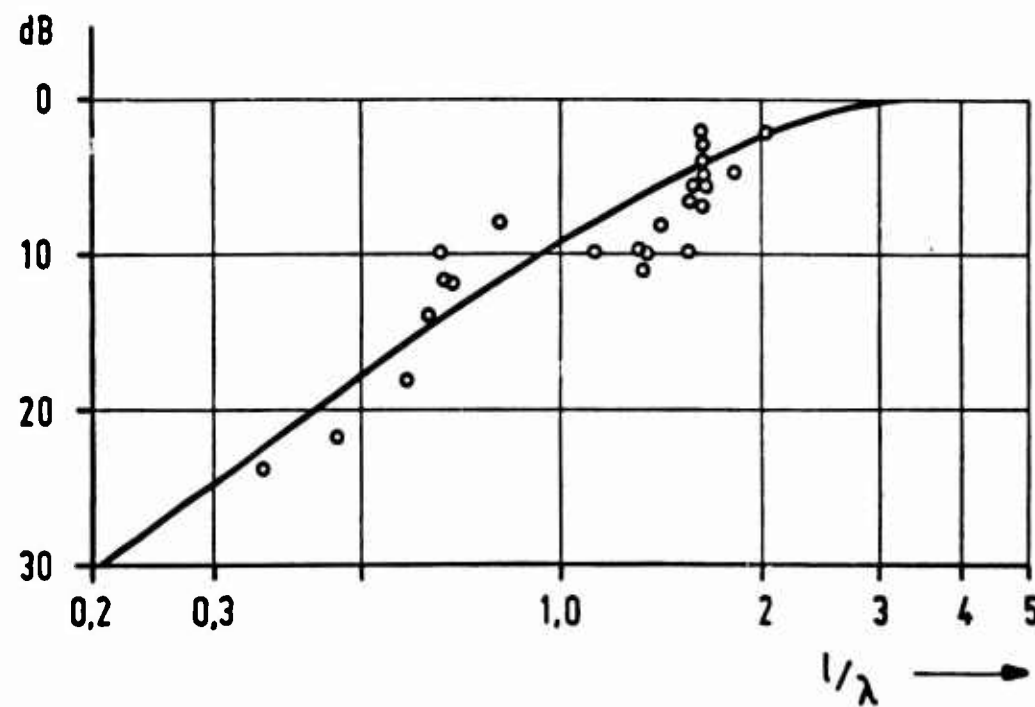


Fig. 2 Theoretical curve calculated after Booker and Gordon (Ref. 1). Single values calculated using forecasting method for measured dB-values.

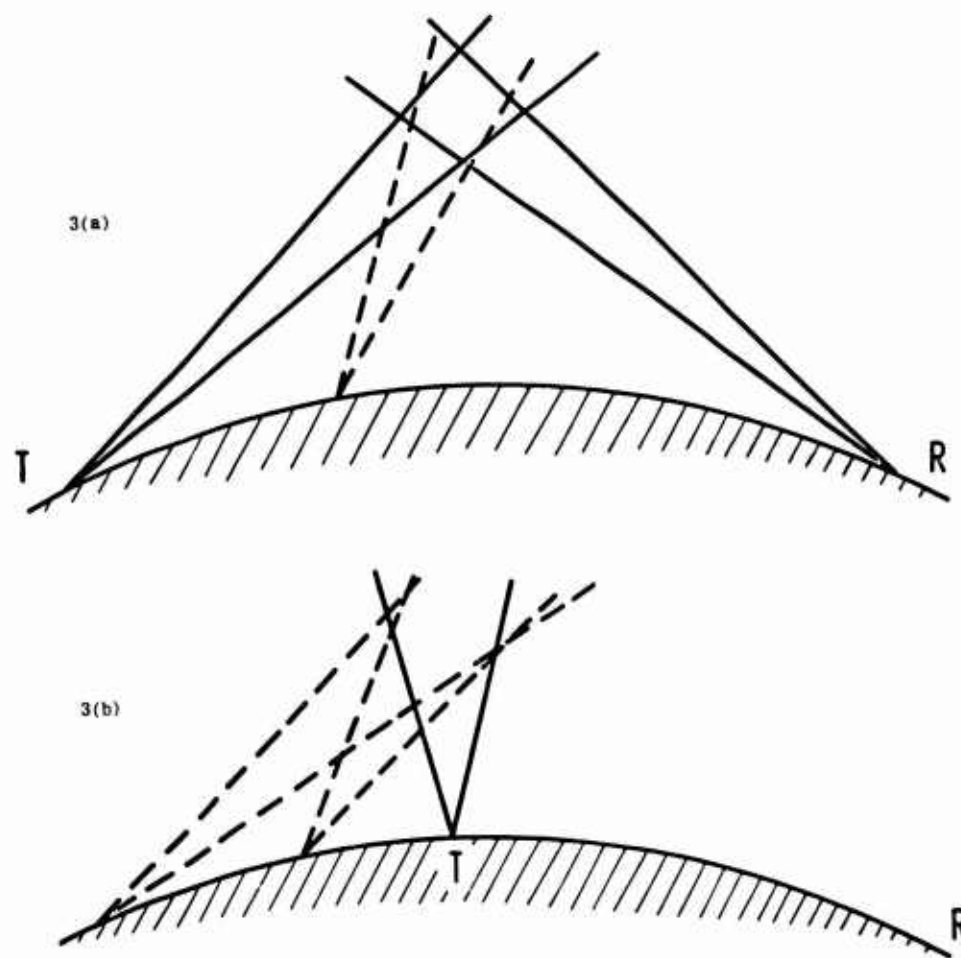


Fig. 3 Scatter links

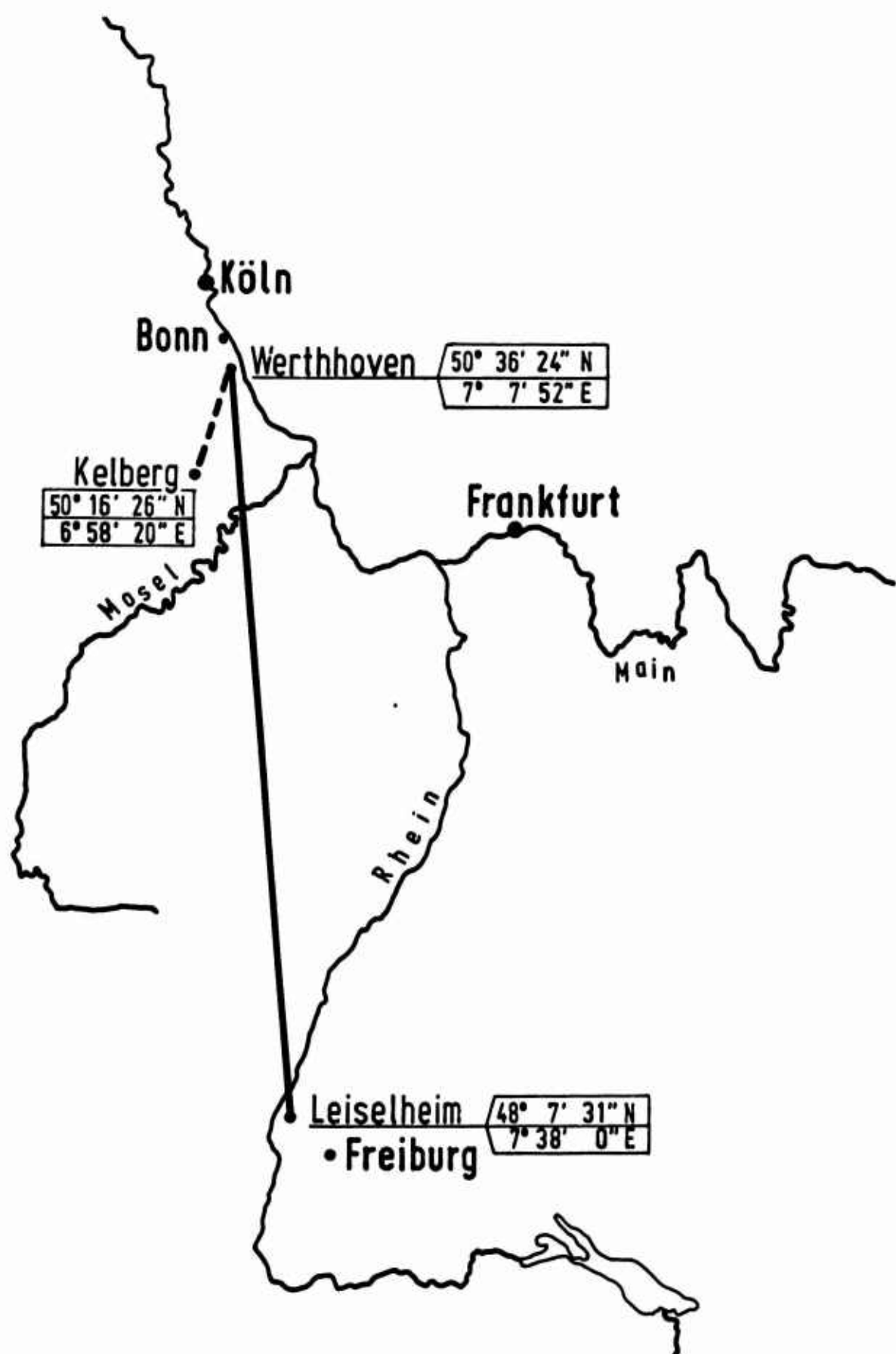
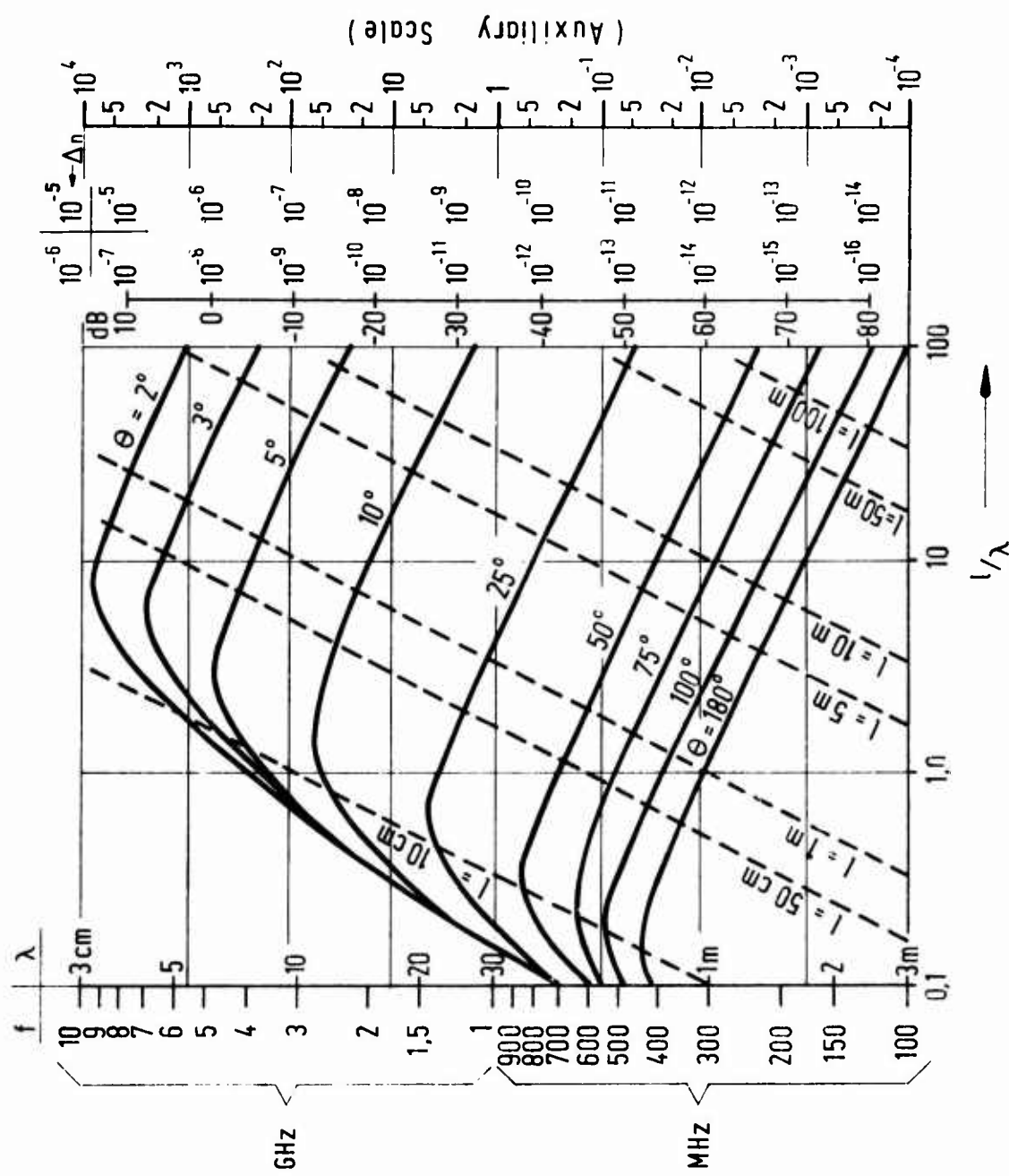


Fig. 4 Tropospheric scatter links

Fig. 5 Nomogram for scatter coefficient [ $1/m$ ]

**PHASE QUADRATURE COMPONENTS OF THE MICROWAVE SCATTERED FIELD  
IN A SHORT TROPOSPHERIC PATH AS RELATED TO THE  
METEOROLOGICAL PARAMETERS**

by

C.I. Beard, W.T. Kreiss, and W.G. Tank

Boeing Scientific Research Laboratories,  
Seattle, Washington 98124, U.S.A.

## SUMMARY

A microwave propagation experiment has been established on a line-of-sight path equipped with extensive meteorological instrumentation to show quantitatively the effect of the atmospheric scatterers on the microwave statistics. A particular microwave technique is used at 10.4 GHz which resolves the received microwave field into its phase quadrature components to provide the statistics of the incoherent scattered field *directly*, since these are the quantities sensitive to the atmospheric fluctuations. The effect of the sphericity of the wavefronts over the scatterers provides an additional descriptive parameter.

The usefulness of the technique in scattering work is to pin down the statistical model of the scattered field, e.g., over a 3.57 km path it shows that the incoherent scattered field lies almost entirely at a phase angle of  $\pm 90^\circ$  to the coherent field and is also normally distributed.

The meteorological instrumentation is unique in that integrated measurements are made of the defining refractivity parameters; i.e., (i) an infrared transmissometer operating in absorption bands of oxygen and water vapor at 1.27 and 1.16 microns, respectively, measures integrated dry air and water vapor partial densities, and (ii) a microwave transmissometer operating in the 22.2 GHz water vapor band measures the integrated water vapor density-to-temperature ratio. Such integrated data admit to direct comparison with the 10.4 GHz near field scattering effects. More conventional meteorological instrumentation is also utilized.

**PHASE QUADRATURE COMPONENTS OF THE MICROWAVE SCATTERED FIELD  
IN A SHORT TROPOSPHERIC PATH AS RELATED TO THE  
METEOROLOGICAL PARAMETERS**

C.I. Beard, W.T. Kreiss, and W.G. Tank

### 1. INTRODUCTION

To study the scattering of electromagnetic waves by atmospheric turbulence, a combined experiment has been set up in which meteorological measurements of the atmospheric structure and its statistics are taken simultaneously with the radio-wave statistics. A particular microwave technique<sup>1</sup>, new to line-of-sight atmospheric measurements<sup>2</sup>, is being used at 10.4 GHz; it can observe the statistics of the phase quadrature components of the incoherent scattered field directly and is sensitive to the effects of spherical wavefronts. The measured microwave scattering effects are being compared in several ways with the simultaneously measured turbulence. With the understanding so gained, it is hoped that these special features of this microwave technique can be exploited as a probe to study atmospheric turbulence in other regions of the atmosphere.

In this experiment three beams in three different wavelength regions, 2.88 cm (10.4 GHz), 1.26 cm (23.8 GHz) (Ref. 3) and near infrared (Ref. 4), traverse the 3.57 km line-of-sight path from a cleared, grassy field (Fig. 1), elevation 136 m, to the 952 m top of a steep ridge, a path elevation angle of 13.2°.

Operation of the 10.4 GHz system will be described first, then the 23.8 GHz and infrared systems, followed by some of the preliminary results to date.

### 2. DESCRIPTION

#### 2.1 The Phase Quadrature Technique

Since the 10.4 GHz system uses the same phase locked equipment described previously<sup>5</sup>, only a brief review, with the aid of Figure 2, is given here. The 10.4 GHz incoherent field is resolved by measuring the phase quadrature components of the instantaneous total received field ( $T$ ) at an instantaneous phase angle  $\theta$ , where  $T$  is the phasor sum of a constant coherent field at a constant phase angle plus the random incoherent field ( $I$ ). The mean values of the two phase quadrature components are thus the components of the coherent field; the fluctuations about the means are the two components of the incoherent field, say  $I_1$  and  $I_2$ . The quadrature axes can be rotated to any phase angle ( $\xi$ ) with respect to the coherent field; however, it has been found on the short path being used that the incoherent component in-phase quadrature to the coherent field is largest. Therefore for convenience in this report  $I_2$  will be called the component at phase quadrature with the coherent field, and  $I_1$  will be the inphase component, with  $\sigma_2^2$  and  $\sigma_1^2$  their respective variances.

This phase quadrature method determines several parameters which may be useful in characterizing the medium:

- (i) The statistics of the phase quadrature components of the incoherent scattered field (such as probability distributions, variances, spectra, correlations, etc.).
- (ii) The incoherent power  $\overline{I^2} = \sigma_1^2 + \sigma_2^2$ .
- (iii)  $K^2 = (\sigma_2^2/\sigma_1^2)_{\max}$  = the maximum ratio of the variances of the phase quadrature components ( $K^2 \geq 1$ ) at whatever value of  $\xi$  this occurs.

(iv) The phase rotation angle ( $\zeta$ ) of the axes to obtain the maximum value of  $K^2$ ; this is the rotation angle of the equiprobability ellipse.

To measure phase it is necessary to return a phase reference from the ridge-top site to the lower site; this is done by an FM 219.5 MHz link. Terrain scattering is minimized by the use of antennas having half-power beamwidths of  $3^\circ$  and primary sidelobes suppressed 25 dB; furthermore one antenna is pointed upward  $13.2^\circ$  at the path angle from the cleared grassy field (Fig. 1), and the other is mounted at the edge of the steeply sloping ridge-top.

## 2.2 23.8 GHz and Infrared Systems

If radio signal statistics are to serve not only as qualitative, but also as quantitative measures of atmospheric refractivity turbulence, then the cause and effect relationship between the characteristics of the random refractivity field and the random signal statistics must be established. To aid in this establishment, the refractivity field characteristics are measured at the site as follows. Radio refractivity, in terms of atmospheric composition, is expressible as

$$N = c_1 \rho_d + c_2 \rho_w + c_3 \frac{\rho_w}{T} .$$

where  $N$  is radio refractivity (the excess of refractive index over unity in parts per million),  $c_1$ ,  $c_2$ , and  $c_3$  are constants,  $\rho_d$  and  $\rho_w$  are the partial densities of dry air and of water vapor, respectively, and  $T$  is temperature. Atmospheric absorption of electromagnetic energy also depends on atmospheric composition, with resonant absorption proceeding according to the path-integrated partial density of the absorbing specie, and off-resonance absorption according to the path-integrated partial density-to-temperature ratio. Resonant absorption is therefore measured in an oxygen band ( $1.27 \mu$ ) and in a water vapor band ( $1.16 \mu$ ) with an infrared transmissometer to define the first two terms of integrated radio refractivity; similar measurements are performed with a microwave transmissometer operating off line center of the 22.235 GHz water vapor line to define the integrated third term. These combined data define integrated refractivity, one parameter governing the near field signal characteristics of the 10.4 GHz phase measurements. Transmissometer measurements therefore isolate the particular feature of the atmosphere active as the causative agent in those signal statistics. That is, it can be specified whether turbulence in the dry air or in the water vapor density field causes the 10.4 GHz signal fluctuations at any given time. Measurements verify the predictions that, in a neutral atmosphere with a finite vertical moisture gradient, water vapor fluctuations are the cause of 10.4 GHz signal fluctuations; whereas in a non-neutral atmosphere with zero moisture gradient, it is temperature fluctuations that generate the fluctuations noted in the 10.4 GHz signals.

Because absorption depends only on the amount, and not on the position, of the absorbing gaseous specie in the propagation path, transmissometer "instrument response functions" to fluctuations in atmospheric composition are specified. This permits interpretation of integrated partial density fluctuation measurements in terms of point statistics, assuming stationarity. Redundant point measurement systems atop a 27 m meteorological tower (Fig. 1) are used to substantiate point statistics inferred from transmissometer measurements. Three-component wind turbulence measurements are also performed with hot-wire anemometers mounted atop the tower.

Although data collection, reduction, and analysis are only partly completed, a number of preliminary results can be reported.

## 3. RESULTS

Standard deviations of 10.4 GHz phase (equivalent to path length variations) of  $2.5^\circ$  have been encountered, and the fluctuations are normally distributed. The sensitivity of

the 10.4 GHz system is illustrated in that a 0.1-N unit change in average refractivity along the path would cause a  $4.5^{\circ}$  phase change, which is as large or larger than the regularly measured standard deviations. The total field amplitude also appears to be normally distributed because the incoherent field is small.

The component of the incoherent field ( $I_2$ ) at phase quadrature to the coherent field possesses a normal probability distribution. The maximum ratio of the variances of the two phase quadrature components  $K^2 = \sigma_2^2/\sigma_1^2$ , ranging from 14 to 60, occurs when the angle  $\xi$  of the phase quadrature axes is approximately the angle of the coherent field, and shows that the incoherent field is primarily at phase quadrature to the coherent field. This result on this short, 3.57 km path agrees with the near-field scattering model of Wheelon and Muchmore<sup>6</sup> and is consistent with observed scale sizes. Previous methods which measured only the magnitude or only the phase of the total received field are not sensitive to the statistical model of the incoherent field, as has been shown<sup>1,2</sup>.

Probability distributions of the small in-phase incoherent component are awaiting digital computation of the magnetic tapes which will compensate for longer term drifts in  $\theta$  and maintain one quadrature axis aligned with the coherent field. This was not possible with the data reported herein which were hand read from strip chart records.

Preliminary results also emphasize that the radio signal statistics respond to atmospheric refractivity turbulence, and not to wind turbulence *per se*. Generally the correlation between simultaneous occurrences of these two turbulences is good. But occasions have been noted when strong refractivity turbulence occurred with little wind turbulence and vice versa, i.e., in a neutral atmosphere with zero vertical moisture gradient strong wind turbulence occurred with little refractivity turbulence, and hence with "quiet" 10.4 GHz signals. In spite of this qualification, on the six days for which reduced data are available, a proportional increase of the variance of the quadrature incoherent component with mean wind speed is found (Fig. 3) up to the highest wind speed observed of 30 miles/hour ( $13.5 \text{ ms}^{-1}$ ).

Although it is too early for general conclusions, the few power spectral densities calculated are illuminating. Power density spectra of the quadrature incoherent field component show slopes ranging from -0.5 to -3. Scale size information extends out to about 1.5 to 2.5 decades smaller than the outer scale size  $L_0$ . Spectral decays similar to those of the quadrature component have been observed in both integrated dry air and water vapor partial density turbulence. Some examples will be given to illustrate different behaviors.

Figure 4 shows a relatively simple power density spectral behavior of the quadrature incoherent field component, having a  $-2.45$  slope on the log-log plot. The abscissa is the frequency of the fluctuations of the envelope of the 10.4 GHz quadrature incoherent field ( $I_2$ ). The abscissa frequency scale is converted to a wavenumber scale by assuming Taylor's hypothesis and dividing frequency by the component of the mean wind perpendicular to the path. The spectrum is thus of the form  $\kappa^{-2.45}$ , where  $\kappa$  is the wavenumber,  $1/l$ , of the eddy of scale length  $l$ . Another spectrum given previously<sup>2</sup> has approximately a  $-2.7$  slope. This is to be compared to the Kolmogoroff-5/3 point spectrum which transforms into a  $-8/3$  spectrum for path-integrated fluctuations. The drooping of the spectrum as  $L_0$  is approached at the low frequency end is also partly caused by the fact that the 10.4 GHz signals are passed through RC high-pass filters of 41-second time constant to remove longer time trends.

A more complicated situation on a different day is displayed in Figure 5(a) for the infrared integrated oxygen density. (These data of 10/20/67 are the first obtained from computer reduction of the magnetic data tapes and thus provide information out to 5 Hz). Implied is an additional turbulence input at mid-frequencies which generates a  $\kappa^{-0.5}$  slope interruption of the steeper decay characterized by slopes (-2.35 and -3.0) bracketing the  $-8/3$  value. The spectrum of the simultaneous 10.4 GHz total phase fluctuations is shown in Figure 5(b); the agreement with the meteorological data of Figure 5(a) is such that the

two graphs can be nearly superimposed. The only difference, the steeper slope of the phase spectrum from 2 to 5 Hz, is believed attributable to the aperture smoothing effect of the 61 cm diameter 10.4 GHz antennas<sup>7</sup>. The 20.3 cm diameter aperture of the infrared telescope should not be a contributing factor in the data of figure 5(a).

An apparently similar energy input is shown in the series of graphs in Figure 6 linking the two microwave and the infrared systems. The two spectra of integrated oxygen and water vapor densities in Figures 6(a) and 6(b) are almost identical in slopes and in "corner" frequency of 1 Hz. In Figure 6(c) the power density spectrum of the 23.8 GHz amplitude fluctuations, which result from both absorption and scattering, has the same spectral slopes with a "corner" at 0.6 Hz. The 10.4 GHz spectrum in Figure 6(d) shows a different quantity this time, the inphase incoherent field component; the slope of its higher frequency portion is in the range of -1.4 to -1.75, which is a less negative slope than the others of Figure 6; its "corner" frequency is about 0.35 Hz. The absorption of the 10.4 GHz signal should be an order of magnitude less than that of the 23.8 GHz signal.

One of the promising exploratory features of this method is the possible use of the ratio  $K^2 = (\sigma_2^2/\sigma_1^2)_{\max}$ . This ratio is sensitive to the sphericity of the illuminating and receiving wavefronts and to the eddy scales. It is suggested<sup>2</sup> that  $K^2$  may be used to explore the eddy wavenumber spectrum by examining  $K^2$  for various frequency "slices" of the power density spectra of the two phase quadrature components of the incoherent field. The low fluctuation frequencies should be associated with the larger scale sizes, and the high fluctuation frequencies with the small scales.  $K^2$  should thus be large at the low frequency end of the spectrum as near-field conditions are approached, and should decrease toward the high-spectral frequencies as far-zone conditions are approached. The first test<sup>2</sup> was made with quadrature component spectral slope of -8/3 and a corresponding inphase component spectral slope of -5/3. The plot of log  $K^2$  versus log f has a slope which is the difference of the two slopes, or -1 in this particular case. On another day the plot of log  $K^2$  versus log f has a slope of zero. Accurate spectra of the in-phase component still await computer reduction of the magnetic tapes before accurate  $K^2$  behavior can be determined. These preliminary indications, however, warrant further investigation.

#### 4. CONCLUSIONS

The phase quadrature technique offers a sensitive method for studying the effects of the atmosphere on the propagation of electromagnetic waves. The consistency of the statistical analyses of the phase quadrature measurements and those of the independent measurements of atmospheric composition demonstrates the exactness, moreover, of the signature of atmospheric structure carried by the near-field signal statistics. The usefulness of the technique as an atmospheric turbulence probe is therefore apparent. The next logical step is to increase the path length severalfold to extend the analyses into the mid-field and far-field regimes, and to compare the measured cross-correlations with the theoretical work of deWolf<sup>8</sup> and Uscinski<sup>9</sup>.

#### ACKNOWLEDGEMENTS

The authors gratefully acknowledge the extraordinary efforts of G.L.Hilt and G.K.Bruce in operating and maintaining the field equipment. We thank W.C.Cook for programming the digital computation of many forms of data, Connie Radford and Nanci Yarno for reading data chart records, and the other field crew members, E.J.Wergin, R.A.Cruz, and H.C.Brooks.

## REFERENCES

1. Beard, C.I. *Statistics of Phase Quadrature Components of Microwave Fields Transmitted Through a Random Medium.* Institute of Radio Engineers, Transactions, Antennas and Propagation, AP-10, November 1962, pp.721-731.
2. Beard, C.I. *Phase Quadrature Components of the 10.4 GHz Scattered Field on a Short Tropospheric Path.* Proceedings Institute of Electrical and Electronic Engineers, Vol.56, August 1968.
3. Kreiss, W.T. *Radio Meteorology,* Boeing Scientific Research Laboratories Review, 1967, p.53.
4. Tank, W.G. *The Measurement of Integrated Refractivity for Evaluating Atmosphere-induced Radar Ranging Errors.* Boeing Scientific Research Laboratories document D1-82-0639, September 1967.
5. Beard, C.I. *Behavior of Non-Rayleigh Statistics of Microwave Forward Scatter from a Random Water Surface.* Institute of Electrical and Electronic Engineers Transactions, Antennas and Propagation, Vol.15, September 1967, pp.649-657.
6. Wheelon, A.D. Muchmore, R.B. *Line-of-Sight Propagation Phenomena - II, Scattered Components.* Proceedings Institute of Electrical and Electronic Engineers, Vol.43, October 1955, pp.1450-1458.
7. Wheelon, A.D. *Radio-Wave Scattering by Tropospheric Irregularities.* Journal of Research, National Bureau of Standards, Vol.63D, September - October 1959, pp.205-233.
8. deWolf, D.A. *Spherical Wave Propagation Through a Random Continuum.* Radio Science, Vol.2, December 1967, pp.1513-1515.
9. Uscinski, B.J. *The Multiple Scattering of Waves in Irregular Media.* Philosophical Transactions of the Royal Society, London, Series A, Vol.262, 14 March 1968, pp.609-643.

'NOT REPRODUCIBLE



Fig.1. Propagation path from cleared field to top of steep ridge at arrow tip. The light serves as the source for the infrared system. The 27 m high instrumented meteorological tower shows in the right of the photograph

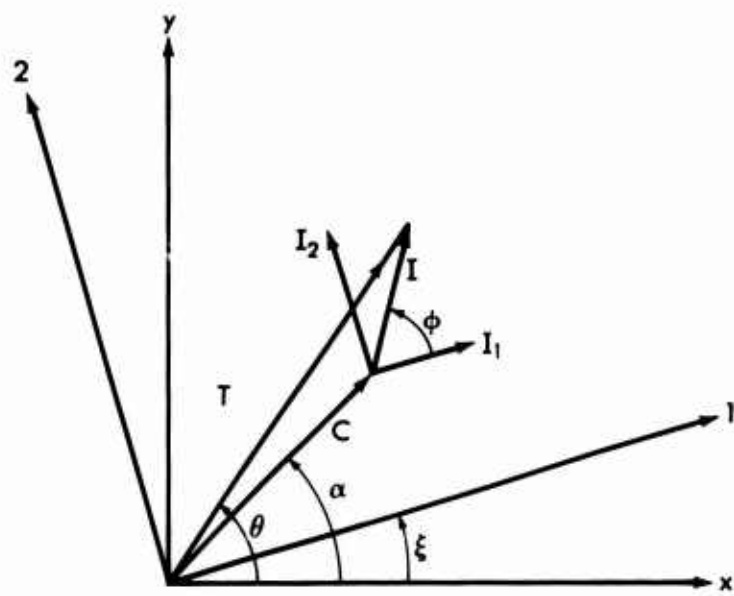


Fig.2. Phasor diagram of the phase quadrature resolution of the fields

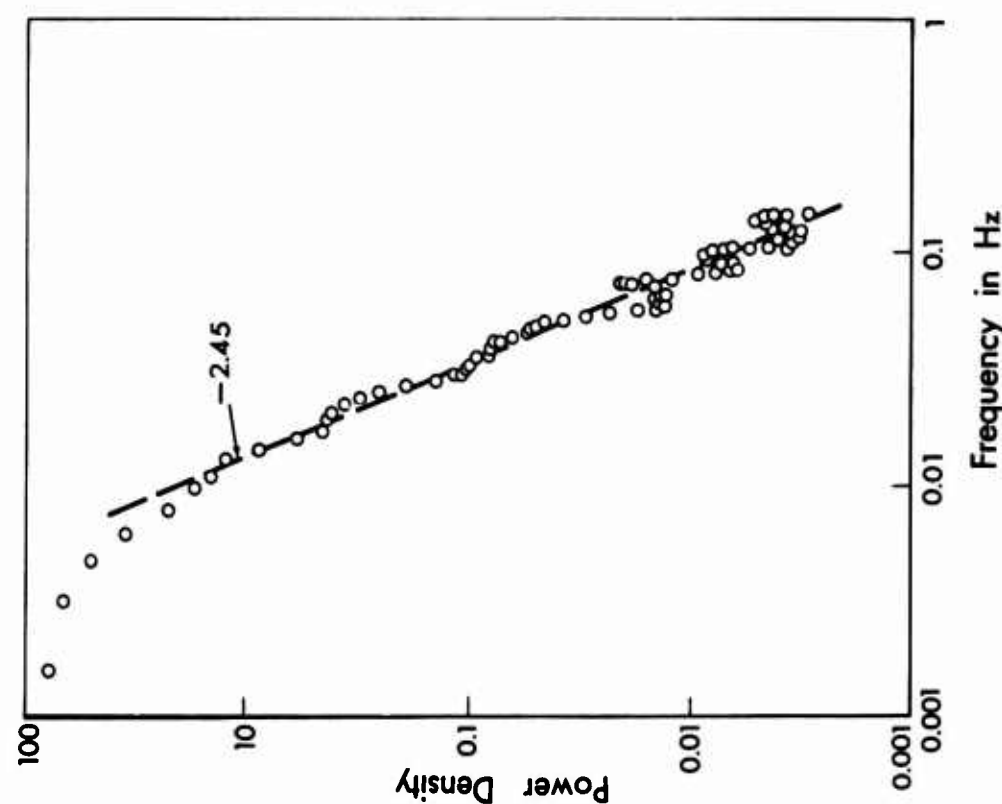


Fig. 4. Example of a power density spectrum of the quadrature incoherent field exhibiting a single decay law. Data of 1 April 1968, 1315 PST. Computed from 854 points read at 2.5 second intervals

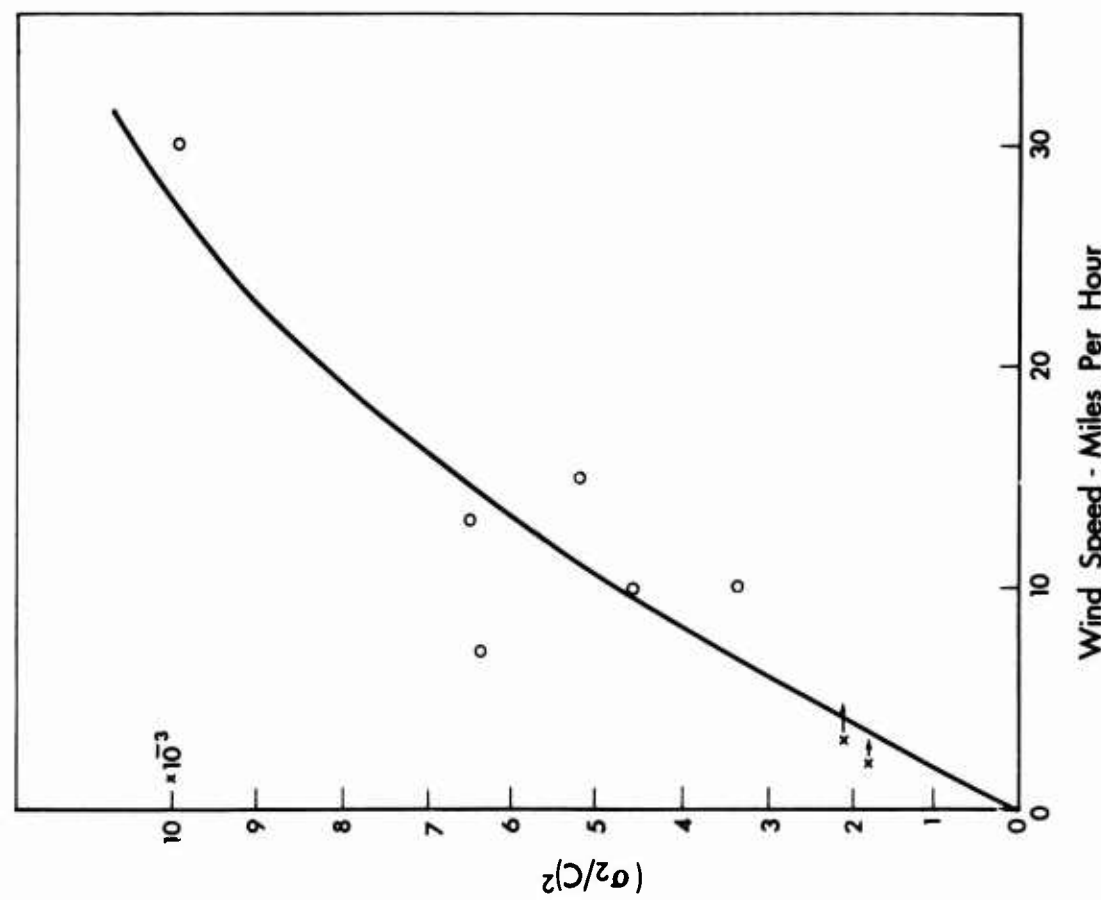


Fig. 3. Variance of quadrature incoherent field versus wind speed

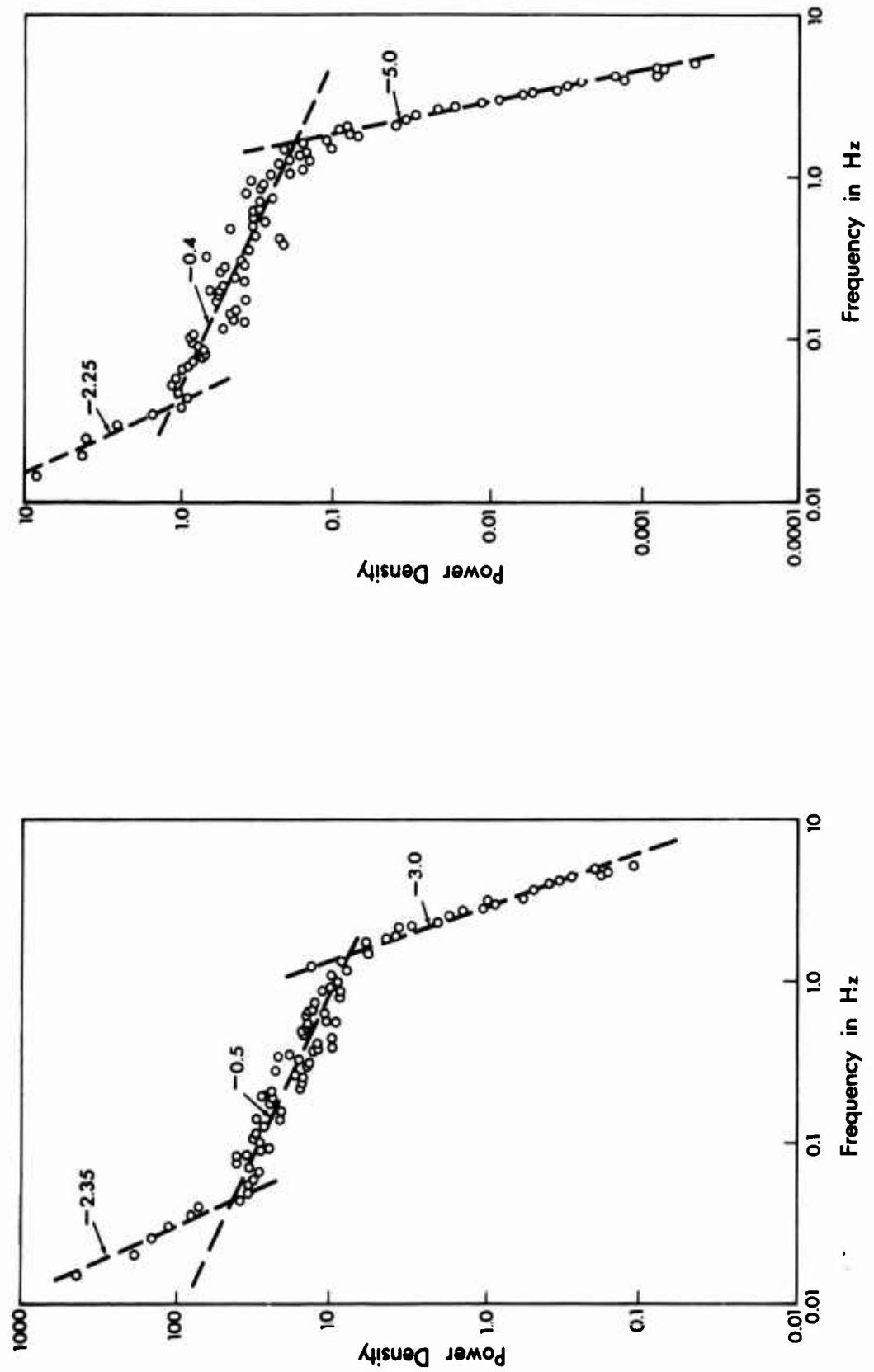


Fig. 5 Infrared and 10.4 GHz spectra showing a complicated decay behavior. Data of 20 October 1968, 1526 PST; 30 minute run sampled at 0.1 second intervals

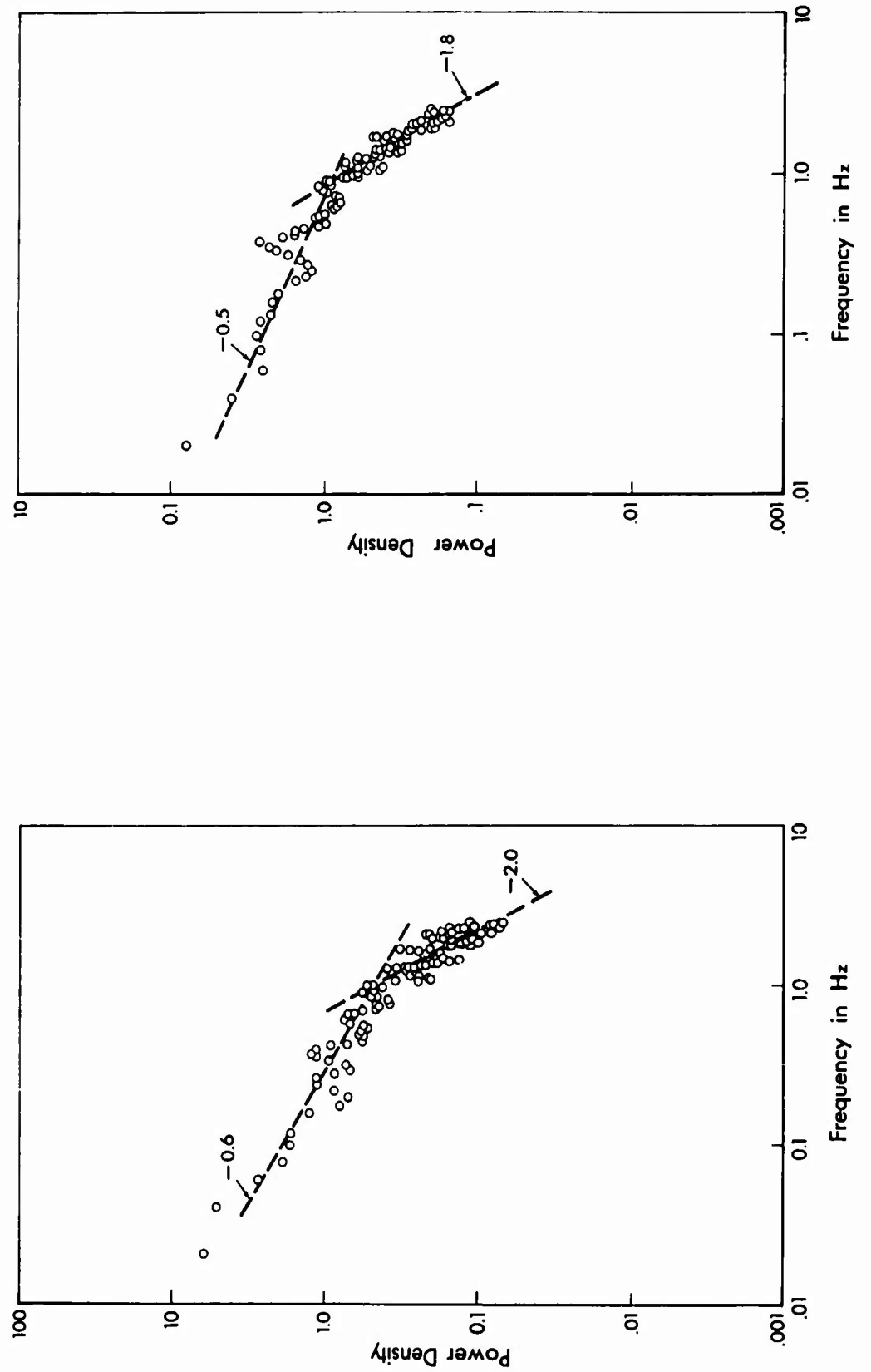
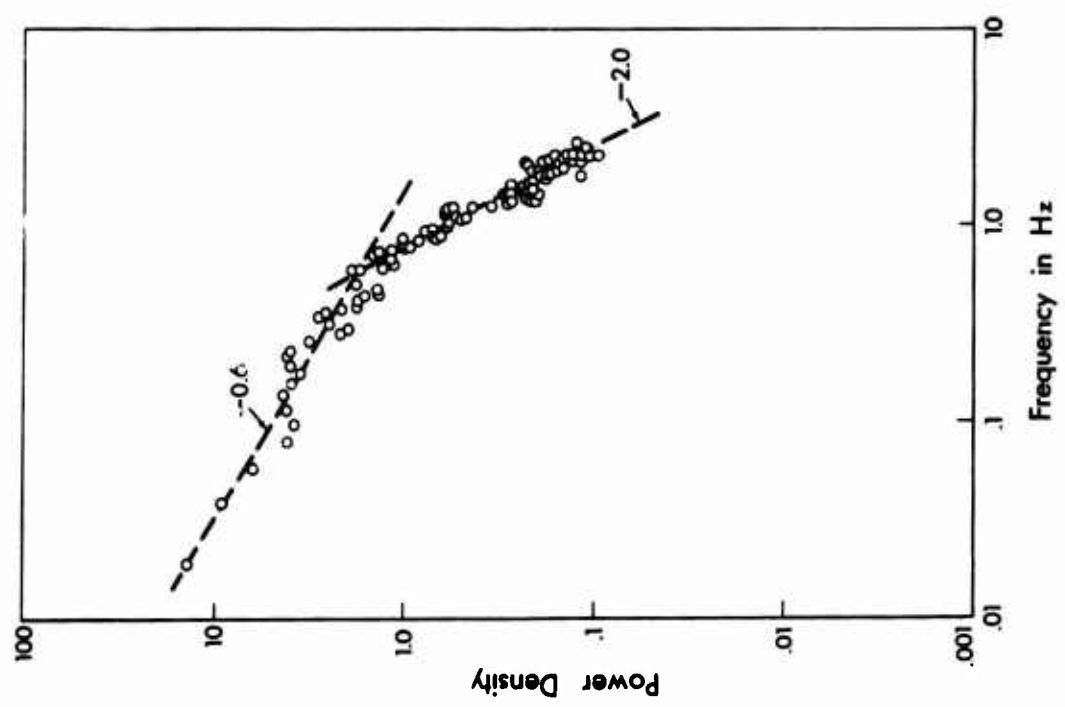
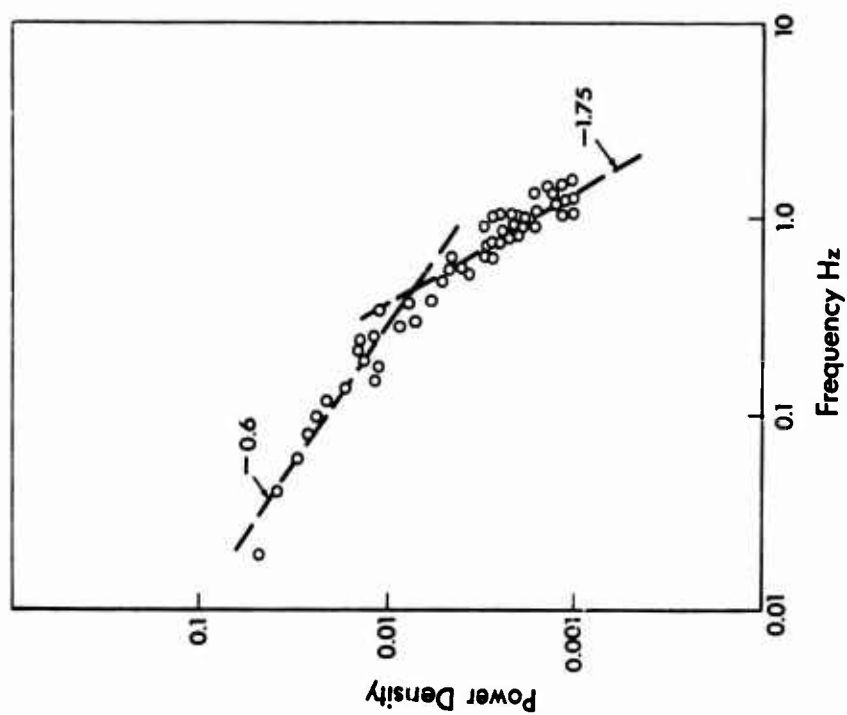


Fig. 6 Interrelations among infrared, 23.8 GHz, and 10.4 GHz power density spectra. Data of 18 July 1968, 1404 PST; 6 minute run read at 0.2 second intervals



(c) 23.8 GHz amplitude



(d) 10.4 GHz in-phase incoherent field

Fig. 6 Concluded

**PHASE AND AMPLITUDE MEASUREMENTS OF  
TRANSHORIZON MICROWAVES WITH A  
MULTI-DATA-GATHERING ANTENNA ARRAY**

by

Donald C.Cox  
Alan T.Waterman, Jr

Systems Techniques Laboratory  
Stanford Electronics Laboratories  
Stanford University, California, USA

## SUMMARY

A versatile vertical antenna array and receiving system which operate at 3.200 GHz have been developed at Stanford University. The array consists of 12 parabolic antennas spaced 1.39 m apart on a tower for a total vertical aperture of 15.24 m (162.5 wavelengths). The equipment samples phase difference between elements and amplitude at each element at rates up to 100 passes per second over the 12 elements.

Data have been processed to produce a conventional array beam  $0.3^{\circ}$  wide which is scanned in elevation to produce angular response patterns. Averaged angular response patterns, which are averages of about 3 minutes of data, are compared with theoretical angular response patterns derived from a scattering model.

The experimental patterns have been divided into three distinct groups:

**Group 1.** These patterns resemble the response of the array to a point source. An appropriate propagation model must predict signal arriving from a narrow region in the atmosphere.

**Group 2.** These patterns can be described by a model predicting a smooth decrease of scattered power with scattering angle at a rate proportional to the inverse  $m^{\text{th}}$  power of the angle, with  $m$  between 4 and 10.

**Group 3.** These patterns are characterized by broadened maxima or two or more maxima. The signals can be explained only by a model which contains a nonuniform scattering mechanism.

## NOTATION

$m$	exponent in model for scattered power
IF	intermediate frequency as used in a superheterodyne receiving system
$\delta$	horizontal change in location of receiving array element along the propagation path caused by motion of the support structure (tower) (cm)
$\vec{k}_c$	wavevector for reference (compensating) signal wavefront ( $\text{cm}^{-1}$ )
$\vec{k}_s$	wavevector for transhorizon signal wavefront ( $\text{cm}^{-1}$ )
$\vec{n}$	unit vector normal to receiving array
$j$	identifying index for an array element where element $j = 1$ is the bottom array element and $j = 12$ is the top array element
$E_j$	amplitude value recorded on magnetic tape for the $j^{\text{th}}$ array element during an array scan (v)
$\Delta\phi_{j, j+1}$	the phase difference value recorded on magnetic tape during an array scan. It is the phase angle by which the output of array element $j$ lags the output of array element $j + 1$ (deg)
$\phi_j$	the phase of the output of array element $j$ for an array scan (deg). The phase is referenced to array element number one (see Equation (1))
$n$	identifying index for an array element where element $n = 1$ is the bottom array element and $n = 12$ is the top array element
$\alpha$	beam pointing angle for the array (deg). (The angle is in elevation)
$P(\alpha)$	array output power with the array beam pointed at an angle $\alpha$ (W)
$E_p(\alpha), E_q(\alpha)$	quadrature components of array output amplitude computed as an intermediate step in computing $P(\alpha)$ (V)
$\gamma$	phase shift constant for the array. (Unit is phase degrees per pointing angle degree)
$\bar{P}(\alpha)$	the average power output of the array with the beam pointed at an angle $\alpha$ (W)
$N$	number of array scans averaged when computing a value for $P(\alpha)$
$i$	a summing index
$\rho$	the scattering angle for a transhorizon propagation path. It is the angle between the wavevector for the wave from the transmitter and the wavevector for the wave scattered to the receiver (deg)
$k_r$	the actual earth's radius is multiplied by $k_r$ to yield an effective earth's radius, which is used in calculating theoretical angular response patterns. The parameter $k_r$ makes a linear correction for refraction which results from the change in refractive index with height in the atmosphere

**PHASE AND AMPLITUDE MEASUREMENTS OF  
TRANSHORIZON MICROWAVES WITH A  
MULTI-DATA-GATHERING ANTENNA ARRAY**

Donald C. Cox  
Alan T. Waterman, Jr

**1. INTRODUCTION**

A versatile vertical antenna array and receiving system which operate at 3.200 GHz have been developed at Stanford University. The equipment has been used in a transhorizon propagation (tropospheric scatter) experiment. The experimental data have been processed to produce a conventional array beam,  $0.3^{\circ}$  wide, which is scanned in elevation to produce angular response patterns. Averaged angular response patterns, which are averages of about 3 minutes of data, are compared with theoretical angular response patterns derived from a scattering model.

The experimental patterns are divided into three distinct groups as follows:

- Group 1.** These patterns resemble the response of the array to a point source. An appropriate propagation model must predict signal arriving from a narrow region in the atmosphere.
- Group 2.** These patterns can be described by a model predicting a smooth decrease of scattered power with increasing scattering angle at a rate inversely proportional to the  $m^{\text{th}}$  power of the angle, with  $m$  between 4 and 10.
- Group 3.** These patterns are characterized by broadened maxima or two or more maxima. The signals can be explained only by a model which contains a nonuniform scattering mechanism.

Unique features of the array and receiving system as applied to transhorizon propagation research are

- (i) The measured parameters are the basic amplitude and relative phase along the arriving wavefront, sampled at each array element. Combining or processing of this basic wavefront information is done after recording.
- (ii) The data are sampled and recorded at rates much greater than the rates of change of atmospheric processes.
- (iii) A reference signal is used to cancel out the effects of relative motion of the array support-structure from the phase data.

The first part of this paper describes the vertical array and receiving system. The remainder of the paper describes the propagation path and presents some experimental results.

**2. VERTICAL ANTENNA ARRAY AND RECEIVING SYSTEM**

The antenna array, which is illustrated by Figure 1, consists of 12 parabolic reflectors spaced at 1.39 m (14.8 wavelengths) intervals on a vertical tower. The array operates at

3.2 GHz and has a total effective aperture of 15.24 m (162.5 wavelengths). The basic measurements made and recorded are amplitude from each of the elements and phase difference between adjacent element pairs. These quantities are sampled element-pair by element-pair in the sequence: amplitude 1, phase difference 1-2; amplitude 2, phase difference 2-3; etc. It takes 10 milliseconds to scan the amplitudes and phase differences of all 12 elements, so that up to 100 scans per second can be made.

Each array element is a 1.22 m (4 ft) parabolic reflector with a vertically polarized dipole feed. The  $5^{\circ}$  half-power beamwidth of these elements determines the azimuth width of the array fan beam. The elements have a gain of about +30 dB and sidelobe levels at least 19 dB down. Each array element is tilted up  $2\frac{1}{2}^{\circ}$  to help suppress foreground reflections.

When the amplitude and phase data are processed to form a conventional, uniformly illuminated, broadside array beam, the half-power beamwidth is  $0.29^{\circ}$  in elevation. This beam can be scanned in elevation. The major grating lobe separation of the array is  $3.88^{\circ}$  and the theoretical minor sidelobe level of 13 dB is essentially achieved. Major array grating lobes which occur outside the  $5^{\circ}$  beamwidth of the elements are reduced in intensity by the rapid decrease in gain of the elements themselves at angles outside the element beamwidth<sup>1,2</sup>. In the application of this array to transhorizon propagation measurements, the major grating lobes above an elevation angle of  $3.88^{\circ}$  are illuminating a region in the common volume from which the signal contribution is negligible. This fact results from the strong angular dependence (scattered power decreases with inverse angle raised to at least the fourth power) of the scattering mechanisms<sup>3-5</sup>. Grating lobes below the horizon illuminate the foreground. On the propagation path used (Fig. 7), a range of hills which determines the horizon from the receiving site provides effective screening of the scattering region from reflections from San Francisco Bay. At distances from the array where the screening becomes ineffective, the foreground is trees, rough ground, etc., and is quite diffuse. Adverse effects from ground reflections have not been observed in the transhorizon path data. Because of all these factors, only the one major array lobe, which scans the sector from the horizon up to  $3.88^{\circ}$ , contributes significantly to the array angular response pattern during a computer-produced beam swing.

Figure 2 is a picture of the array mounted on a 21.3 m (70 ft) tower. The instrumentation trailer which houses the receiving equipment and some of the sampling and calibration equipment can be seen behind the array. The small aluminium boxes, which are visible just behind each reflector, house the first mixer and the 30 MHz IF preamplifier for each array-element receiving channel. The first local oscillator is piped up the tower from the trailer and fed to the mixers through power dividers and approximately equal-length cables.

The measurement of phase on a tower like this is complicated by the fact that tower motion produces a phase shift too. To overcome this complication, a reference signal is transmitted line-of-sight from a source about 1.6 km (1 mile) in front of the array. The information about tower motion contained in the phase of this reference signal is used to remove the effect of the motion from the final phase-difference data.

Figure 3 is a simplified block diagram of an array-element receiving channel. It will be used to illustrate signal flow through one element channel of the receiving system. There are 12 identical receiving channels preceding the electronic commutator.

The transhorizon signal at 3.2000 GHz + 100 kHz and the reference signal at 3.2000 GHz are both received by each array element. In the first mixer they are both mixed with the first local oscillator at 3.230 GHz to produce a 29.9 MHz IF for the transhorizon signal and a 30.0 MHz IF for the reference. The first local oscillator is common to all element channels to preserve relative phases in the mixing process. The first mixers and part of the IF amplifier are mounted in the small aluminum boxes on the tower to minimize cable loss in the signal path. The first mixer noise figure essentially determines the noise figure of the receiving system.

The signal and the reference are separated by quartz crystal filters which have half-power bandwidths of 2 kHz. These narrow-band filters determine the noise bandwidth of the receiving system.

The reference is then further amplified and applied to the second mixer as a second local oscillator. The second mixer is balanced to further suppress reference signal (second local oscillator) noise. Mixing in the second mixer is linear with respect to the transhorizon signal, since that signal is applied to the mixer at a relatively low level. The IF amplifier gain is set so that the reference signal produces adequate d.c. current in the second mixer crystals.

In this mixing process, the transhorizon signal is subtracted from the reference signal. The 100 kHz difference frequency has its amplitude determined by the transhorizon signal amplitude and its phase determined by the phase difference between the transhorizon signal and reference signal. Both signals have traveled the same path from the antenna to the crystal filters. Their phases have been affected almost equally by the same tower motion and by phase drifts in the cables and IF amplifiers. The subtraction in the second mixer then removes these extraneous phase variations from the 100 kHz output. The short-path line-of-sight reference signal is quite stable compared with the transhorizon signal, so that the characteristics of the 100 kHz output are essentially those of the transhorizon signal. It can be shown that the phase error due to motion of an element is  $\delta(\vec{k}_c \cdot \vec{n} - \vec{k}_s \cdot \vec{n})$  where  $\delta$  is the horizontal change in element position along the propagation path,  $\vec{k}_c$  and  $\vec{k}_s$  are the wavevectors for the reference wavefront and the signal wavefront, and  $\vec{n}$  is a unit vector normal to the array. This phase error is less than 0.06 degrees per cm of element motion for the particular reference and signal frequencies and for the actual geometry of the reference, the common volume and the array. That is, element motion as extreme as  $\delta = 10$  cm would cause a phase error of less than  $0.6^\circ$ , which is quite negligible. This 100kHz signal is available continuously from each array element.

The twelve 100kHz signals are applied to the inputs of an electronic commutator. This commutator samples the 100 kHz signals in pairs in a sequence 1-2, 2-3, 3-4, and so forth. The two commutator outputs are connected to a phase detector. One of the outputs is also connected to a linear amplitude detector. The outputs of these detectors are phase difference for adjacent element pairs and amplitude for each element. These are digitized and stored on magnetic tape in computer format by the small, general purpose, digital computer (PDP-8) operating on-line. The 12 elements are scanned in 10 milliseconds.

Tests were run on the system to check the effectiveness of the phase-compensating method which makes use of the reference signal. For this test both the reference and the test signals were transmitted over line-of-sight paths. The phase difference between elements 3 and 10 was measured at the 29.9 MHz crystal filter outputs (Fig. 3) with a 30 MHz phase detector. At the same time the phase difference between the same two elements was measured at the 100 kHz array-element receiving channel outputs, that is, after the signal and reference have been subtracted. Figure 4 is a two-channel chart recorder output. The upper trace is the phase difference for the 29.9 MHz uncompensated outputs for elements 3 and 10. The lower trace is phase difference between the compensated 100 kHz array-element receiving channel outputs for the same two elements. The  $0^\circ$  phase reference for both vertical phase difference scales is arbitrary. The data were taken on a day with little wind, and the tower was relatively steady. At the point where the upper trace begins to oscillate, the guy lines on the tower were pulled to set the tower into oscillation. The somewhat over  $60^\circ$  phase oscillation seen on this trace amounts to somewhat over 1.5 cm of relative tower displacement. The lower trace shows almost no phase shift due to tower motion. It represents the phase difference between the same two elements after the reference is subtracted out by the receiving system. Tower motion of the order of that illustrated on this figure is experienced on windy days.

### 3. ARRAY ANGULAR RESPONSE PATTERNS

For this array, an angular response pattern (beam swing pattern or antenna scan) is obtained from one set of measured amplitude (12 values) and phase difference (11 values) data by computing the array output, point by point, for a series of beam pointing angles. This computation is done from the amplitude and phase data stored on magnetic tape.

The computation of one angular response pattern makes use of one set of amplitude values  $E_1, E_2, \dots, E_j, \dots, E_{12}$  and phase difference values  $\Delta\phi_{1,2}, \Delta\phi_{2,3}, \dots, \Delta\phi_{j,j+1}, \dots, \Delta\phi_{11,12}$ , where the subscripts refer to array elements with 1 at the bottom.  $\Delta\phi_{j,j+1}$  is the phase by which the output of element  $j$  lags the output of element  $j + 1$ . The first step is to compute the phase of each element output with reference to the phase of the output of element number 1. The phase of element 1,  $\phi_1$ , is taken as  $0^\circ$ . For each element  $n$ , for  $n = 2, 3, \dots, 12$ , then

$$\phi_n = \sum_{j=1}^{n-1} \Delta\phi_{j,j+1}. \quad (1)$$

The array output power,  $P(\alpha)$ , as a function of beam pointing angle  $\alpha$  is just the square of the phasor ("vector") sum of the element amplitudes with each phase  $\phi$  shifted linearly with element number to "point" the beam maximum at an angle  $\alpha$ . The computation procedure for  $P(\alpha)$  is to compute

$$E_p(\alpha) = \sum_{n=1}^{12} E_n \cos [\phi_n - (n - 1)\gamma\alpha] \quad (2)$$

and

$$E_q(\alpha) = \sum_{n=1}^{12} E_n \sin [\phi_n - (n - 1)\gamma\alpha], \quad (3)$$

then

$$P(\alpha) = [E_p(\alpha)]^2 + [E_q(\alpha)]^2. \quad (4)$$

The phase shift constant is

$$\begin{aligned} \gamma &= 360^\circ / (\text{grating lobe spacing}) \\ &= 92.71 \text{ phase degrees per pointing angle degree.} \end{aligned}$$

The beam pointing angle  $\alpha = 0^\circ$  corresponds to horizontal at the array. Averaged angular response patterns were produced by averaging the power output from the individual angular response patterns at each elevation angle ( $\alpha$ ) for which the output,  $P(\alpha)$ , was computed. That is,

$$\overline{P(\alpha)} = \frac{1}{N} \sum_{i=1}^N P_i(\alpha). \quad (5)$$

Figure 5 is an angular-response pattern made from data taken over a 10 mile line of-sight path. The vertical scale is relative power plotted on a log scale. The horizontal scale is linear in elevation angle.  $0^\circ$  is the horizontal at the array and for this figure the array is scanning down. The source appears below the array horizontal because the array is located on the side of a hill. The circles and solid curve are the measured angular response pattern. The dashed curve is a theoretical curve for a uniformly illuminated 12-element array. For the main beam the actual and theoretical curves are not distinguishable. Response patterns like this were taken over a signal level range of 33 dB. No deterioration of the response pattern was detected for signal levels 5 dB below the lowest average signal observed during the transhorizon propagation experiment.

The main beam was degraded only  $0.04^{\circ}$  at a level 8 dB below the minimum average signal level.

#### 4. TRANSHORIZON PROPAGATION PATH

Amplitude and relative phase measurements were made on signals propagated over a 164 km (102 mile) transhorizon path between Jackson and Stanford, California. Figure 6 is a map showing the path and Figure 7 is a profile of the path. The profile is plotted with a 4/3 earth radius to take into account standard refractive effects. The height scale is expanded. The common volume for the narrow array beam is about 0.2 km (600 ft) thick in the vertical dimension at the minimum altitude point of the common volume. This point is about 42 km (26 miles) from the receiving array and is about 0.43 km (1400 ft) high.

#### 5. AVERAGED ANGULAR RESPONSE PATTERNS FOR TRANSHORIZON PROPAGATION PATH SIGNALS

The averaged angular response patterns for the actual transhorizon propagation path signals are not presented in chronological order. They have been selected and ordered to illustrate the three distinct groups into which the patterns have been divided.

Averaged angular response patterns from the actual experimental data are compared with theoretical angular response patterns simulated from the path geometry (Fig. 7) and a uniform scattering model<sup>6</sup>. In the model, two adjustable parameters were used. The scattered power was assumed to fall off as  $(1/\theta)^m$ , where  $\theta$  is the scattering angle and the exponent  $m$  is an adjustable parameter in the model. Average refractive effects were accounted for by adjusting the effective earth's radius with a multiplicative constant  $k_r$ , that is, the earth's radius in the model is the actual earth's radius multiplied by  $k_r$ . The theoretical angular response patterns were then simulated by convolving the point source response pattern of the array with the assumed angular distribution of scattered power. Theoretical patterns were computed for many different values of the earth's radius constant  $k_r$  and the scattered power law exponent  $m$ . Effects of the beam patterns of the array elements were also accounted for in the model.

The averaged angular response patterns shown in Figures 8-14 were computed (see Section 3) from amplitude and phase difference data taken over the 164 km transhorizon propagation path. The figures are plots of average power  $P(\alpha)$  as a function of elevation angle  $\alpha$ . The elevation angle  $\alpha = 0^{\circ}$  is horizontal at the array and positive angles correspond to up in elevation. The circles are actual data points which are averages from 4096 antenna scans in elevation taken over a period of about 3½ minutes. The triangles are averages from 3072 scans for the next 2½ minute period. That is, the circles and triangles represent about 6 minutes of consecutive transhorizon path data. The vertical dashed line is at the horizon for a 4/3 earth radius refraction model. The horizontal dashed line is at the half power level. The time indicated is local (Pacific Daylight) time.

The solid curves in Figures 9-14 are the theoretical curves computed from the path geometry and the uniform scattering model. The identifying parameter  $m$  is the exponent in the scattered power law and  $k_r$  is the earth's radius constant. Many theoretical curves were computed and fitted to the data points. The solid curve plotted with each data set represents a "best fit" (by eye) for those cases where a good fit was possible.

Figure 8 is a measured angular response pattern which belongs in Group<sup>1</sup>. This group is generally characterized by stable signals which come from regions in the atmosphere at or very near the horizon and which are very narrow in angular extent. Note that the patterns for the two consecutive time periods represented by the circles and the triangles are almost equal. The solid line is a theoretical angular response pattern for a point source for this figure only. Notice how closely the data points fit the theoretical curve. In particular, notice how deep the nulls are in the actual data. This pattern illustrates

a period of very stable signal conditions with very slow fading with source region *very* narrow in angular extent. This data was taken at about midnight. Signals of this first group occur predominantly late at night or early in the morning when the atmosphere tends to be quite stable.

Figure 9 is another measured angular response pattern from the stable signal group. The solid curve for this figure was computed from the scattering model with scattered power decreasing as  $(1/\theta)^{10}$  and for standard refractive conditions (4/3 earth radius as indicated by  $k_r = 4/3$ ). Note that the actual data points follow the detail in the lobe structure of the theoretical curve quite well, even at levels 20 dB down. This pattern then also indicates that power was coming from a source region of narrow angular extent but, since the nulls are somewhat filled in, some power is coming from higher angles than in the previous figure. The main beam is slightly narrower than the model predicts but the sidelobes are slightly higher. This indicates that the actual scattered power did not vary with angle exactly as the power law assumed in the model. The averaged angular response pattern in Figure 10 belongs in Group 2. It can be described by a model predicting a smooth decrease of scattered power with scattering angle. The actual data points for this averaged angular response pattern fit very closely the theoretical curve which was computed from the model with a scattering law exponent of  $m = 6$ . Again the data points agree with the model quite well even in the detail 20 dB down. The data for the two consecutive time periods which are represented by the circles and triangles define approximately the same curve. This indicates that signal characteristics were quite stationary over the 6 minute time period.

The actual data points for the averaged angular response patterns in Figure 11 lie between the two theoretical curves shown. Again  $m$  is the exponent in the scattering law. The value  $m = 4$  is close to the 11/3 power law which would be predicted on the basis of a Kolmogorov spectrum of turbulence and narrow antenna beams<sup>5,6</sup>. This pattern also belongs in Group 2, with the exponent between 4 and 5. Most of the other experimental angular response patterns which are classified in Group 2 require the use of exponents greater than  $m = 4$  in the theoretical model to produce theoretical curves which will fit the data points. A turbulence model with an intensity decreasing with height or with a spectrum different from the 11/3 power law could probably explain most of the Group 2 data. Note that the theoretical curves which best fit the data points in Figure 11 require an effective earth's radius constant of 5/3 to account for average refractive effects.

Figures 12 and 13 are examples of angular response patterns from Group 3. These averaged angular response patterns cannot be explained by a uniform scattering model. A model which would predict the two maxima seen in these patterns would require a nonuniform mechanism, such as layers or patches of turbulence in the atmosphere. A rather intense localized scattering region seems to be indicated, since the scattered power falls off rapidly with angle above the second maximum. Patterns with broadened maxima or multiple maxima like this one usually occur in the afternoon. It should be emphasized that these examples are only two of many response patterns observed which have a broadened maximum or multiple maxima. In many cases, a secondary maximum in a response pattern appears at about  $\alpha = 3/4^\circ$ , as in Figure 12. This corresponds to a scattering region which has its minimum scattering angle located at an altitude of about 0.5 km (1800 ft) and at about 25% km (16 miles) from the receiving site. The region is above the first range of mountains visible from the receiving site (Fig. 7). The intense scattering region may be caused by winds blowing down San Francisco Bay and up over the row of mountains. Wind measurements made in conjunction with other experiments at Stanford have shown that winds do blow up over these mountains quite consistently. Future experimentation will attempt to isolate the cause of these Group 3 angular response patterns, which are good indicators of atmospheric inhomogeneity.

Figure 14 is an example of an angular response pattern whose maximum does not occur at or near the earth horizon. Also, for this pattern, the scattered power falls off rapidly with elevation angle  $\alpha$  immediately after the maximum, but then at higher angles (greater than one degree) the fall-off of power as a function of elevation angle is more gradual. This

is suggestive of a specular type reflection superimposed on a more diffuse background of scattering, or possibly of an intense scattering region superimposed on a less intense background of turbulent scattering. No theoretical angular response pattern from the uniform scattering model will fit this data. It probably belongs in Group 3.

## 6. CONCLUSION

The experimental averaged angular response patterns in elevation taken with the 12-element vertical antenna array have been classified into three groups by comparing them with theoretical response patterns produced from a uniform scattering model. The three groups and their general signal characteristics are as follows:

- Group 1.** The averaged angular-response patterns for the first group closely resemble the response of the array to a point source or a source narrow in extent in elevation angle. The signal is generally strong and relatively steady with only very slow fading. Signals with the characteristics of this group occur most frequently in the early morning, between midnight and 0800. A propagation model must predict signal arriving from a very narrow region in the atmosphere (like a thin, relatively stable, partially reflecting or refracting layer) to describe the signal characteristics of this group
- Group 2.** The averaged angular-response patterns for this group can be described by a model that predicts that the scattered power decreases smoothly with scattering angle at a rate inversely proportional to the  $m^{\text{th}}$  power of the angle, where  $m$  lies between 4 and 10. The exact value of  $m$  depends on the time period. Signal levels are generally moderate to weak, the signal fades are deep, and the fading rate is moderate. Signals with the characteristics of this group are observed at all times of the day but they occur most frequently in the morning after sun-up and in the evening. A propagation model based on atmospheric turbulence can describe the signal characteristics of this group only if it includes a turbulence intensity that is dependent on height, turbulent regions narrow in vertical extent, or possibly "patches" of turbulence.
- Group 3.** The averaged angular-response patterns for this group are characterized by broadened maxima or two or more maxima when compared with the response pattern for a single point source. Signal levels are generally moderate to weak; the signal fades are deep; and the fading rate is moderate to rapid. Signals with the characteristics of this group occur most frequently in the afternoon. This group of signals cannot be explained by a model that predicts a smooth fall-off of scattered power with elevation angle, that is, by a uniform scattering model. A suitable model must contain in it nonuniform mechanisms (such as layers or patches of turbulence which are more intense in some regions of the atmosphere than in others) to predict a discontinuous or at least nonuniform variation of scattered power with elevation angle.

The uniform scattering model which is based on turbulence theory is not sufficient to predict for all time periods the signal characteristics observed in the experiment. Even during the time periods when a turbulent model predicts the right type of signal variation with angle, modifying factors, depending on atmospheric conditions at the time, are required to make the dependence on angle sufficiently strong. The goal of continuing experimentation with the vertical antenna array is to define more completely the atmospheric structure associated with the three groups of angular response patterns.

## ACKNOWLEDGEMENT

The work reported in this paper was supported by the US Army Electronics Command, Fort Monmouth, New Jersey, USA under Army Contract DA28(043)AMC-01860(E). More detail is given in a Stanford Electronics Laboratories Report TR 2275-1; SEL-67-100; December 1967.

## REFERENCES

1. Waterman, A.T., Jr. *Transhorizon Measurement Techniques.* In "Statistical Methods of Radio Wave Propagation", Pergamon Press, 1960, pp. 212-219.
2. Kraus, J.D. *Antennas*, McGraw-Hill, New York, 1950, pp. 66-74.
3. Friis, H.T. et al. *A Reflection Theory for Propagation Beyond the Horizon.* Bell Systems Technology Journal, Vol. 36, May 1957, pp. 627-644.
4. Staras, H. Wheelon, A.D. *Theoretical Research on Tropospheric Scatter Propagation in the United States, 1954-1957.* Transactions, Institute of Radio Engineers, PGAP, Vol. AP-7, January 1959, pp. 80-87.
5. Wheelon, A.D. *Radio-Wave Scattering by Tropospheric Irregularities.* Journal of Research, National Bureau of Standards - D. Radio Propagation, Vol. 63D, October 1959, pp. 205-233.
6. Cox, D.C. *Phase and Amplitude Measurements of Microwaves Propagated Beyond the Horizon.* PhD Thesis, Technical Report 2275-1 (SEL-67-100), Stanford Electronics Laboratories, Stanford University, California, December 1967.

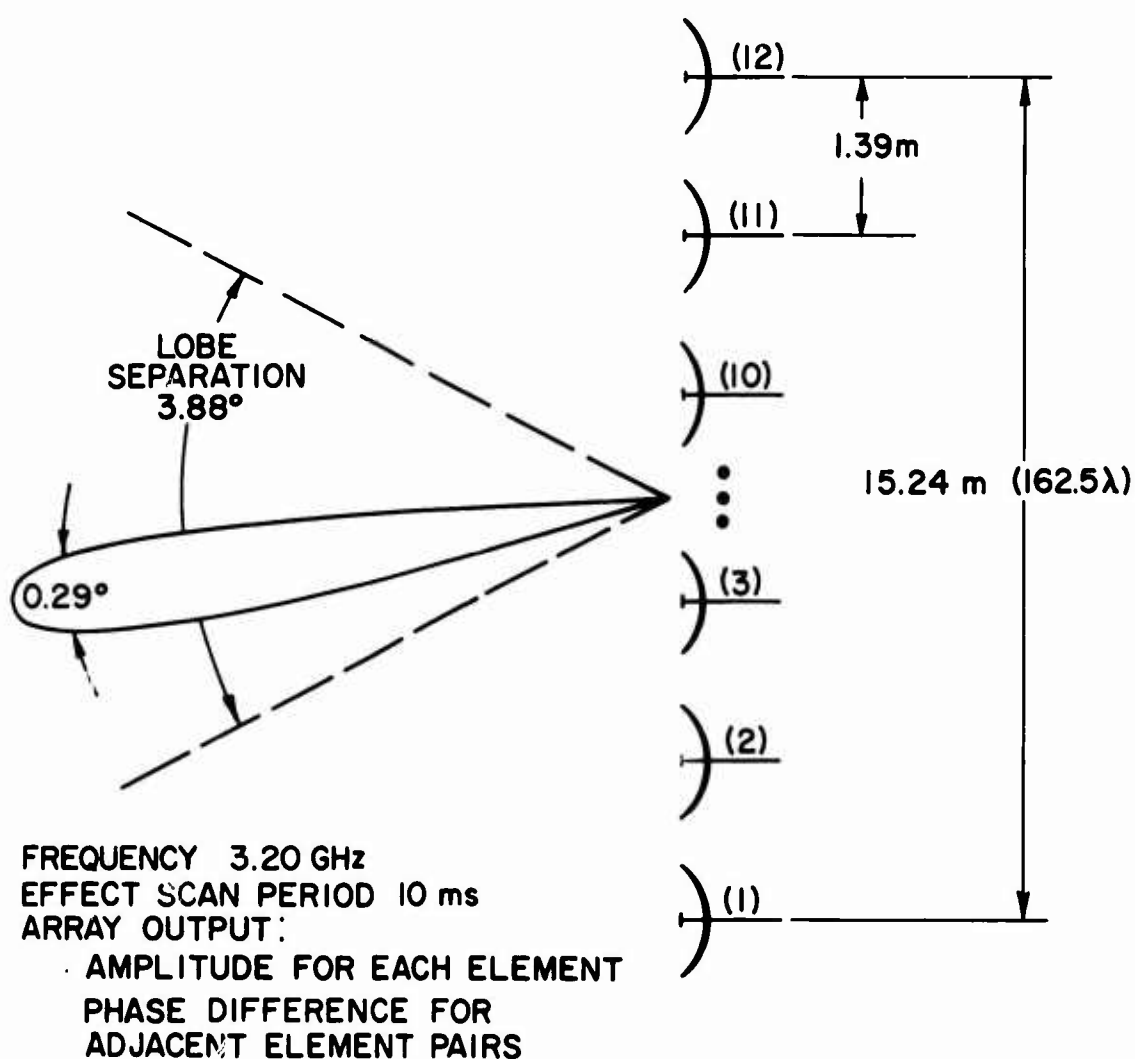


Fig. 1 Receiving array parameters

18-10

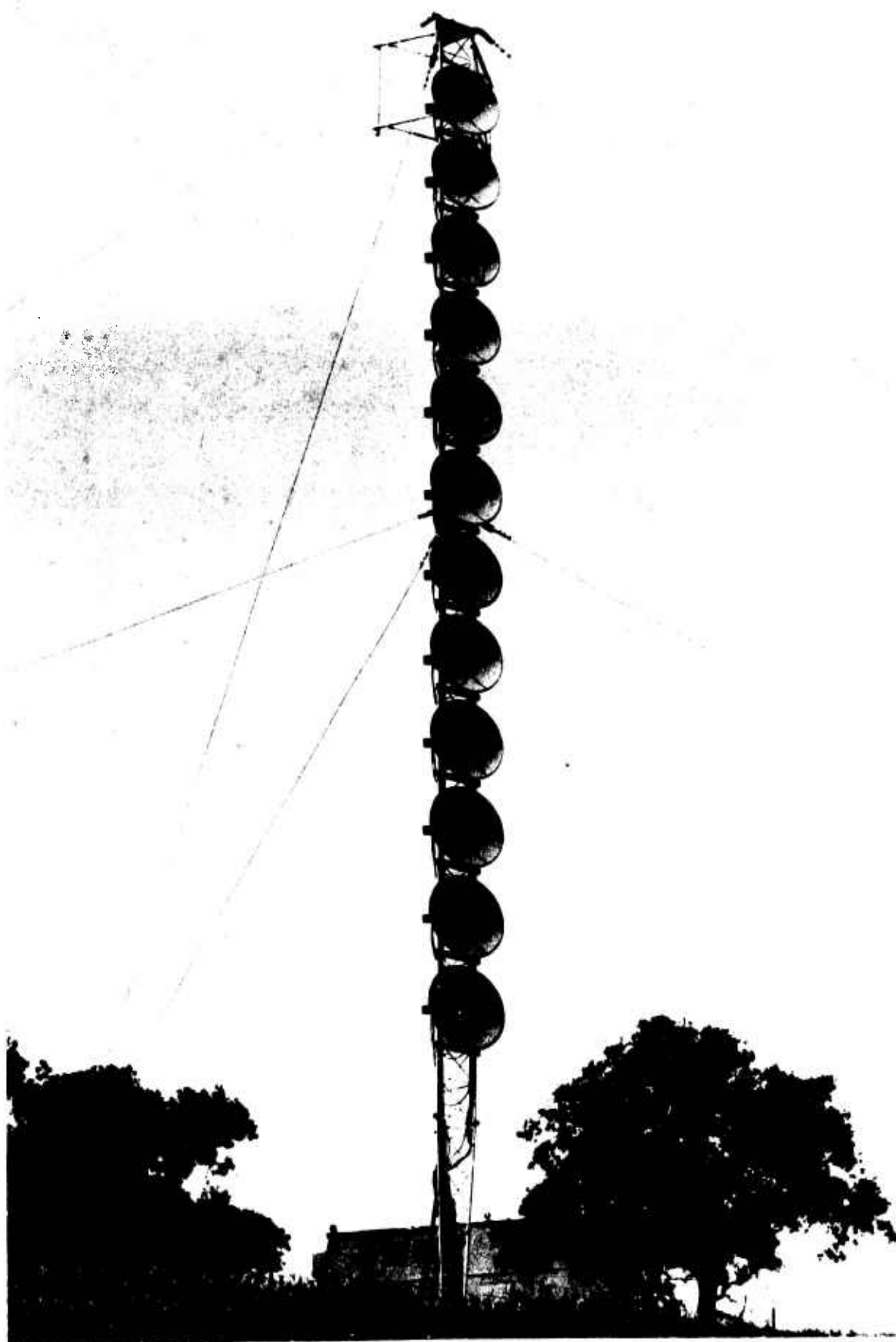


Fig. 2 Receiving array

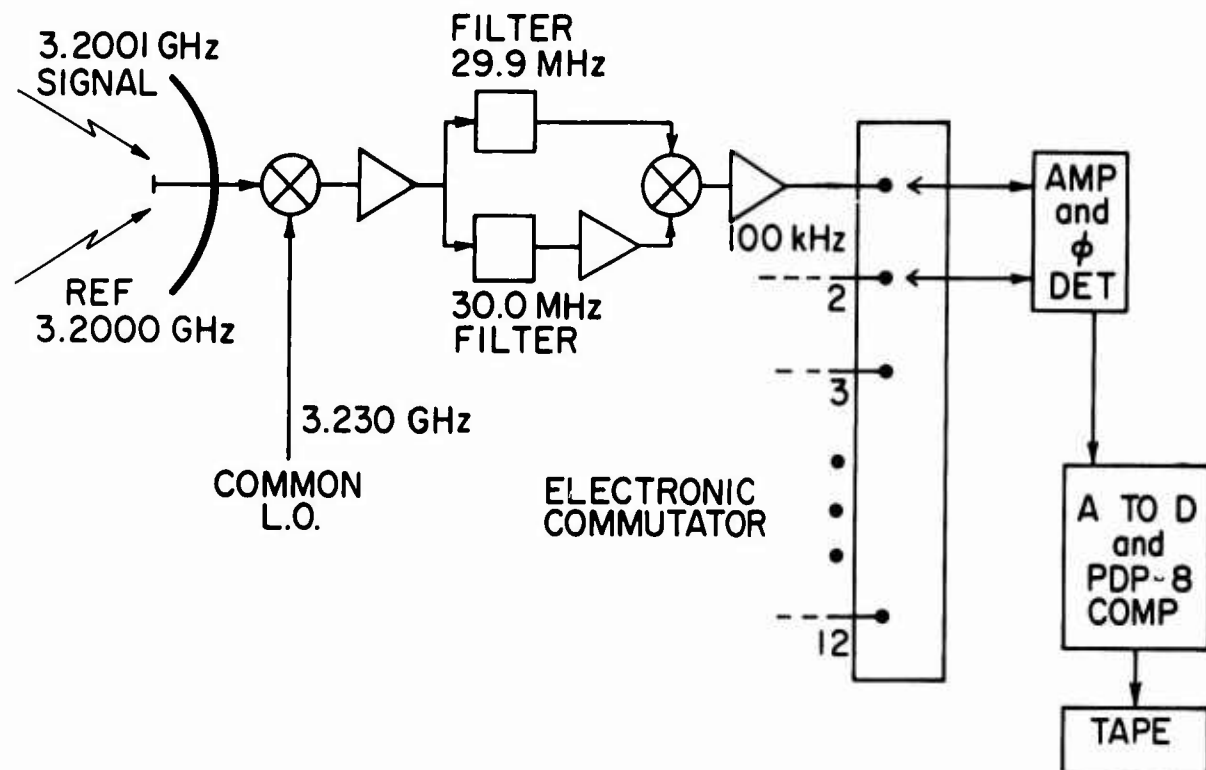


Fig. 3 Simplified block diagram of receiving system

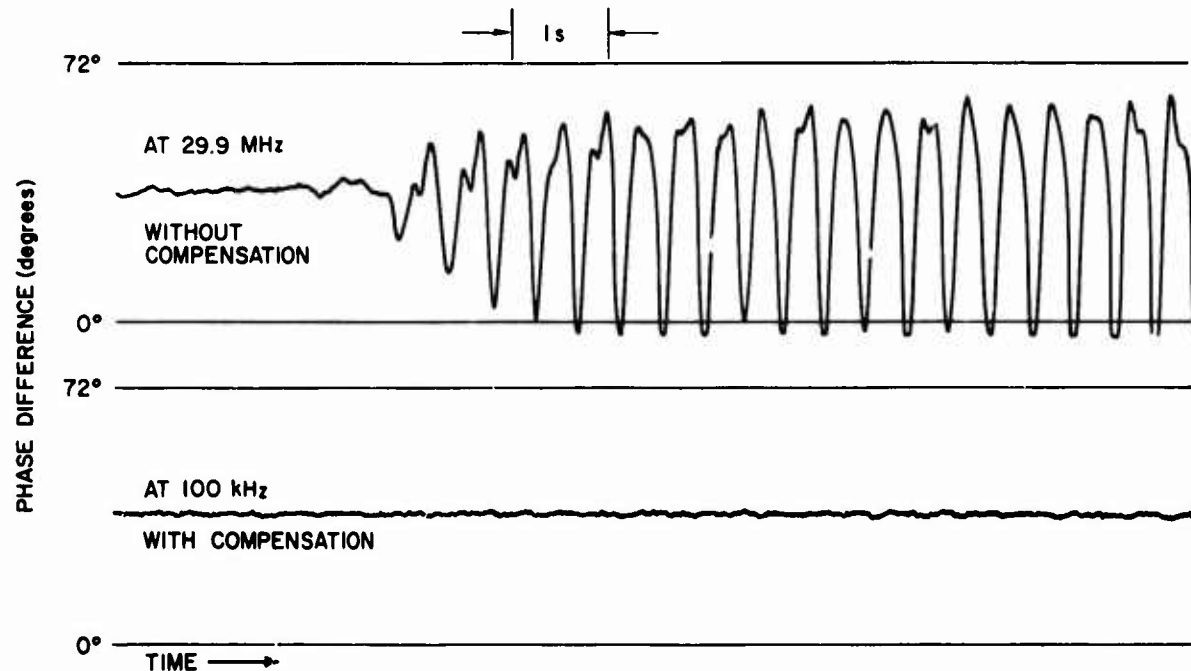


Fig. 4 Phase difference between elements 3 and 10 showing effect of phase compensation

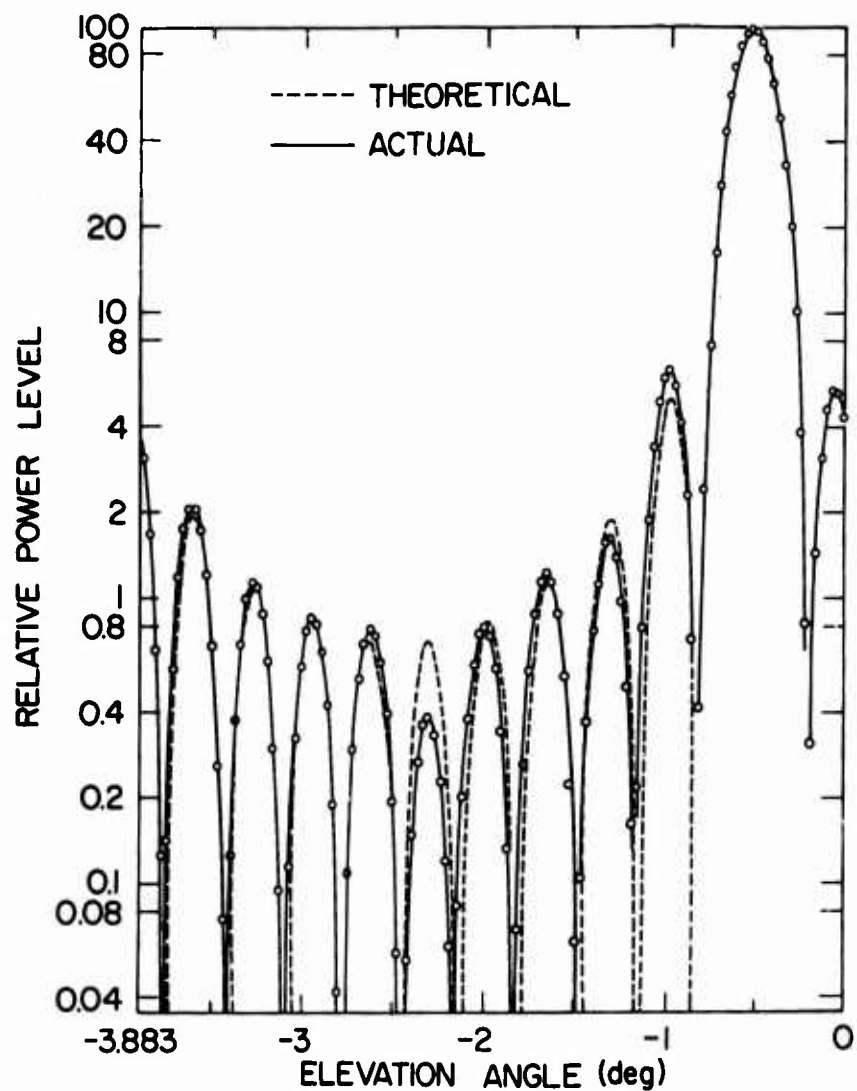


Fig. 5 Averaged angular-response pattern for a line-of-sight path

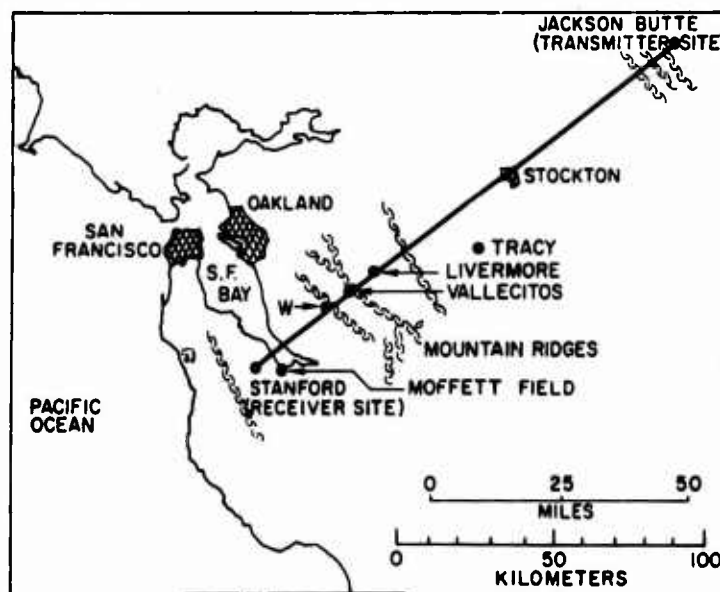


Fig. 6 Map of region surrounding transhorizon propagation path

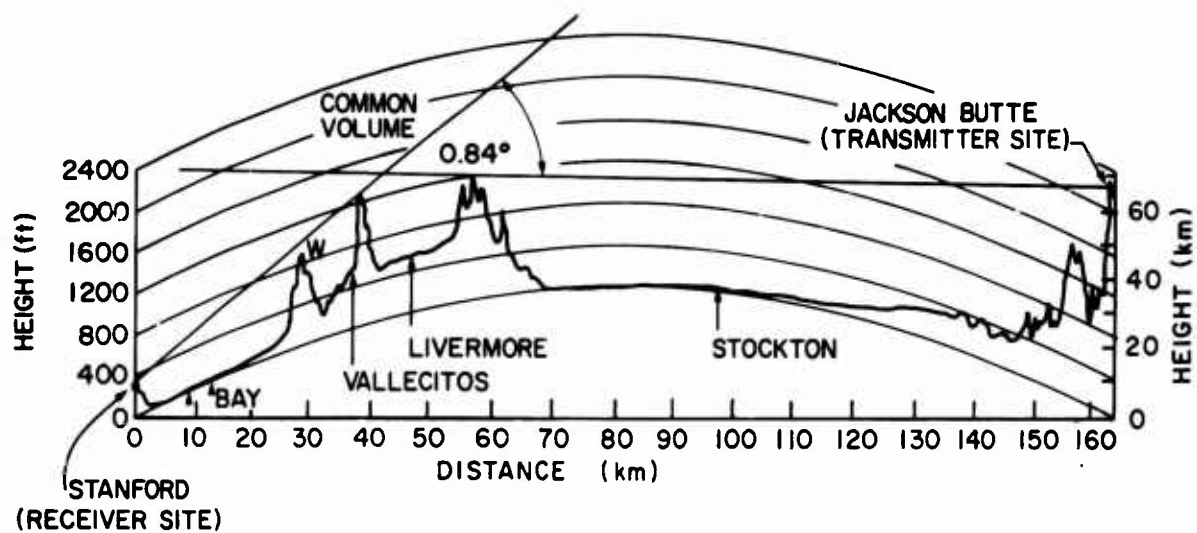


Fig. 7 Profile of transhorizon propagation path

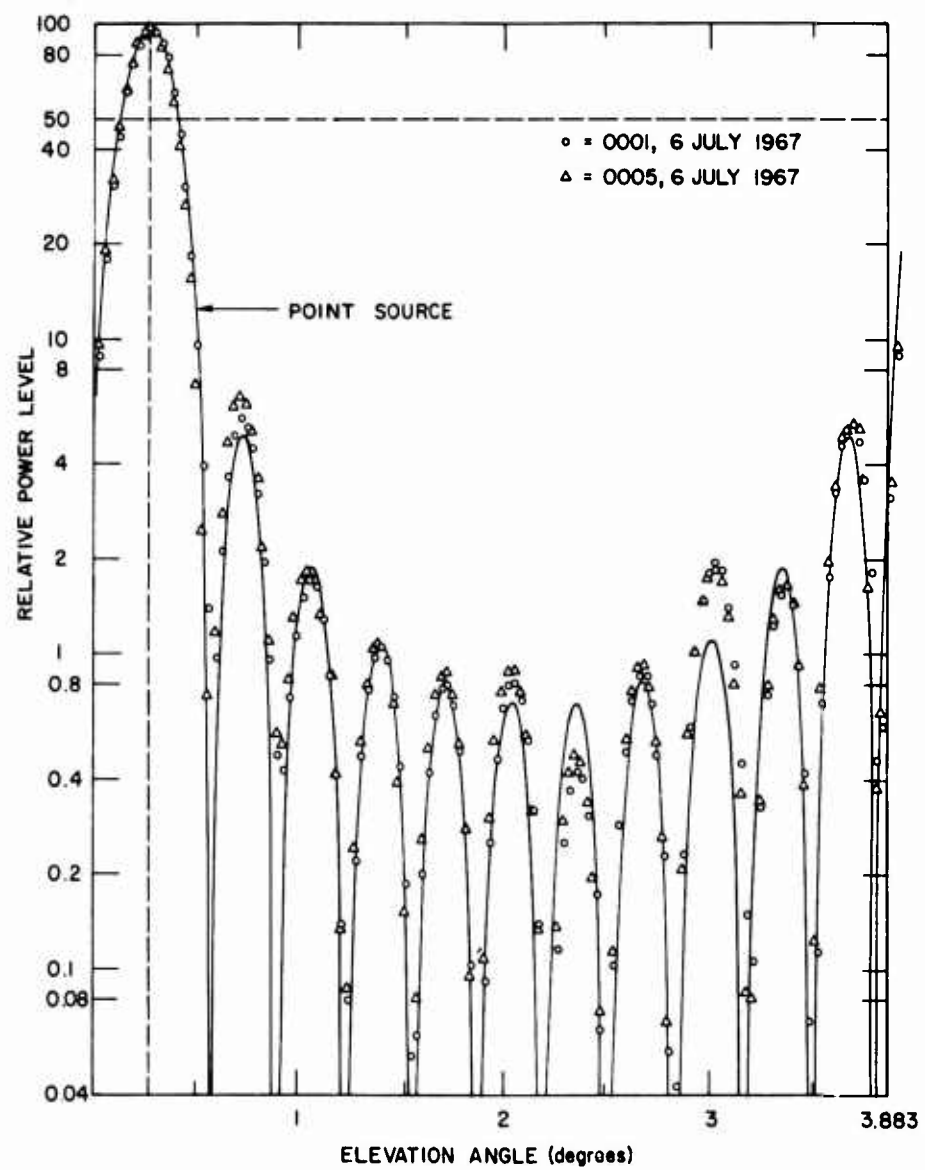


Fig. 8 Averaged angular-response pattern. 0001, 6 July 1967

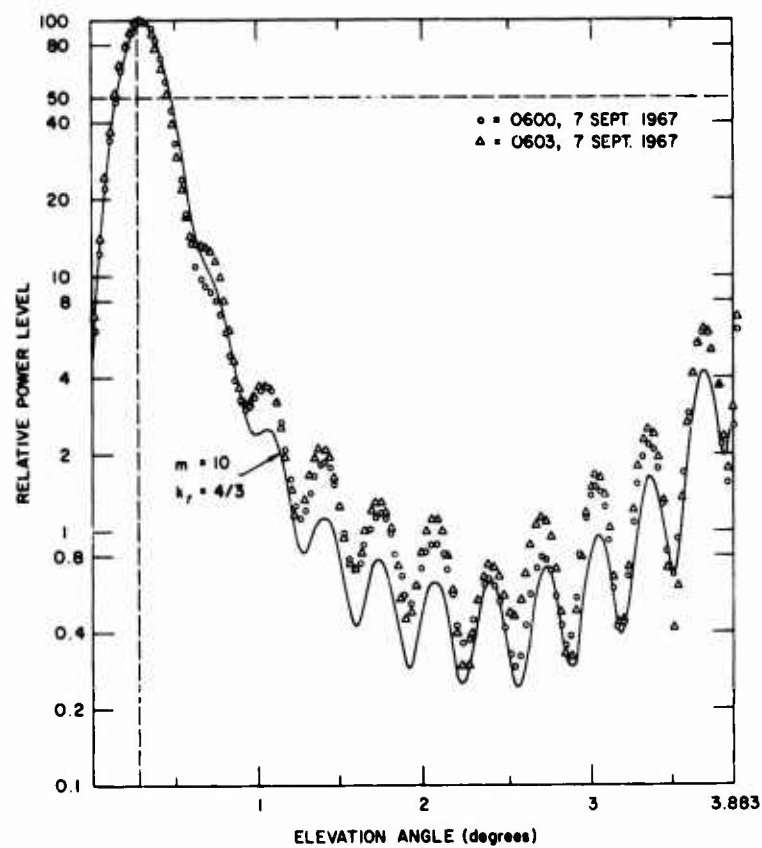


Fig. 9 Averaged angular-response pattern. 0600, 7 September 1967

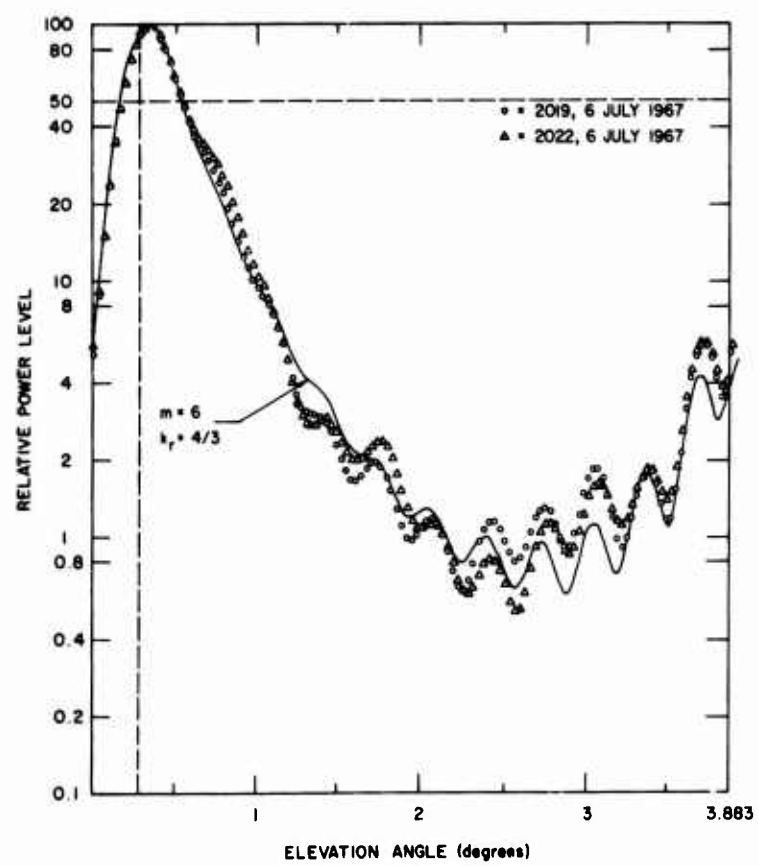


Fig. 10 Averaged angular-response pattern. 2019, 6 July 1967

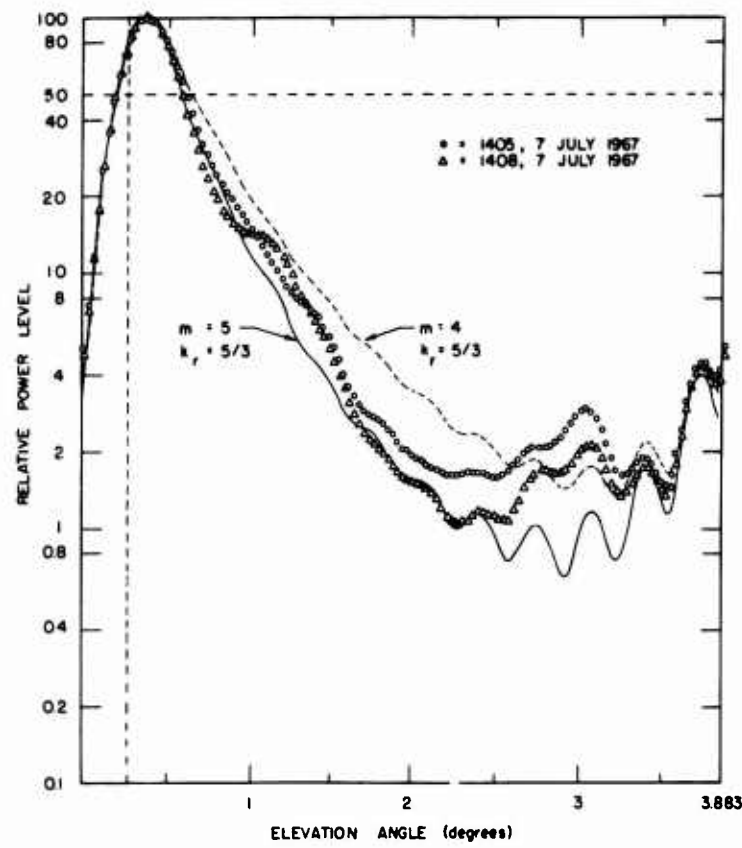


Fig. 11 Averaged angular-response pattern. 1405, 7 July 1967

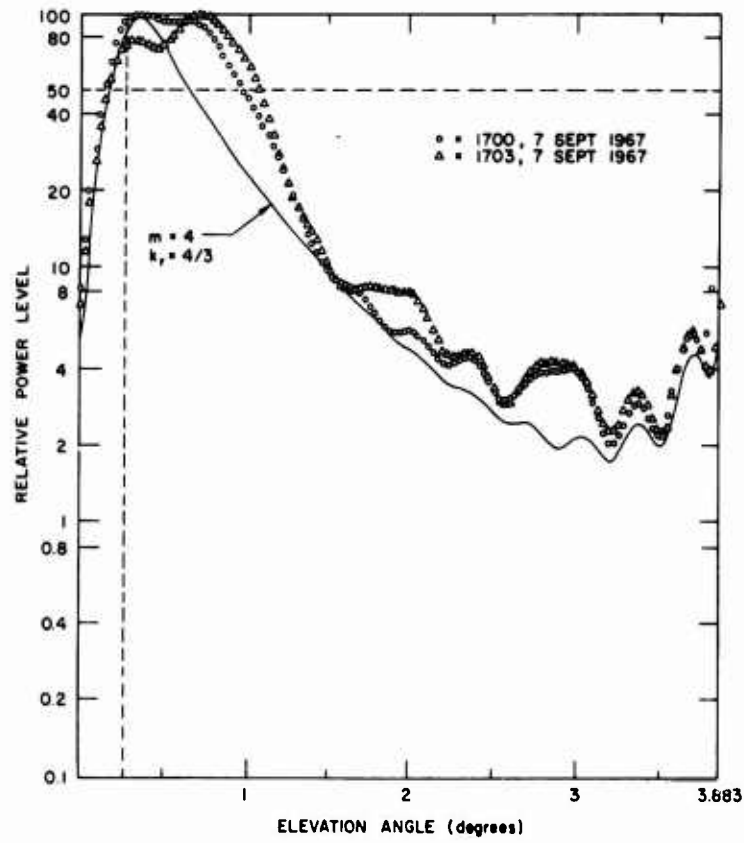


Fig. 12 Averaged angular-response pattern, 1700, 7 September 1967

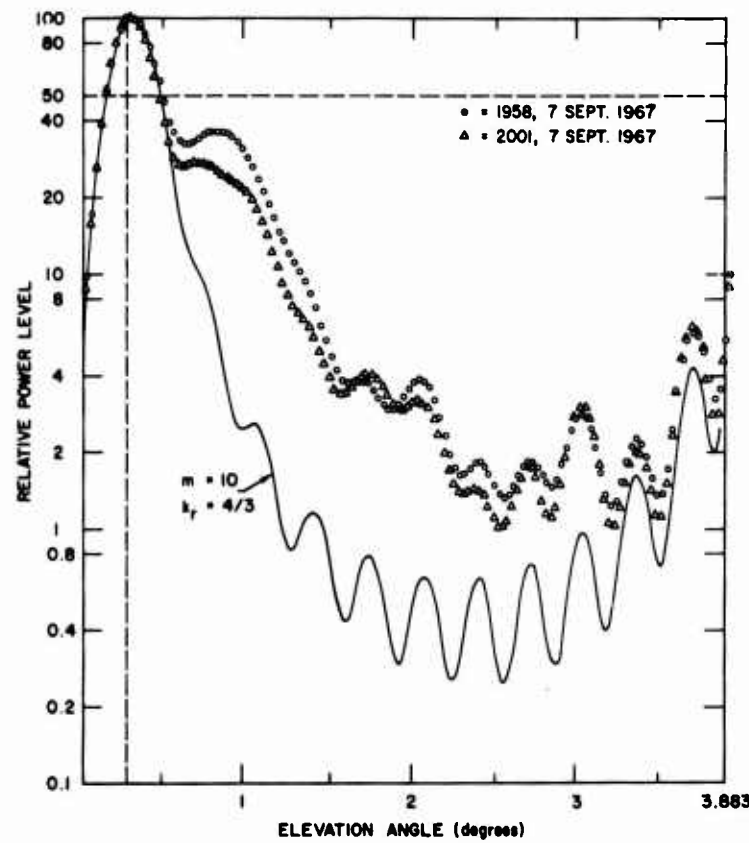


Fig. 13 Averaged angular-response pattern. 1958, 7 September 1967

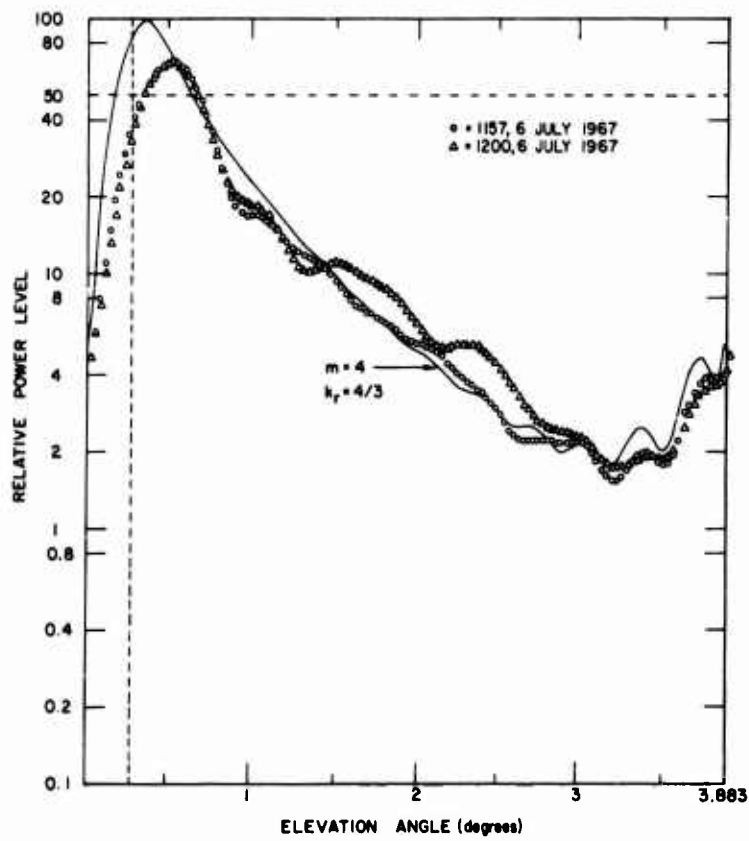


Fig. 14 Averaged angular-response pattern. 1157, 6 July 1967

**THE WAVELENGTH DEPENDENCE OF TROPOSPHERIC  
BEYOND-THE-HORIZON PROPAGATION**

by

**Folke Eklund**

The Swedish Research Institute of National Defence,  
Fack, Stockholm 80, Sweden

**THE WAVELENGTH DEPENDENCE OF TROPOSPHERIC  
BEYOND-THE-HORIZON PROPAGATION**

Folke Eklund

The wavelength dependence of actually received power in relation to free space power has been measured over a 270 km tropospheric scatter path in middle Sweden. The frequencies were 1000 and 3000 MHz and the antennas used were scaled according to the frequencies, giving identical radiation diagrams with the beamwidth  $\alpha = 2.2^\circ$ . The measurements were made during different periods within a year.

The main findings are that the wavelength dependence varies between  $\lambda^{-1}$  and  $\lambda^{+3}$ , and the exponent is correlated with the level of received power. In order to explain the results we found it necessary to consider the received power as the sum of two power terms,  $P_{sc}$ , which is power received from scattering by refractive index variations which are statistically homogeneous and isotropic and  $P_R$ , which is power received from reflections by many small partially reflecting facets within the otherwise homogeneous and isotropic medium. The homogeneous and isotropic refractive index variations are characterised by their "power"-spectrum, which as parameter contains the factor  $C_n^2$ , a measure of the intensity of the refractive index variations.

The facets are characterised by the profile of refractive index through the reflecting surface, the radius of curvature  $R$  of the surface and the maximum tilt, with respect to the horizontal. Furthermore, in order to calculate a numerical value for  $P_R$  we need to know the number of facets per unit volume. We have chosen the following expression for describing the refractive index profile,  $n(z)$ , through the reflecting surface:

$$n(z) = n_0 + \frac{\Delta n}{2} (1 - e^{-(2/z_0)z}) \quad \text{for } z < 0 \quad (1)$$

$$n(z) = n_0 - \frac{\Delta n}{2} (1 - e^{-(2/z_0)z}) \quad \text{for } z > 0. \quad (2)$$

The thickness of the layer causing reflections is defined as  $B = 2z_0$ . The value  $\Delta n$  is the apparent change in refractive index when passing through the reflecting facet.

With this  $n$ -profile the power reflection coefficient becomes

$$|R_0|^2 = \frac{\Delta n^2}{4\psi^4 \left[ 1 + \left( \pi \frac{B\psi}{\lambda} \right)^2 \right]^2}, \quad (3)$$

where  $\psi$  is the grazing angle between the incident ray and the surface of the facet.

The following expressions are obtained for scattered and facet reflected powers, respectively, in relation to free space power,  $P_{FS}$ .

$$\frac{P_{sc}}{P_{FS}} \simeq 0.76 \times 10^{28} \times C_n^2 \left( \frac{dM}{dh} \right)^{-1/3} d^{-11/3} \lambda^{-1/3} \alpha^3, \quad (4)$$

where  $d$  is the distance between transmitter and receiver.

As we have assumed that the refractive index variations follow the  $-11/3$  law we have the  $\lambda^{-1/3}$  dependence for  $P_{sc}/P_{fs}$ .

$$\frac{P_R}{P_{fs}} \simeq \frac{\pi^2 R^2 \phi}{2 \theta_0 d^2} \int_0^{h_{mid}} \frac{N \Delta n^2 (\theta_0 d + 4h)}{\psi \left[ 1 + \left( \frac{8\psi^2}{\lambda} \right)^2 \right]^2} dh . \quad (5)$$

where  $\theta_0$  is the minimum scatter angle of the common volume.

The integration need not be extended beyond the midpcint,  $h_{mid}$ , of the common volume, because  $|R_0|^2$  decreases so rapidly with  $\psi$ .

$P_R/P_{fs}$  is proportional to something between  $\lambda^0$  and  $\lambda^4$ , dependent mainly on the thickness of the facets in relation to the wavelength.

Variations in  $C_n^2$  and  $\Delta n$  are assumed to be the main causes of variations in  $P_{sc}$  and  $P_R$ , respectively. The other parameters are kept constant. However, this assumption is not sufficient if we want to add  $P_{sc}$  and  $P_R$ . We must also know how  $C_n^2$  and  $\Delta n$  are related to each other. There are meteorological reasons for a relation between them, and so we assume a linear relation, with the constant chosen from the maximum of observed values of  $\Delta n$  and  $C_n^2$ . This gives

$$\Delta n = 0.6 C_n^2 \times 10^{10} . \quad (6)$$

The powers can then be added for different values of  $\Delta n$  (or  $C_n^2$ ) and we obtain the results of Figure 1, where

$$A = \frac{P_{sc} + P_R}{P_{fs}} . \quad (7)$$

If we consider the frequency interval 1000 to 3000 MHz, we see that at high signals the wavelength dependence is of the order of  $\lambda^{+2.5}$  and at low signals it is  $\lambda^{-1/3}$ .

We have also calculated the relation between the exponent  $q$  of the wavelength dependence ( $A \sim \lambda^q$ ) and received power in relation to free space power in dB at 1000 MHz and compared it with measured values. The result is shown in Figure 2. The calculated curve agrees reasonably well with the average trend of the measured pointmass.

As we have assumed a relation between  $\Delta n$  and  $C_n^2$ , we also obtain a relation between the levels of received powers at 1000 and 3000 MHz, as shown in Figure 3.

At both the high and the low signal ends there is a  $45^\circ$  dependence between the variations in received powers. The reason is that here the same propagation mechanism is acting at both frequencies - reflection at the high signal end and scattering at the low signal end. At intermediate signal levels the reflection term predominates at 1000 MHz and the scattering term at 3000 MHz, resulting in a slope greater than  $45^\circ$ .

In the experimental data there is a tendency towards a  $45^\circ$  slope at high and low signal levels. In an intermediate section, however, there occur larger variations of the 1000 MHz signal than of the 3000 MHz signal as expected from the propagation model.

The spread of the experimental points in Figures 2 and 3 could be explained in many ways. Thus, for example, the assumed connection between  $\Delta n$  and  $C_n^2$  will certainly change from time to time, and the numerical values of the geometrical parameters describing the reflecting facets will vary.

However, a simple propagation model which considers simultaneous single scattering by a homogeneous and isotropic refractive index structure and facet reflections gives good agreement, on the average, between experimental and calculated results of

- (i) wavelength dependence,
- (ii) the relation between wavelength dependence and received power levels,
- (iii) the relation between received power levels at 1000 and 3000 MHz.

A full account of the experiments and calculations described in this brief contribution is published in Reference 1.

#### REFERENCES

1. Eklund, F.,  
Wickerts, S.  
*Wavelength Dependence of Microwave Propagation Far Beyond  
the Radio Horizon.* To be published in Radio Science,  
November 1968.

19-4

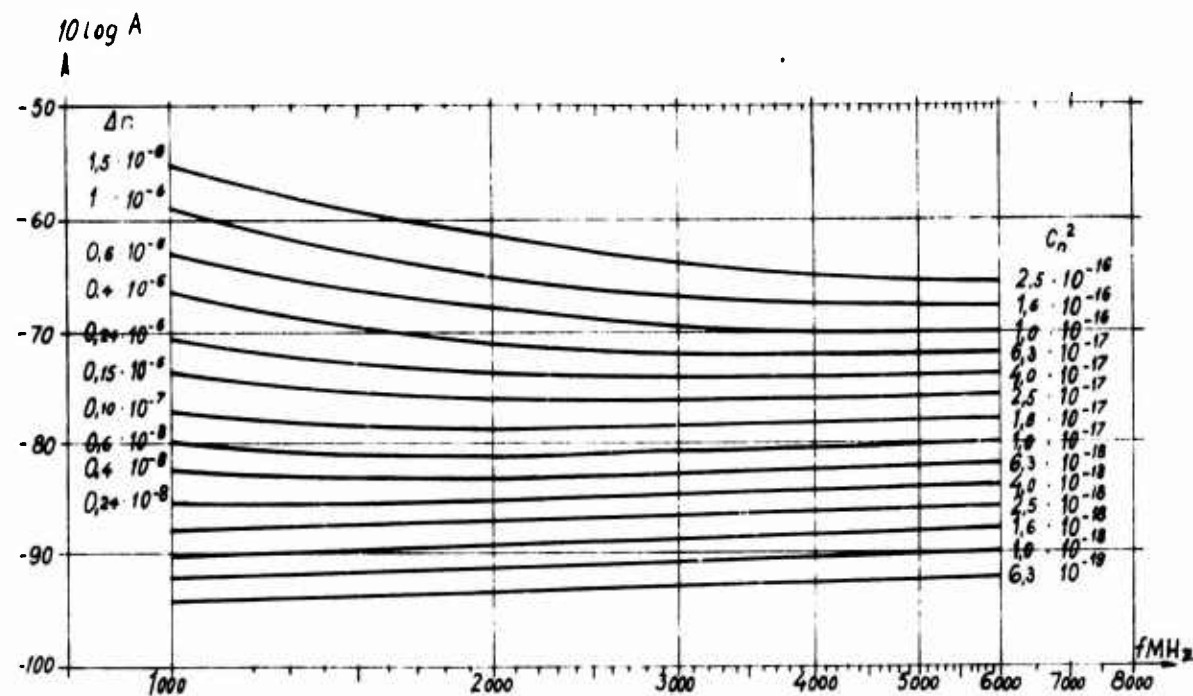


Fig. 1 Frequency dependence of totally received power for different values of  $\Delta n$  and  $C_n^2$

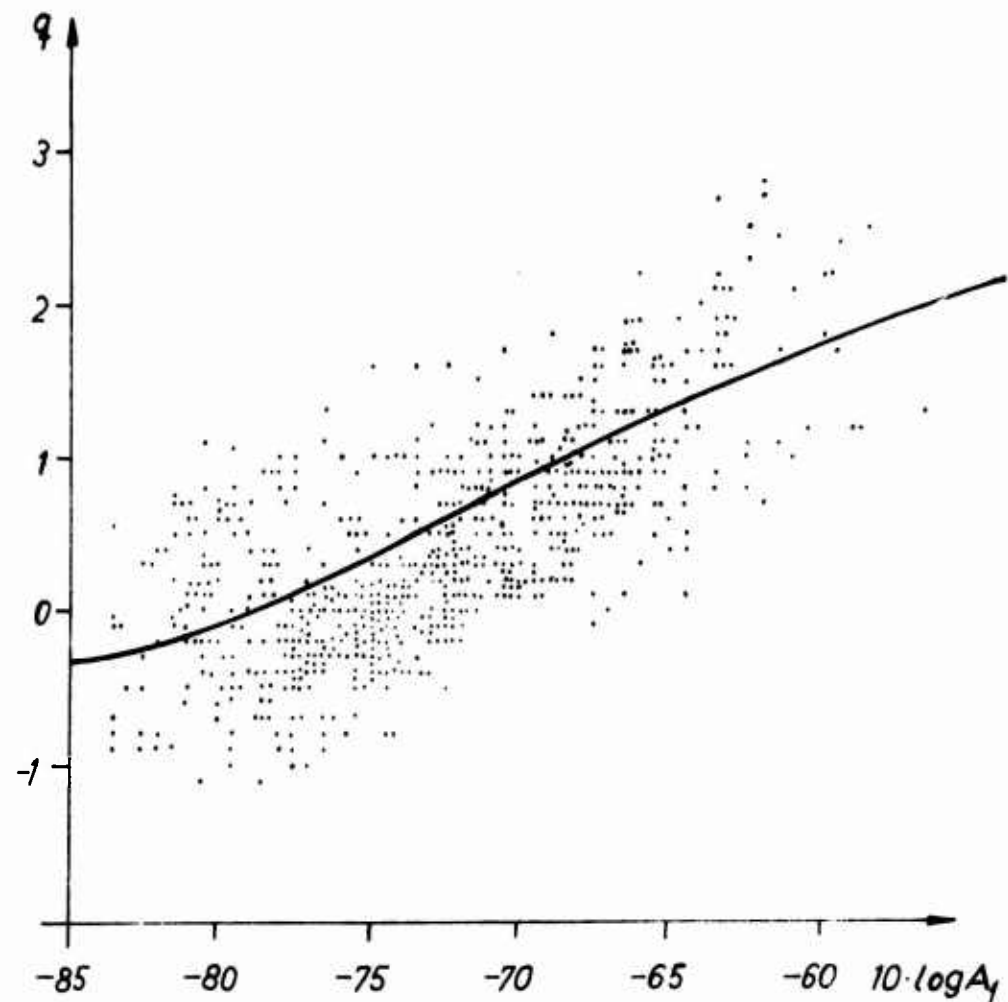


Fig. 2 The exponent of the wavelength dependence as a function of received power at 1000 MHz

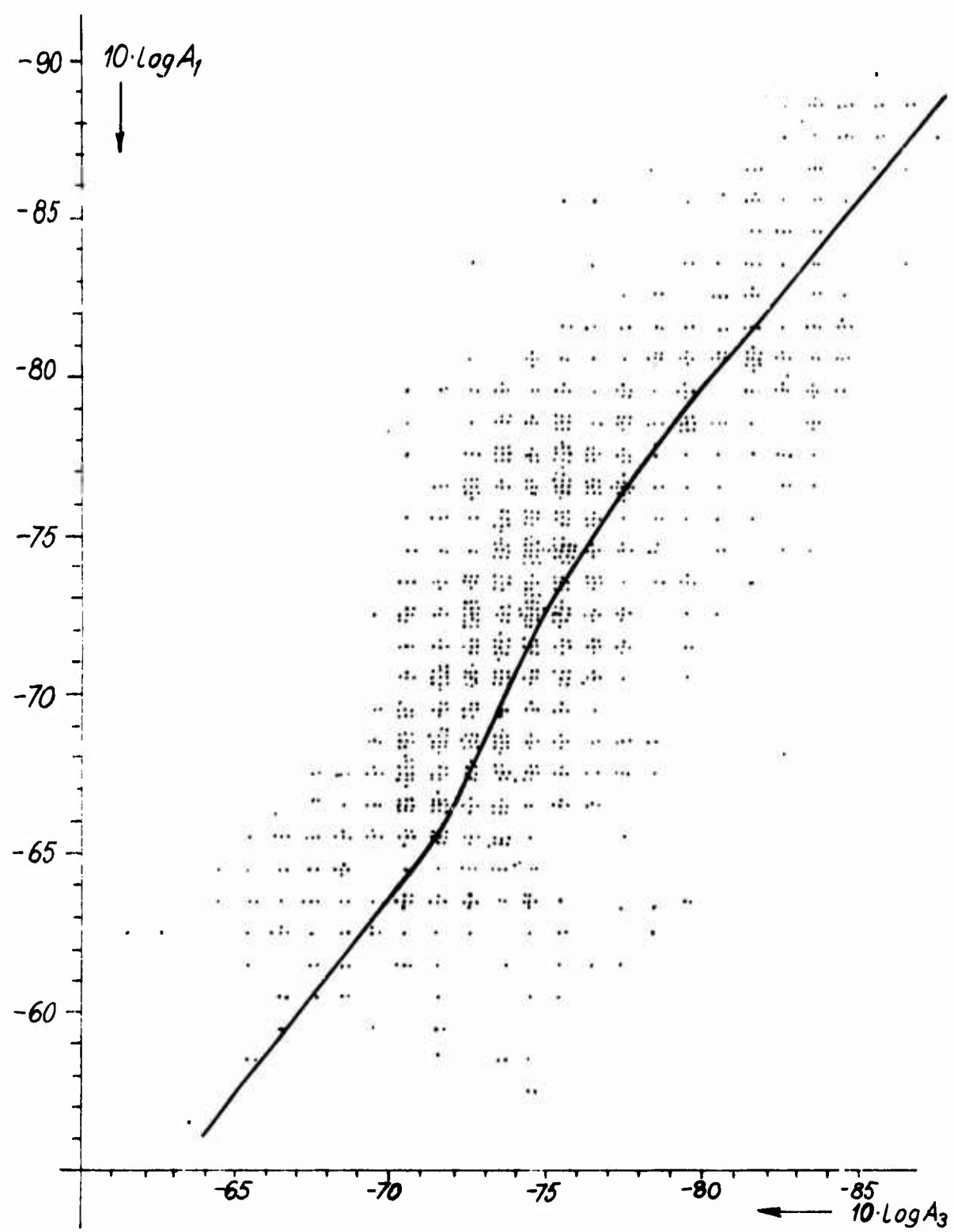


Fig. 3 The signal levels at 1000 MHz as a function of the corresponding values at 3000 MHz

**THE THEORY OF TROPOSPHERIC SCATTERING IN THE  
LIGHT OF NEW PROPAGATION MEASUREMENTS**

by

**L. Fehlhaber**

Research Institute of the FTZ  
(Federal German Post Office)  
Darmstadt, Germany

#### SUMMARY

The structure of the electromagnetic field at the receiving site of a scatter link is caused by a corresponding structure of the refractivity in the common volume. Theoretical investigations have shown that conclusions about the refractivity structure can be drawn from measurements of the structure of the field at the receiving site. The wave number spectrum of the refractivity, deduced in this way, has been shown to agree with the spectrum deduced from turbulence theory. The dependence on height of the inhomogeneities of the refractivity, needed to determine the transmission loss, can usually be calculated from routine radiosonde data. A model of the troposphere is deduced and seems to explain most of the effects of tropospheric beyond-the-horizon propagation.

**THE THEORY OF TROPOSPHERIC SCATTERING IN THE  
LIGHT OF NEW PROPAGATION MEASUREMENTS**

L.Fehlhaber

**1 INTRODUCTION**

Many attempts have been made to investigate the structure of tropospheric refractivity, since Booker and Gordon showed that beyond-the-horizon propagation can be explained by scattering on inhomogeneities of the refractivity. Conventional meteorological measurements, as well as airborne refractometers, showed that the models deduced from turbulence theory are acceptable. It will be shown in this paper that measurements performed in the electromagnetic field at the receiving site of a scatter link allow conclusions to be drawn about the mechanism of propagation. Grosskopf<sup>1</sup> described measurements of this type in detail. They yielded the space-time correlation function of the field, its scale lengths, its horizontal and vertical drift velocities and its fluctuation velocity. It will be shown in Section 2 that the corresponding structure of the troposphere can be deduced from these results. Section 3 deals with the problem of obtaining the height-dependence of the inhomogeneities of the refractivity from routine radiosonde data. A model of the troposphere, deduced from these results, is given in Section 4.

**2. BEYOND-THE-HORIZON PROPAGATION WITH  
FREQUENCIES ABOVE 1000 MHZ**

It is easy to understand that the field structure at the receiving site can be deduced from the corresponding structure of the refractivity  $N$  in the common volume. With scattering, there should be a relation between the two space-time correlation functions of the refractivity and of the field. This relation has been derived by theoretical investigations<sup>2,3</sup> assuming a homogeneous structure. Since this structure certainly is not homogeneous, the relation is only valid over long time-averages. This relation is generally a complicated one, but it becomes somewhat simpler in the limiting case of antennae beams broad enough to comprise the whole beam of scattered radiation, a condition fulfilled in the present measurements.

The spatial correlation function of the field in this case is obtained from that of the refractivity by a simple integration with respect to the coordinate in the direction of propagation. The correlation function of the field is known. The correlation function of refractivity is therefore obtained by solving an integral equation.

A test was made to see whether this method yielded reasonable results when applied to the measurements in the 2000 MHz range. If so, it must be concluded that beyond-the-horizon propagation in this frequency range is due to scattering. The results of this test are now summarized briefly.

The correlation function  $\rho_N$  of the refractivity turned out to be a Norton function of order one-third:

$$\rho_N = N^{1/3} \sqrt{((x/l_x)^2 + (y/l_y)^2 + (z/l_z)^2)}, \quad (1)$$

where  $x$  is the coordinate in the direction of propagation,  $y$  and  $z$  are perpendicular to this direction,  $y$  horizontal,  $z$  vertical.  $l_x$ ,  $l_y$  and  $l_z$  are the scale lengths in these directions and

$$N_\nu = \frac{2^{1-\nu}}{\Gamma(\nu)} |x|^\nu K_\nu(|x|) , \quad (2)$$

$K_\nu$  being a modified Bessel function of the second kind.

The corresponding one-dimensional wave number spectrum

$$S_N = \frac{2\pi\Gamma(5/6)}{\Gamma(1/2)\Gamma(1/3)} (1 + k^2)^{-5/6} . \quad (3)$$

When  $k \gg 1$ , approximately

$$S_N \approx k^{-5/3} . \quad (4)$$

Hence the well known five-third spectrum that Kolmogorov and Oboukhov proposed for the inertial subrange has been derived from the measurements.

Theoretical investigations<sup>2,3</sup> have shown that a very simple relation exists, connecting the scale lengths  $l_x, l_y, l_z$  of the refractivity with the scale lengths  $L_x, L_y$  and  $L_z$  of the field. In the case of a symmetrical path

$$\begin{aligned} L_y &= 2l_y, & L_z &= 2l_z \\ L_x &\rightarrow \infty . \end{aligned} \quad (5)$$

Since the scale lengths of the field are known from the measurements ( $L_y \approx L_z \approx 8 \text{ m}$ ), on the average the scale lengths of the refractivity are

$$l_y = l_z = 4 \text{ m} . \quad (6)$$

The measurements do not provide the scale length  $l_x$  in the direction of propagation. But, since it is a horizontal scale length, it ought to equal  $l_y$ , at least on the average. From these results we infer that the tropospheric structure, causing propagation in the 2000 MHz range, is nearly isotropic.

The temporal variations of the field allow conclusions to be drawn about the corresponding temporal variations of the refractivity. They can both be split up into a drift and fluctuation term. Let  $V_{Dy}$  and  $V_{Dz}$  be the drift components of the field,  $v_{oy}$  and  $v_{oz}$  those of the refractivity. Then, with a symmetrical path,

$$V_{Dy} = 2v_{oy}, \quad V_{Dz} = 2v_{oz} . \quad (7)$$

These relations proved to agree with the measurements, when  $v_{oy}$  was identified with the mean wind component in the common volume.  $V_{Dz}$  was found to be zero. No mean vertical wind therefore exists, as expected.

The vertical component of the fluctuation velocity of the air in the common volume, deduced from the measurements in the field, turned out to be of the order of  $1 \text{ ms}^{-1}$  on the average. By definition, this quantity is root-mean-square deviation of the local wind speed from the mean vertical motion of the air in the whole common volume and is therefore not identical with the vertical turbulence velocity, as measured by meteorological methods. Large scale convective vertical motions are incorporated in the fluctuation velocity as just defined.

Antennae-to-medium coupling losses determined from theory, using the above results, are in good agreement with measured gain losses.

The transmission loss  $A$  relative to free space ought to increase slightly as the frequency  $f$  increases, i.e.

$$A \sim f^{-1/3} . \quad (8)$$

This relation, unfortunately, could not yet be tested by experiment.

These results show that there can be no doubt that beyond-the-horizon propagation in the frequency range between 1500 MHz and 2000 MHz is due to scattering caused by nearly isotropic inhomogeneities of the refractivity. Only in the case of a common volume lying with its main part in the lowest 600 m above ground does a share of partial reflection seem to exist in this frequency range.

### 3. THE DEPENDENCE ON ALTITUDE OF THE INHOMOGENEITIES OF THE REFRACTIVITY

If we want to calculate propagation curves for scatter propagation, not only the correlation function of the refractivity  $N$ , but also the dependence on height of the inhomogeneity  $\bar{N}^2$  must be known. The backscatter measurements with a vertical pointing radar as described by Grosskopf<sup>1</sup> are one of the means of getting this height dependence. A method of calculating an average height dependence using routine radiosonde data is now outlined.

Let us look for the sources of the inhomogeneity  $\bar{N}^2$ . They ought to coincide with the sources of the inhomogeneities of the potential temperature and specific humidity. Inhomogeneity of any exchangeable quantity now needs a steep gradient of this quantity as well as turbulent motion. A small turbulent motion nearly always exists in the troposphere. But there are well mixed regions without any gradient of potential temperature and specific humidity. No inhomogeneity can arise from these regions. The main sources of inhomogeneity therefore will be the regions with a steep gradient of potential temperature, of specific humidity, or of both.

The backscatter measurements using a vertical pointing radar are consistent with this model. The inhomogeneities of the refractivity are concentrated in distinct layers, mostly having short life times.

Using this model, we attempted to calculate the dependence on altitude of the inhomogeneity  $\bar{N}^2$  by means of routine radiosonde data. The data for four months - February, May, August and November 1965 - have been evaluated for this purpose. Instead of describing in detail the method and the theoretical background, Figure 1 shows the result. The inhomogeneity proves to be nearly constant up to an altitude of 1800 m and then decreases exponentially. Up to 4 km approximately, except the lower 500 m, this profile agrees with that found from the backscatter measurements. The existence of the peak at the tropopause was proved by Atlas and Hardy<sup>4</sup> by means of a high power radar.

### 4. A MODEL OF THE TROPOSPHERE

The following model of the troposphere may be deduced from the above results: A large number of scattering leaves with finite extension are embedded in weakly scattering atmosphere. These leaves (or refractivity clouds<sup>5</sup>) are connected with steep gradients of refractivity. In the lower 2 km these leaves presumably are caused by the caps of rising convection bubbles; above 2 km they may be due to inversion layers. Large diurnal variations of the inhomogeneity in the lower 2000 m, with a maximum in the early afternoon, seem to confirm this explanation.

The horizontal extension of the leaves could not be measured by the radar. But a quite different method allows conclusions to be drawn about this quantity. Beyond-the-horizon propagation at 100 MHz must, for many reasons, be due to some mechanism other than scattering. The small fading rate (0.01 Hz) is one of these reasons. It corresponds to horizontal scale lengths of some hundred metres up to some kilometres and hence is not caused by the

isotropic inhomogeneities causing scattering at higher frequencies. The leaves of enhanced inhomogeneity are now connected with steep refractivity gradients. Hence partial reflection at these gradients may be the main cause of beyond-the-horizon propagation at 100 MHz and presumably at frequencies up to at least 500 MHz. We deduce that the measured horizontal scale lengths of some hundred metres up to some kilometres ought to be identical with the horizontal extensions of the leaves of enhanced inhomogeneity.

### 5. CONCLUSIONS

Beyond-the-horizon propagation with frequencies above 1000 MHz seems to be explained best by scattering from nearly isotropic inhomogeneities of the refractivity. The wave number spectrum of the refractivity agrees with that deduced from turbulence theory. The scale lengths in the three directions of space amount to 4 m approximately. Measured diversity spacings, fading rates and antennae-to-medium coupling losses, as well as the wave number spectrum of the field, agree very well with this model.

The scattering inhomogeneities arise in regions with a steep gradient of refractivity. Hence they are concentrated in leaves of finite extension, the so-called refractivity clouds, which reflect the lower frequencies and scatter the higher ones.

On the average the inhomogeneity is constant up to about two kilometres and then decreases at higher altitudes. Near the tropopause a peak of the inhomogeneity is expected.

As shown, this model of the troposphere seems to explain most of the known effects in tropospheric beyond-the-horizon propagation.

### REFERENCES

1. Grosskopf, J. *Experimental Methods to Investigate Receiving Fields with Tropospheric Scatter Propagation.* A paper in this volume.
2. Fehlhaber, L., Grosskopf, J. *Das elektromagnetische Feld am Empfangsort einer troposphärischen Scatterstrecke. I, Die Eigenschaften des Empfangsfeldes und ihre Messung.* Nachrichtentechnische Zeitschrift, Vol. 20, 1967, pp. 511-520.
3. Fehlhaber, L., Grosskopf, J. *Das elektromagnetische Feld am Empfangsort einer troposphärischen Scatterstrecke. II, Die Struktur der Dielektrizitätskonstanten im gemeinsamen Volumen und ihre Wirkungen auf das Empfangsfeld bei Frequenzen über 1000 MHz.* Nachrichtentechnische Zeitschrift, Vol. 20, 1967, pp. 649-657.
4. Atlas, D., Hardy, K.R. *Radar Analysis of the Clear Atmosphere: Angels.* Progress in Radio Science, 1963-1966, Proceedings of the XVth General Assembly of URSI, Munich, pp. 401-469.
5. Fukushima, M., et al. *Statistical Survey of Atmospheric Refractive Index Variations in Japan.* Journal, Radio Research Laboratories, Japan, Vol. 13, 1966, pp. 1-11.

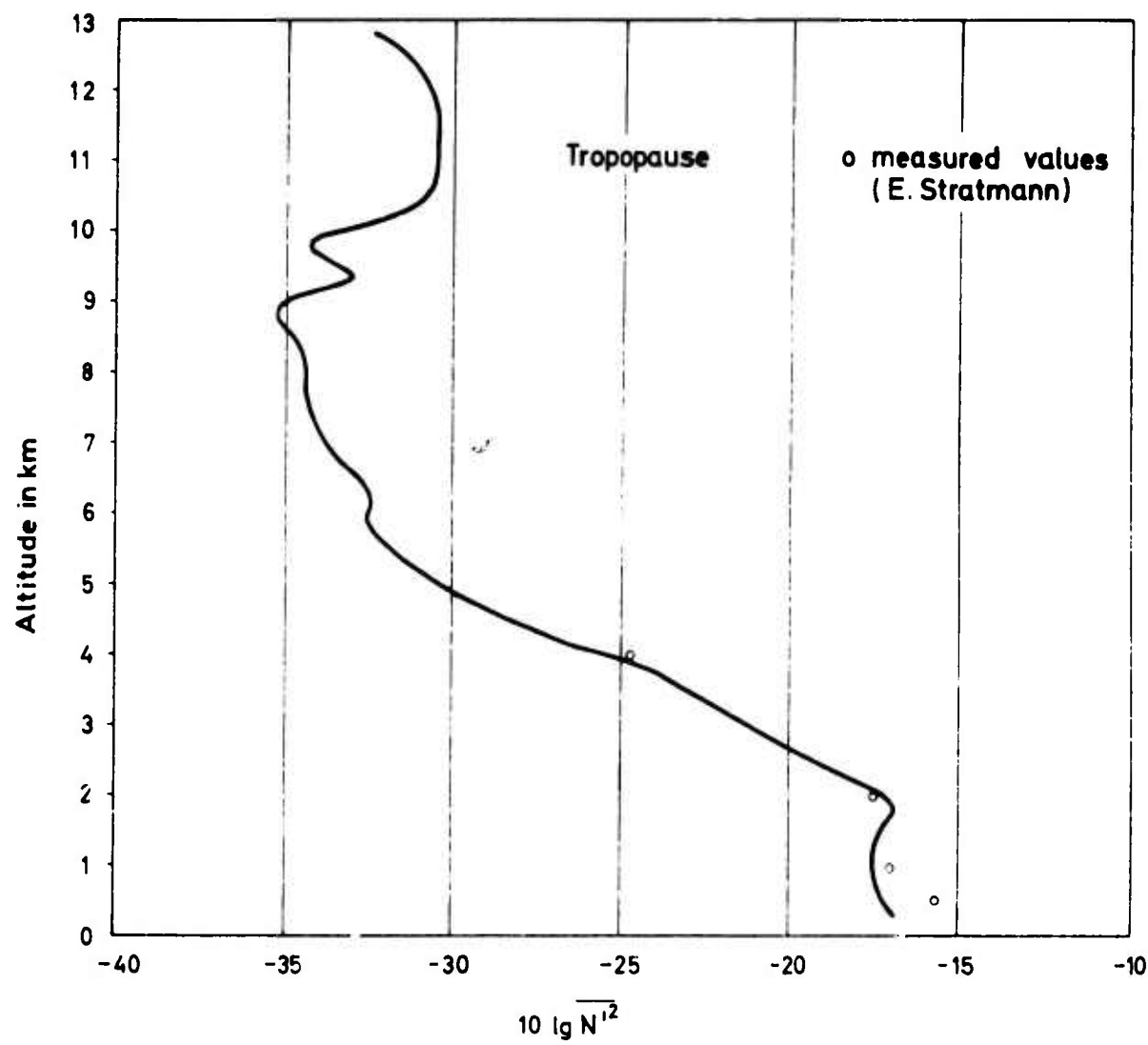


Fig. 1 Dependence on altitude of the inhomogeneity  $\overline{N^2}$  (median value) calculated from routine radiosonde data

MICROWAVE PROPAGATION INFLUENCED BY INTERNAL GRAVITY WAVES

by

Gerda Fengler\* and Gerd Stilke\*\*

\*Institut für Radiometeorologie und Maritime Meteorologie an der Universität  
Hamburg, Institut der Fraunhofer-Gesellschaft.

\*\*Meteorologisches Institut der Universität Hamburg.

## SUMMARY

In the period range of several minutes, wave-like variations of VHF field strength observed on transhorizon links correlate with periodical micropressure variations observed with the aid of sensitive barovariographs. The coincidence of nearly periodical variations of atmospheric pressure and field strength depends on the presence of discontinuities in the vertical profile of the refractive index for microwaves in the lower atmosphere.

Pressure variations in the period range mentioned are caused by internal gravity waves which result in a moving wavy structure of the boundary layers. These rippled layers are thought to influence the fading characteristics of the received field strength on transhorizon microwave links.

## MICROWAVE PROPAGATION INFLUENCED BY INTERNAL GRAVITY WAVES

Gerda Fengler and Gerd Stilke

### 1. INTRODUCTION

For transhorizon links the propagation of UHF and VHF radio waves can most often be related to the mechanism of scattering from areas always existing in the turbulent atmosphere. This propagation mechanism is often modified by reflection from layer-type discontinuities in the lower atmosphere.

Of particular interest is the case of an undulating tropospheric layer. This problem has been studied by Gossard<sup>1</sup>, by discussing the observed parameters of atmospheric internal waves in relation to their implications for radio and radar coverage. Waterman and Strohbehn<sup>2</sup> analysed beam-swinging experiments, assuming a wavy layer moving perpendicular to the radio path. Further work along these lines has been done by Gjessing and Irgens<sup>3</sup>.

The paper presented here deals with the influence of a moving rippled layer on the fading characteristics of VHF signals on transhorizon links. The following topics are discussed:

- (a) Measurements of micropressure variations on the ground, and the analysis of these measurements from which the existence of gravity waves in the lower troposphere is deduced.
- (b) Corresponding measurements of electromagnetic (92.4 MHz) field strength fadings.
- (c) The synthesis of both parameters which results in the phenomenon of reflection from moving wavy boundary surfaces.

### 2. GRAVITY WAVES AND MICROPRESSURE VARIATIONS

The theoretical treatment of gravity waves in a vertically multiple stratified medium leads to wave duct considerations. In the earth's atmosphere, the slow settling of air from a high pressure system produces particularly stable layers and inversions of temperature. If a temperature inversion layer is embedded in layers of less static stability, this layer may act as a duct for gravity waves with periods within a distinct range (e.g. 2 - 20 minutes), depending on the specific stratification.

Figure 1 presents a three-layer model of the lower atmosphere with the fundamental mode of a gravity wave propagating in the inversion layer. Evanescent waves propagate in the adjacent layers. Also shown are the assumed vertical profiles of potential density  $\rho_{pot}$  and potential temperature  $T_{pot}$ , the flow pattern and the vertical profiles of the amplitudes of the streamline components,  $u'$  (horizontal) and  $w'$  (vertical). The amplitudes of the pressure variations  $p'$  due to the wave motion would show the same vertical dependence as the streamline component  $u'$ . Near the ground the pressure variations are of the order of 0.1 mb.

The propagation of these gravity waves, especially in low level ducts (ground-based inversions) may best be seen in vertical cross-sections of the atmosphere. Figure 2 shows the isentropic field, calculated from temperature measurements at six different altitudes up to 250 m on a mast, and the vertical wind component at three altitudes, together with the pressure variations at ground level and the variations of wind direction and wind speed during the passage of a gravity wave.

The speed and the direction of these ducted gravity waves may be deduced from atmospheric pressure measurements by a network of microbarograph stations<sup>4</sup>. As an example, Figure 3 shows the propagation of a wave front at 5-minute intervals.

Marked pressure oscillations due to gravity waves are mostly observed in calm weather conditions. A good coherence sometimes exists between waves recorded at stations farther apart than 100 km.

In the Hamburg area, wave fronts and phase velocities of pressure waves could be deduced every fifth day (long term mean), in comparing phases from at least three microbarograph stations (5 - 10 km apart). The values most frequently obtained, from more than 1000 waves during a three-year period of observation are as follows<sup>5</sup>:

periods:	5 - 15 min
wavelengths:	3 - 15 km
phase velocities:	2 - 20 ms <sup>-1</sup> .

Whenever radiosonde ascents were available at the time of the occurrence of the micro-pressure variations, temperature inversion layers below 3000 m altitude were observed simultaneously. Therefore, it seems justified to associate the observed pressure oscillations with the propagation of gravity waves in atmospheric wave ducts in the lower troposphere.

When it is thin, the wave duct may be replaced by a boundary surface separating two media of different density. In this case the wave is a true surface wave, showing an exponential decrease of amplitude in the vertical direction.

It is estimated that the undulating discontinuity may show vertical displacements up to more than 1/10 of the height of the discontinuity; the amplitudes of the inclination angle often amount to 1° (17.45 mrad) or more.

### 3. EXPERIMENTAL ARRANGEMENT

To investigate the fading characteristics of VHF signals, three radio paths in the northern part of Germany are operated:

Berlin - Hoehbeck  
 Berlin - Hamburg  
 Berlin - Heligoland

with path lengths of 135, 243, and 400 km, respectively (Fig. 4) and frequency 92.4 MHz.

At the receiving stations the field strength is recorded continuously with strip chart recorders at a speed of 12 cm per hour.

In conjunction with these measurements, at all the sites mentioned, simultaneous recordings of air pressure are taken by highly sensitive barographs (Section 2).

Insight into the vertical structure of the troposphere was obtained by the scheduled radiosonde ascents at Schleswig (S), Emden (E), Hannover (H), and Berlin (B), as well as by individual ascents at Bergen (BH).

#### 4. EVALUATION OF THE OBSERVATIONS

##### 4.1 Statistical Results

Comparison of the field strength and micropressure recordings showed that in about 80% of all cases with nearly periodical variations of micropressure, nearly periodical variations of field strength were also observed, if a time delay of one hour between the two recordings was allowed for. The periods of corresponding oscillations range from 2 to 30 minutes, most of them having a duration of about 10 minutes, and the duration of corresponding wave trains extends up to 3 hours.

Detailed investigations covering the measurements of micropressure at Hoehbeck and field strength in Hamburg during the period January 1966 to December 1967 showed that simultaneous periodical variations of both parameters were always correlated - whenever radiosonde ascents were available at the time of observation - with the presence of a layer-type discontinuity below 3000 m altitude, with pronounced vertical variation of the atmospheric refractive module N for microwaves.

Furthermore it became obvious that the coincidence of the variations was most pronounced if the discontinuity in N was situated in the height range from about 500 to 700 m above mean sea level. Otherwise, shorter period oscillations were superimposed on the field strength variations.

The refractive module N for microwaves depends on temperature T ( $^{\circ}$ K), partial water vapour pressure e (mb), and atmospheric pressure p (mb) according to the relation

$$N = (n - 1) \times 10^6 = \frac{77.6}{T} \left( p + \frac{4810}{T} e \right),$$

where n is the refractive index.

As shown in Section 2, internal gravity waves, producing periodical pressure variations on the ground, are ducted in a horizontal layer of higher static stability (higher gradient of potential temperature) than below or above. On the other hand, the propagation of electromagnetic waves depends on the vertical gradient of the refractive index, which is most strongly influenced by the humidity gradient. Since a temperature inversion does not always correspond to the strongest humidity gradient and vice versa, it is evident that no perfect correlation between periodical variations of micropressure and field strength can be expected.

##### 4.2 Analysis of Individual Cases

Some examples of observations may demonstrate the cases in which it is assumed that gravity waves will cause the propagation of electromagnetic waves by oscillating the boundary surface of an atmospheric discontinuity in the common volume of transmitter and receiver.

(A) On 9 June 1966, from 3.00 to 4.30 CET, periodical pressure variations were observed at Hoehbeck with amplitudes of 0.2 mb and periods ranging from 15 to 20 min. If these are compared with the field strength variations recorded at the receiving stations Hoehbeck and Hamburg, it becomes evident that the field strength fadings have nearly the same shape as the pressure variations but that they last from 2.35 to 4.00 CET at Hoehbeck and from 3.10 to 4.40 CET at Hamburg.

By shifting the time scales by up to 25 min the coincidence of the variations becomes obvious (Fig. 5). The available radiosonde ascents indicate a temperature inversion of 3 to 4  $^{\circ}$ C at a height between 250 and 400 m (Fig. 6). The corresponding discontinuity of the refractive module is defined by  $\Delta N = -0.141 \text{ m}^{-1}$ . (Normal atmosphere  $\Delta N = -0.039 \text{ m}^{-1}$ ).

It can be concluded that the pressure variations are due to internal gravity waves and the field strength variations are caused by partial reflections from the moving wavy boundary surface.

To explain the time shift we further assume that the wave pattern of the boundary surface first reached the centre of reflection of the Berlin - Hoehbeck link and about 25 min later the centre of the longer path between Berlin and Hamburg. Since the centre of reflection of the Berlin - Hamburg path is located almost directly over Hoehbeck, it is understandable that the field strength variations of this path were observed almost at the same time as the pressure variations at Hoehbeck.

(B) On 19 February 1966, the variations of micropressure, observed at Hoehbeck from 6.00 to 8.30 CET, and of field strength simultaneously recorded by the Berlin - Hamburg link (Fig. 7) are assumed to correspond to a moving wave pattern at a boundary layer at about 800 to 900 m height (Fig. 8). This layer is characterised by a strong gradient in temperature and refractive module, and a vertical wind shear, as indicated by the Berlin radiosonde ascent.

Here short period fading is superimposed on the long period fadings to a much greater extent than in Example A. This fact corresponds to the greater number of possible ray paths at this height between transmitter and receiver and consequently also to more reflected waves interfering at the receiving station.

(C) The third example (Fig. 9) demonstrates coincident variations of micropressure and field strength which correspond to a ground-based inversion layer more than 1000 m thick (Fig. 10).

On 22 November 1967, a group of wavelike pressure variations with periods of about 8 min was recorded at Hoehbeck as well as in the Hamburg area. This wave group correlated with variations of field strength, first observed at Heligoland, about 20 min later at Hamburg, and 30 min later at Hoehbeck. For this reason it can be concluded that a rippled layer was moving in the direction from Heligoland to Berlin, according to the various reflecting centres of the three radio links.

It is assumed that gravity waves were ducted in the ground-based inversion layer, producing maximum vertical displacements of the surfaces of equal potential temperature and potential refractive module near the upper boundary of the layer at about 1200 m above mean sea level.

As shown in a previous paper<sup>6</sup>, only ground inversions of this thickness can influence the radio wave propagation on links as long as the Berlin - Heligoland path (400 km). Furthermore, the micropressure variations observed in the Hamburg area by a network of eight barograph stations confirm the assumed propagation direction of the gravity wave.

## 5. CONCLUSIONS

Micropressure variations and VHF field strength fadings observed on transhorizon links are correlated. The analysis of the observations leads to the conclusion that the observed fading periods, in the range 2 to 30 minutes, of radio waves reflected from atmospheric discontinuities are due to gravity waves propagating in the lower troposphere.

## REFERENCES

1. Gossard, E.E. *The Reflection of Microwaves by a Refractive Layer Perturbed by Waves.* Institute of Radio Engineers, Transactions on Antennas and Propagation, Vol. AP-10, 1962, pp. 317-325.
2. Waterman, A.T. Strohbehn, J.W. *Reflection of Radio Waves from Undulating Tropospheric Layers.* Journal of Research, National Bureau of Standards, Vol. 67D, 1963, pp. 609-616.
3. Gjessing, D.T. Irgens, F. *On the Scattering of Electromagnetic Waves by a Moving Tropospheric Layer having Sinusoidal Boundaries.* Institute of Electrical and Electronic Engineers, Transactions on Antennas and Propagation, Vol. AP-12, 1964, pp. 51-64.
4. Stilke, G. *Registrierung von Luftdruckwellen im Subschallgebiet.* Zeitschrift für Geophysik, Vol. 33, 1967, pp. 147-154.
5. Stilke, G. *Some Aspects of Micropressure Measurements for the Evaluation of Internal Waves in the Atmosphere.* Proceedings, 1964 World Conference on Radio Meteorology, Boulder, Colorado, 1964, pp. 92-93.
6. Fengler, G. *Untersuchungen der elektromagnetischen Wellenausbreitung im 500 MHz-Bereich über Land unter besonderer Berücksichtigung der meteorologischen Bedingungen.* Berichte des Instituts für Radiometeorologie und Maritime Meteorologie an der Universität Hamburg, Bericht Nr. 8, 1964, p. 158.

21-6

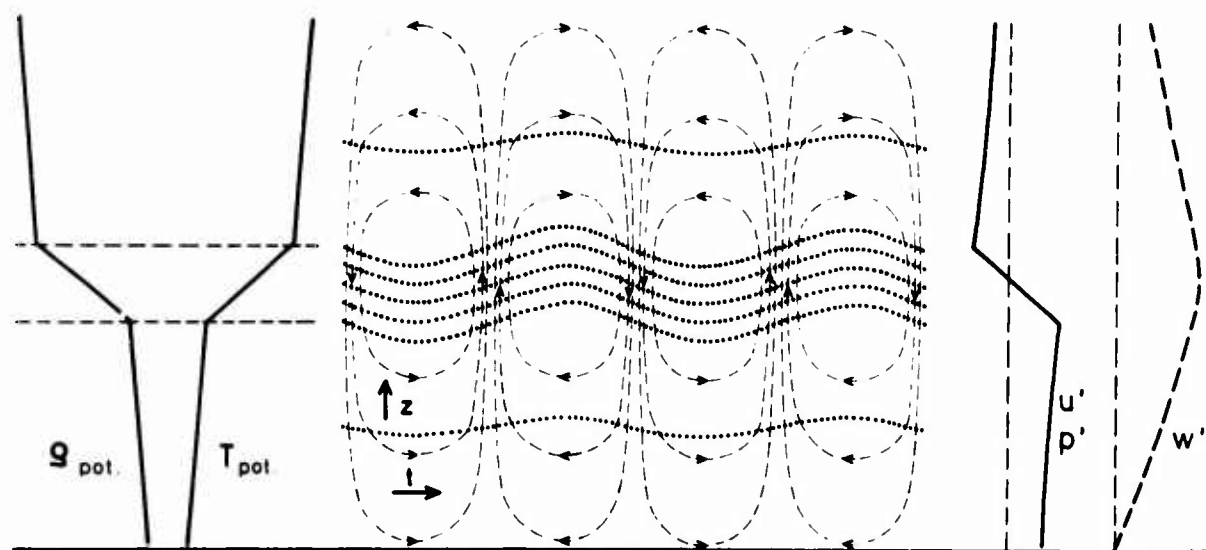


Fig. 1. Three-layer model of the lower atmosphere with ducted gravity waves (fundamental mode), vertical profiles of potential density  $\rho_{\text{pot}}$ , potential temperature  $T_{\text{pot}}$ , perturbation values, and schematic cross-section through the wave pattern

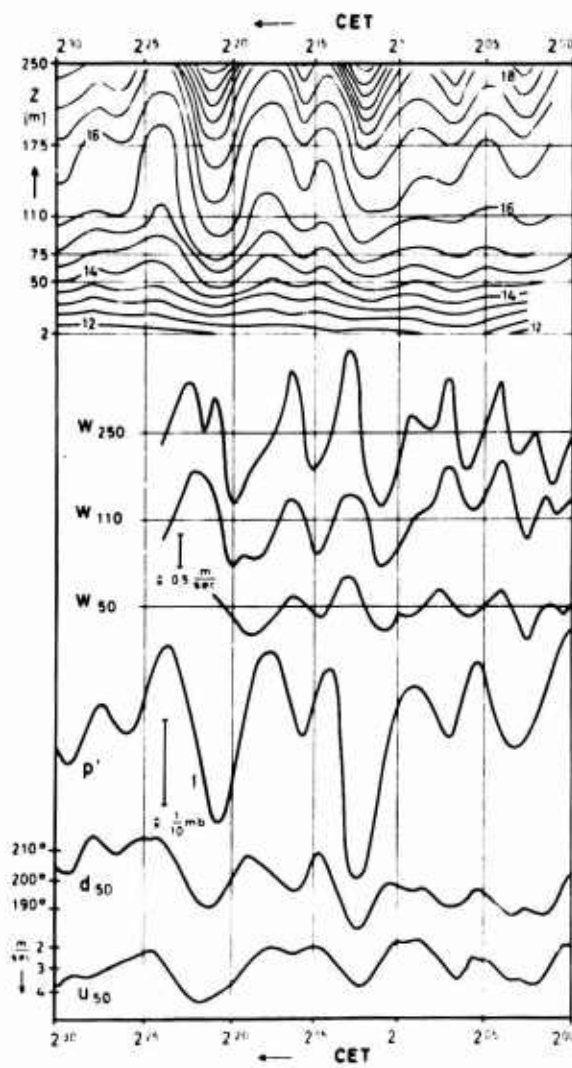


Fig. 2. Gravity wave propagation in a ground-based temperature inversion. Measured cross-section of isentropic surfaces, perturbation values of wind and pressure

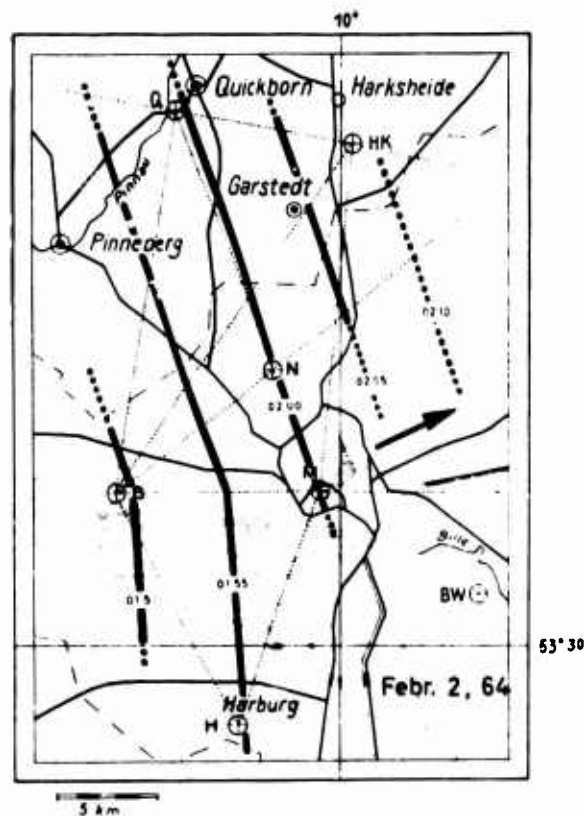


Fig. 3. Gravity wave crossing the Hamburg microbarograph network. Wave front displacement in 5-minute intervals

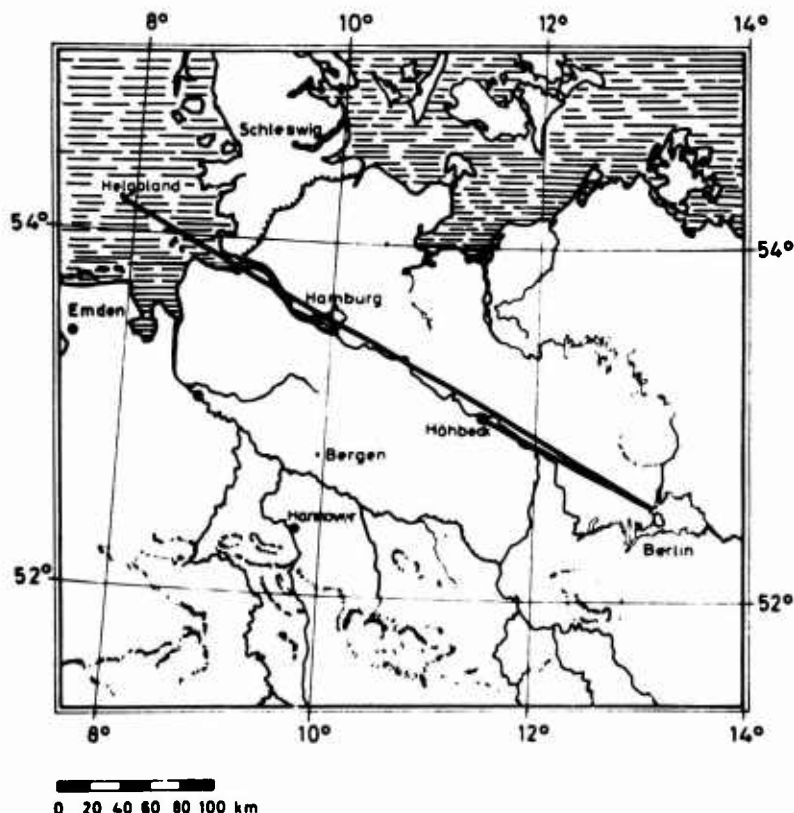


Fig. 4. Geographic location of the radio links and the micropressure stations, as well as the radiosonde stations

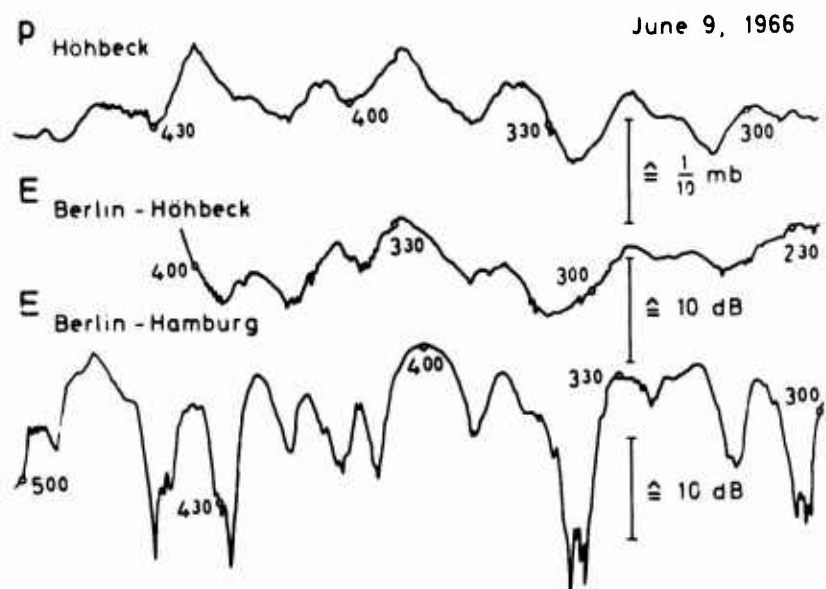


Fig. 5. Recordings of corresponding variations of micropressure  $P$  and field strength  $E$  on 9 June 1966

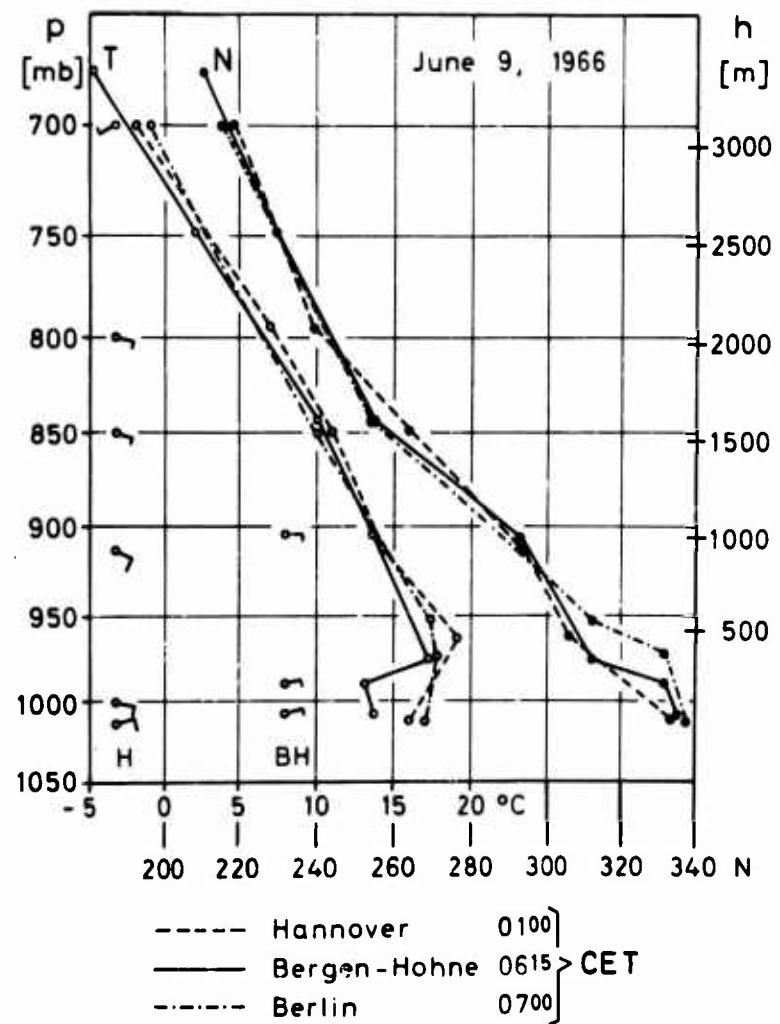


Fig. 6. Vertical profiles of temperature  $T$ , wind, and refractive module  $N$ , derived from radiosonde ascents at various stations on 9 June 1966

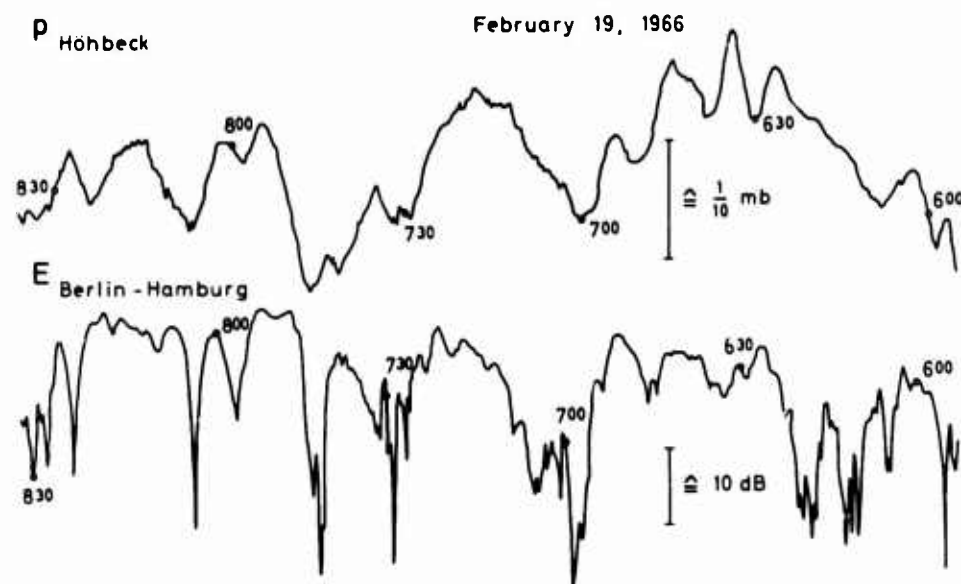


Fig. 7. Recordings of corresponding variations of micropressure  $p$  and field strength  $E$  on 19 February 1966

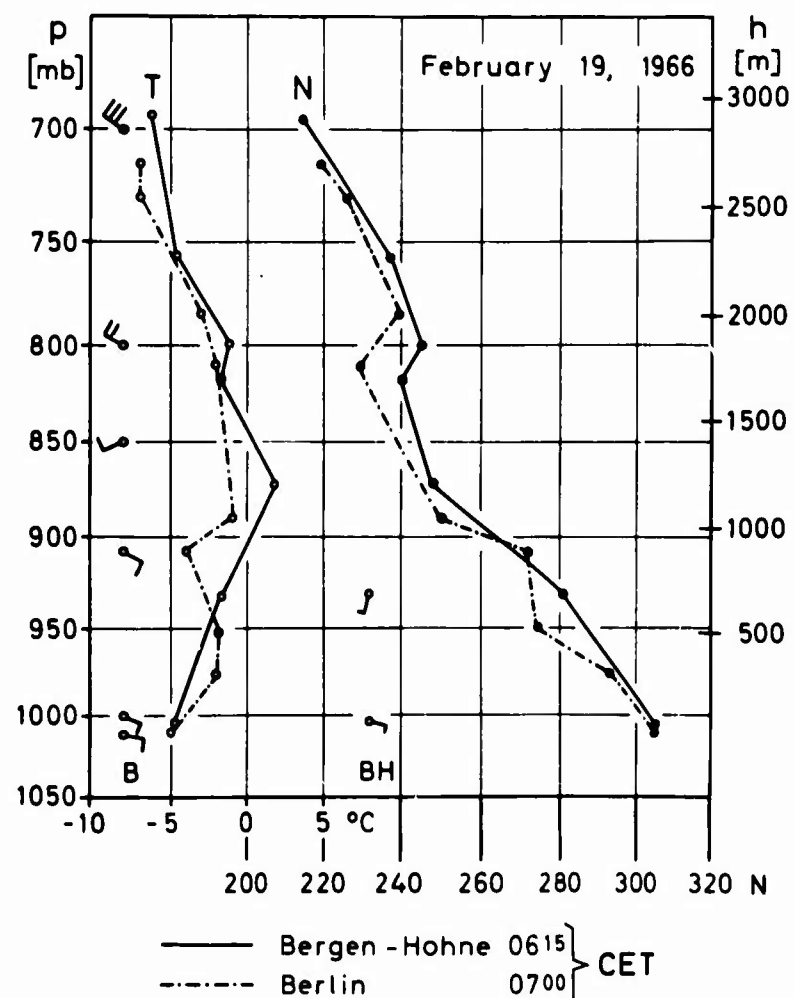


Fig. 8. Vertical profiles of temperature  $T$ , wind and refractive module  $N$ , derived from radiosonde ascents at various stations on 19 February 1966

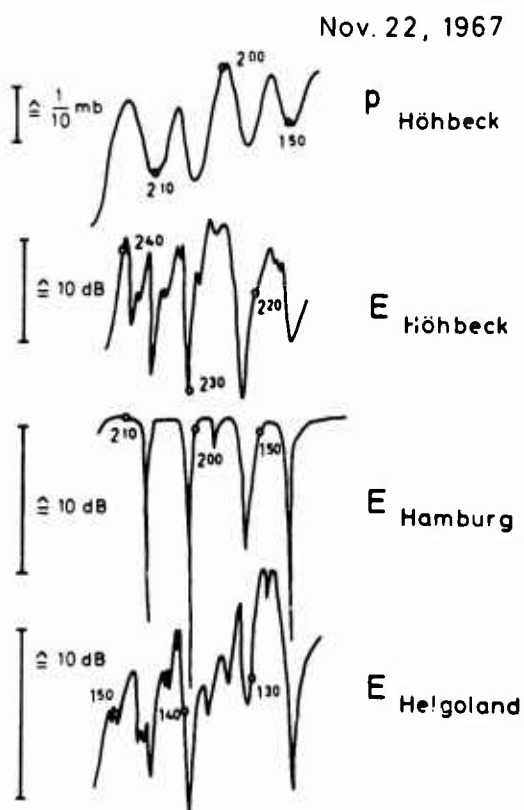


Fig. 9. Recordings of corresponding variations of micropressure  $p$  and field strength  $E$  on 22 November 1967

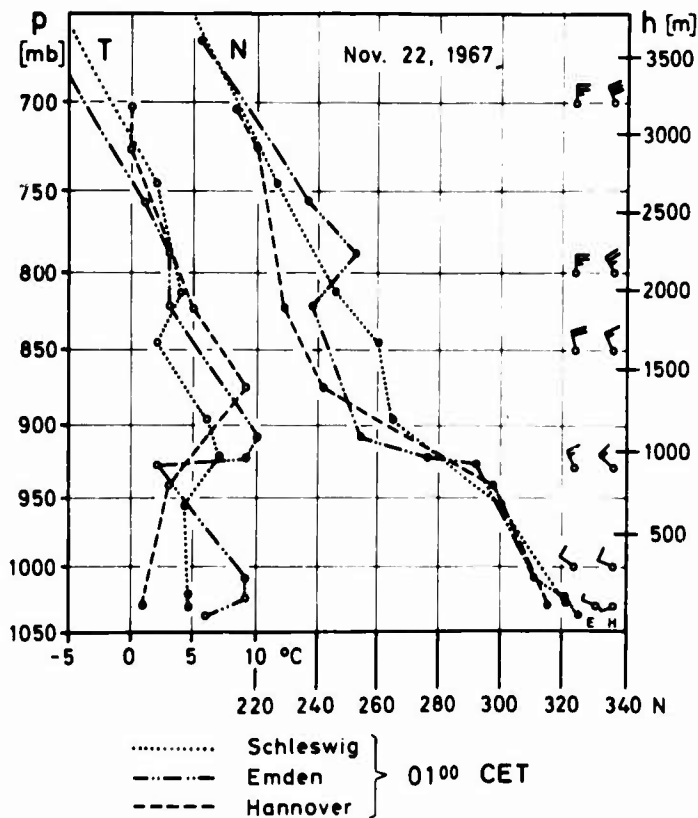


Fig. 10. Vertical profiles of temperature  $T$ , wind, and refractive module  $N$ , derived from radiosonde ascents at various stations on 22 November 1967

**INVESTIGATION OF THE RECEIVING FIELD  
FOR SCATTER PROPAGATION**

by

**J. Grosskopf**

Research Institute of the FTZ (Federal German Post Office)  
at Darmstadt, Germany

#### SUMMARY

Many important parameters of tropospheric scatter propagation can be derived from the statistical structure of the electromagnetic field at the receiving site of a scatter link. This field structure is characterised by its space and time correlation functions. They were measured with a 418 km scatter link in the 2000 MHz frequency range, using an arrangement of three antennae. Analytical expressions for the correlation function and its scale length have been found.

**INVESTIGATION OF THE RECEIVING FIELD  
FOR SCATTER PROPAGATION**

J. Grosskopf

It is well known that in the most general case the field strength occurring in the vicinity of the receiving site is a statistical function of time ( $t$ ) and place ( $x, y, z$ ). These statistical variations are mainly caused by multi-path propagation and its variations with time. As a rule, the field of the distant transmitter does not only arrive from one specific direction, but with an angular spectrum within a cone of rays. The aperture of this cone of rays is a decisive factor for a number of interesting effects concerning the technical characteristics of the receiving arrangements. Such effects are, *inter alia*, antennae-to-medium coupling loss (gain loss), diversity spacing of a diversity installation, transmissible bandwidth, accuracy of bearings taken by means of direction finders and navigational aids, etc.

It is obvious that it must be possible to derive all these effects from the statistical characteristics of the receiving field. These characteristics are represented by the time and space auto-correlation functions and their Fourier transforms, the so-called power and angular spectra. The theoretical principles of the field statistics and the interdependence of the characteristic statistical functions and the propagation characteristics mentioned above have been evolved by many British and American scientists. We have applied them to propagation in the decimetric and centimetric ranges, mainly to the scatter propagation over a 240 km and a 420 km path.

During the tests performed to date the transmitters radiated at discrete frequencies of 2000 MHz and 500 MHz. The transmitters were located in Hamburg and on the Hochblauen, in the southern part of the Black Forest. Reception was at Darmstadt. The Hamburg-Darmstadt and the Hochblauen-Darmstadt paths are 418 km and 242 km respectively. At Darmstadt three antennae were used to observe the variation with time of the transmission loss, the fading frequency and, mainly, the time and space auto-correlation functions. These parameters are the basis for the determination of the most essential propagation effects mentioned above, i.e. the gain loss, the diversity spacing required for two antennae, the transmissible bandwidth, the fading frequencies, etc.

The method used for measuring the auto-correlation functions is very simple. The receiving field is received with two or three low directivity antennae (small diameter  $D = 2$  m, Fig. 1) simultaneously. The envelope curve of the receiving voltage is stored magnetically (period of measurement  $\approx 10$  minutes) and then applied to an electronic correlator for further evaluation. The latter prints the correlation coefficients for the time shifts  $\tau$  in steps of 0.1s to 0.5s with a maximum shift of 7s. In this connection we must ensure that we measure the correlation function.

$$\rho_A(\tau) = \frac{1}{2\tau} \int_{-\tau}^{+\tau} u(t)u(t + \tau) dt = \overline{u(t)u(t + \tau)} \quad (1)$$

of the low frequency variations  $u(t)$  of the envelope curve. It differs from the correlation function  $\rho_{HF}$  of the HF amplitude of the receiving voltage. In 1951 Bramley<sup>1</sup> showed the relations which exist between these two correlation coefficients. The receiver characteristic may also be included. It is always  $\rho_{HF} > \rho_A$ . Hence, the measured  $\rho_A$

must be converted into the corresponding  $\rho_{HF}$  by means of Bramley's relation. As for Rayleigh distribution of the amplitudes,  $\rho_{HF}^2 = \rho_A$  applies approximately. This deals with the time autocorrelation function.

The space autocorrelation function results from the space distribution of the receiving voltage  $u(t)$  over the receiving plane - which is perpendicular to the direction of incidence of the radiation - at a given time. The receiving voltage should be measured in this plane simultaneously at as many and as closely adjacent points as possible. The procedure for the determination of the space autocorrelation function should then be applied to the "mountain" of field strength obtained in this way. The time variable  $t$  would have to be replaced by the space variable  $\xi$  and this method would be too complicated. It can be shown, however, that, with stationary statistical distributions, the time cross-correlation coefficient between the receiving voltages of two antennae set up at the points  $x_0$  and  $x_n$ ,

$$\rho(x_n - x_0) = \rho(\xi) \sim u(t, x_0)u(t, x_n), \quad (2)$$

can be made equal to the space autocorrelation coefficient  $\rho(\xi)$ . Hence, when using three simultaneously recorded receiving points at the same time, we have already three points of the space autocorrelation function, which can be taken to determine the parameters of a particularly appropriate analytical representation of the auto-correlation function. This was done for the scatter link Hamburg-Darmstadt. The function

$$N_\nu(\eta) = \frac{2^{1-\nu}}{\Gamma(\nu)} \left(\frac{\eta}{L}\right)^\nu K_\nu\left(\frac{\eta}{L}\right), \quad \text{with } \nu = 5/6, \quad (3)$$

proposed by Norton, was found to be a particularly appropriate representation. Here,  $K_\nu$  is modified second-kind Bessel function of the  $\nu$ th, order, and  $L$  is the correlation length. For  $y = L$ ,  $N_{5/6}(L) = 0.54$ . The magnitude for the order  $\nu (\nu = 5/6)$  was thoroughly investigated by systematic measurements. It was found that individually the measured auto-correlation functions cannot be assigned to the Norton function of the order  $\nu = 5/6$ , but that it is possible to do so with the monthly average.

This applies, however, only to the horizontal correlation lengths and not to the vertical lengths. In his paper in this volume, Mr Fehlhaber shows that the Norton function  $N_\nu$ , with  $\nu = 5/6$ , can also be substantiated physically. There is a close relation between the auto-correlation function  $\rho_E(\xi)$  at the place of reception and the auto-correlation function  $\rho(\xi)$  of the turbulent medium in which the scatter process takes place. Later this function was used to determine the distribution of the correlation length occurring within a certain period of time. The distributions are listed in Table I.

It is well known that, according to the Wiener-Khintchine theorem, the Fourier transform of the space auto-correlation function  $\rho(\xi)$  is identical with the angular spectrum  $|F(S)|^2$  of the incident scattered power, namely,

$$\rho(\xi/L) = L \int_{-\infty}^{+\infty} |F(LS)|^2 e^{+j(2\pi/\lambda)S\xi} dS, \quad (4)$$

where  $\xi$  is the position coordinate in the plane perpendicular to the direction of radiation, which may be either in the  $y$  or in the  $z$  direction,  $S \approx \sin \nu \approx \nu$  the direction cosine of the scattered radiation with respect to the main direction of incidence and  $|F(SL)|^2$  the power scattered in the direction  $S$ .  $L$  is the scale length of the space auto-correlation function, which can be defined in different ways. If the auto-correlation function is approximated to  $e^{-\xi^2/L_0^2}$  - for instance by a Gaussian function - which is frequently possible, then  $\xi = L_0$  corresponds to the 1/e width of the auto-correlation function. In this case the relevant angular spectrum, also a Gaussian function, has the 1/e angular width:

$$S_s = S_0 = \frac{\lambda}{\pi L_0} . \quad (5)$$

Thus, the aperture of the incoming cone of scattered rays  $S_0$  can be derived from the length  $L_0$  of the auto-correlation function.  $S_s$  is apparently inversely proportional to the length of the auto-correlation function.

To begin with, it is very simple to derive the magnitude of the gain loss and the necessary diversity spacing as a function of the diameter from this magnitude  $S_0$ .

Let us assume that the pattern of the main beam of the receiving antenna can be approximated by

$$e^{-S^2/S_A^2} . \quad (6)$$

Experience has shown that this is a fair approximation for antenna patterns with a higher directivity. In general, the main beam of the antenna cuts a certain portion out of the cone of the incident scattered rays with the aperture  $S_s$ . This portion depends upon the size of the cone of scattered rays,  $S_{ges}$ , actually received by the antenna according to the relation

$$e^{-S^2/S_{ges}^2} = e^{-S^2/S_s^2} e^{-S^2/S_A^2} \quad \text{with} \quad \frac{1}{S_{ges}^2} = \frac{1}{S_s^2} + \frac{1}{S_A^2} . \quad (7)$$

By means of the Wiener-Khintchine relation it is possible to assign a new auto-correlation function to this effective angular spectrum modified by the antenna aperture. For a Gaussian behaviour of the auto-correlation function we obtain a new correlation length

$$L = \frac{\lambda}{\pi S_{ges}} = \frac{\lambda}{\pi S_s} \sqrt{1 + \frac{S_s^2}{S_A^2}} = L_0 \sqrt{1 + \frac{S_s^2}{S_A^2}} . \quad (8)$$

$S_s$  is the  $1/e$  width of the cone of rays setting up the receiving field and  $L_0$  the relevant correlation or diversity spacing at which the correlation decreases to  $1/e$ . Apparently,  $L_0$  is assumed for  $S_A \gg S_s$ , i.e. for a very weak directivity of the receiving antenna. When replacing the aperture of the cone of scattered rays, from (5), by  $S_s = \lambda/\pi L_0$  and the antenna aperture (half-power beamwidth) by the antenna diameter  $2S_A = 70 \lambda/D$ , we obtain

$$L = L_0 \sqrt{1 + (0.43 D/L_0)^2} . \quad (9)$$

For antennae having very large diameters of  $D \gg L_0$ ,  $L \approx 0.43 D$ , and if they are set up so as to touch each other, the condition for a good diversity effect with  $\rho < 1/e$  is therefore always met.

The gain loss results from similar considerations. We obtain the formula

$$\frac{\Delta G}{dB} = 10 \log \left( 1 + \frac{S_s^2}{S_A^2} \right) = 10 \log \left( 1 + \frac{A}{\pi L_0^2} \right) = 10 \log \left[ 1 + \left( 0.43 \frac{D}{L_0} \right)^2 \right] = 20 \log \frac{L}{L_0} , \quad (10)$$

where  $A$  is the effective area of the antenna and  $D$  is the antenna diameter. The loss  $\Delta G$  of the antenna gain for the reception of scatter radiation with respect to free-space radiation concentrated on one direction is expressed in dB. Table II shows the results of the gain loss measurements from on the Hamburg - Darmstadt path.

Furthermore, we were interested in the angle of elevation of the central axis of the cone of scattered rays at the receiving site. For this purpose, the field received from Hamburg over the 418 km scatter path was observed at Darmstadt with the help of a two-antenna interferometer. The two 2 m receiving paraboloids forming the interferometer were arranged vertically one above the other at a distance of 2 m. The two receiving voltages were combined alternately in anti-phase for two minutes and in-phase for one minute. At the same time the phase difference between the antennae was continuously shifted in steps of  $0.0917^\circ$  corresponding to the 1.6 mrad angle of elevation. Another 30-step phase shifter was used for this purpose. The angular range within which the minimum of reception is to be expected in the case of anti-phase and the maximum in the case of in-phase is covered during a period of about  $30 \times 3 = 90$  minutes. The receiving amplitude is recorded by an ink recorder and evaluated manually (Fig. 2).

The theory of the measurement is quite simple. The incoming powers (square-law detection) in the maximum and minimum of the 30-step scan are proportional,

$$P_{\max} \sim 1 + \rho \quad \text{and} \quad P_{\min} \sim 1 - \rho, \quad (11)$$

where  $\rho$  is the correlation coefficient  $\rho(d)$  of the two antennae set up at a d/m space. The position of the minimum within a scan indicates the angle of elevation;  $P_{\max}$  and  $P_{\min}$  are used to determine the correlation coefficients and, for a fixed space  $d$  between the two interferometer antennae, the correlation length  $L_z$ , and from that the angular aperture of the cone of scattered rays. The following mean values were obtained from 15 measurements made during the period from 20 October 1967 to 1 December 1967 in the morning and the early afternoon. The mean value of  $L_z$  was  $\bar{L}_z = 8.6 + 0.30$  m, the half-power beamwidth of the cone of scattered rays was  $\theta_H = 0.25^\circ \pm 0.01^\circ \cong 4.4$  mrad, the angle of elevation with respect to the horizontal was  $\alpha = 1.9$  mrad and the angle of elevation with respect to the horizon was  $\gamma = 0.3^\circ \cong 18' \cong 5.25$  mrad. Consequently, the best direction of radiation for this path is  $0.3^\circ$  above the horizon.

The tropospheric influence on the transmission loss of a scatter link can be indicated by a scatter parameter  $S = (1/l) \overline{(\Delta\epsilon/\epsilon)^2}$ , where  $\overline{(\Delta\epsilon/\epsilon)^2} \sim (\Delta\epsilon)^2$  is the mean square variation of the permittivities of the inhomogeneous scattering medium (troposphere) and  $l$  is a measure for the space correlation length of the inhomogeneities.

In order to calculate the transmission loss it is necessary to determine experimentally the magnitude  $(\Delta\epsilon/\epsilon)^2$ , which is a function of time and height. This was done on the basis of aerological balloon and refractometer ascents. An article by Norton, et al<sup>2</sup>, included a graphical representation of  $S$  as a function of  $h$ . Here  $S(h)$  is constant up to a height of 1 km. For heights exceeding 1 km it decreases with  $h^{-2}$ . For vertical incidence in the troposphere, i.e. for  $\theta = \pi$ , the scatter coefficient of the troposphere is

$$\sigma \sim S \sim \left( \frac{\Delta\epsilon}{\epsilon} \right)^2 \frac{1}{l} \quad . \quad (12)$$

for  $4\pi l/\lambda \gg 1$ .

At this stage it is natural to investigate the vertical structure of the troposphere existing in the case of vertical incidence by means of a vertical radar. The scatter parameter  $S$  is immediately derived from the scatter coefficient measured in this connection. At Darmstadt such measurements were made on wavelengths of 10 cm and 3 cm. The 10 cm radar has a peak power of 80 kW. The 3m transmitting and receiving parabolas were installed side by side in the ground, so as to suppress secondary radiation. Within a height range from 300 to 7000 m the echoes returning from the troposphere could be measured quantitatively with satisfactory accuracy. Below 300 m some trouble was caused by secondary radiation and overshooting of the circuits, due to the basic impulse; above 7000 m it was generally impossible to separate tropospheric noise and receiver noise. The echoes arriving simultaneously from all heights were separated by means of gate circuits with

variable delay line, which scanned the height range between 300 m and some 7000 m in steps of 150 m.

Some of the height profiles of the scatter parameter  $S$  are plotted in Figures 3 and 4. Figure 3 shows the profiles of the 16 and 17 May 1966. Here the  $S$  values are higher at noon (1200 h) than in the morning (0600 h). Up to a height of 2 km the curve of  $S$  is nearly constant; then it slopes steeply. Figure 4 indicates the average value for 10 days and shows the magnitude  $q = 10 \log (\Delta \epsilon / \epsilon)^2 (1/l)$ . In general, the profiles were taken on clear, cloudless days (clear air turbulence).

It is evident that this convenient, comparatively cheap method allows the spatio-temporal variability to be continuously observed better and more completely than is possible by means of radiosondes and refractometer measurements.

In this way we investigated the correlation between the height profile characteristics and the respective atmospheric conditions, the diurnal variation of the height profiles, the appearance and disappearance of layers, the stability in time of these layers, and the diurnal and seasonal variations. It would take too long to discuss these items in detail.

A particularly striking phenomenon was studied more thoroughly. It is the occurrence of echoes known as "angels". The distribution of their spatio-temporal occurrence was investigated, and it was found that in many cases the radiation from the "angels" can be considered as isotropic (simultaneous reception at two receiving points separated up to 2 km). Figure 5 shows the A-scope of a typical angel; Figure 6 indicates the amplitude-time response of some angels separated from the other echoes by means of a gate circuit. In order to obtain the space auto-correlation function for the scatter field, even with vertical incidence, two or three receiving antennae set up side by side are now used simultaneously. The space auto-correlation function thus determined allows one to draw conclusions about the angular aperture of the cone of scattered rays and the structure (blob size) of the scattering medium.

In 1950 Briggs, et al<sup>3</sup> indicated how it is possible to derive the characteristic velocities which determine the fluctuation of the receiving fields from the time auto-correlation function and the time cross-correlation function of the voltages of two adjacent antennae. An example of a record of the auto-correlation function and cross-correlation function of two antennae set up at a distance  $d$  is given in Figure 7. Some marked points of this graph (e.g., the maximum of the cross-correlation function, the displacement of this maximum with respect to the maximum of the auto-correlation function, the intersection point of the two correlation functions, etc.) allow, *inter alia*, the determination of the "drift velocity"  $v$  at which the receiving field mountain seems to drift over the reception point. Another velocity that can be determined is the "characteristic velocity"  $v_c$  which would be recorded as residual velocity by an observer moved with the field strength pattern at the drift velocity  $v$ . It is the mean square velocity of the statistical disordered movement superimposed on the ordered drift movement. It is obvious that these velocities will be closely related to the meteorological characteristics causing the field fluctuations. The experiment showed that the drift velocity of the receiving field is almost equal to double the velocity of the wind transverse to the direction of propagation. (Correlation between  $r = 0.8 - 0.95$ .) The "characteristic velocity"  $v_c$  determines the fading frequency of the received scatter radiation.

It is easy to understand that the fading frequency caused by movements in the multi-path system must be approximately proportional to the expression

$$f_s [\text{Hz}] = \frac{2 \sin (\theta/2)}{300} f [\text{MHz}] v [\text{ms}^{-1}] , \quad (13)$$

i.e., proportional to the vertical component  $v$  of the velocity of the scattering or reflecting object and the sine of the scatter angle  $\theta/2$ . Hence, the fading frequency derived from the auto-correlation function in the case of vertical incidence must be  $1/\{\sin(\theta/2)\}$  times the fading frequency occurring in the case of oblique angle propagation. This fact was substantiated by a comparison of the fading frequencies on the Hamburg-Darmstadt path (418 km) and of the vertical radar.

Finally, the space auto-correlation function length  $L$  can be used to determine another technically interesting parameter, the transmissible bandwidth. We have seen that the correlation length  $L$  determines the angular aperture  $\vartheta$  of the cone of rays incident at the point of reception. The aperture  $\vartheta$  again determines the size of the common volume, and consequently the greatest possible propagation difference, in a simple, purely geometrical manner. Thus, the transmissible bandwidth is already fixed. For  $\Delta f/L$  we find the relation

$$\frac{\Delta f}{f} = \frac{2L}{d\theta}, \quad (14)$$

where  $d$  is distance and  $\theta$  is scatter angle.

It has been shown in how many ways the auto-correlation and cross-correlation functions can be used to solve a number of technical problems without further hypotheses, by measurements in the receiving field. It is clear that it is not possible to cover all relevant problems in this brief survey.

#### REFERENCES

1. Bramley, E.N. Proceedings of the Institution of Electrical Engineers, Vol. 98, 1951, p. 19.
2. Briggs, B.H. et al. Proceedings of the Physical Society, Vol. B63, 1950, p. 106.
3. Norton, K.A. et al. Proceedings of the Institute of Radio Engineers, Vol. 43, 1955, p. 1488.

TABLE I

Horizontal correlation length  $L_y$  and vertical correlation length  $L_z$ .  
Hochblauen-Darmstadt

Percentage of time	1	10	50	90	99
$L_y/m$	13.4	10.4	4.0	2.6	2.2

## Hamburg-Darmstadt

Percentage of time	1	10	50	90	99
$L_y$	18.8	13.1	8.1	4.8	-
$L_z$	14.5	11.0	7.3	4.7	3.3

TABLE II

Gain loss on the 418 km path Hamburg-Darmstadt ( $\lambda = 0.175$  m)  
Diameter of the Hamburg transmitting antenna: 9 m  
Diameter of the Darmstadt receiving antennae: 9 m, 5 m and 2 m.

Combination 9/9 working to 9/2				
	9.6	6.5	5.2	dB
Percentage of time exceeded	10.0	50.0	90.0	
Combination 9/9 working to 9/5				
	5.7	4.2	2.9	dB
Percentage of time exceeded	10.0	50.0	90.0	

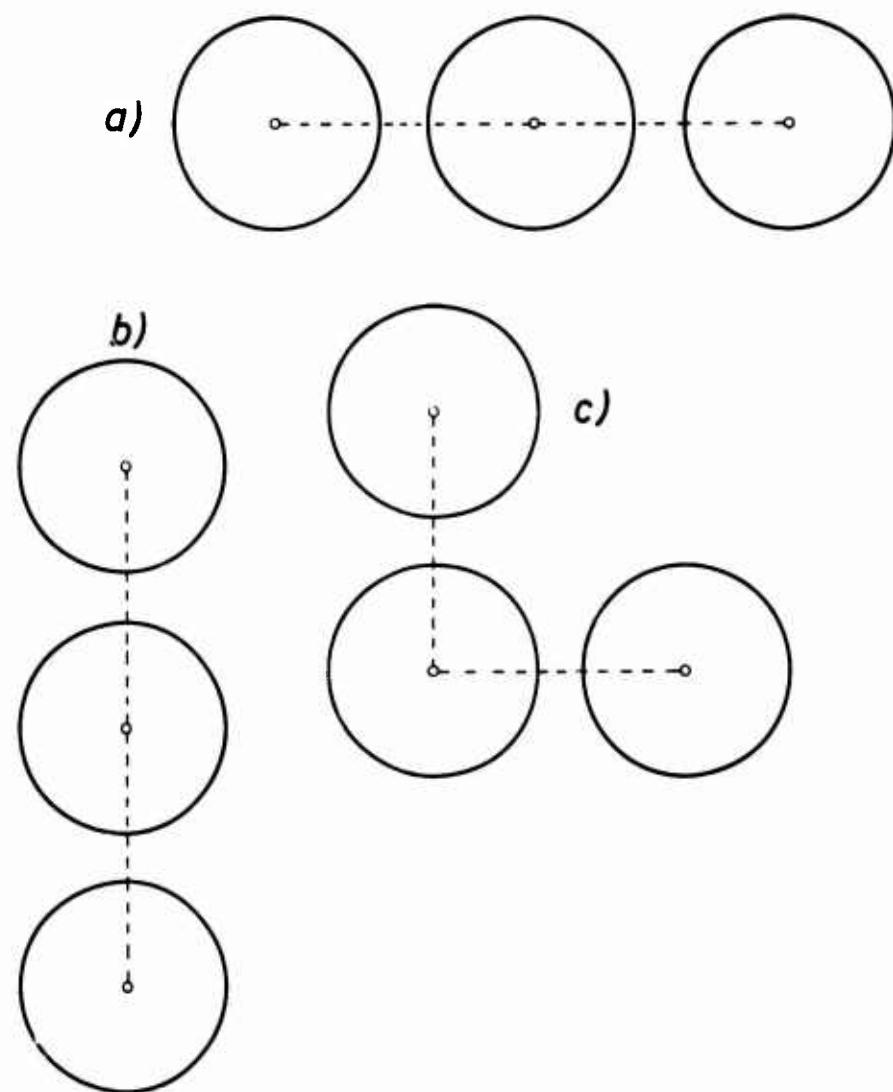


Fig. 1 Antenna arrangement to record the time and space correlation functions

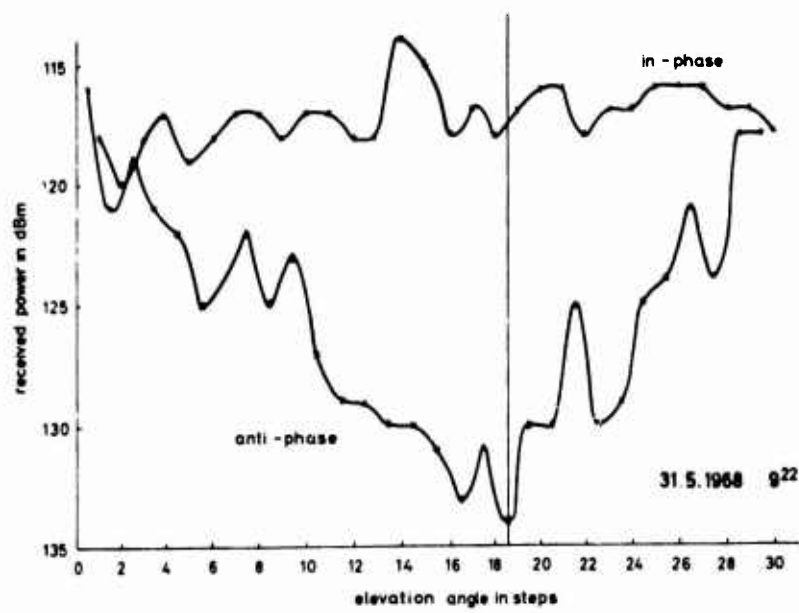


Fig. 2 Interferometer measurements on the Hamburg - Darmstadt path

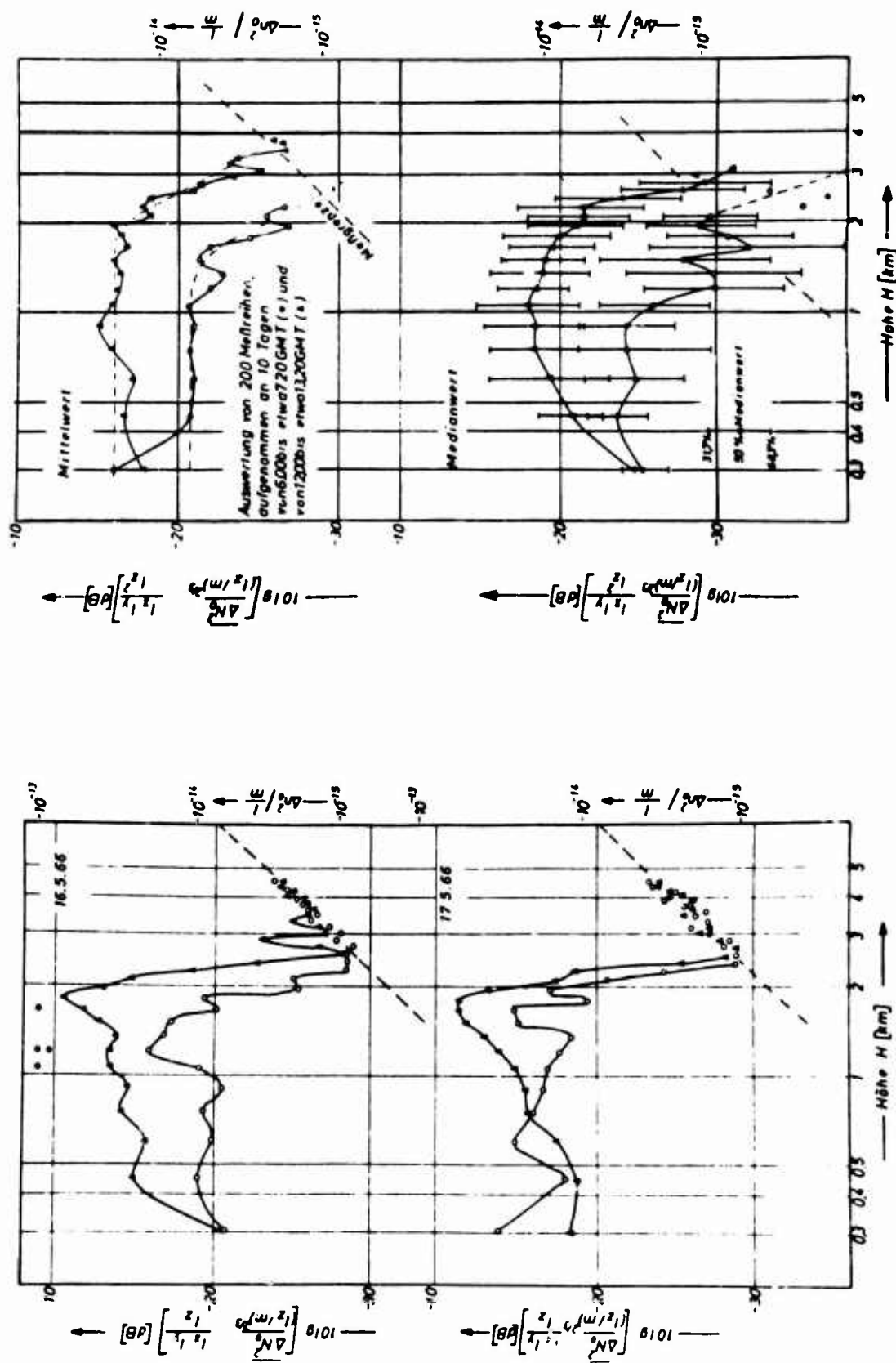


Fig. 4 Average values of the height profiles over ten days

22-10

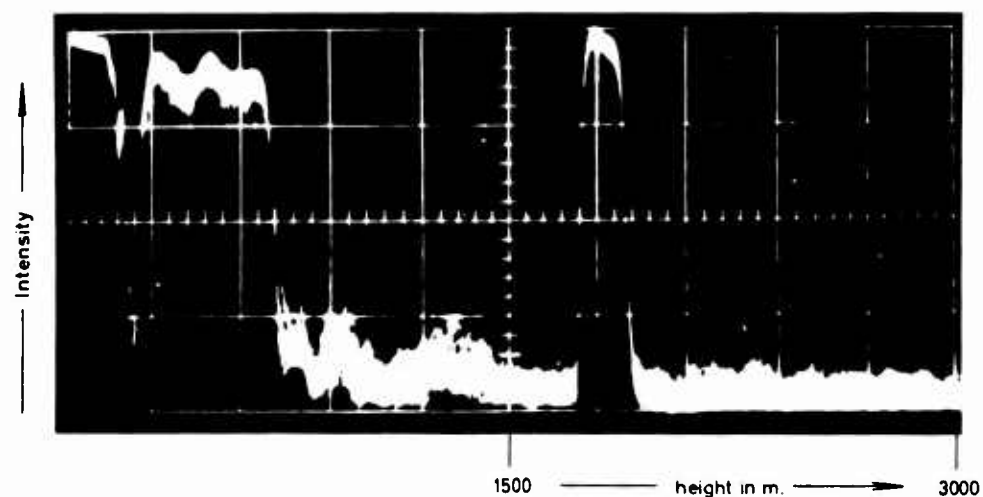


Fig. 5 A-scope of an angel

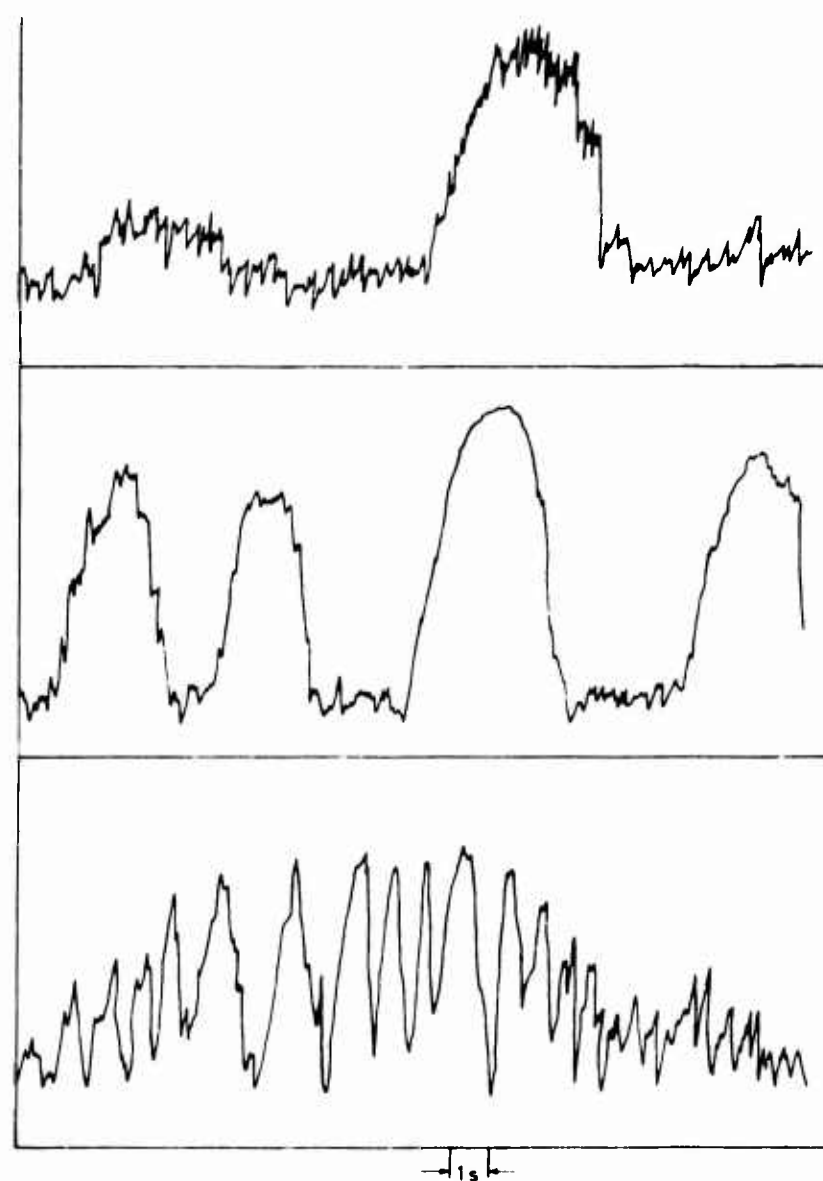


Fig. 6 Amplitude-time response of some angels

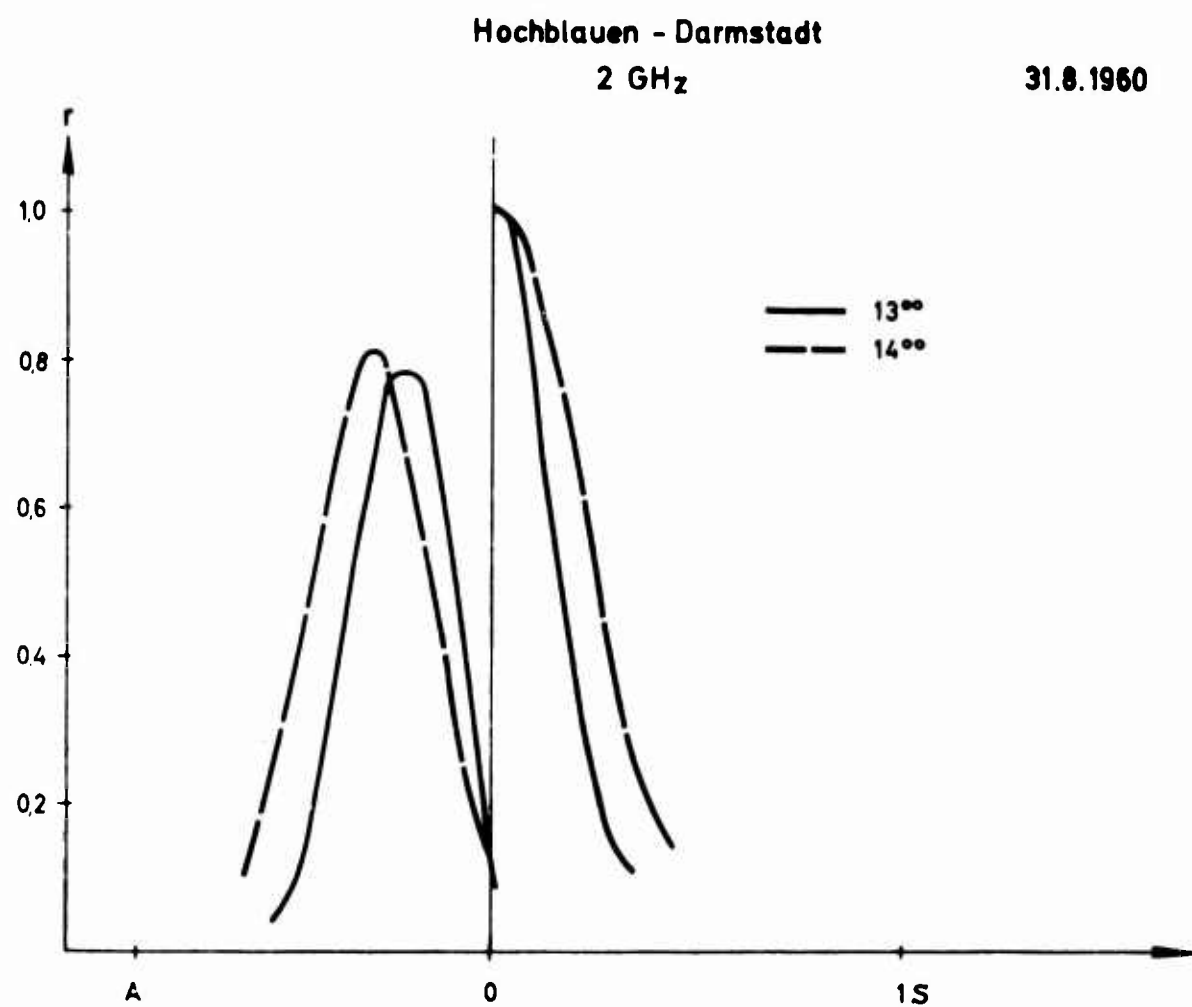


Fig. 7 Auto-correlation function and cross-correlation function

**ELECTROMAGNETIC SCATTERING FROM AIR CURRENTS**

by

**H. N. Kritikos**

The Moore School of Electrical Engineering  
University of Pennsylvania  
200 S. 33 St.  
Philadelphia, Pa. 19104, USA

## SUMMARY

The scattering of a plane monochromatic electromagnetic wave incident on an air current is studied by considering a jet stream in a homogeneous dielectric fluid to be its idealized model. Starting with a differential equation for the reflection coefficient a solution is obtained for a parabolic velocity transition. The results show that, to a first order in  $\beta$ , reflections can only take place at forward scattering, large angles of incidence and transitions which are of the order of a wavelength. Reflections at normal incidence, i.e. backscatter, is of one order of magnitude in  $\beta$  below those of oblique incidence. For wind shears of  $0.1 \text{ sec}^{-1}$  measured over a distance of 100 m, an angle of incidence of  $85^\circ$  and a frequency of 50 MHz, the reflection coefficient is of the order of  $R = 10^{-10}$ .

## NOTATION

$\beta$	= $v/c$ , where $v$ is the velocity of the medium
$\beta_0$	= $v_{\max}/c$ , where $v_{\max}$ is maximum velocity of parabolic velocity profile
$c$	the velocity of light, $= 10^8$ m/sec
$d/2$	thickness of parabolic transition
$\omega = \omega_1 = \omega_2$	angular frequency of incident, transmitted, and reflected wave
$\mathbf{v}$	velocity vector of moving medium
$\mathbf{e}_x$	unit vector in $x$ direction
$v$	magnitude of the velocity vector
$E_0$	magnitude of incident electric field
$E_y$	$y$ component of incident electric field
$H_{x,z}$	$x$ and $z$ components of incident magnetic field
$\theta$	angle between $k_2$ and $\tilde{\mathbf{v}}$ in Laboratory frame
$\theta_1$	angle of refraction in Laboratory frame
$\mathbf{k}_1$	propagation vector in incident wave
$k_1$	magnitude of propagation constant of incident wave
$k_{1x}$	$x$ component of propagation constant of incident wave
$k_{1z}$	$z$ component of propagation constant of incident wave
$k'_2$	magnitude of propagation constant of refracted wave in right half space with respect at Laboratory frame
$k_2$	magnitude of propagation constant of refracted wave in right half space with respect to its rest frame
$k'_{2x,z}$	$x,z$ component of propagation constant of refracted wave in right half plane with respect at Laboratory frame
$n$	index of refraction
$n'$	apparent index of refraction of the moving right half space with respect to the Laboratory frame
$R$	reflection coefficient for oblique incidence
$R_n$	reflection coefficient for normal incidence
$R_0$	first order in $\beta_0$ reflection coefficient, $R = R_0 \beta_0$
$Z$	wave impedance of dielectric

## ELECTROMAGNETIC SCATTERING FROM AIR CURRENTS

H.N.Kritikos

### 1. INTRODUCTION

The study of electromagnetic propagation in moving dielectrics has led to a number of contributions of both theoretical and applied interest. The theoretical contributions have provided largely to the understanding of the basic nature of electromagnetic phenomena. The applied results, on the other hand, have uncovered and pointed out new mechanisms responsible for the scattering of electromagnetic waves in moving dielectric streams. A result of these investigations has been the realization that a jet stream in a homogeneous idealized fluid with the same index of refraction in its rest frame scatters electromagnetic waves<sup>1</sup>. In this paper an extension to the theory of scattering from jet streams is made. The magnitude of the reflection coefficient from highly idealized models of air currents is determined and the optimum manner for possible observation of such scattering is discussed.

### 2. REFLECTION FROM A STEP DISCONTINUITY IN VELOCITY

Consider the idealized case of a dielectric fluid in laminar flow, which is characterized by an index of refraction  $n$  in its proper frame. A step discontinuity in velocity exists such that with respect to the left half space the right half is moving uniformly along its boundary with a velocity  $v = e_x v$  (see Figure 1). A plane wave with a wave vector  $k_1$  is incident from the left to the interface. The components of the field vectors are

$$E_y = E_0 e^{ik_1 x} \left[ e^{ik_1 z} + R e^{-ik_1 z} \right] \quad (1)$$

$$H_x = - \left( \frac{E_0}{Z} \right) \cos \theta e^{ik_1 x} \left[ e^{ik_1 z} - R e^{-ik_1 z} \right] \quad (2)$$

$$H_z = \left( \frac{E_0}{Z} \right) \sin \theta e^{ik_1 x} \left[ e^{ik_1 z} + R e^{-ik_1 z} \right], \quad (3)$$

where  $Z = \sqrt{\mu/\epsilon}$  is the impedance of the dielectric.

Although the reflection coefficient has been calculated previously<sup>1</sup>, for the sake of clarity a simplified version will be given here.

With respect to a laboratory frame fixed to the medium in the left half space the apparent index of refraction  $n'$  of the right-hand half space to a first order in  $\beta$  is

$$n' = n - (n^2 - 1) \beta \cos \rho'. \quad (4)$$

$\beta = v/c$ ,  $v$  = velocity of the medium,  $c$  = speed of light in vacuum.  $\rho'$  is the angle between the velocity vector  $v$  and the propagation vector  $k'_2$ .

For an angle of transmission  $\theta_1$  one has  $\theta' = \pi/2 - \theta_1$ . The propagation constant  $k'_2$  in the right half plane becomes

$$k'_2 = \frac{\omega_n}{c} \left[ 1 - \frac{(n^2 - 1)}{n} \beta \sin \theta_1 \right]. \quad (5)$$

To find the angle of transmission  $\theta_1$ , one recognizes that

$$\omega_1 = \omega_2 = \omega \quad (6)$$

$$\text{and } k_{1x} = k'_{2x} \quad (7)$$

$$\text{or } k \sin \theta = k'_2 \sin \theta_1. \quad (8)$$

To a first order in  $\beta$  and  $\{(n^2 - 1)/n\} \beta \sin \theta \ll 1$  one obtains

$$\sin \theta_1 = \sin \theta - \left( \frac{n^2 - 1}{n} \right) \beta \sin^2 \theta. \quad (9)$$

The z component of the propagation vector  $k'_2$  is

$$k'_{2z} = \sqrt{(k'^2 - k_{1z}^2)}. \quad (10)$$

To a first order in  $\beta$  one has

$$k'_{2z} = \frac{\omega_n}{c} \cos \theta \left[ 1 - \frac{(n^2 - 1)}{n} \beta \frac{\sin \theta}{\cos^2 \theta} \right]. \quad (11)$$

The reflection coefficient is therefore given by

$$R = \frac{k'_{2z} - k_{1z}}{k'_{2z} + k_{1z}} \quad (12)$$

$$\text{or } R = \frac{(n^2 - 1)}{2n} \frac{\sin \theta}{\cos^2 \theta} \beta. \quad (13)$$

For normal incidence it has been shown that the reflection coefficient  $R_n$  is

$$R_n = \frac{1 - n^2}{2n} \beta^2. \quad (14)$$

It is interesting to notice therefore that scattering at normal incidence is one order of magnitude in  $\beta$  below that of oblique incidence. The results for the case where the electric vector is in the plane of incidence are identical to those derived above.

### 3. THE PARABOLIC VELOCITY PROFILE

Since in a number of applications the velocity change takes place gradually, it is instructive to construct models of such transitions and study their scattering properties. One such model is a jet stream with a parabolic velocity profile (see Figure 2). A convenient method of finding the reflections of such a profile is to derive a differential equation for the reflection coefficient  $R$  by using the principle of invariant imbedding. It has been shown previously<sup>1</sup> that the differential equation is of the Riccati type and is

$$\frac{dR}{dz} = \frac{dk_z}{dz} \frac{1}{2k_z} - 2ik_z R - \frac{dk_z}{dz} \frac{1}{2k_z} R^2, \quad (15)$$

where  $k_z$  given by equation for a parabolic velocity profile of the form

$$\beta = \beta_0 \left[ 1 - \left( \frac{2z}{d} - 1 \right)^2 \right]. \quad (16)$$

The solution to a first order in  $\beta_0$ , and for  $(n^2 - 1/n) \beta_0 \tan \theta \sec \theta \ll 1$ ,

is  $R = R_0 \beta_0 + R_1 \beta_0^2 + \dots, \quad (17)$

where  $R_0 = \frac{i(1-n^2)}{nk_z d} \frac{\sin \theta}{\cos^2 \theta} \left[ \frac{2z}{d} - 1 - \frac{1}{ik_z d} \right] + Ce^{-2ik_z z}, \quad (18)$

where  $C$  is a integration constant determined by the boundary conditions. Two cases of conditions are recognized: A complete jet stream of thickness  $d$ . A transition section of thickness  $d/2$  leading to a half infinite space moving uniformly with a velocity  $v$ . (see Figure 2).

The solution for the parabolic jet stream with boundary condition has been given elsewhere<sup>1</sup>.

For the parabolic transition with the boundary condition  $R(z = d/2) = 0$  one has

$$R = \beta_0 \frac{(n^2 - 1)}{n} \tan \theta \sec \theta \frac{1}{k_z d} \left[ 1 + \frac{1}{ik_z d} \left( 1 - e^{-ik_z d} \right) \right]. \quad (19)$$

A discussion and an evaluation of the above expression appears in the next section.

#### 4. SCATTERING FROM AIR CURRENTS

The results of the previous sections can be applied to a highly idealized model of air currents which exist in the upper atmosphere. One such air current is the jet stream which in the northern hemisphere runs approximately from west to east at an altitude of 10 km. The maximum reported velocity is in the vicinity of 100 m/sec. The thickness of the jet stream is a difficult parameter to determine because of its irregular nature. Estimates, however, place it in the order of magnitude of 5 km. Since, even for HF, it is too large to act as a resonant scatterer, one is led into an examination of the fine structure of wind profile. Data for the fine structure of the wind distribution are given in terms of the wind shear<sup>2</sup>. Estimates for the wind shear at an altitude of 10 km measured over intervals of 100 m are of the order of  $0.1 \text{ sec}^{-1}$ , i.e., over a distance of 100 m a change of wind velocity of 10 m/sec takes place. If one makes the idealized assumption that the transition region can be modeled by a parabolic profile, the results of the previous section can be applied here. For an index of refraction  $n = 1.00015$ , typical of an altitude of 10 km and a velocity change of  $v = 10 \text{ m/sec}$  ( $\beta_0 = 10^{-7}$ ), the reflection coefficient has been calculated for a range of thickness (see Figure 3). The results show that significant reflections occur only for large angles of incidence and transition regions of the order of a few wave lengths. As an example consider a forward scatter experiment of a 50 MHz signal from a transition region of 100 m thickness, ( $d/2 = 100 \text{ m}$ ,  $kd = 210$ ) at an altitude of 10 km and angle of incidence of  $85^\circ$  with a transmitter receiver separation of 230 km. From Figure 3, the reflection coefficient is found to be  $R = 1.1 \times 10^{-10}$ .

### 3. CONCLUSIONS

The results derived from the idealized models of air currents show that, to a first order in  $\beta$ , reflections can only take place at forward scattering with large angle of incidence,  $85^\circ < \theta < 90^\circ$ , and wavelengths which are of the order of magnitude of the width of the velocity transitions. In addition, it is required that the incident propagation vector is parallel or antiparallel to the velocity vector of the air current. For the jet stream at a height of 10 km, having wind shears of  $0.1 \text{ sec}^{-1}$ , an angle of incidence of  $\theta = 85^\circ$  and a frequency  $f = 50 \text{ MHz}$ , the estimated reflection coefficient is of the order  $10^{-10}$ . It is expected that in practice many other factors such as inhomogeneities and turbulence will alter the above idealized predictions. These effects are difficult to estimate because of their complexity and lack of data pertaining to this altitude. It should be pointed out, however, that since the jet stream in the northern hemisphere runs from west to east, with a width of several hundred miles, it should scatter electromagnetic energy coherently.

From the results of this paper it appears that at present the optimum arrangement for detecting such reflections rests with forward scattering of high power HF radar pulses.

### ACKNOWLEDGMENT

The author would like to express his appreciation to Professor Papas, of the California Institute of Technology, for his initial suggestion of the problem and his kind guidance.

### REFERENCES

1. Kritikos, H.N.  
et al. *Electromagnetic Reflectivity of Nonuniform Jet Streams*,  
*Radio Science*, Vol. 2 (New Series) September 1967, p. 991.
2. Valley, S.L. *Handbook of Geophysics and Space Environment*. Air Force  
Cambridge Research Laboratories, Office of Aerospace  
Research, USAF, 1965, pp. 4-19 to 4-23.

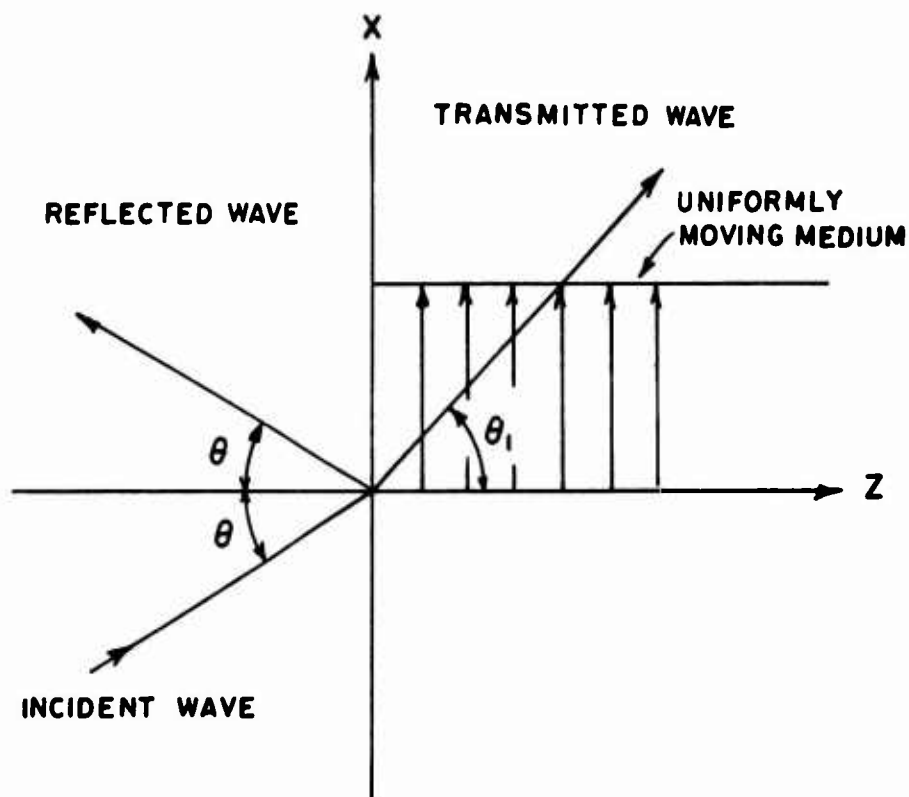


Fig. 1 Reflection from a step discontinuity in velocity

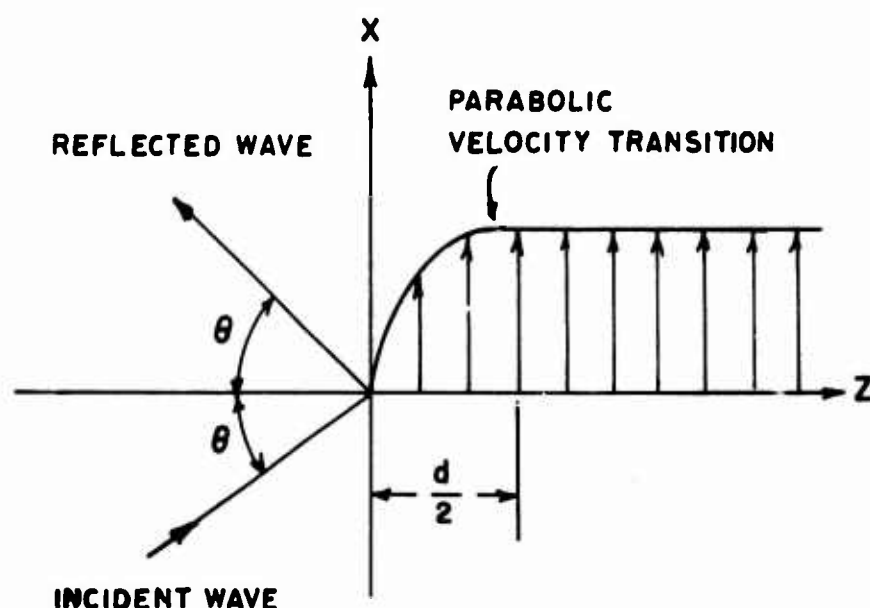


Fig. 2 Reflection from a parabolic transition

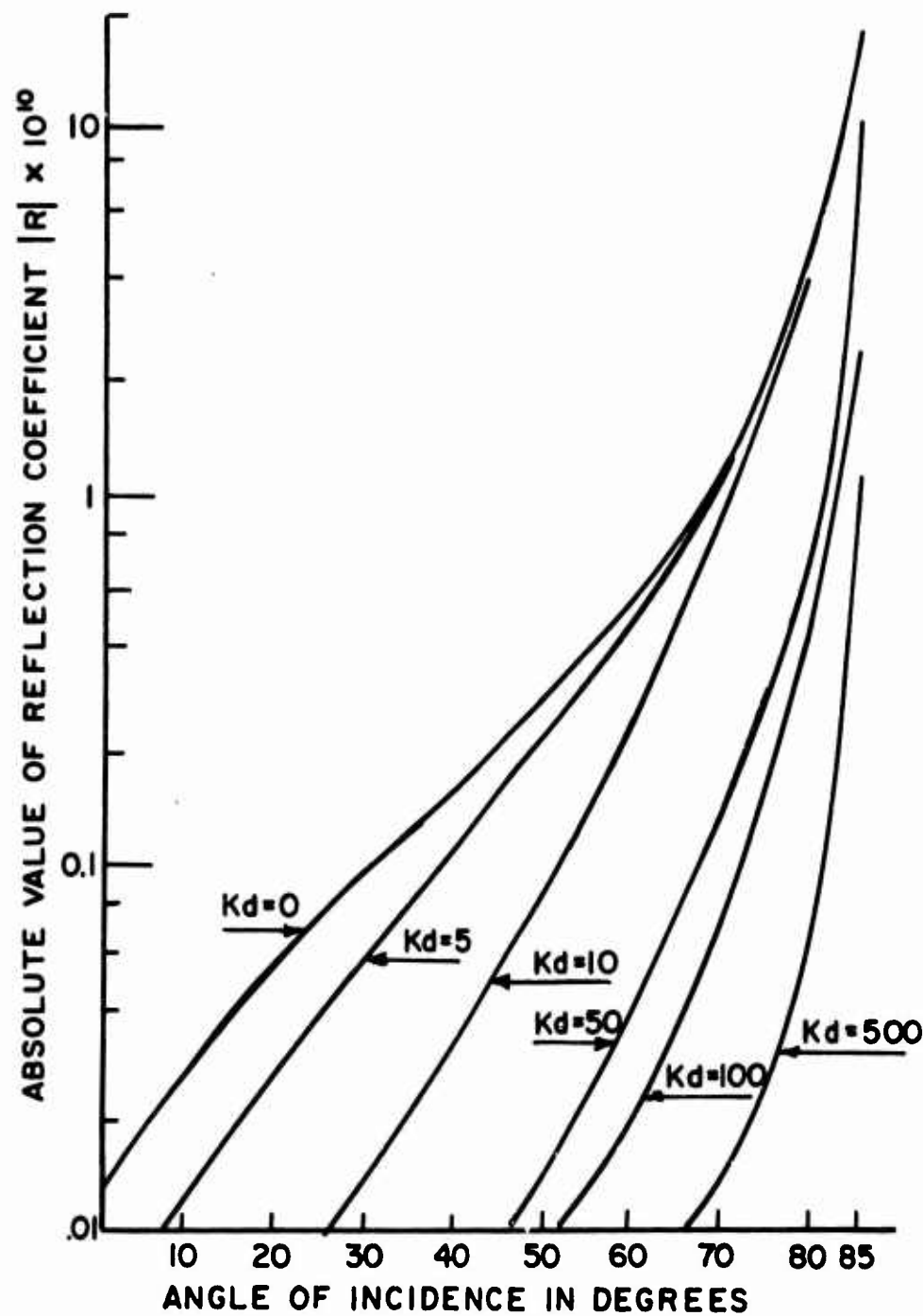


Fig. 3 The absolute reflection coefficient  $R$  versus angle of incidence  $\theta$  for a parabolic transition of thickness  $d/2$ . The index of refraction corresponding to an altitude of 10 km is  $n = 1.00015$ . The velocity change is  $v = 10 \text{ m/sec}$  ( $\beta_0 = 10^{-7}$ ).

**TROPOSPHERIC SCATTER PROPAGATION AT 16 GHZ  
OVER A 500 KM PATH**

by

**Uve H.W.Lammers\*, Edward E.Altshuler\*  
and John W.B.Day†**

**\* Air Force Cambridge Research Laboratories  
L.G.Hanscom Field, Bedford  
Massachusetts, USA**

**† Defense Research Telecommunications Establishment  
Shirley Bay, Ottawa 4, Ontario, Canada**

#### SUMMARY

A forward scatter experiment is carried out to study tropospheric structure with high resolution antennas. Synchronous, computer controlled beam swinging techniques render two-dimensional cuts of the troposphere covering up to 2000 km<sup>2</sup> in a 10 minute raster scan. High stability CW signals are used for Doppler and spectral studies within the 5 km<sup>3</sup> troposcatte volume.

## TROPOSPHERIC SCATTER PROPAGATION AT 16 GHZ OVER A 500 KM PATH

Uve H.W. Lammers, Edward E. Altshuler and John W.B. Day

### 1. INTRODUCTION

Forward scattering techniques have been widely used in the past for communication and to some extent for the exploration of structural properties of the troposphere. Due to the commercial interest, however, communication links seem to have reached a higher level of perfection than radiometeorological forward scatter systems. Data from troposcatter paths designed for communication purposes were quite often used for tropospheric studies, and those scatter experiments especially planned to investigate the troposphere were limited in their capabilities, e.g. sensitivity or spatial resolution. Nevertheless, it has been pointed out that forward scatter systems or bistatic radars might have a great future in determining meteorological parameters of general interest such as clear air turbulence (CAT) or similar phenomena<sup>1</sup>.

The purpose of the troposcatter experiment to be described in this paper is to obtain direct information on the composition of the troposphere by using a very small scattering volume which can be rapidly scanned in arbitrary directions. Depending on the scan mode, one- or two-dimensional cuts through the troposphere are possible. Because of the time alone which is necessary to perform a three-dimensional scan, the complete picture that can be obtained from moving tropospheric structures is of limited value. The transmitted CW signal has a very narrow bandwidth; therefore spectra received from particular portions of the troposphere can be analyzed for frequency spread and Doppler shift, i.e. turbulence and wind-speed.

### 2. THE TROPOSCATTER EQUIPMENT

The trans-horizon path between Prospect Hill Radio Observatory, Waltham, Massachusetts, and Shirley Bay, Ottawa, Ontario, has a length of 500 km. It is believed that 15.7 GHz is the highest frequency at which a troposcatter propagation experiment has ever been conducted. The AFCRL 29 ft (8.85 m) MM-Wave Antenna is located on top of Prospect Hill at an elevation of 160 m and the precision 30 ft (9.15 m) DRTE Antenna is at a site 81 m above sea level. The antennas are horizontally polarized and have similar electrical characteristics with free space beamwidths of approximately  $0.14^\circ$ , 60 dB gain, and sidelobe levels below 19 dB. At the minimum elevation angles of  $0.12^\circ$  and  $0.50^\circ$ , respectively, the above beamwidths lead to a common volume approximately 0.7 km in height and width and 10 km in effective length.

Since the system is designed for conducting Doppler and spectral studies of the scattered signals, both transmitter and receiver local oscillators are high stability low frequency crystal types. Frequency multiplication and phase-locking techniques are used to generate appropriate microwave signals of high spectral purity (3 dB width better than 15 Hz).

Figure 1 shows a block diagram of the transmitter. A Varian VA-882 Klystron with 60 dB gain and 26 MHz bandwidth in the efficiency mode tuning is used in the final stage. The receiver block diagram presented in Figure 2 shows a standard phase-lock version with a balanced crystal mixer input. Two intermediate frequencies are employed (60 MHz and 10 MHz),

the latter one with a minimum filter width of 3 kHz. The lowest phase-lock loop bandwidth is about 125 Hz, yielding a -140 dBm sensitivity of the receiver. An automatic gain control loop (AGC), which utilizes a synchronous detector, is used to provide a monitor of received signal level. The AGC voltage is digitized by an analog/digital converter. The output is sampled in real time by a digital computer and recorded, with time and antenna position, on magnetic tape. A sampling rate of up to 100 per second can be used; the standard rate, however, is 10 per second.

### 3. PATH PARAMETERS AND SCAN PROCEDURES

The map (Fig. 3) indicates the approximate location of the trans-horizon path. BED-Bedford and OW-Ottawa are within a few kilometers from the actual transmitter and receiver sites. Radio soundings of the troposphere are taken at 0000 hours and 1200 hours Greenwich time at Maniwaki, Ottawa, Albany, and Nantucket. Additional weather information is obtained from other stations along or near the path, as indicated on the map.

The profile in Figure 4 shows significant elevations along the path. The horizon elevation angles of the transmitting antenna (horizon distance approximately 70 km) and of the receiving antenna (horizon distance approximately 4 km) lead to a minimum height of 5 km above ground for the common scatter volume. A maximum height of 15 km has been used for all scans as a compromise between limited speed and acceleration of the antennas and the objective to obtain an instantaneous picture of the troposphere. Some of the scan procedures are depicted in this graph, the most significant ones being the wide and narrow raster scans along the great circle path.

The common volume is scanned up and down 20 times in a square wave fashion, covering a portion of  $\pm 100$  km (C-D) or  $\pm 50$  km (B-E), respectively, from midpath. Vertical soundings (A-F) have been taken at the minimum scatter angle position (225 km from Ottawa) and horizontal scans were obtained perpendicular to the path at various heights within A-F. Other scan modes, such as horizontal scans along the path or constant scatter angle scans, produced less obvious results and are omitted from this presentation. For all these scans the antennas were pre-programmed by computer and synchronism within 100 msec was maintained; this is equivalent to 1/5 beamwidth deviation with the highest antenna speed used. The actual up or down scan was done by moving the antennas in either one- or two-step linear approximation, depending on the type of program. A standard 4/3 earth radius correction was applied for scans along the great circle path, whereas no correction to the real earth curvature seemed to be a reasonable approximation perpendicular to the path.

### 4. TROPOSCATTER RESULTS

Signals were received at almost all times during the tests, except for short periods when real deep fading occurred. This was due to poor scattering from the troposphere and possibly cancellation of partial signals as well as to attenuation through precipitation. Peak signals reached a level 50 dB above the receiver noise.

Only a small number of the recordings are presented here. Figure 5 displays four narrow raster scans along the path indicating the height of the reflection, as calculated from the antenna elevation angles versus the distance from the receiver site. Every 5 km division on the abscissa represents the position of an upsweep or downsweep of the scatter volume; the signal amplitude is plotted horizontally with a scale of 7.5 dB per smallest division. The zero signal level always coincides with the vertical line that starts from the distance mark on the abscissa. To give this kind of presentation a quasi-third-dimension, the areas underneath the signal envelopes were filled in black. At least to some degree, the black-to-white ratios of particular portions of the plot thus indicate the reflectivity of the respective volumes of the troposphere. Due to the scale used, the black areas sometimes overlap.

Thirty seconds are required for one upsweep or downsweep of the common volume. As a result, it takes 10 minutes to complete one raster scan. Figure 5 shows, in four stages, vanishing tropospheric layers. It is assumed that the well defined layer in the 0620 and 0630 hour samples (Greenwich time) is the tropopause. The radio soundings from the four stations mentioned earlier show the tropopause at 14 - 15 km height. The upper two scans, which were taken 10 minutes apart, reproduce remarkably well. Since this was noticed in all similar cases it is believed that the scan time per picture is compatible with the stationarity of the troposphere. Only two layers show up in these two graphs (four have been observed as a maximum so far) but definitely some additional structure can be seen in the broad lower layer. Like a wedge, the height of strong reflectivity rises from the left to the right and finally disappears. The scan taken at 0730 hours shows rather marked changes with respect to the first two. The upper layer has partly disappeared and shows an inclination towards the Boston side, as does the lower layer. The region producing strongest signals has moved further to the Boston side, too. At 0830 hours the layers are shown merging together. Looking at subsequent up and down lines of the raster one can see that the changes in the signal level are as gradual as one might expect from the changes in tropospheric structure.

Temperature and windspeed recordings from the 0000 hours radio soundings are presented in Figure 6. As stated before, they yield tropopause heights from 14 - 15 km.

The pictures taken on 24 June at about the same time (Figure 7) indicate a different tropospheric composition. The returns are marginal towards the Boston side at 0420 hours and more or less spread all over the observed height range towards Ottawa. One hour later the reflectivity becomes higher at the right side of the picture and a layer seems to form at a height varying from 12.5 - 10.5 km. This composition changes again, at 0620 hours, when the layer in the preceding scan disappears. Then a region of low reflection, like a blob, shows up in the midpath position at 13.5 km along with a short layer at the same height on the Boston side. Finally, at 0720 hours a single broad V-shaped structure forms with hardly any enhanced regions, as far as signal amplitude is concerned.

Wide raster scans render similar results to the narrow ones. The two samples in Figure 8 are taken on 24 and 27 June. A raster twice as wide, but with the same number of up and down scans along the path, covers an area 200 km long and 10 km high.

A different type of display is used for the samples of vertical and horizontal soundings in Figure 9, which were taken at 2110 and 2120 hours on 25 June. The horizontal axis is a time axis with the 30-sec markers indicating the start of a vertical up or down sweep at a fixed position (225 km from Ottawa) in the 2110 hours scan. Obviously, the tropospheric composition did not change very much during this 10-minute interval. A strong signal from 6.5 km occurs in every sweep, as well as a range of very weak returns between 11 and 14 km. The signal level from about 14.5 km is somewhat stronger. One might be tempted to interpret this kind of display as a two-dimensional one, with layering etc. like the ones shown before. However, this is only possible to such an extent as one can assume a constant velocity, unidirectional motion of the troposphere. From the wind profiles, one must conclude that in general this is not the case. As in the 2120 hours horizontal scan which was taken at the same position along the path and at a height of 6 km, only the variation of particular profiles with time can be observed. On the vertical axis the distance off the great circle has been chosen with 10 km equivalent to slightly more than  $2.3^\circ$  in antenna azimuth angle change. No explanation other than a foreground obstruction at the receiver site has been found for the deep null at about - 5 km which shows up in all horizontal scans. However, some lobing with no relation to the angular position of the antenna sidelobes seems to be present over the whole width of the scan. Optimum measured azimuth angle, as indicated by zero km distance, and calculated azimuth direction coincide within a tenth of a degree. Again, the horizontal scans are rather consistent over the 10-minute interval.

A series of vertical soundings on the great circle path, 225 km from Ottawa, are given in Figure 10. Strong reflections from 5 - 11 km at 0500 hours and a weaker one around 12.5 km move upward in the following scans. The quite well defined 12.5 km reflection spreads out and combines with the lower region. Both upper and lower boundaries of the reflections

are diffuse at 0630 hours but at 0800 hours, when the lower boundary now is at 6.5 km, the height range of signals has contracted and looks well defined again.

The spectrum of the calibrator multiplied by the receiver first local oscillator spectrum (Fig. 11(a)) is obviously narrower than the 15 Hz filter of the spectrum analyzer can resolve, since it has a 3 dB width of approximately 15 Hz. Spectral measurements of the actual transmitter signal yield a similar curve. Two samples of a wide variety of troposcatter spectra obtained so far are given in Figure 11(b). These spectra were recorded with about a 2-minute separation, using the same filter width as before and the same sweep of 500 Hz/min. The antennas were pointing towards the minimum scatter angle position along the path. Both spectra (1 and 2) consist of a sharp first peak and a broader second peak 4 to 5 dB lower. The frequency range of low power density in between differs roughly by 10 dB, however. One might interpret these spectra as the result of scattering from a highly reflective region of constant velocity and another region somewhat more turbulent and of a velocity different from the first one.

### 5. FUTURE IMPROVEMENTS

Only a few characteristic results could be presented here, due to limited space as well as due to the fact that the experiment itself is still in a developmental stage. Experience has to be obtained how to use this forward scatter system effectively. Other scan modes will be implemented in the near future, such as horizontal raster scans and high raster scans (up to 25 km) along the path. The system sensitivity will be improved and frequency diversity will be used.

No doubt exists that there are limitations to probing the troposphere with a high resolution forward scatter system. As with all remote microwave sensing techniques, the sensor itself is subject to tropospheric influences. It is believed, however, that more and useful information can be gathered from the troposphere than was hitherto possible.

### ACKNOWLEDGEMENTS

The authors would like to thank Mr. S. Gitelson and Mr. J. Frazier of AFCRL, and Mr. K.S. McCormick and Mr. W. Pawziuk of DRTE for helping to set up and operate the equipment.

### REFERENCE

1. Atlas, D.  
et al. *Bistatic Microwave Probing of Refractively Perturbed Clear Atmosphere.* Journal of Atmospheric Science, Vol. 25, 1968,  
pp. 257-268.

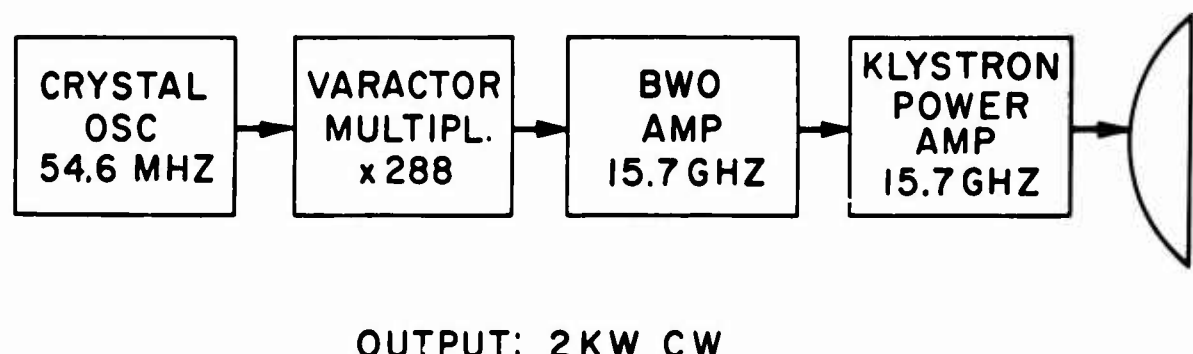


Fig. 1 Transmitter block diagram

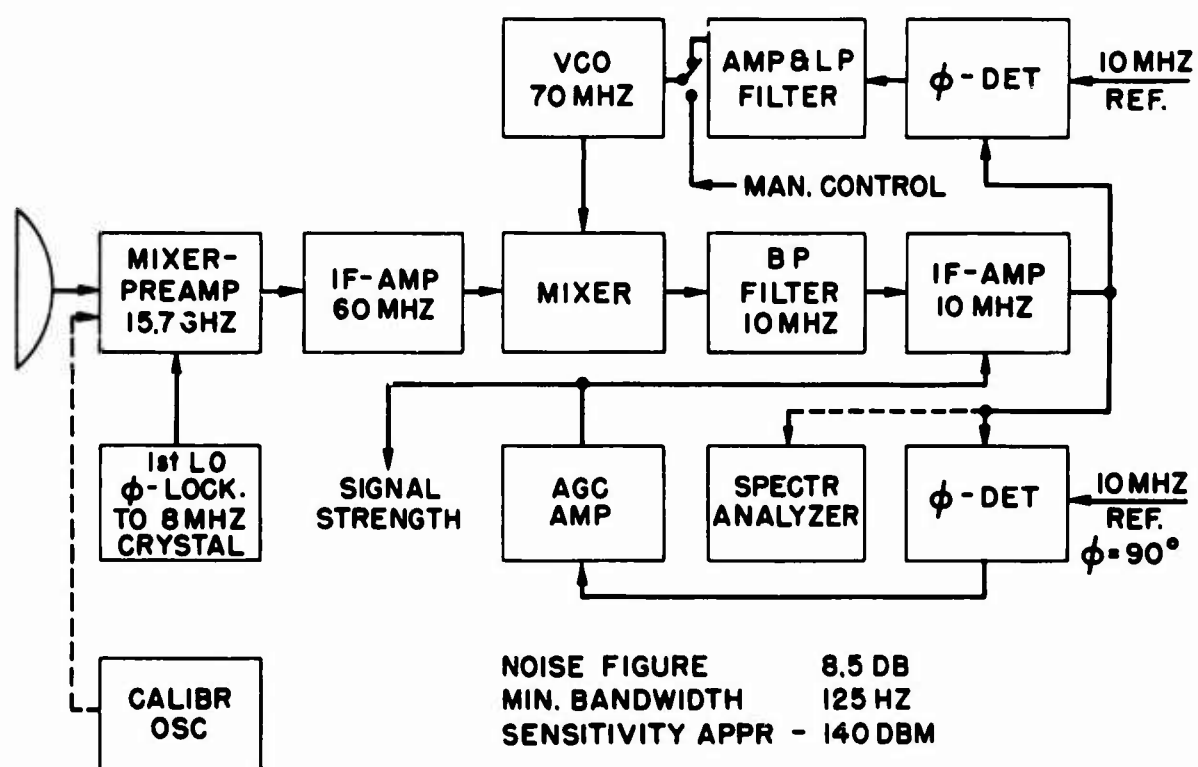


Fig. 2 Receiver block diagram



Fig.3 Map with path parameters

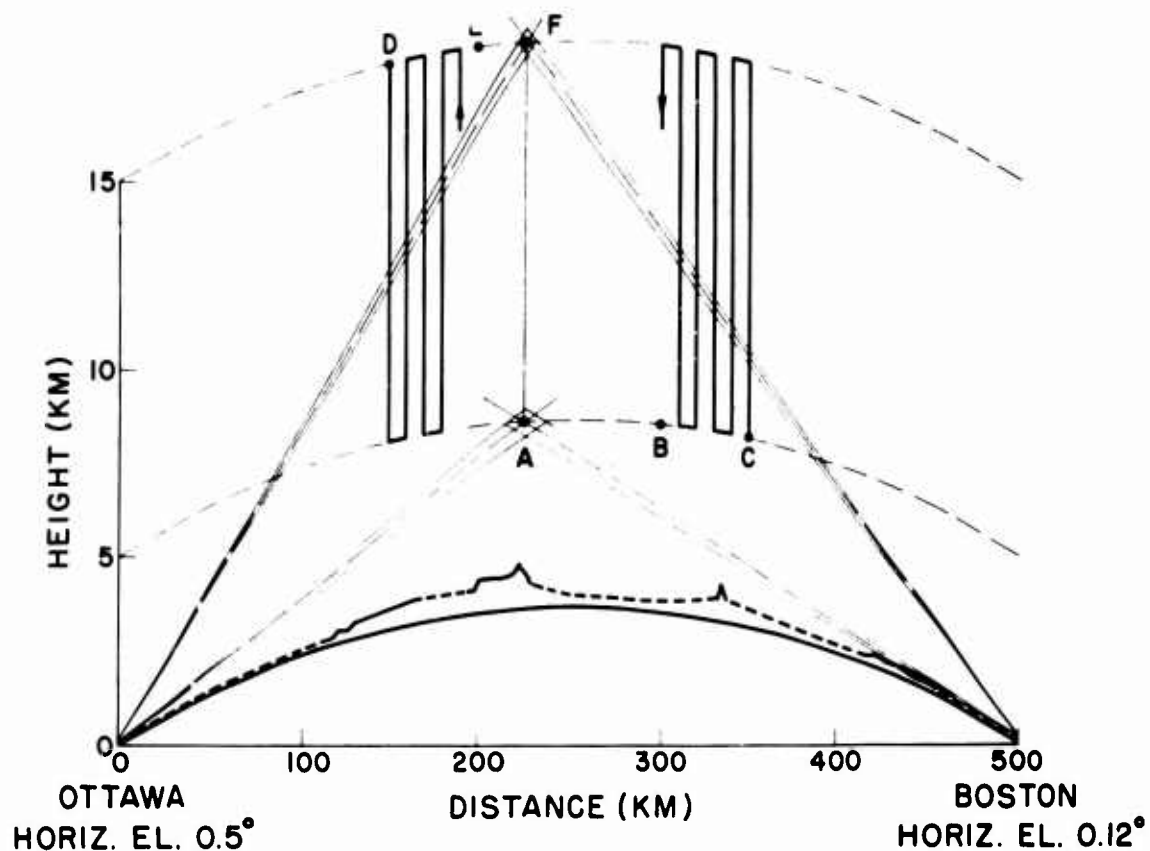


Fig. 4 Profile and scan modes along troposcatter path

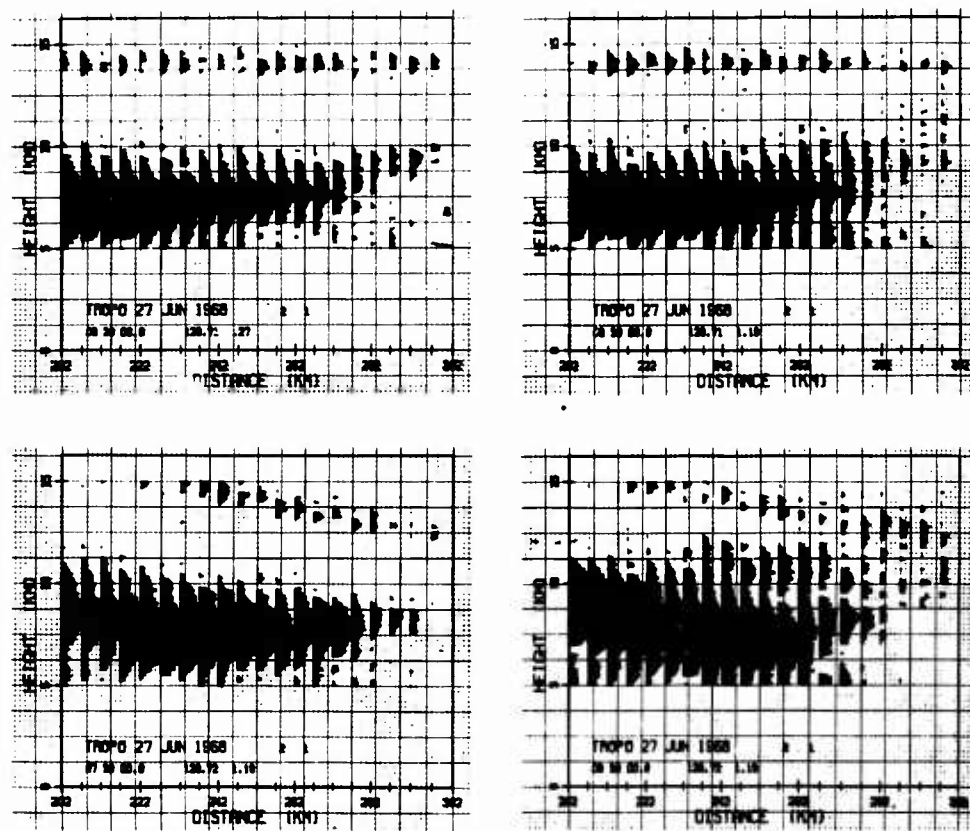


Fig. 5 Vanishing tropospheric layers. (Tropopause at 14 km)

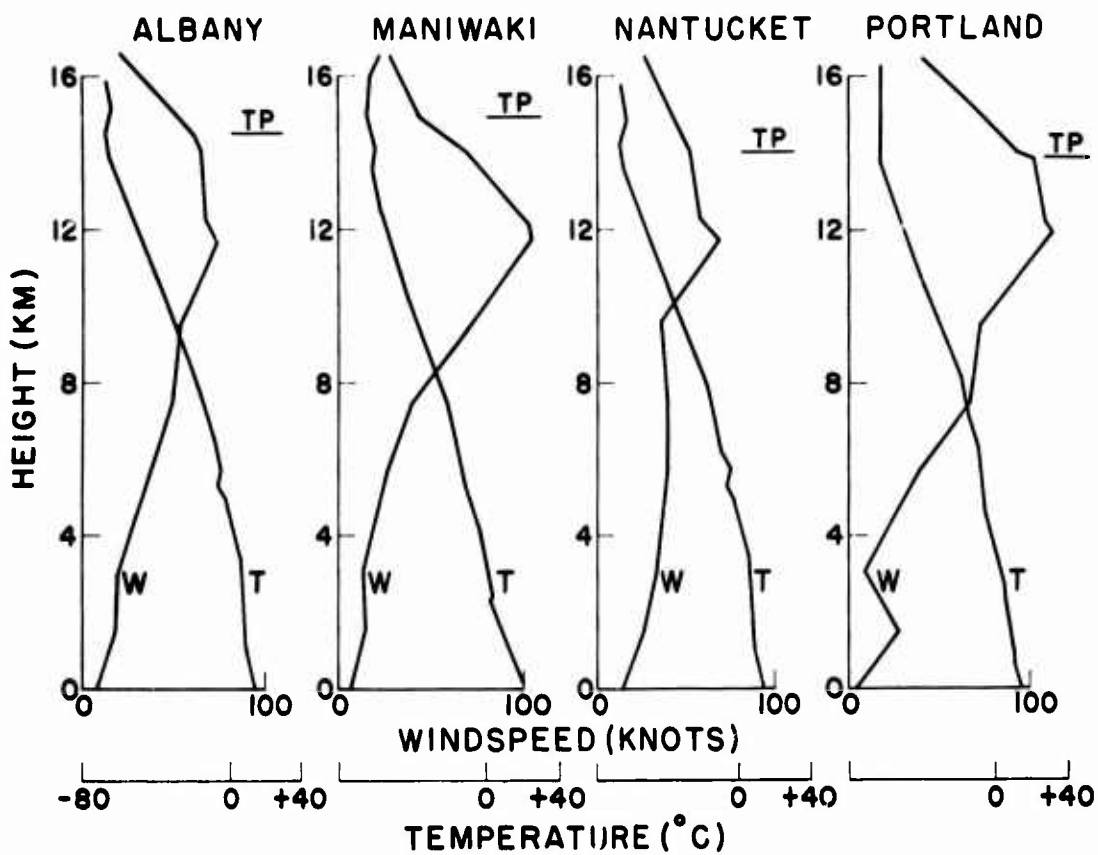


Fig. 6 Radiosonde data from stations close to the troposcatter path

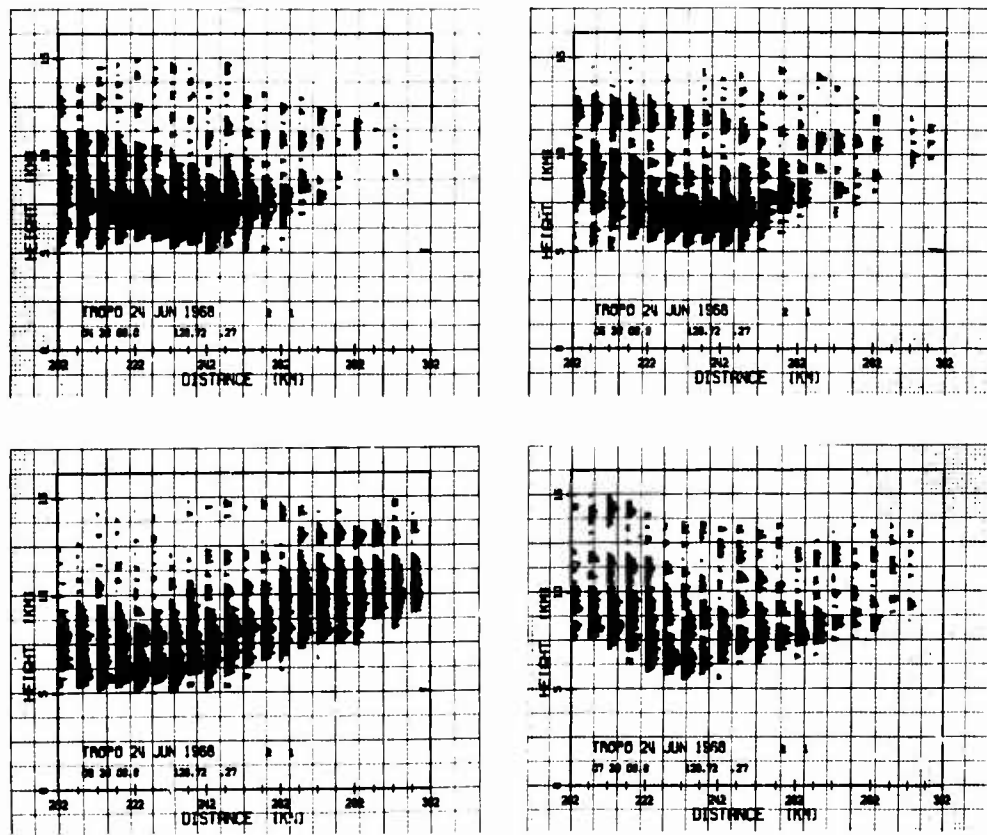


Fig. 7 Various structures forming and disappearing in a quasi-homogeneous troposphere

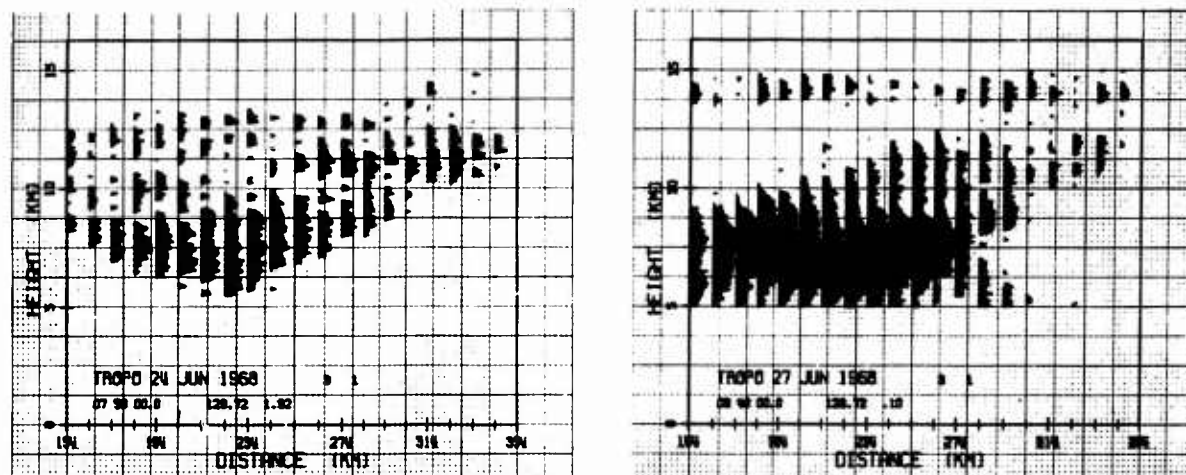


Fig. 8 Samples of wide raster scans

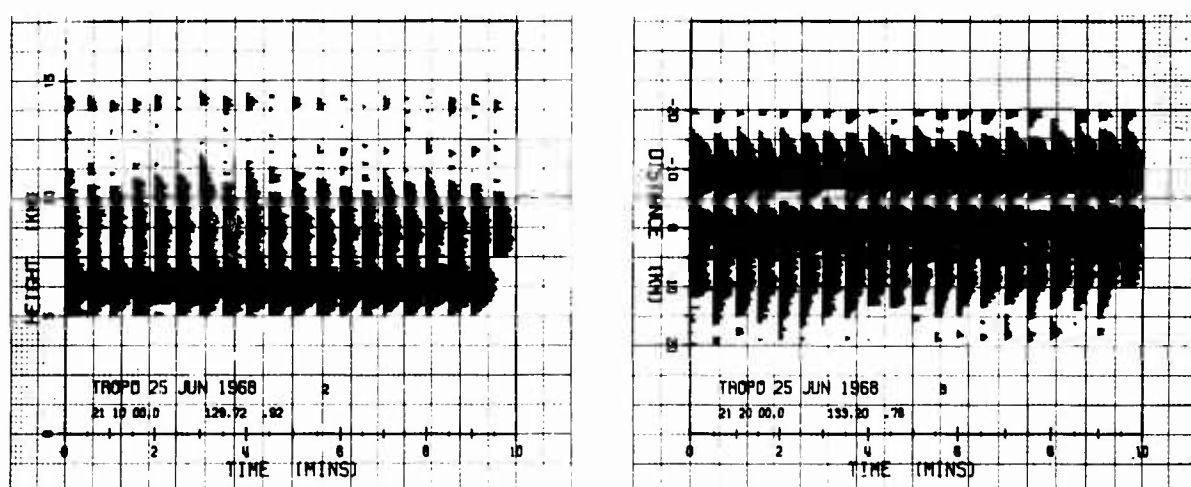


Fig. 9 Samples of vertical and horizontal midpath scans

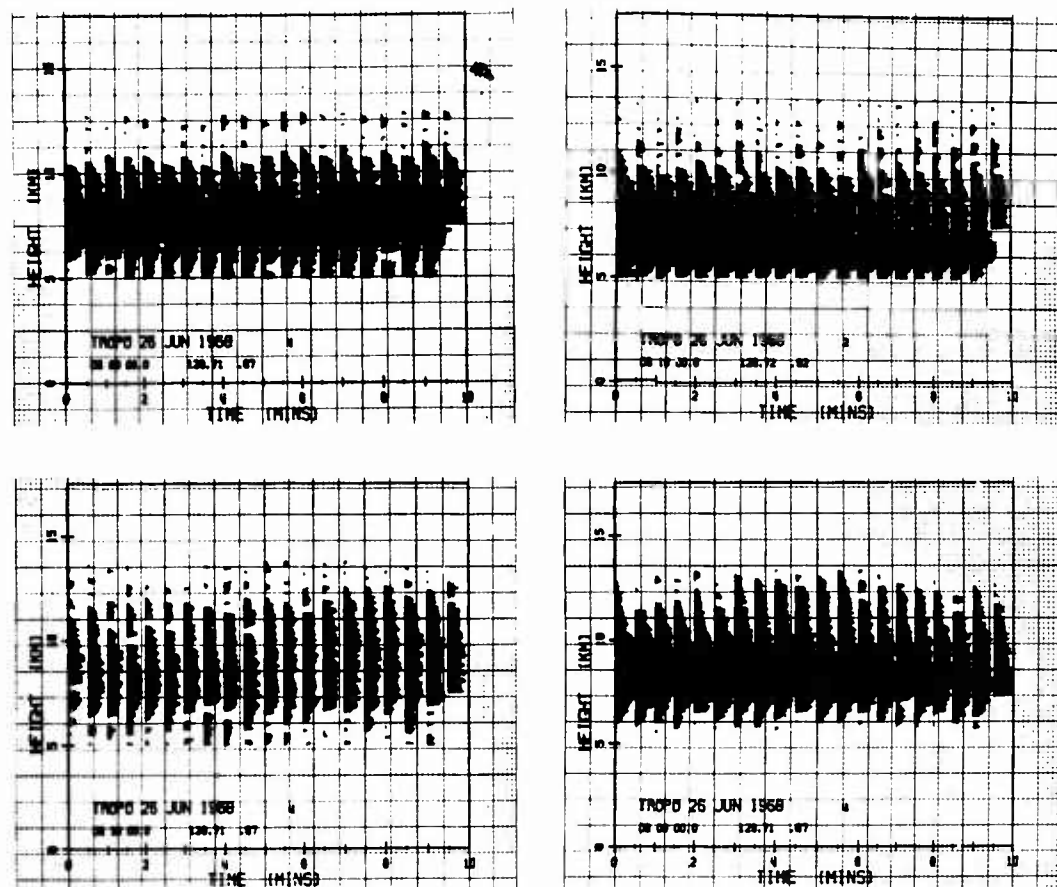


Fig. 10 Midpath vertical scan showing varying height of reflections

**NO PHASE-LOCK, SWEEP 500 HZ / MIN  
SPECTRA OF 16 GHZ SIGNALS 28 JUNE 68 0324 GMT**

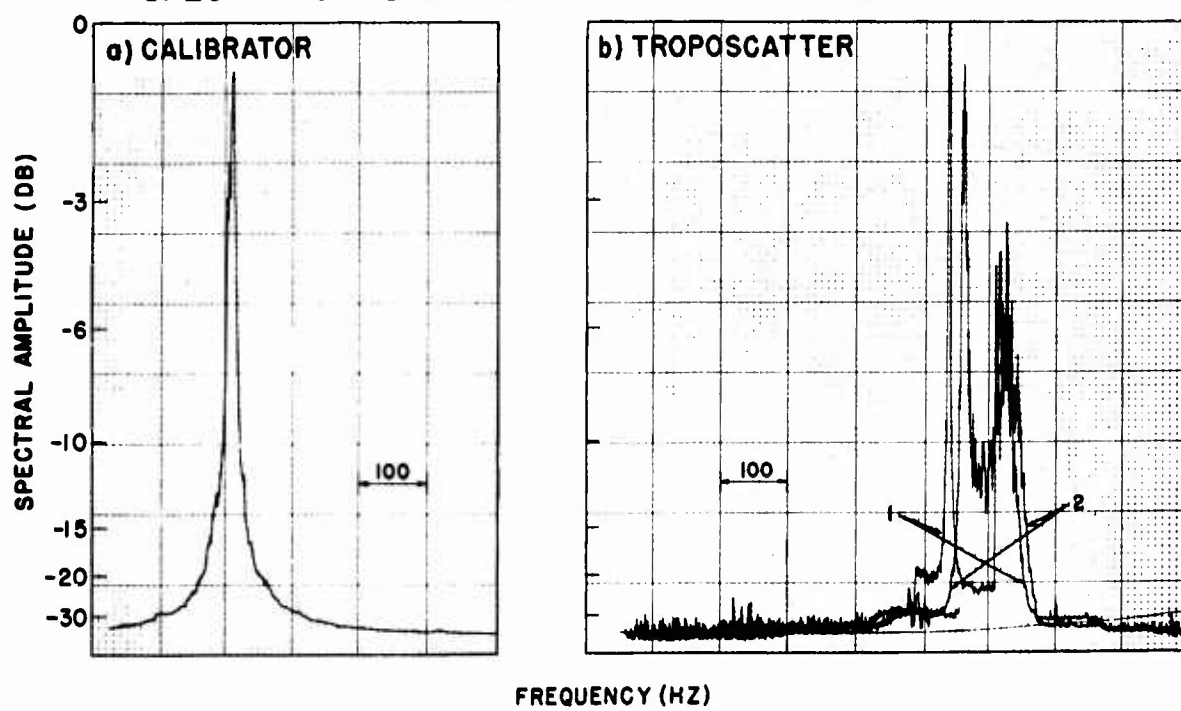


Fig. 11 Spectra of 16 GHz signals

**USING THE TROPOSPHERIC VOLUME OF A QUASI-BACKSCATTER  
LINK TO INVESTIGATE THE SCATTER MECHANISM**

by

R.Menzel and Kh.Rosenbach

Department of Telecommunications,  
Forschungsinstitut für Hochfrequenzphysik - FHP,  
5321 Werthhoven, Nr. Bonn,  
Federal Republic of Germany

## **SUMMARY**

In conjunction with other work on disturbing effects of scatter mechanism undertaken by the Department of Telecommunications, this contribution presents a detailed description of first results obtained in a quasi-backscatter direction.

The first part of the paper refers to the effect of diffraction paths between transmitter and receiver and possibilities of accounting for these paths; it includes the comparison between values calculated theoretically and experimental determinations on selected paths over hilly terrain. The second part quotes experimental data obtained with the quasi-backscatter link and includes a detailed discussion on measured values in relation to values expected theoretically. Considerable work has been done on possible field-strength fluctuations caused by changing meteorological conditions in the relevant scatter volume. Results obtained are interpreted in relation to data originating from other scatter links operated by the Department. Future plans of the project are discussed.

**USING THE TROPOSPHERIC VOLUME OF A QUASI-BACKSCATTER  
LINK TO INVESTIGATE THE SCATTER MECHANISM**

R. Menzel and Kh. Rosenbach

**1. INTRODUCTION**

In conjunction with other work on disturbing effects of scatter mechanism undertaken by the Department of Telecommunications, it was intended to investigate scattering also with respect to side-scattering and backscattering. It was of particular interest to evaluate the data with respect to a change in the scale of turbulence, and so investigations were made on a communication link with an antenna system radiating vertically.

The transmitter of this link is situated on a hill in the Eifel, as shown in Figure 1, and is operated on a frequency of approximately 140 MHz. In accordance with the intention of investigating the scatter mechanism using the side-scattering and backscattering of this special link, we had to place the receiving terminal as near as possible to the transmitting station in order to find side-scattering, or even backscattering. For this reason the receiving system was set up at a point where the power received over the diffraction path from side lobes of the transmitting antenna was negligible in comparison with the scattered power.

In this connection we had to find a way of computing for diffraction paths. To make a comparison between values calculated theoretically and those obtained experimentally, results were obtained on the diffraction path Hochkelberg - Werthhoven, as shown in Figure 1.

**2. MULTIPLE DIFFRACTION OF RADIO WAVES OVER  
ROUNDED OBSTACLES**

Since the theory of diffraction of radio waves over one or more obstacles has already been described in several papers<sup>1-5</sup>, we may at once deal with the calculation of our diffraction paths. In Figures 2 and 3 you see both diffraction paths. On both paths there are two intervening hills, which we treated as rounded obstacles. A method described by Deygourt<sup>1</sup> was applied to the computation of these diffraction paths (Fig. 4). The diffraction loss associated with the main hill is computed first as if this hill were alone. The diffraction loss associated with the second hill is then calculated by considering the propagation around the main hill-receiver with virtual sources above the main obstacle. Then the diffraction loss below free space loss is given by

$$a_{MD} = a_{m1} + a'_{m2} . \quad (1)$$

The single diffraction losses were computed by a method described in Reference 4. The diffraction loss for a rounded obstacle and irregular terrain, shown in Figure 5, is defined as

$$a_{m1}(v, \rho) = a(v, 0) + a(0, \rho) + \mu(v, \rho) , \quad (2)$$

where  $v$  is the dimensionless parameter defined by

$$v = \pm 2\sqrt{(\Delta r/\lambda)} , \quad (3)$$

and  $\rho$  is a dimensionless index of curvature for the crest radius. For the diffraction path Hochkelberg - Staffel the following values were computed:

$$\begin{aligned} a_{m1} &= 42 \text{ dB} \\ a'_{m2} &= 30 \text{ dB} . \end{aligned}$$

Then the whole diffraction loss below free-space loss is

$$a_{ms} = (42 + 30) \text{ dB} = 72 \text{ dB} .$$

For the diffraction path Hochkelberg - Werthhoven we obtained

$$a_{mw} = (23 + 13) \text{ dB} = 36 \text{ dB} .$$

As the same side lobe of the transmitting antenna pointed towards Staffel and Werthhoven we had a good comparison between the power received at Werthhoven and the one to be expected at Staffel. The theoretically calculated values agreed fairly well with those obtained experimentally at Werthhoven. Thus we could be certain that the power received at Staffel must be mainly scattered power. A typical recording of the diffraction path Hochkelberg - Werthhoven is shown in Figure 6.

### 3. SCATTER PROPAGATION AT ONE LOCATION

The investigations were made, as already mentioned, with a side-scatter, or even a backscatter, link and the path geometry is shown in Figure 7. The scatter angles were between  $75^\circ$  and  $115^\circ$  and the antenna beamwidths were  $40^\circ$  for the transmitting antenna and  $37^\circ$  for the receiving antenna. The distance between transmitter and receiver is about 24 km. The signal received is predominantly due to scattering in the troposphere, which can be seen in Figure 8 which shows some typical curves of the power received, although the exact definition of the appropriate scatter volume is difficult, owing to the mixed diffraction and scatter paths present. The effective scatter volume is considered to extend from a minimum altitude of 3.0 km up to about 4 - 5 km, for the purposes of calculation.

The power  $P$ , scattered to a receiver at a distance  $D$  from the transmitter, and relative to the free-space power  $P_{fs}$ , is

$$\frac{P}{P_{fs}} = KD^2 \int \frac{\sigma(\theta, \chi)}{R_T^2 R_R^2} dV , \quad (4)$$

where  $R_t$  is the distance from transmitter to scattering element,  $R_r$  is the distance from scattering element to receiver, and the integration is over the tropospheric scatter volume.  $K = (1 + |\rho|^2)^2$  is introduced to account for the reflection coefficient  $\rho$  of the ground. From theories currently available<sup>5-11</sup> of determining the power scattered by the troposphere we decided to use the one by Booker and Gordon<sup>6</sup> which gives, for the scattered power,

$$\sigma(\theta, \chi) = \frac{\delta_p^2 (2\pi l/\lambda)^3 \sin^2 \chi}{\lambda [1 + \{(4\pi l/\lambda) \sin \theta/2\}^2]^2} . \quad (5)$$

where  $\theta$  is the angle between the direction of incidence and the direction of scattering,  $\delta_n^2$  is the mean-square deviation of the dielectric constant of the atmosphere from the mean value,  $l$  is the scale of turbulence,  $X$  is the angle between the incident field and the direction of the line to the receiver and is approximately  $90^\circ$  and  $\lambda$  is the wavelength. For the theoretical calculation of our scatter link we have used, as a representative value for the turbulence, a refraction index variation of  $\delta_n = 10^{-5}$  with a scale length  $l = 4$  m and  $K = 1$ . The scattered power below the free-space value is then of the order of 90 dB. This agreed with the average of those values obtained experimentally.

Our particular receiving terminal has been operational for only a few weeks. First results have been evaluated on the basis of average field strength over periods of half a day. The curve so obtained, shown in Figure 9, has been compared with the air temperature determined from radiosonde ascents and with the refractive index also derived from radiosonde ascents. Although the correlation coefficient with respect to refractive index variations yielded the low value expected, because of the short period covered, the correlation with regard to air temperature proved to be much more promising. The coefficients are 0.25 for refractive index and 0.79 for air temperature, respectively. A similarly close correlation between the scattered power and air temperature at two metres altitude has been mentioned in work by Stratmann<sup>12</sup>. However, the air temperature measured at two metres cannot be regarded as representative of the temperature inside the volume.

In relation to a comparison of the results obtained with those of another scatter link operated by the Department of Telecommunications, it is interesting to evaluate the data with respect to a change in the turbulence scale. The different frequencies permit reasonably reliable values to be obtained. In a first analysis, variations in field strength occurring simultaneously, if the slightly different geographical location is allowed for, yield two values of changes in the dimensions of turbulent blobs which should be identical under perfect conditions. A number of such single cases has been evaluated and good agreement in the length changes has been found to exist in 90% of them.

#### 4. CONCLUSIONS

Considering that this vertical scatter system was constructed to supply scatter data on a frequency yielding  $l/\lambda$  ratios which permit a more omni-directional scatter pattern, the first results reported in this paper seem to prove that the system will fulfil its purpose. In addition, a number of possible diffraction paths allows interesting studies to be made of the variations of such links with respect to changes in the mixture between diffraction and scatter paths and due to variations in the meteorological conditions. Work will continue and further results will be the subject of a later paper.

#### ACKNOWLEDGEMENTS

The authors wish to express their thanks to all collaborators, in particular to Miss Fassbender and Mr. Giesen for preparing the manuscript and to Miss Drolshagen and Mr. Becker for data evaluation.

The work was sponsored by the Ministry of Defence, Federal Republic of Germany, under Research Contract No.T 833-1-203/5.3, and is published with their permission.

## REFERENCES

1. Deygout, J. *Multiple Knife-Edge Diffraction of Microwaves.* Institute of Electrical and Electronic Engineers, Transactions on Antennas and Propagation, Vol. AP-14, July 1966, p. 480.
2. Carlson, A.B. Watermann, A.T. *Microwave Propagation over Mountain-Diffraction Paths.* Institute of Electrical and Electronic Engineers, Transactions on Antennas and Propagation, Vol. AP-14, July 1966, p. 489.
3. Neugebauer, H.E.J. Bachynski, M.P. *Diffraction by Smooth Cylindrical Mountains.* Proceedings, Institute of Radio Engineers, Vol. 46, pp. 1619-1627.
4. Rice, P.L. et al. *Transmission Loss Predictions for Tropospheric Communication Circuits.* US National Bureau of Standards, Technical Note NBS 101 (revised), 1966.
5. Du Castel, F. *Radiowave Propagation beyond the Horizon.* Pergamon Press, 1966.
6. Booker, H.G. Gordon, W.E. *A Theory of Radio Scattering in the Troposphere.* Proceedings, Institute of Radio Engineers, Vol. 38, April 1950, p. 401.
7. Villars, F. Weisskopf, V.F. *On the Scattering of Radio Waves by Turbulent Fluctuations of the Atmosphere.* Proceedings, Institute of Radio Engineers, Vol. 43, October, 1955, p. 1232.
8. Gordon, W.E. *Radio-Scattering in the Troposphere.* Proceedings, Institute of Radio Engineers, Vol. 43, January 1955, p. 23.
9. Ortwein, N.R. et al. *Properties of Tropospheric Scattered Fields.* Proceedings, Institute of Radio Engineers, Vol. 49, April 1961, p. 788.
10. Staras, H. *Forward Scattering of Radio Waves by Anisotropic Turbulence.* Proceedings, Institute of Radio Engineers, Vol. 43, October 1955, p. 1374.
11. Booker, H.G. De Bettencourt, J.T. *Theory of Radio Transmission by Tropospheric Scattering Using Very Narrow Beams.* Proceedings, Institute of Radio Engineers, Vol. 43, March 1955, p. 281.
12. Stratmann, E. *Ergebnisse der Troposondenmessungen in Darmstadt.* National URSI Convention, Germany, 1967. Kleinheubacher Berichte, Bd. 12, pp. 131-138.

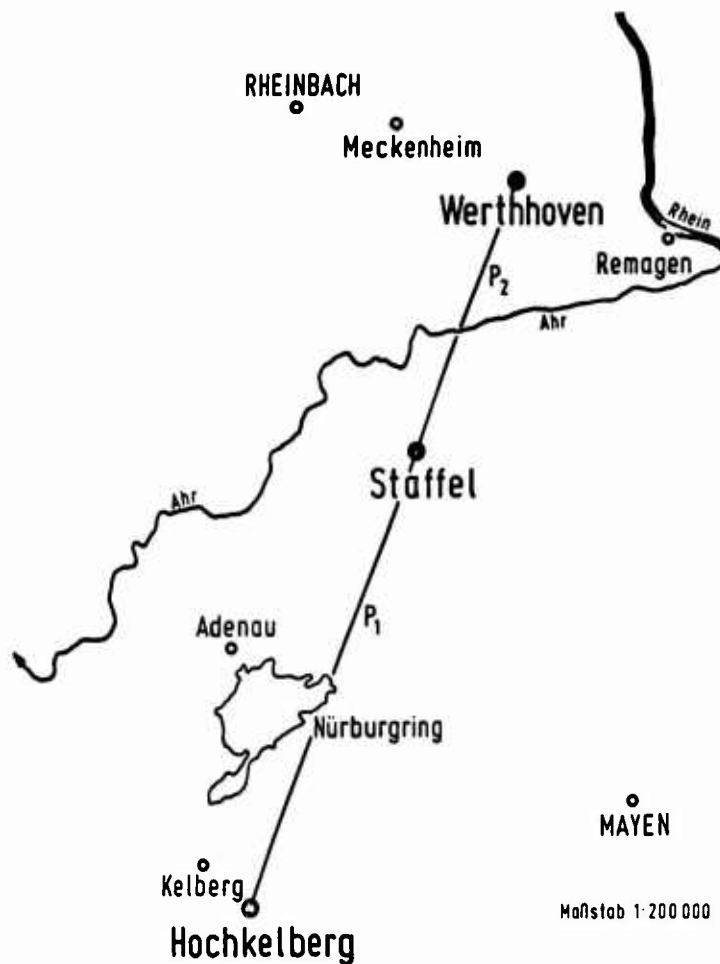


Fig. 1 Hochkelberg-Werthhoven path

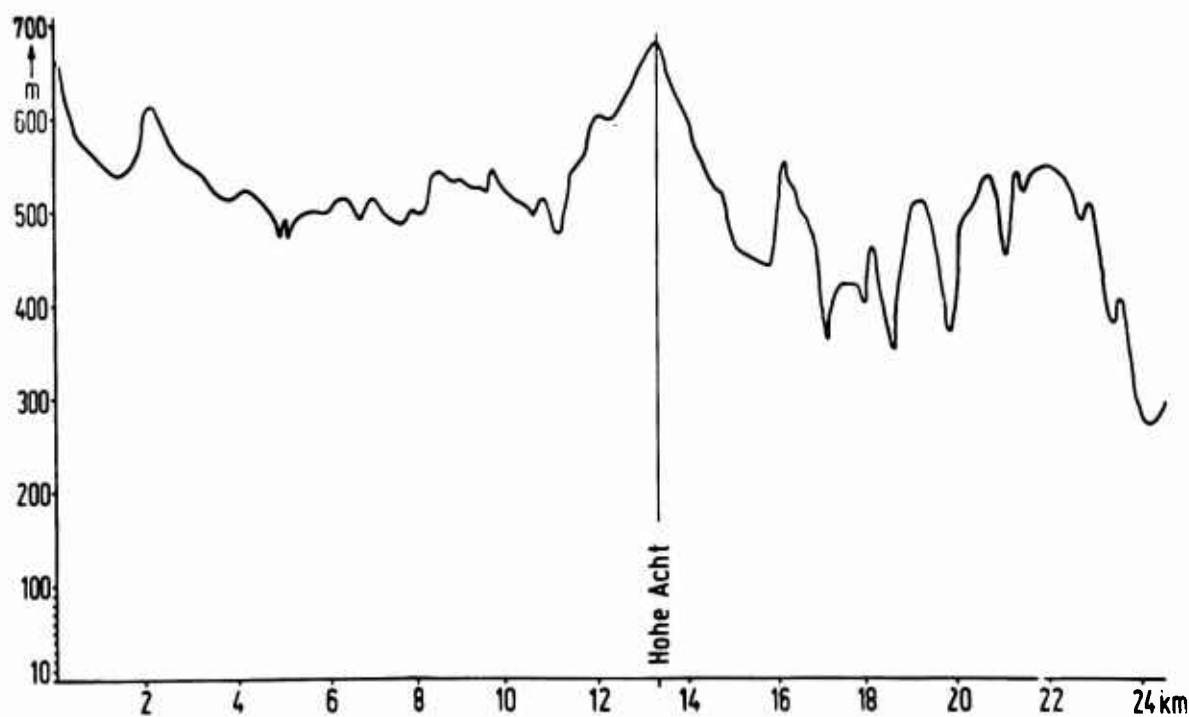


Fig. 2 Path profile Hochkelberg-Staffel

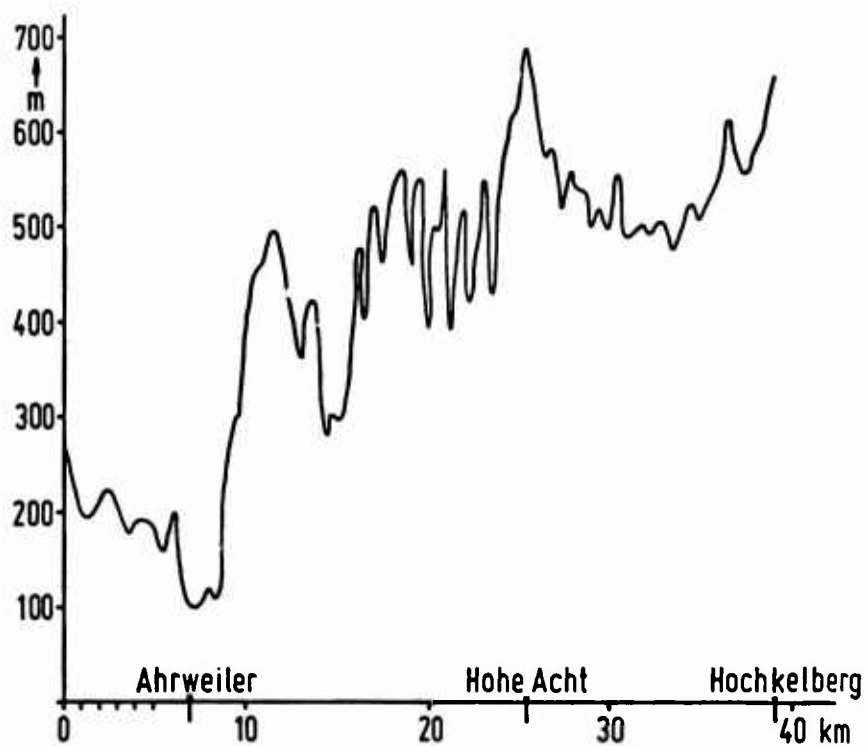


Fig. 3 Path profile Werthhoven-Hochkelberg

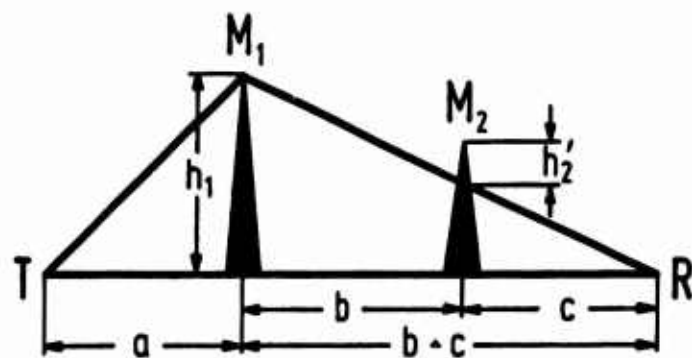


Fig. 4 Double knife-edge approximation. (Symbols as in Reference 1)

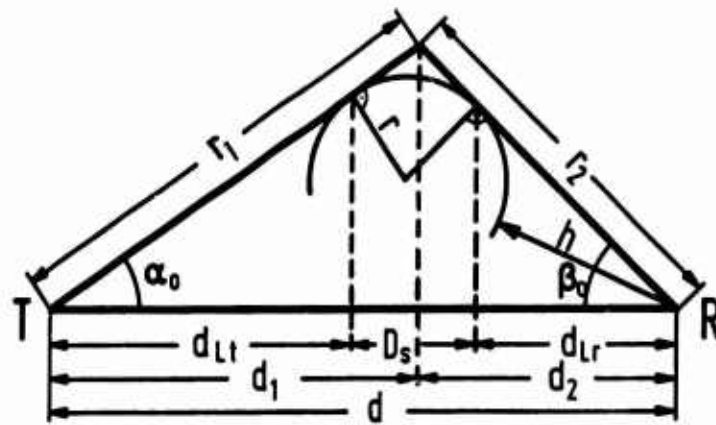


Fig. 5 Isolated rounded obstacle. (Symbols as in Reference 4)

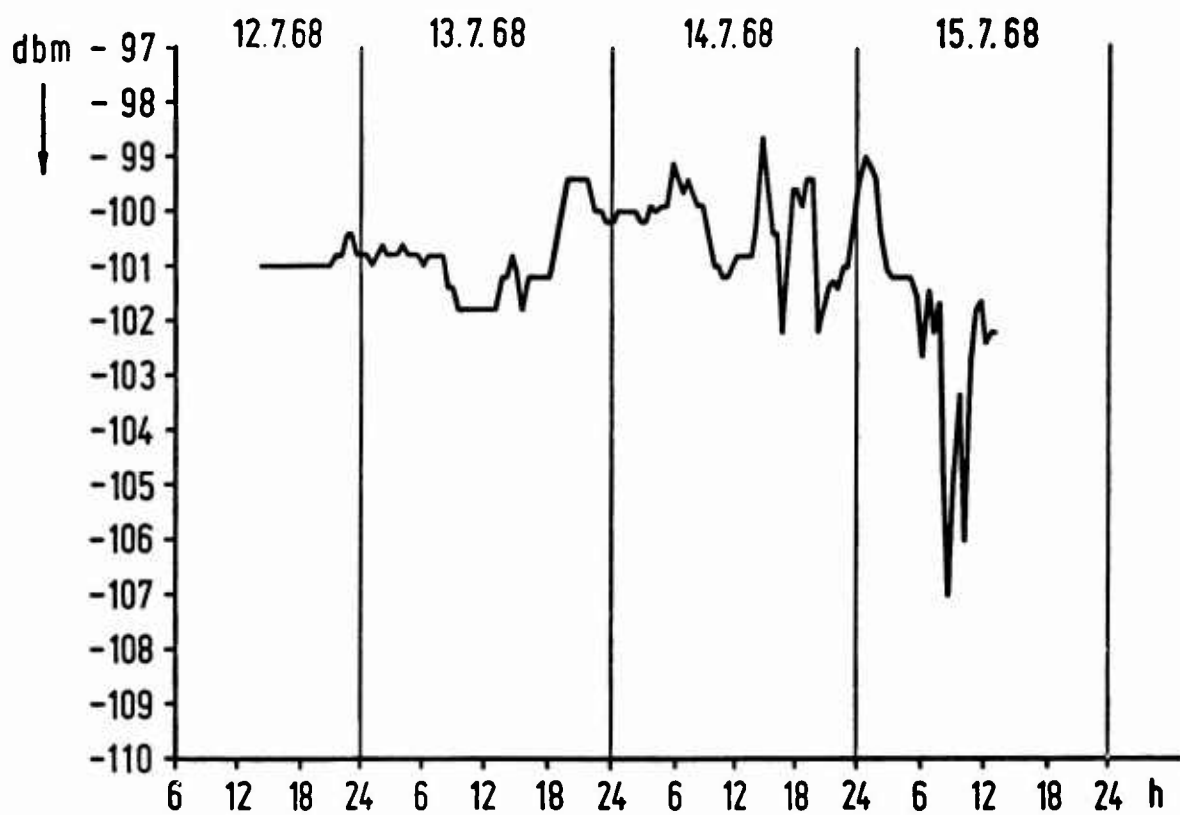


Fig.6 Average power received versus time at Werthhoven

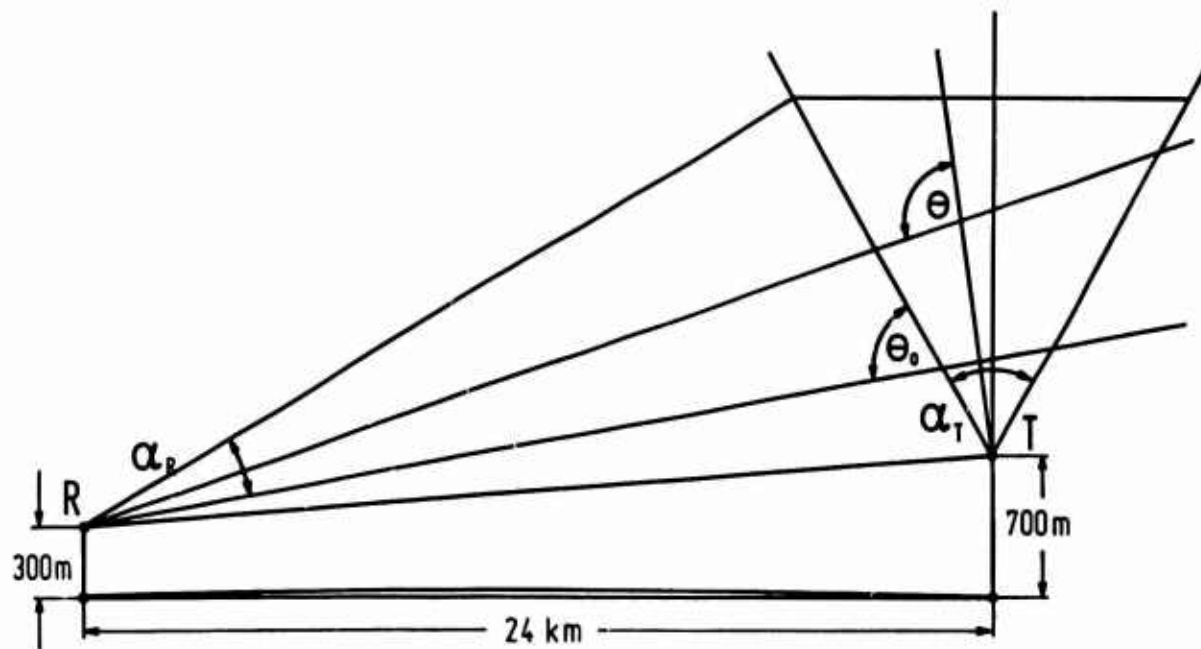


Fig.7 Tropospheric scattering geometry

25-8

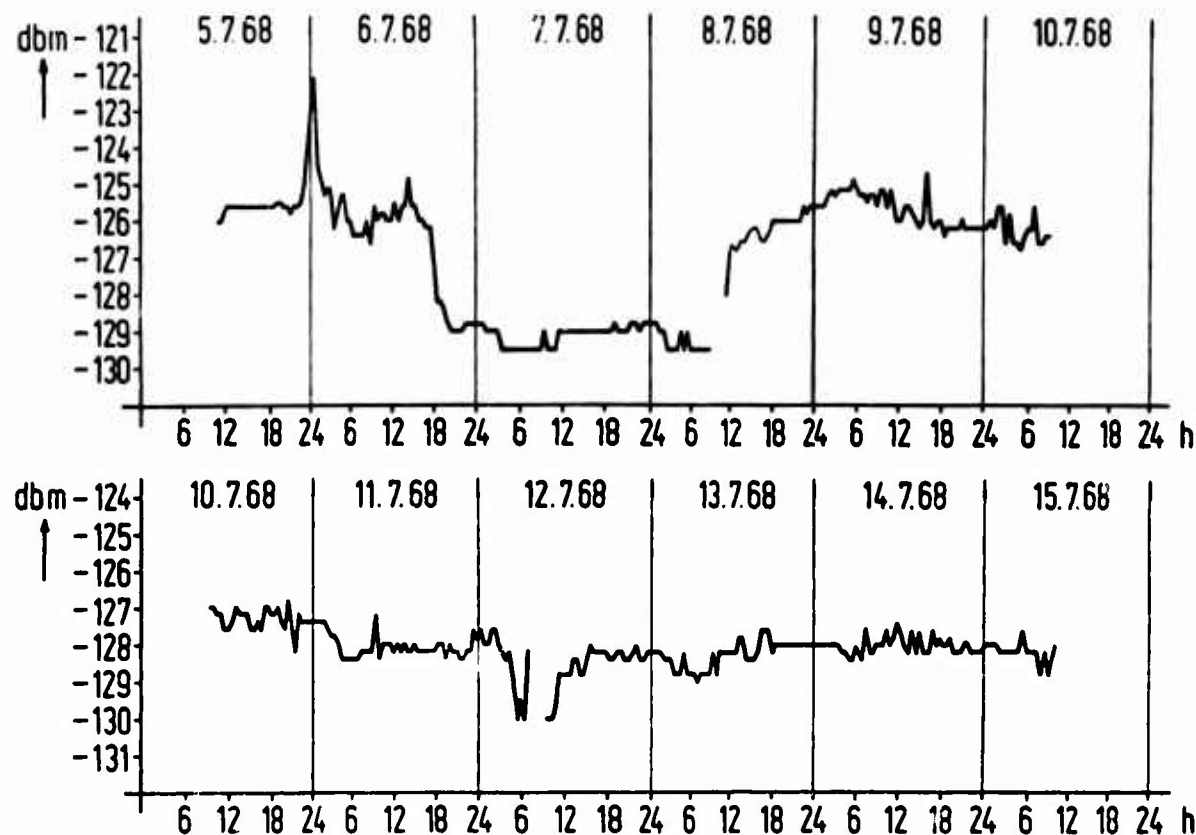


Fig. 8 Average power received versus time at Staffel

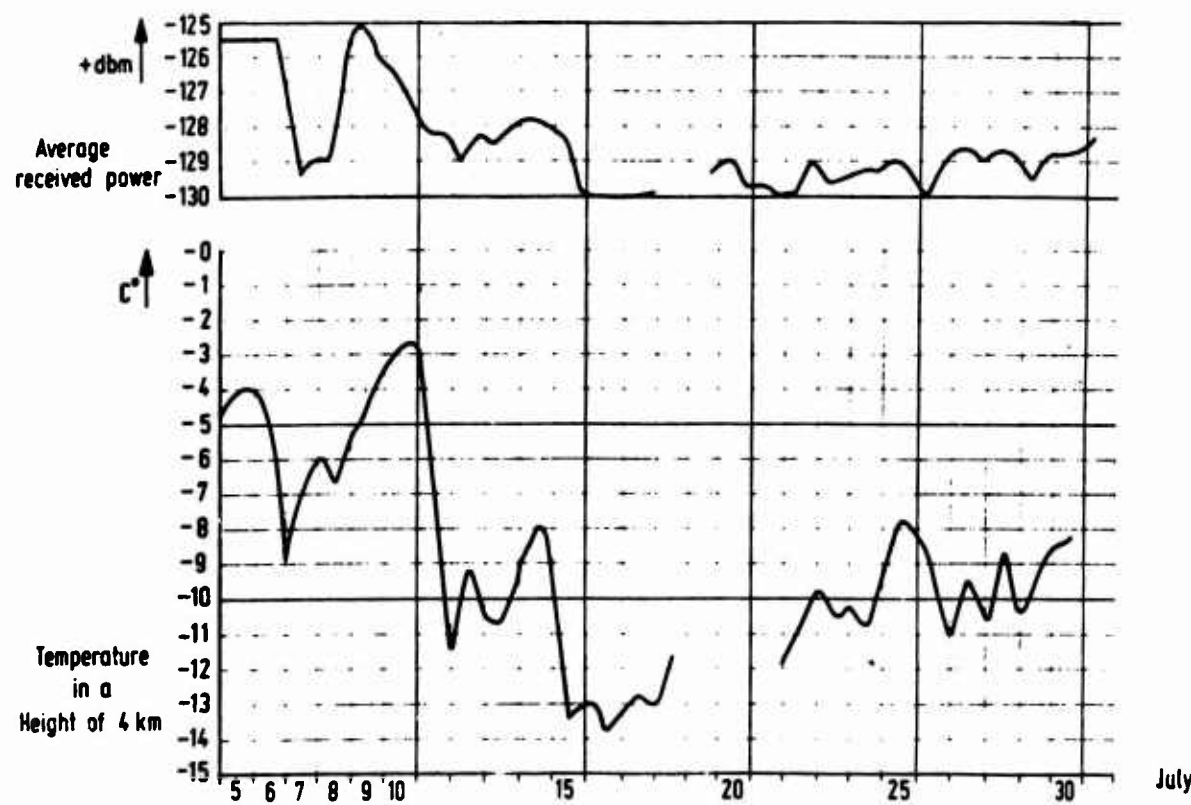


Fig. 9 Comparison of the temperature in the scatter volume and the average power received

**NOTES ON THE THEORY OF TROPOSCATTER MODULATION DISTORTION**

by

**A. Wasiljeff**

Department of Information Processing,  
Forschungsinstitut für Hochfrequenzphysik - FHP  
5321 Werthhoven, nr. Bonn  
Federal Republic of Germany

This work was sponsored by the Ministry of Defence, Federal Republic of Germany, under  
Research Contract No. T 833-1-203 and is published with the Ministry's permission.

## SUMMARY

Intermodulation distortion caused by tropospheric effects can be calculated either by the theory of Beach and Trecker, assuming one weak echo, or by the multi-echo theory of Sunde. A compromise between these conflicting theories seems to be Bremmer's "few echoes" theory published some years before the two papers just mentioned. It deals with the distortion of FM modulation waves by a tropospheric scatter mechanism of the Booker-Gordon type.

The present paper gives a generalisation of the theory including autocorrelation functions of the Norton type. The scattered field of modulated waves can be described with the help of a six-fold integral including the statistical parameters of the dielectric constant. The evaluation of this integral leads to a convenient approximation:

The field at the receiver may be considered as being made up of a small number of components which show unequal amplitudes and different delays with respect to the component arriving first.

A physical interpretation of this mathematical approximation shows a main signal followed by one strong and several weak echoes. This point of view may give a simple explanation of a negative correlation between field strength received and intermodulation, which cannot be explained by either the one-weak-echo theory or the multi-echo theory.

The frequency-multiplex signal is represented by a pre-emphasized band-limited Gaussian noise. The aim of this paper is to calculate the intermodulation of such a signal caused by the tropospheric effects described. For this purpose Sunde's formula which gives the second-order distortion of pre-emphasized noise in a closed form is generalised to third- and fourth-order distortion.

## NOTES ON THE THEORY OF TROPOSCATTER MODULATION DISTORTION

A. Wasiljeff

## 1. INTRODUCTION

Many investigations of the tropospheric scatter propagation of monochromatic radio waves have been reported. Though it is formally possible to obtain any complicated signal by Fourier analysis, if the spectral behaviour of the system is known, there is still a need for special investigation of signals that are modulated in a more complicated manner. Only a few papers deal with the intermodulation distortion of troposcatter links that are used for multi-channel telephony.

In the present paper we consider troposcatter systems in which the composite signal wave from a group of carrier telephone channels in frequency-division multiplex is transmitted by frequency modulation.

The multiplex system can be represented in an idealized form. For a sufficiently large number of channels the signal can be replaced for calculation and test purposes by a band of pre-emphasized Gaussian noise. Such a random noise signal simulates a composite speech signal.

For studies of interchannel-modulation distortion, the input energy corresponding to some particular speech channel is removed. The received output of the originally clear channel represents the intermodulation distortion.

Some years ago Beach and Trecker<sup>1</sup> described a method for predicting the magnitude of interchannel modulation in frequency-modulated troposcatter systems. They stated that the geometry of a tropospheric scatter path suggests a multi-path problem, and that components of the signal reflected from successively higher points in the atmosphere are delayed behind the earliest arriving component.

These echoes are the cause of the distortion occurring in the FM transmission of frequency-division multiplex, which adds to other distortion energy generated by nonlinearities in equipment. To facilitate calculations Beach and Trecker adopted the "one-weak-echo" theory of Bennet, Curtis and Rice<sup>2</sup>, omitting the multi-path transmission model.

The one-weak-echo theory was originally devised to estimate the interchannel interference due to echoes with small amplitudes caused by mismatched lines. Extrapolating these results, Beach and Trecker calculated the troposcatter modulation distortion caused by a single so-called "worst" echo. They added empirical corrections based upon comparison of calculated values with experimental measurements. A further approach was suggested by Sunde<sup>3</sup>. He regarded the received wave as a multiplicity of sine wave components arriving over many transmission paths with varying amplitudes and phases. With the aid of methods similar to those used in the analysis of the statistical properties of random noise, Sunde calculated the probability distribution of quadratic phase distortions for phase non-linearity of random multi-path transmission. On this premise he determined the intermodulation distortion in FM multiplex troposcatter systems.

The multi-echo theory of Sunde yields results that are similar to those obtained by the one-weak-echo theory of Beach and Trecker in spite of the difference of the assumed physical mechanisms. A compromise between these contradicting theories seems to be Bremmer's "few-echoes theory" published some years before the two previous papers mentioned<sup>4</sup>. It deals with the distortion of frequency modulated waves by a tropospheric scatter mechanism of the Booker-Gordon type<sup>5</sup>.

The present paper gives a generalisation of Bremmer's theory, including autocorrelation functions of the Norton type<sup>6</sup>.

## 2. GENERALISATION OF BREMMER'S THEORY

If the electromagnetic field of the transmitter is assumed to have a time dependence  $f(t)$ , the field which reaches the receiver after having been scattered by any tropospheric volume element will have the time dependence

$$f[t - (R_1 + R_2)/c] = f[t - \tau(P)] , \quad (1)$$

where  $R_1$  denotes the distance from the transmitter to the volume element,  $R_2$  the distance from the volume element to the receiver, and the argument  $t - \tau(P)$  expresses the delay conditioned by the path from the transmitter to the scattering volume element and from there to the receiver.

Let  $\Delta\epsilon$  be the local deviation of the dielectric constant,  $dV$  the volume element. If we exclude the contributions due to successive scatterings by more than one volume element, i.e. restriction to single scattering, we may write for the Hertz field at the receiving point

$$\Pi = \frac{1}{4\pi\epsilon_0 R_1 R_2} \iiint \Delta\epsilon(P) f[t - \tau(P)] dV , \quad (2)$$

where the integration is performed over the scattering volume. The corresponding field of the electric vector may be obtained by existing methods<sup>7</sup>. For the following study of phase distortion and intermodulation it is sufficient to consider formula (2).

The mean square of (2) shows the dependence of the scattered field on the spatial auto-correlation function of the dielectric constant.

$$B(r) = \langle \Delta\epsilon(P)\Delta\epsilon(P') \rangle \quad (3)$$

$$\begin{aligned} \langle \Pi^2 \rangle &= \text{constant} \times \left\langle \iiint \Delta\epsilon(P)f[t - \tau(P)] dV \iiint \Delta\epsilon(P')f[t - \tau(P')] dV' \right\rangle \\ &= \iiint \left\{ \iiint B(r)f[t - \tau(P')] dV' \right\} f[t - \tau(P)] dV . \end{aligned} \quad (4)$$

In this manner the scattered field of modulated waves can be described with the help of a six-fold integral including the statistical parameters of the dielectric constant.

The integral may be evaluated with the aid of the following approximations:

Because of the large distances in scatter propagation the scattering volume proves to be concentrated near the mid-plane between receiver and transmitter and the scattering volume dimensions may be considered as small compared with the distances  $R_1$  and  $R_2$ .

The rapid decrease of the autocorrelation function allows us to extend the integration limits of the inner integral in Equation (4).

We assume the scattering space to be isotropic and its statistical properties to be homogeneous with respect to time.

Using the well-known Fourier relation between autocorrelation function and spectral density

$$\phi(k) = \frac{1}{(2\pi)^3} \iiint \cos(kr) B(r) dV , \quad (5)$$

and assuming a time dependence of the signal in the form

$$f(t) = \cos[\Omega_c t + \varphi(t)] , \quad (6)$$

we finally get

$$J = \text{constant} \times \iiint f^2[t - \tau(P)] \phi\left(\frac{\Omega_c}{c} 2 \sin \frac{\theta}{2}\right) dV . \quad (7)$$

In the case of the Booker-Gordon correlation we get from Equation (7) the results given by Bremmer (formula (16) of Reference 4). Since the Norton correlation function<sup>6</sup> has some properties which describe the physical situation of inhomogeneities in a turbulent flow, we shall use it in the calculations presented in this paper.

Introducing a delay time function analogous to that defined by Bremmer, we can write the integral (7) as a convolution product of this function and the time function  $f^2(t)$ .

$$J = \text{constant} \times \int_{-\infty}^{+\infty} D(x) f^2(t-x) dx , \quad (8)$$

where the distortion function is given by

$$D(t) = \iiint \delta[(t - \tau(P))] \phi\left(\frac{\Omega_c}{c} 2 \sin \frac{\theta(P)}{2}\right) dV \quad (9)$$

and  $\delta(t)$  denotes the Dirac function.

The Fourier transform of Equation (8) yields the product of the corresponding spectra of  $f^2(t)$  and Equation (9). The resulting integral can be evaluated using the method of stationary phase and other asymptotic methods similar to that given in Reference 4.

The evaluation leads to a convenient approximation. The field at the receiver may be considered as being made up of a small number of components which show unequal amplitudes and different delays with respect to the component arriving first.

The delay times depend on the geometry of the scattering volume. The amplitudes determining the relative weights of the various delayed contributions are composed of a geometrical factor and of another factor which depends on the assumed behaviour of the dielectric constant. Thus we have, from (7),

$$J = \text{constant} \times \{ r_0 \cos[2\Omega_c(t-t_0) + 2\varphi(t-t_0)] + \\ + r_1 \cos[2\Omega_c(t-t_1) + 2\varphi(t-t_1)] + r_2 \cos[2\Omega_c(t-t_2) + 2\varphi(t-t_2)] + \dots \} , \quad (10)$$

where  $\Omega_c$  denotes the carrier frequency,  $t_i$  the various delay times,  $r_i$  the echo amplitudes, and  $\varphi(t)$  the phase modulation of Equation (6).

After tedious calculations, similar to those given by Bremmer<sup>4</sup> we finally obtain, for the first echoes,

$$\left. \begin{aligned} R_1 &= \frac{-2\left(1 + \frac{2\psi}{\theta}\right)^{\frac{1}{2}}}{\left(1 + \frac{\psi}{\theta}\right)^2} \left\{ \begin{aligned} &\left( \frac{1 + \frac{\Omega^2}{c^2} l_0^2 \theta^2}{1 + \frac{\Omega^2}{c^2} l_0^2 (\theta + \psi)^2} \right)^n \\ &\left( \frac{1 + \frac{\Omega^2}{c^2} l_0^2 \theta^2}{1 + \frac{\Omega^2}{c^2} l_0^2 (\theta + 2\psi)^2} \right)^n \end{aligned} \right\} \\ R_2 &= \frac{1}{\left(1 + \frac{2\psi}{\theta}\right)^3} \end{aligned} \right\} \quad (11)$$

$$T_1 = \frac{a \theta^2 \psi}{c 4}; \quad T_2 = \frac{a \theta}{c 2} (\theta \psi + \psi^2), \quad (12)$$

where we have introduced relative echoes  $R_1 = r_1/r_0$  and difference delay times  $T_1 = t_1 - t_0$ ;  $a$  is the modified earth radius,  $l_0$  the correlation length of the dielectric constant, and  $c$  the velocity of light. In the case of Norton correlation we have  $n = 11/6$ . The angles  $\theta$  and  $\psi$ , which are determined by the boundaries of the scattering volume, are illustrated in Figure 1. Since the influence of further echoes is only noticeable in higher order corrections we may neglect them in a first-order approximation.

For a numerical example we choose  $\theta = 0.041$  radian,  $\psi = 0.0235$  radian,  $l_0 = 1.5$  m, carrier frequency  $\Omega_c = 895$  MHz. Thus we obtain

$$T_1 = 0.22336 \mu\text{sec}, \quad T_2 = 0.70277 \mu\text{sec},$$

$$R_1 = -0.3863, \quad R_2 = 0.01302.$$

The distortion by scatter propagation transforms the frequency-modulated signal into various contributions, each of which is undistorted but is characterised by a specific delay time. We notice that the first calculated echo amplitude is not small, contrary to the assumption of Beach and Trecker; on the other hand, there is a rapid decrease of terms in the expansion in question; therefore we can confine ourselves to some few echoes, neglecting terms of higher order. Thus we have a compromise between the one-weak-echo theory of Beach and Trecker and the multi-echo theory of Sunde.

### 3. COMPUTATION OF DISTORTION

The final computation of the distortion in the case of FM is based on the assumption that the differences of the delay times are small compared with the reciprocal central frequency of the low-frequency modulation function, i.e., the relative change of the low-frequency modulation function is small over the difference-delay intervals in question. However, there will be no restriction on the magnitude of the amplitude of the various echoes.

The distortion proves to be equivalent to that due to the passage of the undistorted signal through a network with a non-linear phase characteristic.

$$\phi_d(t) = a_0 + a_1 M(t) + a_2 M^2(t) + a_3 M^3(t) + a_4 M^4(t) + \dots \quad (13)$$

$M(t)$  denotes the low frequency modulation function. From this formula we get the frequency-modulation distortion by differentiation:

$$M_d(t) = a_1 \frac{d}{dt} M(t) + a_2 \frac{d}{dt} M^2(t) + a_3 \frac{d}{dt} M^3(t) + a_4 \frac{d}{dt} M^4(t) + \dots \quad (14)$$

The coefficients  $a_n$  have been calculated from (10) with the aid of a digital computer. The calculation is briefly outlined in the Appendix. The rather complicated coefficients contain terms with harmonic functions of the large variable  $x = \Omega_c t_0$ , where  $\Omega_c$  denotes the carrier frequency and  $t_0$  the delay time caused by the distance from transmitter to the central point of scattering volume and from there to the receiver. We can replace this large variable in the argument of the sine or cosine functions in question by a random variable distributed uniformly in the interval  $0 \leq x \leq 2\pi$ . Averaging over many trials we finally get the mean values of the coefficients  $a_n$ . For our numerical example we obtain

$$a_2^2 = 3.906 \times 10^{-28} \text{ sec}^4, \quad a_3^2 = 3.744 \times 10^{-41} \text{ sec}^6, \quad a_4^2 = 4.598 \times 10^{-54} \text{ sec}^8.$$

On the premise of formulae (13) and (14), intermodulation noise in frequency modulation transmission can be evaluated. As already mentioned, the frequency-division-multiplex signal, generally used for transmission of voice channels, can be represented by a pre-emphasized band-limited Gaussian noise. Sunde<sup>3</sup> investigates a non-linear tropospheric phase characteristic, developed on other premises, neglecting distortion terms of orders higher than the second. However, he points out that results given by Rice<sup>8</sup> for random variables indicate that there is no correlation between the second- and third-order distortion term, so that distortion from the second-order term will combine on a power addition basis with distortion from the third-order term. Sunde emphasizes that there may be a negative correlation factor between the second- and fourth-order distortion terms. Hence the distortion produced by the fourth-order term will be subtracted on the average on an amplitude basis from the second-order distortion. Sunde presumes that the fourth-order distortion term may play an important role in reducing intermodulation noise as the effective frequency deviation is increased.

A formula of Sunde's which gives the second-order distortion of a pre-emphasized basic power spectrum in a closed form can be generalized to third- and fourth-order distortion. The corresponding formulae are given in the Appendix of this paper.

The autocorrelation function of the output phase distortion of Equation (13) is given by

$$\psi_{\text{output}}(\tau) = q_0 + q_1 \psi_{\text{in}}(\tau) + q_2 \psi_{\text{in}}^2(\tau) + q_3 \psi_{\text{in}}^3(\tau) + q_4 \psi_{\text{in}}^4(\tau) \quad (15)$$

The coefficients  $q_i$  are calculated from the coefficients  $a_i$  in the Appendix, using the characteristic function methods described by Rice<sup>8</sup>. The terms  $q_2$ ,  $q_3$  and  $q_4$  cause second-, third- and fourth-order distortion of the corresponding baseband power spectrum.

The output power spectrum of Equation (15) can be obtained with the aid of the Wiener-Kinchin theorem. Figure 2 shows the power spectra of second-, third- and fourth-order distortion corresponding to a baseband spectrum with 10 dB pre-emphasis. For the numerical example of the tropospheric scatter path described above, the signal to intermodulation ratio has been calculated in the top channel as a function of the root-mean-square frequency deviation. It is shown in Figure 3.

The inserted measured values are results from a similar troposcatter test link between Leiselheim and Werthhoven. They are used with the kind permission of Mr. Albrecht and Dr Schmitt. A comparison shows fairly good agreement, which lies inside the usual limits of troposcatter theories and measurements. A more detailed analysis which takes into consideration the lack of symmetry of the tropospheric scatter volume may give further information.

#### 4. CORRELATION BETWEEN FIELD STRENGTH AND INTERMODULATION DISTORTION

The great advantage of the few-echoes theory outlined in this paper is an explanation of a correlation between field strength and signal-to-intermodulation ratio which cannot be obtained by either the one-weak-echo theory or the multi-echo theory.

Beach and Trecker try to explain the observed correlation between intermodulation and path loss, i.e., a negative correlation between field strength and intermodulation, by assuming that minimum refractivity corresponds to minimum bending of radio waves, that yields maximum time delay for an echo of given amplitude and therefore maximum intermodulation. This argument, which may be valid for an average value of intermodulation and field strength taken over a long time period, cannot explain the observed correlation between short-time fading of field intensity and signal-to-intermodulation ratio.

However, from the theory presented in this paper, we can calculate the momentary field intensity and signal-to-intermodulation ratio.

The author believes that the short time variation of received field intensity and intermodulation can be explained by random variation of the large variable  $x = \Omega_c t_1$  in the argument of the sine and cosine functions used in the calculations of the few-echoes theory. To prove this conjecture many thousand trials of calculation of signal-to-intermodulation ratio and field strength have been performed on a digital computer simulating the random variation of  $x$  by a random variable distributed uniformly in the interval  $0 < x < 2\pi$ . Figure 4 shows a partial sketch of the calculated simulation. The expected correlation of field strength and signal-to-intermodulation ratio is evident. Calculation from some thousand trials yields a correlation coefficient of 0.7, which is in very good agreement with the correlation coefficient 0.72 measured by Schmitt on the troposcatter test link between Leiselheim and Werthhoven<sup>9</sup>.

#### ACKNOWLEDGMENTS

The author wishes to thank Prof. H. Bremmer and Prof. G. Eckart for helpful comments and suggestions, and to acknowledge preparation of the manuscript by Mr Niephaus and Miss Fassbender.

## APPENDIX

## A1. Coefficients of Nonlinear Phase Characteristic

Equation (14) can be written in the form

$$\left. \begin{aligned} M_d(t) &= \left( \frac{d}{dt} M(t) \right) \{ a_1 + 2a_2 M + 3a_3 M^2 + 4a_4 M^3 + \dots \} \\ &= - \left( \frac{d}{dt} M(t) \right) \{ b_0 + b_1 M + b_2 M^2 + b_3 M^3 + \dots \} \end{aligned} \right\} \quad (A1)$$

We can also write Equation (10) as

$$\sum_{i=1}^N r_i \cos \phi_i = A \cos(\phi_0 + \phi_d), \quad (A2)$$

where we have written, for abbreviation,

$$\phi_i = 2\Omega_c(t-t_i) + 2\varphi(t-t_i).$$

From Equation (A2) we obtain

$$\phi_0 + \phi_d = \arctan \frac{\sum_{i=0}^N r_i \sin \phi_i}{\sum_{i=0}^N r_i \cos \phi_i}. \quad (A3)$$

Differentiation yields

$$2\Omega_c + 2M + 2M_d = \frac{\sum_{i=0}^N \sum_{k=0}^N r_i r_k \frac{d\phi_k}{dt} \cos(\phi_k - \phi_i)}{\sum_{i=0}^N \sum_{k=0}^N r_i r_k \cos(\phi_k - \phi_i)}. \quad (A4)$$

Assuming, that the relative change of the low frequency modulation function  $M(t)$  is small over the delay intervals in question we can approximate as follows:

$$\frac{d\phi_k}{dt} \approx 2\Omega_c + 2M - 2t_k \frac{dM}{dt}. \quad (A5)$$

Thus we obtain from Equation (A4)

$$M_d(t) = \left( \frac{d}{dt} M \right) \cdot \frac{\sum_{i=0}^N \sum_{k=0}^N r_i r_k t_k \cos(\phi_i - \phi_k)}{\sum_{i=0}^N \sum_{k=0}^N r_i r_k \cos(\phi_i - \phi_k)}. \quad (A6)$$

Comparison of (A1) and (A6), yields the form

$$b_0 + b_1 M + b_2 M^2 + b_3 M^3 = \frac{c_0 + c_1 M + c_2 M^2 + c_3 M^3}{d_0 + d_1 M + d_2 M^2 + d_3 M^3} , \quad (A7)$$

which yields

$$\begin{aligned} b_0 &= \frac{c_0}{d_0} ; & b_1 &= \frac{1}{d_0} (c_1 - b_0 d_1) ; \\ b_2 &= \frac{1}{d_0} (c_2 - b_1 d_1 - b_0 d_2) ; & b_3 &= \frac{1}{d_0} (c_3 - b_2 d_1 - b_1 d_2 - b_0 d_3) . \end{aligned}$$

Thus we can calculate the coefficients  $a_1$  of Equation (A1). The coefficients  $c_n$  and  $d_n$  are given by

$$\left. \begin{aligned} c_n &= \sum_{i=0}^N \sum_{k=0}^N r_i r_k t_k \frac{1}{n!} 2^n (t_i - t_k)^n \cos \left( 2\Omega_c (t_i - t_k) + \frac{n\pi}{2} \right) \\ d_n &= \sum_{i=0}^N \sum_{k=0}^N r_i r_k \frac{1}{n!} 2^n (t_i - t_k)^n \cos \left( 2\Omega_c (t_i - t_k) + \frac{n\pi}{2} \right) . \end{aligned} \right\} \quad (A8)$$

## A2. Higher Order Distortion of a Bandlimited Power Spectrum with Pre-Emphasis

Formula (15) describes the output autocorrelation function of a non-linear phase characteristic. The coefficients  $q_i$  can be calculated by a method described by Rice<sup>8</sup> using the characteristic function of normal noise, which yields the higher moments of the distribution necessary for the calculation of  $\psi_{\text{output}}$ . The resulting relation between the coefficients  $q_i$  and  $a_i$  is

$$\begin{aligned} q_2 &= 2a_2^2 + 24a_2 a_4 \psi_{in}(0) + 72a_4^2 \psi_{in}^2(0) , \\ q_3 &= 6a_3^2 , \quad q_4 = 24a_4^2 ; \end{aligned} \quad (A9)$$

Since the output power spectrum of (15) is obtained with the aid of the Wiener-Khinchin theorem by Fourier integration, we get the corresponding power spectra of  $n^{\text{th}}$  order distortion by  $n$ -fold convolution of the baseband power spectrum. The output power spectrum corresponding to Equation (14) can be obtained from the calculated spectrum by multiplication with the square of the corresponding frequency.

Assuming pre-emphasized bandlimited Gaussian noise the background spectrum is given by

$$\left. \begin{aligned} p(x) &= k(1+cx^2) & \text{if} & \quad |x| < 1 \\ p(x) &= 0 & \text{otherwise} . \end{aligned} \right\} \quad (A10)$$

with  $x = f/f_g$  being the limitation of frequency band. The convolutions of (A10) may be performed graphically or numerically. Sunde has given a closed expression of the first convolution, corresponding to second-order distortion<sup>3</sup>. This may be generalized to third- and fourth-order distortion.

$p_n$  being the  $n^{\text{th}}$  convolution of (A10) we have, assuming an even power spectrum  
 $p(x) = p(-x)$ ,

$$\left. \begin{aligned} p_2(x) &= p(x)*p(x) = \frac{k^2}{2} \sum_{i=1}^5 d_i x^i && \text{if } 0 \leq x \leq 2 \\ &= 0 && \text{if } x \geq 2, \end{aligned} \right\} \quad (\text{A11})$$

with

$$d_0 = 2 + \frac{4}{3}c + \frac{2}{5}c^2, \quad d_1 = -(1 + 2c + c^2),$$

$$d_2 = 2c + \frac{2}{3}c^2, \quad d_3 = -\frac{2}{3}c, \quad d_4 = 0, \quad d_5 = -\frac{c^2}{30}.$$

$$\left. \begin{aligned} p_3(x) &= p_2(x)*p(x) = \frac{k^3}{4} \sum_{v=0}^5 d_v \sum_{m=0}^{v+3} A_{mv} x^m + B_{mv} x^{m+1} + C_{mv} x^{m+2} && \text{if } 0 \leq x \leq 1 \\ &= \frac{k^3}{4} \sum_{v=0}^5 d_v \left\{ P - Q_v x + R_v x^2 + \sum_{m=0}^{v+3} (-1)^m G_{mv} x^m + (-1)^{m+1} E_{mv} x^{m+1} + \right. \\ &\quad \left. + (-1)^{m+1} F_{mv} x^{m+2} \right\} && \text{if } 1 \leq x \leq 3 \\ &= 0 && \text{if } x \geq 3, \end{aligned} \right\} \quad (\text{A12})$$

with

$$A_{mv} = [(-1)^m + 1] \left[ \binom{v+1}{m} \frac{1}{v+1} + \binom{v+3}{m} \frac{c}{v+3} \right],$$

$$B_{mv} = \frac{2c}{v+2} \binom{v+2}{m} [(-1)^m - 1],$$

$$C_{mv} = \frac{c}{v+1} \binom{v+1}{m} [(-1)^m + 1],$$

$$P_v = \left[ \frac{(-2)^{v+1}}{v+1} + \frac{(-2)^{v+3}}{v+3} c \right], \quad Q_v = \frac{2c}{v+2} (-2)^{v+2},$$

$$R_v = -\frac{c}{v+1} (-2)^{v+1},$$

$$G_{mv} = \left( \frac{1}{v+1} \binom{v+1}{m} + \frac{c}{v+3} \binom{v+3}{m} \right),$$

$$E_{mv} = -\frac{2c}{v+2} \binom{v+2}{m}, \quad F_{mv} = \frac{c}{v+1} \binom{v+1}{m}.$$

$$p_4(x) = p_3(x) * p(x) = \frac{k^4}{8} \sum_{v=0}^5 d_v S_v \quad (A13)$$

$$\begin{aligned} S_v &= \sum_{\mu=1}^5 \left\{ u_{\mu v} ((-1)^\mu - (-1)^\mu (1+x)^\mu) + \sum_{m=0}^{v+3} [v_{\mu m v} ((-1)^{m+\mu} - (-1)^{m+\mu} (1+x)^{m+\mu}) + \right. \\ &\quad \left. + \omega_{\mu m v} ((1-x)^{m+\mu} - (-1)^{m+\mu})] \right\} \quad \text{if } 0 \leq x \leq 2 \\ S_v &= \sum_{\mu=1}^5 \left\{ u_{\mu v} (1-x)^\mu - (-3)^\mu \right\} + \sum_{m=0}^{v+3} v_{\mu m v} ((1-x)^{m+\mu} - (-3)^{\mu+m}) , \quad \text{if } 2 \leq x \leq 4 \\ S_v &= 0 \quad \text{if } x \geq 4 , \end{aligned}$$

with

$$\begin{aligned} u_{1v} &= P_v (1 + cx^2) , \quad u_{2v} = \left[ \frac{Q_v}{2} (1 + cx^2) + cx P_v \right] , \\ u_{3v} &= \left[ \frac{R_v}{3} (1 + cx^2) + \frac{P_v}{3} c + \frac{2}{3} cx Q_v \right] , \quad u_{4v} = \frac{c Q_v}{4} + cx \frac{R_v}{2} , \quad u_{5v} = \frac{c R_v}{5} , \\ v_{1mv} &= G_{mv} (1 + cx^2)/(m+1) , \quad v_{2mv} = [E_{mv} (1 + cx^2) + 2cx G_{mv}] / (m+2) , \\ v_{3mv} &= [F_{mv} (1 + cx^2) + c G_{mv} + 2cx E_{mv}] / (m+3) , \\ v_{4mv} &= (c E_{mv} + 2cx F_{mv}) / (m+4) , \quad v_{5mv} = c F_{mv} / (m+5) , \\ \omega_{1mv} &= (1 + cx^2) A_{mv} / (m+1) , \quad \omega_{2mv} = [B_{mv} (1 + cx^2) + 2cx A_{mv}] / (m+2) , \\ \omega_{3mv} &= [c A_{mv} + (1 + cx^2) C_{mv} + 2cx B_{mv}] / (m+3) , \\ \omega_{4mv} &= (c B_{mv} + 2cx C_{mv}) / (m+4) , \quad \omega_{5mv} = c C_{mv} / (m+5) . \end{aligned}$$

Although the formulae given in the Appendix may look quite complicated, they considerably facilitate calculations. For example, the direct numerical integration of the convolutions of the baseband power spectrum with 10 dB pre-emphasis, took about three-quarters of an hour, with the aid of a digital computer, whereas a calculation based on the formulae presented here, was done in a few minutes. Moreover, we can calculate the convolution of any desired pre-emphasis with the aid of these formulae.

## REFERENCES

1. Beach, C.D.  
Trecker, J.M.  
*A Method for Predicting Interchannel Modulation Due to Multi-path Propagation in FM and PM Tropospheric Radio Systems.* Bell Systems Technical Journal, Vol. 42, January 1963, pp. 1-36.
2. Bennett, W.R.  
et al.  
*Interchangeable Interference in FM and PM Systems under Noise Loading Conditions.* Bell Systems Technical Journal, Vol. 34, May 1955, pp. 601-635.
3. Sunde, E.D.  
*Intermodulation Distortion in Analog FM Troposcatter Systems.* Bell Systems Technical Journal, Vol. 35, January 1964, pp. 399-437.
4. Bremmer, H.  
*Distortions in Tropospheric Scatter Propagation.* Philips Telecommunication Review, Vol. 18(3), 1957, pp. 137-154.
5. Booker, H.G.  
Gordon, W.E.  
*A Theory of Radio Scattering in the Troposphere.* Proceedings, Institute of Radio Engineers, Vol. 40, 1950, p. 401.
6. Norton, K.A.  
*Carrier Frequency Dependence of the Basic Transmission Loss in Tropospheric Forward Scatter Propagation.* Journal of Geophysical Research, Vol. 65, 1960, p. 2029.
7. Eckart, G.  
*Über die Streuung elektrischer Wellen an Zonen dielektrischer Turbulenz.* Bayerische Akademie der Wissenschaften, Heft 76.
8. Rice, S.O.  
*Mathematical Analysis of Random Noise.* Bell Systems Technical Journal, Vol. 23, 1944, p. 282 and Vol. 24, 1945, p. 46.
9. Schmitt, F.  
*Über Intermodulationsmessungen bei troposphärischer Streuausbreitung.* National URSI Convention, Germany, 1967. Kleinheubacher Berichte, Bd. Nr. 12, 1967, pp. 139-145.

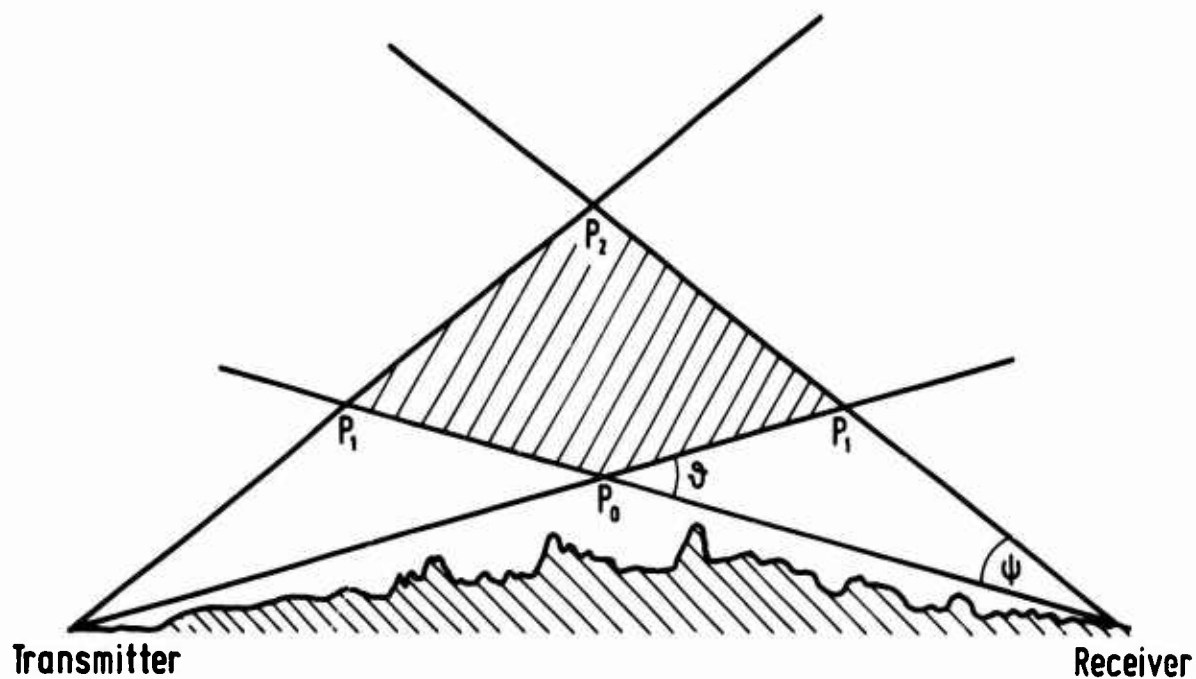
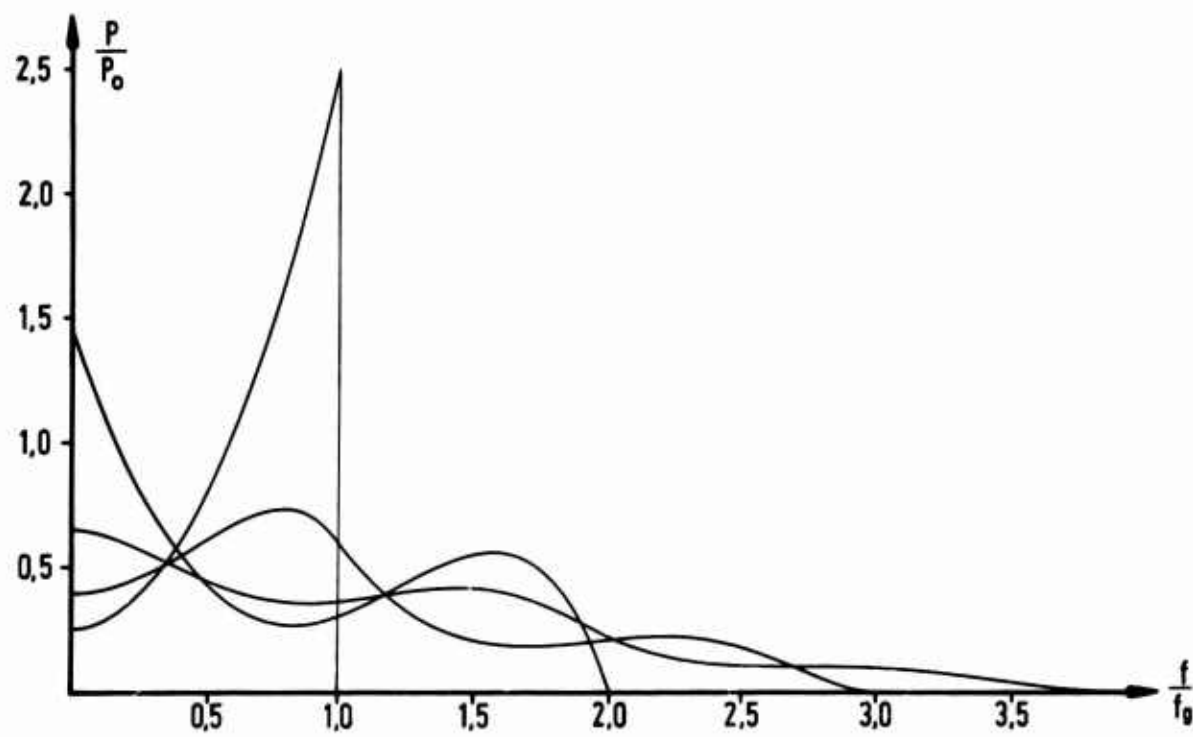


Fig. 1 Idealised tropospheric scattering volume

Fig. 2 Power-spectra obtained by convolutions of a base-band spectrum  
with 10 dB pre-emphasis

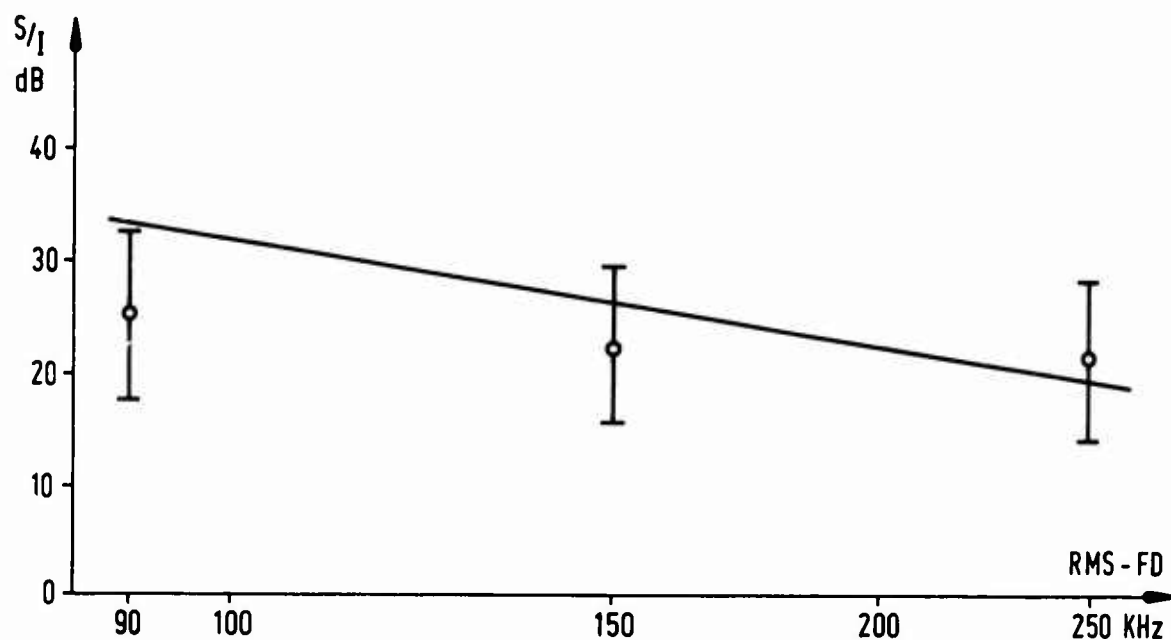


Fig. 3 Signal-to-intermodulation ratio versus root-mean-square frequency deviation

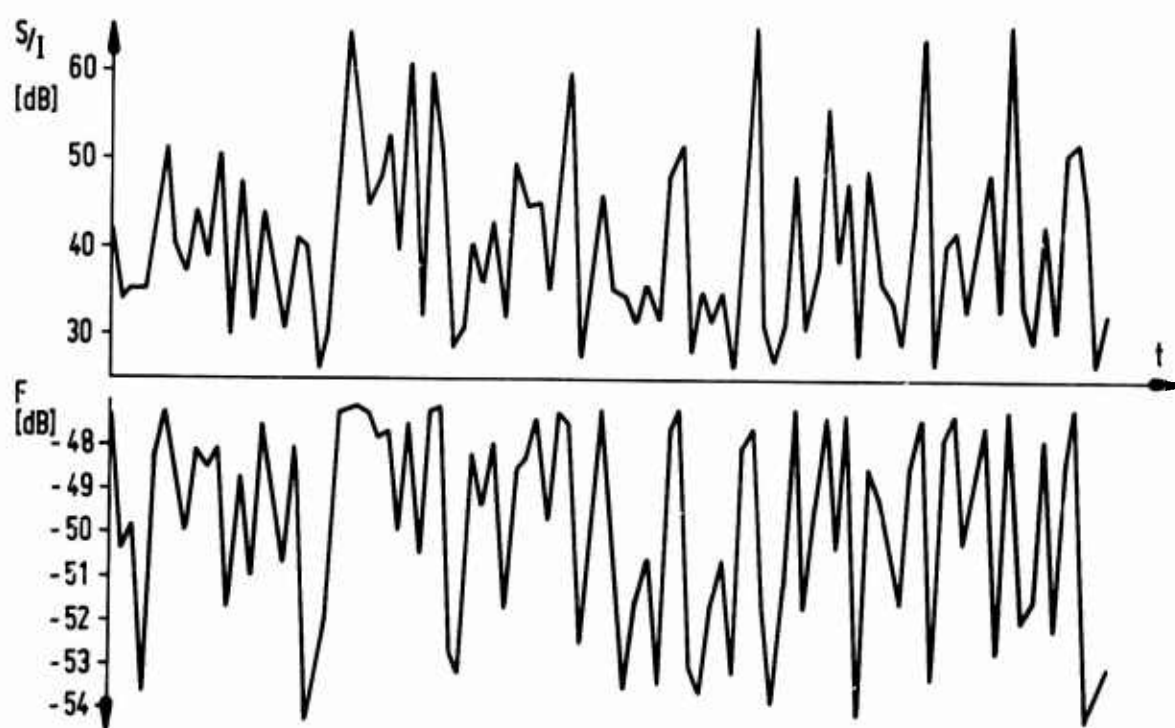


Fig. 4 Signal-to-intermodulation ratio, S/I, and field intensity F

### DISCUSSION ON PAPERS PRESENTED IN SESSION III (TROPOSPHERIC SCATTER)

*Discussion on Paper 15: "Scattering of radio waves from regular and irregular time varying refractive index structures in the troposphere", by D.T.Gjessing.*

**Dr H.N.Kritikos:** Do you, Dr Gjessing, have any evidence that the assumption of the homogeneous turbulence necessary for the derivation of the Oboukhov spectrum is valid? Is there any evidence that the frequency dependence of the scattering cross-section favours any one of the proposed models?

**Dr D.T.Gjessing:** Our experiments show that in general the atmospheric structure is neither homogeneous nor isotropic. Within a limited spatial region (scattering volume when this is small), however, the structure is probably sufficiently homogeneous to permit use being made of Oboukhov's results. Similarly, in most of the cases the isotropy properties are such that one would not expect to introduce a large error when writing  $E(K) = 4\pi K^2 \Phi(K)$ . This means that the Oboukhov  $K^{-5/3}$  one-dimensional spectrum gives rise to a  $K^{-11/3}$  three dimensional spectrum which is the one measured in radio experiments. As pointed out in my survey paper, we measure  $\Phi(K)$  directly in beamswinging experiments, and if  $\Phi(K) \sim K^{-n}$ , then the wavelength dependence of the scattering cross-section  $\sim \lambda^{n-4}$ . Our beamswinging experiments show that the median value of  $n$  is  $11/3$ . The exponent  $n$  is, however, strongly dependent on atmospheric stability.

*Discussion on Paper 16, "Theoretical analysis of medium-dependent fluctuations with tropospheric scatter links, and comparison with new experimental data, including side-scatter characteristics", by H.J.Albrecht.*

**Dr E.N.Bramley:** You mentioned, Dr Albrecht, the importance of multiple scatter under conditions when the scale length of turbulence is sufficiently reduced. Does this mean that single scatter theory is then inadequate to explain the experimental data?

**Dr H.J.Albrecht:** For many scatter links, the influence of multiple scatter is negligible. However, in a very general sense, multiple scattering may have an effect upon the relationship between intermodulation and field strength, as shown by published data under certain conditions.

**Dr Gerda Fengler:** Dr Albrecht, you have found a correlation between signal decrease and age of passing cold fronts. I should be interested to know (a) if there exists a dependence on the direction in which the cold fronts are passing over the radio link and (b) what is the correlation coefficient between the two parameters (signal decrease and age of passing cold front)?

**Dr H.J.Albrecht:** Not possessing means of steering the direction of cold fronts, we have to accept what the troposphere offers, and that is a predominantly West-to-East direction for 90% of the cases observed since 1965. With regard to your second question, reference is made to one of my earlier publications (Reference 4 in my paper) for the exact value, the order of magnitude being 0.8 to 0.9.

**Dr N.C.Gerson:** Several general comments may be made about the sizes of the irregularities allowing tropospheric scatter. Neglect for the moment frontal effects and consider only the average size distribution. The spectrum of available sizes undoubtedly is a function of the air masses involved. Arctic or cold polar air masses undoubtedly have median irregularity sizes which are appreciably smaller than those in equatorial air masses. Over equatorial ocean areas irregularities of large size may be expected which persist for relatively long time periods because of the homogeneity of the underlying surface. The presence of this condition should allow the use of tropospheric scatter of lower frequencies and should permit scattering at lower radiated powers for longer periods of time.

*Discussion on Paper 19, "Wavelength dependence of microwave propagation far beyond the radio horizon," by F.Eklund.*

**Dr H.N.Kritikos:** I should like to ask Dr Eklund how the ratio between the two species is established. Is it very critical? Since rapid fluctuations arise from turbulent scattering, is it possible to differentiate between the two species by filtering techniques?

**Dr F.Eklund:** The ratio between the scattered and facet-reflected powers is mainly determined by the assumed relation between  $\Delta n$  and  $C_n^2$ . We have assumed a linear relationship between these parameters where the proportionality constant is determined from the maximum of observed values. It is not very critical, since the model is intended to describe average conditions. The spread of the experimental points about the theoretical line could, at least to some extent, be explained by a varying linear relationship between  $\Delta n$  and  $C_n^2$ . With regard to your second question, experiments have shown that the facet-reflected signals come approximately along the great circle path, while scattered signals come from a wider horizontal angular interval. This probably means that the fading characteristics are a little bit different and it could maybe offer a possibility of sorting out facet-reflected and scattered signals to some extent, by some kind of signal handling.

**Dr J.Ramasastri:** Could you please give a quantitative estimate of what the final result would be if one assumed a slightly different relationship between  $\Delta n$  and  $C_n^2$ ?

**Dr F.Eklund:** The scattered power is proportional to  $C_n^2$ , and the facet-reflected power is approximately proportional to  $\Delta n^2$ ; so, if you change the slope of the linear relationship between  $\Delta n$  and  $C_n^2$ , it is obvious how the power terms will change. For example, if we change the relation from  $\Delta n = 0.6 C_n^2 \times 10^{10}$  to  $\Delta n = 0.3 C_n^2 \times 10^{10}$  the reflected power will decrease by 6 dB when  $C_n^2$  is held constant. The change would mainly mean that we have to go to a lower frequency to get a dominant contribution from the reflection mechanism.

*Discussion on Paper 20, "Results of the theory of tropospheric scattering, derived from propagation measurements", by L.Fehlhaber, and on Paper 22, "Experimental methods to investigate receiving fields with tropospheric scatter propagation", by J.Grosskopf (presented by L.Fehlhaber).*

**Mr G.C.Rider:** Dr Fehlhaber, in making coupling loss measurements, is the quoted loss of 1 dB for the 2 m dish a measured or computed value? Have echoes due to particulate matter and birds also been observed on the X-band vertical incidence radar together with the targets attributed to inversion layers and convective caps?

**Dr L.Fehlhaber:** The coupling loss of the 2 m antenna has not been measured, but was taken from a CCIR curve. The measurements yielded only relative coupling losses. Echoes from birds, insects and so on (that is, angels) have often been seen but these effects have not been included in the backscatter results.

*Discussion on Paper 24, "Tropospheric scatter propagation at 16 GHz over a 500km path", by U.H.W.Lammers and E.E.Altshuler (presented by Dr Lammers)*

**Professor I.Ranzi:** Did you, Dr Lammers, determine the median value or the minimum value of the basic propagation loss for the 500 km distance? I had the impression that such a loss was lower than we may now theoretically predict. Such data are of great interest for the sharing problems connected with the use of such frequencies for communication satellite systems.

**Dr U.H.W.Lammers:** We did, of course, calculate the medium signal levels to be expected for a 500 km path using a frequency of 15.7 GHz. The results obtained from several theories were quite discouraging, when we tried to establish the troposcatter link. Experimentally we found that a received signal was available almost any time with properly pointed antennas.

**Dr N.C. Gerson:** It would be expected that your results, which are very interesting, would show some correlation and perhaps distinctive features depending upon the type of air mass over the volume concerned. Also, frontal passages may perhaps allow characteristic changes in reflectivity and signal strength. Have any of these aspects been investigated? What is the possibility that the returns which you indicated as arising from the tropopause actually represent a double-hop reflection from a tropospheric scattering surface?

**Dr U.H.W. Lammers:** As I mentioned, the troposcatter program described was initiated only very recently. This is the first, mostly qualitative, presentation of results. Though we have a wealth of meteorological information from the test periods conducted so far, we did not have a chance to correlate meteorological and radio data to a great extent. We have very carefully checked the angular position and level of the antenna, since we were afraid of irregular returns like the one mentioned, or main beam-side lobe and side lobe-side lobe propagation. The fact that there is only one layer (at 14 km height), and the fact that this layer is completely straight and horizontal, is sufficient evidence for its actual presence. One would not obtain such a simple result in the other cases mentioned, considering the rather complicated scanning procedure.

*Discussion on Paper 21, "Microwave propagation influenced by internal gravity waves", by Gerda Fengler and Gerd Stilke (presented by Gerda Fengler)*

**Mr W.G. Burrows:** Would the author please give some details of ground profile structure of the paths used in this experiment?

**Mr G. Fengler:** The terrain between the transmitter and all three receiver stations is nearly flat. There are no hills higher than 100 m. 25% of the 400 km path from Berlin to the isle of Heligoland is over the North Sea.

**Dr K. Davies:** In the USA we have observed atmospheric waves in the F-region with periods of about 2 to 5 minutes. These are associated with severe weather fronts. Did Dr Fengler observe any particular weather conditions during her observations on gravity waves?

**Dr G. Fengler:** The occurrence of gravity waves is mostly associated with two kinds of weather conditions:

- (a) With high pressure systems over middle or northern Europe, when discontinuities in density and refractive index are formed by outgoing radiation.
- (b) With approaching warm fronts, when discontinuities are formed by advection, i.e., warm and dry air is overflowing cold and wet air. This case corresponds to the one Dr Davies mentioned.

**Mr T.J. Elkins:** We at AFCRL have noticed fading, very similar to that which Dr Fengler described, by observing nearly stationary satellites at 400 MHz, near the horizon. Without having meteorological data, we came tentatively to the same conclusion regarding internal tropospheric waves. Can Dr Fengler (a) give an estimate of the discontinuity in radio refractive index which she observed and (b) say precisely how these gravity waves produce the observed fluctuations in field strength?

**Dr G. Fengler:** The gradients in the discontinuities of the refractive index derived by routine radiosonde ascents, are about 0.2 N/m, i.e., about 5 times stronger than in the well-mixed atmosphere (0.04 N/m). With a more sensitive instrumentation of the radiosondes the gradients would appear to be far stronger. Concerning your second question, I assume that the energy of the electromagnetic waves will be reflected by a boundary surface having a wavy structure. This wave pattern will move with the direction and velocity of the gravity wave. The incident transmitter beam will therefore periodically find the same wave pattern, i.e., the same reflection conditions. Hence the interference field at the receiving station will periodically have the same form, i.e., the fading structure of the received field strength will have a period corresponding to the velocity of the gravity waves.

Dr H.J. Albrecht: I should like to comment on Mr Elkin's remark that fluctuations in signals observed from satellites just above the horizon might be explained by the influence of gravity waves. In most cases, such fluctuations are found to be caused by ground reflections rather than tropospheric effects. I have the following question to Dr Fengler: Has any statistical analysis been made and, if so, what were the correlation coefficient and the statistical significance?

Dr G. Fengler: A statistical analysis has been made covering a two-year period (compare Section 4.1 of my paper). During this period about 320 cases with pressure variations due to internal gravity waves were measured and evaluated. In about 80% of these cases a coincidence with field strength fadings of nearly the same periods was observed.

Dr H.J. Albrecht: As a rule the correlation coefficient between refractive index and field strength has a low value unless periods extend over at least one month. If cases of coincidence between pressure and field strength fluctuations have been observed every fifth day, the occurrence probability of high pressure areas with inversion layers must be very high. Can this be confirmed?

Dr G. Fengler: I have already answered to Dr Davies's question that the occurrence of internal gravity waves is not only associated with high pressure systems, but also with weather fronts. Both meteorological conditions are related to radio meteorological events due to inversion layer structures. Reference is made to previous papers and to publications in preparation.

*Discussion on Paper 23, "Electromagnetic scattering from air currents", by H.N.Kritikos.*

Dr J. Ramasastry: I have the following questions for Dr Kritikos: Are the reflection coefficients shown by you "power" or "amplitude" reflection coefficients? Why did you assume the model in which the air current discontinuity moves normal to the plane of incidence? Couldn't it be oblique? The "total reflection" mentioned by you is not quite the same as the total reflection from a stationary mirror. Don't you agree?

Dr H.N. Kritikos: The coefficients are amplitude reflection coefficients. With regard to your second question; from all the evidence we have, the only stable air currents are those which move along their boundaries. Those which move obliquely break down into a turbulent state. I do agree with your last comment. The difference lies in the phase of the reflection coefficient, whose sign depends on the relative direction of the velocity of the current with respect to the incident field.

Dr C. Fengler: Is there a dependence in reflection coefficient on parallel and antiparallel direction to the interface of the air current?

Dr H.N. Kritikos: The magnitude of the relection coefficient is the same. The phase, however, changes sign.

RADIO WAVE SCATTERING FROM THE IONOSPHERIC D-REGION

by

J. B. Gregory

Institute of Space and Atmospheric Studies,  
University of Saskatchewan,  
Saskatoon, Canada

## SUMMARY

The topic of partial reflections and scattering of radio waves vertically incident upon the lower ionosphere is reviewed. Present knowledge is summarized, in relation to heights of occurrence of partial reflections and their seasonal and diurnal variation, thicknesses of scattering regions, height profiles of scatter strength and their variations, and angular spectra of reflected waves. Theoretical treatments of perturbations in electron density and collision frequency are examined. The outstanding lack of knowledge concerns processes in the fluid atmosphere which cause these perturbations. Existing radio wave theories are essentially descriptive, and the application of more complex formulations requires a corresponding advance in physical understanding. The relation of vertical backscattering and oblique forward scattering is discussed. Applications of scattering to the determination of electron densities below 100 km, to the measurement of winds above 65 km, and to detection of particle influx are discussed. New developments in relation to the influence of atmospheric circulation on the aeronomy of the lower ionosphere are outlined.

## RADIO WAVE SCATTERING FROM THE IONOSPHERIC D-REGION

J. B. Gregory

### 1. INTRODUCTION

This review will discuss the phenomena involved in the partial reflection and scattering of radio waves vertically incident upon the lower ionosphere. The altitudes involved are those below 100 km, with a present lower limit of about 50 km. These altitudes include part of the stratosphere, the mesosphere and part of the lower thermosphere, and thus extend above and below the D-region. Restriction of the direction of incidence to vertical, or near-vertical, permits this form of scattering to be distinguished from oblique, forward scattering, though these two forms have some features in common. The exclusion of total reflection phenomena directs attention away from mean values of properties of the lower ionosphere towards perturbations of those values. The reflected energy is generally a small fraction of incident energy, i.e. the scattering is weak. It is thus possible to derive information about mean values of macroscopic properties, such as electron densities and collision frequencies, from a study of the scattered waves.

The subject thus defined proves to be remarkably complex. It involves not only magneto-ionic theory, but also the physics of irregularities in neutral and ionized constituents of the atmosphere. (The term irregularity will be used here as denoting a volume, without limitation on geometrical form, in which the value of some property of the atmosphere differs from that in the surroundings. The term perturbation will be applied to the change of value of that property as compared with some mean value, e.g., of the surroundings.) Little is known about the mechanism of generation of irregularities, though much has been hypothesized, for example that turbulence is the main dynamical process involved. This uncertainty affects the application of magneto-ionic theory to the scattering process. Existing magneto-ionic theory appears to be adequate to describe the propagation of the scattered waves, particularly when a generalized form is employed. Advances in treatment of the electromagnetic aspects of scattering are thus dependent on a better understanding of the physics and fluid dynamics of the irregularities.

Experimental studies of the topic are basically dependent on ability to detect weak scattered or partially reflected waves. Thus the history of the subject is that of development or application of techniques which permit adequate observations. In this respect, the most useful technique is that of pulse transmission at a single medium frequency (MF), with adequate transmitter power, e.g. 100 kW peak; some antenna gain, e.g. 15 dB over an isotropic radiator, and good receiving conditions, e.g. a low-noise site and receiver of low noise factor. Current techniques provide adequate sensitivity, but improvements in height and angular resolutions are desirable.

This survey will deal briefly with the development of the subject, and will summarize the relatively small body of information on the characteristics of scattering. A discussion of theoretical approaches and current problems of treatment will follow. A final section will deal with some applications of scattering to measurements of ionospheric properties and winds.

## 2. HISTORICAL DEVELOPMENT

Experimental studies of D-region scattering had an uncertain start. They were stimulated by the work of Appleton (1930), who deduced the existence of free electrons below the E-region of the ionosphere from evidence of radio wave absorption. A D-region, located around 60 km, was postulated by him. At that time, the reflection of waves from the ionosphere, after oblique incidence, had been established, but the direct detection of reflections of vertically incident waves from heights below E-region had not been achieved. Between 1932 and 1947, several workers attempted this latter objective. In retrospect, it is evident that the frequencies employed were such that only partial reflection from the D-region was likely to have occurred. Nevertheless, a number of claims were made that D-region reflections had been detected.

It is difficult to decide how much reliance may be placed upon these early claims. A review of some twenty papers published prior to 1947 fails to identify any particular work as a starting point for vertical incidence studies of the D-region. Perhaps the most significant point which emerges is that, in order to achieve similar results in a reliable and reproducible manner, equipment of much superior performance is now found to be essential. A reading of early papers shows that some workers were not aware of the limitations of their equipment, and claimed impossible results. Others undoubtedly noted reflections from ranges between 5 and 90 km, but failed to interpret these correctly. For example, reflections from hills and from objects on the surface of the earth appear to have been mistaken by several workers for reflections from the atmosphere below 50 km. A prevalent cause of confusion has been the reflection of radio waves from the surface of the sea. Well defined sea echoes from 20 to 80 km range, overlapping with atmospheric reflections at altitudes down to 70 km, have been observed on many occasions. Thus from coastal and island sites there have originated observations which cannot be accepted as describing high altitude phenomena, but which were made the basis of deductions concerning the lower ionosphere. Failure to recognize ground and sea returns of transmitted pulses has persisted until recent date.

During 1939-1945, a series of oblique transmissions of MF waves, together with measurements of pulse delay times, established the existence of reflections from altitudes down to 75 km. Likewise the study of atmospherics and VLF and LF propagation from 1936 to 1951 yielded some estimates of altitudes of reflections. The first reliable pulse soundings at vertical incidence, specially designed to study the lower ionosphere, appear to have been those of Helliwell, et al.<sup>1</sup> (1951), who used frequencies of 100 kHz and 325 kHz to obtain reflections from 90 to 130 km at night. The first daytime results which fit into the recognizable pattern of D-region scattering appear to be those of Dieminger and Hoffman-Heyden<sup>2</sup> (1952), who reported reflections from pulse transmissions for frequencies between 1.5 and 4.0 MHz, at altitudes between 75 and 100 km. About the same time, Gnanalingam and Weekes<sup>3</sup> (1952) reported reflections down to 75 km, using a frequency modulation technique.

A significant advance was made by Gardner and Pawsey<sup>4</sup> (1953). Working at a very low noise site, they detected reflections down to about 70 km, and studied such characteristics as fading. They also made measurements of ratios of amplitudes of the two circularly polarized components, and obtained values of electron density through calculations of differential absorption coefficients. Reference to this differential absorption experiment (DAE) is made in Section 6.2. A further step was the introduction by Gregory<sup>5,6</sup> (1956, 1961) of techniques which provided adequate sensitivity and height resolution. These included the use of aerial arrays of improved gain, use of a common aerial for transmission and reception, the radiation of pulses less than 25 microseconds in length, and systematic change of receiver gain to resolve reflections. He showed the existence of echoes down to 55 km or less in daytime, and examined their altitude structure (Section 3.3). Titheridge<sup>7</sup> (1962) made a similar investigation, using the frequency modulation apparatus of Gnanalingam.

All the experimental studies described above were made at frequencies not greater than 7 MHz. This situation accords with the decrease of radio wave reflection coefficient from a given irregularity with increasing radio frequency in the MF and HF ranges. At higher frequencies, e.g. 50 MHz, only apparatus with high transmitter power, e.g. 1 MW, and very large aerial gain, offers the possibility of detection of vertical incidence reflections from below E-region. Bowles<sup>8</sup> (1958) detected reflections at 41 MHz in a temperate zone, and Flock and Balsley<sup>9</sup> (1967) have reported reflections at 49.9 MHz in the equatorial zone. The occurrence of these reflections has not been as frequent or as consistent as those observed at MF. At a frequency of 430 MHz, incoherent backscatter equipment has detected energy returning from altitudes of 55-70 km (Lalonde<sup>10</sup>, 1966), but the interpretation of these reflections is still a matter of debate. Since 1962, attention has been directed away from the characteristics of the scattering process towards its utilization as a means of deriving macroscopic properties of the atmosphere, such as electron densities.

Theoretical study of electromagnetic aspects of partial reflections and scattering at vertical incidence may be considered as a special case of studies of oblique scattering, such as those made by Booker<sup>11</sup> (1959). At medium frequencies, it is desirable that theoretical treatments include the effects of collisions, of the earth's magnetic field, and of differences in phase paths of ordinary and extra-ordinary components of scattered waves. Flood<sup>12</sup> (1968) has modified Booker's treatment to take account of absorption of the radiation incident upon different parts of the scattering volume (see Section 4.3).

### 3. SCATTERING PHENOMENA

#### 3.1 General

The aim of a study of partial reflections and scattering from heights below 100 km is ideally a quantitative description of the strength of the scattered waves in terms of location, time and propagation conditions. Such a description would presumably imply that the appropriate mechanisms of scattering or reflection had been correctly identified. Sufficient evidence exists to show that, at times, more than one mechanism operates, in the altitude range between 50 km and 100 km. This point may be confirmed by reference to Figure 1, which shows a selected record of a vertical incidence pulse transmission at 2.3 MHz made at 79°S (Scott Base). Visible in this record are some reflections at altitudes of 59 and 68 km which might well be considered as arising from a specular reflection process. At higher altitudes, between 73 and 90 km, and above 92 km, more rapid time variations of the reflections are evident. These might be consistent with turbulent scattering. At present, information is available as to the heights and thicknesses of scattering regions or reflecting layers, and their strengths, as a function of time of day and season, for only a few latitudes. Statistical studies of the time variation of the strength of the scattered reflections (fading) are available in less quantity.

Elementary theories of the radio wave reflection process show that the reflection coefficient of a given irregularity is proportional to the fractional change in refractive index,  $\Delta n/n$ . The dominant factor in determining the altitudes at which scattering occurs is the presence of free electrons, and the strength of scattering depend upon the electron density at a given altitude. Electron density profiles are known to be variable with solar zenith angle, with season, with changes in solar ionizing radiation, e.g. soft X-ray fluxes, and with influx of corpuscular radiation, e.g. solar protons at high geomagnetic latitudes. Belrose<sup>13</sup> (1963) and Knecht<sup>14</sup> (1965) have summarized information on electron density below 100 km. Seasonal average noon profiles of electron densities at a middle latitude have recently been presented by Gregory and Manson<sup>15</sup> (1968).

Scattering at vertical incidence has been observed at high geomagnetic latitudes, poleward of the auroral zones, where solar proton influxes causes large increases in electron densities below 80-100 km (Gregory<sup>16</sup>, 1962). Similar scattering has been observed in the auroral zones, where electron precipitation causes increases below 120 km (Holt, Landmark and Lied<sup>17</sup>, 1962). The various studies mentioned in Section 2 show that scattering occurs

throughout mid-latitudes, certainly to  $30\text{-}35^{\circ}$  geographic. For latitudes close to and including the equator, little information is available, though satisfactory measurements of electron densities have been made by the differential absorption method at  $19^{\circ}\text{S}$  (Thrane et al.<sup>18</sup>, 1968).

### 3.2 Heights of Reflection

Dieminger<sup>19</sup> (1952), observing at  $52^{\circ}\text{N}$  from 1949 to 1952, noted reflections down to 75 km in the middle of the day. However, his equipment did not permit the resolution of individual reflecting structures. Gardner and Pawsey<sup>4</sup> (1953) observing for a total of less than 20 days in 1951 and 1952 at  $34^{\circ}\text{S}$ , noted reflections which they grouped into two divisions, namely, "90 km", which referred to those between 80 and 110 km, and "70 km" which referred to those below 80 km. Gnanalingam and Weekes<sup>3</sup> (1952) reported reflections from heights between 75 and 80 km, and also above 90 km, at  $52^{\circ}\text{N}$ . A larger body of data was obtained by Gregory<sup>5,6</sup> (1956, 1961) at  $43^{\circ}\text{S}$ . His observations were made automatically at hourly intervals throughout 1956-1958, and mid-day thereafter. The heights of occurrence of observed partial reflections varied considerably. However, when data were assembled into histograms of occurrence, by months, reflections were found to occur most frequently in regions whose lower boundaries were close to 55, 61, 66, 74 and 86 km. A further region, possibly totally reflecting at times, was found at 95 km. Reflections near 86 km continued throughout day and night, whereas lower reflections were essentially of day-time occurrence only. Lowest altitudes were reached around noon.

All the foregoing measurements were made at frequencies between 1.4 MHz and 3 MHz. Titheridge<sup>7</sup> (1962) working at  $52^{\circ}\text{N}$ , used a lower frequency of 720 kHz. From an analysis of 40,000 recorded heights obtained during 1957 and 1958, he reported that reflections tended to occur from heights of about 71, 80, 90 and 100 km. The observations by Gregory and Titheridge comprise the bulk of available data, and both sets of data suggest that the occurrence of preferred heights is a real phenomenon in the atmosphere. It may be noted that, at a higher latitude of  $69^{\circ}$ , though under conditions of particle influx, observations by Holt et al.<sup>17</sup> (1962) also revealed a tendency for preferred heights around 63, 73, possibly 77, and 83 km. Belrose and Burke<sup>20</sup> (1964) have published a limited sample of their observations, from which the reflections which occurred at greatest strengths have been omitted. It is therefore not possible to compare their data with that of other workers.

The existence of preferred heights of scattering is inferred from assemblages of data, and requires to be interpreted in a statistical sense, i.e., for a sample observation, the probability of occurrence of a reflection at a preferred height is larger than the probability of occurrence at other heights. Data presented as histograms usually show reflections at all heights, but the matter of continuity of reflections throughout all heights at a particular time requires closer examination (see Section 3.3). Before the existence of preferred heights can be accepted as verified, it is necessary to investigate at least two factors. These are the height resolution possible in a given experimental arrangement and the presence of bias in scaling of records. Height resolution is determined by matters such as pulse length, and antenna polar diagram, in pulsed equipment. Bias usually occurs as a personal factor in scaling of records, e.g. in interpolation of tenths.

The work of Gregory and of Titheridge has been examined in these aspects. Gregory (unpublished) has recently arranged for an independent re-examination of his data and, apart from some anticipated changes in personal bias, has had his original findings confirmed with only minor modifications. Some, but not all, of Titheridge's data show evidence of bias. For both investigators, it appears that the technical characteristics of their equipment permitted good height resolution. The effects of oblique reflections in each experiment are more difficult to assess. It is concluded that the existence of preferred heights of reflection, under the particular conditions of observation in the two experiments, is a real phenomenon. The agreement which Titheridge purported to find between his and Gregory's data is not well established, however, due to the structure of reflecting regions.

### 3.3 Structure of Reflecting Regions

Studies of amplitudes of reflections as a function of altitude and time reveal that reflecting regions exist. These may be discrete, i.e. separated by altitude intervals in which amplitude is below detection level, or continuous, i.e. extending throughout a range of altitudes. (See, for example, height-time records in Gregory<sup>5</sup> (1956), obtained using a pulse length of ten microseconds at half-power points.) Discrete reflections are more prevalent below 80 km, and continuous reflections above that height. By applying a swept-gain technique, Gregory (unpublished) has been able to show that reflecting regions have thicknesses ranging from less than 1 km to more than 5 km. The mean thickness increases with altitude. The probability of occurrence of these regions decreases with increasing thickness. Greatest probability of occurrence is in winter, particularly when the wind flow in the mesosphere is disturbed by the passage of a planetary or cyclonic wave (Gregory and Manson<sup>21</sup>, 1968). No detailed studies have been made on the characteristics of irregularities within these reflecting regions. The hypothesis that the latter are also regions of turbulent shear flow of air is plausible (see Section 4.4).

### 3.4 Amplitude of Scattered Waves

The amplitude of partially reflected or scattered waves has been measured only at the earth's surface. Thus, after allowance is made for the parameters of a given experimental arrangement, the amplitudes are governed both by the amount of ionospheric absorption between the surface and the altitude of reflection, and by the nature of the reflection process. To date, only data representing amplitudes uncorrected for absorption have been published. Gregory<sup>22</sup> (1967) has presented a set of height profiles of monthly mean noon scatter strength, relative to a fixed strength, for the years 1956-1957, at 1.75 MHz. Apart from a number of minor features, all the profiles show a general increase in strength with height to the maximum altitude reported, 95 km. Between 55 and 95 km, the mean strength increased by an amount varying between 35 and 50 decibels, with greatest increase in winter. The existence of a winter increase is confirmed by other workers, e.g. Titheridge<sup>7</sup> (1962).

Day-to-day variations of the recorded amplitude at the earth's surface, as a function of altitude, are considerable, reaching as much as 70 decibels in the height range 80-100 km. The respective effects of the scattering process and of absorption have not yet been separated in regard to these variations.

### 3.5 Seasonal Variations of Amplitude

A winter increase in amplitude of scattered waves was early observed by Dieminger<sup>19</sup> (1952). Seasonal variations in amplitude have been examined by Gregory<sup>22</sup> (1967), who grouped data for noon periods, 1956-1959, into four altitude ranges of 10 km each between 55 and 94 km. When data for similar months were assembled, a winter maximum was found in all four altitude ranges. The ratio of winter-to-summer amplitudes was largest in the 75-84 km interval, being about 18 dB at these altitudes. An important feature, which is also relevant to studies of VHF forward scattering, is the occurrence of both a winter and a summer maximum, above 75 km. Although the winter maximum dominates at all altitudes, the summer maximum increases with altitude, so that a semi-annual variation is pronounced in the region above 75 km. This variation applies to amplitudes which are uncorrected for absorption. The related variations of electron densities in the same altitude ranges are discussed in Section 7.

### 3.6 Diurnal Variation of Amplitude

The tendency for reflection amplitudes to reach a maximum at noon was noted by early workers. Gardner and Pawsey<sup>4</sup> (1953) found that the "70 km" group of reflections increased in amplitude from sunrise to noon, then decreased, to disappear after sunset. Their "90 km" group tended to decrease to a shallow minimum at noon, presumably because of the effect of ionospheric absorption. Gregory (unpublished) has noted the appearance, around

sunrise and sunset, of weak reflections at low altitudes, e.g. 60 km. The origin of these reflections is believed to be related to the formation of a minor maximum of electron densities by incident cosmic radiation. Such a maximum has been inferred by Deeks<sup>23</sup> (1966) and Bain and May<sup>24</sup> (1967).

It is to be noted that wide variations in diurnal behaviour are encountered, so that the trends described above must be considered as representative, rather than as actual, behaviour on a given day.

### 3.7 Diurnal Variations of Altitude

The diurnal variations of amplitude just described may be re-interpreted as variations of altitude by plotting contours of constant amplitude. One such amplitude, in a given experimental system, is the value which is just detectable, for example, photographically. A smooth variation, with lowest altitude at noon, might be expected for reflections of smallest detectable amplitude if solar control predominates. While this situation does occur at times, notably when scattering is continuous in altitude, an alternative behaviour is also evident. Gregory<sup>6</sup> (1961) showed that many reflections persisted at essentially the same altitude throughout daylight hours, or underwent changes, including appearance and disappearance, which were not related to solar zenith angle. A dynamical origin of this latter behaviour was postulated.

### 3.8 Angular Spectrum

The scattering of waves from a partially reflecting region of the atmosphere may be treated as a diffraction effect, in which the angular spectrum and the complex amplitude of the waves leaving the region are related as a Fourier transform pair. In order to determine the corresponding angular spectrum, measurements must be made over an area which includes the largest significant scale sizes in the diffraction pattern. If the diffraction pattern did not change with time, such a measurement would present little difficulty. However, the pattern is found to move and to change its geometry while moving. The experimental requirement is then to sample the pattern simultaneously throughout the significant area. This requirement has not been achieved in any studies reported to date. Corresponding information on the angular spectrum is thus not yet available.

An alternative approach to this problem is through the determination of the spatial correlogram which describes the form of the diffraction pattern on the ground. Kelleher<sup>25</sup> (1966) has attempted this determination for reflections from E- and F-regions. A similar experiment, involving a series of spaced antenna, is desirable to determine D-region characteristics. Awe<sup>26</sup> (1961) has made measurements using two antenna only, on reflections from 90 km altitude. He reported lower values of correlation coefficient than were obtained by Briggs and Phillips<sup>27</sup> (1950) for the E-region, implying a larger spread of angles of downcoming waves from the 90 km altitude region. It is likely that the angular spectra of waves reflected below the E-region are very variable with altitude and time.

Awe has also studied the fading of 90 km reflections. He found that the mean fading speed was approximately three to four times the speed of fading of E-region reflections. A wide range of fading speeds, varying with altitude and time, can be noted in published data. The significance of these amplitude variations, in relation to wind and electron density profiles, remains to be established.

## 4. THEORETICAL TREATMENTS

### 4.1 General

In this section some discussion will be given of attempts to establish theoretical descriptions of the radio wave partial reflection and scattering processes. It should be noted that such descriptions are essentially confined to electromagnetic processes,

since the atmospheric processes, to which the scattering may ultimately be ascribed, are not yet identifiable with any certainty. It is thus necessary to assume a model of the electromagnetic process; more specifically, the geometry of the reflectors of scatterers must be postulated.

#### 4.2 The Fresnel Discontinuity

The simplest and perhaps most useful approach is one which invokes partial reflection at an extended horizontal irregularity in refractive index, as distinct from volume scattering. The horizontal extent of the irregularity is assumed sufficient to fill the first Fresnel zone, for vertically incident waves. This dimension is typically of the order of 3 km, for MF waves, at mesospheric altitudes. If the medium below the irregularity has a refractive index of  $n_1$ , and that above the boundary has an index of  $n_2$ , the reflection coefficient,  $R$ , at normal incidence, for the electric field intensity is given by

$$R = \left| \frac{n_2 - n_1}{n_2 + n_1} \right| \quad (1)$$

(Budden<sup>28</sup>, 1961). The same expression can be shown to apply (Thrane<sup>29</sup>, 1966) to the ordinary (O) and extra-ordinary (X) circularly polarized waves when the propagation direction coincides with that of the magnetic field. A quasi-longitudinal approximation is useful in many situations, and hence the reflection coefficients,  $R_X, R_O$  for such a model of an irregularity may be calculated for application in many experimental situations. In practice,  $n_2$  and  $n_1$  are usually not known, and equivalent values of  $R_X$  and  $R_O$  are determined from measurements of amplitudes of reflections on the basis of the model described. It is found that the equivalent reflection coefficients are in the range from  $< 10^{-5}$  to  $> 10^{-2}$ , usually increasing in magnitude from altitudes of approximately 50 km up to E-region. These values have usually been determined in the presence of ionospheric absorption of unknown extent.

A more complicated geometry of irregularity involves a series of small reflecting structures, for each of which a reflection coefficient can be calculated. This model was first discussed by Gardner and Pawsey<sup>4</sup> (1953) in connection with the differential absorption experiment using partial reflections. These authors deduced that, provided equality of phase paths for O and X waves is maintained for each irregularity, the ratio  $R_X/R_O$  is the same as that calculated for a single extended plane horizontal irregularity. This point is discussed further in relation to the differential absorption experiment (Section 6.2).

#### 4.3 Volume Scattering

The case of volume scattering has been considered by Booker<sup>11</sup> (1959), primarily for application at VHF, where the effect of the earth's magnetic field and electron collisions with neutral particles may be neglected. In place of a model of an irregularity structure, the autocorrelation function which describes the spatial distribution of the radio wave irregularities must be assumed.

A scattering cross-section,  $\sigma$ , which is the power scattered per unit solid angle, per unit incident power density per unit volume, is then calculable as

$$\sigma = \left| \frac{\Delta\epsilon}{\epsilon} \right|^2 \frac{\pi^2 \sin^2 X}{\lambda^2} P[k(l_2 - l_1), k(m_2 - m_1), k(n_2 - n_1)], \quad (2)$$

where  $\epsilon$  = permittivity of medium

$X$  = angle between scattering direction and incident electric vector

$\lambda$  = wavelength

$P(l, m, n)$  = Fourier transform of  $\rho(x, y, z)$ , the autocorrelation function of  $(\Delta\epsilon/\epsilon)$ .

$l, m, n$  = direction cosines of scattering (2) and incidence (1) directions.

Booker suggests a number of possible forms of  $\rho(x, y, z)$ . Of these, the simple Gaussian form

$$\rho(x, y, z) = \exp \left\{ -\frac{1}{2} \left( \frac{x^2}{a^2} + \frac{y^2}{b^2} + \frac{z^2}{c^2} \right) \right\}, \quad (3)$$

where  $a, b, c$  are scale lengths, has been most often used in VHF forward scatter. No experimental tests appear to have been made of the suitability of any of the forms of  $\rho(x, y, z)$  for application to MF back scattering.

Booker's theory has been extended by Flood<sup>12</sup> (1968) to take account of absorption in the scattering volume. Flood assumed that the latter is in the form of a horizontal slab, whose vertical thickness  $\delta h$  is determined by the pulse duration  $\tau$ .

$$\text{i.e. } \delta h = C \frac{\tau}{2}. \quad (4)$$

He assumed also that plane waves are incident upon this slab from below. Flood showed that in these circumstances the expression for a scattering cross-section  $\sigma$ , as defined above, is not unique, since it involves the pulse length as one of the volume-determining factors. The quasi-longitudinal approximation to the generalized (Sen and Wyller<sup>30</sup>, 1960) magneto-ionic theory was used throughout in the derivation of radio wave refractive index.

The relevance of Flood's theory to studies of back-scattering appears to be limited. The geometry of the scattering volume is determined by the radiated pulse packet, and is essentially in the form of a spherical cap, rather than that of a horizontal slab. Experimental evidence (Section 3.3) suggests also that there is not a continuum of back-scattered echoes, but rather that layers exist in which scattering occurs. Hence the actual scattering volume is defined by the intersection of a spherical cap with a horizontal layer. It is to be noted that in such a volume the angle of propagation of the scattered waves, with respect to the magnetic field, varies in practice from zero to about 45°. In such volumes also, both the electron density and the electron collision frequency may change appreciably with altitude, while within the radial thickness defined by  $C\tau/2$ . Thus, in the determination of cross-sections, the volume averaging process is not easily described by an analytical expression. Finally, Flood shows that four or more planar discontinuities, within the spherical cap, give rise to backscattering cross-sections which are identical with those of the volume scattering case.

#### 4.4 Selection of Appropriate Theory

In view of the considerable increase in calculation entailed by the adoption of the volume scattering hypothesis, it is desirable that some assessment be made in practice of the need to use the latter. A test may be made by observing the effect of increase of transmitted pulse length. For Fresnel discontinuities, the amplitude of the reflected pulse remains unchanged. Austin and Manson<sup>31</sup> (1968) have shown that this test yielded results more consistent with the concept of plane discontinuities than with that of a scattering volume.

#### 4.5 Physical Quantities Involved

Regardless of the choice of scattering model, it is necessary to decide which physical parameters are involved in the determination of the mean and perturbed radio wave refractive index. Gallet<sup>32</sup> (1955) has shown that the scattering which results from fluctuations in the density  $\rho$  of the neutral gas alone, is insufficient to account for observations. The existence of an electron density  $N$  is basic; since a change  $\Delta N$  in electron density,

or a change  $\Delta\nu$  in collision frequency  $\nu$ , will then cause a change  $\Delta n$  in refractive index. The relative importance of the perturbations  $\Delta N$  and  $\Delta\nu$  has been discussed by several workers. Gardner and Pawsey<sup>4</sup> (1953) assumed that only perturbations  $\Delta N$  existed. Pigott and Thrane<sup>33</sup> (1966) and Manson<sup>34</sup> (1966) pointed out that the inclusion of a term  $\Delta\nu$  would modify the calculated values of  $R$ , the reflection coefficient in Equation (1). Thrane et al.<sup>18</sup> (1968) have evaluated the effect of the ratio

$$\alpha = \frac{\Delta\nu/\nu}{\Delta N/N} \quad (5)$$

upon the ratio  $R_x/R_0$ , which is used in the differential absorption experiment. However, they derived values of  $\alpha$  for two special cases of atmospheric motion, namely, adiabatic and isothermal expansion of masses of air. Gregory and Manson<sup>15</sup> (1968) re-examined the possible role of these processes in the atmosphere and, after considering observational evidence, concluded that perturbations  $\Delta\nu$  in collision frequency  $\nu$  did not occur in sufficient magnitude to affect the calculated values of  $R$ .

Thus, at present, theoretical calculations concerning the magnitudes of reflection coefficients may well be based on a simple, plane irregularity model, with perturbation in electron density only. For calculations concerning the height region 70-85 km, where  $\nu \approx \omega$ , the wave angular frequency, the Sen and Wyller<sup>30</sup> (1960) generalized magneto-ionic theory is usually employed. This theory has not yet received a rigorous test of its applicability to aspects of radio wave scattering. Quasi-longitudinal approximations, using the generalized theory, have been utilized (Belrose and Burke<sup>20</sup>, 1964) but, with the availability of adequate computing facilities, the theory is now usually applied without approximation. When the direction of propagation does not coincide with that of the magnetic field, coupling between the right- and left-hand circularly polarized waves takes place. However Thrane<sup>29</sup> (1966) has shown that, for conditions typical of the upper mesosphere, the coefficients of reflection which describe the coupling are some three orders of magnitude less than the coefficients for the separate waves, provided large changes in collision frequency do not occur. As discussed above this seems a reasonable assumption.

### 5. RELATION TO VHF FORWARD SCATTERING

The heights at which oblique forward scattering at VHF occurs were determined by Bailey et al.<sup>35</sup> (1955), and by Pineo<sup>36</sup> (1956). Daytime values were in the range 60-86 km, while night heights were generally between 85 and 90 km. Gregory<sup>37</sup> (1957) made a comparison between heights of vertical incidence reflections at 1.75 MHz and those of forward scattering at VHF as determined by Pineo. These two sets of data were obtained in opposite hemispheres, but the agreement was sufficient to suggest that the two forms of scattering originated in the same range of altitudes. No satisfactory test has been made which would show whether the same volume of the atmosphere was simultaneously capable of sustaining both the forward and the vertical incidence scattering; evidence is now available which shows that the two forms have some common seasonal characteristics. The relation between the scattering cross-sections for the two situations is not known. Bailey et al.<sup>35</sup> found a semi-annual variation of noon signal intensity for a VHF path centred at 40°N, in USA. Ellyett and Leighton<sup>38</sup> (1958) examined a longer series of data for the same path and found that the same variation occurred throughout an eight-year period which included sunspot minimum. This variation, which includes one maximum in mid-summer and another, more variable in epoch, in winter, is essentially the same as found by Gregory<sup>16</sup> (1962) for the strengths of 1.75 MHz noon partial reflections, and by Gregory and Manson<sup>15</sup> (1968) for noon electron densities (see Section 7). In these last two investigations, the semi-annual variation was strongest above 80 km. Thus, despite the uncertainty of height determination in the oblique process, there is further support for the concept that the main contribution to the background, or non-meteor, component of VHF scatter is in the region 80-90 km during daytime. Since Ellyett and Leighton showed that a solar cycle effect was present in the strength of VHF forward scatter, it is possible to predict a similar effect in the strength of partial reflections at MF and most probably in the electron densities in the region 80-90 km.

## 6. APPLICATIONS OF SCATTERING AND PARTIAL REFLECTIONS

### 6.1 General

Three main, and several minor, applications of radio wave backscattering have been made to date. These include the determination of electron densities below about 90 km, using measurements of differential absorption, the derivation of radio-wave winds, and the detection of solar proton influx at high geomagnetic latitudes. These will now be briefly described.

### 6.2 The Differential Absorption Experiment (DAE)

This experiment was developed by Gardner and Pawsey<sup>4</sup> (1953) and has since been employed by several groups at a number of latitudes. The original paper may be consulted, since the experiment remains unchanged in its essentials. The ratio of the extraordinary and ordinary wave reflection coefficients,  $R_x/R_0$ , is calculated for conditions of electron density  $N$  much less than critical (i.e.  $n \sim 1$ ), and for assumed collision frequency profiles,  $\nu = \nu(h)$ . The values of this ratio, as observed at the ground, are modified by differential absorption, for which the indices are  $k_x$  and  $k_0$ . The ratio at ground,  $A_x/A_0$ , is measured for several naturally occurring reflection heights,  $h_2, h_1$ , etc. Then it may be shown that

$$\frac{[\log_e(R_x/R_0)_2 - \log_e(R_x/R_0)_1] - [\log_e(A_x/A_0)_2 - \log_e(A_x/A_0)_1]}{2(k_x - k_0)/N(h_2 - h_1)} = \bar{N}, \quad (5)$$

where  $\bar{N}$  is now the mean electron density between the heights  $h_2$  and  $h_1$ . The experiment has been described by several workers, including Belrose and Burke<sup>20</sup> (1964). An assessment of the method, its accuracy, and the assumptions involved, has been given by Gregory and Manson<sup>21</sup> (1968).

Using this method, profiles of electron densities in disturbed conditions (Holt et al.<sup>17</sup>, 1962), and in undisturbed conditions at various latitudes (Belrose et al.<sup>39</sup>, 1966, Thrane et al.<sup>18</sup>, 1968, Gregory and Manson<sup>15</sup>, 1968) have been determined.

### 6.3 Wind Measurements in the Mesosphere

The determination of motion in the ionosphere from observations of the diffraction pattern at the ground, using three spaced receivers, has been described by Briggs et al.<sup>40</sup> (1950). The method was originally applied to reflections from E- and F-regions. In the D-region, and especially below 75 km, the motion of electrons is dominated by collisions with neutral particles. Fraser<sup>41</sup> (1968) utilized partial reflections to determine the drift of diffraction patterns. The method relies on apparatus of sufficient sensitivity to detect weak partial reflections. The interpretation to be made of the drift velocities derived from measurements has been the subject of much discussion (see for example, the report of the proceedings of St.Gallen Symposium; Journal of Atmospheric and Terrestrial Physics, Vol. 30, May 1968). However, Fraser has shown that, below 100 km, the monthly mean zonal winds derived by this method are in satisfactory agreement with data obtained by other methods.

### 6.4 Particle Influx Studies

Partial reflections, at vertical incidence, have been utilized by Gregory<sup>16, 42</sup> (1962, 1963) to determine the time variations of the influx of solar protons, at high geomagnetic latitudes, and to make estimates of residual ionization during the polar winter night. This application parallels the use of VHF forward scattering by Bailey<sup>43</sup> (1959) for studies of proton and electron influx around and poleward of the auroral zone.

## 7. DYNAMICAL PROCESSES IN THE ATMOSPHERE

The uncertainty which surrounds the origin of the scattering processes in the atmosphere has been mentioned in Section I, and examples of situations which may correspond to turbulent scattering have been cited in Section 3.3. Other observations tend to favour the adoption of a single irregularity concept. However, the evidence that a seasonal increase of scattering strength occurs, in winter and summer, at both MF (Gregory<sup>22</sup>, 1967) and at VHF (Ellyett and Leighton<sup>38</sup>, 1958, suggests that the processes involved must be closely related to characteristics of atmospheric circulation.

Similar evidence is available from studies of irregularities in the lower ionosphere. Fraser and Vincent (private communication) have used three spaced receivers to measure the sizes of ground diffraction patterns for partially reflected MF waves. They have made measurements of fading periods, and have detected changes in phase path at vertical incidence. A decrease in size of ground pattern, in time of reflections, and in fading period, was noted in both summer and winter. All three changes are consistent with the occurrence of more complex irregularity structures in summer and in winter.

Gregory and Manson<sup>15</sup> (1968) have reported results of five years' observations of noon electron densities below 90 km, for a quiet sun period, at 44°S. They derived mean profiles for four seasons, and examined the coefficient of variation (standard deviation/mean) in height intervals of 65-79 km, and 80-88 km. They also examined the range of values in each season. An increase was noted in mean noon electron densities, in winter and spring, by comparison with those in summer, between 79 and 88 km. The increase in values of electron densities in the same altitude interval, from fall to winter, coincided with the period of establishment of the winter eastward polar vortex at mid-latitudes. Likewise, the coefficient of variation was found to have a maximum in winter, which varied with altitude, being greatest in the region 65 to 69 km.

The summer period was characterized by low values of electron density, particularly when these were amended to correspond to constant solar zenith angle, and also a decreased coefficient of variation at all altitudes.

Gregory and Manson related these finds to work by Bossolasco and Elena (1963) and Gregory (1965), which supports the concept of interaction between the dynamics of the atmosphere, and the aeronomy of the lower ionosphere. In particular, they showed that the changes in electron densities and in their coefficients of variation were consistent with present knowledge of the penetration of planetary ( $\lambda \approx 10,000 - 4000$  km) and cyclonic ( $\lambda \approx 4000 - 2000$  km) waves, present in the upper troposphere and ne stratosphere, and attaining altitudes which are determined by the existing mean wind profiles below approximately 100 km. Insufficient data existed to permit an estimate of the effects of these waves in transporting ionizeable material, especially in the region of greatest seasonal effects, estimated to be between 82 and 96 km. A comparison of temperatures at 86 km, derived from radio wave winds at the same location, and electron densities around the same altitude, showed some similarities of seasonal trend.

This investigation did not demonstrate how the penetration of planetary and cyclonic waves might actually bring about an increase in scattering or reflection coefficients, such as is observed at altitudes where the winter increase of electron densities is not large, e.g. between 55 and 64 km. It remains to be demonstrated whether gravity waves (Hines<sup>44</sup>, 1960) or atmospheric turbulence, or both, can be clearly linked to an alteration in local conditions of wind flow below 100 km, which might follow from the passage of major waves.

### ACKNOWLEDGEMENTS

It is a pleasure to acknowledge helpful discussions with Drs G.J. Fraser, A.H. Manson, E.V. Thrane and R.A. Vincent.

## REFERENCES

1. Helliwell, R.A.  
et al. *The Fine Structure of the Lower Ionosphere.* Journal of Geophysical Research, Vol. 56, 1951, pp. 53-62.
2. Dieminger, W.  
Hoffman-Heyden, A.F. *Reflections of Short Waves at Heights Less than 100 km.* Naturwissenschaften, Vol. 39, 1952, pp. 84-85.
3. Gnanalingam, S.  
Weekes, K. *Weak Echoes from the Ionosphere with Radio Waves of Frequency 1.42 Mc/s.* Nature, Vol. 170, 1952, p. 113.
4. Gardner, F.F.  
Pawsley, J.L. *Study of the Ionospheric D-region Using Partial Reflections.* Journal of Atmospheric and Terrestrial Physics, Vol. 3, 1953, pp. 321-344.
5. Gregory, J.B. *Ionospheric Reflections from Heights Below the E-region.* Australian Journal of Physics, Vol. 9, 1956, pp. 324-342.
6. Gregory, J.B. *Radio Wave Reflections from the Mesosphere. I. Heights of Occurrence.* Journal of Geophysical Research, Vol. 66, 1961, pp. 429-445.
7. Titheridge, J.E. *The Stratification of the Lower Ionosphere.* Journal of Atmospheric and Terrestrial Physics, Vol. 24, 1962, pp. 283-296.
8. Bowles, K.L. *Observation of Vertical Incidence Scatter from the Ionosphere at 41 Mc/s.* Physics Review Letters, Vol. 1, 1958, p. 454.
9. Flock, W.  
Balsley, B.B. *VHF Radar Returns from the D-region of the Equatorial Ionosphere.* Journal of Geophysical Research, Vol. 72, 1967, pp. 5537-5541.
10. Lalonde, L.M. *Incoherent Backscatter Observations of Sporadic-E.* Journal of Geophysical Research, Vol. 71, 1966, pp. 5059-5066.
11. Bocke, H.G. *Radio Scattering in the Lower Ionosphere.* Journal of Geophysical Research, Vol. 64, 1959, pp. 2164-2177.
12. Flood, W.A. *Revised Theory for Partial Reflection D-region Measurements.* Journal of Geophysical Research, Vol. 73, 1968, pp. 5585-5598.
13. Belrose, J.A. *Present Knowledge of the Lowest Ionosphere.* In "Radio Wave Propagation", edited by W.T. Blackband, Pergamon, 1963, pp. 3-23.
14. Knecht, R.W. *The Distribution of Electrons in the Lower and Middle Ionosphere.* Progress in Radio Science, edited by G.M. Brown, Elsevier, Amsterdam. Vol. 3, 1965, pp. 14-45.
15. Gregory, J.B.  
Manson, A.H. *Electron Densities in the Dynamic Atmosphere Below 100 km. II. Electron Densities and Atmospheric Circulation.* Journal of Atmospheric and Terrestrial Physics. (In the press.)
16. Gregory, J.B. *Residual Ionization in the Polar Lower Ionosphere.* Journal of Geophysical Research, Vol. 67, 1962, pp. 3829-3841.

17. Holt, O.  
et al.  
*Observations of Electron Density and Collision Frequency During Polar Radio Blackout Conditions.* Proceedings of the Fifth Technical Meeting of the Fifth Ionosphere Research Committee of AGARD, edited by N.C.Gerson, Pergamon, 1962, p. 318.

18. Thrane, E.V.  
et al.  
*Measurements of D-region Electron Densities During the International Quiet Sun Years.* Journal of Atmospheric and Terrestrial Physics, Vol. 30, 1968, pp. 135-150.

19. Dieminger, W.  
*On the Causes of Excessive Absorbtion in the Ionosphere on Winter Days.* Journal of Atmospheric and Terrestrial Physics, Vol. 2, 1952, pp. 340-349.

20. Belrose, J.S.  
Burke, M.J.  
*Study of the Lower Ionosphere Using Partial Reflection.* Journal of Geophysical Research, Vol. 69, 1964, pp. 2799-2818.

21. Gregory, J.B.  
Manson, A.H.  
*Electron Densities in the Dynamic Atmosphere Below 100 km. I. Differential Absorption Measurements.* Journal of Atmospheric and Terrestrial Physics. (In the press.)

22. Gregory, J.B.  
*Mesospheric Electron Densities at 43°S.* Published in "Proceedings of DRTE/AFCRL Conference on Ground Based Radio-wave Propagation Studies of the Lower Ionosphere". Defence Research Board, Ottawa, Canada, 1967.

23. Deeks, D.G.  
*D-region Electron Distributions in Middle Latitudes Deduced from the Reflection of Long Radio Waves.* Proc. Roy. Soc., Vol. A291, 1966, pp. 413-437.

24. Bain, W.C.  
May, B.R.  
*D-region Electron Density Distributions from Propagation Data.* Proceedings, Institution of Electrical Engineers, Vol. 14, 1967, pp. 1593-1597.

25. Kelleher, R.F.  
*Some Characteristics of the Ground Diffraction Pattern Caused by the Vertical Reflection of Radio Waves from the Ionosphere.* Journal of Atmospheric and Terrestrial Physics, Vol. 28, 1966, pp. 99-102.

26. Awe, O.  
*The Fading of Radio Waves Weakly Scattered at Vertical Incidence from Heights Near 90 km.* Journal of Atmospheric and Terrestrial Physics, Vol. 21, 1961, pp. 142-156.

27. Briggs, B.H.  
Phillips, G.J.  
*A Study of the Horizontal Irregularities of the Ionosphere.* Proceedings of the Physical Society, Vol. B63, 1950, p. 907.

28. Budden, K.G.  
*Radio Waves in the Ionosphere.* Cambridge University Press, 1961, p. 108.

29. Thrane, E.V.  
*Experimental Studies of the Structure of the Ionospheric D-region.* Norwegian Defence Research Establishment, Report 54, Kjeller, Norway, 1966.

30. Sen, H.K.  
Wyller, A.A.  
*On the Generalization of the Appleton-Hartree Magneto-Ionic Formulas.* Journal of Geophysical Research, Vol. 65, 1960, pp. 3931-3950.

31. Austin, G.L.  
Manson, A.H.  
*On the Nature of the Irregularities which Produce Partial Reflections of Radio Waves from the Lower Ionosphere (70-100 km).* Radio Science. (In the press.)

32. Gallet, R.M. *Aerodynamical Mechanisms Producing Electronic Density Fluctuations in Turbulent Ionized Layers.* Proceedings, Institute of Radio Engineers, Vol. 43, 1955, pp. 1240-1252.

33. Piggott, W.R. *The Effect of Irregularities in Collision Frequency on the Amplitude of Weak Partial Reflections.* Journal of Atmospheric and Terrestrial Physics, Vol. 28, 1966, pp. 311-314.

34. Manson, A.H. *Comments on the Theory of the Differential Absorption Experiment.* Journal of Geophysical Research, Vol. 71, 1966, pp. 3783-3785.

35. Bailey, D.K. et al. *Radio Transmission at V.H.F. by Scattering and Other Processes in the Lower Ionosphere.* Proceedings, Institute of Radio Engineers, Vol. 43, 1955, pp. 1181-1230.

36. Pineo, V.C. *Oblique Incidence Measurements of the Heights at which Ionospheric Scattering of VHF Radio Wave Scattering Occurs.* Journal of Geophysical Research, Vol. 61, 1956, p. 165.

37. Gregory, J.B. *The Relation of Forward Scattering of VHF Radio Waves to Partial Reflection of M.F. Waves at Vertical Incidence.* Journal of Geophysical Research, Vol. 62, 1957, pp. 383-388.

38. Ellyett, C. Leighton, H. *Solar Cycle Influence on the Lower Ionosphere on VHF Forward Scatter.* Proceedings, Institute of Radio Engineers, Vol. 46, 1958, pp. 1711-1716.

39. Belrose, J.S. et al. *Propagation of Radio Waves at Frequencies Below 300 Kilocycles.* In AGARDograph 74, Pergamon Press, Oxford, 1966.

40. Briggs, B.H. et al. *The Analysis of Observations on Spaced Receivers of the Fading of Radio Signals.* Proceedings of the Physical Society, Vol. B63, 1950, pp. 106-492.

41. Fraser, G.J. *Seasonal Variation of Southern Hemisphere Mid-latitude Winds at Altitudes of 70-100 km.* Journal of Atmospheric and Terrestrial Physics, Vol. 30, 1968, pp. 707-714.

42. Gregory, J.B. *Particle Influx at High Latitudes. II. Solar Protons.* Journal of Geophysical Research, Vol. 68, 1963, pp. 3097-3107.

43. Bailey, D.K. *Abnormal Ionization in the Lower Ionosphere Associated with Cosmic Ray Flux Enhancements.* Proceedings, Institute of Radio Engineers, Vol. 47, 1959, pp. 255-266.

44. Hines, C.O. *An Interpretation of Certain Ionospheric Motions in Terms of Atmospheric Waves.* Journal of Geophysical Research, Vol. 64, 1959, p. 2210.

NOT REPRODUCIBLE

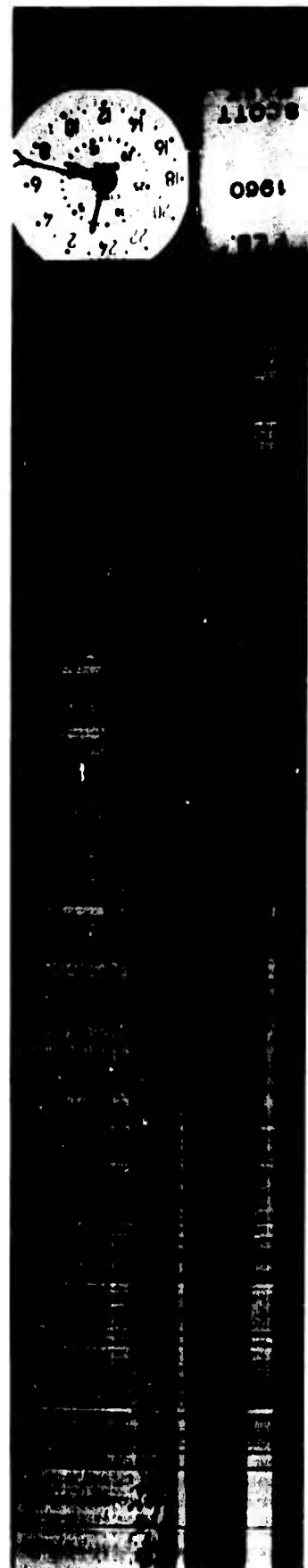


Fig. 1 Sample height-time record, taken at Scott Base, Antarctica, 79°S. The working frequency was 2.3 MHz. White marks at the bottom indicate a reduction in receiver sensitivity by steps of 6 dB, and occur at half-minute intervals. Height markers are at 10 km intervals, with first marker at 30 km. At bottom, the trailing edge of the transmitter pulse shows. At 59 km, and again at 67 km, stable reflections appear. From 74 to 90 km, a weak scattering region is evident. Above 90 km, a stronger reflecting region exists. E-region can be seen as a distinct region at about 103 km. (Time runs from left to right.)

DRIFT MEASUREMENTS BY USE OF D-REGION PARTIAL REFLECTIONS

by

Arne Haug\* and Olav Holt\*\*

\*The Auroral Observatory, Tromsø, Norway

\*\*Norwegian Defence Research Establishment, Kjeller, Norway.

## SUMMARY

Preliminary results are given from an experiment in progress where Mitra's method of drift measurements in the ionosphere is applied to D region partial reflections. Measurements are taken at Lavangsdalen, a low noise level site near Tromsø, Norway.

Partially reflected waves of frequency 2.75 MHz are received on four loop aerials. The spacing between the aerials is of the order of one wavelength. The experimental apparatus is briefly described. The fadings are recorded on four-channel magnetic tape and an analogue computer is used in the correlation analysis.

Drift measurements have been made down to 60 km, but normally the reflections come from the region 70 - 100 km.

Height profiles of electron density are measured simultaneously by the technique (Ref.1) due to Gardner and Pawsey.

Since the observations have only just begun, it is too early to draw any conclusions about seasonal variations in the D-region winds, etc.

The purpose of the paper is merely to show the feasibility of the method.

## DRIFT MEASUREMENTS BY USE OF D-REGION PARTIAL REFLECTIONS

Arne Haug and Olav Holt

### 1. INTRODUCTION

This paper presents some preliminary results from an experiment where the spaced receiver method of drift measurements is applied to D-region partial reflections.

The spaced receiver method has been applied on a routine basis for many years by various workers. It has mainly been used, however, for measurements in the E- and F- region and only a few measurements have been made in the D-region, for instance by Fraser<sup>23</sup>.

The spaced receiver method is well known and we shall only sum up the method briefly. Time delays between the fading of amplitudes recorded by spaced antennas are interpreted as a drift of a ground amplitude pattern, related to the diffraction screen of the reflecting layer. The movements and structure of the ground pattern is, in principle, detectable by three antennas not in a straight line and is, in the classical analysis, assumed to be simply related to movements and structure in the reflecting screen. Recently a collection of reviews and investigations on drift measurements has been published by Kaiser and Müller<sup>4</sup>.

Observations of D-region drift by partial reflections started regularly in Tromsø in December 1967. Measurements are now being taken on one or two days a week.

At least some of the difficulties that arise in the interpretation of spaced receiver measurements in the E- and F- region also seem to occur in the D-region studies and are briefly discussed in this paper.

### 2. EXPERIMENTAL EQUIPMENT AND METHOD OF ANALYSIS

The present experiment is taking place at Lavangsdalen, south of Tromsø ( $69.5^{\circ}\text{N}$ ,  $19.3^{\circ}\text{E}$ ). The transmitting equipment consists of a pulsed transmitter with 50 kW peak power and 12 horizontal half-wave dipoles arranged to give 11 dB vertical gain relative to a single half-wave dipole. The frequency used is normally 2.75 MHz. At the receiver end, four crossed-loop aerials, placed approximately one wavelength apart, as shown in Figure 1, are used.

Circularly polarised receiving aerials have been used to avoid polarisation fading between the two magneto-ionic components. This is important for D-region studies because the two partially reflected magneto-ionic components have comparable amplitudes.

In theory three aerials are needed, but in practice the consistency and reliability of the method may be checked continuously by using four aerials.

At the field site the partial reflections are also detected by a separate receiving system, in order to calculate electron density profiles of the D-region at the same time.

A block diagram of the receiving and recording equipment for these drift measurements is given in Figure 2. The signals from the different antennas are fed through pre-amplifiers into four separate receivers. A height-scan oscilloscope is used to monitor the height

interval of interest. A gate of variable width, usually 5 km, is set at the height where the partial echoes occur, and the signal amplitudes within the gate are recorded on four-track magnetic tape. A four-channel pen recorder is connected for visual display of the fading records. Partial reflections of sufficient strength normally occur at 2 - 4 distinct heights in the height range 60 - 100 km. For the full correlation analysis, which is carried out by means of an analogue computer, it is necessary to have fading records of at least three minutes duration at each height. The required auto- and cross-correlation functions are calculated and plotted automatically.

Figure 3 shows an example of these functions calculated from a three-minute period of observation. The functions shown in the figure are not normalised.

The parameters required to determine the drift are read off from the functions plotted. The final calculation of drift velocity and ground amplitude pattern parameters are then made by a digital computer programmed for the classical procedure of spaced receiver studies (Phillips and Spencer<sup>5</sup>, Fooks<sup>6</sup>).

### 3. RESULTS

Since the observations have only just begun, it is too early to draw any definite conclusions from the records. At the present stage we shall therefore only present some examples of the results. Figure 4 shows examples of E-W and N-S components of drifts obtained on three days in February, March and May 1968. The drifts have typical velocities of  $10-50 \text{ m sec}^{-1}$ . Many records show a change in drift direction with height, with a shift of direction in the components between 90 and 100 km. The records from 22 May show a marked change in the height structure during the  $2\frac{1}{4}$ -hour interval between the records. During other periods of measurement the drift at a certain height has been observed to be stable during a long time interval, as shown in Figure 5. Both the drift direction and magnitude at 60 km height were fairly stable during these two hours. Generally, the amplitude pattern seems to be elongated in the SE-NW direction.

It was mentioned that four receiving aerials are used in the experiment, in order to check the reliability and accuracy of the method. From the four aerials, three different triangles are obtained. The correlation functions illustrated in Figure 3 give drift velocities for the three triangles that agree within 7% from the mean. The drift directions agree within  $\pm 15^\circ$ . Figure 6 shows correlation functions from a period earlier the same day at 95 km height. In this case the velocities agree within 17% and directions within  $\pm 35^\circ$ . It is tempting to connect this larger spread in the results to the fact that the cross-correlation functions for this period are more asymmetric, which may again be attributed to a velocity dispersion of fading frequency components. This will be discussed later.

In the analogue computations, the frequency spectrum of the amplitude fading is also plotted for the different receiver channels. In order to resolve the lowest part of the frequency spectrum, a few records of 20-minutes duration have been made. Figure 7 shows the amplitude spectrum for a record of echoes from 90 km height. In addition to the original spectrum plot, a smooth line has been drawn.

Several authors have suggested that velocity dispersion may take place in the drift, i.e. that the observed fading pattern results from a number of frequency components travelling with different velocities (Downe and Maude<sup>7</sup>, Jones and Maude<sup>8</sup>, Briggs and Golley<sup>9</sup>). Some of the results suggest a dispersion relation where the phase velocity is proportional to frequency. This means that the phase difference,  $\phi$ , between two points on the ground is the same for all frequencies

Using the fading frequency spectrum of Figure 7 (solid line), and the assumption that the phase velocity is proportional to frequency, the cross-correlation functions have been calculated for different values of the phase difference  $\phi$ . The results from this calculation is

shown in Figure 8. Curves for  $180^\circ < \phi < 360^\circ$  may be obtained from a mirror image of the curves in the figure.

Apparent time delays may thus be due to dispersion effects. According to correlation theory cross-correlation functions have the same overall shape as the auto-correlation functions but have lower correlation values and may be time-displaced. However, in the results, functions with asymmetric shapes, which deviate appreciably from the shape of the auto-correlation functions, are often observed.

In the analysis, we have found examples of functions with shapes very similar to those shown in Figure 8. The idea of dispersion seems thus to be a fruitful approach to explain some of the observed correlation functions. It has been suggested to use the skewness of the functions to separate the records which cannot be analysed by the normal method (Briggs and Golley<sup>9</sup>). The apparent dispersion may be due to velocity gradients in the finite height interval which is observed, to oblique reflections from lower heights where the drift velocities may be different, or to real dispersion at a certain height, i.e. moving turbulence or waves with different velocities.

#### 4. CONCLUSIONS

From the preliminary results obtained in this experiment it is seen that the classical drift analysis is not applicable for all records. A necessary, but possibly not sufficient, criterion for the exclusion of records may be a measure of skewness of the cross-correlation functions. The idea of velocity dispersion of fading frequency components seems to be a fruitful approach to explain the asymmetric correlation functions.

#### ACKNOWLEDGEMENTS

The equipment was designed by Mr B. Bjelland and Mr R. Larsen, who has also taken part in the observations.

The computation of the curves shown in Figure 8 is due to Mr Helge Petterson, to whom the authors are also indebted for many helpful discussions.

## REFERENCES

1. Gardner, F.F.  
Pawsey, J.L.  
  
Journal of Atmospheric and Terrestrial Physics, Vol.3, 1953,  
p. 321.
2. Fraser, G.J.  
  
Journal of Atmospheric Science, Vol. 22, 1965, pp. 217-218.
3. Fraser, G.J.  
  
Journal of Atmospheric and Terrestrial Physics, Vol.30, 1968,  
pp. 707-719.
4. Kaiser, T.R.  
Müller, H.G.  
  
Journal of Atmospheric and Terrestrial Physics, Vol.30, 1968,  
pp. 657-1063.
5. Phillips, G.J.  
Spencer, M.  
  
Proc. Roy. Soc. Series B, Vol. 68, 1955, pp. 481-492.
6. Fooks, G.F.  
  
Journal of Atmospheric and Terrestrial Physics, Vol.27, 1965,  
pp. 979-989.
7. Downe, W.H.  
Maude, A.D.  
  
Journal of Atmospheric and Terrestrial Physics, Vol.30, 1968,  
pp. 897-902.
8. Jones, D.  
Maude, A.D.  
  
Journal of Atmospheric and Terrestrial Physics, Vol. 30, 1968,  
pp. 975-977.
9. Briggs, B.H.  
Golley, M.G.  
  
Journal of Atmospheric and Terrestrial Physics, Vol.30, 1968,  
pp. 963-973.

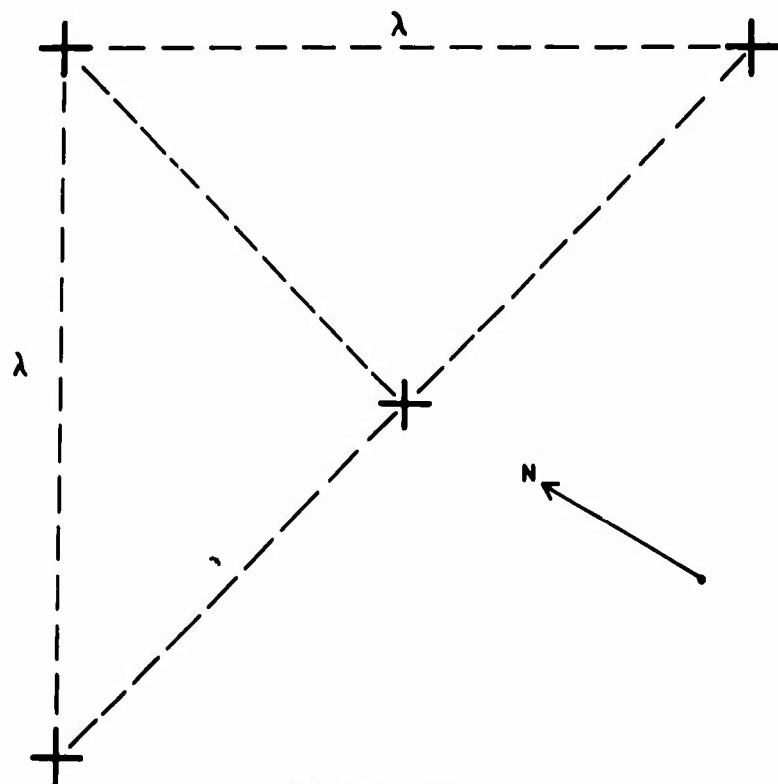


Fig. 1. Configuration of receiving aerials

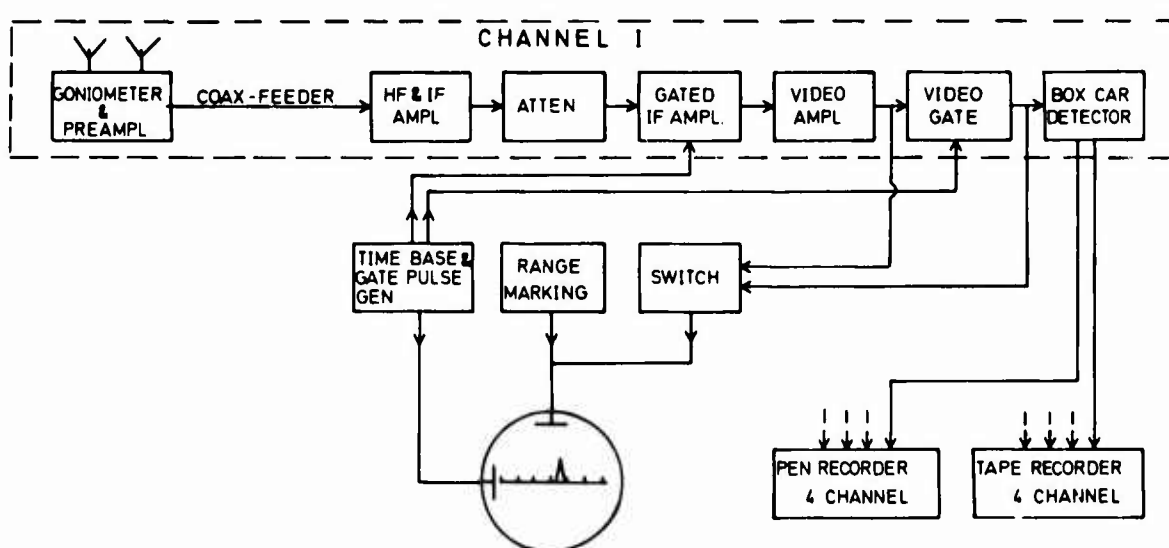


Fig. 2. Block diagrams of receiving and recording equipment

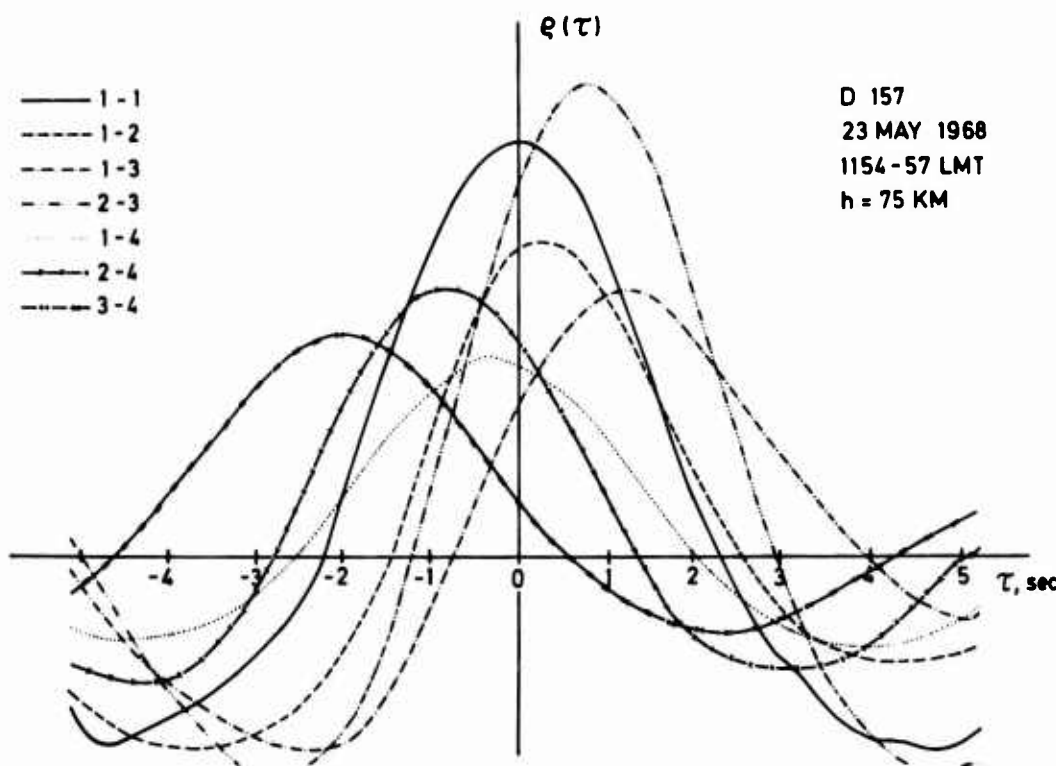


Fig. 3. Examples of auto- and cross-correlation functions from a three-minute period of observation

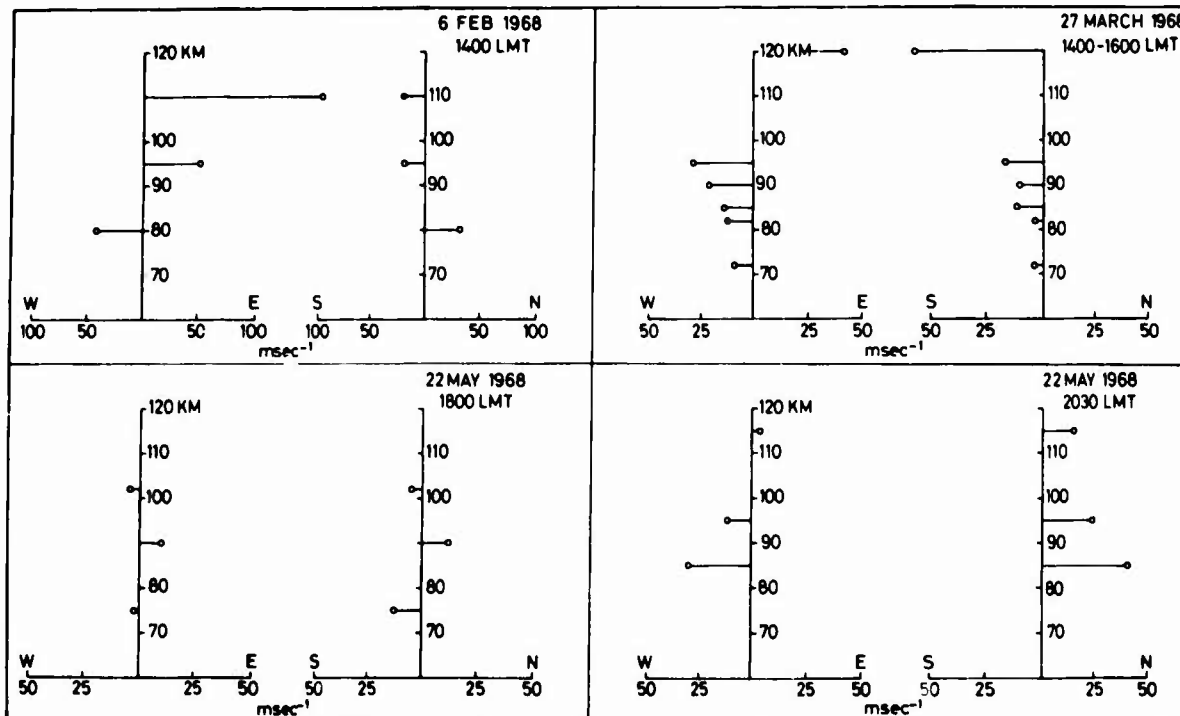


Fig. 4. E-W and N-S components of drift velocities obtained on three days in February, March and May 1968

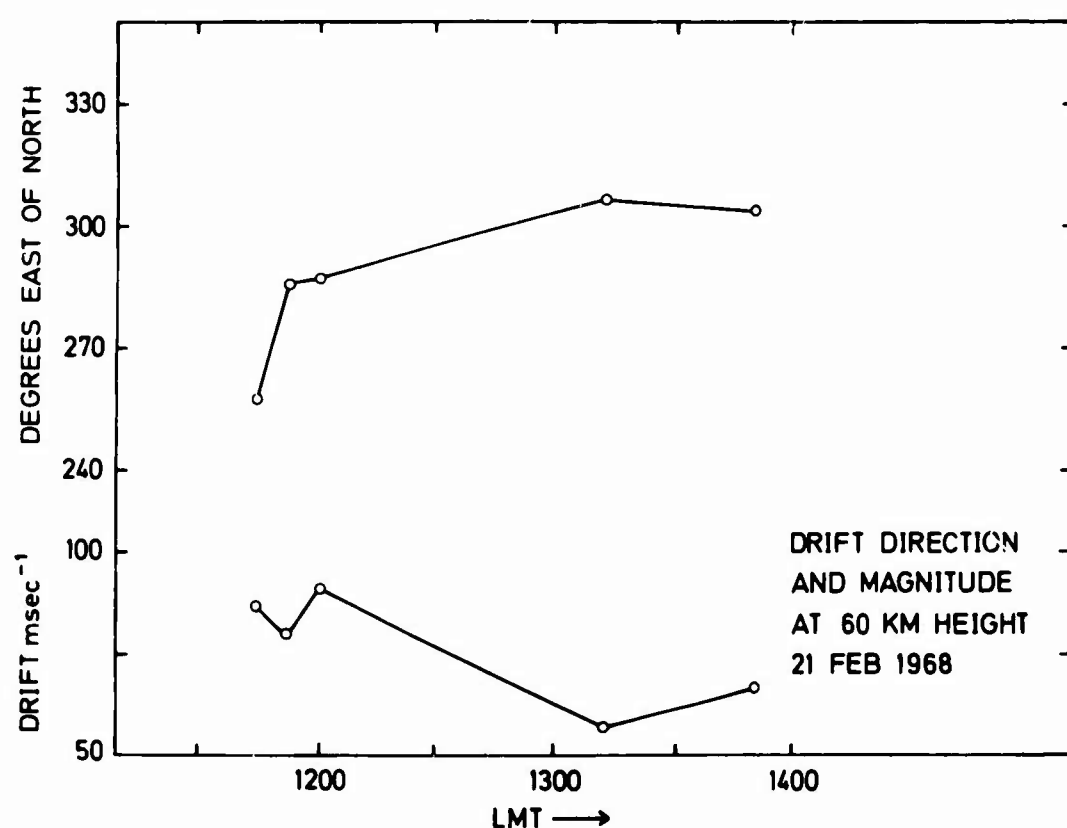


Fig. 5. Direction and magnitude of drift velocity at 60 km height, 21 February 1968

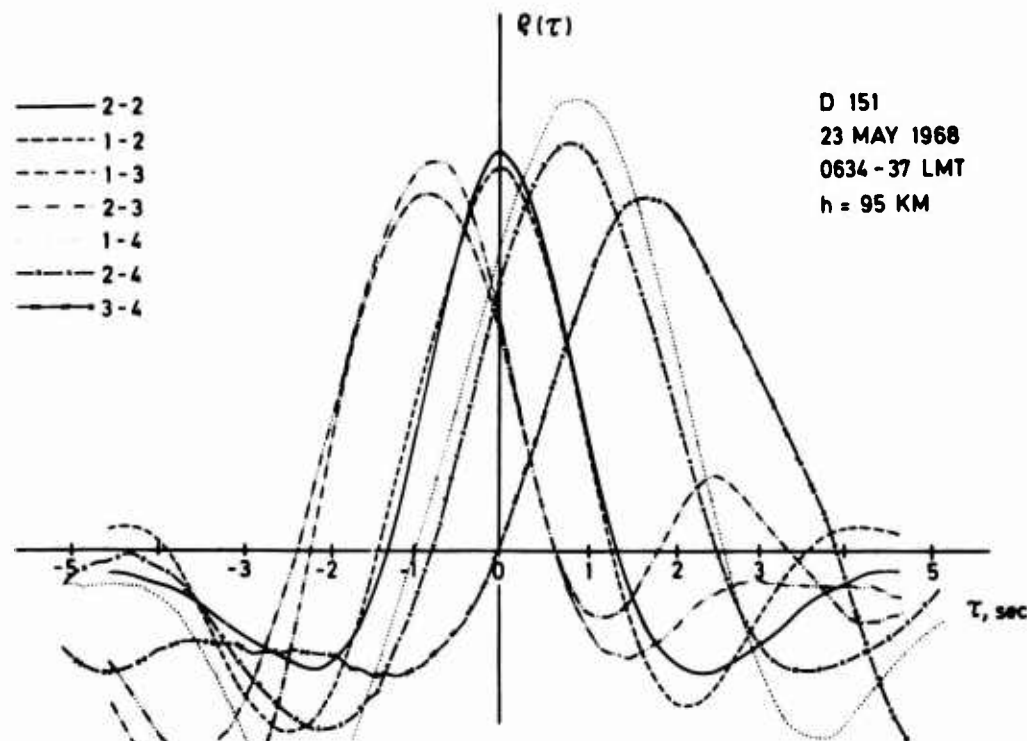


Fig. 6. Auto- and cross-correlation functions from a recording at 95 km height, 23 May 1968

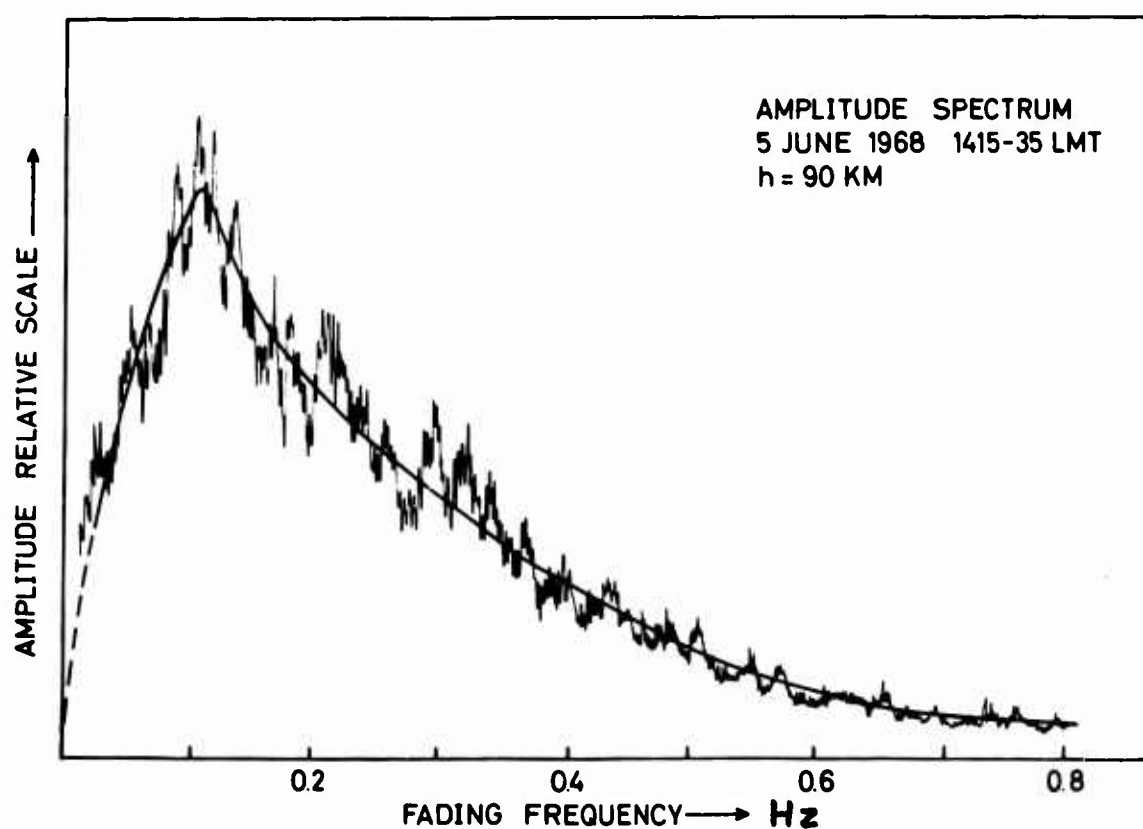
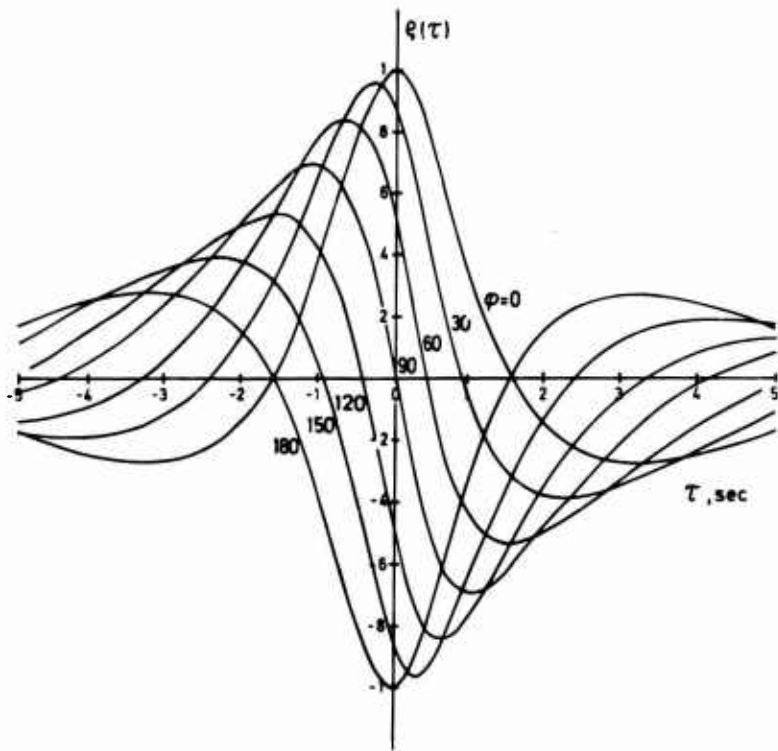


Fig. 7. Amplitude spectrum of a fading record from 5 June 1968

Fig. 8. Cross-correlation functions for various phase differences,  $\phi$ , assuming a dispersion relation with constant  $\phi$  for all frequency components, and using the amplitude spectrum of Figure 7

**DISCUSSION ON THE PAPERS PRESENTED IN SESSION IV  
(D-REGION PARTIAL REFLECTIONS).**

*Discussion on Paper 28: "Radio wave scattering from the ionospheric D-region", by J.B.Gregory.*

**Dr J.Ramasastray:** I should like to ask Dr Gregory if the transport mechanism he mentioned is strong enough to produce any measurable electric fields; in other words, is a dynamo action important in the D-region?

**Dr J.B.Gregory:** The region between 75 and 100 km is a mixed one, in which collisions still determine the mean motion of the electrons. Therefore a dynamo action should not be of importance.

**Dr K.Davies:** A planetary wave can only redistribute (not create) ionization. Can you expand on this point?

**Dr J.B.Gregory:** The concept of a wave does indeed imply a redistribution, e.g., of the overhead mass of air. Thus, locally, a redistribution of ionizable constituents may be expected. If electrons could be considered a conservative property of the atmosphere, they would be similarly redistributed. Thus a travelling wave creates a time variation, at one location, of these quantities. The observations show the existence of such time variations.

**Dr E.V.Thrane:** How does the seasonal variation in the northern hemisphere, as observed for example by Belrose, Bode and Hewitt (Radio Science Journal of Research, Vol.68D, 1964, p.1319), compare with your measurements in the southern hemisphere? Off-vertical reflections impose a limitation on the interpretation of the partial reflection data. At which height do you feel that such reflections become important in your experiments?

**Dr J.B.Gregory:** From measurements of MF absorption at two northern and two southern mid-latitudes, we are able to show a common seasonal variation. We have reworked electron density data published by Belrose, and find the same increase in mean electron densities, 80-86 km, in winter at Ottawa ( $45^{\circ}\text{N}$ ) as exists as Christchurch ( $44^{\circ}\text{S}$ ). In answer to your second question, our technique of measuring the ratio  $A_x/A_o$  required that the two reflections show dependent fading. This requirement was usually not satisfied above 90-95 km, indicating that oblique echoes were present at these altitudes. Our data were limited to altitudes below 90 km for this reason.

*Discussion on Paper 29: "Drift measurements by use of D-region partial reflections", by O.Holt and A.Haug (presented by A.Haug)*

**Dr E.N.Bramley:** Are the drift speeds you quoted, Mr Haug, those of the ground diffraction pattern, or have they been divided by two to give the ionospheric drift speed?

**Mr A.Haug:** The drift speeds have been divided by two. It should perhaps be mentioned that there has been some discussion in the literature recently about whether the simple geometric model that gives the factor of two is correct.

**THOMSON SCATTER AS A COMMUNICATION MODE**

by

**Allen M. Peterson**

**Stanford Research Institute  
Menlo Park, California 94025  
and  
Stanford, University  
Stanford, California  
USA**

## SUMMARY

Scattering of radio waves by density fluctuations of free electrons (Thomson scatter) in the upper region of the ionosphere offers possibilities for long distance communication in the VHF and UHF bands.

While high transmitter power and large antennas would be required, the communication capacity of this propagation mode would decrease only slowly with distance for path lengths up to about 4000 km. A wide range of frequencies could be used, with the 100 to 1000 MHz range being the most likely for practical application.

In Thomson scatter, a Doppler spreading of the transmitted spectra occurs as a result of the thermal motion of the ions which constrain the electrons in the scattering volume. The noise-like nature of the received signal would preclude the use of conventional modulation and detection techniques. Instead, the use of incoherent communications techniques involving frequency shift and/or pulse position modulated transmission and simple power observation (radiometer) in the receiving process would be necessary.

## THOMSON SCATTER AS A COMMUNICATION MODE

Allen M. Peterson

### 1. INTRODUCTION

All charged particles are capable of scattering electromagnetic waves as shown first by J.J. Thomson<sup>1</sup> in 1906. Gordon<sup>2</sup>, in 1958, was the first to suggest that radar technology had advanced to the point that it should be possible to observe "Thomson" scattering by free electrons in the ionosphere. He suggested that the total echo power should be equal to the echo power from a single electron multiplied by the number of electrons, and the spectrum should have a Gaussian shape with a characteristic width determined by the thermal motion of the electrons.

That same year, Bowles<sup>3</sup>, using a 50-MHz radar, detected a scatter signal from the ionosphere of about the predicted intensity but with much narrower spectrum. Bowles<sup>4</sup> suggested that the narrow spectrum resulted from the fact that the electrons are constrained in their motion by the ions, so that the spectral width should correspond to the ion motion for all radio wavelengths, long compared to the Debye shielding distance of the ions. He also argued that the echo spectrum should show amplitude modulation corresponding to the ionic gyrofrequencies and their multiples whenever the incident and scattered rays make equal angles with the earth's magnetic field.

Detailed and continuing theoretical studies of Thomson scattering from the ionosphere have been carried out by many people, including the following: Dougherty and Farley<sup>5,6</sup>; Farley<sup>7,8</sup>; Fejer<sup>9,10</sup>; Hagfors<sup>11</sup>; Moorcroft<sup>12,13</sup>; Perkins and Salpeter<sup>14</sup>; Renau<sup>15</sup>; Rosenbluth and Rostoker<sup>16</sup>; and Salpeter<sup>17</sup>. A very readable and thorough discussion of this work is contained in a recent report by Evans<sup>18</sup>.

Since the original experiments by Bowles, a number of radar systems have been designed specifically for Thomson scatter studies of the ionosphere and lower magnetosphere. Listed in Table I are the major radar facilities that have been constructed for such studies. This table also lists the parameters of these facilities.

The facilities indicated in Table I have permitted a wide variety of important studies of the ionosphere and lower magnetosphere, including (i) the measurement of electron densities to heights of several thousand km, (ii) the measurement of ionospheric electron and ion temperatures, and (iii) the measurement of winds and travelling ionospheric disturbances. Discussion of Thomson scatter observations may be found in the following papers and reports: Bowles<sup>19</sup>; Carlson and Gordon<sup>20</sup>; Evans<sup>18</sup>; Evans and Lowenthal<sup>21</sup>; Farley<sup>22</sup>; Petit and Reyssat<sup>23</sup>.

Based on theory and radar observations, it appears that Thomson scattering of radio signals can provide a useful propagation mode for long-distance communication in VHF and UHF bands. The scattering region of most importance for communication purposes will be the ionosphere near the maximum electron density portion of the F-region. Though the communication capacity would be limited and large antennas and high powers would be required, the capacity should decrease slowly with increasing distance to about 4000 km. A wide band of frequencies should be usable, with 100 to 1000 MHz being the most likely region for application.

## 2. SCATTERED POWER AND CHANNEL CHARACTERISTICS

The Thomson scatter radar cross-section for a free electron is given by the expression

$$\sigma_e = 4\pi(h_e \sin \psi)^2 = 10^{-28} \sin^2 \psi \text{ m}^2, \quad (1)$$

where the classical electron radius  $r_e = e^2/m_e c^2$ , and  $\psi$  is the polarization angle, i.e. the angle between the direction of the incident electric field and the direction to the observer. The  $\sin \psi$  term enters because the scattering polar diagram of each excited electron is similar to that of a Hertzian dipole. As mentioned earlier, electrons in the ionosphere are constrained in their motion by the ions, and as a result the observed radar cross-section  $\sigma$  differs in a number of ways from  $\sigma_e$  given by Equation(1). The following approximation for the radar cross-section was obtained by Buneman<sup>24</sup> for the case in which  $T_e > T_i$  in the ionosphere:

$$\sigma = \sigma_e \left\{ \frac{1}{1 + \left(\frac{4\pi D}{\lambda}\right)^2} + \frac{1}{\left[1 + \left(\frac{4\pi D}{\lambda}\right)^2\right] \left[1 + \left(\frac{4\pi D}{\lambda}\right)^2 + \frac{T_e}{T_i}\right]} \right\}$$

for  $T_e/T_i \leq 3$ . (2)

where

$D = (4\pi N e^2/m_e)^{1/2}$ , the Debye length

$N$  = electron density

$e$  = electron charge

$m_e$  = electron mass

$T_e$  = electron temperature

$T_i$  = ion temperature

$\lambda$  = radio wavelength.

When  $(4\pi D/\lambda) \ll 1$ , the spectrum width is proportional to thermal velocity of the ions and, when  $(4\pi D/\lambda) \gg 1$ , the width is proportional to the thermal velocity of the electrons. With present experimental radars, it is not possible to detect signals when  $(4\pi D/\lambda) > 1$ . This situation would also prevail for communication purposes. It is, therefore, important to choose an operating wavelength  $\lambda$  for which  $(4\pi D/\lambda) \ll 1$ . Under this constraint, the radar cross-section can be represented by the following simplified equation:

$$\sigma = \sigma_e \left[ \frac{1}{1 + \frac{T_e}{T_i}} \right] \text{ for } T_e/T_i \leq 3. \quad (3)$$

Using  $\sigma$ , as given by Equation (3), and assuming a communication path geometry as shown in Figure 1, the ratio of received signal-power to noise-power can be written

$$\frac{S}{N} = \left( \frac{1}{KT_a B} \right) \left( \frac{P_t G_t}{(4\pi R_1)^2} \right) \left( \frac{nV\sigma}{(4\pi R_2)^2} \right) \left( A_T \right) . \quad (4)$$

where

$$K = 1.38 \times 10^{-23} \text{ (Boltzmann constant)}$$

$T_a = T_c + T_R$ , where  $T_c$  is the effective antenna temperature, determined primarily by cosmic noise, and  $T_R$  is the receiver noise temperature ( $^0\text{K}$ )

$B$  = receiver bandwidth in Hz, assumed equal to or greater than the bandwidth ( $B_s$ ) of the scatter signal.

$P_t$  = transmitted power (watts)

$G_t$  = transmitting antenna gain over an isotropic radiator

$R_1$  = range from transmitter to scattering volume (m)

$R_2$  = range from scattering volume to receiver (m)

$V$  = scattering volume, i.e., volume common to transmitting and receiving antenna beams ( $\text{m}^3$ )

$n$  = electron density in scattering volume (electrons/ $\text{m}^3$ )

$A_r$  = aperture of receiving antenna ( $\text{m}^2$ ).

In the Thomson scatter process, Doppler spreading of the signal occurs as a result of the thermal motions of the ions in the scattering region. A continuous-wave single-frequency transmission will be received as a noise-like signal with bandwidth  $B_s$ . Based on the work of Fejer<sup>10</sup> and Moorcroft<sup>12</sup>, the following approximation for the bandwidth may be written for the communication path geometry as

$$B_s = \frac{4 \cos \phi}{\lambda} \sqrt{\left( \frac{2K T_i}{m_i} \right)} . \quad (5)$$

where

$\phi$  = half the included angle between the rays from the scattering volume to the transmitter and receiver.

$\lambda$  = radio wavelength (m)

$T_i$  = ion temperature ( $^0\text{K}$ )

$m_i$  = ionic mass.

In the F region of the ionosphere, which is of primary importance for communication purposes, the dominant ion is  $O^+$ . Based on this,

$$B_s \approx \frac{240 \sqrt{T_i}}{\lambda} \cos \phi . \quad (6)$$

For forward scatter, consider the case of identical transmitting and receiving antennas of height  $H$ , and width  $W$ . The use of identical transmitting and receiving antennas is indicated by scattering volume considerations. Since the useful scattering volume is that common to the two antenna beams, if the lobe patterns of the antennas do not match, power and system sensitivity are wasted. For simplicity, also assume  $R_1 = R_2 = R$  and use the following relationships:

$$G_t = 4\pi A/\lambda^2 = 4\pi n A_0 / \lambda^2$$

$$\beta \approx \lambda/H \text{ radians (half power vertical beamwidth)}$$

$$\gamma \approx \lambda/W \text{ radians (half power vertical beamwidth)}$$

$$\begin{aligned}
 A_0 &= WH \text{ (m}^2\text{)} \\
 \eta &= A_R/A_0 \\
 V &= \frac{2}{3} \left( \frac{\gamma \beta^2 R^3}{\sin 2\phi} \right) = \frac{2}{3} \left( \frac{\lambda^3}{WH^2} \right) R^3 .
 \end{aligned} \tag{7}$$

Using these relationships, the received signal-to-noise ratio can be written from Equation (5) as

$$\frac{S}{N} \approx \frac{P_t \eta^2 W n \sigma \lambda}{12\pi K T_a B_s R \sin 2\phi} . \tag{8}$$

Equation (8) shows that the signal-to-noise ratio is inversely proportional to range to the first power, not  $1/R^4$  as in the conventional radar equation. Thus, the path length has only a small effect on the system sensitivity. Also,  $S/N$  is proportional to antenna width, but, to a first approximation, is independent of antenna height. Thus, to increase signal-to-noise ratio for a given total antenna area,  $W$  should be made as large as possible. Fortunately, an antenna with large width and small height is the easiest type to fabricate. However,  $H$  must be large enough to provide a vertical beamwidth ( $\beta = \lambda/H$ ) which is narrow enough to confine the vertical extent of the scattering volume to the high electron density part of the F-region. Thus, for a scattering volume 200 km in vertical extent, and for a long transmission path ( $2R = 4000$  km), the vertical beamwidth must be limited to  $\beta \approx 0.1$  radian. This requires that  $H \approx 10\lambda$ . More detailed calculations, based on realistic ionospheric electron density profiles, have confirmed that optimum antenna vertical dimensions will be in the  $10\lambda$  to  $15\lambda$  region.

A signal transmitted over an electron scatter communications path will not only be spread in frequency but also in time. Because the signal is propagated by volume scattering, a time delay exists between energy scattered from different regions of the volume. The maximum multipath distance is given by

$$\Delta R = \frac{2R\beta}{\tan \phi} = \frac{2R\lambda}{H \tan \phi} \text{ m} . \tag{9}$$

The multipath time delay is

$$\tau_{\text{mult}} = \frac{\Delta R}{C} = \frac{2R\lambda}{CH \tan \phi} \text{ sec} . \tag{10}$$

The size of the scattering volume also places a constraint on the minimum pulse width to be used in a pulsed transmission system or since the transmitted pulse must fill the common volume in order for the calculated  $S/N$  to be realized. The minimum pulse width is found to be

$$\tau_{\text{min}} = \frac{RB}{C} \tan \phi = \frac{R\lambda}{CH} \tan \phi \text{ sec} . \tag{11}$$

### 3. COMMUNICATION TECHNIQUES

The noise-like nature of the Thomson scatter would preclude the use of conventional modulation and detection techniques. Instead, the use of incoherent communication techniques involving frequency shift and/or pulse position modulated transmission and simple power observation in the reception process would be necessary.

The incoherent channel involves received signal energy determination following appropriate frequency filtering and time gating to minimize the additive noise background. The predetection filter should have a bandwidth equal to the spectrum spread  $B_s$ , since additional bandwidth adds only noise and not signal power. Frequency shifts for information encoding must be at least as large as  $B_s$ , plus the bandwidth of the transmitted pulse. Similarly, pulse-position shifts should be as large as the duration of the transmitted pulse, plus any multipath delay time  $\tau_{\text{mult}}$ . By using  $m$  possible pulse positions consisting of  $m_f$  frequency-shift positions and  $m_t$  time positions, it is possible to encode  $\log_2(m)$  bits of information for each transmitted pulse. This "large alphabet", or multiple-bit encoding, can markedly increase the transmitted information rate under conditions in which either extra frequency positions or extra pulse time positions are available. Extra pulse positions will not ordinarily be available, except where high peak-power, low average-power transmissions are utilized. Extra frequency positions can, in principle, always be used provided frequency allocations permit the extra total bandwidth.

For Gaussian distribution of amplitude fading, the envelope of the amplitude is characterized by a Rayleigh distribution. If our communication system consisted of two channels, we would determine the state of the message by simply comparing the energy levels in the two channels. The means of the envelope distributions in the two channels would be separated by  $(S+N)/N$  dB. Hence, we would determine the error rate by calculating the fraction of time the channel containing noise only would exceed that containing noise plus signal. This can be accomplished by evaluating the appropriate integrals,

$$\text{error rate} = \int_{-\infty}^{\infty} p(x) \int_x^{\infty} p(y) dy dx = \int_{-\infty}^{\infty} p(x) [1 - P_x(y)] dx, \quad (12)$$

where

$p(y)$  is the probability density function of the noise channel,  
 $p(x)$  is the probability density function of the signal noise channel,

$$P_x(y) = \int_{-\infty}^x p(y) dy,$$

and the ratio of the means of  $p(x)$  and  $p(y)$  indicates the S/N ratio.

The error rate can be evaluated for various S/N. For an alphabet size ( $m$ ) greater than two, the error rate would be approximately  $(m-1)$  times the fraction of time  $N > (S+N)$ . In deriving expressions for error rate, it is useful to represent received signal and noise energies by sums of instantaneous power observations taken at intervals separated in time by  $1/B_s$ . When the bandwidth is  $B_s$ , sampling at intervals of  $1/B_s$  yields independent or uncorrelated samples of noise or noise-like signal. If the signal pulse interval is of duration  $\tau$ , then there are  $d = \tau B_s$  samples of signal and noise which can be summed or averaged to increase the probability that a signal has been observed. For high signal-to-noise ratios, fewer independent samples need be averaged to reduce the error rate to a given level than for low signal-to-noise ratios. Hence, shorter duration signal pulses can be used at high signal-to-noise ratios than at low. Of course, high signal-to-noise ratios imply high transmitter power levels and hence may be either impossible to achieve or inefficient in the use of power.

Figure 2 shows the results of calculation\* of two channel error rate (percent of time noise exceeds signal plus noise) as a function of the received signal-to-noise ratio, with order of diversity  $d = \tau B_s$  as a parameter. The curves of Figure 2 can be used to estimate the performance of Thomson scatter signals after having calculated the signal-to-noise ratio from Equation (8), and the scatter bandwidth  $B_s$  from Equation (6). Minimum possible signal diversity  $d = \tau B_s$  would occur if a pulse length  $\tau_{\text{min}}$  (Equation (11)) were utilized for transmission. For this case, the received pulse length would be  $\tau = \tau_{\text{min}} + \tau_{\text{mult}}$ . If, for error-rate considerations, a larger order of diversity were required, longer duration transmitted pulses would be utilized.

---

\* Private communication from J. Petriceks and M. Baron of Stanford Research Institute.

Analyses by Harris<sup>25</sup> and Kennedy and Lebow<sup>26</sup> have determined that optimal system performance, as indicated by the minimum value of the ratio  $E_b/N_0$ , occurs when the signal-to-noise ratio is approximately three.  $E_b$  is the energy per bit of information transmitted, and  $N_0$  is the noise power per unit bandwidth (Hz). For a given pulse transmission system

$$\left. \begin{aligned} \frac{E_b}{N_0} &= \frac{P_t \tau}{N_0 \log_2(m)} \\ &\approx \frac{Sd}{B_s N_0 \log_2(m)} \\ &= \frac{d(S/N)}{\log_2(m)} \end{aligned} \right\} \quad (13)$$

In practice, for optimal performance, the transmitter power and pulse length would be adjusted so that received  $(S/N) = 3$  would provide the required error rate  $\epsilon$  for a given alphabet size  $m$ . System operation at higher or lower signal-to-noise ratios would require higher peak power or longer pulses which would result in higher than optimum values of  $E_b/N_0$ , i.e. require more energy per transmitted information.  $S/N \approx 3$  represents an optimum choice of diversity in combatting the combined effects of receiver noise fluctuations and scatter signal fluctuations. Operation at signal-to-noise ratios in the range between one and ten will ordinarily prove satisfactory and will increase the required energy by less than a factor of two from the optimum value.

As an example of a possible communication application of Thomson scatter, consider its use for teletype transmissions. One 60-word-per-minute teletype channel requires a 30-bit-per-second information rate. For illustrative purposes, assume an error rate  $\epsilon = 10^{-3}$  is required, and the following system parameters are chosen:

$$\begin{aligned} \lambda &= 1 \text{ m} \\ w &= 100 \text{ m} \\ n &= 10^{12} \text{ electrons/m}^2 \\ T_e/T_i &= 1 \\ T_i &= 1500^\circ \text{K} \\ T_a &= 100\lambda^{2,3} = 100^\circ \text{K} \\ R &= 2000 \text{ km.} \end{aligned}$$

From Equations (3), (6), and (8), we find that

$$\begin{aligned} B_s &= 3 \times 10^3 \text{ Hz} \\ S/N &= P_t \eta^2 \times 10^{-4}. \end{aligned}$$

Now, if we assume  $\eta^2 = 0.3$ , and  $S/N = 3$ , we obtain

$$P_t = 10^5 \text{ watts.}$$

Using Figure 2 for a single teletype circuit ( $m = 2$ ), an error rate of  $\epsilon = 0.1\%$  and  $S/N = 3$  requires that the diversity  $d = 16$ . From the relationship  $d = \tau B_s$  we obtain the required pulse length

$$\tau = \frac{d}{B_s} = \frac{16}{3 \times 10^3} = 5.3 \times 10^{-3} \text{ sec.}$$

For single-channel 60-wpm teletype and the assumed system parameters, 30-pulses-per-second are required, of peak power  $10^5$  watts each, pulse of duration 5.3 milliseconds. If a continuous duty transmitter of  $10^5$  watts were available, a much higher bit rate would be possible, approximately 180 bits/sec, or the equivalent of six 60-wpm teletype circuits. Alternatively, S/N might be reduced from optimum and the pulse length increased (hence increasing d) to allow a single teletype channel at reduced peak power.

A more attractive alternative might be to increase the alphabet to size  $m$  to increase the communication rate. For example, if  $m = 16$ , each pulse will encode  $\log_2(16) = 4$  bits of information. For  $m = 16$ , the error rates portrayed in Figure 2 are increased by a factor  $(m - 1) = 15$ . For optimum system performance ( $S/N = 3$ ), the diversity  $d$  must be increased to about  $d = 23$ , requiring an increase in pulse length to  $\tau = d/B_S = 23/(3 \times 10^3) = 7.7 \times 10^{-3}$  seconds. Since each pulse encodes four bits, a  $10^5$  watt transmitter would be able to transmit approximately 500 bits/sec, equivalent to sixteen teletype channels.

It should be noted that these calculations are based on the most favorable assumptions of electron density  $n$ , and receiving antenna noise temperature  $T_a$ . The electron density in the scattering region might, at times, be as much as a factor of ten lower than the assumed  $10^{12}$  electrons/m<sup>2</sup>. The assumed antenna temperature,  $T_a = 100^{\circ}\text{K}$ , might not be realizable, particularly at the low-lost angles required for the longest transmission paths for which sidelobe illumination of the warm ground may be unavoidable. These factors would require correspondingly higher powers to be utilized if the rates given are to be maintained or, alternatively, the transmission rates must be reduced.

#### REFERENCES

1. Thomson, J.J. *Conduction of Electricity Through Gases*. Cambridge, University Press, 1906, p. 321.
2. Gordon, W.E. *Incoherent Scattering of Radio Waves by Free Electrons, with Applications to Space Exploration by Radar*. Proceedings, Institute of Radio Engineers, Vol. 46, 1958, pp. 1824-1829.
3. Bowles, K.L. *Observations of Vertical Incidence Scatter from the Ionosphere at 41 Mc/sec*. Physical Review Letters, Vol. 1, 1958, pp. 454-455.
4. Bowles, K.L. *Incoherent Scattering by Free Electrons as a Technique for Studying the Ionosphere and Exosphere: Some Observations and Theoretical Considerations*. National Bureau of Standards, Journal of Research, Vol. 65D, 1961, pp. 1-13.
5. Dougherty, J.P. Farley, D.T. *A Theory of Incoherent Scattering of Radio Waves by a Plasma*. Proc. Roy. Soc., Jones A. Vol. 259, 1960, pp. 79-99.
6. Dougherty, J.P. Farley, D.T. *A Theory of Incoherent Scattering of Radio Waves by a Plasma. III; Scattering in a Partly Ionized Gas*. Journal of Geophysical Research, Vol. 68, 1963, pp. 5473-5486.
7. Farley, D.T. *The Effect of Coulomb Collisions on Incoherent Scattering of Radio Waves by a Plasma*. Journal of Geophysical Research, Vol. 69, 1964, pp. 197-200.

8. Farley, D.T. *A Theory of Incoherent Scattering of Radio Waves by a Plasma. IV, The Effect of Unequal Ion and Electron Temperatures.* Journal of Geophysical Research, Vol. 71, 1966, pp. 4091-4098.

9. Fejer, J.A. *Scattering of Radio Waves by an Ionized Gas in Thermal Equilibrium.* Canadian Journal of Physics, Vol. 38, 1960, pp. 1114-1133.

10. Fejer, J.A. *Scattering of Radio Waves by an Ionized Gas in Thermal Equilibrium in the Presence of a Uniform Magnetic Field.* Canadian Journal of Physics, Vol. 39, 1961, pp. 716-740.

11. Hagfors, T. *Density Fluctuations in a Plasma in a Magnetic Field, with Applications to the Ionosphere.* Journal of Geophysical Research, Vol. 66, 1961, pp. 1699-1712.

12. Moorcroft, D.R. *On the Power Scattered from Density Fluctuations in a Plasma.* Journal of Geophysical Research, Vol. 68, 1963, pp. 4870-4872.

13. Moorcroft, D.R. *On the Determination of Temperature and Ionic Composition by Electron Backscattering from the Ionosphere and Magnetosphere.* Journal Geophysical Research, Vol. 69, 1964, pp. 955-970.

14. Perkins, F.W. Salpeter E.E. *Enhancement of Plasma Density Fluctuations by Non-Thermal Electrons.* Physical Review, Vol. 139A, 1965, pp. 59-62.

15. Renau, J. *The Cross Section for Scattering of Electromagnetic Waves from an Ionized Plasma in Thermal Nonequilibrium.* Journal of Geophysical Research, Vol. 67, 1962, pp. 3624-3626.

16. Rosenbluth, M.N. Rostoker, N. *Scattering of Electromagnetic Waves by a Nonequilibrium Plasma.* Physics of Fluids, Vol. 5, 1962, pp. 776-788.

17. Salpeter, E.E. *Electron Density Fluctuations in a Plasma.* Physical Review, Vol. 120, 1960, pp. 1528-1535.

18. Evans, J.V. *Design Considerations for a Thomson Scatter Radar.* Aeronomy Report No. 17, University of Illinois, Urbana, Illinois, April 1967.

19. Bowles, K.L. *Measuring Plasma Density in the Magnetosphere.* Science, Vol. 139, 1963, pp. 389-391.

20. Carlson, H.C. Gordon, W.E. *Radar Spectrographic Estimates of Ionic Composition from 225 to 1400 Kilometers for Solar Minimum Winter and Summer Conditions.* Journal of Geophysical Research, Vol. 71, 1966, 5573-5578.

21. Evans, J.V. Lownethal, M. *Ionospheric Backscatter Observations.* Planetary and Space Science, Vol. 12, 1964, pp. 915-944.

22. Farley, D.T. *Ionospheric Temperature and Composition Measurements at the Geomagnetic Equator.* Annales de Géophysique, Vol. 22, 1966, pp. 448-453.

23. Petit, M.  
Reyssat, M. *La Station de Reception du Sandeur Ionosphérique à Diffusion, Francais.* L'Onde Electrique, Vol. 46, March 21-24, 1966.

24. Buneman, O. *Scattering of Radiation by the Fluctuations in a Non-Equilibrium Plasma.* Journal of Geophysical Research, Vol. 67, 1962, pp. 2050-2053.

25. Harris, D.P. *Techniques for Incoherent Scatter Communication.* Institute of Radio Engineers, Transactions on Communications Systems, June 1962, pp. 154-160.

26. Kennedy, R.S.  
Lebow, I.L. *Signal Design for Dispersive Channels.* Institute of Electrical and Electronic Engineers, Spectrum, March 1964, pp. 231-237.

TABLE I  
Parameters of Existing Thomson Scatter Radars

<i>Location and Affiliation of Facility</i>	<i>Position</i>	<i>Operating Frequency (MHz)</i>	<i>Type</i>	<i>Antenna</i>	<i>Effective Antenna Aperture A<sub>d</sub> (dB over 1 m<sup>2</sup>)</i>	<i>T<sub>s</sub> (°K)</i>	<i>Peak Power (kW)</i>
Jicamarca (Peru), ITSA/ESSA	76.9°W 11.9°S	49.92	Vertical pulse	290 m × 290 m dipole array	45.0	6,000	4,000
Arecibo (PR), Cornell U.	66.75°W 18.3°N	I 40.12 II 430.0	Vertical pulse Vertical pulse	300 m spherical reflector	43.7 41.7	10,000 300	2,500 2,000
Millstone Radar (Westford, Mass.), MIT Lincoln Lab.	71.5°W 42.6°N	I 440.0 II 1295.0	Vertical pulse Oblique pulse	68 m 25 m parabolas	32.2 22.8	200 150	3,000 4,000
Nancay (France), CNET	Transmitter at 2.19°E 44.65°N St. Santin de Maurs) Receiver at 2.19°E 47.37°N (Nancay)	935.0	Bistatic CW transmitter vertical  Receiver Oblique	20 m × 100 m reflector  40 m × 200 m reflector	30.0	600	75
Malvern (England), RRE	2.14°N 52.09°N	400.0	Vertical pulse	45.5 m parabola	28.5	200	10,000
Stanford (Calif.), SRI	37.40°N 122.17°W	1290.0	Oblique pulse	27 m parabola	23.0	200	5,000

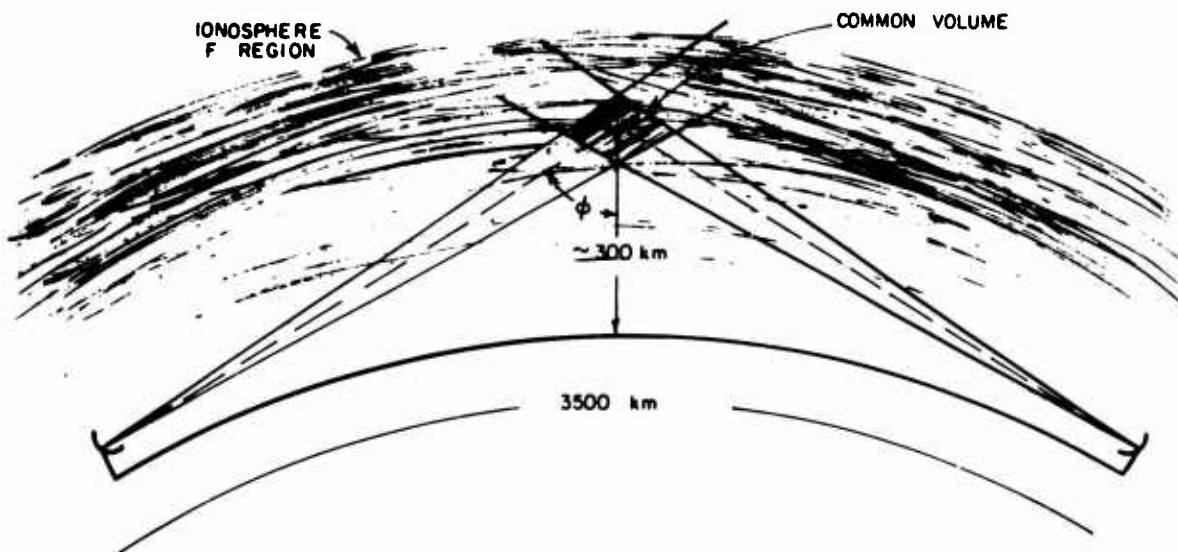


Fig. 1 Communication path geometry

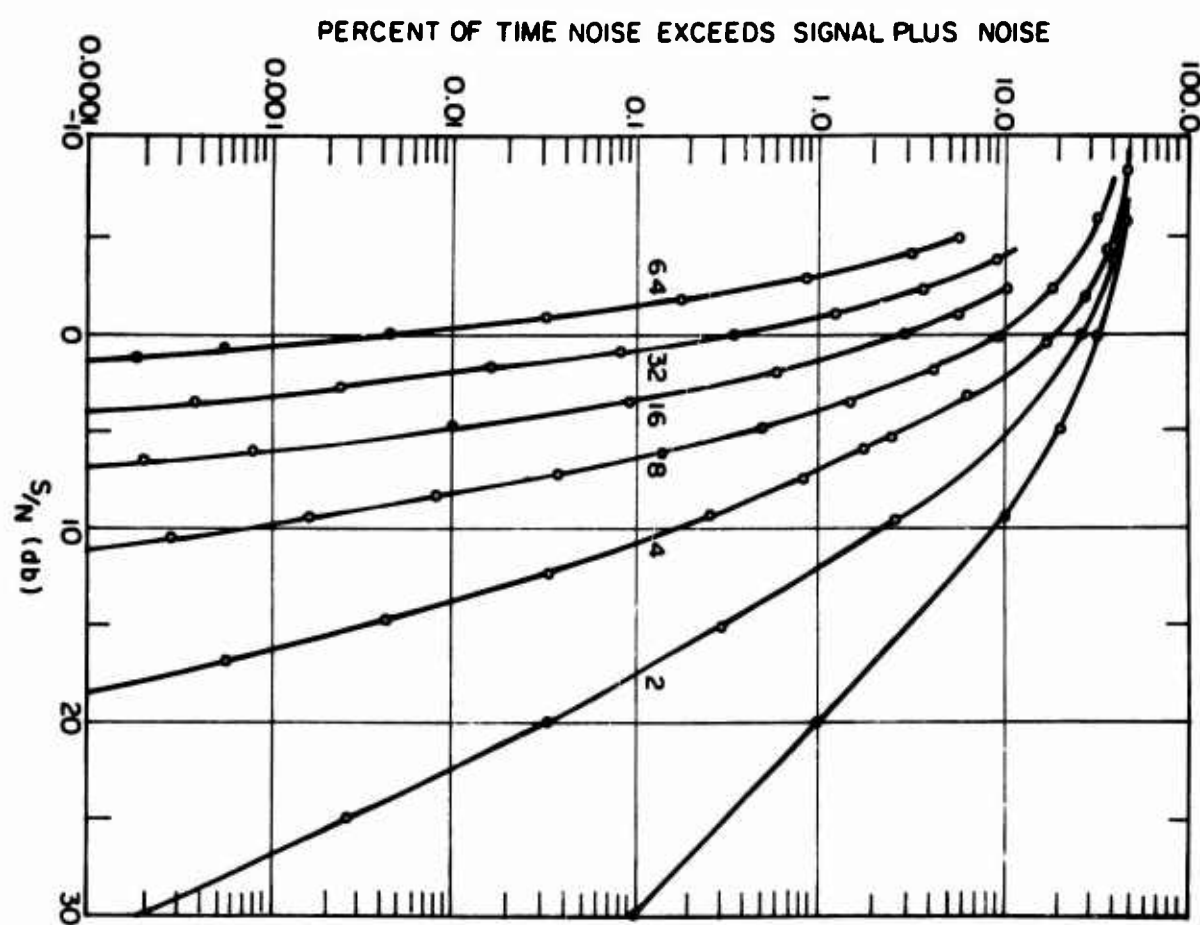


Fig. 2 Percent of time noise exceeds signal plus noise versus signal-to-noise ratio with order of diversity as a parameter

**INCOHERENT SCATTER OBSERVATIONS OF THE E-REGION**

by

**G. N. Taylor**

Royal Radar Establishment,  
Malvern, Worcestershire, England

## SUMMARY

The method of measuring profiles of electron concentration  $N_e$  versus height in the lower ionosphere with a pulsed incoherent scatter radar is described. The lowest measurable  $N_e$  is determined partly by equipment sensitivity and partly by the plasma Debye length becoming comparable with the radar wavelength. Incoherent scatter yields good E-region profiles in conditions which defeat the ionosonde, e.g. at night-time, during blanketing  $E_s$  or high absorption, and when  $N_e$  is not increasing monotonically with height. It also gives much better temporal coverage than sounding rockets. Some typical mid-latitude summer profiles for both night-time and day-time are presented. Plots of the heights of well-defined peaks against time illustrate the relative stability of the normal- and sporadic-E peaks, and the large number of abnormal propagation modes that can exist for short periods.

## INCOHERENT SCATTER OBSERVATIONS OF THE E-REGION

G. N. Taylor

### 1. INTRODUCTION

The technique of incoherent scattering has been extensively used for obtaining information about the charged particle concentrations and temperatures in the ionospheric F-region<sup>1</sup>, and has also recently begun to be used in the E-region. The results presented here are concerned with the detailed structure and variability of the electron concentration profile between 90 and 170 km altitude at a mid-latitude station in summer. The information about stratification, time variations and night-time profiles is more detailed and complete than that given by other techniques, and would be suitable for precise calculations of absorption, group delay and propagation modes in communication systems.

### 2. APPLICATION OF PULSED INCOHERENT SCATTER RADAR TO THE E-REGION

The mechanism of scattering, which is essentially caused by thermal fluctuations of refractive index in the plasma, has been extensively discussed in the literature<sup>2,3,4</sup> and it is sufficient here to quote a simplified equation giving the received signal-to-noise power ratio,  $\eta$ , for a vertically looking radar system:

$$\eta = K \frac{P_T A N_e \sigma \tau}{R^2 T_B} . \quad (1)$$

Here  $P_T$  is the peak transmitted power,  $A$  is the effective area of the receiving aerial,  $N_e$  is the electron concentration,  $R$  is the range (the same as the height,  $h$ , in this case),  $T$  is the system noise temperature,  $B$  is the receiver bandwidth,  $\tau$  is the pulse duration,  $\sigma$  is the scattering cross-section per electron and  $K$  is a constant. For the normal mode of scattering, in which the signal spectrum is broadened by an amount characteristic of the thermal velocities of the ions,

$$\sigma = \sigma_e \left( 1 + \frac{T_e}{T_i} \right) , \quad (2)$$

where  $\sigma_e$  is the Thomson electron scattering cross-section and  $T_e, T_i$  are the electron and ion temperatures respectively.

Equation (2) holds true<sup>5</sup> as long as

$$\lambda_0 \gg 4\pi\lambda_D , \quad (3)$$

where  $\lambda_0$  is the radar wavelength and  $\lambda_D$  is the Debye length in the plasma, proportional to  $(T_e/N_e)^{1/2}$ . When  $\lambda_0 \gtrsim 4\pi\lambda_D$ , a significant proportion of the scattered power originates from the classical Thomson process, with a spectral spread corresponding to the thermal velocities of the electrons rather than the ions. Because of its broad bandwidth, this "electronic" component of the scatter signal is effectively lost, and thus  $\sigma$  is reduced below the value given by Equation (2). This situation, which occurs both at low heights, in the D-region, and at great heights, around 2000 km, determines the region of the ionosphere from which it is possible to get useful information by the incoherent scattering technique for a given  $\lambda_0$ . It is assumed that the occurrence of collisions between electrons and heavy particles has no effect on  $\sigma$  (Ref. 4).

For E-region observations,  $\tau$  and  $B$  in Equation (1) must be chosen so that adequate height resolution is achieved. In general, a radar pulse length not greater than the plasma scale height is used; if very fine structure such as that of sporadic-type layers is to be resolved, a pulse length much shorter than the scale height is needed. The short pulses required for E-region work have a relatively large intrinsic frequency spread, much larger than the additional spread due to the thermal motion of the scattering centres. Thus direct temperature measurements are very difficult to make and some assumption has to be made about the value of  $T_e/T_i$  in Equation (2). Fortunately, it is now fairly certain that  $T_e/T_i = 1$  at all heights below 140 km (References 6 and 7); thus, from Equation (2),

$$\sigma = \sigma_e/2 \quad (4)$$

and observed profiles of  $\eta$  versus  $h$  can be converted to  $N_e(h)$  profiles provided that an absolute calibration of the system is available. This calibration is most conveniently provided by measurements of the E-layer critical frequency,  $f_c E$ , from a nearby ionosonde.

### 3. COMPARISON WITH OTHER TECHNIQUES FOR E-REGION MEASUREMENTS

The main information given by the present observations is the profile of  $N_e$  versus height. It is relevant to compare this technique with others, and in particular with ionosondes and sounding rockets: no technique for observing the E-region from an orbiting satellite is yet available.

The ground-based ionosonde has been used for many years and gives accurate values of  $N_e$  at peaks and points of inflection, but less reliable measurements at other parts of the profile. This is especially true of "valleys", which are difficult to delineate, and whose presence affects the interpretation of echoes from regions lying above them. Normal ionosondes also give little information about regions whose penetration frequencies lie below the lower frequency limit of the instrument. The lowest accessible value of  $N_e$  is commonly about  $10^{10} \text{ m}^{-3}$ ; this limit is reduced for special low frequency ionosondes, but these can be successfully operated only in areas remote from sources of interference, and have so far yielded much less information than the higher frequency instruments. Ionosondes also run into difficulty in the presence of blanketing sporadic-E layers, or of high absorption; in these cases information about the E-region profile is much reduced or is missing altogether.

Sounding rockets allow various techniques to be used for measuring the profile, including in situ sampling and radio propagation methods. Very accurate measurements with excellent height resolution can be obtained, which do not suffer from the limitations of the ionosonde in measuring low values of  $N_e$  and detecting the extent of valleys. Rocket measurements can thus provide a "snapshot" of the  $N_e$  profile at one place and time, but only a very incomplete picture of time variations, because of the difficulty and expense of organising launches.

Incoherent scatter radar has the advantage of all ground-based techniques in obtaining measurements as a function of time at a fixed place. Since the scattering cross-section is extremely small (typically  $10^{-4} \text{ m}^2$  for a pulse volume), the radar can "see through" maxima of  $N_e$  and accurately determine the profile shape in the valleys. Absolute values of  $N_e$  are less reliable than those obtained from ionograms, but the whole profile is readily calibrated by a few spot ionosonde measurements. The minimum detectable  $N_e$  is limited in principle by relation (3), ceasing to be true for large Debye lengths, but in practice also by the equipment sensitivity. For the present equipment, these two limits occur in the E-region at the same value of  $N_e$ , about  $6 \times 10^8 \text{ m}^{-3}$ . Time resolution is normally about 5–10 minutes but can be improved, at the expense of some loss of sensitivity, by reducing the signal integration period. Height resolution can be made at least as good as that of an ionosonde, but approaches that of the best rocket measurements only at the cost of considerably decreased sensitivity. Since group delay in the scattering medium

is negligible, the absolute heights of features on the profile can be measured very easily, with an uncertainty due only to the finite length of the transmitted pulse.

Thus incoherent scatter radar has many of the advantages of both ionosondes and sounding rockets: its main disadvantage is the complexity of the equipment, which restricts the number of places in which it can be used.

#### 4. EQUIPMENT

The results presented in Section 5 were obtained with a vertically-looking pulsed incoherent scatter radar equipment at the Royal Radar Establishment, Malvern, England, at a geographical position of  $52.1^{\circ}\text{N}$ ,  $2.3^{\circ}\text{W}$ , and a magnetic dip angle of  $67.7^{\circ}$ . The observations were made on three days in May 1968 and it is not claimed that all the features observed are necessarily of daily occurrence, though most of them are probably typical of the season.

The equipment operates at a frequency of 400.50 MHz (74.9 cm wavelength) with a peak transmitted power of 7 MW and a repetition frequency of  $150\text{ s}^{-1}$ . The pulse duration was chosen to be  $33\mu\text{s}$  (5 km radar length), to give adequate height resolution for the E-region. The receiver front end is a varactor diode parametric amplifier; the system noise temperature is  $150^{\circ}\text{K}$  and the receiver bandwidth is 40 kHz. The aerial is a fixed front-fed vertically pointing paraboloid of aperture diameter 43 m; the feed is in the plane of the aperture, in order to minimise the gain in far-out sidelobes of the polar diagram, and thus eliminate as much clutter signal as possible.

Circular polarisation is used, generated in a waveguide turnstile junction, which also provides passive isolation between the transmitter and the receiver. The total passive isolation, due partly to the properties of the turnstile junction, and partly to the use of a vertex plate in the aerial, is 50 dB. Thus only about 70 W peak power leaks through to the receiver input from the transmitter, and this is further reduced by gas discharge and solid state limiters. The total receiver protection appears to be quite adequate, as no recovery effects are observed after the transmitter pulse.

The received signal was incoherently integrated in 30 range intervals, each equal in width to the radar pulse length, for periods of 5 minutes; frequent comparison runs with the receiver off-tuned by 100 kHz were made, to determine the baseline from which the integrated signal was measured. Permanent clutter echoes were present at ranges up to 70 km; between 70 and 90 km strong echoes occurred randomly, with durations seldom exceeding a few minutes. These latter echoes are thought to be due to aircraft passing through the near horizontal sidelobes of the aerial: if any of them were of natural origin it would be impossible to distinguish them.

#### 5. RESULTS

The  $N_e$  profiles presented here were obtained by normalising the scattered power at the observed height of the E-region peak (about 110 km) to  $N_{mE}$  measured by the ionosonde at Slough, 130 km distant. At night, when  $f_0E$  is below the range of the ionosonde, the daytime calibration was extrapolated to lower signal levels. Corrections were applied for varying system sensitivity, and for departures from the small Debye length approximation when  $N_e$  was small. In the absence of independent temperature measurements, no correction for  $T_e/T_i$  differing from unity was possible, and thus the profiles became progressively more uncertain above 140 km by day. Errors in  $N_e$  are probably about 10% below 140 km by day, and about 20% at all heights during the night.

It is of considerable interest to know whether there is a valley in the profile above the normal E-layer. During the present observations a small valley was usually seen during the daytime, though it sometimes disappeared, apparently more or less at random. Figure 1

shows typical examples of daytime profiles with and without valleys, and a profile showing multiple stratification.

A very noticeable feature of many of the profiles, both during the day and the night, was the presence of sporadic-type layers, which appeared as spikes which were clearly unresolved in height. These sporadic layers were seen for a considerable proportion of the time, and usually appeared to be superimposed on a normal profile. Figure 2 shows daytime profiles, one with a slight, one with an intense, and one with a double, sporadic layer: since these peaks are unresolved, the peak electron concentrations are lower limits.

The night-time profiles were extremely variable in form, with  $N_e$  usually less than  $5 \times 10^9 \text{ m}^{-3}$  below 170 km, except possibly in sporadic-type layers. Between 110 and 140 km height there was usually at least one prominent peak, sometimes resolved and sometimes of sporadic type. Above 140 km,  $N_e$  became too low to be reliably measured in the hours before dawn. Between 100 and 105 km another persistent, though much smaller, peak was often observed, and is believed to be due mainly to integrated coherent echoes from meteors, and is thus not a true ionospheric layer. Figure 3 shows some profiles illustrating these night-time features.

During the day the profiles are usually contaminated with clutter echoes at heights below 90 km. A few runs were, however, apparently clear of clutter, and with these the profiles can be extended down into the upper D-region. Some typical results obtained at two times of day are shown in Figure 4 and compared with a recent mean profile, based on VLF propagation measurements in England, published by Bain and May<sup>8</sup>. The incoherent scatter results are of the right order of magnitude, but are subject to considerable uncertainty, as a fairly large Debye length correction factor has been applied. The residual clutter level is not known, but it would appear to be significant below 80 km.

Lastly, to present a more systematic picture of the present data, in Figures 5 and 6 are plotted the heights at which all clearly defined peaks and points of inflection occurred on the profiles during two periods of time. Figure 5 is for a period from noon until just before sunset, which is at 2110 h at 100 km height. The normal E-region peak can be seen from 1200 h to 1500 h, but is obscured by a sporadic layer most of the time after 1500 h; height deviations of  $\pm 5$  km from the average value occur fairly randomly. The features around 165 km are probably at the F1-layer peak as normally defined, though this may be partly suppressed by the absence of a temperature correction to the profile. Many other features between 120 and 160 km can be seen, but these are mostly transient.

Figure 6 covers a period from midnight till several hours after dawn, which is at 03 h at 100 km height. The most interesting feature is a persistent sporadic-type layer, which appears to move steadily downwards from 140 km and merges with the normal E-layer peak at dawn. The peak which has been attributed above to meteor echoes is clearly visible at about 105 km from 0100 h onwards: at dawn this gradually becomes swamped by normal scatter echoes from the ambient ionisation, first becoming a point of inflection and then disappearing.

## REFERENCES

1. Evans, J.V. *Ground-Based Measurements of Atmospheric and Ionospheric Particle Temperatures.* In "Solar-Terrestrial Physics", Academic Press, London, 1967, p. 289.
2. Fejer, J.A. *Scattering of Radio Waves by an Ionized Gas in Thermal Equilibrium in the Presence of a Magnetic Field.* Canadian Journal of Physics, Vol. 39, 1961, p. 716.
3. Dougherty, J.P., Farley, D.T. *A Theory of Incoherent Scattering of Radio Waves by a Plasma.* Proc. Roy. Soc., London, A, Vol. 259, 1960, p. 79.
4. Waldteufel, P. *Introduction de l'Effet des Collisions Elastiques dans l'Equation de Boltzmann d'un Gaz Faiblement Ionisé: Application à la Diffusion Incohérente d'une Onde Electromagnétique par l'Ionosphère.* Annales de Géophysique, Vol. 21, 1965, p. 106.
5. Buneman, O. *Scattering of Radiation by the Fluctuations in a Nonequilibrium Plasma.* Journal of Geophysical Research, Vol. 67, 1962, p. 2050.
6. Carru, H., et al. *Mesures de Températures Electroniques et Ioniques par Diffusion Incohérente.* Journal of Atmospheric and Terrestrial Physics, Vol. 29, 1967, p. 351.
7. Evans, J.V. *Electron Temperature and Ion Composition in the F1 Region.* Journal of Geophysical Research, Vol. 72, 1967, p. 3343.
8. Bain, W.C., May, B.R. *D-Region Electron-Density Distributions from Propagation Data.* Proceedings, Institution of Electrical Engineers, Vol. 114, 1967, p. 1593.

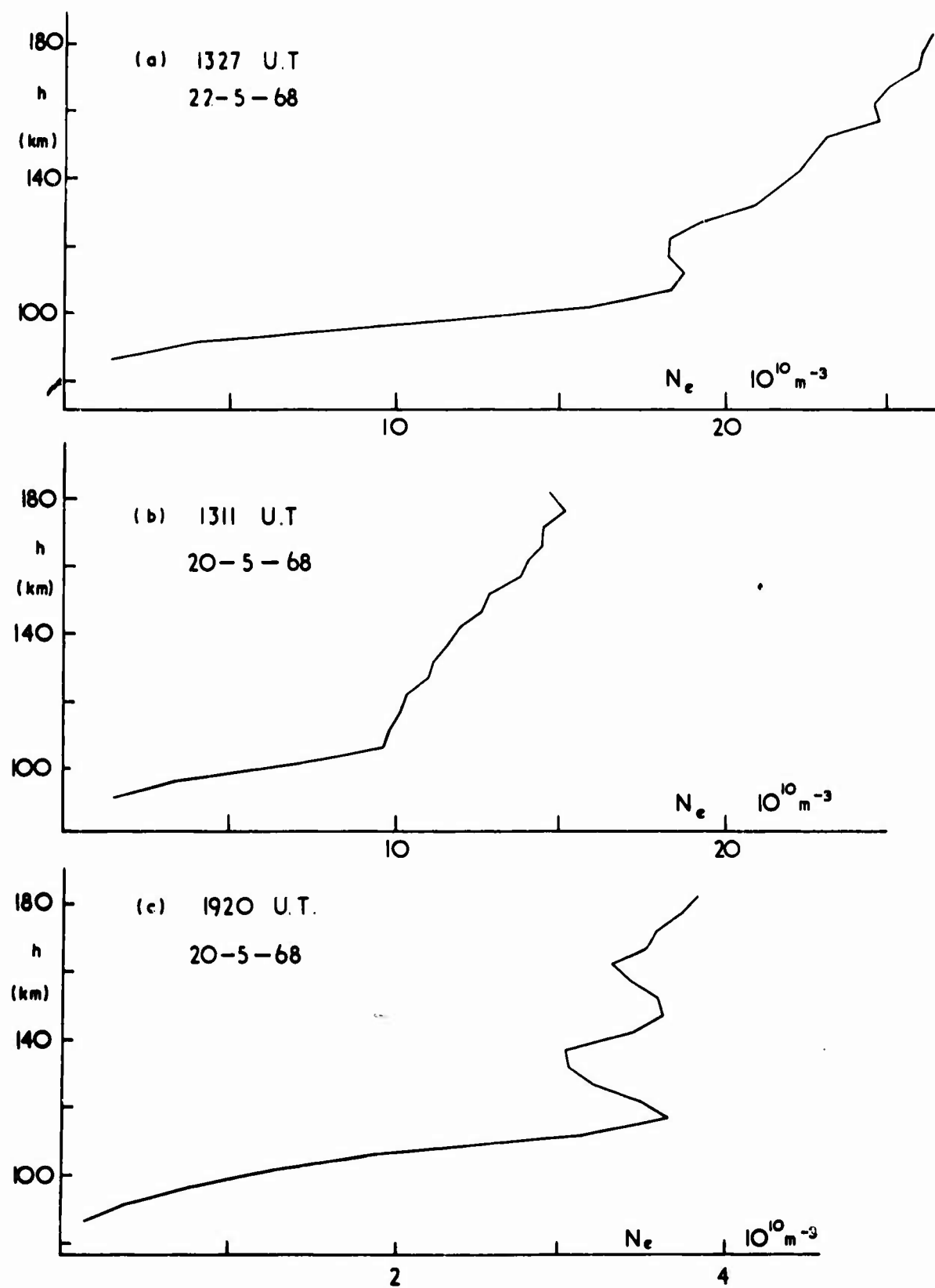


Fig. 1 Daytime profiles of electron concentration  $N_e$  versus height  $h$  showing:  
 (a) normal profile with valley above the E-peak, (b) normal profile  
 without valley, (c) profile with multiple stratification. Time on this  
 and subsequent Figures is UT ( $0^\circ\text{W}$  Mean Time)

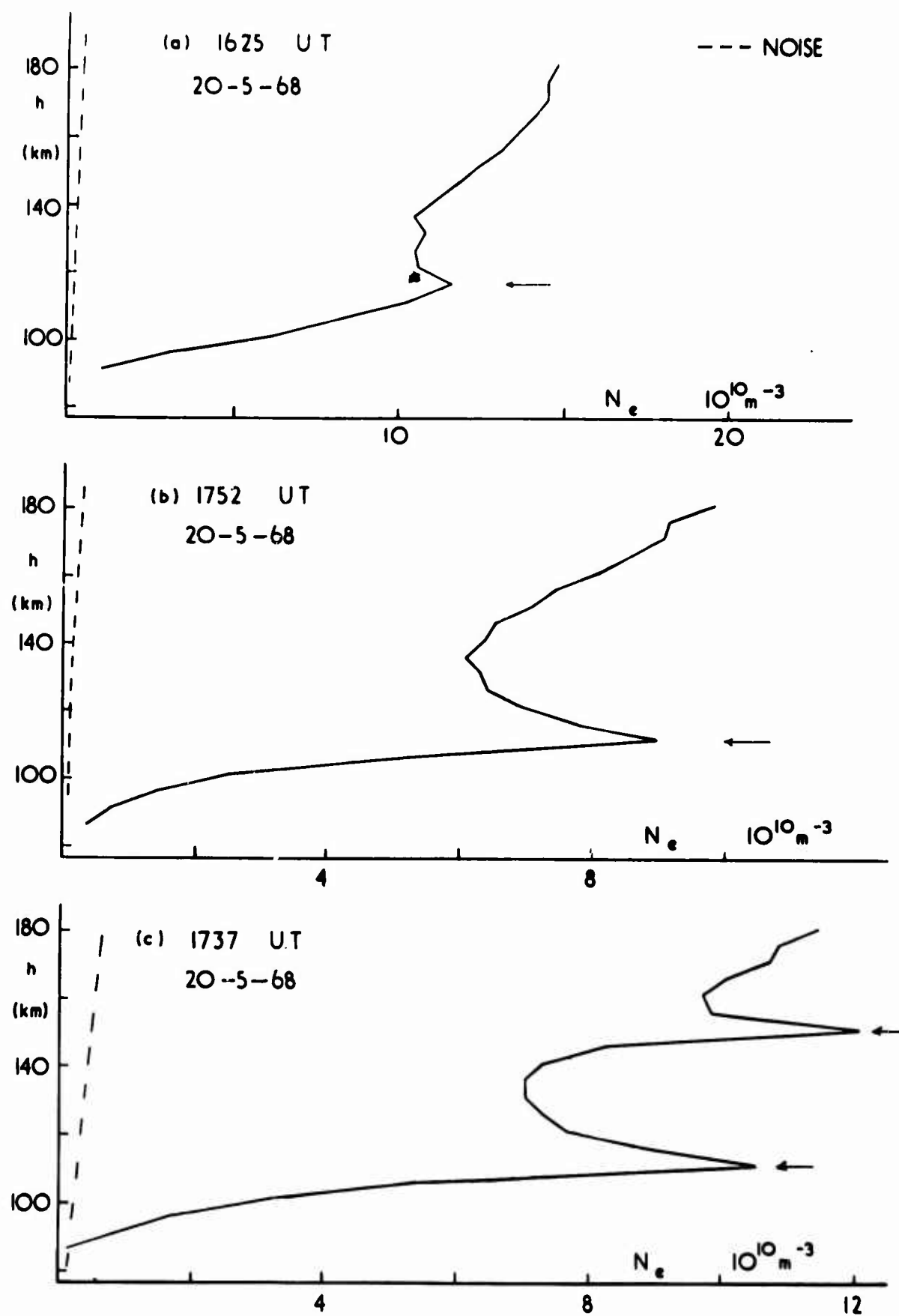


Fig. 2 Daytime  $N_e(h)$  profiles showing: (a) slight, (b) intense, (c) double, sporadic-E layers

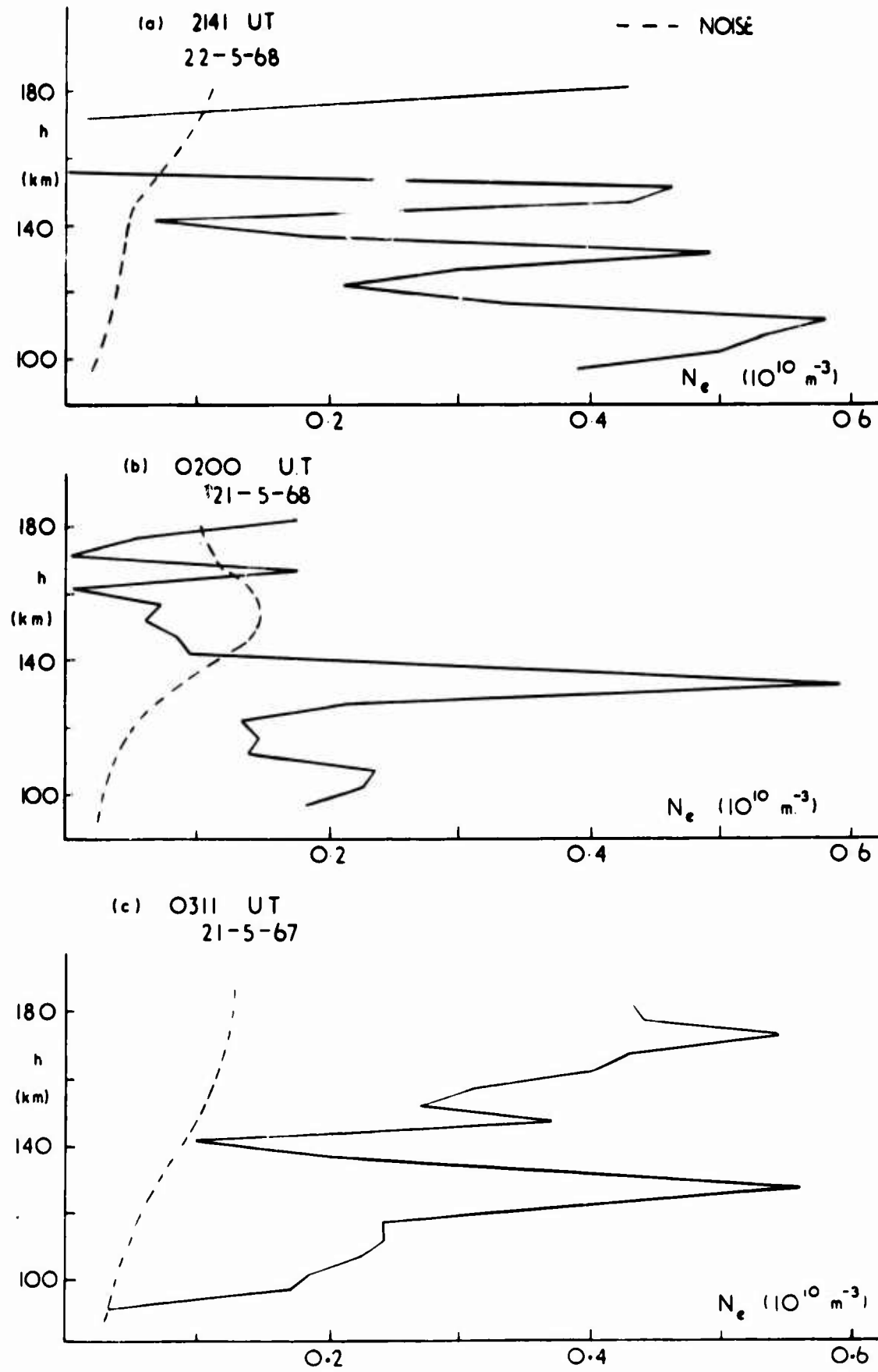


Fig. 3 Night time  $N_e(h)$  profiles: (a) just after sunset, showing irregular structure; (b) 1 hour before dawn, showing meteor echo peak at 105 km, sporadic-type layer at 130 km, and very low  $N_e$  above 140 km; (c) just after dawn, showing night-time structure beginning to be "filled-in" by photoionisation

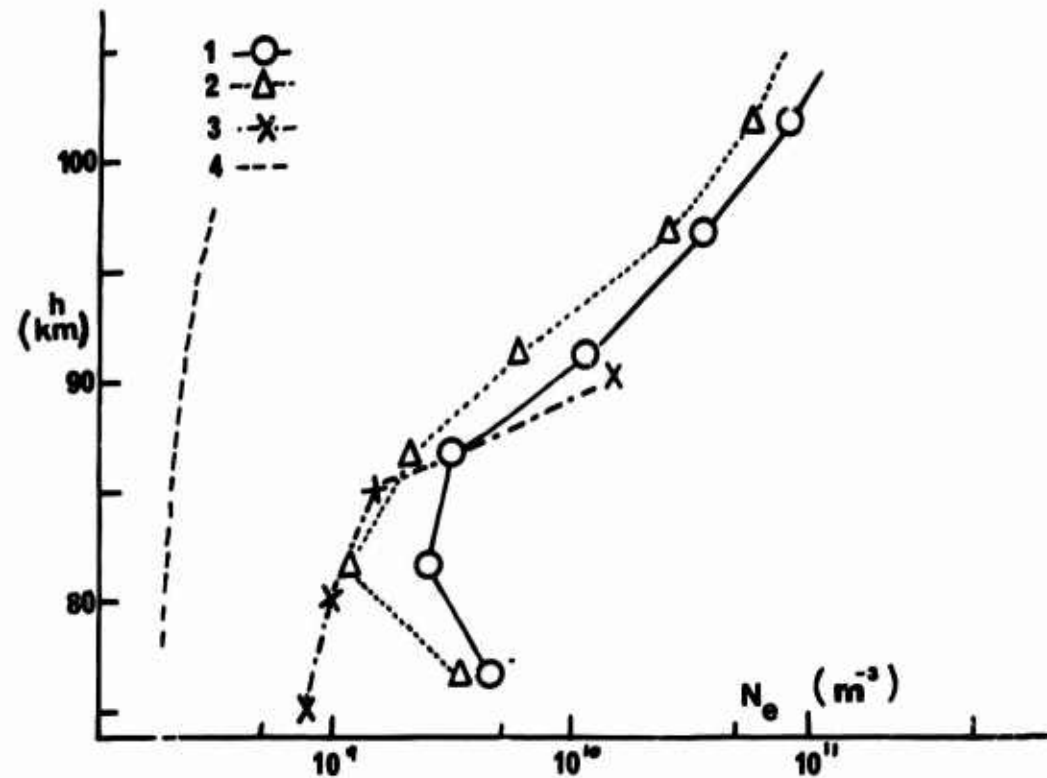


Fig. 4 Daytime  $N_e(h)$  profiles between heights of 80 and 100 km, from selected clutter free recordings: (1) 1210 UT, 20th May 1968. (2) 1740 UT, 20th May 1968. (3) Mean profile for noon, summer, sunspot maximum, from VLF propagation results (Ref. 8). (4) Noise level

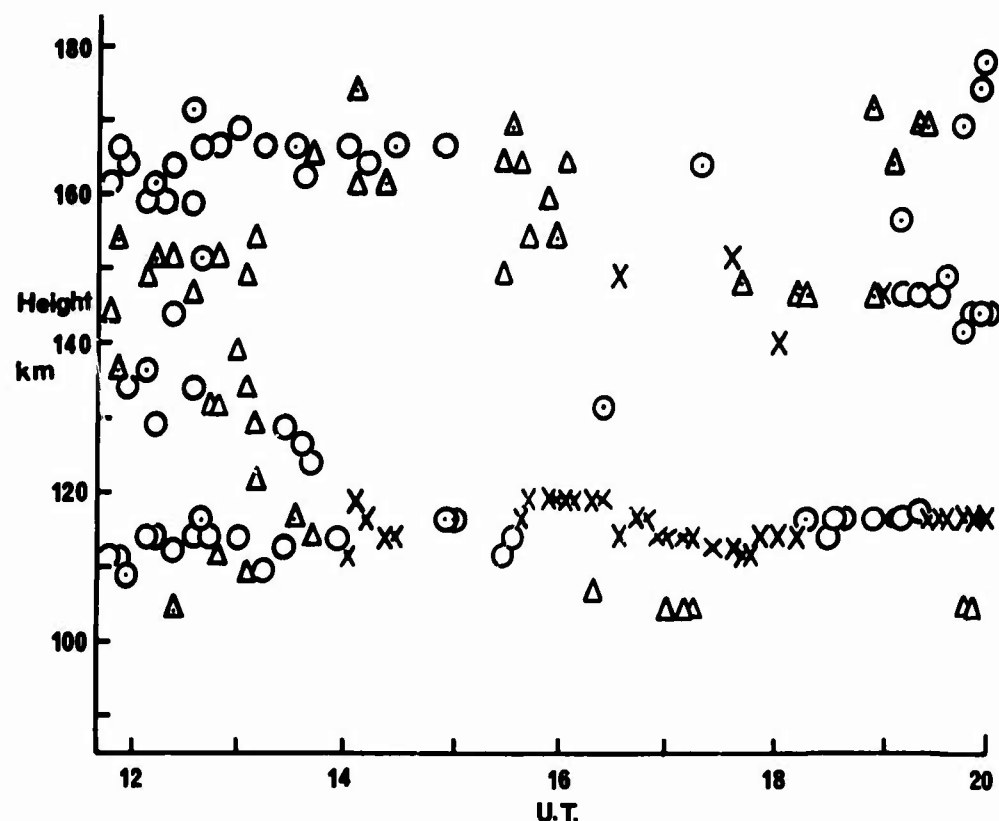


Fig. 5 Heights of resolved peaks,  $\circ$ ; sporadic-type peaks,  $X$ ; and well-marked points of inflection,  $\Delta$ ; from 12 to 20 h UT on 20th May 1968

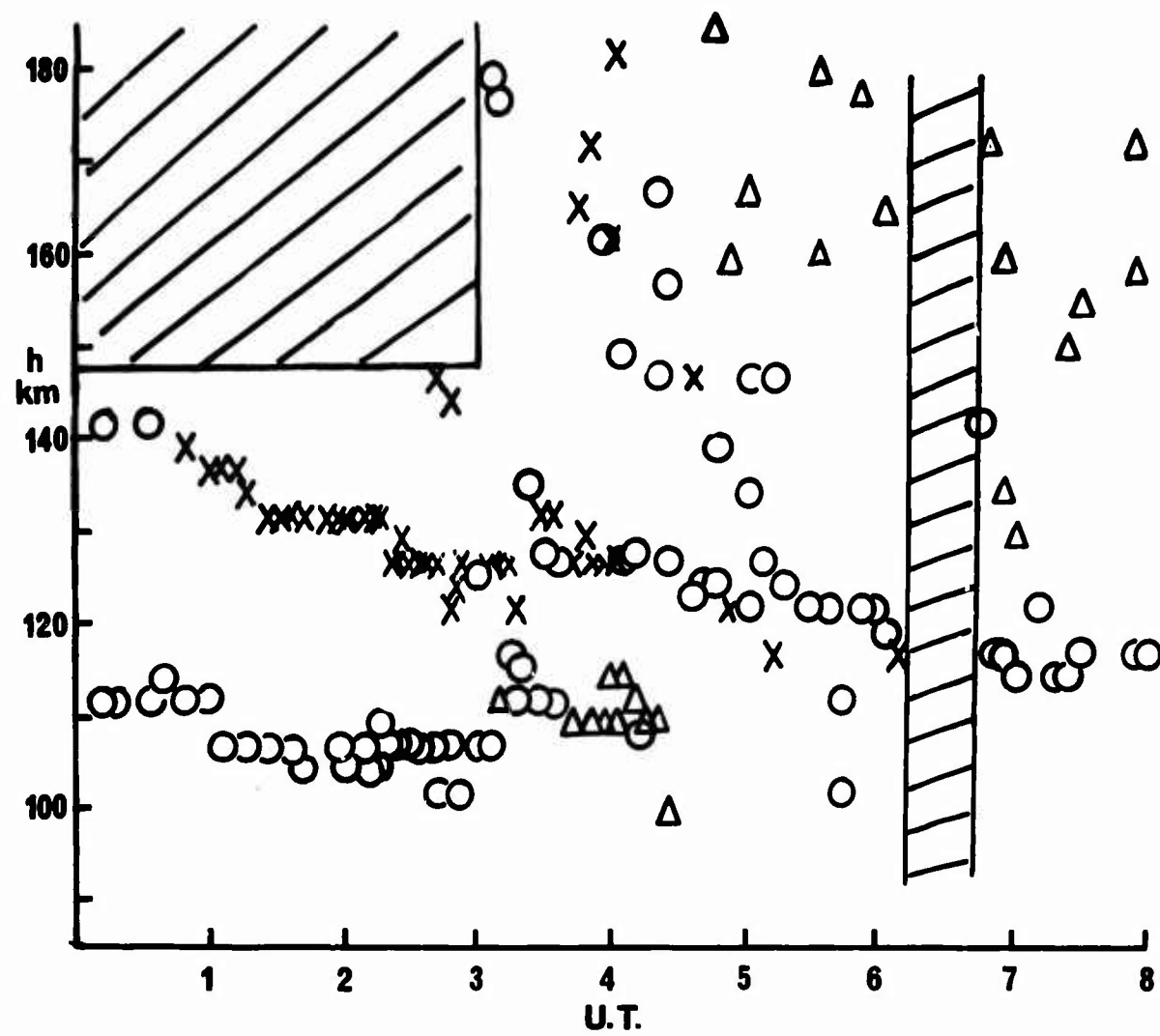


Fig. 6 As Figure 5, from 00 to 08 h UT on 21st May 1968. In shaded areas data was unreliable or missing

## DISCUSSION ON THE PAPERS PRESENTED IN SESSION IV (THOMSON SCATTER)

*Discussion on Paper 31, "Thomson scatter as a communication mode", by A.M.Peterson  
(presented by R.Cohen)*

**Professor E.D.R.Spearman:** What assumption is made as to the width  $W$  of the transmitting and receiving antennas?

**Dr R.Cohen:** 100 meters.

**Dr N.C.Gerson:** What effect would the beaming of 100 kW have upon the normal F2-region? What interactions would result?

**Dr R.Cohen:** That is an interesting question, since D.T.Farley (Journal of Geophysical Research, Vol.68, 1963, p.401), also wondered about it, so he calculated the ionospheric perturbations that would be produced by the powerful incoherent-scatter transmissions being used at incoherent-scatter facilities for ionospheric diagnostics. Deviative absorption in the F-region of this radio-frequency energy heats the electron gas, causing the electron temperature  $T_e$  to increase, and the accompanying diffusion of the heated electrons along the geomagnetic field lines results in a dilution of the electron concentration  $N_e$  in a volume near  $h_{\max}$ , the height of a maximum electron concentration. Farley found that, even at the lowest frequency then being employed for incoherent scatter (at the Jicamarca Radar Observatory in Peru), the effects were minimal, since the exploring frequency (about 50 MHz) was so much greater than the typical penetration frequencies (order of 10 MHz). At  $h_{\max}$  (for the Jicamarca radar) he obtained an elevation in  $T_e$  of about 10%, and a corresponding reduction in  $N_e$  of about 5%. The way to really produce a significant ionospheric perturbation, as described by Farley, is to heat at a frequency just above the penetration frequency, then to lower the heating frequency appropriately as the penetration frequency is thereby reduced.

*Discussion on Paper 32, "Incoherent scatter observations of the E-region", by G.N.Taylor.*

**Dr J.Ramasastry:** I should like to clarify a remark made by the chairman which might give the impression that Dr Taylor's measurements were the first measurements of incoherent scatter in the E-region. To my knowledge such observations, using both Thomson scatter and bottomside ionosonde techniques, have been made at Arecibo, Puerto Rico.

**Dr G.N.Taylor:** I was, of course, aware of the work done at Arecibo, and also at Millstone Hill and by the CNET group in France. However, I believe the Malvern installation is the only peaked incoherent backscatter radar in Europe, and the only one at medium/high latitudes which is capable of making measurements at vertical incidence, and also capable of making E-region measurements at night.

**Dr I.Paghis:** Would you please comment on the reproducibility of the "normal" E-region on consecutive profiles, with the equipment integration time of 5 minutes? Since vertical ionosonde data were not available at the site, but only at a distance of about 130 km, do you consider that sporadic E may have influenced some of the apparently normal E-region profiles?

**Dr G.N.Taylor:** The height of the normal E-layer peak stays constant from one run to the next, but the depth of the valley above it is somewhat variable, sometimes becoming zero, as shown in Figure 1 of my paper. Other features, such as subsidiary peaks between E and F1, are usually visible on at least two consecutive profiles (10 minutes duration), but usually do not last for more than about 20 minutes. In answer to your second question, the distinction between normal and sporadic-type E-peaks is rather arbitrary, and there appears to be a continuous gradation between them. We cannot distinguish between very thin, very dense Es-layers, and thicker, less dense layers if both are unresolved in height. We have not yet attempted any detailed comparisons of our data with measurements from a nearby ionosonde.

**Professor E.D.R. Shearman:** The author stated that it was not possible to measure with an ionosonde the electron density above a maximum in the  $N(h)$ -curve. There is a method, originated by Whitehead, in which the ordinary and extraordinary traces are used together to deduce the electron density above such a maximum. It would be instructive to compare the direct incoherent scatter measurements with such deduced values from ionosonde measurements.

**Dr G.N. Taylor:** It would certainly be very useful to make this comparison.